KfK 3513 B
April 1983

General and Special Engineering Materials Science —Ciencia General y Especial de los Materiales —

Vol. II
- Special Engineering Materials Science - Nuclear Materials under Normal Reactor Operation Conditions

K. Anderko, K. R. Kummerer, G. Ondracek
Institut für Material- und Festkörperforschung

Kernforschungszentrum Karlsruhe

KERNFORSCHUNGSZENTRUM KARLSRUHE

Institut für Material- und Festkörperforschung

KfK 3513 B

General and special engineering materials science
- Ciencia General y Especial de los Materiales -

Vol. II - Special engineering materials science - nuclear materials under normal reactor operation conditions.

K. Anderko, K.R. Kummerer, G. Ondracek

Kernforschungszentrum Karlsruhe GmbH, Karlsruhe

Kernforschungszentrum Karlsruhe GmbH
ISSN 0303-4003

Preface and Summary

The present report about general and special engineering materials science is the result of lectures given by the authors in two terms in 1982 at Instituto Balseiro, San Carlos de Bariloche, the graduated college of the Universidad de Cuyo and Comision Nacional de Energia Atomica, Republica Argentina. These lectures were organised in the frame of the project "nuclear engineering" (ARG/78/020) of the United Nations Development Program (UNDP) by the International Atomic Energy Agency (IAEA).

Some chapters of the report are written in English, others in Spanish. The report is subdivided into three volumes:
Volume I treats general engineering materials science in 4 capital chapters on

- the structure of materials
- the properties of materials
- materials technology
- materials testing and investigation

supplemented by a selected detailed chapter about elasticity plasticity and rupture mechanics.
Volume II concerns special engineering materials science with respect to nuclear materials under normal reactor operation conditions including

- reactor clad and structural materials
- nuclear fuels and fuel elements
- nuclear waste as a materials viewpoint

Volume III - also concerning special engineering materials science - considers nuclear materials with respect to off-normal ("accident") reactor operation conditions including

- nuclear materials in loss-of-coolant accidents
- nuclear materials in core melt accidents.

December 1982 Gerhard Ondracek

P R O L O G O

La presente serie de tres informes procede de un curso de dos semestres sobre ciencias de los materiales en que los autores participaron como docentes invitados en el Instituto Balseiro, para estudiantes de la carrera de Ingenieros Nucleares de la Universidad de Cuyo en San Carlos de Bariloche, dentro del proyecto "Nuclear Engineering" (ARG/78/020) del Organismo Internacional de Energía Atómica (OIEA), United Nations Development Program (UNDP). Los diferentes capítulos están escritos en idioma inglés o español.

El primer informe trata de la ciencia general de los materiales y está subdividido en capítulos sobre:

- la estructura de los materiales
- la tecnología de los materiales y
- el ensayo de materiales

y se completa mediante un capítulo selecto donde se profundiza el tema de las características mecánicas: elasticidad, plasticidad y mecánica de la fractura.

El segundo informe sobre ciencia especial de los materiales trata de los materiales de reactores bajo condiciones normales de funcionamiento del reactor:

- materiales de vaina y de estructura del reactor,
- combustibles nucleares y elementos combustibles,
- desecho nuclear como problema de material.

El tercer informe - también sobre ciencia especial de los materiales - trata de los materiales de reactores bajo condiciones de accidente:

- materiales de reactores en el accidente con pérdida de refrigerante
- materiales de reactores en el accidente de fusión del núcleo del reactor.

Diciembre de 1.982 Gerhard Ondracek

Vorwort und Zusammenfassung

Allgemeine und spezielle Werkstoffkunde

Der vorliegende Report über allgemeine und spezielle Werkstoffkunde ist das Ergebnis von Vorlesungen, die die Autoren über zwei Semester 1982 am Institut Balseiro, dem Graduierten-College der Universität von Cuyo und der Comision Nacional de Energia Atomica in San Carlos de Bariloche, Argentinien, gehalten haben. Die Vorlesungen wurden im Rahmen des Projektes Kerntechnik (ARG/78/020) des Entwicklungsprogramms der Vereinten Nationen (UNDP) veranstaltet und von der Internationalen Atomenergiebehörde (IAEA) in Wien organisiert.

Einige Kapitel des Reports sind in Englisch geschrieben, andere in Spanisch. Der Report gliedert sich in drei Bände:
Band 1 behandelt die Grundlagen der allgemeinen Werkstoffkunde in 4 Kapiteln über

- den Aufbau von Werkstoffen
- die Eigenschaften von Werkstoffen
- die Werkstofftechnologie
- die Werkstoffprüfung und -untersuchung,

die ergänzt werden durch ausgewählte Kapitel über Elastizität, Plastizität und Bruchmechanik.
Band 2 betrifft spezielle Werkstoffkunde und zwar Reaktorwerkstoffe unter normalen Betriebsbedingungen eines Kernreaktors und behandelt

- Reaktorhüll- und Strukturwerkstoffe
- Nukleare Brennstoffe und Brennelemente
- Nuklearen Abfall und seine Behandlung als Werkstoff

Band 3 betrifft ebenfalls spezielle Werkstoffkunde und behandelt Reaktorwerkstoffe unter Störfallbedingungen, wie den Kühlmittelverlust-Unfall und den Core-Schmelzunfall.

Dezember 1982 Gerhard Ondracek

Content/Indice

Part I: Nuclear Clad and structural materials - iron and iron alloys and steels (K. Anderko)

Part II: Nuclear moderator, absorber, shielding and coolant materials as well as nuclear fuels and fuel elements (K.R. Kummerer)

Parte III: Desechos nucleares: un problema de materiales

(G. Ondracek)

PART I:

Nuclear clad and structural materials - iron and iron alloys and steels

K. Anderko

A. Introduction: Origin of the iron isotopes

At the time of the "Big Bang" ("Urknall") only H and He existed within the universe. Heavier elements up to atomic weight 56 (iron isotope) formed by stepwise fusion in the center of stars. No further synthesis is possible in this way since this isotope of medium size is the most stable nucleus.

The element iron, however, consists of 4 stable isotopes (A = 54,56,57,58) as may be seen from an extract of the Karlsruhe chart of nuclides (see Table I). Black isotopes are stable, red ones transmutate by positron decay (β^+) or electron capture (ε), blue ones by negatron (β^-) decay.

How then the stable iron isotopes (57,58) have been formed? One hypothesis assumes the following: Big stars, of more than 10 sun masses, burn relatively fast (millions of years), forming a center of gaseous iron. The iron nuclei capture electrons of the electron gas, which lowers the gas pressure which is mainly due to the electrons. The equilibrium between gas pressure and inertia forces is disturbed which leads to a sudden break-down of the iron core. An extreme densification occurs in that all protons and electrons are combined to neutrons. Hereby gigantic energies are freed which explode the outer shell of the star. In this "supernova" explosion probably all of the heavier elements (A > 56) are formed. Only two such supernovae events appear to have been

occured within historic times within our milky way (1572 and 1604). A residue of a more remote supernova event (in 1054) is the famous cancer nebula. In the center of such nebulae extremely densified neutron stars are assumed to exist (sometimes perhaps also "black holes").

Table I

	52	53	54	55	56	57	58	59	60	61	
26	red	red	black	red	black	black	black	blue	blue	blue	
	$\beta^+\gamma$	$\beta^+\gamma$	5.8	ε	91.7	2.1	0.3	$\beta^-\gamma$	β^-	$\beta^-\gamma$	At % or decay type
	26		28		30		32		34		

number of protons

number of neutrons

B. The Iron - carbon - system

1) Historical development

Fe-C-alloys as main test field of early metallography (correlation of solidification and solid state transformation reactions with microstructure)

1864: H.C. Sorby ("Pearlite")

1878: A. Martens

Ordering of vast amount of observations by physico-chemical principals:

1873: W. Gibbs, then B. Roozeboom:
Phase rule, Thermodynamics of heterogeneous equilibrium

1900: First (incomplete) Fe-C-phase diagram
But the simultaneous occurrence of cementite and graphite was not fully understood.

1904/05: E. Heyn, G. Charpy: Double diagram Fe-cementite, Fe-graphite

Last essential addition:

1930: W. Köster: α-Fe-phase field
Age hardening by C (and N)

2) General constitution and designations

Double diagram (Fig.: 1)

full lines: Fe-cementite system (metastable)

broken lines: Fe-graphite system (stable)

Remarks as to the relative position of corresponding lines in the double diagram:

Lines are not far separated. This is due to the fact that there is no large difference in stability between carbide and graphite.

One-phase fields of the metastable system are more extended (melt, γ)

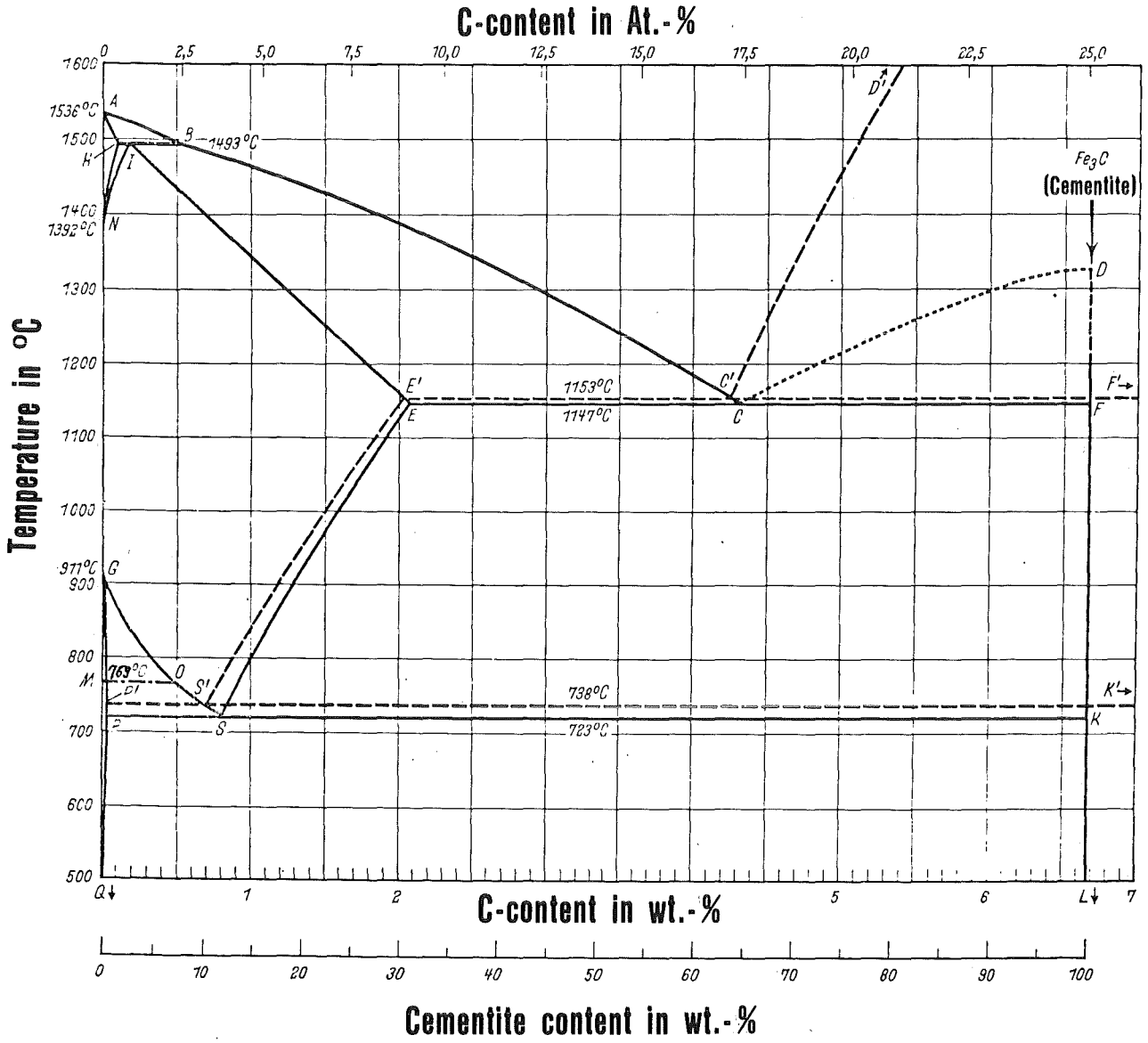
C-content in At.-%
0
2,5
5,0
7,5
10,0
12,5
15,0
17,5
20,0
22,5
25,0
1600
1536°C
A
1500
H
I
B
1493°C
1400
1392°C
N
1300
1200
1100
1000
911°C
G
900
800
M
769°C
O
P
S'
S
E'
E
1153°C
1147°C
C'
C
D'
Fe3C
(Cementite)
D
F'
F
738°C
723°C
K'
K
700
600
500
Q
L
Temperature in °C
1
2
5
6
7
C-content in wt.-%
0
10
20
30
40
50
60
70
80
90
100
Cementite content in wt.-%

Fig. 1

Energy consideration (1000 °C, schematic):

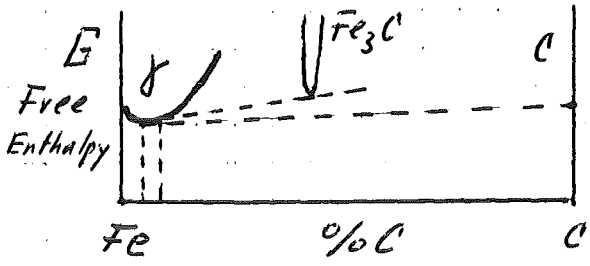

Nucleation of metastable Fe_3C occurs much more readily than that of graphite (especially at low C contents and at fast cooling rates).

Below 1.7% C under normal conditions solidification always occurs according to the Fe-cementite system. At C contents above 1.7% both types of solidification may be active. At fast cooling cementite formation, at slow cooling graphite formation is favored.

Solidification exclusively according to the stable system rarely occurs - only at very slow cooling and in the presence of certain alloying elements like silicon (cast irons >2%C). Cementite may be decomposed to graphite by long-time annealing of white cast irons (→malleable cast iron, with ferritic or pearlitic matrix).

We are mainly concerned with steels, with the greatest tonnages produced in the range up to 0.3%C.
Only in rare instances is steel used with a little more than 1% C (razor blades, cutlery).
Steels contain carbon only in the form of carbide; the occurrence of graphite due to wrong chemical analysis or wrong heat treatment leads to early failure: "Schwarzbruch" (black fracture).
So, further considerations can be concentrated on the $Fe-Fe_3C$-system.

Designations for arrests in temperature-time curves for pure iron (and the $Fe-Fe_3C$-system):

A_4 :	δ/γ-transformation	1392 °C (1665 K)
A_3 :	γ/α-transformation	911 °C (1184 K)
A_2 :	magnetic transformation (α)	769 °C (1024 K)
A_1 :	eutectoid transformation	723 °C (996 K)
A_o :	magnetic transformation(Fe_3C)	210 °C (483 K)

Those temperatures are equilibrium data; with practical cooling or heating rates the arrests occur at somewhat lower or higher temperatures, resp.

A_r : on cooling curves (r=refroidissement)

A_c : on heating curves (c=chauffage)

So, for instance, A_{r3} or A_{c3}.
Those designations are also used with hypoeutectoid steels, so A_{r3} means begin of ferrite precipitiation (at $\overline{GOS}$) from austenite.

These letter designations of equilibrium lines were introduced by W.C. Robert-Austen and B. Roozeboom and have been accepted internationally. Further example: $\overline{ES}$ = line of beginning precipitation of (secondary) cementite from austenite.

3) The metastable system $Fe-Fe_3C$ (Fig. 2)

Melts above 4.3%C (hypereutectic) precipitate primary cementite followed by the eutectic ledeburite. Melts below 4.3%C (hypoeutectic) precipitate Fe(C) solid solution and - if above 2.06%C - followed again by ledeburite.
Between 0.51 and 2.06%C the only solidification product is austenite = f.c.c. Fe(C) solid solution.

At low C contents the primary solidification product is b.c.c. δ-Fe(C). $\overline{AB}$ is the liquidus, $\overline{AH}$ the solidus for these alloys. At 1493 °C a peritectic reaction occurs :

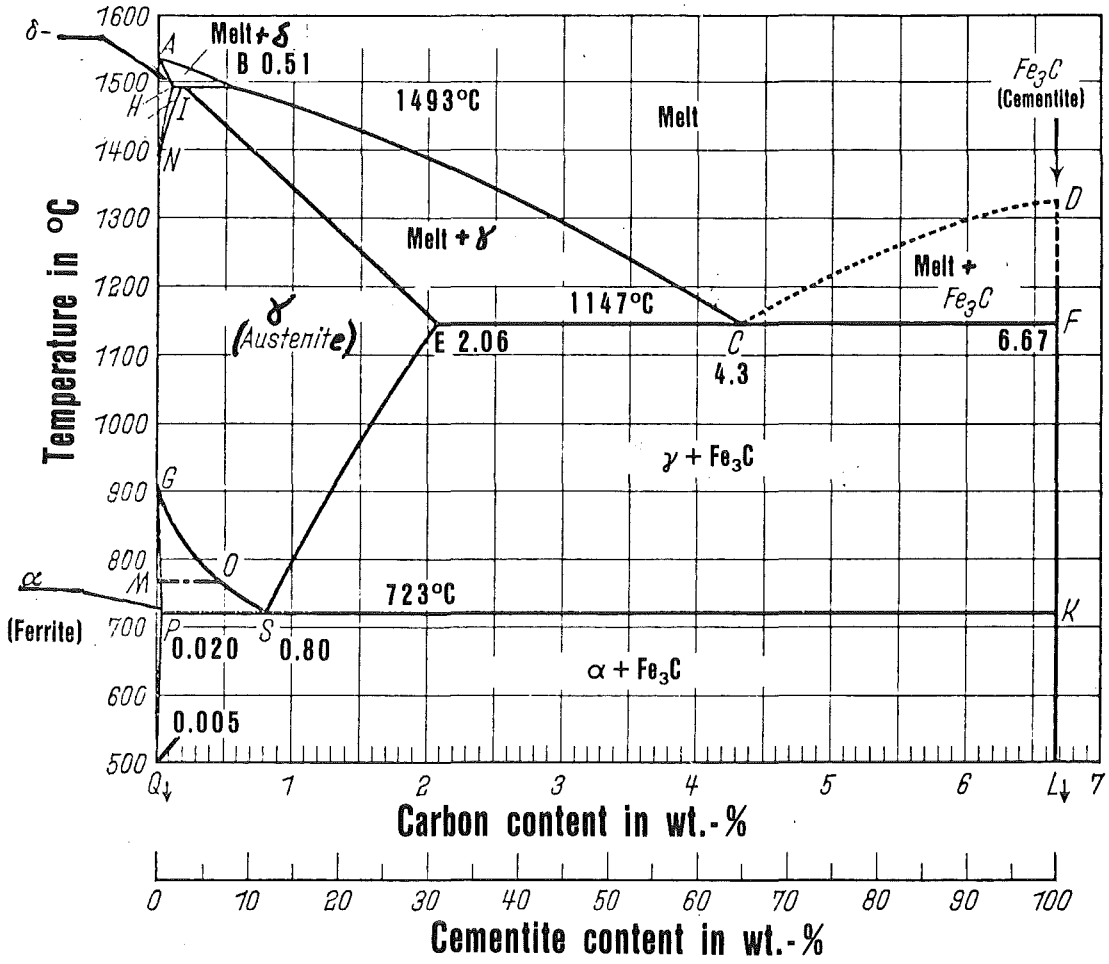
H = 0,10
I = 0.16%C
δ-
Melt+δ
B 0.51
1493°C
Melt
Fe3C
(Cementite)
Melt + γ
Melt +
Fe3C
γ
(Austenite)
1147°C
E 2.06
C
4.3
6.67
γ + Fe3C
α
(Ferrite)
723°C
0.020
0.80
α + Fe3C
0.005
Temperature in °C
Carbon content in wt.-%
Cementite content in wt.-%

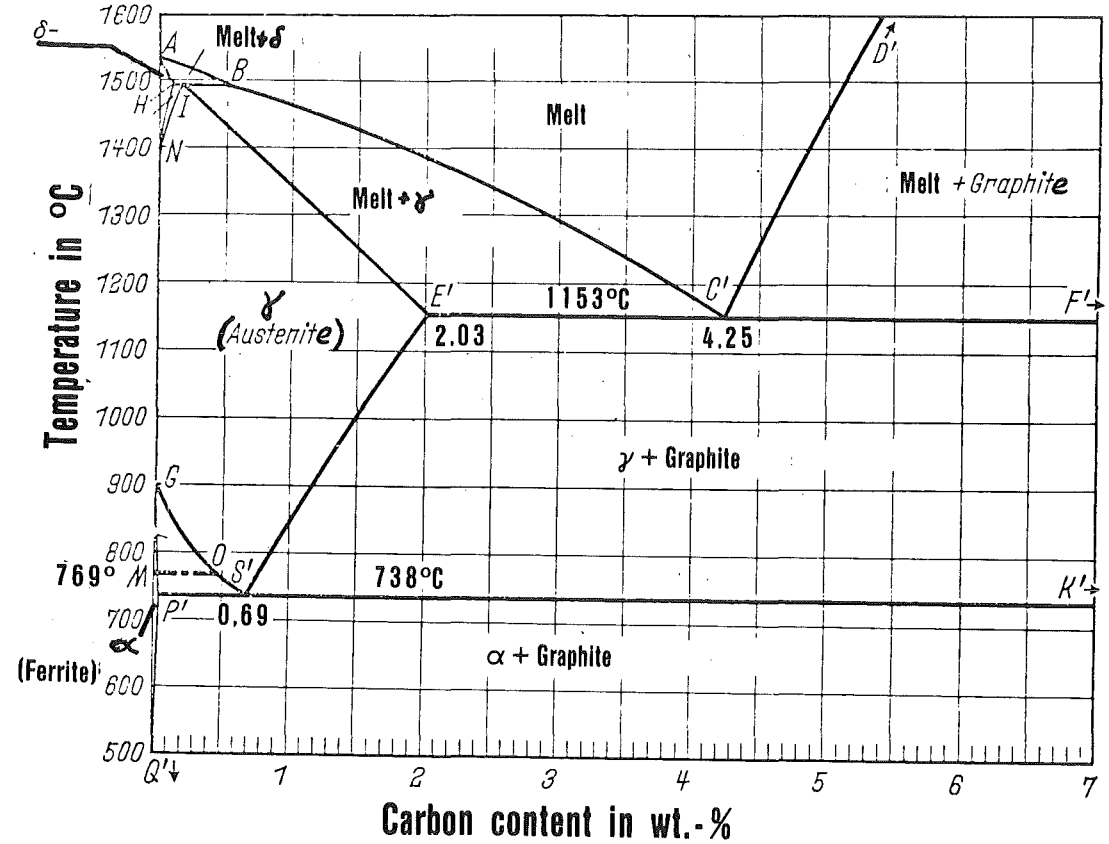
δ-
Melt+δ
Melt
Melt + Graphite
Melt + γ
γ
(Austenite)
1153°C
2.03
4.25
γ + Graphite
769°
738°C
0,69
α
(Ferrite)
α + Graphite
Temperature in °C
Carbon content in wt.-%

Fig. 2 + 3

δ,H (0.10) + Melt, B (0.51) = γ, I (0.16)

At carbon contents above I (0.16), δ disappears. At carbon contents below I (0.16), melt disappears (further transformation $\delta \rightarrow \gamma$ by solid state reaction along $\overline{HN}$, $\overline{IN}$).
This peritectic reaction has only secondary effects on the structure of steels at room temperature. (segregation or coring effects, if not removed by diffusion during hot working and heat treatment).
At slow cooling of solidified alloys with > 0.8%C, secondary cementite is precipitated from austenite along $\overline{ES}$. In alloys below 0.8%C, ferrite is precipitated along $\overline{GOS}$ below A_3 (911 ^{o}C). At 723 ^{o}C the eutectoid reaction occurs :

γ,S (0.80) = α, P (0.02) + Fe_3C, K (6.7)

Latent heat of transformation relatively small (1 kcal/Mol to be compared with heat of fusion, 3.7 kcal/Mol).

The eutectoid structure is called <u>pearlite</u>.

Computation of ratio of ferrite and cementite (in wt% of the total alloy) by means of the lever rule:

$$\text{wt\%Ferrite} = \frac{6.67 - 0.80}{6.67 - 0.02} \quad (\times 100) = 88,3$$

wt% cementite = 11.7

Since the densities of the two components are similar (7.86 and 7.4), the lamellae of α-Fe and Fe_3C have respective widths of about 8:1.
The maximum solid solubility of ferrite (α) for carbon is 0.02% (at 723 ^{o}C). On cooling below that temperature, <u>tertiary cementite</u> is precipitated along $\overline{PQ}$. Precipitation occurs in the ferrite grain boundaries and for this reason it may lead to embrittlement effects (thin sheets).

Dias 11-13, 18, 19, 21 - 24, 26, 28, 29, 31 will be shown for illustration.

4) The stable system Fe-graphite

This system is shown in Fig. 3 .
The position of the eutectic (in wt-%C,T) is close to the point C of the ledeburite-eutectic, however according to the lever-rule the graphite eutectic contains more γ-phase than does ledeburite.

The line $\overline{E'S'}$ runs to the left of $\overline{ES}$; in the region between, the γ-phase is supersaturated with respect to graphite, but not saturated with respect to cementite. Thus the only possible precipitation in this region is that of elementary graphite.

Below the eutectoid point S' (0.69 wt-%C, 738 ^{o}C) ferrite P' coexists with graphite. However, graphite amounts to less than 1 wt-% in this mixture. As was said before, the equilibrium state ferrite + graphite is (fortunately) hard to reach in lower carbon alloys (long-time annealing, silicon alloying).

Dias 36,37,39,41,42 will be shown for illustration.

5) Transformations of Austenite

The alloys follow the equilibrium lines of the phase diagram only under conditions of (very) slow cooling. With faster cooling rates undercooling of the transformations occurs. In those lower temperatures regimes diffusion processes necessary for establishing the equilibrium states are partially or fully suppressed.

As a consequence metastable states and transformation mechanisms differing from the usual nucleation-and-growth type will develop.

With steels, one differentiates mainly between 3 types of transformations:

Pearlite range	("Perlitstufe")
Bainit range	("Zwischenstufe")
Martensite range	("Martensitstufe")

A good survey is given by Fig. 4 showing the shifting of the γ/α -transformation temperatures of a hypoeutectoid steel with increasing cooling rate.

5.1. Transformation in the Pearlite Range

At slow cooling (low undercooling) only pearlite is formed. The influence of cooling rate is, however, quite remarkable. At higher rates the Ar_3 and Ar_1 points are depressed, finally merging into a single arrest point Ar'.
This means that the ferrite precipitation in hypoeutectoid steels along GOS is restrained and finally (above 0.5 %C) completely suppressed. The explanation for this behaviour is given by Fig. 5 , showing an undercooling diagram for the pearlite range. Only in region II the undercooled austenite is oversaturated relative to both ferrite and cementite and the transformation will start with pearlite formation.

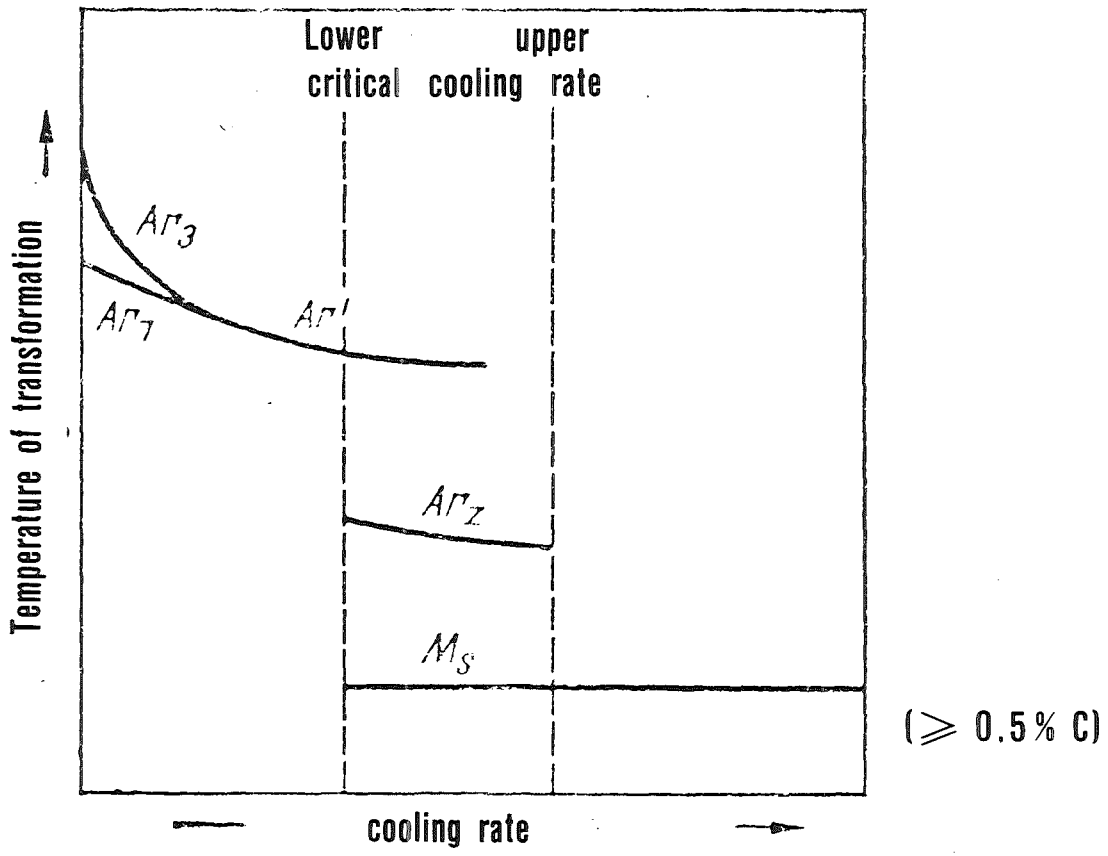

Fig. 4 Shift of γ/α-transformation of a hypoeutectoid steel with increasing cooling rate (Schematic)

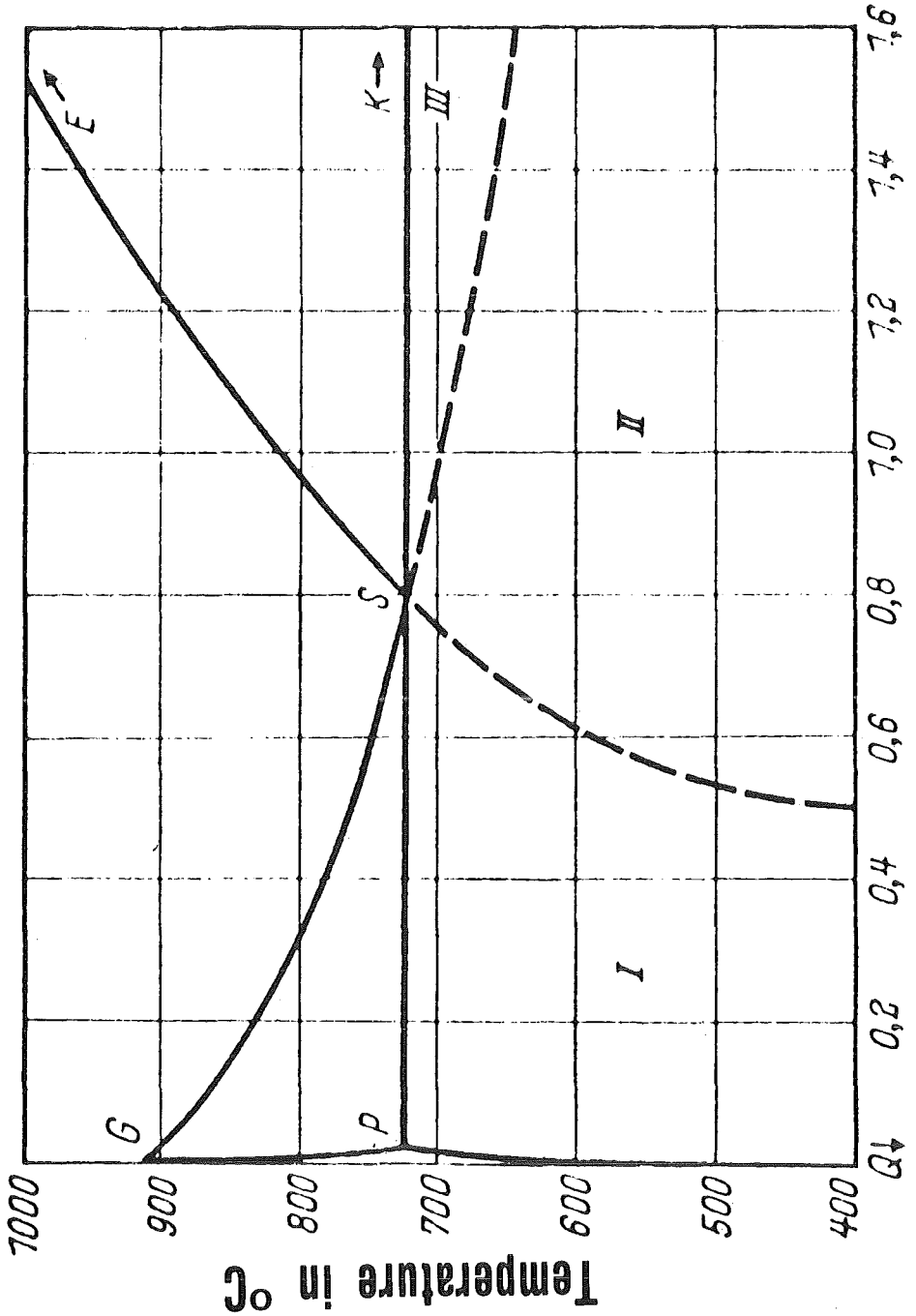
Temperature in °C
1000
900
800
700
600
500
400
Carbon content in wt.-%
0,2
0,4
0,6
0,8
1,0
1,2
1,4
1,6
E
K
III
II
I
S
G
P

Fig. 5

In hypoeutectoid steels proeutectoid ferrite precipitation is normally nucleated at the grain boundaries. With coarse austenite grain and elevated cooling rates, those ferrite precipitates may also occur within the grains, aligned along specific crystallographic planes:
Widmannstätten structure (Fig. 6). -

Pearlite: Alternate plates of ferrite and Fe_3C, with ferrite as the continuous phase. Formation by nucleation and growth. Active nucleus probably Fe_3C. Heterogeneous nucleation (at grain boundaries, residual Fe_3C particles).

Rate of (isothermal) pearlite formation as a function of temperature. Factors are:

a) Nucleation rate
b) Growth rate
   b1) diffusion rate
   b2) diffusion length (interlamellar spacings)
   b3) Energy gain (driving force)

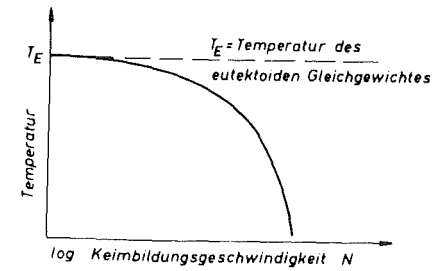

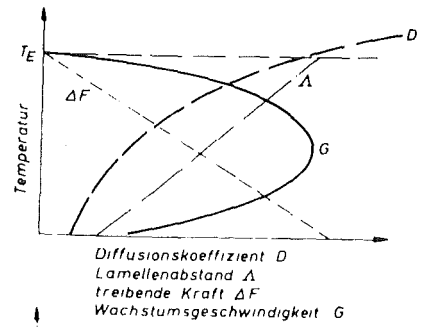

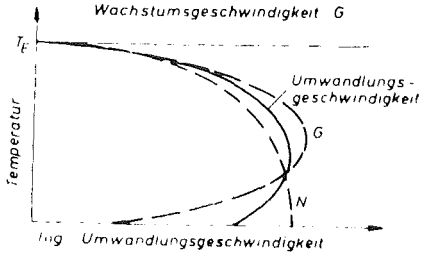

T_E Eutectoid temperature
N Nucleation rate
Λ Interlamellar spacing
ΔF Driving Force
G Growth Rate

Umwandlungsgeschwindigkeit = Rate of Transformation

(taken from H. Böhm, Einführung in die Metallkunde, Bibliographisches Institut, 1968)

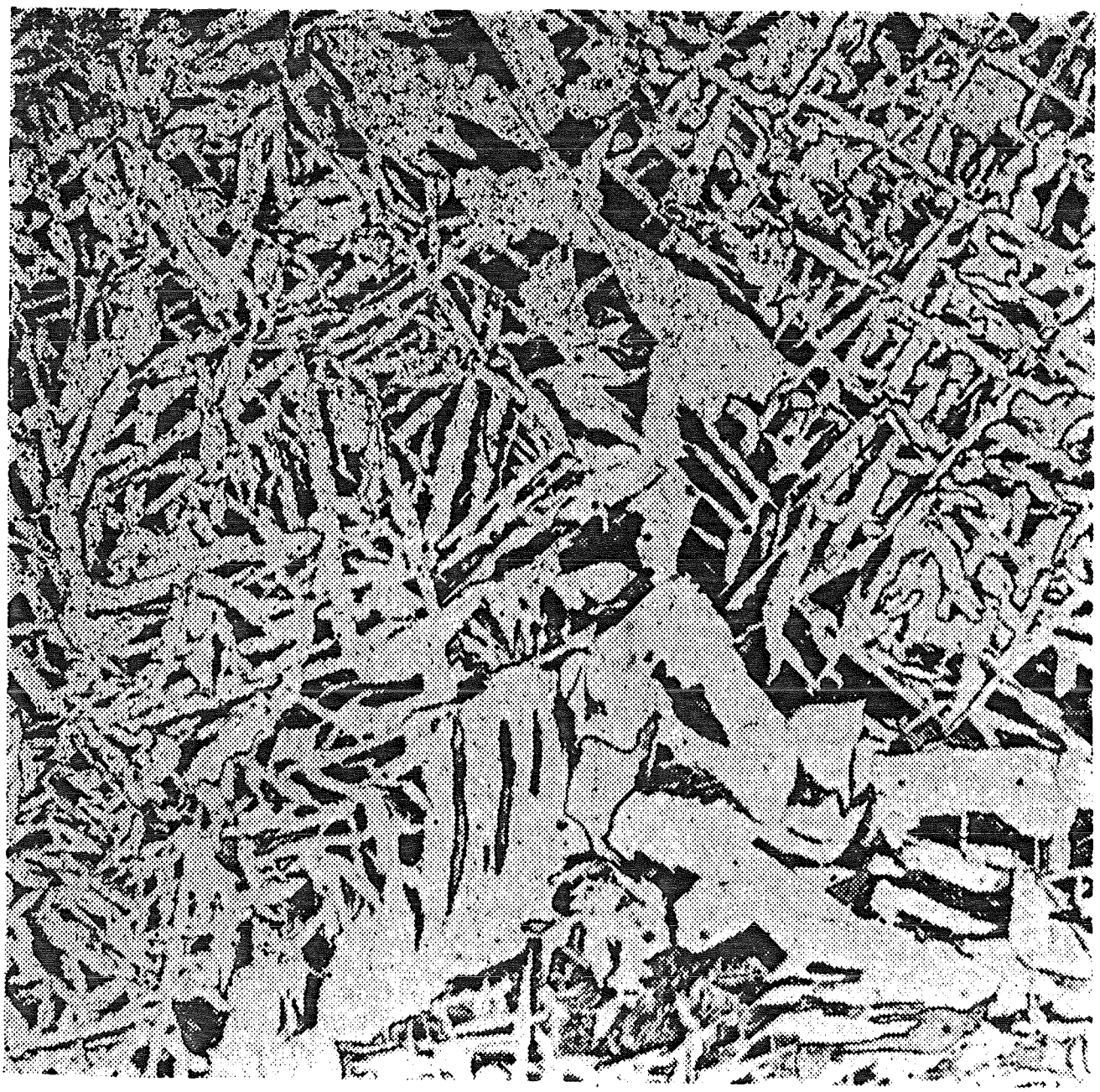

Fig.-6-

The interlamellar spacings at isothermal transformation

700°C	1 µm
600°C	0.1 µm

are independent of austenite grain size (contrast to size of martensite needles): "not structure sensitive".
Since the growth rates parallel and vertical to the lamellae are nearly equal, the "pearlite nodules" are usually spherical.

5.2. Transformation in the Martensite Range

Preventing diffusion processes by quenching from the austenite phase field (> upper critical cooling rate) leads to a diffusionless shear transformation, the martensitic transformation.

General remarks on transformations:

1. Nucleation and growth-type:

Example: Pearlite formation from undercooled austenite
(non-equilibrium irreversible transformation)

Progress of transformation
at constant temperature
("isothermal"),
Nucleation and transformation are
time dependent

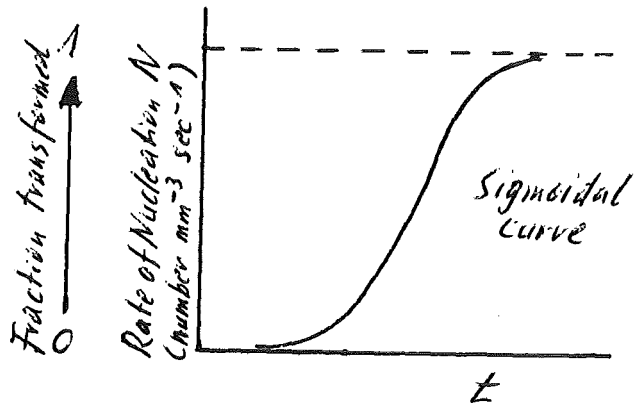

Fraction transformed

$$f(t) = 1 - e^{(-\pi/3)NG^3t^4}$$

(Johnson, Mehl 1939)

(T and growth rate G = constant)

Thermally activated diffusion processes (displacement of atoms relatively to their neighbours over distances greater than the interatomic ones).

2. Martensitic transformations

Progress of transformation only by change in T which increases driving force (free energy difference).

Martensite (heterogeneous) nucleation requires no thermal activation, therefore no time dependence ("athermal") [1)]

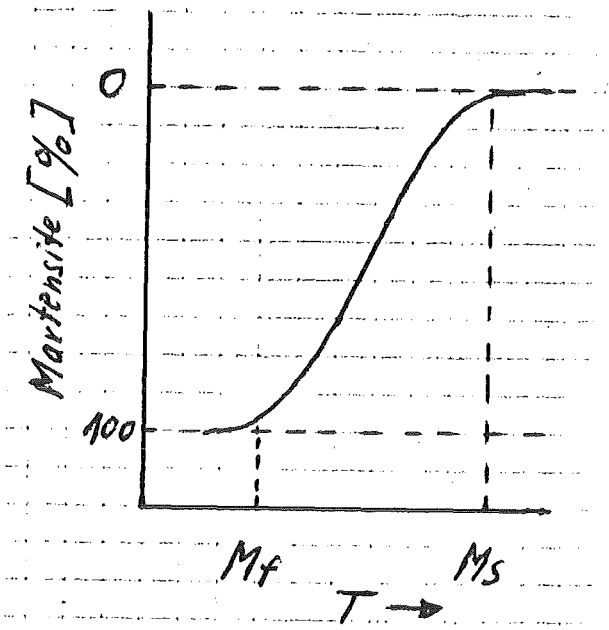

Diffusion-less shear transformation:
Atoms moving (suddenly and cooperatively) only a fraction of the interatomic distance.

(A new piece of terminology has evolved:
martensitic: "military transformation", because rearrangement of atoms occurs in a orderly disciplined manner.
nucleation and growth: "atoms behave as civilians, each following their individual routes along the broad reaction path" (Nutting).)

Examples showing characteristic differences:

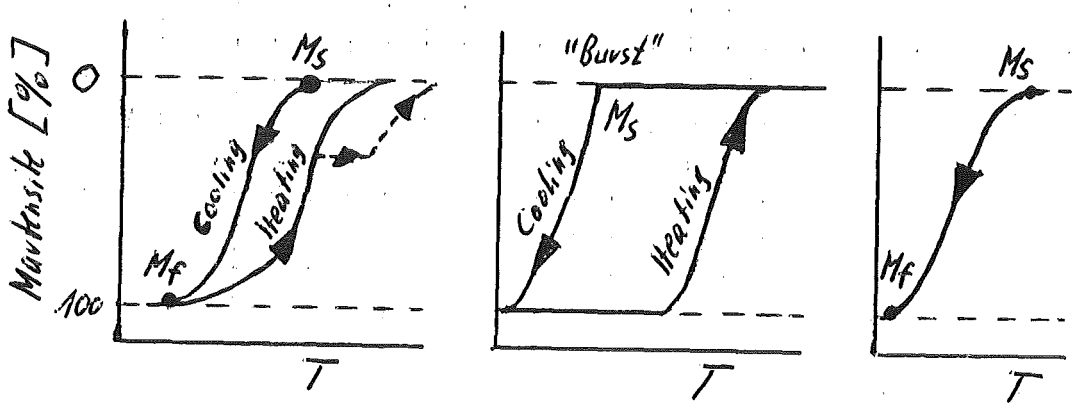

Indium-Thallium	Fe-Ni	Fe-C
Movement of single interface. Reversible, hysteresis $2^{o}C$ Stabilization	Small lens-shaped plates which grow very rapidly to their final size. Progress of transformation by nucleation of additional plates. Reversible, hysteresis 420^{o} (with ε_{pl}:$100^{o}C$) Stabilization in cooling and heating)	Plates, formation time 10^{-7}s. Progress as under Fe-Ni. Not reversible (decomposition even under moderate reheating)

[1] Small amounts of austenite may be transformed to martensite isothermally.

Note: stabilization means there is a secondary, though negative, time effect on the transformation.

In the Fe-C system, the result of the martensitic transformation is a tetragonally distorted α-Fe lattice. The distortion increases with increasing C-content.

The variation of M_s and M_f-temperatures with C-content in C-steels is shown in Fig. 7 .
The size of the martensite plates or needles depends on the prior austenite grain size, inclusion content and the fraction of still untransformed austenite ("structure sensitive").

TEM investigations have revealed that, depending on the transformation temperature, there exists two slightly different types of martensite: Fig. 8 .

5.3. Transformation in the Bainite Range

Above the lower critical cooling rate (see Fig. 4) the pearlite transformation will decrease and finally cease. Instead, at

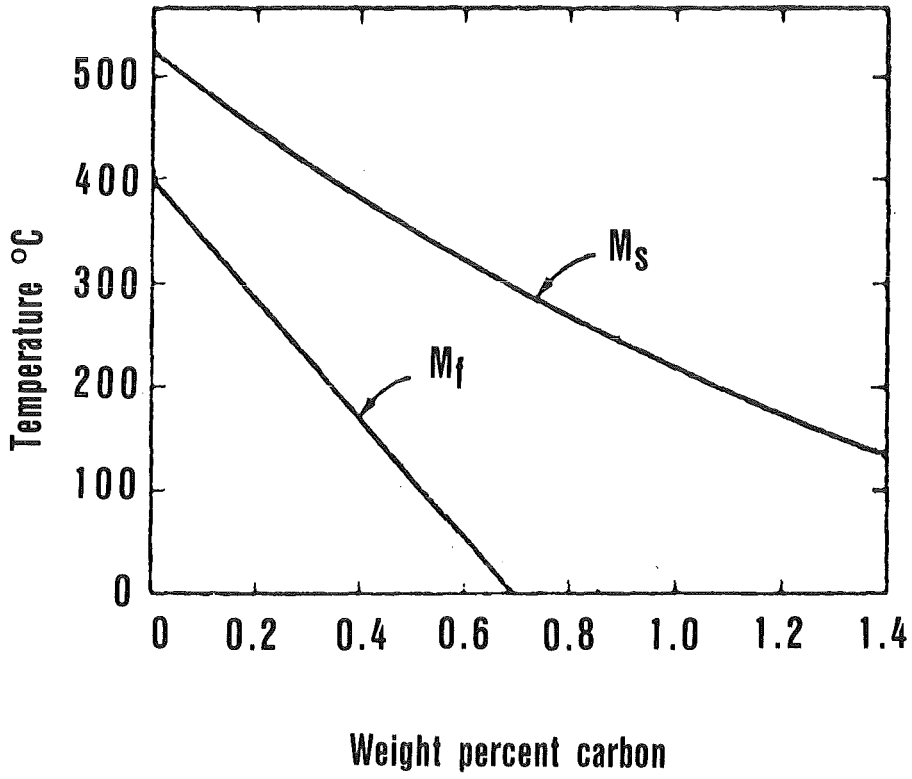

Fig. 7 Variation of M_S and M_f with carbon concentration in steel. (Troiano, A. R., and Greninger, A. B. Metal Progress, 50, 303 [1946].)

Favored by lower transformation temperatures
Low internal dislocation density,
C atoms on normal interstitial sites. —

Macroscopic shear by twinning

Twinned lenticular mart.

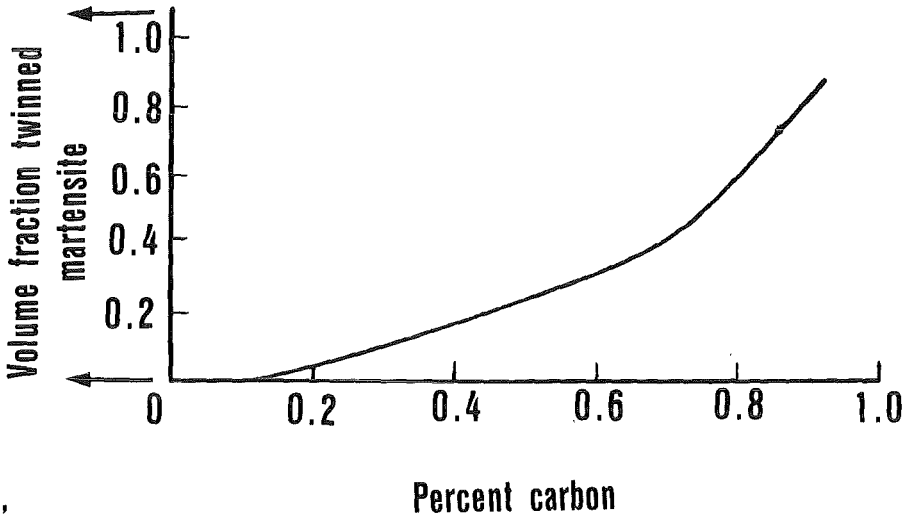

Lath martensite

High internal dislocation
density (10^{11}-10^{12} cm^{-2}),
arranged in plate-shaped cells.
C atoms segregate around dislocations,
even after a rapid quench. —

Macroscopic shear by slip

Fig. 8 Curve showing the volume fraction of twinned martensite as a function of the carbon concentration.
(Speich. G. R., TRANS AIME, 245, 2553 [1969])

lower temperatures, a new type of transformation occurs, that of the bainite range ("Zwischenstufe").

It is characterized by the fact that at temperatures below 500°C diffusion of Fe and of substitutional alloying elements (Mn, Ni, Cr) practically ceases whereas C atoms are still able to diffuse. Not too surprising, therefore, the bainite reaction exhibits a dual nature. In a number of respects it reveals properties that are typical of a nucleation and growth type of transformation (pearlite), but, at the same time is shows an equal number that would classify it as a martensitic type of reaction:

	Pearlite range	Bainite range	Martensite range
•Diffusion of C	+	+	-
•Diffusion of substit. alloying elements	+	-	-
•T=Thermally activated A=Athermal transformation	T	T	A
•Complete transformation (just below start temp.)	+	-	-
•Growth shape	Spheres	Plates	Plates
•Nucleated by	Fe_3C	Ferrite	(heterogeneously)

The dualism is also evident from the following diagrams of isothermal transformations:

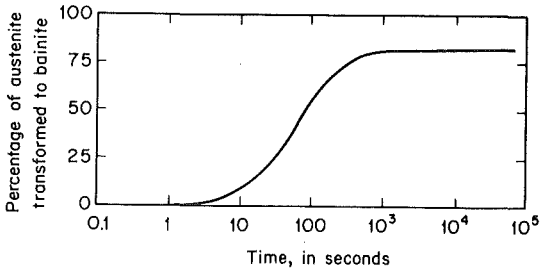

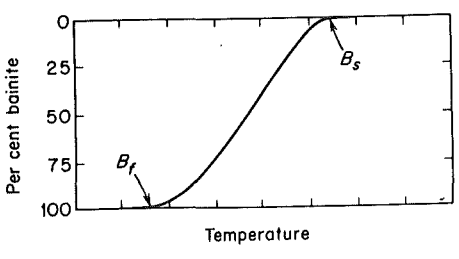

Bainite is a mixture of ferrite and carbide.
Differences to pearlite:

a) Ferrite supersaturated with C and alloying elements.
b) Structure.

Each bainite plate is composed of a volume of ferrite in which carbide particles are embedded.
One differentiates between upper and lower bainite.

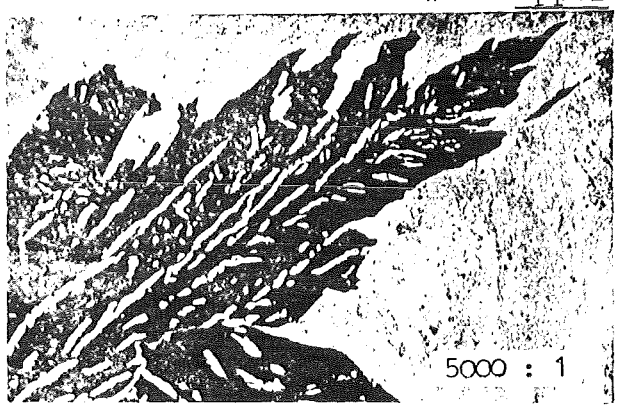

Upper bainite (475°C)
5000 x
Fe_3C-particles paralleling length of ferrite plate

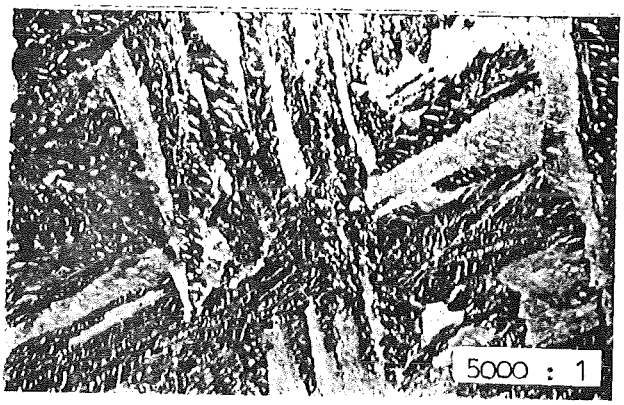

Lower bainite (325-250°C)
5000 x
ε-carbide ($Fe_{2.4}$ C?), smaller in size and as cross-striations (55° to axis of plate)

In the upper bainite range the carbide particles may even be seen in a light microscope at high magnification. In the lower bainite range carbide precipitation is more incomplete and in such a fine dispersion that EM-techniques are required.

In Fe-C alloys there occurs an overlapping of the pearlite and bainite transformation ranges at around 500°C. On the other hand, in alloyed steels both transformation ranges are well separated. This can best be shown by means of so-called Time-Temperature-Transformation (TTT) diagrams in which, of course, also the martensitic transformation may be plotted.

5.4. Time-Temperature-Transformation (TTT) diagrams

Two types

isothermal transformation
(to be read along time axis)

continuous cooling
(to be read along plotted cooling rate lines)

Examples: a) Alloy steels of good hardenability:

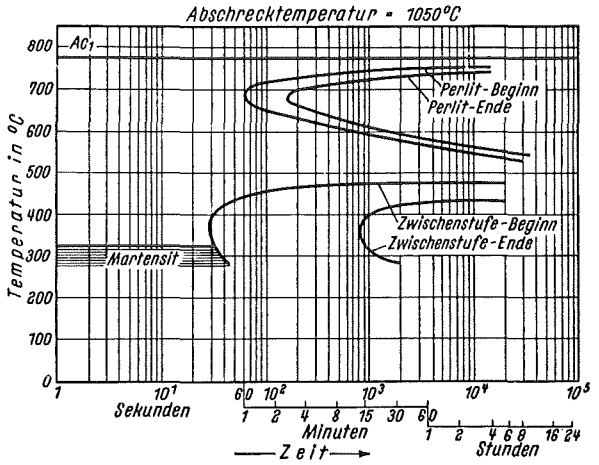

Isothermal TTT-diagram
0.45C, 3.5Cr
The pearlitic and bainitic transformation ranges are well separated in those steels.

(Abschrecktemperatur = Quenching temperature
Beginn = Start
Zwischenstufe = Bainite range
Stunden = hours)

Note: Minima in incubation times follow from opposing effects:

Pearlite: With decreasing temperature thermodynamic instability of austenitic increases and diffusion rates of C and Fe decrease.

Bainite: With decreasing temperature the driving force for the shearing transformation of austenitic increases, but the diffusion rate of C decreases.

At temperatures just below B_S (="Zwischenstufe Beginn"), austenite does not transform completely to bainite.-

In the heat treatment cycle called "Austempering" the workpiece (alloy steel) is therefore cooled rapidly to a temperature in the lower bainite region and is held at that temperature so that the section transforms completely to bainite (residual stresses and distortion minimal). Likewise, in "Martempering" an alloy steel workpiece, it is cooled rapidly to a temperature just above Ms and held there until the piece attains a uniform temperature, then cooled slowly (air cooling) through the martensitic range. This procedure causes martensite to form more or less simultaneously throughout the entire section, thereby holding transformational stresses at a very low level, minimizing distortion and danger of cracking.

b) Low alloyed steels:

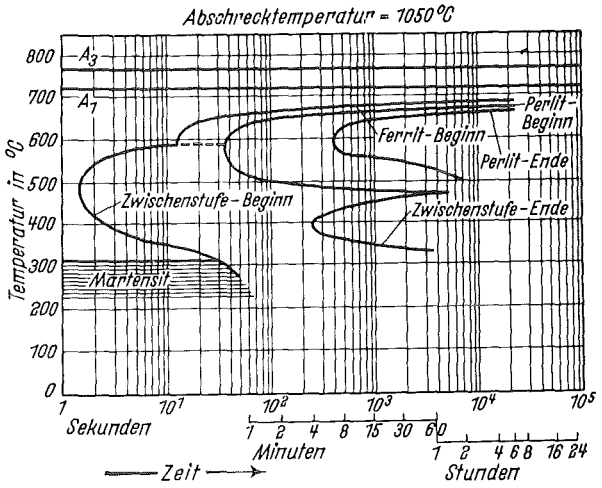

Isothermal
0.43C, 1.67 Mn, 0.10 V

There is overlapping of the pearlite and bainite transformation ranges.
Transformation at 500°C starts with bainite formation which after 2 minutes is followed by pearlite formation.

Comparison = Shift of lines (s. 24a) !

c) Carbon steel:

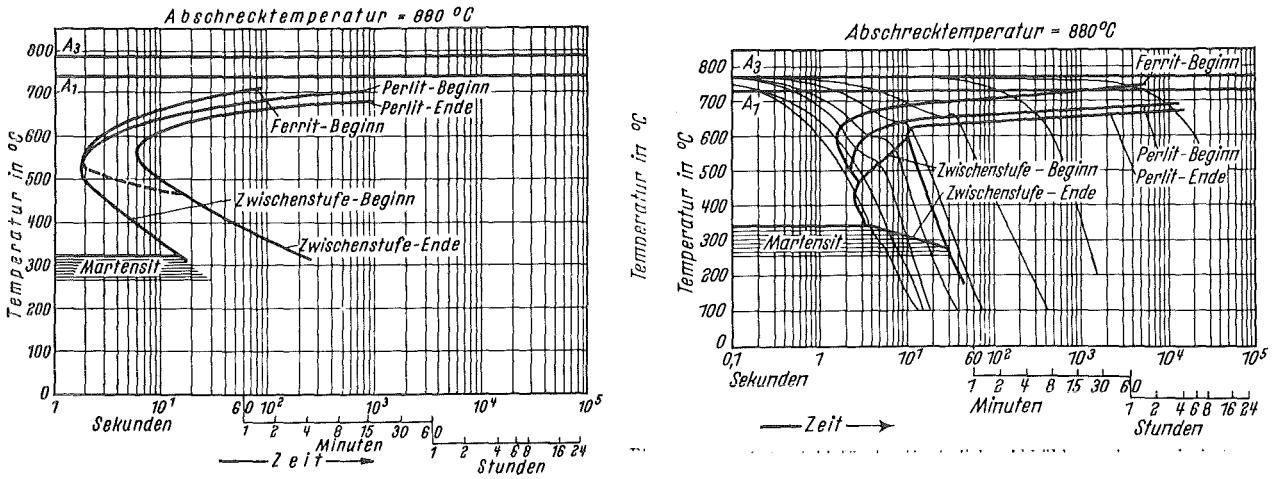

0.45 % C

Isothermal Continuous

There is a smooth and continuous transition between pearlite and bainite (both are not athermal). Due to the lack of substitutional solid solution elements the pearlite reaction occurs early.

Fig. 9 shows the influence of different cooling rates on the microstructure of a eutectoid Fe-C-steel.

Full anneal: Furnace cooled from austenitizing temperature
(Power supply of furnace shut off).
24 h to room temperature.
Transformation close to equilibrium
(coarse pearlite in case of eutectoid steel).

Normalization: Intermediate cooling rate by pulling
the specimens out of the austenitizing furnace
(air cooling). Transformation at 600-500°C.
(Fine pearlite in case of eutectoid steel).

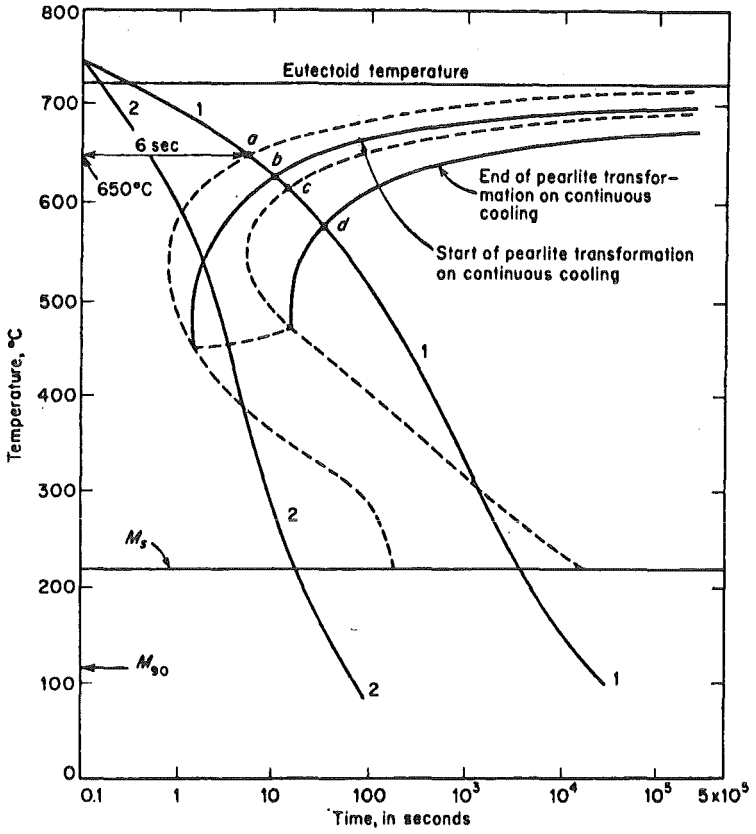

Fig. 18.1 The relationship of the continuous cooling diagram to the isothermal diagram for an eutectoid steel (schematic). (After *Atlas of Isothermal Transformation Diagrams,* United States Steel Corporation, Pittsburgh, 1951.)

reached the 650° C isothermal at the end of 6 sec and may be considered to have been at temperatures above 650° C for the entire 6-sec interval. Because the time required to start the pearlite transformation is longer at temperatures above 650° C than it is at 650° C, the continuously cooled specimen is not ready to form pearlite at the end of 6 sec. Approximately, it may be assumed that cooling along path 1 to 650° C has only a slightly greater effect on the pearlite reaction than does an instantaneous quench to this temperature. In other words, more time is needed before transformation can begin. Since in continuous cooling an increase in time is associated with a drop in temperature, the point at which transformation actually starts lies to the right and below point *a*. (The location of this point may be estimated with the aid of several appropriate assump-

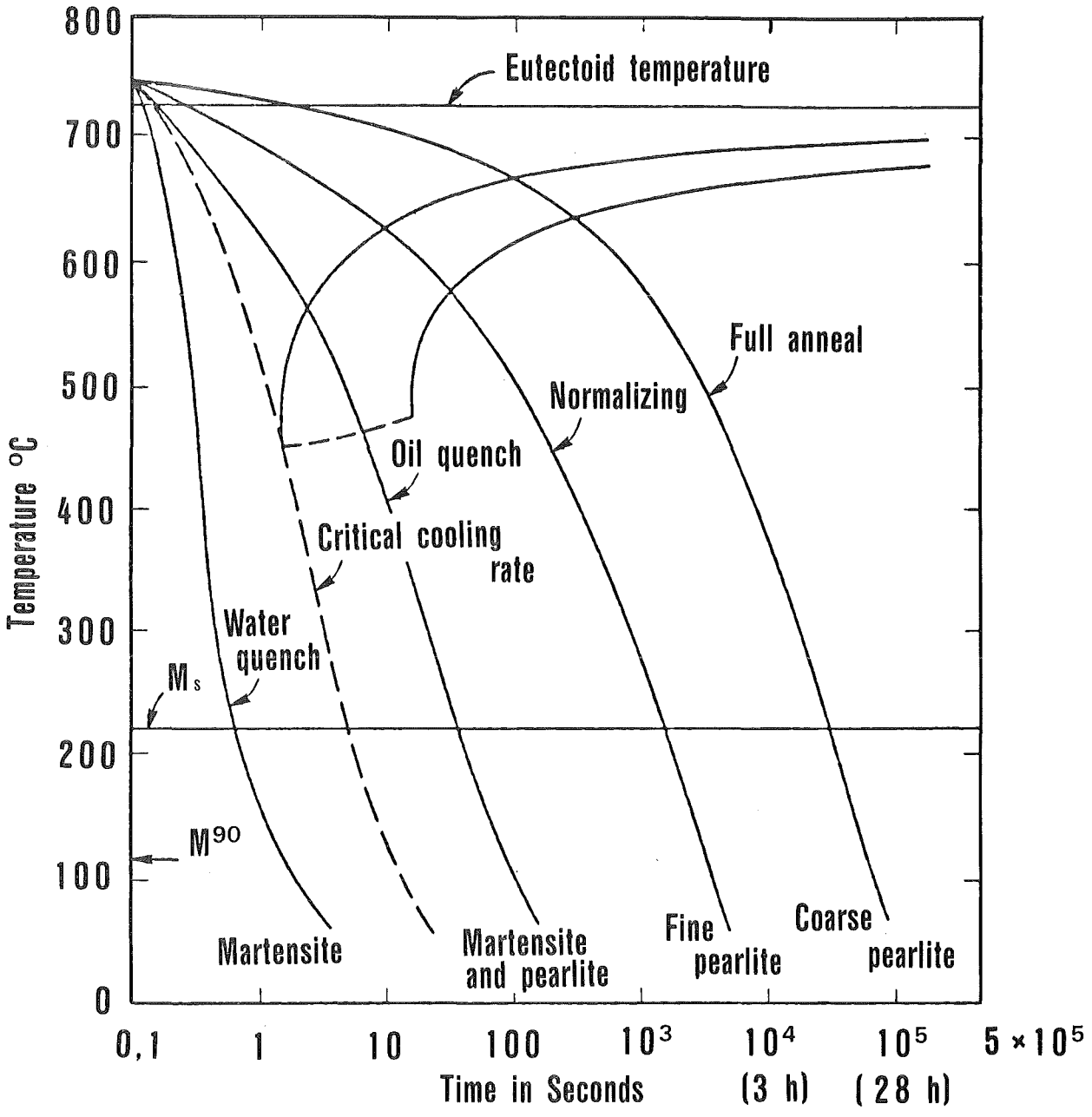
800
700
600
500
400
300
200
100
0
Temperature °C
Eutectoid temperature
Full anneal
Normalizing
Oil quench
Critical cooling rate
Water quench
M_s
M^{90}
Martensite
Martensite and pearlite
Fine pearlite
Coarse pearlite
0,1
1
10
100
10^3
10^4
10^5
5×10^5
Time in Seconds
(3 h)
(28 h)

Fig. 9

5.5. Tempering

Steels rapidly cooled from the austenite phase field are not in a thermodynamically stable state. On reheating into temperature regimes of sufficient high diffusion rates (time, temperature!) microstructural changes will occur.

Pearlitic and bainitic structures will not be greatly modified by tempering: With Fe-C alloys only spheroidization and coarsening of cementite will occur.

A pure martensite structure is very brittle and therefore of little practical use. To improve ductility and stability, a tempering treatment is almost always used. In this tempering martensite decomposes stepwise into undistorted ferrite and cementite. The single steps may overlap each other and they progress the faster the higher the temperature of tempering. The 4 stages that can be differentiated in Fe-C-alloys are collected ~~in Fig.~~ below .

(A fifth stage of tempering exists with alloy steels: precipitation of alloy carbides (>540°C), which leads to "secondary hardening", and eventually of intermetallic compounds)

Stage 1: ~ 0-200°C

< 0.2 C | > 0.2 C

Segregation of C to lath dislocations and boundaries (max. 0.2 %).

Martensite still slightly tetrag. distorted

no carbide precipitation | + ε-carbide ($Fe_{2.4}C$) visible in TEM

Light microscope:

Dark etching

(Only small amount of isothermal martensite formation from austenite below 100°C)

Stage 2: $\sim$ 100-300°C

Retained austenite → bainite
(cubic ferrite + ε-carbide)

(Positive length changes;
Simple exponential rate law

$$\text{rate} = \frac{1}{t} = A \cdot \exp\ (-Q/RT)$$

Decomposition controlled by diffusion of
C in austenite)

Thus after the 1. and 2. stage of tempering, the microstructure will exhibit: Martensite (still tetr. distorted) + eventually ε-carbide and Bainite (cubic α+ε-carbide).

Stage 3: Formation of cubic ferrite + Fe_3C
(at 200°C: rod-shaped transition phase)
at 250°C: ferrite + Fe_3C
at 500-600°C: recovery of dislocations in
the ferrite lath boundaries
(→ low-dislocation-density
acicular ferrite)
At short time tempering below A_1 the acicular (needle) structure persists, only the cementite coarses.
600-700°C: Prolonged tempering leads in C-steels
to recrystallization (equiaxed ferrite)

Stage 4: Growth of the spheroidal Fe_3C-particles
(Ostwald ripening)

Literature to Chapter B

The manuscript is mainly based on

Das Zustandsschaubild Fe-C und die Grundlagen der
Wärmebehandlung der Fe-C-Legierungen
4. Auflage, 1961,
Verlag Stahleisen mbH, Düsseldorf, Germany

Lichtbildvortrag "Die Fe-C-Diagramme"
2. Auflage, 1964,
Beratungsstelle für Stahlverwendung,
Düsseldorf, Germany

Physical Metallurgy Principles by R.E. Reed-Hill,
2. edition, 1973, D. van Nostrand Co, New York

Metals Handbook, Vol. 1, Properties and Selection:
Irons and Steels, 9. edition, 1978,
American Society for Metals.

H. Böhm, Einführung in die Metallkunde, Bibliographisches
Institut, Mannheim/Wien/Zürich 1968

C. Alloy Steels

1) Steel Designation Systems

Many different designation systems may be (and were) used: Composition, finishing methods, strength, product form. Nowadays there is a tendency to prefer the classification according to chemical composition.

1.1. Federal Republic of Germany

Rough classification:

- Unalloyed (=C-)steels
  (< 0.5 Si, < 0.8 Mn, < 0.1 Al or Ti)
- Low and medium alloyed steels
  (≤ 5% alloying elements)
- Highly alloyed steels
  (> 5% alloying elements)

1.1.1. Unalloyed construction steels (Baustähle, Massenstähle) will normally not be further heat treated by the user. Therefore designation according to strength level:

St 38 = steel (Stahl) with a minimum tensile strength of 380 N/mm^2.

1.1.2. Unalloyed carburizing and tempering steels (Einsatz- und Vergütungsstähle) will normally be further heat treated by the user(carburized, quenched, tempered):

Designation according to chemical composition:

Rule: C for carbon, followed by its content in

$\frac{1}{100}$ wt - %

example: C 15 = average carbon content 0.15 wt %.

further indications:

k for low P- and S-content
example: Ck 10

m for specified S-content
example: Cm 45

1.1.3. Low and medium alloyed steels:

Rule:
- First figure(s) = carbon content in $\frac{1}{100}$ wt-%
- Main alloying elements, sequence according to average wt-% content.
- At the end: Figures for alloy content

Multiplicators:

4 for Cr, Co, Mn, Ni, Si, W
10 for Al, Be, Cu, Mo, Nb, Pb, Ta, Ti, V, Zr
100 for P, S, N, Ce
1000 for B

examples: 15 Mn 3 = 0.15 wt-%C (0.12-0.18)
0.8 wt-%Mn

29 CrMoV 9 = 0.29 wt-%C
2.3 wt-% Cr and lower Mo and V contents.

1.1.4. Highly alloyed steels:

Rule: X, followed by
C-content in $\frac{1}{100}$ wt-%, followed by main alloying elements, at the end: figures for alloy content (Without multiplicators)

Examples: X6 CrNi 18 11
= steel with 0,06 wt-%C,
18 wt-% Cr and 11 wt-%Ni

X10 NiCrMoTiB 15 15
= steel with 0,10 wt-%C,
15 wt-%Ni, 15 wt-%Cr and
lower Mo, Ti and B contents.

1.1.5. Superalloys:

Examples: NiFeCr12Mo
= Ni-Fe-alloy with 12 % Cr and some Mo

CoCr25NiW
= Cobalt-base, 25 wt-%Cr and lower Ni- and W-contents.

1.2. USA

The most widely used systems for designation are also based on chemical composition.

AISI-SAE system for carbon and low-alloyed steels
(Metals handbook, 9th ed.)

Numerals and digits	Type of steel and nominal alloy content
Carbon Steels	
10XX(a)	Plain carbon (Mn 1.00% max)
11XX	Resulfurized
12XX	Resulfurized and rephosphorized
15XX	Plain carbon (max Mn range—1.00 to 1.65%)
Manganese Steels	
13XX	Mn 1.75
Nickel Steels	
23XX	Ni 3.50
25XX	Ni 5.00
Nickel-Chromium Steels	
31XX	Ni 1.25; Cr 0.65 and 0.80
32XX	Ni 1.75; Cr 1.07
33XX	Ni 3.50; Cr 1.50 and 1.57
34XX	Ni 3.00; Cr 0.77
Molybdenum Steels	
40XX	Mo 0.20 and 0.25
44XX	Mo 0.40 and 0.52
Chromium-Molybdenum Steels	
41XX	Cr 0.50, 0.80 and 0.95; Mo 0.12, 0.20, 0.25 and 0.30
Nickel-Chromium-Molybdenum Steels	
43XX	Ni 1.82; Cr 0.50 and 0.80; Mo 0.25
43BVXX	Ni 1.82; Cr 0.50; Mo 0.12 and 0.25; V 0.03 min
47XX	Ni 1.05; Cr 0.45; Mo 0.20 and 0.35
81XX	Ni 0.30; Cr 0.40; Mo 0.12
86XX	Ni 0.55; Cr 0.50; Mo 0.20
87XX	Ni 0.55; Cr 0.50; Mo 0.25
88XX	Ni 0.55; Cr 0.50; Mo 0.35
93XX	Ni 3.25; Cr 1.20; Mo 0.12
94XX	Ni 0.45; Cr 0.40; Mo 0.12
97XX	Ni 0.55; Cr 0.20; Mo 0.20
98XX	Ni 1.00; Cr 0.80; Mo 0.25
Nickel-Molybdenum Steels	
46XX	Ni 0.85 and 1.82; Mo 0.20 and 0.25
48XX	Ni 3.50; Mo 0.25
Chromium Steels	
50XX	Cr 0.27, 0.40, 0.50 and 0.65
51XX	Cr 0.80, 0.87, 0.92, 0.95, 1.00 and 1.05
Chromium Steels	
50XXX	Cr 0.50 } C 1.00 min
51XXX	Cr 1.02 } C 1.00 min
52XXX	Cr 1.45 } C 1.00 min
Chromium-Vanadium Steels	
61XX	Cr 0.60, 0.80 and 0.95; V 0.10 and 0.15 min
Tungsten-Chromium Steel	
72XX	W 1.75; Cr 0.75
Silicon-Manganese Steels	
92XX	Si 1.40 and 2.00; Mn 0.65, 0.82 and 0.85; Cr 0.00 and 0.65
High-Strength Low-Alloy Steels	
9XX	Various SAE grades
Boron Steels	
XXBXX	B denotes boron steel
Leaded Steels	
XXLXX	L denotes leaded steel

(a) XX in the last two digits of these designations indicates that the carbon content (in hundredths of a percent) is to be inserted.

example:

4422 0.35-0.45% Mo
0.20-0.25% C
(0.70-0.90% Mn)
(0.15-0.30% Si)

AISI-System: Standard Grades of Wrought Stainless and Heat-Resisting Steels

The first digit defines a major series:

200 series: austenites in which some Ni has been replaced by Mn and N.

300 series: Ni-stabilized austenites.

400 series: Cr-steels with up to 2.5 % Ni; some can be hardened by quenching and tempering ("martensitic steels"), the others are classified as "ferritic".

500 series: Cr-steels with 4-6 % Cr.

AISI type	Nominal composition, % C	Mn, max	Si, max	Cr	Ni	Other(a)
Austenitic Steels						
201	0.15 max	7.50(b)	1.00	16.00 to 18.00	3.50 to 5.50	0.25 max N
202	0.15 max	10.00(c)	1.00	17.00 to 19.00	4.00 to 6.00	0.25 max N
301	0.15 max	2.00	1.00	16.00 to 18.00	6.00 to 8.00	....
302	0.15 max	2.00	1.00	17.00 to 19.00	8.00 to 10.00	....
302B	0.15 max	2.00	3.00(d)	17.00 to 19.00	8.00 to 10.00	....
303	0.15 max	2.00	1.00	17.00 to 19.00	8.00 to 10.00	0.15 min S
303(Se)	0.15 max	2.00	1.00	17.00 to 19.00	8.00 to 10.00	0.15 min Se
304	0.08 max	2.00	1.00	18.00 to 20.00	8.00 to 12.00	....
304L	0.03 max	2.00	1.00	18.00 to 20.00	8.00 to 12.00	....
305	0.12 max	2.00	1.00	17.00 to 19.00	10.00 to 13.00	....
308	0.08 max	2.00	1.00	19.00 to 21.00	10.00 to 12.00	....
309	0.20 max	2.00	1.00	22.00 to 24.00	12.00 to 15.00	....
309S	0.08 max	2.00	1.00	22.00 to 24.00	12.00 to 15.00	....
310	0.25 max	2.00	1.50	24.00 to 26.00	19.00 to 22.00	....
310S	0.08 max	2.00	1.50	24.00 to 26.00	19.00 to 22.00	....
314	0.25 max	2.00	3.00(e)	23.00 to 26.00	19.00 to 22.00	....
316	0.08 max	2.00	1.00	16.00 to 18.00	10.00 to 14.00	2.00 to 3.00 Mo
316L	0.03 max	2.00	1.00	16.00 to 18.00	10.00 to 14.00	2.00 to 3.00 Mo
317	0.08 max	2.00	1.00	18.00 to 20.00	11.00 to 15.00	3.00 to 4.00 Mo
321	0.08 max	2.00	1.00	17.00 to 19.00	9.00 to 12.00	5 × C min Ti
347	0.08 max	2.00	1.00	17.00 to 19.00	9.00 to 13.00	10 × C min Cb-Ta
348	0.08 max	2.00	1.00	17.00 to 19.00	9.00 to 13.00	10 × C min Cb-Ta, 0.10 max Ta
Martensitic Steels						
403	0.15 max	1.00	0.50	11.50 to 13.00	....	....
410	0.15 max	1.00	1.00	11.50 to 13.50	....	....
414	0.15 max	1.00	1.00	11.50 to 13.50	1.25 to 2.50	....
416	0.15 max	1.25	1.00	12.00 to 14.00	....	0.15 min S
416(Se)	0.15 max	1.25	1.00	12.00 to 14.00	....	0.15 min Se
420	0.15 min	1.00	1.00	12.00 to 14.00	....	....
431	0.20 max	1.00	1.00	15.00 to 17.00	1.25 to 2.50	....
440A	0.60 to 0.75	1.00	1.00	16.00 to 18.00	....	0.75 max Mo
440B	0.75 to 0.95	1.00	1.00	16.00 to 18.00	....	0.75 max Mo
440C	0.95 to 1.20	1.00	1.00	16.00 to 18.00	....	0.75 max Mo
501	0.10 min	1.00	1.00	4.00 to 6.00	....	0.40 to 0.65 Mo
502	0.10 max	1.00	1.00	4.00 to 6.00	....	0.40 to 0.65 Mo
Ferritic Steels						
405	0.08 max	1.00	1.00	11.50 to 14.50	....	0.10 to 0.30 Al
430	0.12 max	1.00	1.00	14.00 to 18.00	....	....
430F	0.12 max	1.25	1.00	14.00 to 18.00	....	0.15 min S
430F(Se)	0.12 max	1.25	1.00	14.00 to 18.00	....	0.15 min Se
446	0.20 max	1.50	1.00	23.00 to 27.00	....	0.25 max N

The term "martensitic" is somwhat misleading as it is applied to tempered or annealed material in which the martensite has been more or less widely decomposed. Thus the name is given on the basis of the behaviour during heat treatment.-

Much more stringent rules are imposed on the supplier if one orders materials according to standard specifications. The most comprehensive and widely used standard specifications are those of the American Society for Testing and Materials (ASTM). Such a specification is a published document ("Annual Book of ASTM Standards").
An example well-known to nuclear engineers is that of the Standard Specification ASTM A 508 for "Quenched and tempered vacuum-treated carbon and alloy steel forgings for pressure vessels". It imposes on the supplier requirements as to the manufacturing process (melting, forging, heat treatment), chemical composition, mechanical properties, non destructive Inspection and so on.

Literature: Stahl-Eisen-Liste
5. Auflage 1975, 6. Auflage 1977
Verlag Stahleisen mbH, Düsseldorf

Metals Handbook
8. edition, Vol. I (1961)
9. edition, Vol. I (1978)
American Society for Metals, Metals Park,
Ohio (USA).

2) General Influence of Alloying Elements

Low alloyed steels have principally similar properties as unalloyed C-steels; however, the alloying additions are aimed at to improve special properties:

- better hardenability at milder quenching (less distortion and less danger of crack formation)
- higher yield point at similar hardness
- higher toughness at high strength
- higher elastic limit and therefore higher fatigue strength
- better high temperature strength

Highly alloyed steels (> 5%) may exhibit properties not shown by C- or low alloyed steels:

- corrosion resistance (passivity)
- oxidation resistance at high temperatures
- cutting ability at red-hot-temperatures (cutting tools for high-speed machining)
- special physical properties (magnetic, electric, expansion).

In alloyed steels mainly the same phases occur as already known from Fe-C-alloys. New phases are: alloy carbides, intermetallics (σ-FeCr for instance), elements like Pb (or Cu).

The alloying elements can be divided into two groups depending on whether they close or open the γ-field. Fig. 1 indicates a clear dependence on the position of the elements in the Periodic Table. The only inconsistency appears to be the behaviour of C and N; however, this is easy to understand because all interstitial elements open the γ-field due to sites of smaller strain energy available in the fcc lattice.

Fig. 1

Periodic Table of Elements

(International atomic weights, 1955)

M = preferentially in matrix
C = preferentially in carbide
—— closing
--- opening
μ-loop

1 H 1.0080																	2 He 4.003
3 Li 6.940	4 Be 9.013											5 B 10.82	6 C 12.011	7 N 14.008	8 O 16.0000	9 F 19.00	10 Ne 20.183
11 Na 22.991	12 Mg 24.32											13 Al 26.98	14 Si 28.09	15 P 30.975	16 S 32.066	17 Cl 35.457	18 Ar 39.944
19 K 39.100	20 Ca 40.08	21 Sc 44.96		22 Ti 47.90	23 V 50.95	24 Cr 52.01	25 Mn 54.94	26 Fe 55.85	27 Co 58.94	28 Ni 58.71	29 Cu 63.54	30 Zn 65.38	31 Ga 69.72	32 Ge 72.60	33 As 74.91	34 Se 78.96	35 Br 79.916	36 Kr 83.80
37 Rb 85.48	38 Sr 87.63	39 Y 88.92		40 Zr 91.22	41 Nb 92.91	42 Mo 95.95	43 Tc (99)	44 Ru 101.1	45 Rh 102.91	46 Pd 106.4	47 Ag 107.880	48 Cd 112.41	49 In 114.82	50 Sn 118.70	51 Sb 121.76	52 Te 127.61	53 I 126.91	54 Xe 131.30
55 Cs 132.91	56 Ba 137.36	57 La 138.92	58 to 71	72 Hf 178.50	73 Ta 180.95	74 W 183.86	75 Re 186.22	76 Os 190.2	77 Ir 192.2	78 Pt 195.09	79 Au 197.0	80 Hg 200.61	81 Tl 204.39	82 Pb 207.21	83 Bi 209.00	84 Po 210	85 At (210)	86 Rn 222
87 Fr (223)	88 Ra 226.05	89 Ac 227	90 to ?															

Lanthanides	58 Ce 140.13	59 Pr 140.92	60 Nd 144.27	61 Pm (145)	62 Sm 150.35	63 Eu 152.0	64 Gd 157.26	65 Tb 158.93	66 Dy 162.51	67 Ho 164.94	68 Er 167.27	69 Tm 168.94	70 Yb 173.04	71 Lu 174.99
Actinides	90 Th 232.05	91 Pa 231	92 U 238.07	93 Np (237)	94 Pu (242)	95 Am (243)	96 Cm (245)	97 Bk (249)	98 Cf (249)	99 Es	100 Fm	101 Md (256)	102 No	

The best-known example for an opening γ-field is the Fe-C-system. Fe-Cr (Fig. 2) and Fe-Si are examples for systems with closed γ-loops. There are also systems in which closing of the γ-loop is prevented by the interaction of an intermetallic phase (Fe-Nb, Fig. 3).

Systems with a closed γ-loop exhibit alloys which are purely ferritic up to the melting point. The limiting concentration is, however, generally much dependent on the C-content: thus binary Fe-Cr alloys are ferritic above about 13 % Cr, whereas a carbon addition of only 0.25 % shifts the limiting Cr-concentration to 24 %.

Those ferritic steels show no α/γ-transformation. Thus they cannot be normalized, hardened or tempered. A grain refinement treatment requires plastic deformation plus recrystallization. A well-know representative of a ferritic steel is the transformer steel (0.05 % C, 3-4 Si), a magnetically soft steel for the cores of transformers.

Half-ferritic steels consist of non-transformable δ-ferrite + other phases:

a) 0.22 % C, 17 % Cr, 1.7 % Ni:
   At high T: δ + γ
   After slow cooling from 1100°C: δ + Pearlite
   After quenching: δ + Martensite

b) 0.1 % C, 1.7 % Si, 15.4 % Mn, 10.8 % Cr, 1 % Ti:
   At all temperatures between 1250 and 20°C: δ + γ
   (not hardenable)

In systems exhibiting an open γ-field the A_3-point is lowered by the alloy addition. There are consequently alloys which are austenitic from RT to the m.p. Again they cannot be quench-hardened and grain refinement is only possible by cold deformation and recrystallization (The danger of coarse grain formations is, however, lower than with ferritic steels due to the higher recrystallization temperature of the austenite). Austenites normally exhibit low yield strengths but also a high degree of strain hardening by cold working.

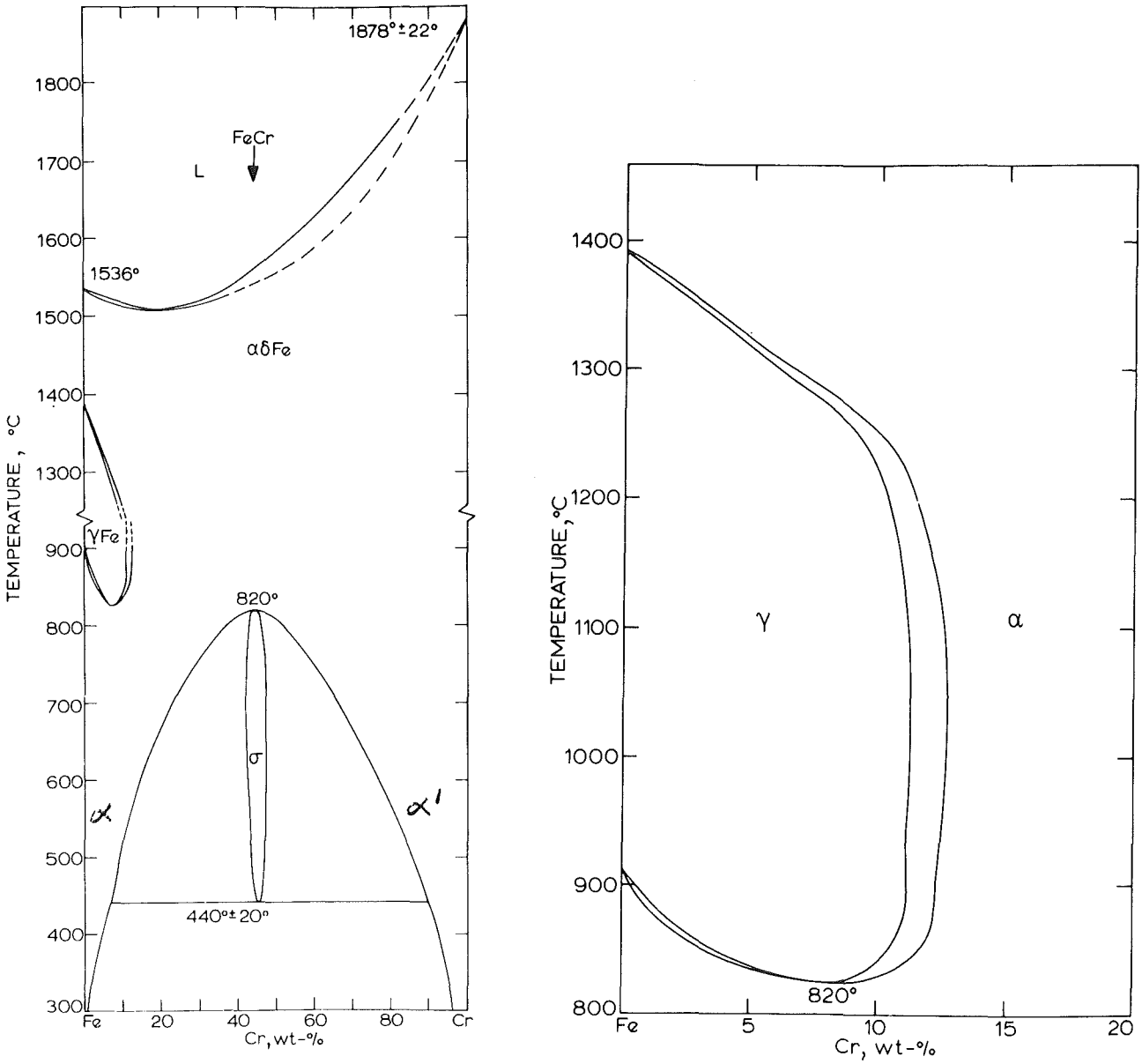

Fig. 2 Fe-Cr system

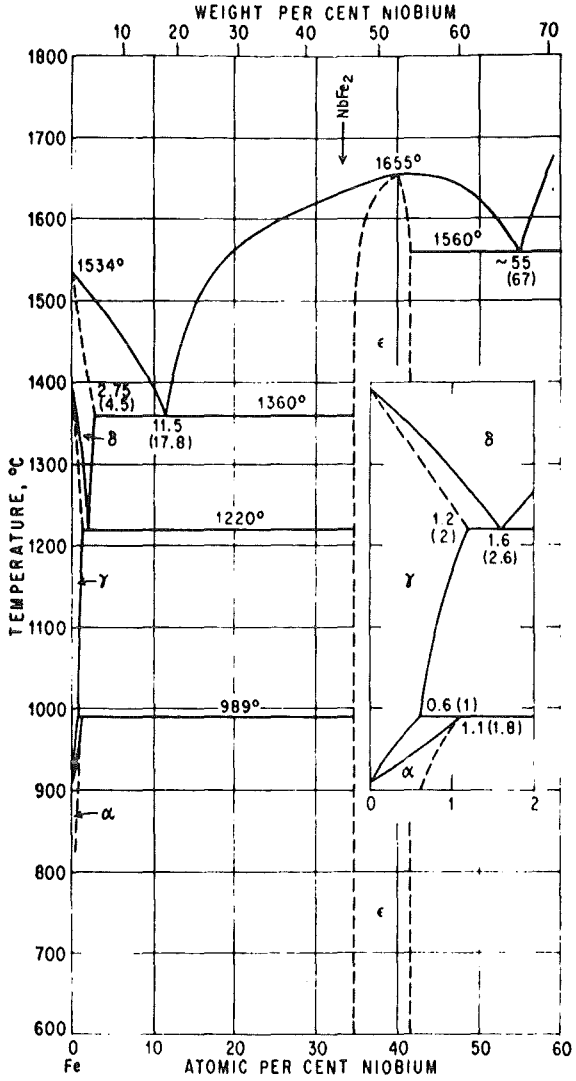

Fig. 3 Fe-Nb system

The study of the transition between an open and a closed γ-field inside a ternary phase diagram is always an interesting and presumptuous task. Fig. 4 gives a schematic example for the special case that the two alloying elements A and B may form a continuous solid solution with each other.

In carbon-containing multinary systems the phase relations are even more complicated. The partition of an alloy addition between the matrix and a carbide phase then depends on the trend to carbide formation. Information on those aspects is also given in Fig. 1.

At low concentrations of a weak carbide former this element may be taken up in cementite as mixed crystal: $(Fe, X)_3C$. Examples are: $(Fe, Mn)_3C$, $(Fe, Cr)_3C$, $(Fe, Si)_3C$.

At higher concentrations of a weak carbide former, but already at low concentrations of a strong carbide former alloy carbides (Sonderkarbide) are formed. Examples are Cr_7C_3, Mo_2C, W_2C, V_4C_3, TiC, NbC. Frequently the alloy carbides contain also Fe in solid solution: $(Fe, Cr)_{23}C_6$ = "$M_{23}C_6$", $(Fe, Cr)_7C_3$.

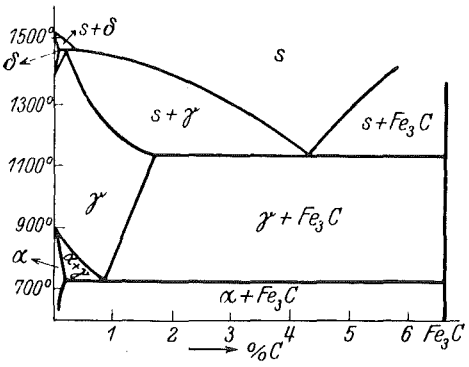

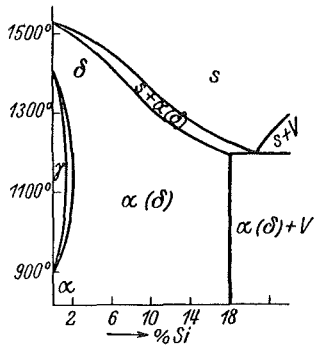

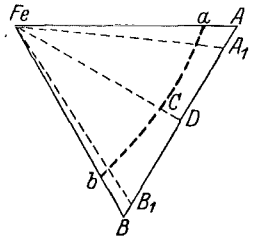

Abb. 159. Konzentrationsdreieck des Teilsystems FeAB.

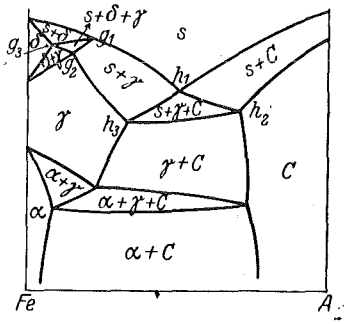

Abb. 160. Schnitt FeA_1 (vgl. Abb. 159).

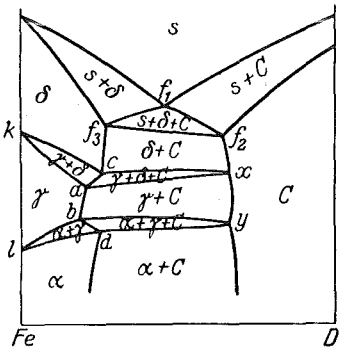

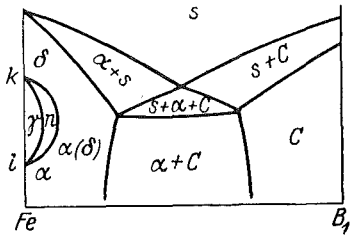

Fig. 4: Transition between an open and a closed γ-field inside a ternary diagram Fe-A-B

3) Specific effects of certain elements

Distinction between alloying and residual elements.

Mn: Normally present in all commercial steels.
Deoxidizer (reduced hot shortness)
Desulfurizer (MnS stringers improve machinability)
Solid solution strengthening of ferrite
Greatly increases hardenability

Cr: In low-alloy steels it serves to increase hardenability, high-temperature strength and resistance to oxidation and corrosion.
Alloy contents of 10-27 % Cr lead to the classes of martensitic and ferritic stainless steels with usable hot strengths up to 650°C.

Ni: In low-alloy steels it serves to increase hardenability and low-temperature toughness.
Furthermore solid solution strenghtening of ferrite.

A survey of the microstructure of higher alloyed Ni-C-steels is given in Fig. 1 (Guillet).

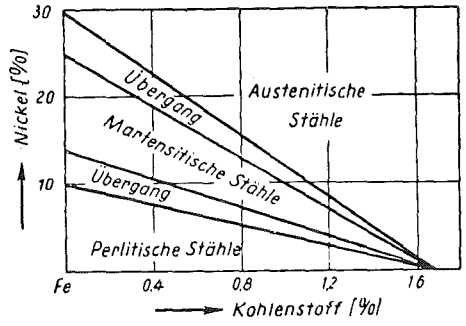

The austenitic alloys (up to 80 % Ni) are well-known for their special physical properties:
hard and soft magnetic materials
thermal expansion coefficient
(Invar)

Alloys with 18-30 wt % Ni are furthermore the base for the so-called Maraging steels (high-strength steels due to precipitation of intermetallic compounds out of a low-carbon martensite matrix).

Mo: is unique in the extent to which it increases the high-temperature tensile and creep strength of steels (slow diffusion). It also increases the hardenability of steels and minimizes the susceptibility to temper embrittlement.

V: Additions up to 0.05 % increase the hardenability. It is generally added to inhibit grain growth during heat treatment, thereby improving strength and toughness of hardened and tempered steels. -

Fig. 2 summarizes the solid solution hardening effect of some elements in α-Fe. Si and Mn show the strongest effect.

From this the term hardenability has to be differentiated. Good hardenability means, that a low cooling rate is sufficient to suppress the pearlite decomposition and to reach a (hard) bainitic or martensitic structure. From the metallic elements Co is the only one known to decrease hardenability. The presence of Co in steel increases both the rate of nucleation and of growth of pearlite so that steels containing Co are more difficult to harden than those that do not contain it.

A relative measure of hardenability is given by empirical "Hardenability Multiplying Factors" in the following Table:

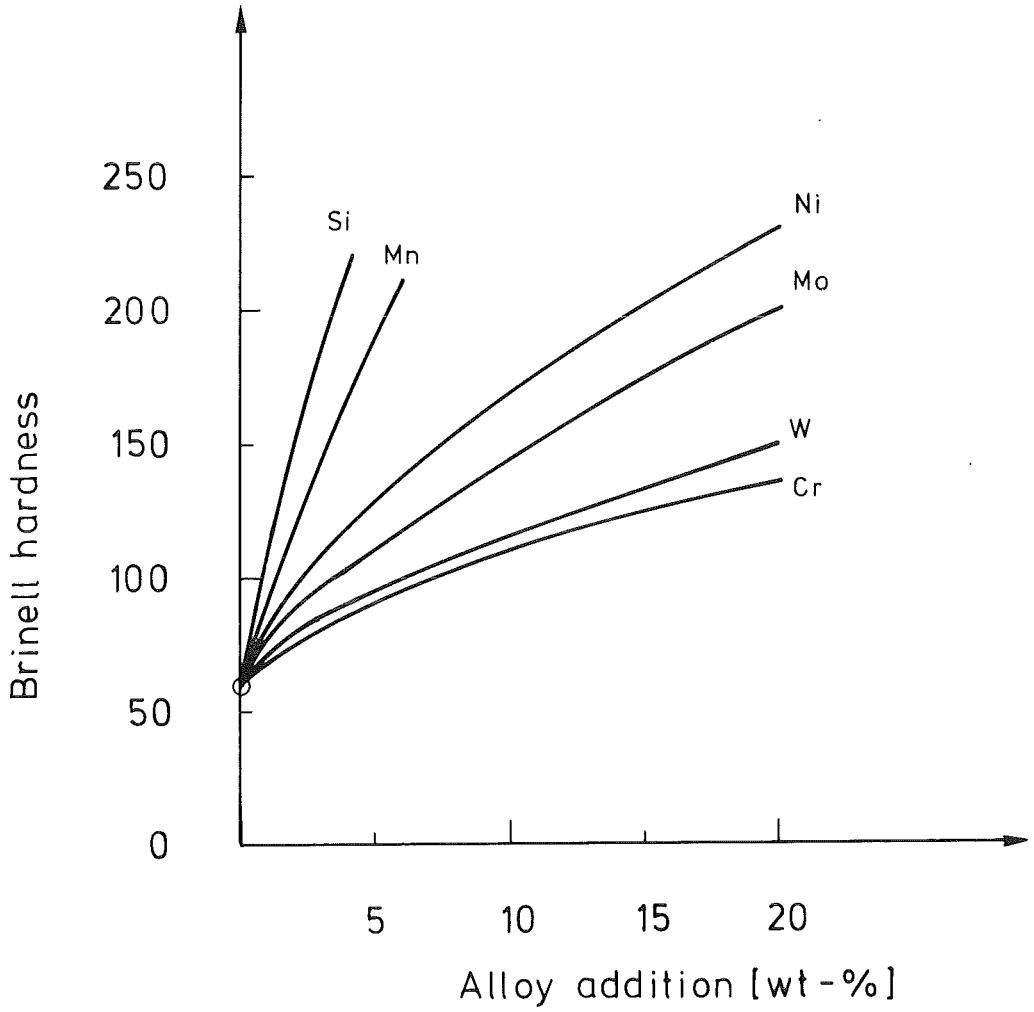

Fig. 2 : Brinell hardness of binary α-Fe-solid solutions

Hardenability Multiplying Factors.*

Percent	Mn	Si	Ni	Cr	Mo
0.05	1.167	1.035	1.018	1.1080	1.15
0.10	1.333	1.070	1.036	1.2160	1.30
0.15	1.500	1.105	1.055	1.3240	1.45
0.20	1.667	1.140	1.073	1.4320	1.60
0.25	1.833	1.175	1.091	1.54	1.75
0.30	2.000	1.210	1.109	1.6480	1.90
0.35	2.167	1.245	1.128	1.7560	2.05
0.40	2.333	1.280	1.146	1.8640	2.20
0.45	2.500	1.315	1.164	1.9720	2.35
0.50	2.667	1.350	1.182	2.0800	2.50
0.55	2.833	1.385	1.201	2.1880	2.65
0.60	3.000	1.420	1.219	2.2960	2.80
0.65	3.167	1.455	1.237	2.4040	2.95
0.70	3.333	1.490	1.255	2.5120	3.10
0.75	3.500	1.525	1.273	2.62	3.25
0.80	3.667	1.560	1.291	2.7280	3.40
0.85	3.833	1.595	1.309	2.8360	3.55
0.90	4.000	1.630	1.321	2.9440	3.70
0.95	4.167	1.665	1.345	3.0520	
1.00	4.333	1.700	1.364	3.1600	

Abstracted from *U.S.S. Carilloy Steels*, U.S. Steel Corp., Pittsburgh, 1948

From the elements listed, Mn and Mo have the highest, Ni the lowest hardenability effect (wt % basis).

(For a well-presented treatment of the use of these factors, see Reed-Hill, Physical Metallurgy Principles, van Nostrand Co., 1973).

To reach an optimization of properties, a combination of element additions is generally necessary. For instance, a Ni addition is particularly effective when used in combination with Cr and Mo; the resulting steel possesses high strength, toughness and hardenability (LWR pressure vessel steel!)

As an example for the phase relations encountered in more complex systems, we will have a closer look on the Fe-Cr-Ni ternary system (V.G. Rivlin, G.V. Raynor, Intern. Metals Reviews, 1980, No. 1, 21-38).

Binary systems: Fe-Cr (See p.37)
Fe-Ni (Fig. 3)
Cr-Ni (Fig. 4)

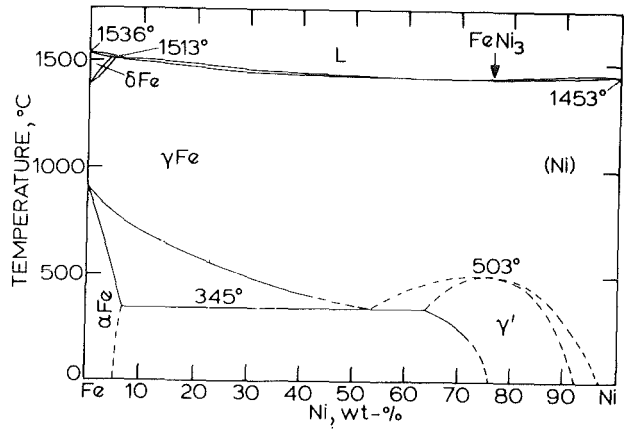

Fig 3

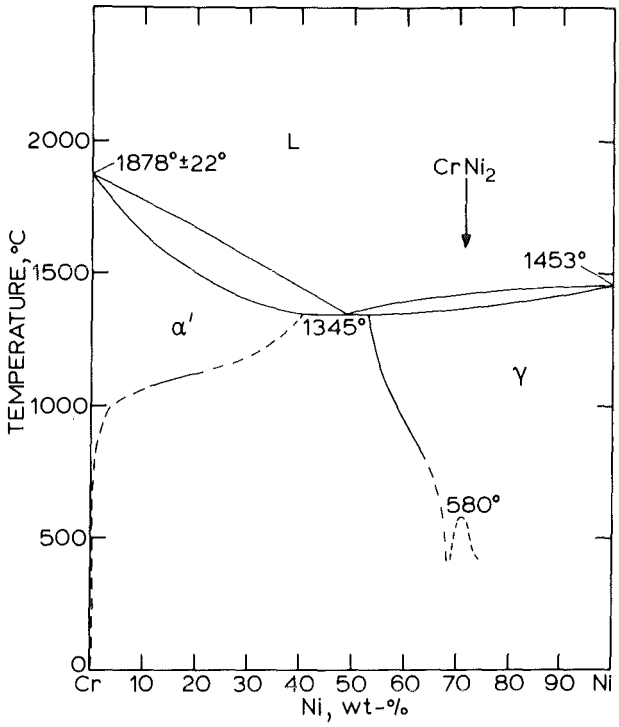

Fig. 4

In the Fe-Cr-system σ forms below 820 °C and decomposes eutectoidally at around 440 °C. However, all reactions involving σ are extremely sluggish due to the very small differences in free enthalphy. So metastable α and α' can easily form at the expense of σ above 440 °C (easier nucleation of α'-precipitation).

The boundaries of the γ-loop are very sensitive to interstitial solute content (C,N).

Fe-Ni: γ decomposes eutectoidally at 345 °C. However, at normal cooling rates γ is retained at RT above 30 wt % Ni.

Ternary Fe-Cr-Ni

Liquidus surface (Fig. 5): There is a univariant line running from the Fe-Ni peritectic to the Cr-Ni eutectic. It, however, passes through a minimum just below 1300°C (49 % Cr - 8 % Fe - 43 % Ni). Here the peritectic and eutectic tie-triangles, respectively, become a tie-line connecting the 3 phases that are in equilibrium at the T-minimum (see Fig. 6 and 7 , taken from F.N. Rhines, Phase Diagrams in Metallurgy, McGraw-Hill 1956, p. 153).

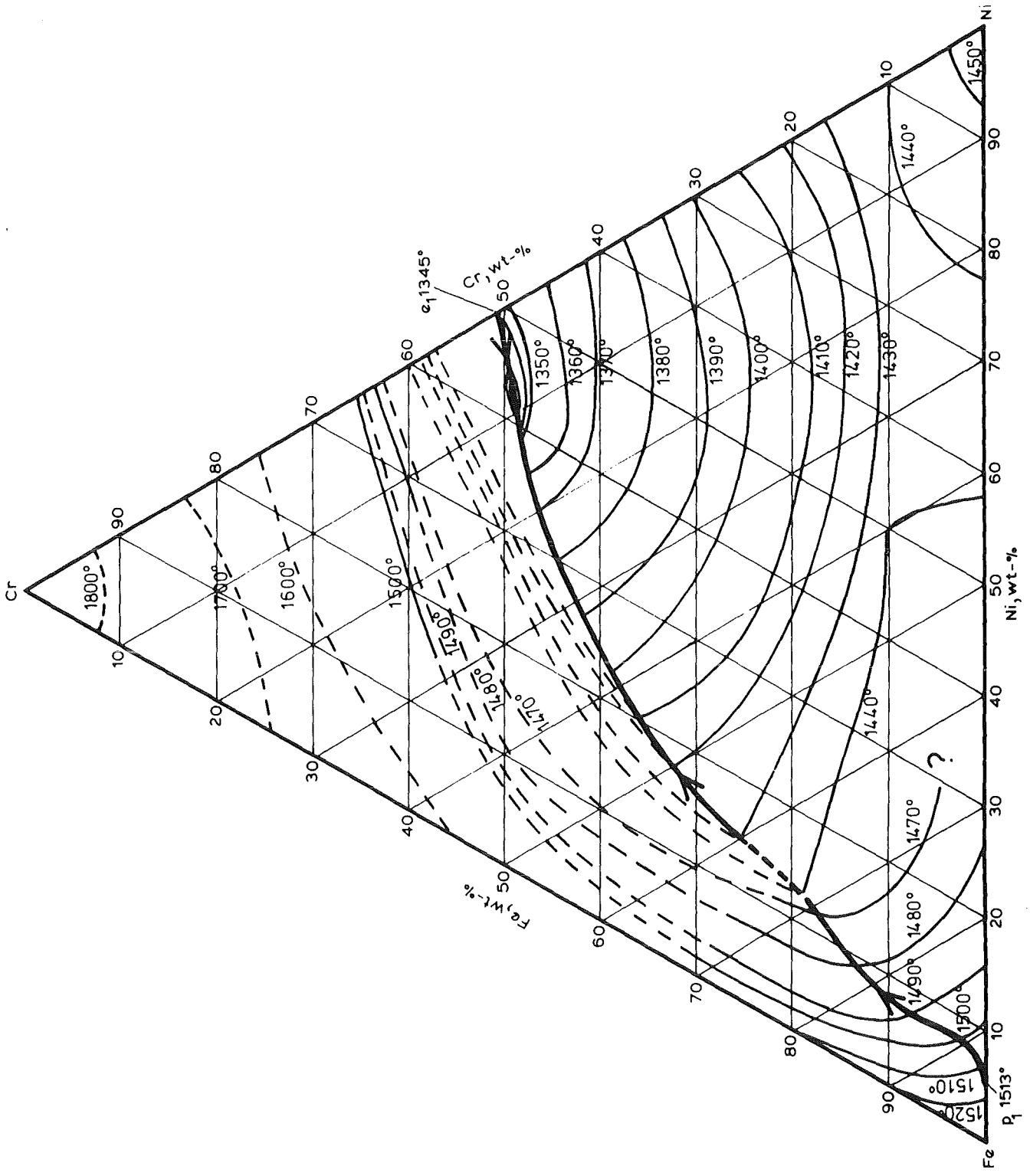

Fig. 5 : Liquidus projection of Fe-Cr-Ni system

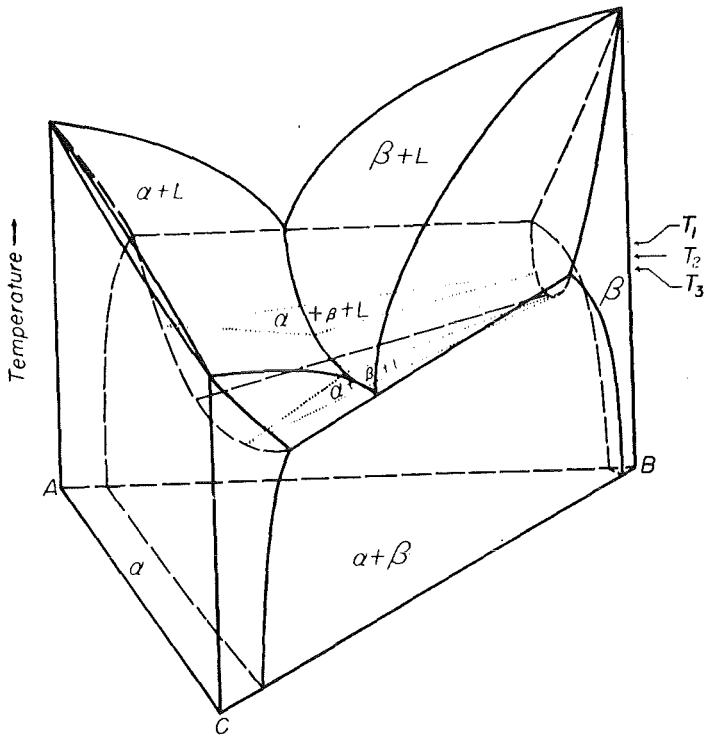

Fig. 6 : Three-phase region reduces to a tie-line at a temperature minimum

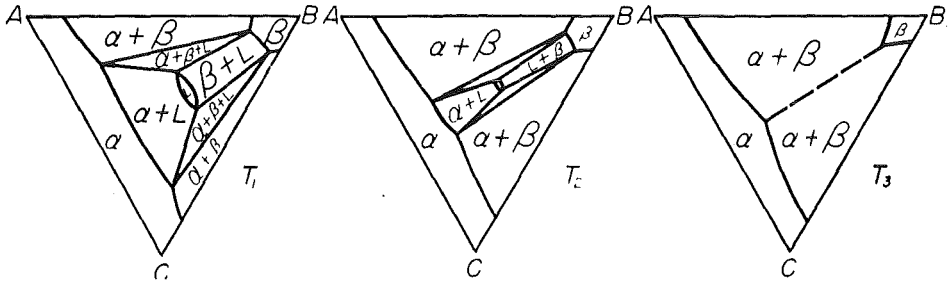

Fig. 7 : Isotherms through the space diagram of Fig. 6

The solidus projection of Fig. 8 shows the two solid solution (bcc and fcc) surfaces and the gap between, bridged by tie-lines.

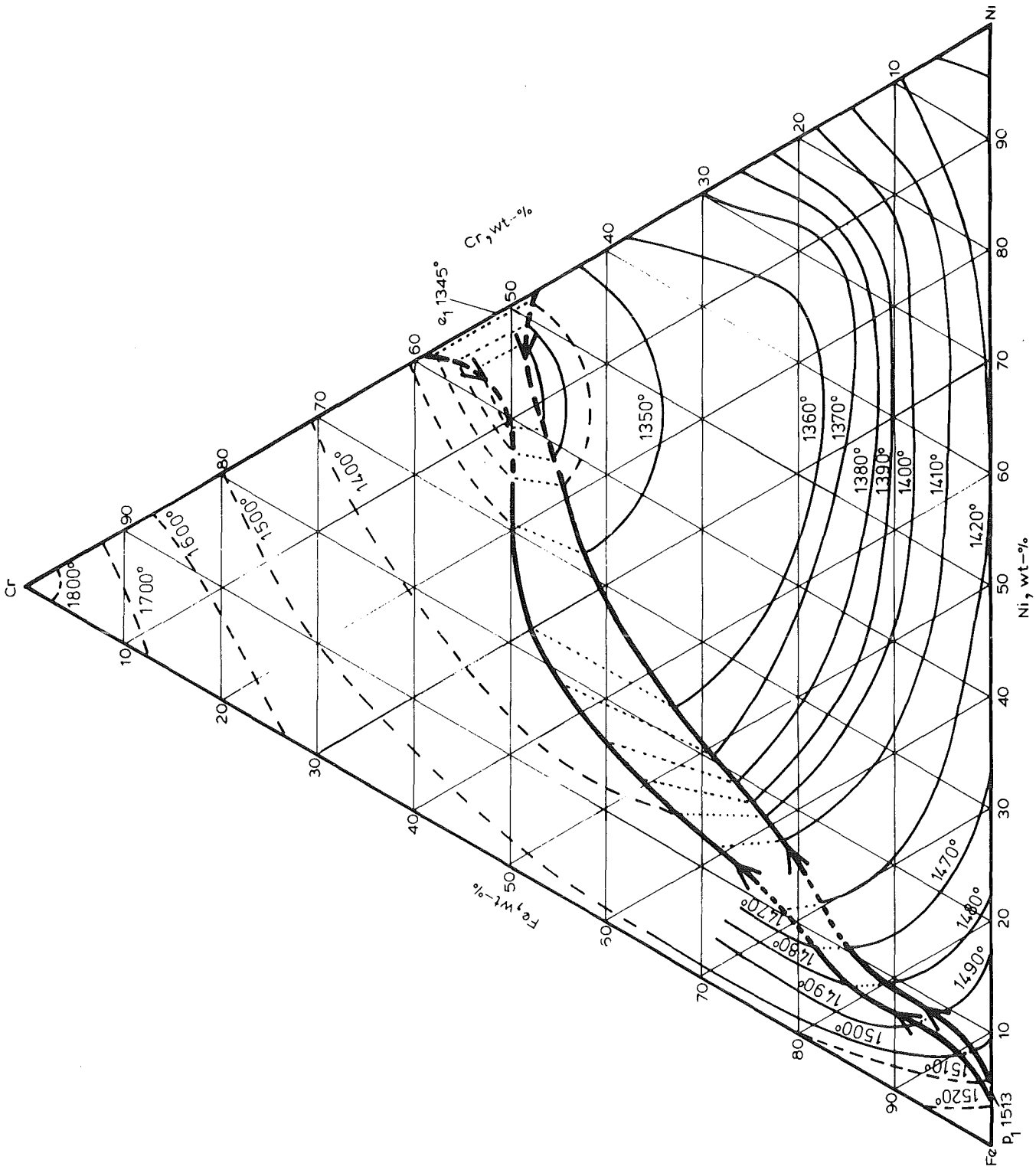

Fig. 8 : Solidus projection of Fe-Cr-Ni system

As one sees, the intermetallic compound σ plays no part in the melting equilibrium.

Isothermal sections: Solid phase equilibria between 1300 and 1000°C are determined solely by the co-existence of γ and α. The two-phase field (α + γ) widens as the T falls (compare the solidus projection with the 1000°C isotherm of Fig. 9).

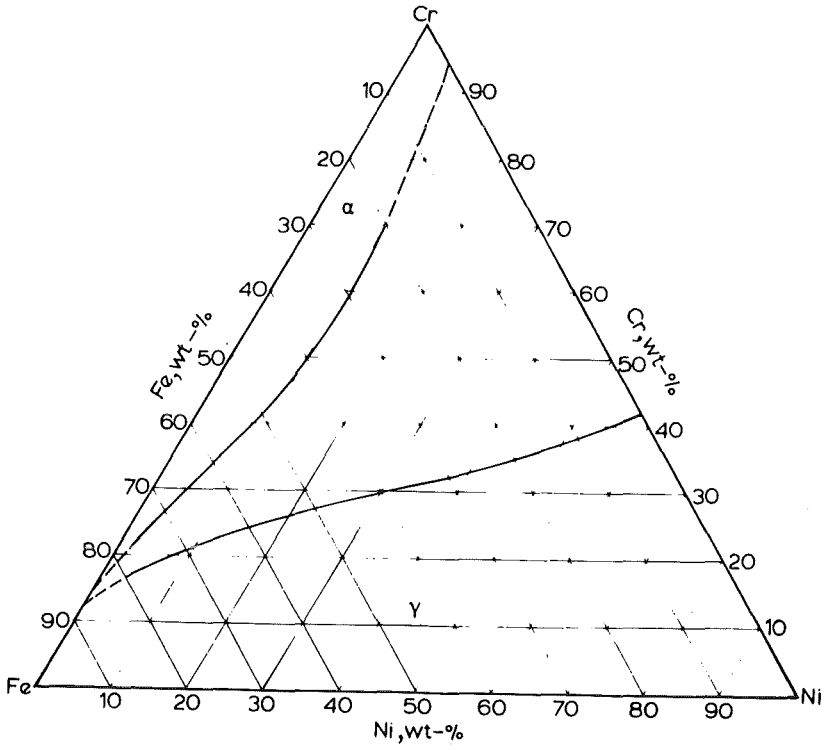

Fig. 9 : 1000°C isotherm of Cr-Fe-Ni system

The σ-phase in the ternary Fe-Cr-Ni system has an upper temperature limit which is higher than in the binary Fe-Cr system (950-960°C to be compared with 820°C). Therefore σ appears in the 900°C isotherm (Fig. 10).

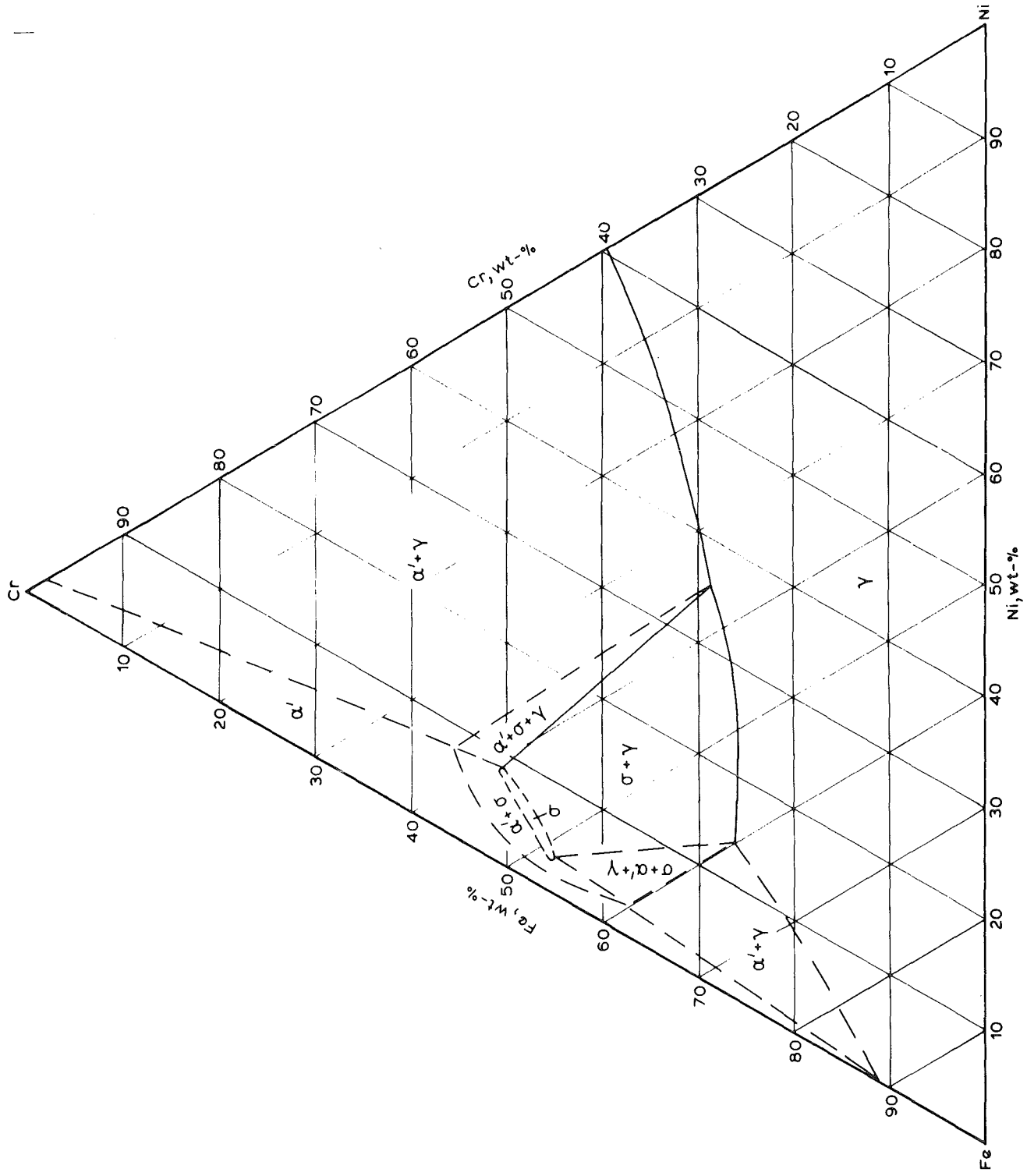

Fig. 10 : 900°C isotherm of the Fe-Cr-Ni system

At lower temperatures the establishment of the phase boundaries affords intermediate cold work and extended anneals.

The narrow homogeneity range of σ inside the ternary diagram (below 10 % Ni) expands at lower T to include the Fe-Cr edge: Fig. 11 , 650°C-isotherm.

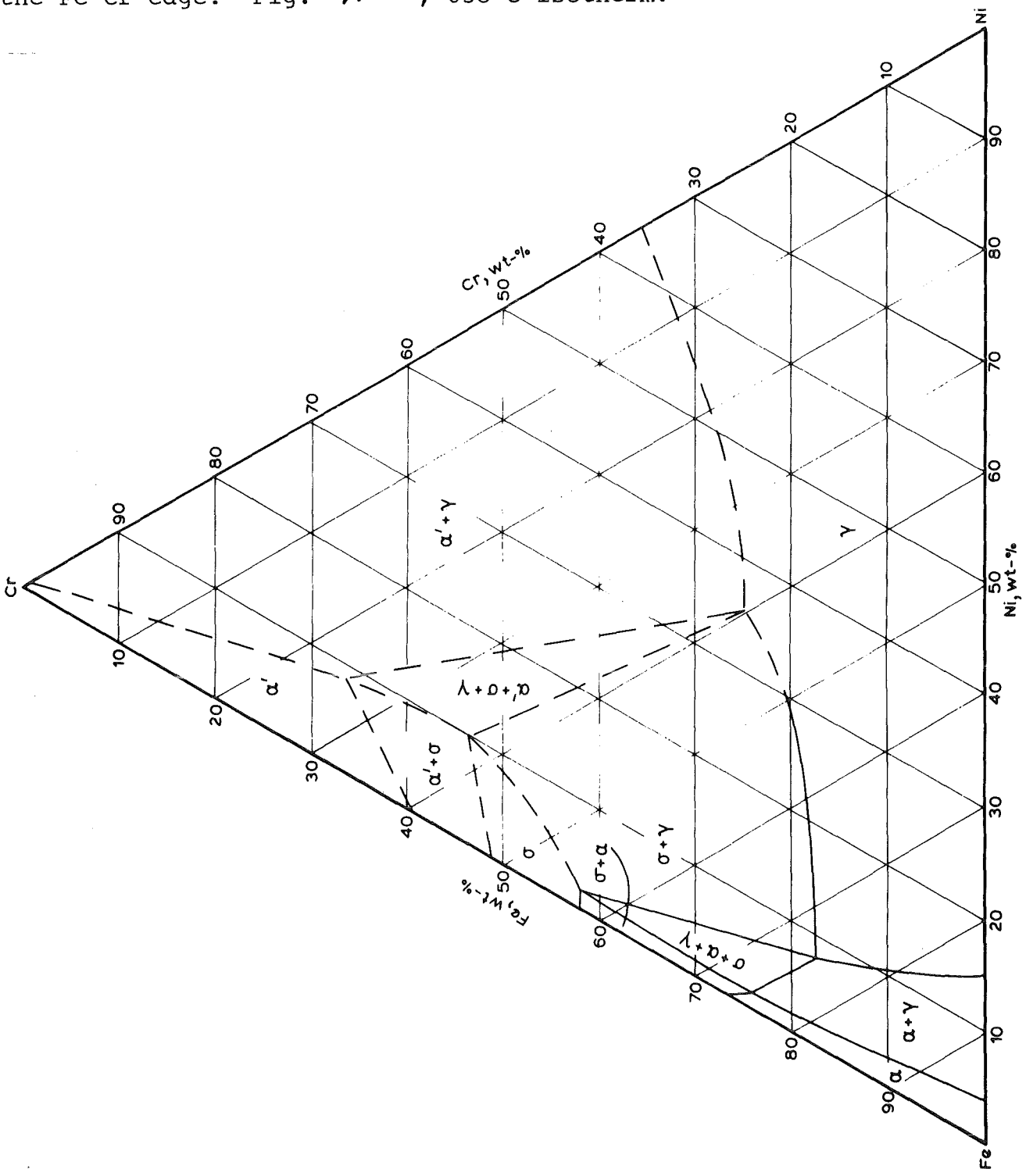

Fig. 11 : 650°C-isotherm of the Fe-Cr-Ni system

No truly ternary compounds have been found in the Fe-Cr-Ni system (all phases, including σ, are derived from the respective binary alloys).

The shape of the γ-phase field and its T-dependence plays obviously an important rôle in the swelling resistance of austenitic Fe-Cr-Ni-alloys.

Further Literature to C2,3 (besides that quoted in the text)

H. Schumann, Metallographie, Leipzig, 1962 and later editions

R.W. Cahn, Physical Metallurgy, North-Holland Publ. Co. and American Elsevier Publ. Co., 1974

M. Hansen, K. Anderko, Constitution of Binary Alloys, McGraw-Hill, New York, 1958 and Supplements by R.P. Elliott (I) and F.A. Shunk (II)

G. Masing, Ternäre Systeme, Leipzig 1949

F.N. Rhines, Phase Diagrams in Metallurgy, Mc Graw-Hill 1956

4.) Steels for Nuclear Reactors

The structural steels for nuclear power plants (PWR, BWR, LMFBR) are principally the same materials as commonly used in pressure systems of fossil-fueled power plants. There are minor - but important - restrictions as to residual elements, for instance Co and Cu.

To minimize corrosion products in LWR's ("crud" - adversely affecting heat transfer, fuel element life and maintenance), the inner surfaces of components in contact with pressurized water consist of austenitic steel. That means that the pressure vessel and other large diameter components of PWR's, as well as the portions of the primary system of BWR's exposed to water, are weld-overlay clad by austenitic steel - the base material being low-alloy fine grain ferritic steel. Steam piping and other components in the steam portion of BWR's are therefore usually unclad ferritic steel.

In addition to loadings by stresses and temperature, the effects of neutron and gamma fluxes have to be considered in nuclear reactor primary systems. So we will also have to deal with radiation damage of the steels and with changes induced in the (water) coolant by the radiation (stress corrosion).

Most existing and planned LMFBR's use austenitic stainless steels and Ni-base alloys as major construction materials for the (low pressure) vessel, piping and core internals.

4.1 Melting practices

The quality required for reactor steels makes it necessary to use special melting practices.
The furnaces used are shown in Fig. 1 - 3

Fig. 1 **Schematic diagram of electric-arc furnace**

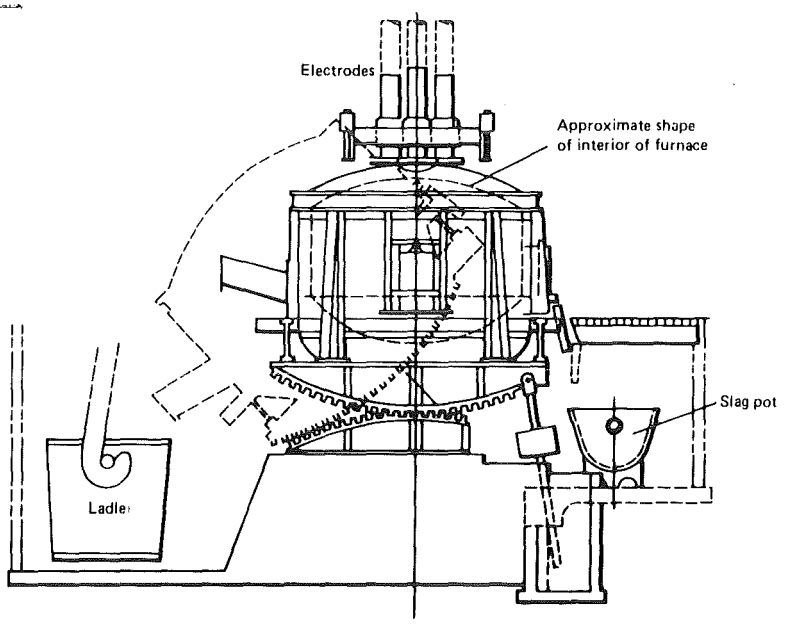

Fig. 2

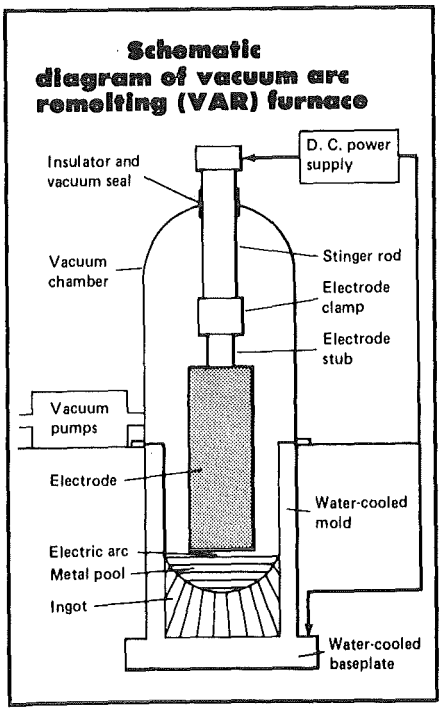

Low residual elements, except sulfur

Fig. 3

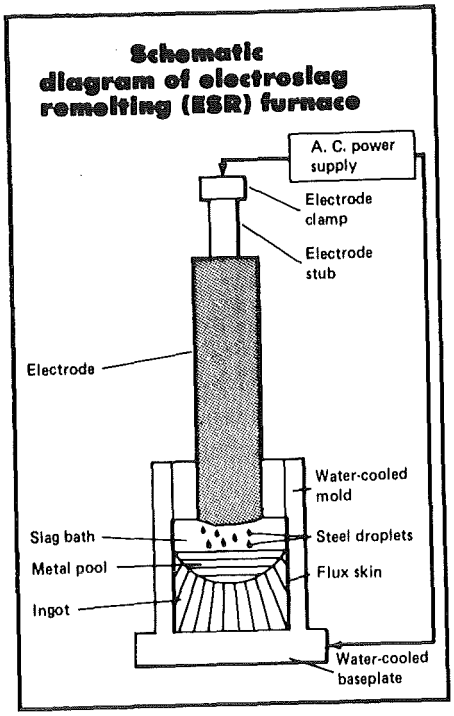

especially effective in removing sulfur

Furthermore

Vacuum induction melting (VIM) furnaces are used. This treatment leads to steels with minimum amounts of gas porosity and nonmetallic inclusions.

In the following typical examples are given for melting practices.

LWR, pressure vessel steel:
Electric are furnace, melt argon-treated and vacuum cast

LWR pressure vessel screws (27 NiCrMo 14 6; 34 CrNiMo 6):
Electric are furnace, electroslag remelting (ESR)

LMFBR, cladding and wrapper:
Melting in VIM
Remelting in VAR

LMFBR, tubes for heat exchanger (12 % Cr)
VAR + ESR

Literature to (4.1)

Metals Handbook, 9. ed., Vol. 1, 1978

4.2 Irradiation Damage and Irradiation Effects

Before we deal with specific steels the general effects of neutron irradiation will be considered.

The primary microscopic "irradiation damage" precedes the appearance of technologically important gross changes in the solids ("irradiation effects"). Irradiation damage analyses attempt to predict the number and configuration of the point defects (vacancies, interstitials) produced by the bombarding particles. Only the surviving point defects (can be as low as 1 %) lead to the macroscopic irradiation effect (Olander, 1976).

The following table gives some more differentiating information:

	Irradiation Damage	Irradiation Effects
Sequence	Primary	Secondary
Time	$< 10^{-11}$ s	10^{-3} s to months
Temperature	No importance (particle energy >>kT)	Highly T dependent [exp(-E/kT)]
Notions	PKA	
	Displacement cascade	Void swelling
	Depleted zone	In-pile-creep
	Focusing, Crowdion	Hardening
	Channeling	Embrittlement
	Transmutation	
	Activation	

4.2.1 Irradiation Damage

Due to elastic interactions between neutrons and lattice atoms the latter may be displaced. The (maximum) transmitted energy U_{max} depends on the energy of the knocking particle E_k and the mass relation of the knocking partners

(hard sphere-model):

$$U_{max} = E_k \cdot \frac{4\ M_1 \cdot M_2}{(M_1+M_2)^2}$$

At low neutron energies E_k, for instance 1 keV, U_{max} is in order of size of the displacement energy for lattice atoms (Wigner energy, $\sim$ 40 eV). That means that single isolated Frenkel defects are produced.

At high neutron energies (> 0.1 MeV) U_{max} becomes 100 keV or more; the lattice atom (primary knock-on atom, PKA) becomes a projectile itself and produces a sequence of collisions (displacement cascade). Only a very crude description of the PKA effects is possible by the hard sphere model; a more realistic picture is obtained if atomic interaction potentials, inelastic energy losses (ionization) as well as the periodicity of the crystalline lattice are considered.

Fig. 4 gives a picture of a displacement cascade.

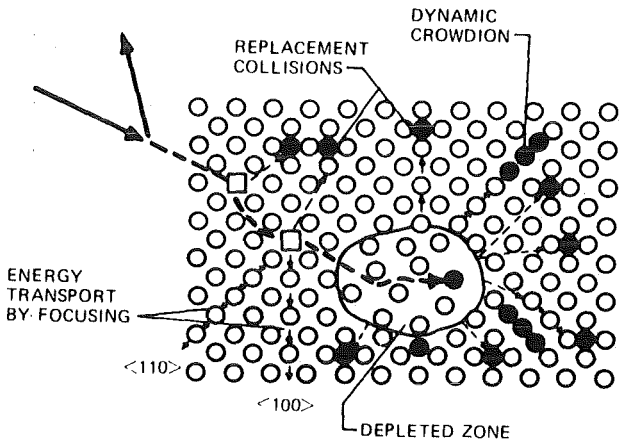

Fig. 4 Displacement cascade
□ vacancy ● Interstitial atom
—— Path of neutron - - - Path of PKA

Replacement collisions yield close Frenkel pairs (high probability of recombination).

There are, however, two mechanisms which lead to a much larger separation of vacancies and interstitials: Focusing and channeling.

Focusion refers to the transfer of energy and atoms by nearly head-on collisions along a row of atoms. (A-seldom-precise head-on collision is not required; the angle between the knock-on and the axis of the row of atoms is reduced in each successive collision: "focused collision sequence".)

A vacant lattice site appears at the starting location of the collision sequence and an interstitial is found far down the line of atoms: "focused replacement" or "dynamic crowdion". (Crowdion = extra atom squeezed into a line of atoms. The dynamic condition is a crowdion in motion. See Olander, 1976).

Channeling is the complementary process whereby atoms move long distances in the solid along open directions in the crystal structure. In this case the moving atom is kept in its channel by glancing collisions with the atomic rows that serve as walls.

Focusing and channeling affect both the number and configuration of displaced atoms in a cascade. Focused or channeled atoms may constitute the bulk of the displaced atoms that escape recombination with vacancies and, therefore, may be mainly responsible for "irradiation effects" controlled by the interstitials (such as void growth, in-pile creep).

Of special interest is the formation of the so-called depleted zone at the end of range for the PKA (more closely spaced displacement collisions with decreasing kinetic energy of the PKA). It is assumed that this zone immediately collapses into a planar vacancy cluster which is visible in

the TEM as a so-called "black-dot" damage.

Inelastic collisions between neutrons and lattice atoms produce new isotopes or elements via (n,p)-, (n,α)-, (n,γ)-, (n,2n)-reactions. Those transmutations which result in long-life isotopes emitting hard γ- (and β-) radiation lead to undesirable activation of the components themselves and- via corrosion products - also of the whole cooling circuit. We will have a closer look on activation below.

The inelastic collisions do produce further displacement damage via the energetic recoils.

Examples: 1) $^{10}B + n \rightarrow {}^{7}Li(0.9\ MeV) + {}^{4}He(1.5\ MeV)$
(TEM observations have revealed concentric circular "Halos" or rings of dislocation loop damage surrounding boron-rich precipitates, located at the ends of the trajectories of the recoiling He and Li ions)

2) (n,γ): atoms can absorb thermal neutrons, the subsequent recoil of the atoms upon emission of the γ-rays creates displacement damage.

We will have now a closer look on the activation of metallic constituents of steel. Due to their high cross section for absorption, σ_a, thermal neutrons are mainly responsible for the activation.

Element	σ_a[barn] thermal neutrons	σ_a[barn] fast neutrons (0.1 MeV)
Fe	2.53	$6.1 \cdot 10^{-3}$
Cr	3.1	$6.8 \cdot 10^{-3}$
Co	37.0	$11.5 \cdot 10^{-3}$
Ni	4.8	$12.6 \cdot 10^{-3}$
Mn	13.2	$25.6 \cdot 10^{-3}$
Mo	2.7	$71.0 \cdot 10^{-3}$
Nb	1.15	$100.0 \cdot 10^{-3}$

The next table given more data on the activation of important alloying elements by thermal neutrons (F.Rapatz, 1962)

Element	Isotope to be activated	Percentage of this isotope in the element	σ act (cross sect. for activ. (barns)	Active Isotope	Half life time	β (MeV)	γ (MeV)
1	2	3	4	5	6	7	8
Ti	Ti^{50}	5,34	0,14	Ti^{51}	5,8 min	1.9,2.2	0,32
V	V^{51}	99,76	4,5	V^{52}	3,8 min	2,5	1,44
Cr	Cr^{50}	4,3	11	Cr^{51}	27,8 d	-	0,32
Mn	Mn^{55}	100	13,4	Mn^{56}	2,58h	0,65-2,81	0,82-2,13
Fe	Fe^{58}	0,3	0,9	Fe^{59}	46 d	0,27-1,56	0,19-1,3
Co	Co^{59}	100	2,0	Co^{60}	5,28 a	0,3 -1,48	1,17-1,33
Ni	Ni^{64}	1,1	2,6	Ni^{65}	2,5 h	0,6- 2,1	0,37-1,49
Cu	Cu^{63}	69	3,9	Cu^{64}	12,8 h	0,37	1,34
	Cu^{65}	31	1,8	Cu^{66}	5,1 min	1,59 2,63	1,04
Nb	Nb^{93}	100	1,0	Nb^{94}	6,6 min	1,3	0,415
Mo	Mo^{98}	23,75	0,13	Mo^{99}	68 h	0,45-1.23	0,04-0,78
Ta	Ta^{181}	100	19	Ta^{182}	111 d	0,18-0.51	0,06-1,2
W	W^{186}	28,4	34	W^{187}	24 h	0,62 1,3	0,07-0,77

The higher the values in column 3 and 4, the more of the active isotope (column 5) is formed.

Fe itself is only weakly activated.
Mn is heavily activated, however, its half-life time is short (2.58 h).

Co and Ta are the most inconvenient elements as regards activitation.
Even if the Co-content in a pressure vessel steel is kept at 0.02% (200 ppm), it means that a 1000t vessel contains 200 kp Co, which gives an enormous amount of activition.

Fig. 5 shows the increase of the induced radioactivity [Ci · g^{-1}] with time at a neutron flux of 10^{10} n· cm^{-2} · s^{-1}. Saturation is reached early (late) with isotopes of low (high) half-life time. Examples are V and (Co).

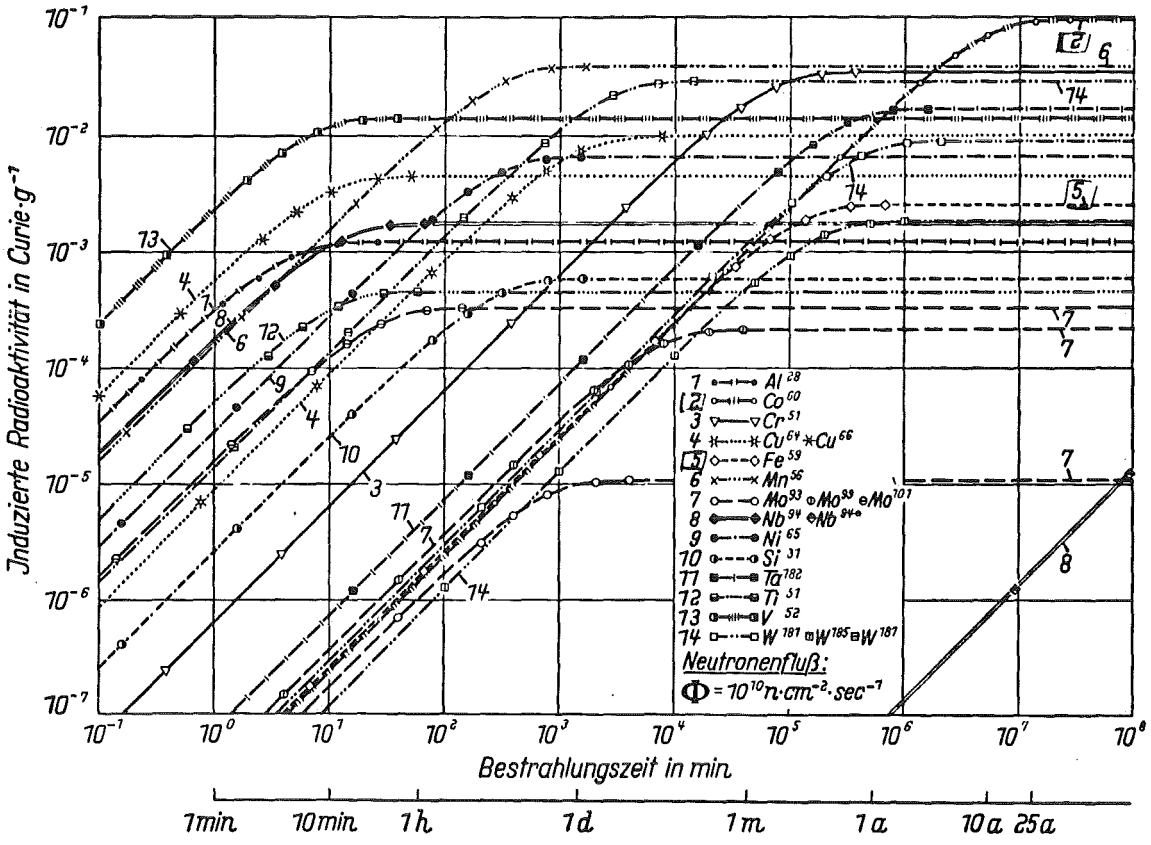

Fig. 5

Of even more interest is the decrease rate of the induced radioactivitiy from the saturation levels (Fig. 6).

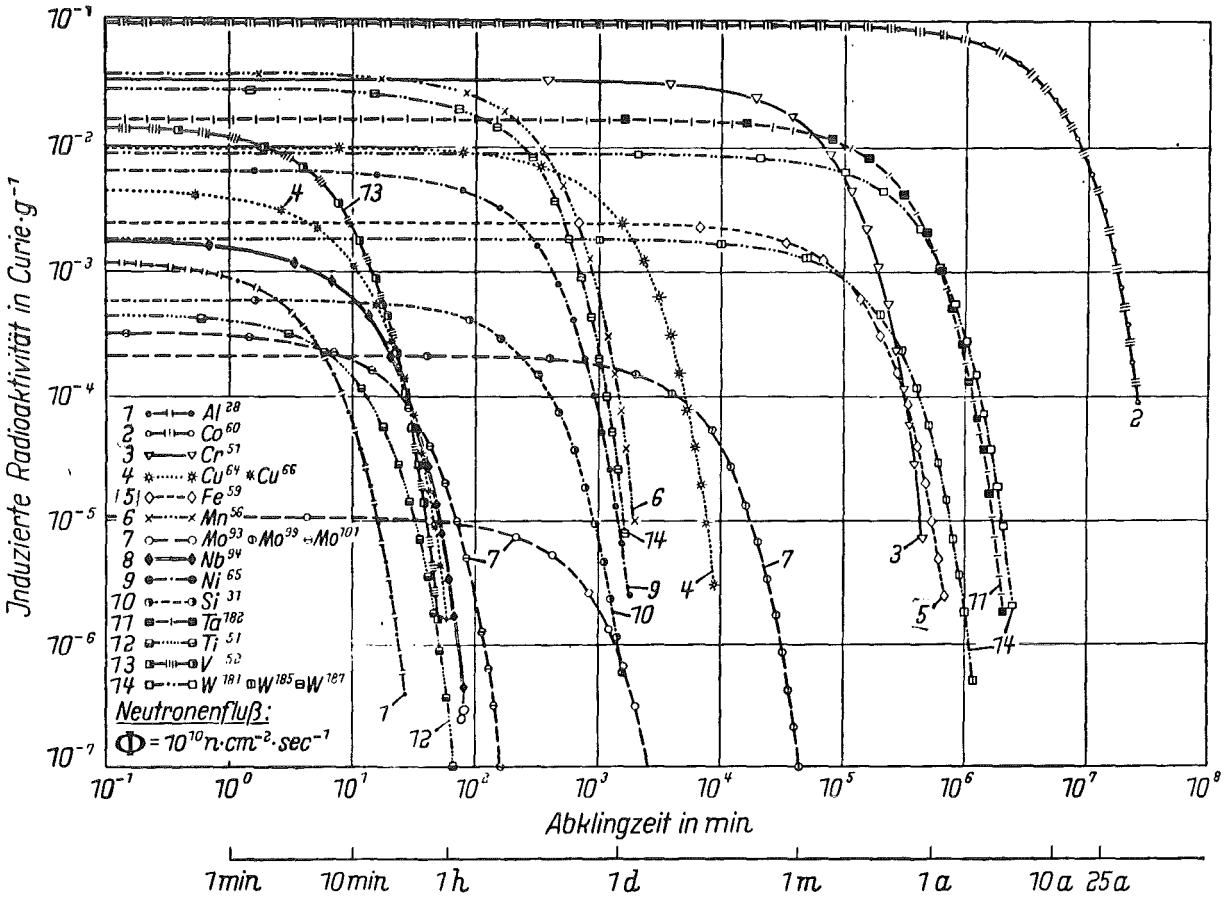

Fig. 6

-life

The group of the long half time isotopes Co^{60}, Cr^{51}, Fe^{59}, Ta^{182} and W is clearly separated. Inconveniently Cr^{51} und Fe^{59}, which are to be found in all alloyed steels, belong to this group (Gebhard, Thümmler, Seghezzi, 1964).

In connection with the consideration of inelastic collisions between neutrons and lattice atoms we will have a closer look also on the helium production rates by means of (n,α)-reactions

Thermal flux: The primary source of He in steel is due to the reaction

$$B^{10} + n^{1} \rightarrow Li^{7} + He^{4} \quad \text{(cross section 3000 barns)}$$

Even the small quantities of B in stainles steel (between 5 and 60 ppm) produce substantial quantities of He. Natural B contains only 20 % B^{10}, however, and therefore it is burned out of the cladding early in the life of a fuel element.

A second source of helium is the following two-step reaction involving thermal neutrons and Ni:

$$Ni^{58} + n^{1} \rightarrow Ni^{59} + \gamma$$
$$Ni^{59} + n^{1} \rightarrow Fe^{56} + He^{4}$$

The effective cross-sections for these reactions are 4.4 and 13 barns, respectively.

Fast flux

Preliminary remark: As to be seen from the table,

$\phi_f = 10^4 \cdot \phi_{th}$ in a LMFBR

$\phi_f \simeq \phi_{th}$ in a LWR and

$\phi_{tot,LMFBR} = 10^2 \cdot \phi_{tot,\ LWR}$

Comparison of Typical 1000-Mw(e) Oxide Reactors

	LWR	LMFBR
Fissile species enrichment	3% ^{235}U in ^{238}U	15% ^{239}Pu in ^{238}U
σ_f, barns	550	1.8
Core-averaged neutron flux, n cm^{-2} sec^{-1}		
Thermal	3×10^{13}	1×10^{11}
Fast (> 0.2 MeV)	5×10^{13}	8×10^{15}
Burnup, %	3	10
Fast fluence, n/cm^2	3×10^{21}	3×10^{23}
Irradiation time (at full power), years	2	1.5

The "fast" (n,α) reactions with steel alloying or impurity elements set only in above a threshold energy of the order 1 to 5 MeV. The cross-sections are given in the table.

Effective (n,α) Cross Sections in a Fission-Neutron Spectrum

Element	$\sigma_{(n,\alpha)eff}$, mb
Cr	0.2
Fe	0.23
Ni	4.2
N	41
B	623

The higher flux in a fast reactor and its lower material cross-section as compared with a thermal reactor, lead to the following He concentrations in 304 SS exposed to LMFBR and LWR spectra:

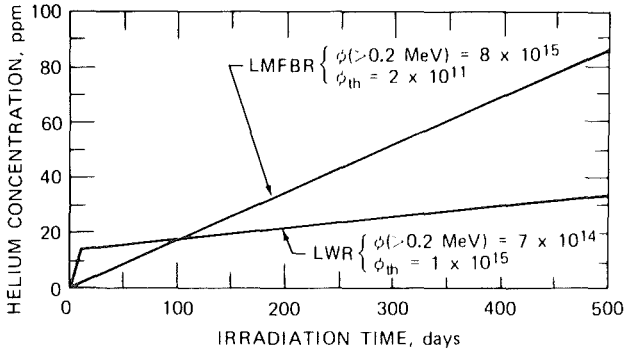

Helium concentration in type 304 stainless steel exposed to LMFBR and LWR flux spectra. [After A. DePino, Jr., *Trans. Amer. Nucl. Soc.*, 9: 386 (1966).]

The discontinuity in the He production rate in the thermal reactor is due to burnout of B^{10}. The continued rise in He concentration is due to threshold (n,α) reactions in the fast component of the neutron flux (2-step reaction not considered). Cross-over after ≃ 100 days. After 1 1/2 years the fast cladding reaches 100 ppm He.

4.2.2. Irradiation effects

The development of the primary irradiation damage into new structural configurations, which are in thermal equilibrium and which are responsible for the technological irradiation effects, is highly temperature and time dependent (Boltzmann factor, exp (-E/kT), in the expression for the rate of thermodynamic processes or migratory events).

At a very low irradiation T ($T/T_M=0$)

- interstitials and vacancies are immobile

- vacancy clusters are formed, as we have seen at the sites of the depleted zones.

$$N_c \simeq \emptyset \cdot t$$

$$S_c \simeq E_n \qquad \text{(cluster size } S_c\text{, neutron energy } E_n\text{)}$$

However, the increase of black dot damage with neutron fluence is lower than theoretically expected due to an anneling effect in overlapping cascades

- transmutation products

  Via (n,p), (n,α) ..... reactions

Fig. 7 gives a survey of the more complex phenomena at higher irradiation temperatures.

Above $T/T_M = 0.1$ (-100^oC for steel) the self-interstitials (Si) become mobile:

- Recombination of mobile Si with vacancies
- Annealing of Si at V-loops (planar) or -clusters (3-dim.) $N_L \sim (\phi\, t)^n$, with $n \leqslant 0.5$
- Agglomeration of Si to (small) loops and on solute atoms
- Onset of irradiation creep: Si move preferentially to dislocations and to favorably oriented i-loops.

Above $T/T_M = 0.3$ ($\sim 250^oC$ for ferritic steel) vacancies also become mobile:

- Recombination of mobile Si and mobile V
- Agglomeration of V to voids (swelling above threshold fluence)
- Complex formation of V with solute elements.

One can conclude that for a LWR pressure vessel (operating at about 300 ^oC) defect clusters stabilized or nucleated by solute trace elements (like Cu) are responsible for the observed embrittlement effects.

Also annealing (saturation) effects are to be expected due to mobile Si and V.

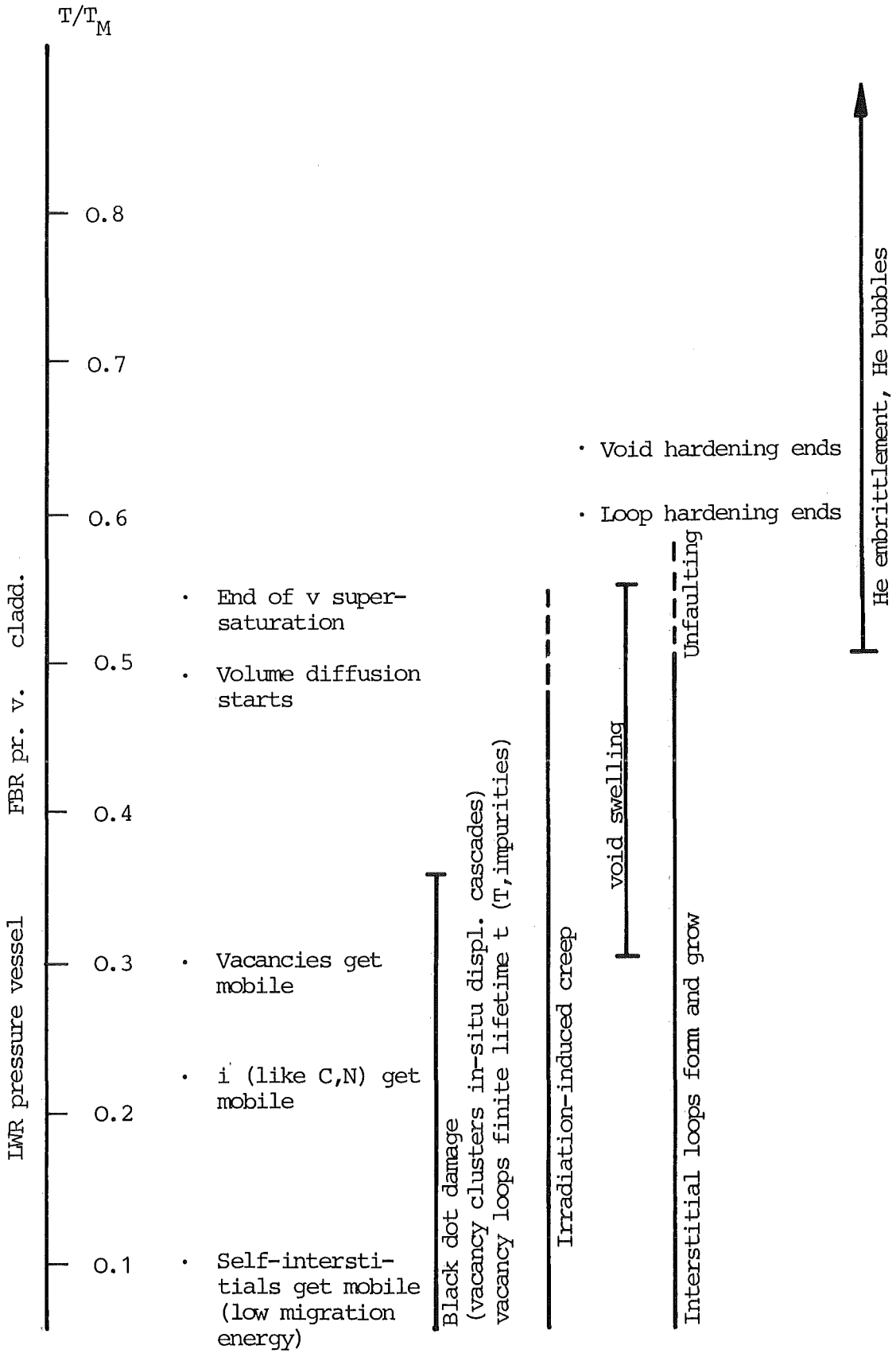

Fig. 7 (new): Temperature dependence of irradiation effects

At T/T_M= 0.5 (≈550°C for steel) the mean diffusion paths of atoms including generated transmutation products (He) become comparable to the grain sizes of the steel. The agglomeration of He as gas-bubbles dominates the mechanical behavior by reducing the ductility (especially austenites).

At high fast-neutron fluences (> 10^{21} n/cm^2) dislocation loops and voids grow to large sizes. These large effects require appreciable time to anneal out even in high-T mechanical tests. Complete recovery of the radiation hardening does not take place until temperatures in excess of 800°C (0.65 T_m). At still higher T only He bubbles remain. These are not numerous enough to cause appreciable hardening, however reduce ductility dramatically at T up to the melting point.

There is another irradiation effect, besides void swelling, which may lead to permanent deformation of structural materials: In-pile creep. It is a creep process, below the temperature regime of thermal creep, under the influence of a fast neutron flux. The SIPA-theory explains this phenomenon by the Stress-Induced Preferential Absorption of interstitials by favorably oriented dislocation loops and edge dislocations. The in-pile creep behavior is of great importance for the cladding and wrapper material of a LMFBR.

Literature to (4.2)

D.R.Olander, Fundamental Aspects of
Nuclear Reactor Fuel Elements,
Technical Information Center, Office of
Public Affairs, Energy Research and Development
Administration, USA, 1976.

K.Ehrlich, "Irradiation Behavior of Reactor Vessel Steels"
Joint JEN-KfK-Seminar, Madrid, 1980.

F. Rapatz, "Die Edelstähle", Springer-Verlag, 1962

E. Gebhardt, F. Thümmler, H. Seghezzi, "Reaktorwerkstoffe",
Teubner-Verlag, Stuttgart, 1964.

4.3 LWR-steels and their properties

We will limit the scope of our consideration to the inner (spherial) shell of the containment("Reaktorsicherheitsbehälter") and mainly to the pressure retaining primary components located inside. (Fig. 1,2)

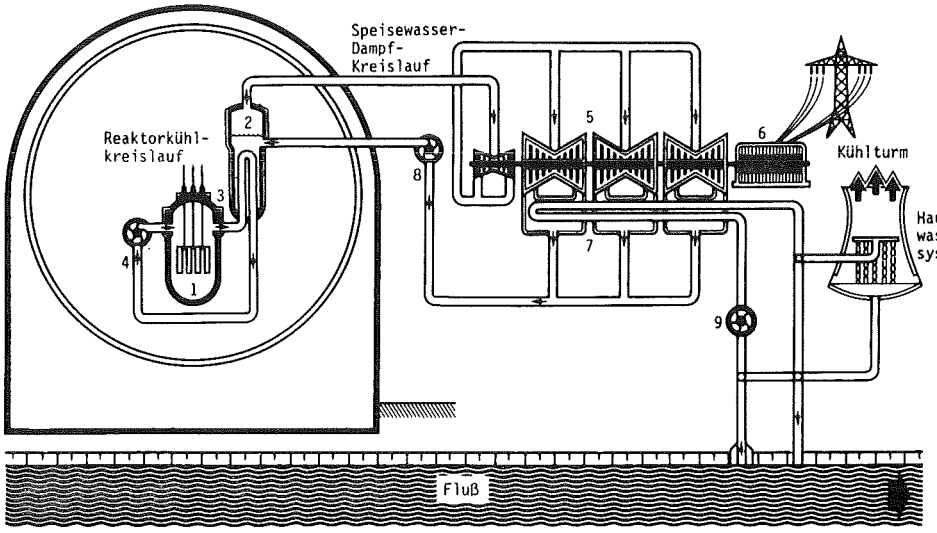

1 Reaktorkern
2 Dampferzeuger
3 Reaktordruckbehälter
4 Hauptkühlmittelpumpe
5 Turbine
6 Generator
7 Kondensator
8 Hauptspeisewasserpumpe
9 Hauptkühlwasserpumpe

Fig. 1
PWR

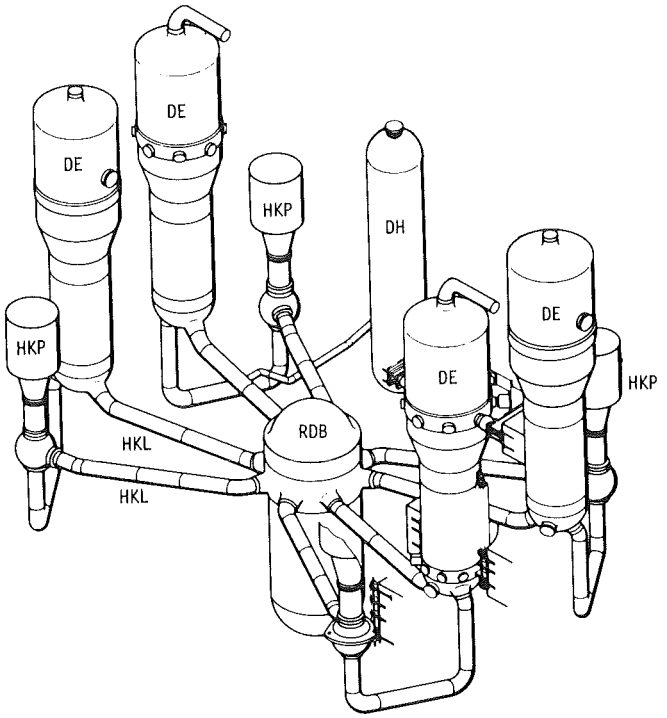

DE = Dampferzeuger
DH = Druckhalter
HKL = Hauptkühlmittelleitung
HKP = Hauptkühlmittelpumpen
RDB = Reaktordruckbehälter

Fig. 2
Components of the primary cooling Systsem of a PWR (Reaktorkühlkreislauf

The main components are =

RDB = Reaktordruckbehälter = Pressure vessel
DH = Druckhalter = pressurizer
HKL = Hauptkühlmittelleitung = Primary piping
HKP = Hauptkühlmittelpumpen = Main cooling pumps
DE = Dampferzeuger = Vapor generator

The pressure retaining system consists of RDB, DH, HKL, Main pumps housings, lower primary chamber and U-tubing of the DE. Their integrity is the barrier against a type of loss of coolant accidents.

All these components belong to "Anforderungsstufe 1"; to meet the stringent material requirements, the appropriate melting and working processes have to be used.

4.3.1 Inner shell (Sicherheitsbehälter) = Steels in use are of the type CMn or CMnNi, both Al-killed and fine-grain steels

CMn	StE 36	(E=Elektroofen)
CMnNi	15 MnNi63	(1.6210)

we will have a closer look on 15 MnNi 63.
Chemical composition (melt).

	C	Si	Mn	P	S	Cu	Cr	Ni
min.	0,12	0,15	1,20	-	-	-	-	0,50
max.	0,18	0,35	1,65	0,015	0,005	0,06	0,15	0,85

	AL ges	As	Mo	Sn	Ti	Nb	N	V
min.	0,020	-	-	-	-	-	-	-
max.	0,050	0,015	0,05	0,010	0,020	0,004	0,015	0,020

This steel is used in the normalized condition, exhibiting a ferrite + pearlite structure. Compare the Time-Temperature-Transformation diagramm of Fig. 3 !

In the normalized state this steel exhibits a yield strength $R_{p0.2}$ = 370 MPa and a fracture elongation A = 22 %.
An advantage of this steel is that at thicknesses $\leq$ 38 mm no stress relief annealing after welding is necessary (for simple geometrical configurations like a sphere and after a 100 % non-destructive test of all welds).

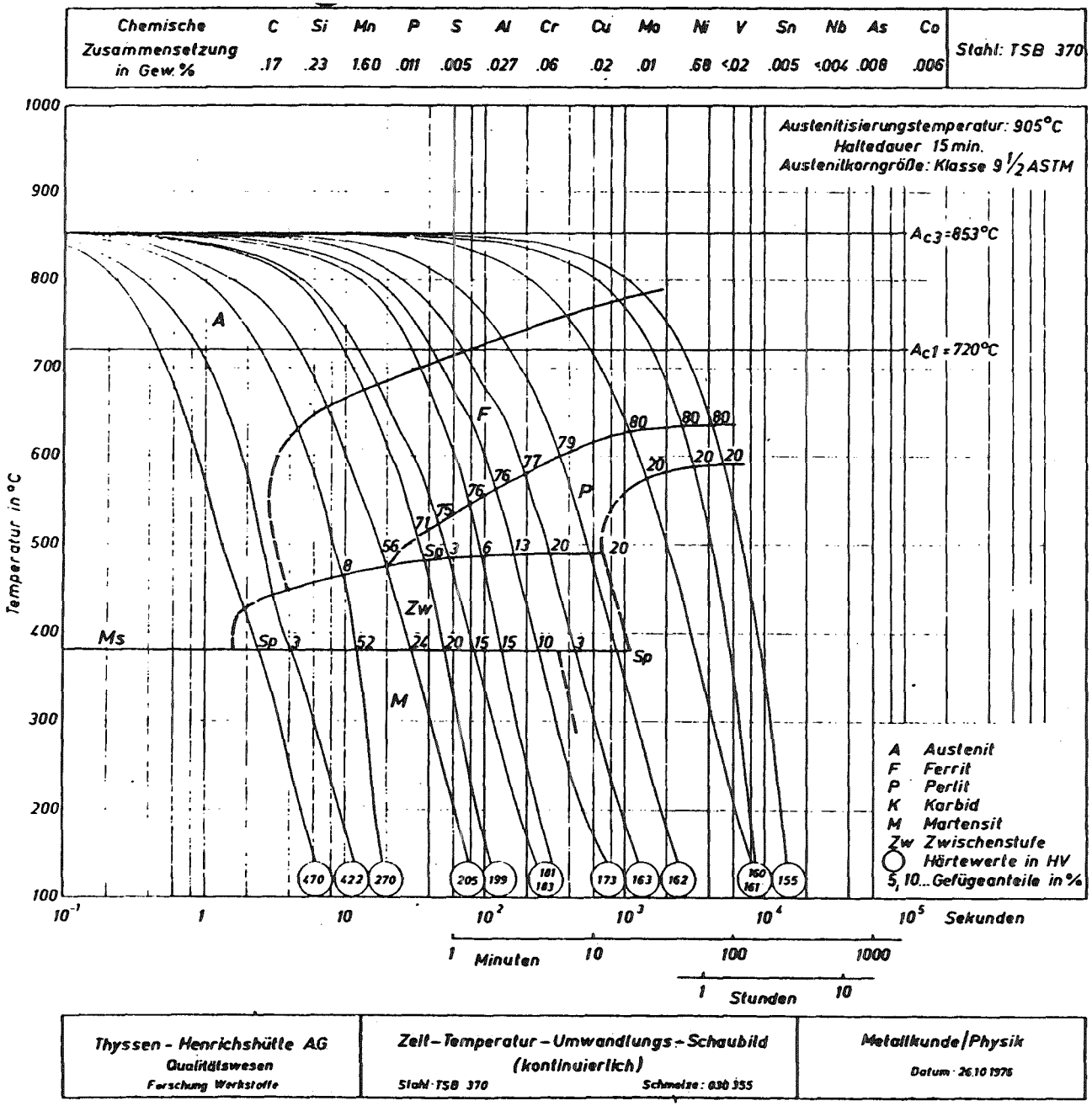
Chemische Zusammensetzung in Gew.%
C .17
Si .23
Mn 1.60
P .011
S .005
Al .027
Cr .06
Cu .02
Mo .01
Ni .68
V <.02
Sn .005
Nb <.004
As .008
Co .006
Stahl: TSB 370
Austenitisierungstemperatur: 905°C
Haltedauer 15 min.
Austenitkorngröße: Klasse 9 1/2 ASTM
Ac3=853°C
Ac1=720°C
Temperatur in °C
A Austenit
F Ferrit
P Perlit
K Karbid
M Martensit
Zw Zwischenstufe
Härtewerte in HV
5, 10... Gefügeanteile in %
Sekunden
Minuten
Stunden
Thyssen - Henrichshütte AG
Qualitätswesen
Forschung Werkstoffe
Zeit-Temperatur-Umwandlungs-Schaubild
(kontinuierlich)
Stahl: TSB 370
Schmelze: 030 355
Metallkunde/Physik
Datum: 26.10.1976

4.3.2 Pressure vessel

a) General Information

For safety reasons a failure of the pressure vessel (and of the pressurizer) must be prevented.
For this reason a quality and safety assurance program unparalleled in the history of technology is presented for the fabrication and operation of these components (Literature: U.Rösler, H.Cerjak, VDI-Berichte Nr. 302,1977).

Fig. 4 shows exploded views of pressure vessels.
The vessel to the left is fabricated using forgings and plates, the other two using forgings only.

- Segregation zones in the ingot center are removed by punching out of core
- Longitudinal welds are avoided ($\sigma_t = 2\ \sigma_l$).

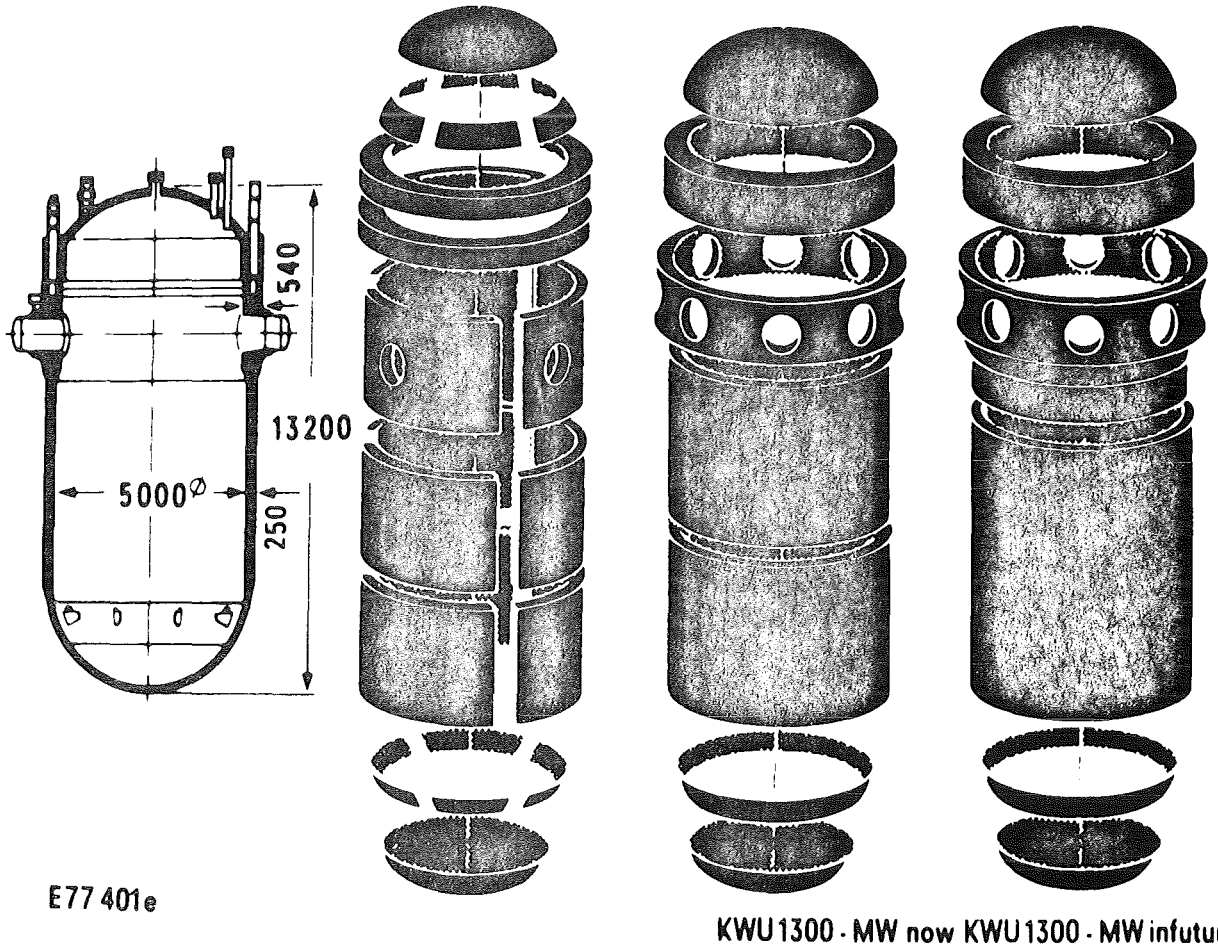

Reaktordruckbehälter für 1300 MW DWR

Fig. 4 Pressure vessel for 1300 MWe PWR(KWU)

The requirements for pressure vessel steels are:

a) Sufficient strength (hardenability) and toughness
b) low scatter of property data in the component
c) good weldability
d) applicability of non-destructive testing methods and easy failure detection
e) low irradiation embrittlement
f) high microstructural stability (40 years of operation)
g) corrosion resistance as to cooling medium.

In the western world two types of steel have been developed for pressure vessels and other pressure retaining primary components. These are low-alloyed, fine-grained and toughened (quenched + tempered)+) steels of the types

NiMoCr : 22 NiMoCr 37 or ASTM A 508 cl. 2
(1.6751)

MnMoNi : 20 MnMoNi 55
(1.6310)
or ASTM A 508 cl. 3 (forgings)
ASTM A 508 gr. B (plates)

The chemical analyses and main mechanical properties at RT and 350°C are given below.

+) This treatment results in a bainitic or bainitic-martensitic microstructure.

	ASTM A 508 class 2	22NiMoCr 37 KWU-Spez. WS 1.1	ASTM A 533 grade B class 1	ASTM A 508 class 3	20 MnMoNi 55 KWU-Spez. RE-WS 1.1
C	< 0,27	0,17-0,25	≤ 0,25	0,15-0,25	0,17-0,25
Si	0,15-0,35	0,10-0,35	0,15-0,30	0,15-0,35	0,15-0,30
Mn	0,50-0,90	0,50-1,00	1,15-1,50	1,20-1,50	1,15-1,50
P	≤ 0,025	≤ 0,012[1)]	≤ 0,035	≤ 0,025	≤ 0,012[1)]
S	≤ 0,025	≤ 0,015	≤ 0,040	≤ 0,025	≤ 0,015
Cr	0,25-0,45	0,25-0,50	-	-	≤ 0,20
Mo	0,55-0,70	0,50-0,75	0,45-0,60	0,45-0,60	0,45-0,60
Ni	0,50-0,90	0,60-1,00[1)]	0,40-0,70	0,40-0,80	0,40-0,80
Co	n.s.	≤ 0,030	n.s.	n.s.	≤ 0,030
Ta	n.s.	≤ 0,030	n.s.	n.s.	≤ 0,030
Al	n.s.	≤ 0,050	n.s.	n.s.	≤ 0,050
Cu	n.s.	≤ 0, 10[1)]	n.s.	n.s.	≤ 0,10[1)]
V	≤ 0,05	≤ 0,05	n.s.	≤ 0,05	≤ 0,03
Ultimate tensile strength N/mm² RT	550-725	560	522-689	550-725	560
Ultimate tensile strength N/mm² 350°C	n.s	490	527	n.s.	490
Yield strength N/mm² RT	345	392	344	345	392
Yield strength 350°C	n.s	343	285	n.s.	343
Tensile elongation % RT (Lo=5d$_o$ or 2 in)	18	19	18	18	19
Tensile elongation % 350°C (Lo=5d$_o$ or 2 in)	n.s	14	n.s	n.s	14
Reduction of area % RT	38	45	n.s.	38	45
Reduction of area % 350°C	n.s.	n.s.	n.s.	n.s.	n.s.
Impact energy J (Iso-V-Notch spec) Test-T 0°C or 4,4°C	a 41 LV 34 (4.4°C)	64 52 (0°C)	n.s. n.s	41 34 (4.4°C)	64 52 (0°C)

1) For parts outside the core region: Cu up to 0,18 %; P up to 0,015; Ni up to 1,20

n.s..... not specified
a ..... average
LV ..... lowest single value

Typical heat-treatment temperatures (for 20 MnMoNi 55) are: Quenching: 870-930°C, Tempering: 630-690°C.

The fine grain results from a controlled Al(0.02-0.05%) and eventually V-addition.
The two steel types NiMoCr and MnMoNi are nearly identical. There is, however, one difference: MnMoNi(1.6310) shows less susceptibility to the formation of stress-relief cracks, resulting in less repair work during fabrication.

The fabrication and testing steps for a pressure vessel forged ring are shown in Fig. 5.

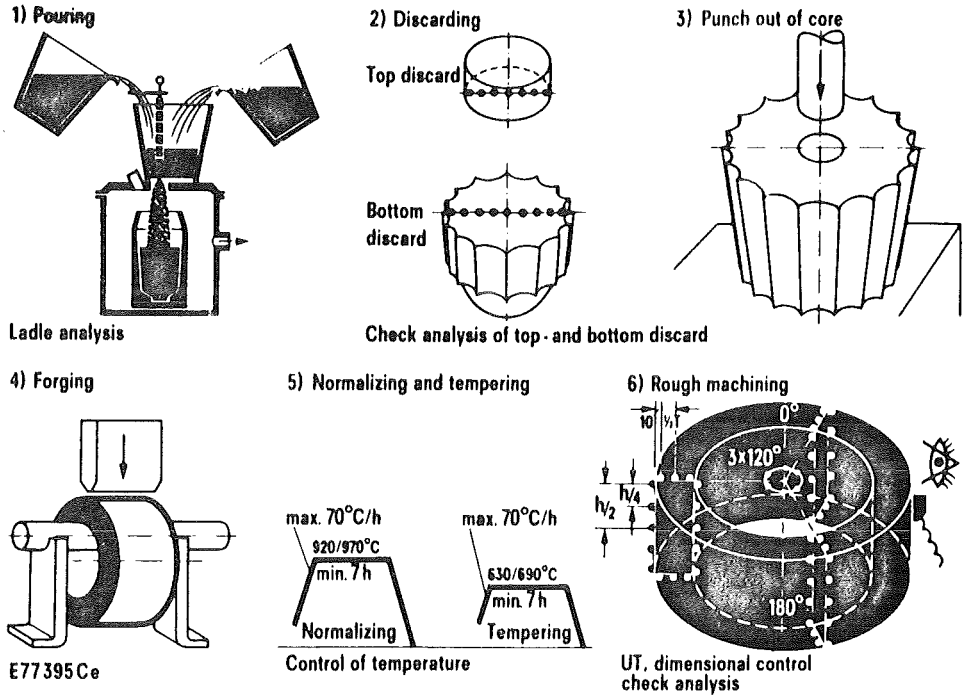

Bild 11. Herstellungs- und Prüfgeschichte eines RDB-Schmiederinges, Teil 1

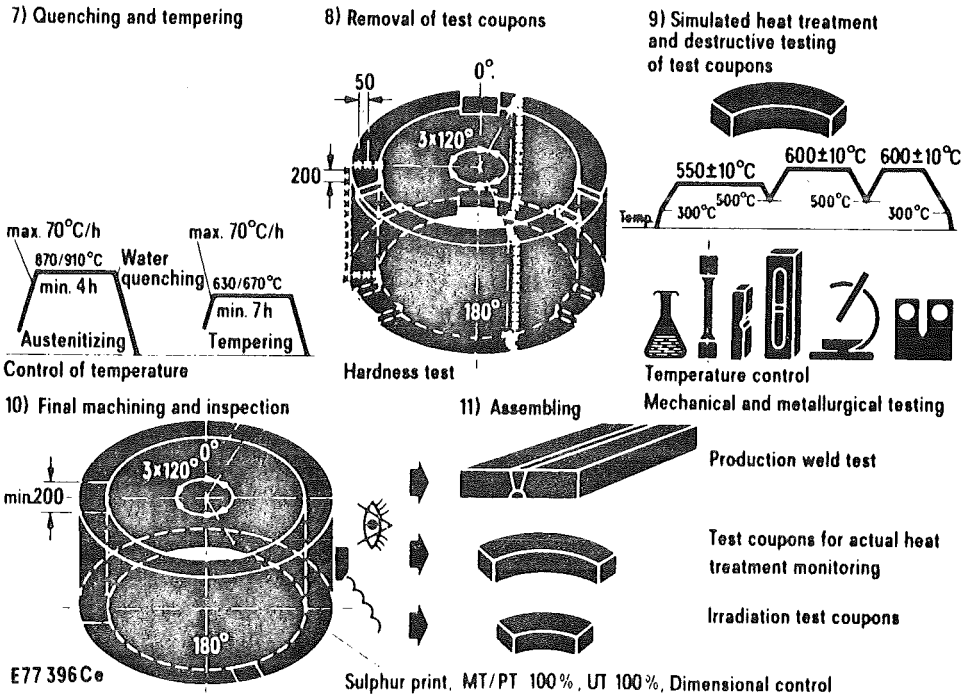

Bild 12. Herstellungs- und Prüfgeschichte eines RDB-Schmiederinges, Teil 2

Fig. 5

Remarks: (2) Discard: Analyses to determine extent of macro-segregation

(4) and (5) : T control during those steps to assure a homogeneous and testable microstructure.

(9) Simulation of effect of stress relief annealing on test coupons: Tensile, impact, drop weight (Pellini), K_{Ic}-testing.

The continuous TTT-diagram of the steel 20MnMoNi 55 is shown in Fig. 6 . One sees that to avoid the pearlite nose the temperature must be brought down to 600°C within less than 3 minutes.

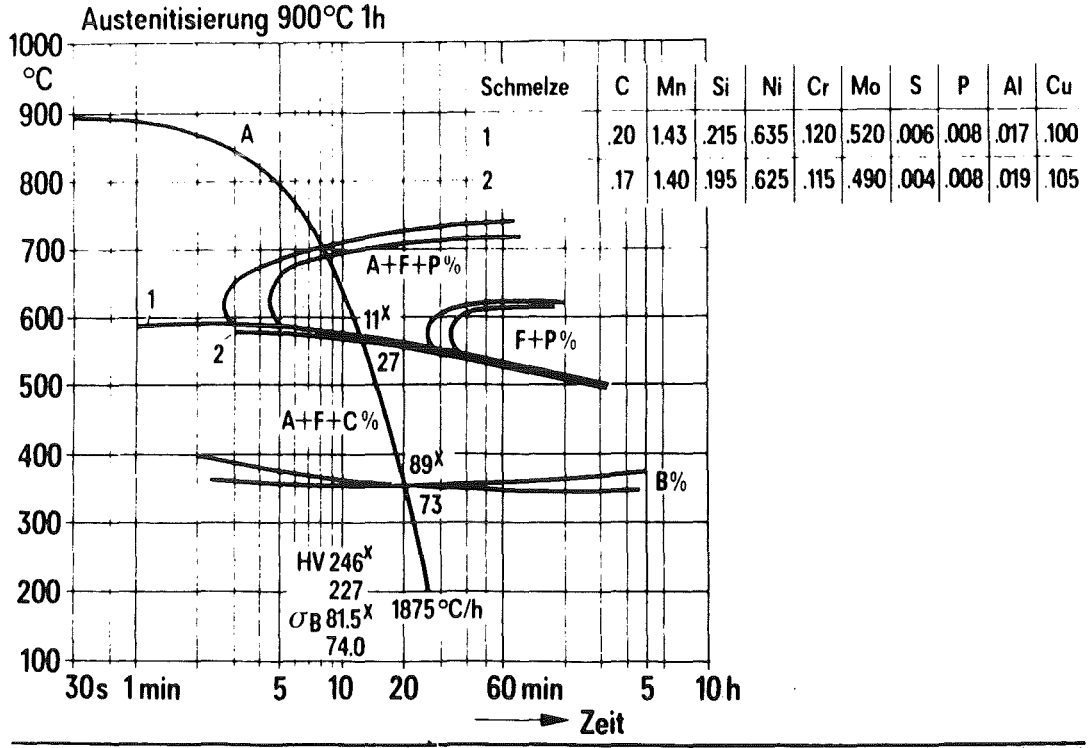

Fig 6 : 20 Mn Mo Ni 55, ZTU-Diagramme

In the center of thick walls as with pressure vessel flanges (560 mm) the lower quenching rate leads to a higher ferrite content. As Fig. 7 shows, the influence on mechanical properties is nevertheless small (including the upper shelf impact energy). However, the impact transition temperature is remarkably shifted to higher T (see $0^{o}C$ data line).

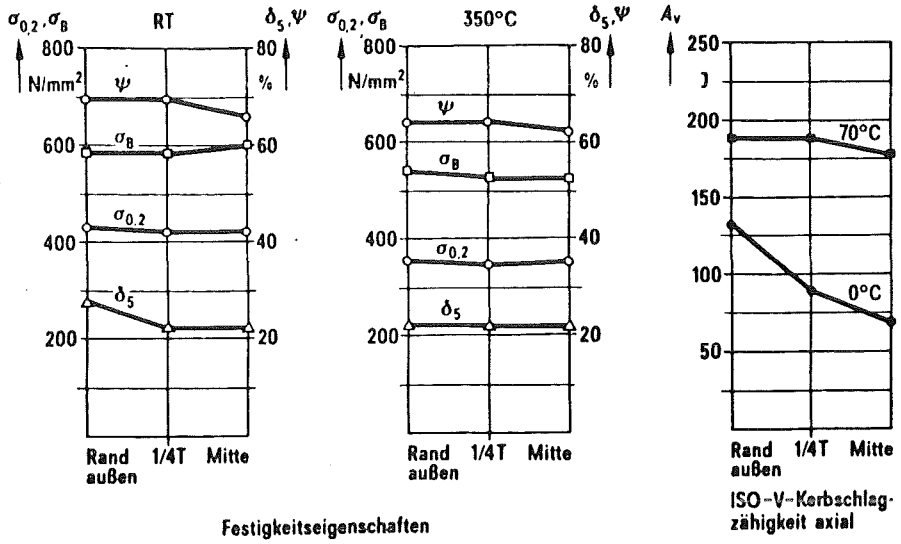

Fig. 7: 20 Mn Mo Ni 55: Mechanische Eigenschaften über den Querschnitt (560 mm) Mantelflansch, Probenlage axial

E76493

Early US-reactors were constructed of stainless-clad steel manufactured by a roll-bonding process (Dresden I, Shipping-port). Today all commercial reactors are lined with stainless steel by the weld overlay process.

b) Welding

Weld processes are used to connect the different (forged) parts of the pressure vessel and to clad the inside with a corrosion resistant austenitic steel.

The weld cladding is done by the submerged arc strip cladding process. The strip electrode may be 60 mm wide, with the arc burning under a blanket of granular fusible basic material. The corrosion resistance is secured by the choice (KWU) of a stabilized austenite (X 5 CrNiNb 19 9, 1.4551), the absence of cracks by a careful supervision of welding parameters including a controlled δ-ferrite content.

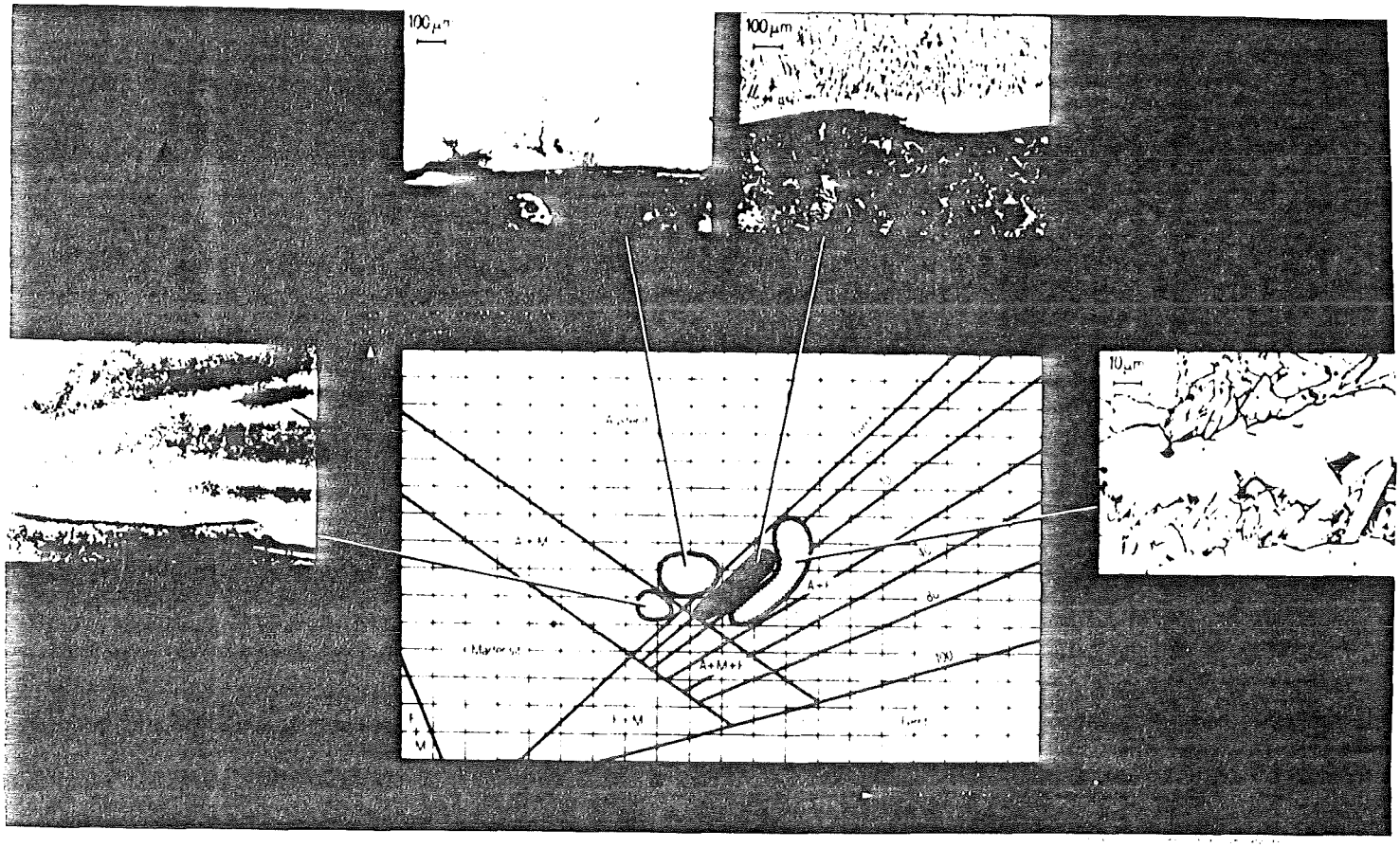

Fig. 8: Various microstructures at austenitic weld clads

Fig. 8 shows a Schaeffler-diagram in which the dark shaded area gives the best results.

In the following we will deal with the mechanical testing of weldments and with the problem of weld cracks, which has gained much publicity.

A weld consists mainly of 3 areas = weldment, heat affected zone (HAZ) und base material.
Fig. 9 shows mechanical properties across those areas.

Kraftwerk Union

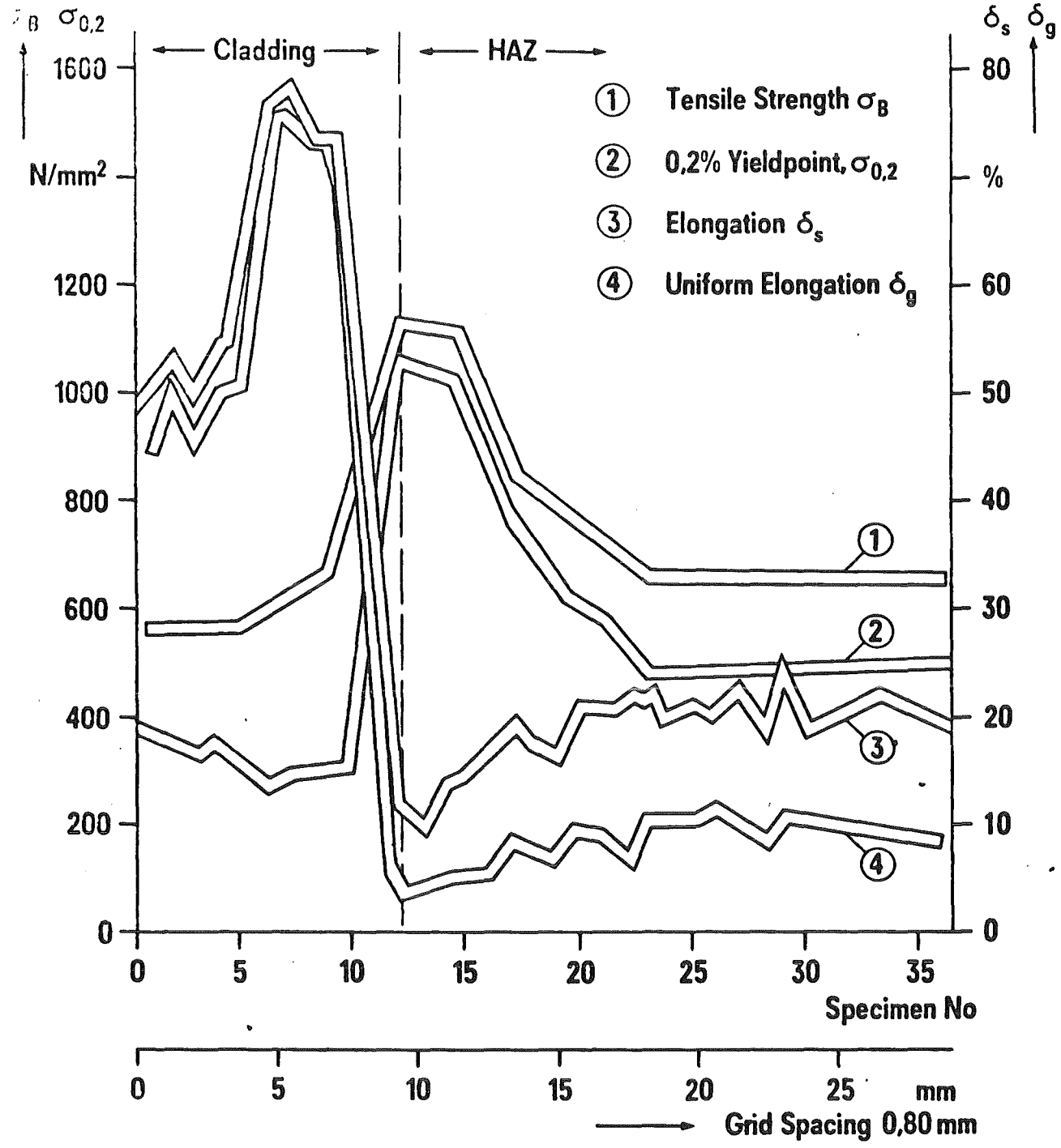

Tensile Tests with Micro Rectangular Tensile Specimens; Stripcladding

E 80 1259 Ce

Fig. 9

A survey of mechanical testing methods is collected in Fig. 10.
Note the micro tensile specimen with a 0.5 x 2 mm cross section (length 21 mm).

Type of Test	Sampling Location	Cross Section of Sample	Material Property
Tensile Test	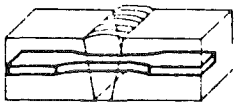	Arbitrary	Tensile Strength of the Softest Region
Technological Bend Test		Arbitrary	Deformability of the Weld Joint
Notch Bar Impact Bending Tests CVN Specimen	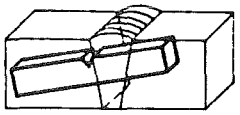	8×10 mm	Notch Impact Toughness Lateral Expansion Proportion of Ductil Fraction of the Notch Region
Drop-Weight Test	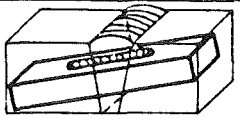	19×50 mm	NDT-Temperature of the Notch Region
Fracture Mechanics Test CT Specimen	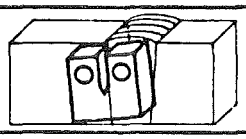	Specimen Thickness Times Diameter of the Plastic Zone	da/dN, K_{IC}, COD of the Notch Region
Wide Plate Test	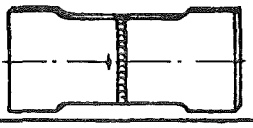	500×30 mm	K_{IC}, COD of the Notch Region
Vickers Hardness Test	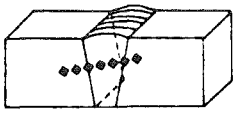	µm Range	Hardness Traverse of the Weld Joint
Tensile Test Micro Rectangular Tensile Specimen	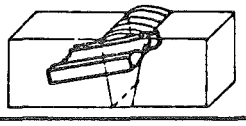	0,3×1 mm or 0,5×2 mm	E-Modul, Yieldpoint Tensile Strength Elongation Grid Spacing: 0,6 mm
tch Bar Impact Bending Tests with Micro-Specimen	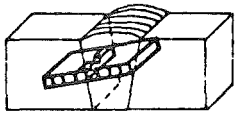	3×3 mm	Notch Impact Toughness Grid Spacing: 3,3 mm
Drop-Weight Test	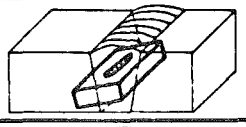	19×50 mm	NDT-Relation between All-Weld- +Base Material +HAZ
Fracture Mechanics Test CT-Specimen	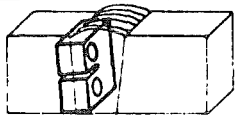	Specimen Thickness Times Diameter of the Plastic Zone	da/dN, K_{IC}, COD Relation between All-Weld- +Base Material +HAZ

Testing of HAZ

Kraftwerk Union

It is important to note that in nuclear reactor technology the same requirements (testing, properties) have to be fulfilled for welds as for the base material.-

The phenomenon of stress-relief cracking, SRC (Relaxationsrissbildung) has already been mentioned. Two types may by differentiated

- the "classical" stress-relief cracks in the coarse grain region of the HAZ, parallel to the weld direction, and

- the underclad cracks in the coarse grain region of the HAZ, vertically to the weld direction

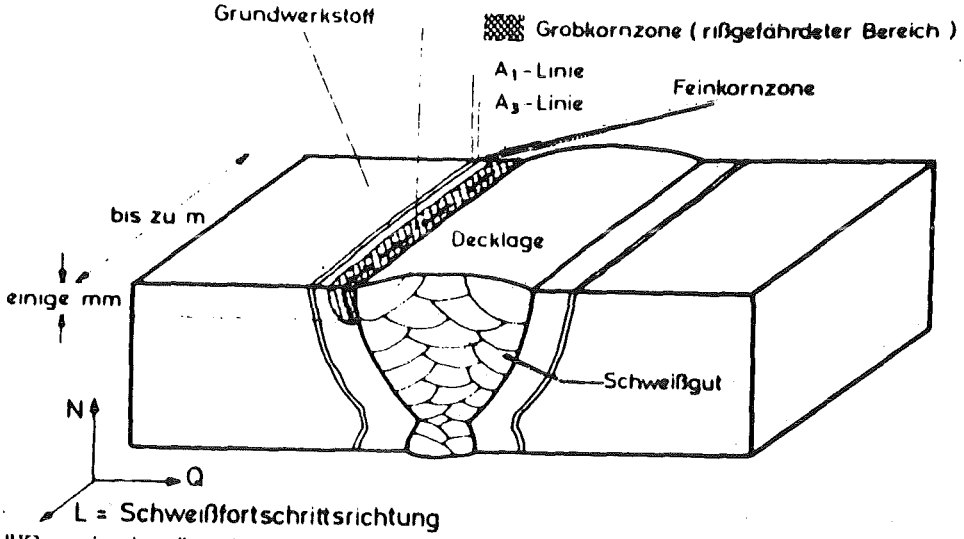

"Klassischer" Nahtflankenriß (stress relief crack) schematisch

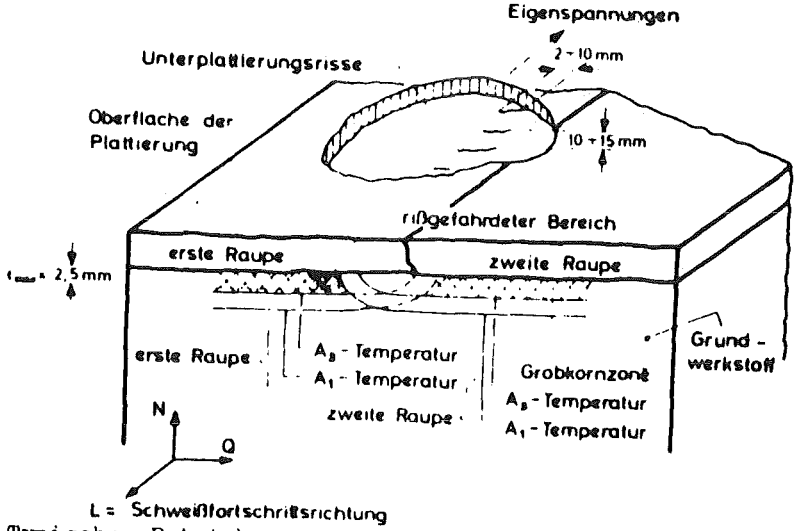

Typischer Entstehungsort und Lage von Unterplattierungsrissen (schematisch)

Mainly research at MPA Stuttgart (Germany) helped to solve this problem which once led to appreciable difficulties during production.
It was shown that the so-called strain induced embrittlement is a pre-stage of SRC. This embrittlement depends on the contents of special carbide formers (Mo, V, Nb) and of impurities. The success of counter-measures could be demonstrated by a so-called "weld simulation technique". It consists in principle of 3 steps.

- Giving the same heat tretment to a large sample as is to be endured at a certain HAZ-area during welding (heating/cooling cycle).

- Performing a short time creep test at stress relief temperature, to simulate relaxation of welding stresses and transformation stresses. Establishing a creep-rupture-elongation curve as a function of time.

- Measuring the tensile and notch-impact properties of samples which show low creep-rupture elongation.

An example for creep test results is shown in Fig. 11

The weld simulation tests did show differences in behaviour for areas of different structure but did not show spezial SRC-susceptibility or strain induced embrittlement for any of the areas present in the HAZ.

Kraftwerk Union

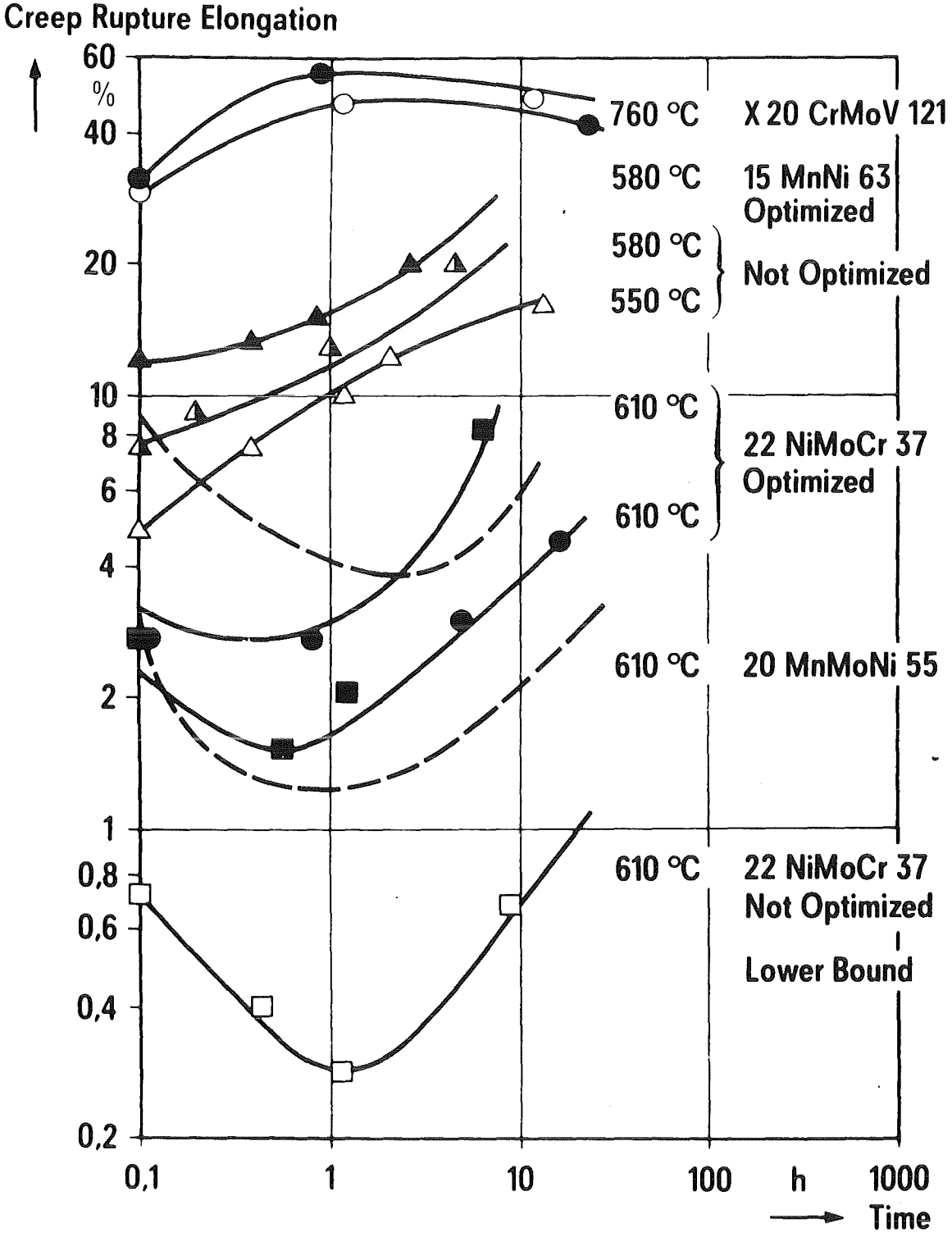

Improvement of Creep Rupture Elongation in 1300° C / H_2O-Quenched Condition

(Simulation of HAZ – Structure), (Ref. VDEh)

E 80 1238 e

Embrittlement by hydrogen which may enter the steel during welding (and as a result of a corrosion reaction during operation) is not considered a serious problem in pressure vessel steels. Delayed fractures resulting from the presence of hydrogen have only be observed in steels much higher in strength than those used for pressure vessels (Sterne, Steele, Nucl. Eng. and Design 10, 1969, 305).

c) Criteria for Toughness

The quality guide-lines in the Fed. Rep. of Germany are widely based on the "Reference NDT-Concept" which has been developed in the USA (ASME Code, Section III, NB 2300). In certain respects, however, the german guide lines are even more stringent.

The system is based on
- the Nil Ductility Transition Temperature (NDTT)
- the impact energy
- linear elastic fracture mechanics (K_{Ic})

The NDTT of ferritic steels are determined by the Pellini Drop-weight-Test (ASTM Standard Method, E 208-69). This Test, developed in 1952, has been extensively used to investigate the conditions required for initiation of brittle fractures in structural steels of 5/8 in. (15,9 mm) minimum thickness.
The Drop-weight-Test employs simple beam specimens specially prepared to create a crack in their tensile surface at an early time interval of the test. The impact load is provided by a guided, free-falling weight with an energy of 350 to 1650 J, depending on the specimen size and the yield strength of the steel to be tested.

Fig. 12 shows the machine and the test conditions used.

Standard Drop-Weight Test Conditions

Type of Specimen	Specimen Size, in. (mm)	Span, in. (mm)	Deflection Stop, in. (mm)	Yield Strength Level, ksi (MPa)	Drop-Weight Energy for Given Yield Strength Level[a]	
					ft-lbf	J
P-1	1 by 3½ by 14 (25.4 by 89 by 356)	12.0 (305)	0.3 (7.6)	30 to 50 (210 to 340)	600	800
				50 to 70 (340 to 480)	800	1100
				70 to 90 (480 to 620)	1000	1350
				90 to 110 (620 to 760)	1200	1650
P-2	¾ by 2 by 5 (19 by 51 by 127)	4.0 (102)	0.06 (1.5)	30 to 60 (210 to 410)	250	350
				60 to 90 (410 to 620)	300	400
				90 to 120 (620 to 830)	350	450
				120 to 150 (830 to 1030)	400	550
P-3	⅝ by 2 by 5 (15.9 by 51 by 127)	4.0 (102)	0.075 (1.9)	30 to 60 (210 to 410)	250	350
				60 to 90 (410 to 620)	300	400
				90 to 120 (620 to 830)	350	450
				120 to 150 (830 to 1030)	400	550

[a] Initial tests of a given strength level steel shall be conducted with the drop-weight energy stated in this column. In the event that insufficient deflection is developed (no-test performance) an increased drop-weight energy shall be employed for other specimens of the given steel.

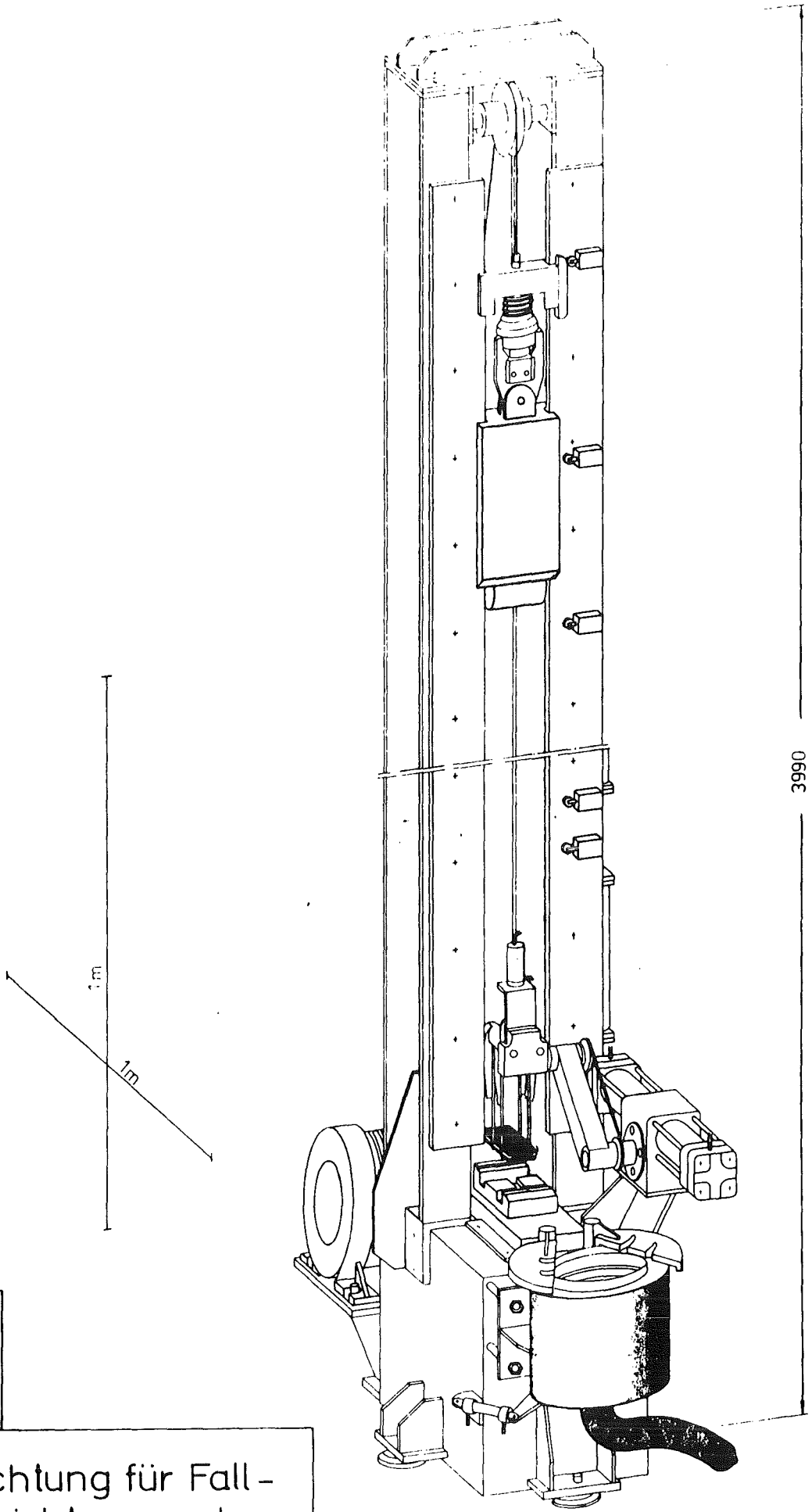

GKSS

Einrichtung für Fall-gewichtsversuche

By the anvil construction (Fig. 13)
the specimens are prevented by a stop from deflecting more than a few mm.
The crack-starter weld is deposited on the tension surface of the specimen. The weld finally is notched at the center of the bead length (Fig. 14).

The test is conducted by subjecting a series of specimens of a given material to a single impact load at a sequence of selected temperatures to determine the maximum T at which a specimen breaks (the "NDTT").

The test evaluates the ability of the steel to withstand yield point loading in the precence of a small flaw which forms after a minute bending of the test specimen. A specimen is considered broken if fractured to one or both edges of the tension surface. Typical examples of break performance are shown in Fig. 15.

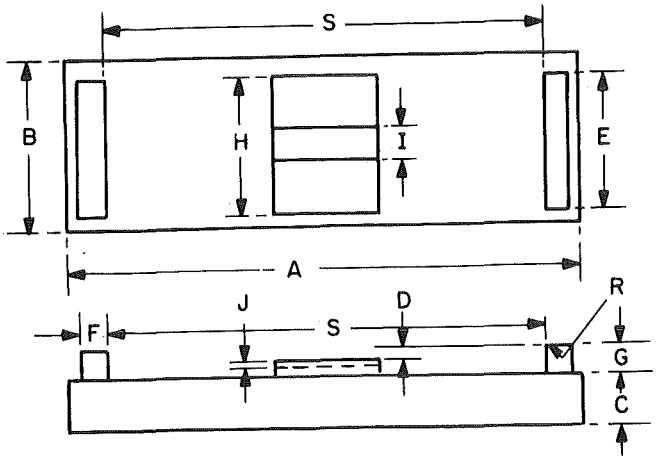

Fig. 13

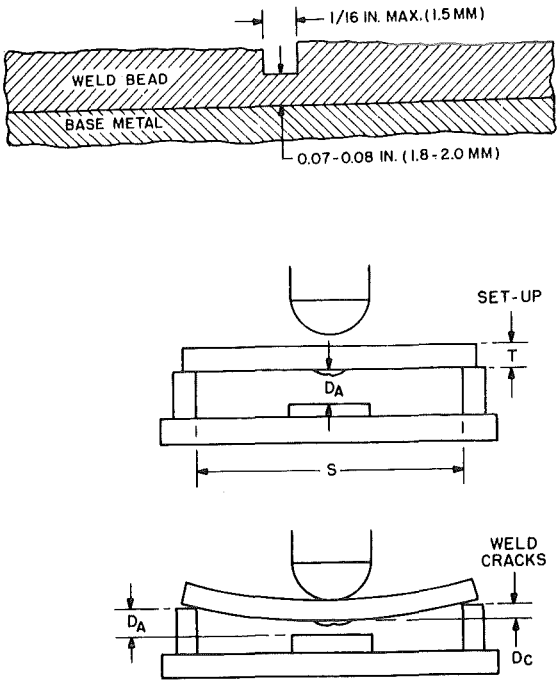

YIELD POINT LOADING IN PRESENCE OF SMALL CRACK IS TERMINATED BY CONTACT WITH STOP
Drop-Weight Test Method.

Fig. 14

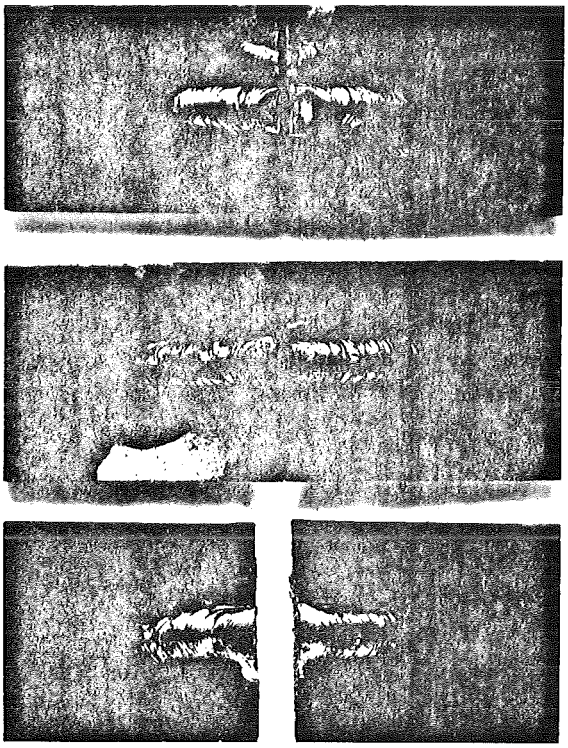

Typical Examples of Broken Drop-Weight Specimens. Fracture Reaches to at Least One Edge.

Fig. 15

The impact energy [J] is measured using the ISO-V-specimen.

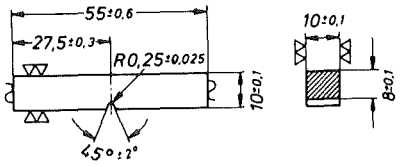

ISO-Spitzkerbprobe (ISO-V-Probe)

(1 J = 0.102 kp · m)

Fracture mechanics tests are carried out using CT-specimens (see section "welding"). Fracture toughness (K_{IC}) data as a function of T for base metal, weld metal and the HAZ are plotted in Fig. 16.
The lower limit curve is used for design (see below)

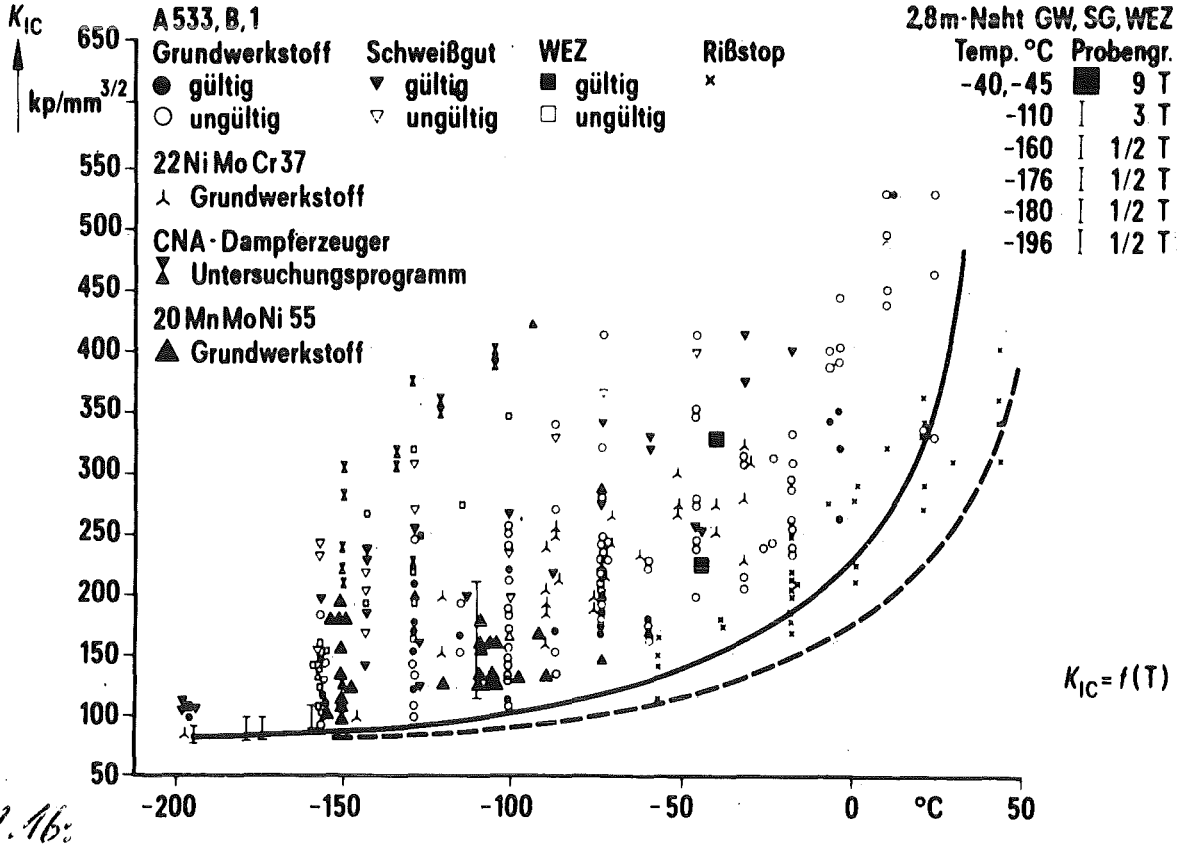

Fig. 16:
Bruchzähigkeit als Funktion der Temperatur Werkstoffe: A 533, B 1, 22 NiMoCr 37, 20 MnMoNi 55

The "Reference NDT-concept" forms the basis for the Acceptance Standards in both the USA and the Federal Republic of Germany. The main points of the German version are as follows (RSK-Leitlinien für Druckwasserreaktoren, 2. Ausgabe, 24.1.1979):

- For ferritic materials (base, weld as well as HAZ) the reference temperature RT_{NDT} must be at least 33 K below both, the lowest operational temperature and the temperature of the vessel pressure test. RT_{NDT} is established as follows:

a. Determine the nil-ductility transition temperature T_{NDT} by drop-weight tests.

b. At a temperature not greater than T_{NDT} + 33 °C xx) each specimen of the Charpy C_v-(Iso-V-transversal specimen-) test shall exhibit at least 0.9 mm lateral expansion and not less than 68 J absorbed impact energy. When these requirements are met, $T_{NDT} = RT_{NDT}$.

   Furthermore in the upper shelf each (transversal) specimen must exhibit at least 100 J.

c. In the event that the requirements of (b) are not met ($\lesssim$ 68 J, 0.9 mm), conduct additional C_v-tests on transversal specimens to determine the temperature T_{C_v} at which they are met. In this case the reference temperature $RT_{NDT} = T_{C_v} - 33$ °C. Thus, the reference temperature RT_{NDT} is the higher of T_{NDT} and /$T_{C_v} - 33$ °C/.

In the USA there are additional requirements under consideration to ensure adequate fracture toughness (NB-2330). Linear elastic fracture mechanics procedures limit the allowable loadings (Appendix G of the ASME Boiler and Pressure Vessel Code, Section III (12.1972), "Protection Against Nonductile Failure").

---

xx) According to Pellini and Puzak, at and above (NDT +33°C) ferritic steels are within the upper shelf region. (even in the presence of large flaws, there is no danger of instable crack growth with ferritic steels under yield point loading. See Möller, Wärme 84, Heft 5, S.99)

Fig. 17 shows a curve which gives "the relationship which can be conservatively expected between the critical, or reference, stress intensity factor, K_{IR}, and a temperature which is related to the reference nil ductility temperature, RT_{NDT}. This curve is based on the lower bound of static, dynamic and crack arrest critical K_I values measured as a function of temperature .....".

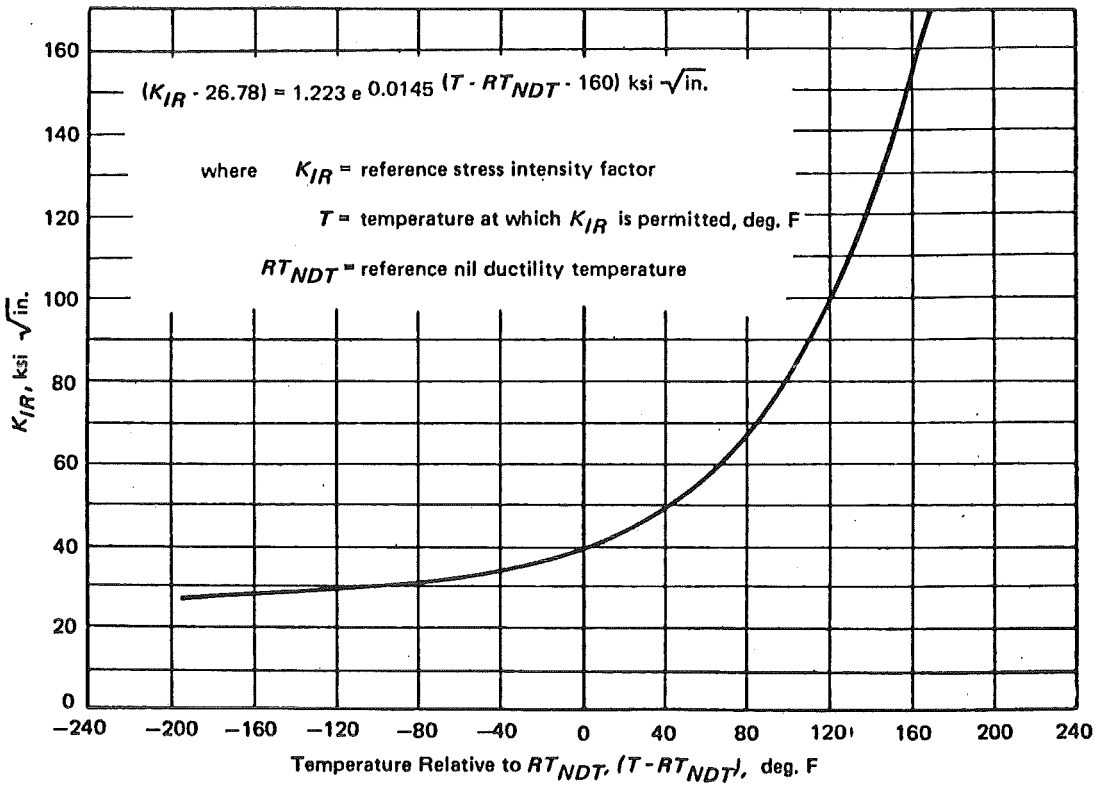

Fig. 17

This curve is valid for ferritic steels with a yield strength at RT of 345 MPa or less. For higher yield strength materials (as, for instance, 1.6310 and 1.6751!), not exceeding 621 MPa, this curve may also be used provided fracture mechanics data are available on at least three heats of the material. Where these higher yield strength materials are to

be used in conditions where radiation may affect the material properties, the effect of radiation on the K_{IR} curve must be determined.

We have seen that the Reference NDT-concept is a system interrelating the NDT-temperature, impact energy and linear elastic fracture mechanics.

For thin-walled components and elevated temperatures elasto-plastic fracture mechanics (COD, J-Integral) is more suited. Developmental work for LWR is underway.

d) Irradiation effects

In chapter (4.2) we came already to the conclusion that for a LWR pressure vessel the planar defect clusters (vacancy and interstitial agglomerates) must be the important radiation effect. In this section we will see how the properties are affected by irradiation and how far the phenomena are understood.

The yield strength as a function of neutron fluence and T is given in Fig. 18 and 19 (Steel ASTM A 533 B).

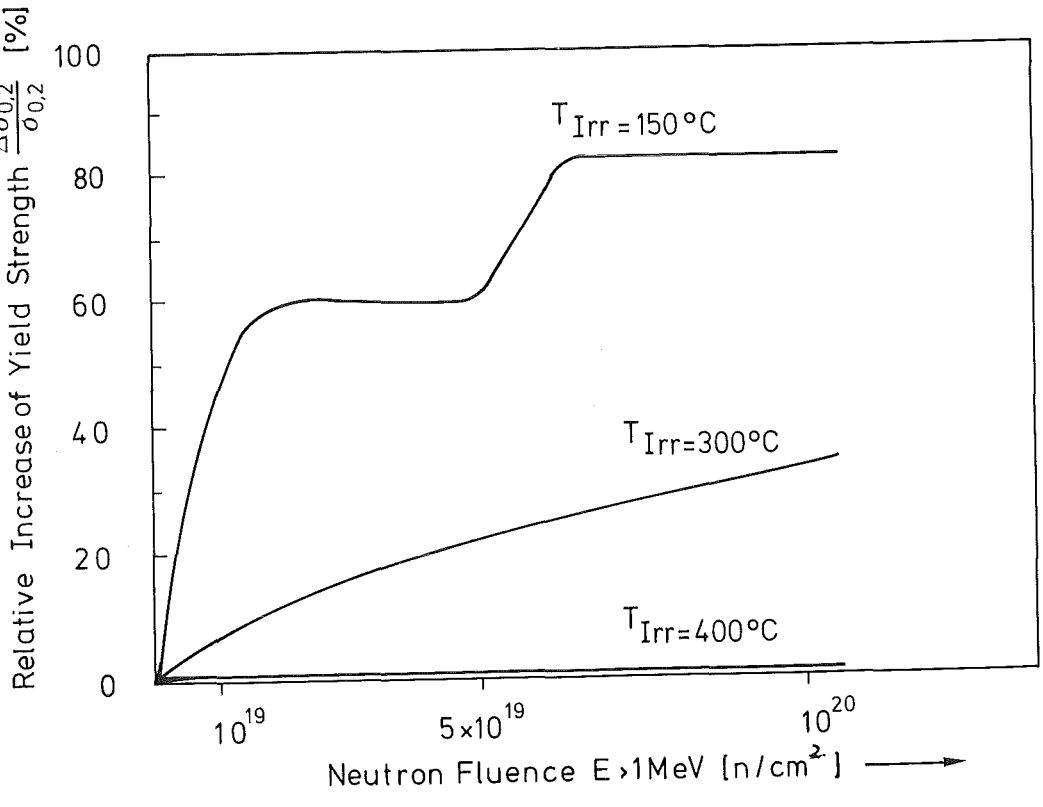

Fig. 18

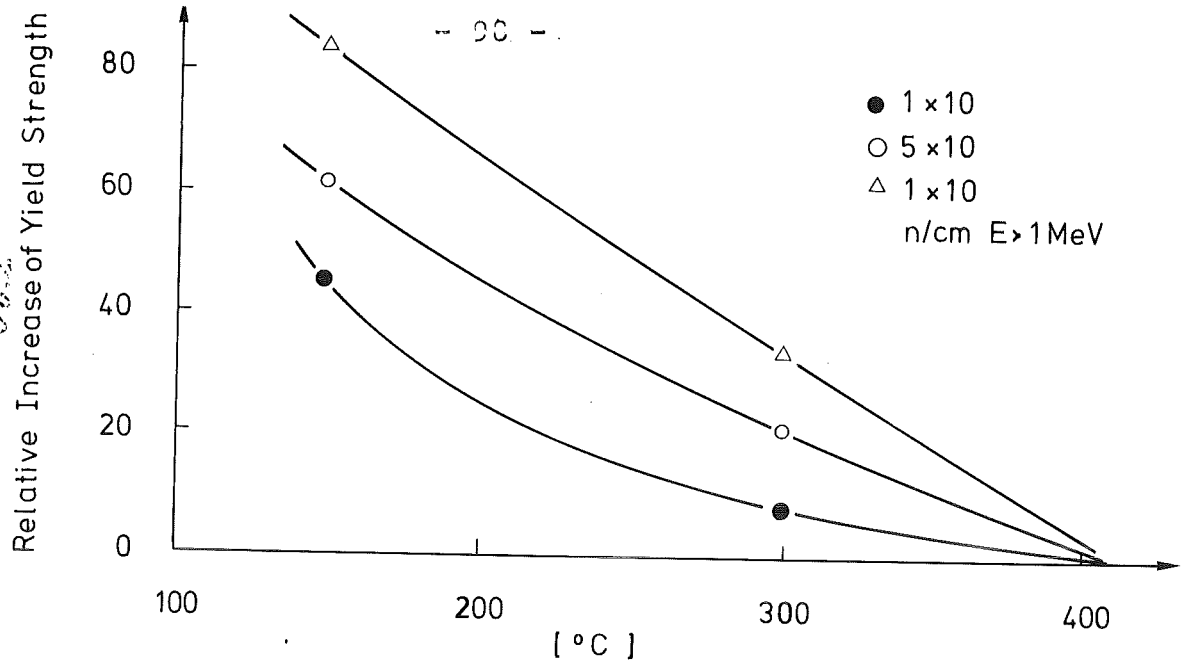

Fig. 19 Increase of yield strength in dependence of irradiation temperature for ASTM A 533 B

At $5 \cdot 10^{19}$ n_s/cm^2 the relative increase of yield strength is about 60 % at 150°C, 20 % at 300°C and 0 % at 400°C. At 150°C, apparent saturation effects (two steps) occur. Heat treatment after irradiation (annealing) has the same effect as high T irradiation: at higher T defects anneal out.

As regards impact properties, irradiation affects both the transition temperature and the upper shelf energy. The former is increased and the latter depressed by irradiation (Fig. 20).

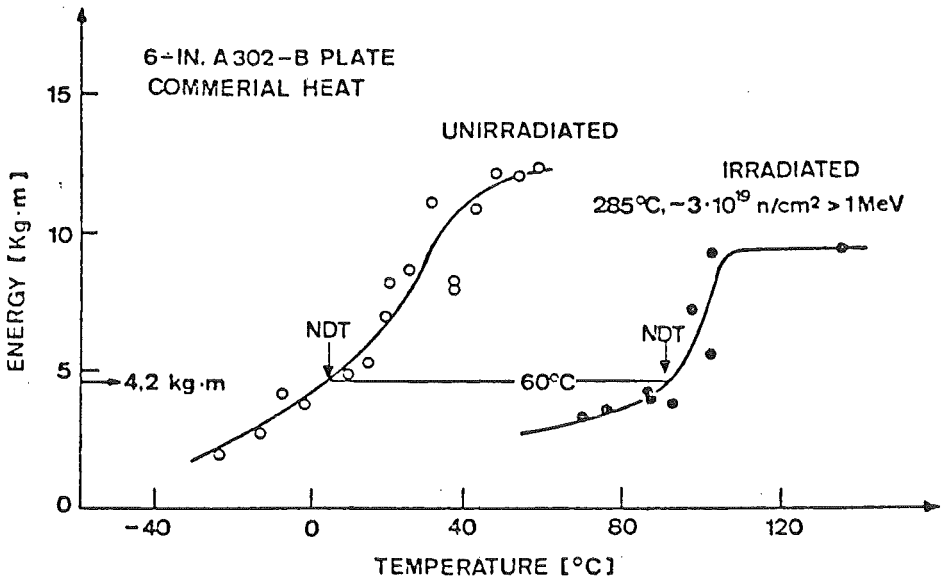

Fig. 20 Charpy-V notch impact data for irradiated A 302-B steel (after Steele, 1966)

The dependence of TT and Upper Shelf Energy on fluence and irradiation temperature is given in Fig. 21 :

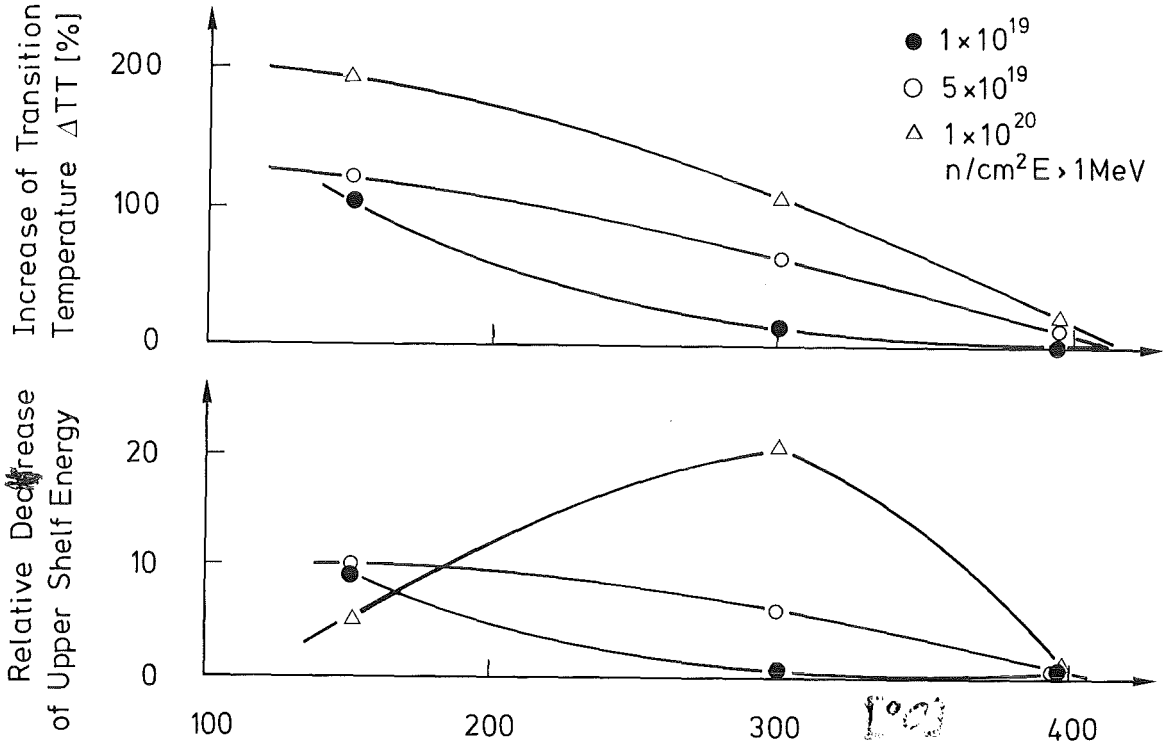

Fig. 21 Comparison of NDTT-transition with increase of upper shelf energy in dependence of irradiation temperature for ASTM A 533 B (Pachur, 1980)

By comparison with Fig. 19 one recognizes that the T-dependence of the irradiation induced increases of yield strength and transition temperature are similar. This may show that both phenomena are caused by the same defect clusters (vacancy aggregates? Bush, 1974). Mainly the transition temperature (TT) shift after irradiation at higher temperatures (290°C) is influenced by residual substitutional elements like Cu, P, As and V. Fig. 22 shows the effect of Cu. By decreasing Cu from > 0.15 % to ≤ 0.10 %, the irradiation induced TT-shift for plate, weld and HAZ material is greatly reduced. A further reduction in maximum allowable Cu content to ≤ 0.06 % (best steelmaking practice) will not substantially further improve the 550°F (288°C) radiation resistance (Hawthorne et al., 1979).

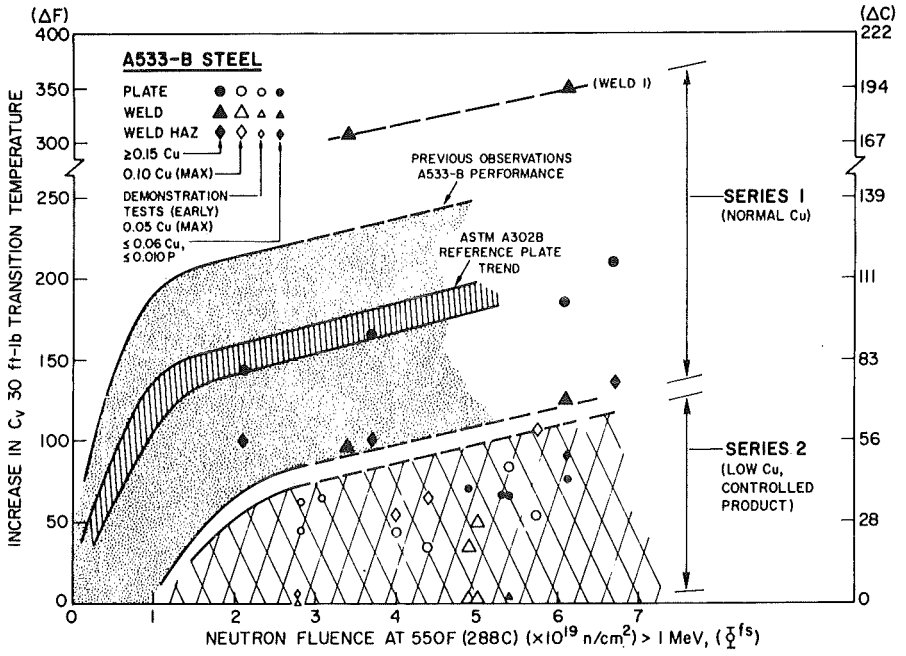

Fig. 22

Charpy C_V 41J transition-temperature elevations were less than 56°C and upper-shelf energy degradations were about 13 % with fluences of 5 to $7 \cdot 10^{19}$ n/cm^2 (E> 1 MeV).

The fact that at a irradiation temperature of 230°C the damage (ΔTT) is independent of the level of residuals, whereas at 290°C appreciable damage is only shown in high residual steels points to a dynamic recovery effect. We know from Section (4.2.2) that at the lower T level only interstitials are mobile, whereas at the higher T also vacancies become mobile. Therefore vacancies appear to be responsible for the dynamic recovery effect. A stable Cu-vacancy binding obviously stabilizes the defect clusters responsible for embrittlement. This may be a direct stabilization mechanism or act via enhanced nucleation of the defect clusters.

Quite recently (1980) D. Pachur has started to analyse those hardening and embrittling phenomena using hardness and impact tests. By annealing at different T he could show that various processes, characterized by specific activation energies, occur in different T ranges (Fig. 23):

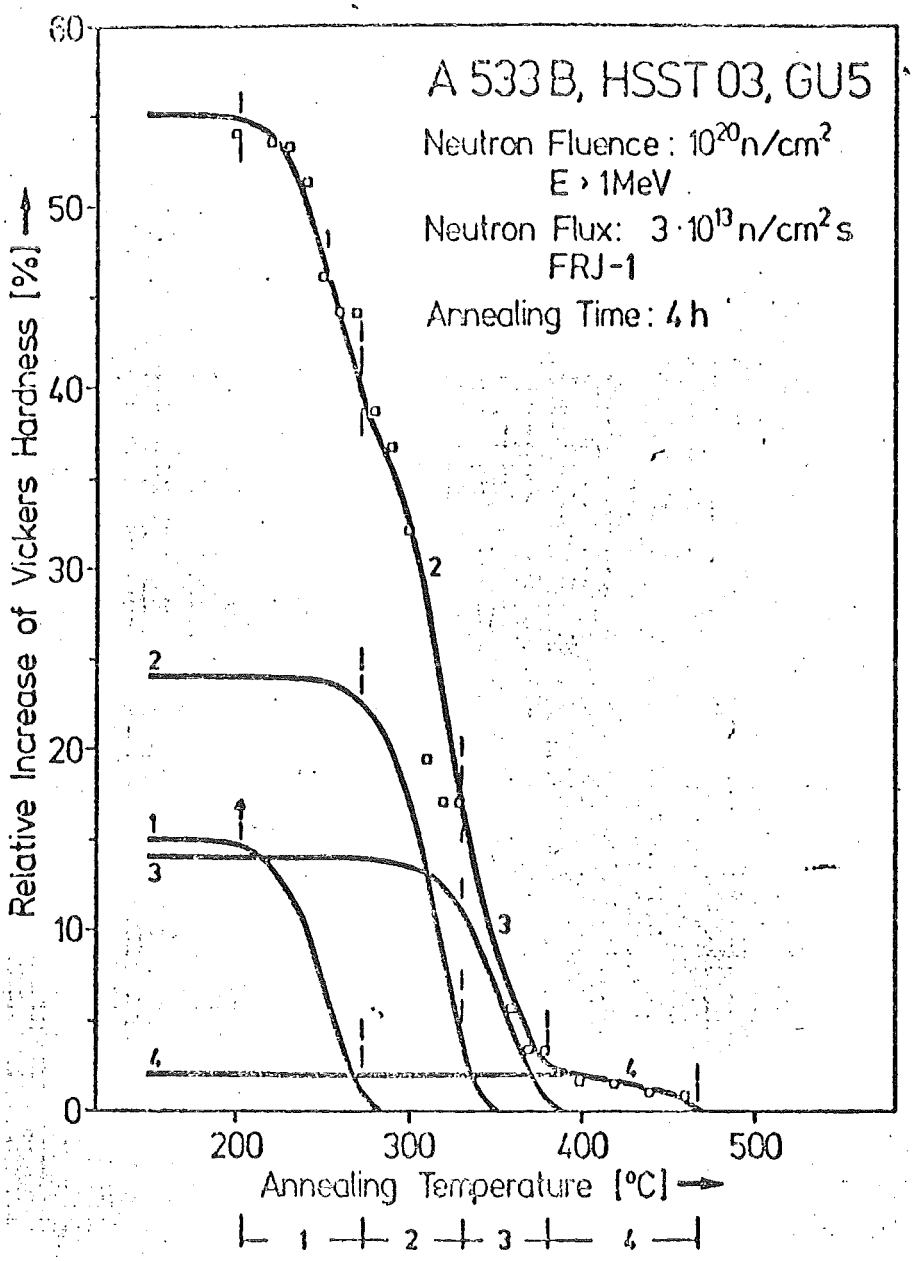

Fig. 23 Recovery of the Relative Increase of Vickers Hardness for Steel A Irrad. at 150 °C as a Function of Annealing Temperature.

It can be seen that the hardness increase due to a 150°C-irradiation recovers on annealing (4 h) and that the total hardness curve may be looked upon as composed of 4 hardening contributions. No. 1 starts to anneal out at about 200°C, No. 2 at 290°C, No. 3 at 310°C and No. 4 above 400°C.

A question of great practical importance is whether there is a dose-rate effect. Surveillance samples removed from (U.S.) commercial LWR's appear to show Charpy upper shelf energy and transition temperature shifts which are much less than would be predicted from (accelerated) test reactor data. The fluxes were 10^{10} (surveillance) and 10^{11}-10^{14} $n/cm^2 \cdot s$ ($E > 1$ MeV), respectively. It has been postulated that at low flux the embrittlement will saturate at a rather low fluence level due to self-annealing phenomena. This would mean that accelerated (high flux) tests give conservative results.

The present data base, however, is too limited to suggest regulatory changes at this time.

The best way to reduce the problem of embrittlement (especially NDTT shift) is to lower the expected neutron fluence in the beltline region at the end of life-time. This has been realized in modern design of pressure vessels (enlarged space between core and pressure vessel wall, which is filled with water and

steel-layers, acts as a radiation shield), see the table.

Table

Some operational Parameters for Pressure Vessel Steels of Light Water Reactors

	PWR	BWR
Operational Temperature [°C]	285-316	285-316
Operating Life-time [years]	40(1)	40(1)
Accumulated fluence [n/cm^2, E>1 MeV]	5×10^{18}(2) - 5×10^{19}	10^{18}
Effective fast flux [$n/cm^2 \cdot s$, E>1 MeV]	5×10^{9} - 5×10^{10}(3)	1×10^{9}

(1): with an availability factor of 0.8 the effective operation period is 32 years,

(2): accumulated fluence is dependent upon the geometry; e.g. modern PWR's of Biblis-Type lie in the range of 5×10^{18} n/cm^2 at the end of life,

(3): typical neutron fluxes used for irradiation experiments of reactor pressure vessels: 10^{11} - 10^{14} n/cm^2 (E > 1 MeV)

The NDT-shift at the end of life fluence of $5 \cdot 10^{18}$ n/cm^2 (E > 1 MeV) will be < 30°C with modern pressure vessel steels containing $\leq$ 0.10 % Cu. (The German "RSK-Leitlinien" prescribe an end of life fluence of maximal $1 \cdot 10^{19}$ n/cm^2

(E > 1 MeV). Fig. 24 shows the KWU design curves for the steels 20 MnMoNi 55 and 22 NiMoCr 37 for T_{Irr}=290°C.

The observed recovery effects principally open the possibility to remove the irradiation induced embrittlement in the beltline region of a pressure vessel by a thermal annealing treatment. This option may become important for the first generation of LWR's with their higher residual element content. "Wet annealing" at 350°C is not as efficient as a treatment at a somewhat higher T. An upper T limit is given by the danger of temper embrittlement.

Erhöhung der Übergangstemperatur, ΔNDT-T

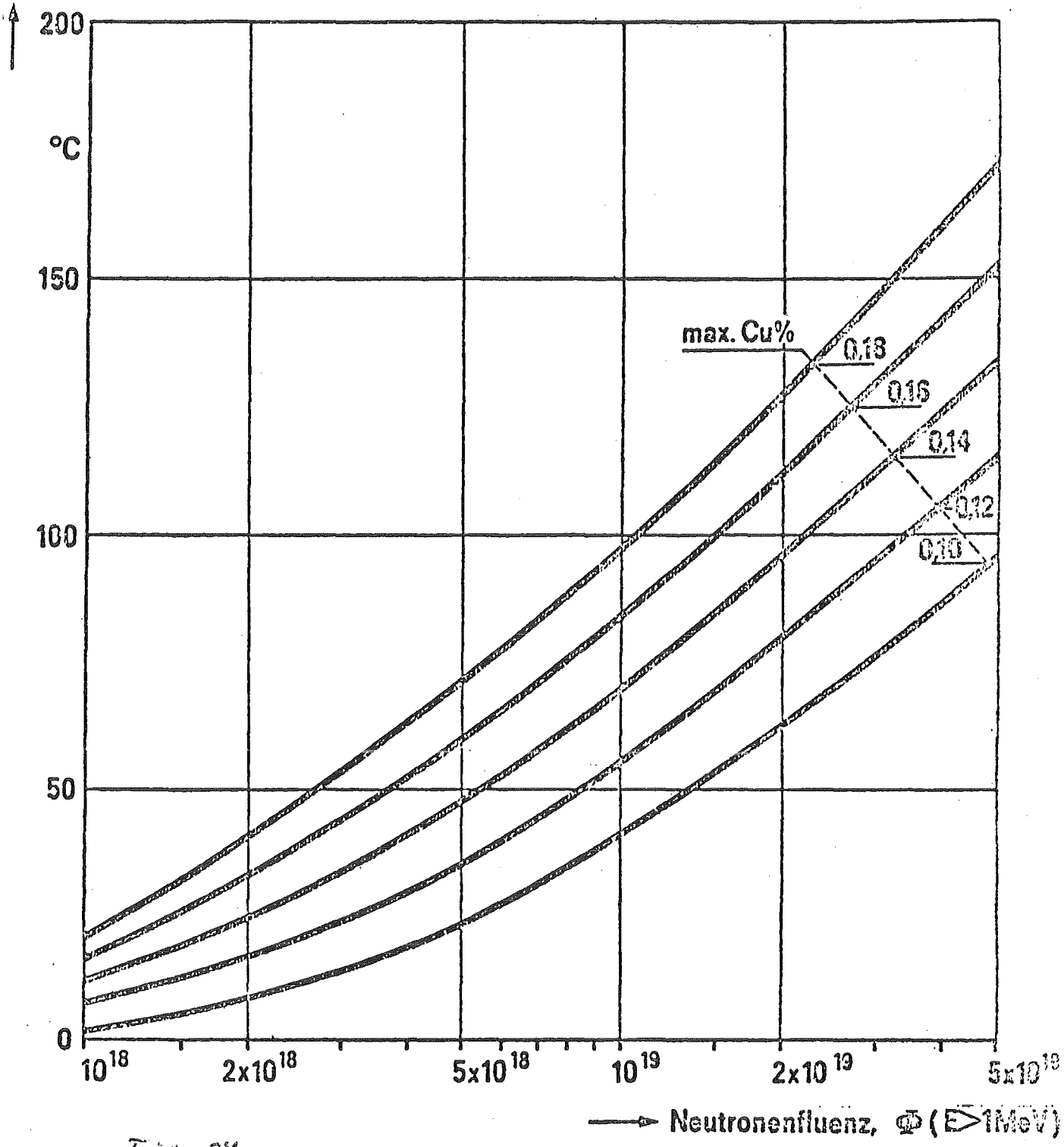

Fig. 24

Auslegungskurven zur Vorausberechnung der Strahlenversprödung der RDB-Stähle 20MnMoNi55 und 22NiMoCr37 für DWR und SWR (Bestrahlungstemperatur ca. 290 °C)

4.3.3 Pressure Vessel Internals

A survey of the components inside the pressure vessel of a (KWU-) PWR is given by the longitudinal and cross sections of Fig. 25 and 26 . The core with the (193) fuel elements rests on the lower support plate (Unterer Rost) which forms the bottom of the core barrel (Kernbehälter, Kernmantel). Going upwards there follows the upper core plate (Gitterplatte) and the upper (top) support plate (Oberer Rost mit Deckplatte).

The core is wrapped by the core shroud (Kernumfang). The core barrel has a wall thickness of 40-50 mm. This component as well as the lower and upper support plate and the upper core plate are made of massive austenitic steel 1.4550 (X10 CrNiNb 18 9) in the solution annealed state.

The cold cooling water passes the ringshaped Downcomer and moves upwards between the fuel pins towards the outlet.

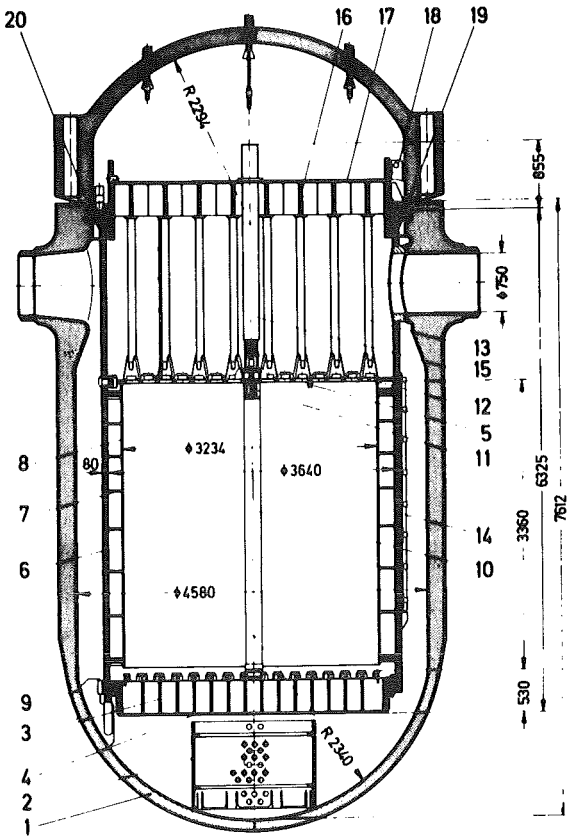

Längsschnitt durch den Reaktordruckbehälter mit Einbauten [2]

1 Druckbehälter
2 Siebtonne
3 Unterer Rost
4 Stauplatte
5 BE-Zentrierstifte
6 Kernbehälter
7 Formblech
8 Kernumfassung
9 Kernbehälter-Begrenzung
10 Brennelement
11 Steuerstab
12 Gitterplatte
13 Stütze
14 Bestrahlungskanal
15 Steuerstabführung
16 Oberer Rost
17 Deckplatte
18 Anhängeöse
19 Niederhalter
20 Zentrierung

Fig. 25
Longitudinal Section

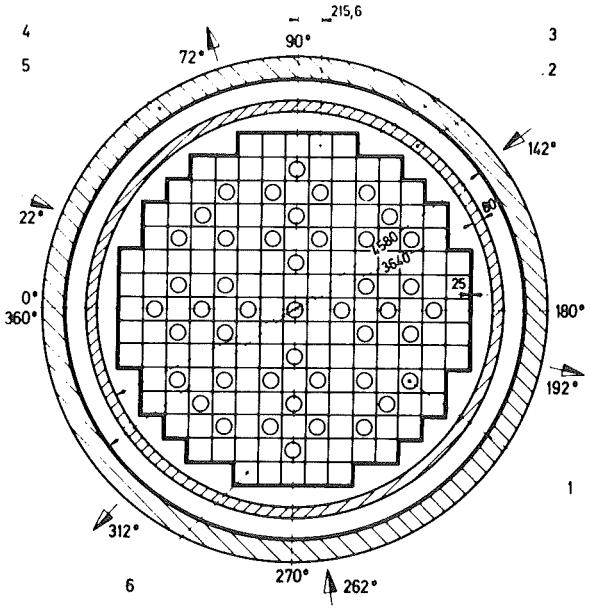

Querschnitt durch den Kern eines Druckwasserreaktors

1 Brennelement mit Steuerelement
2 Kernbehälter
3 Kernumfassung
4 Reaktordruckbehälter
5 Austenitische Plattierung
6 Brennelement

Fig. 26
Crosssection

4.3.4 Other pressure retaining primary components

The main components of the primary system of a PWR had already been shown on p. 71 . It can generally be said that there are either weld-overlay clad ferritic or fully austenitic.

Like the pressure vessel, the following components are made of weld-overlay clad (1.4551) 20 MnMoNi 55 - steel

- Primary piping (Hauptkühlmittelleitungen), up to 800 mm ∅
- Pressurizer (Druckhalter)
- Pump housings (Gehäuse der Hauptkühlmittelpumpen)
- Primary chamber of the steam generator

The primary piping of KWU-reactors is based on seamless (Mannesmann) pipes, diameter about 650 mm, wall thickness 50 mm.

The pressurizer release tank (Abblasebehälter), the accumulator (Druckspeicher) for emergency cooling and their piping are fully austenitic, of types

- 1.4550 X10 CrNiNb 18 9
- 1.4541 X10 CrNiTi 18 9
- 1.4571 X10 CrNiMoTi 18 10

For castings 1.4581 G-X7 CrNiMoNb 18 10 is under consideration.

Of special importance within the pressure retaining primary system are the bundles of U-shaped tubes in the steam generator (SG). They constitute a critical barrier between primary and secondary cooling circuits.

A longitudinal cross-section of a PWR-Steam generator is shown in Fig. 27 . The primary coolant, entering the primary chamber, flows through the U-shaped tube bundles. The secondary coolant water is on the outside of the tubes and forms a free surface within the upper part of the SG (Fig. 1, p. 71). Above this surface devices for vapour drying are installed.

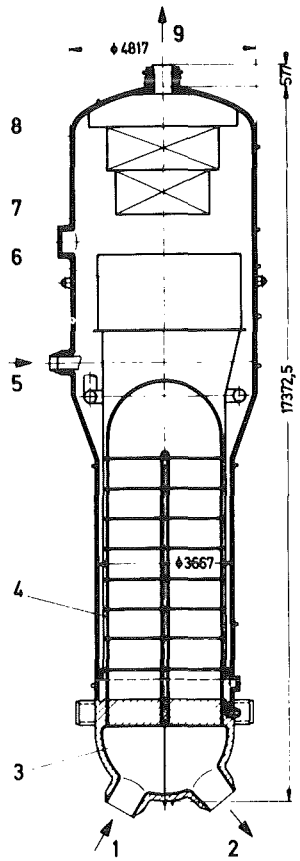

Fig. 27

Schnitt durch einen Dampferzeuger

1 Primäreintritt
2 Primäraustritt
3 Sammler (Primärkammer)
4 Rohrbündel
5 Speisewassereintritt
6 Grobabscheider
7 Dampfraum
8 Feinabscheider
9 Dampfaustritt

The corrosion conditions by the primary and secondary coolant are quite different. The primary water conditions are quite clear and defined (by KWU) as follows:

		Dauerbetrieb	zulässige Abweichungen bei An- und Abfahrbetrieb und in Störfällen
Lithium-7-Hydroxid	ppm ^{7}Li	1–2	0–7
Wasserstoff	ppm H_2	2–4	1–5
Sauerstoff	ppm O_2	<0,005	<0,1
Chlorid	ppm Cl	<0,2	<1
Borsäure	ppm B	0–2500	–
pH-Wert bei 25 °C		5–10,5	–
Leitfähigkeit bei 25 °C	$\mu S \times cm^{-1}$	<30	–

(Dauerbetrieb = long time operation

zulässige ... = admissible deviations during go and stop transients and in disturbances)

LiOH is added for p_H-control and also formed as a secondary product of the $^{10}_{5}B(n,\alpha)^{7}_{3}Li$ transmutation reaction. A slightly elevated pH of about 9 is desired to suppress corrosion effects.

Boric acid is used for "shim control"

(Initial surplus reactivity is necessary to compensate for "neutron poisons" - ^{135}Xe, $^{149,151}Sm$, ^{155}Eu, ^{157}Gd - formed by transmutations within the oxide fuel; by by-pass-filtering, and burn-out of ^{10}B, the total

boron content is held at the necessary level). In a BWR the "shim control" is carried out heterogeneously by control rod positioning.

H_2-additions serve to inhibit the radiolytic formation of O_2 which - like Cl'-ions - enhances corrosive attacks.

A high purity of the primary coolant is secured by continuous by-pass cleaning in ion-exchangers (50-60°C).

Data on the general corrosion of certain materials under primary conditions is collected in the table:

	Zeit [Tage]	Gesamtmetallverlust [µm/Jahr]	Metallabgabe an das System [mg/dm² × Monat]
Alloy 600	120-300	1,4	1,5
Alloy 800	120-300	0,6	0,5
Alloy 801	150-210	0,5	0,5
Stahl			
W.Nr. 1.4301	180-240	0,3	1,0
W.Nr. 1.4550	120	1,1	1,7
W.Nr. 1.4541	120	1,7	1,8

Thus the corrosion rate is about 1 µm/a. This low value is negligible with respect to design life of the equipment. However, the release of corrosion products is of more importance considering radiation protection, maintenance and repair.

The conditions on the outer (feed water) side of the steam generator tubes are more complex. Although the predominant part of the outer tube surfaces is covered by water of specified purity (Table), there may be in certain location - dependent on thermohydraulic factors and impurity levels due to, for instance, condenser leaks - depositions as well as chemical reactions which lead to specific corrosion effects.

		Dauerbetrieb	zulässige Abweichungen bei An- und Abfahrbetrieb und bei Störfällen	Speisewasser
pH-Wert bei 25 °C		8,8–9,5	7–10,7	8,8–9,5
Leitfähigkeit bei 25 °C	µS×cm^{-1}	<50	-	<2
Sauerstoff	ppm O_2	-	-	<0,005
Hydrazin	ppm N_2H_4	-	-	0,010–0,020
Phosphat	ppm PO_4	2–6	<50	-
Molverhältnis	Na/PO_4	2,0–2,6	<3,0	-
Chlorid	ppm Cl	<1	<20	-
Kieselsäure	ppm SiO_2	<4	-	-
Eisen	ppm Fe	-	-	<0,02
Kupfer	ppm Cu	-	-	<0,003

Table: Dampferzeugerwasser

Thus steam blanketing or crevices lead to depositions and concentration of hydroxyl ions (pH > 11) which may cause (caustic) stress corrosion. To minimize this danger chemical additions are made to the feed water (Speise-wasser):

- A mixture of secondary and tertiary Na-phosphat (Na^+/PO_4^{-3} = 2-2.6),
- Hydrazine (mild alcaline action, also oxygen remover), so-called "zero-solids procedure".

To understand the material choice for the SG-tubes a more detailed consideration of the possible corrosion mechanisms has to be made:

General (weight-loss) corrosion
Stress-corrosion (SC):

a) Transcrystalline (TSC)
b) Intercrystalline (ISC)

Intercrystalline corrosion (IC)
Pitting corrosion (Lochfraß) PC)
Denting corrosion

Susceptibility to both types of SC is covered by the so-called Coriou-diagram of Fig. 28 .

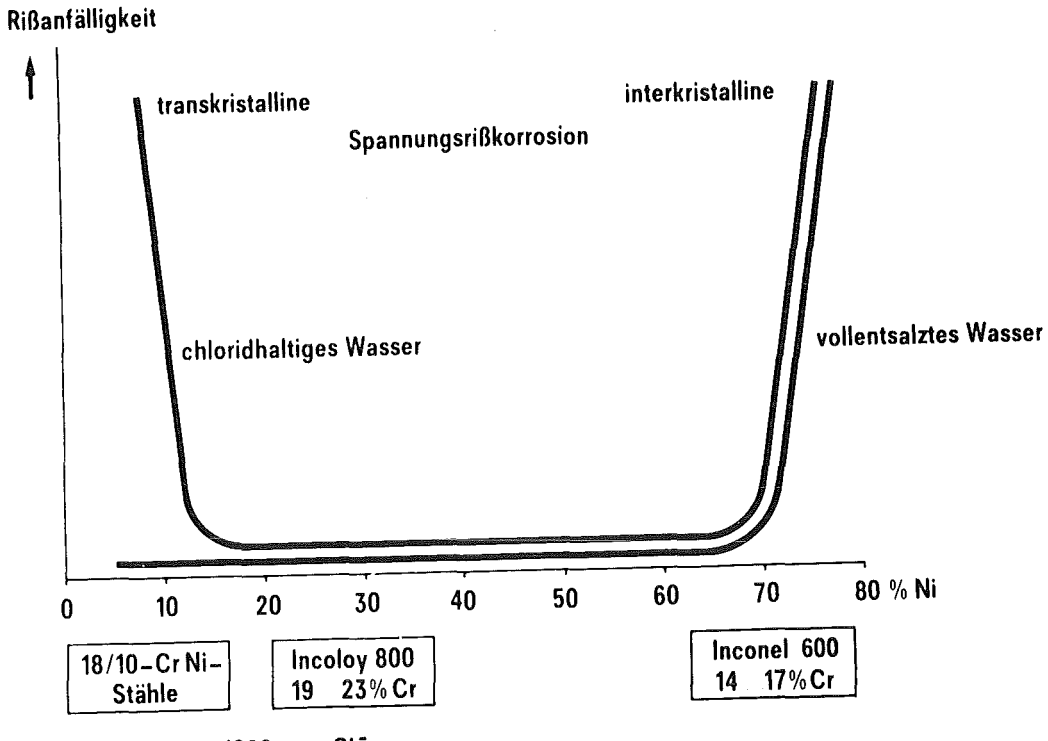

Fig. 28 : Einfluß des Ni-Gehaltes auf die SpRK-Anfälligkeit austenitischer Legierungen

18/10-type CrNi-steels (even stabilized or low C-versions which are immune against ISC) may show catastrophic TSC if chloride-ions and or oxygen are present. This is the reason why those steels were only used in the first reactor generation as HX-tubes. To solve this corrosion problem two philosophies have been followed. In the US and in France, for instance, the high-Ni Inconel 600 (2.4816,NiCr15Fe8) has been used because it is not prone to chloride-ion induced TSC. With this material, however, there is the danger of ISC (high σ, OH, traces of Pb). However, great improvements are possible by minimization of fabrication-induced residual stresses and by special heat treatment leading to a particular type of carbide precipitation at the grain boundaries. - On the other hand, in West Germany (KWU) the lower Ni-alloy Incoloy 800 (1.4876, X10NiCrAlTi 3220), in an optimized version, has been preferred. This alloy offers a good compromise as regards non-susceptibility to both TSC and ISC. The resistance against IC and ISC was improved by an increased Ti/C-ratio (Fig. 29), that against TSC and PC by elevated Cr- and Ni-contents. Moreover the chloride content in the secondary water can be strictly monitored, controlled and kept below 1 ppm. (For accident conditions, KWU gives the limitation of $\leq$ 1000 h operation within 2 years with $Cl' < 20$ ppm).-

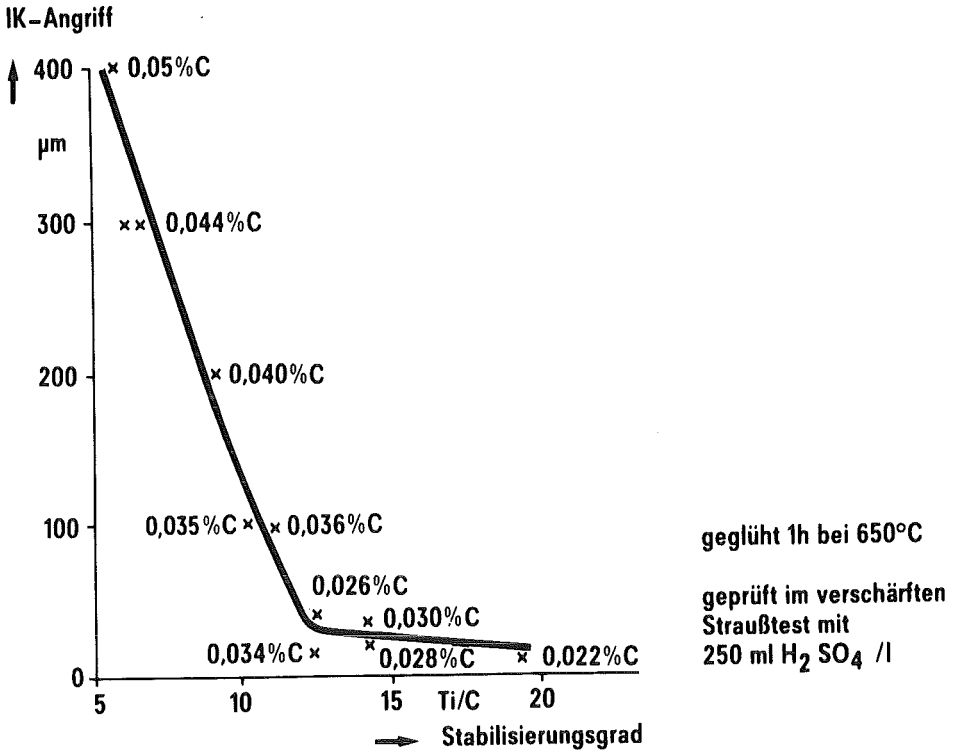

Fig. 29 Abhängigkeit des IK-Angriffs bei Incoloy 800 vom Stabilisierungsgrad.

"Denting" is a very special failure which occurred in US-american nuclear reactors. It describes the indentation of the SG-tubes in the region of the distance plates by a fast growing corrosion layer within the slit between the two parts mentioned (Fig. 30). The denting effect could be reproduced in the KWU-laboratory. It could be shown that it only occurs if rigid tube distance plates are made of un- or low-alloyed steel and if the pH is strongly lowered by a hydrolytic reaction within the narrow slit.

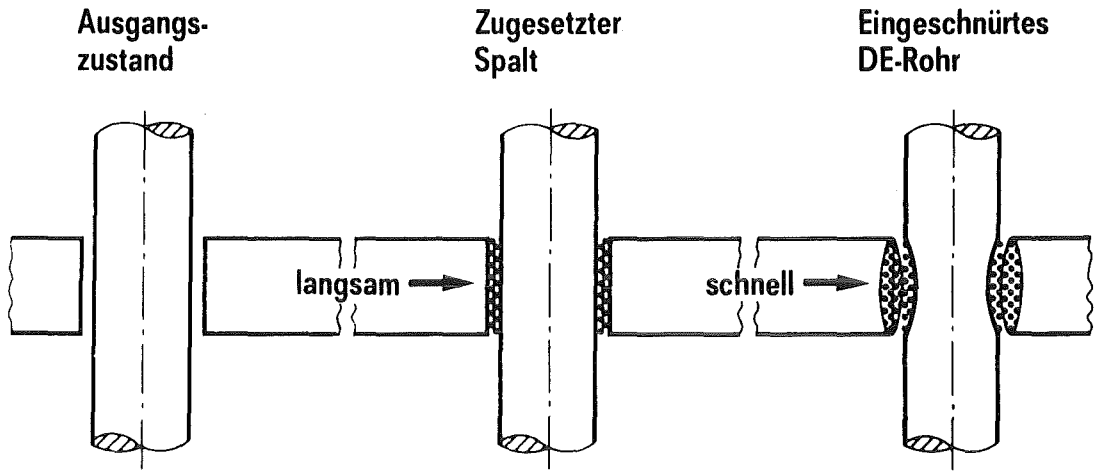

Fig. 30 Entstehen von "Denting" an DE-Rohren

Denting does not occur if the distance plates are made of highly alloyed stainless steel and/or Na-phosphate conditioning has been applied to the water.

4.3.5 Steels for the Secondary Circuit

The tubes for the Feedwater (Speisewasser)- und Steam-Circuit of about 400 and 600 mm diameter, respectively, have to serve under conditions like those in conventional power stations. The operational temperature is below the creep range. Therefore low-alloyed steels can be used.

Previously in Germany the steel WB 35 (1.8817, 17MnMoV 6 4) was used. After air quenching and tempering (luftvergütet) a bainitic-ferritic microstructure resulted.

More recently the steel WB 36 (1.6368, 15NiCuMoNb 5) has been used which after water quenching and tempering becomes fully bainitic.

The composition and mechanical properties of those steels are compiled in the table.

Bezeichnung nach DIN 17 006	WB 35	WB 36
Werkstoff-Nr. nach DIN 17 007	1.8817	1.6368
Technische Lieferbedingungen nach DIN, VdTÜV bzw. ASTM	VdTÜV W-Bl. 376	VdTÜV W-Bl. 377 und 262 4.67 Ergänzung
Chemische Zusammensetzung in %		
C	≤ 0,19	≤ 0,17
Si	0,20 . . . 0,50	0,25 . . . 0,50
Mn	1,40 . . . 1,70	0,80 . . . 1,20
P	0,035	0,035
S	0,035	0,035
Cr		
Mo	0,20 . . . 0,50	0,25 . . . 0,50
	V ≤ 0,19	Ni 1,00 . . . 1,30
		Cu 0,50 . . . 0,80
		Nb ca. 0,02
Mechanische Eigenschaften bei Raumtemperatur		
Wärmebehandlungszustand	vergütet	vergütet
Zugfestigkeit kg/mm²	60 . . . 75	62 . . . 77
Streckgrenze kg/mm² mind.	44	44
Bruchdehnung ($L_o = 5\ d_o$) % mind.	16	16
Mechanische Eigenschaften bei erhöhter Temperatur		
Streckgrenze in kg/mm² bei einer Temperatur in °C von		
200	38	39
250	37	38
300	36	37
350	35	36
400	32	34
450	–	–
500	–	–
550	–	–

According to the KWU materials concept of 1977 for low alloyed steels (Fig. 31)

it is possible that in future WB35 and WB36 will be replaced by the steels 20 MnMoNi 55 and 15MnNi 63, which we know from the discussion of the primary components and the inner shell, respectively.

Type		Steel*)
C	Aluminum Killed (Fine Grain)	St 37.3
C Mn		StE 26 to 36 (17 Mn 4 to 19 Mn 5)
C MnNi		15 MnNi 63
C MnNiMo		20 MnMoNi 55
C MnNiMoCr		22 NiMoCr 37 (Optimized)
Cast Steel		
C Mn		GS C 25
C MnNiMoCr		GS 18 NiMoCr 37

*) Impurity Specification Corresponding to Safety Class of the Component

Fig. 31

Low Alloy Steels for Plate, Forging, Pipe and Castings after General KWU Steel Concept

E 77 1054 e

Literature to 4.3

S.H. Bush, Structural Materials for Nuclear Power Plants, J. Testing and Evaluation 2, 1974, 435-462

U. Rösler, H. Cerjak, VDI-Berichte Nr. 302, 1977, 127-136

W. Debray, KWU-Erlangen, Lecture at Dechema, Frankfurt/M., 1979

W. Möller, Wärme 84, 1978, 99-101

W. Debray, Joint JEN-KfK-Seminar "Materials for Reactor Vessels and Components", Madrid 1980

D. Pachur, "Apparent Embrittlement Saturation and Radiation Mechanisms of Reactor Pressure Vessel Steels", Proc. ASTM Tenth Int. Symp. Rad. Mat. Savannah, USA June 3-5, 1980

J.R. Hawthorne et al., ASTM STP 683, 1979, 235-251

C. Leitz, KWU-Erlangen, Summary of IAEA-Specialist Meeting, Vienna, 1979

K.E. Stahlkopf, G.R. Odette, T.U. Marston, Radiation Damage Saturation in Reactor Pressure Vessel Steels: Data and Preliminary Model, J. Mechan. Eng., 1980, 265-272

N. Wieling, KWU-Seminar, Erlangen, 1978

S.H. Bush, J. Testing and Evaluation 2, 1974, 435-462

M.A. Cordovi, Inco-Conference Kyoto, Japan, 1972

S. Leistikow, in PHYSICS AND CONTEMPORARY NEEDS, Vol. 4 1980, Edited by Riazuddin, Book available from: Plenum Publishing Corp. 227 West 17th Street, New York, N.Y. 10011, pages 325-381

D. Smidt, Reaktortechnik, Verlag G. Braun Karlsruhe, 1976

D. Smidt, Reaktor-Sicherheitstechnik, Springer-Verlag 1979

Deutsche Risikostudie Kernkraftwerke, Verlag TÜV Rheinland, 1979

K. Kummerer, Werkstoffe der Kerntechnik, G. Braun-Verlag Karlsruhe, 1980

4.4 LMFBR-steels

4.4.1 General remarks

A comparison between 1000 MWe thermal and fast reactors is shown in the table (Olander, 1976).

Comparison of Typical 1000-Mw(e) Oxide Reactors

	LWR	LMFBR
Fissile species enrichment	3% ^{235}U in ^{238}U	15% ^{239}Pu in ^{238}U
σ_f, barns	550	1.8
Core-averaged neutron flux, n cm^{-2} sec^{-1}		
Thermal	3×10^{13}	1×10^{11}
Fast (>0.2 MeV)	5×10^{13}	8×10^{15}
Burnup, %	3	10
Fast fluence, n/cm^2	3×10^{21}	3×10^{23}
Irradiation time (at full power), years	2	1.5

It is to be noted that

- total flux $\phi_{t,F.R.} = 100 \cdot \phi_{t,Th.R.}$
  This large flux increase leads to a higher power production per unit volume in the fast reactor although the fission cross sections are much lower (see Chapter 4.21).
- Burnup in a fast reactor is higher for economic reasons. This, of course, leads to a higher neutron loading of the metallic materials (n/cm^2, E > 0.1 MeV):

	Thermal reactor	Fast reactor
Cladding	$5 \cdot 10^{21}$	$2 \cdot 10^{23}$
Pressure vessel/Tank	$1 \cdot 10^{19}$	$1 \cdot 10^{21}$

Of course, the temperatures also are higher in a fast reactor.

The neutron energy spectra for 2 thermal and 3 fast reactors are given in Fig. 1.
Fast reactors exhibit a single peak neutron distribution. Thermal reactors have two widely separated peaks (see BR2). In a thermal reactor the fluences for E > 0.1 MeV and E > 1.0 MeV are essentially the same, whereas in a fast reactor the E > 0.1 MeV fraction may be much larger than the E > 1.0 MeV value.

A survey of the principal design features of a LMFBR is given in Fig. 2. The main components are: Reactor tank, primary pumps, primary tubing, intermediate heat exchanger (which separates the primary and secondary sodium circuits), secondary pumps, secondary tubing, vapor generator; tertiary circuit with vapor turbines.

There are two different modes for the arrangement of the components, the

loop system (SNR 300, FFTF, Clinch River)
pool system (Superphénix, PFR)

In the loop system the components of the primary circuits are connected by tubing (SNR 300 : 200 m length) whereas in the pool system a single tank contains the whole primary circuit. For a discussion of the "pros and cons" of the two systems the reader is referred to |Smidt, 1979|.[1)]

---

1) D. Smidt, Reaktorsicherheitstechnik, Springer-Verlag, 1979.

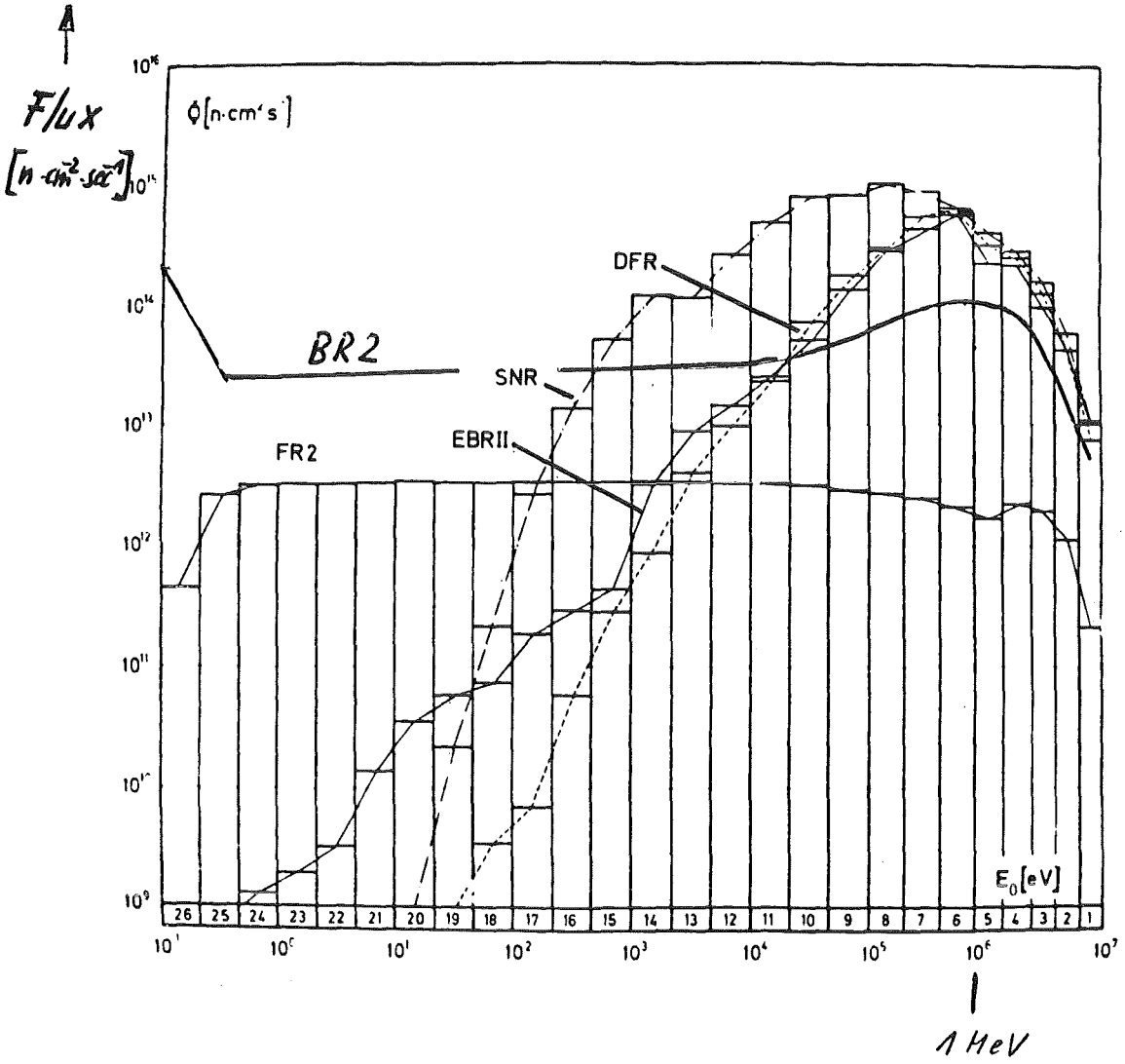

Fig. 1: Verschiedene Reaktorspektren in der 26-Gruppensatz-Darstellung

Kern-Material

- Hüllrohre 1.4970
- Abstandshaltegitter 1.4981
- BE.-Kasten 1.4981
  [oder Ferrite 12% Cr
  1.4914 , 1.4923]

$T = 400 - 700^{\circ}C$

$\phi_s \cdot t = 1{,}5 \cdot 10^{23}$ $n \cdot cm^{-2}$ (>0,1 MeV)

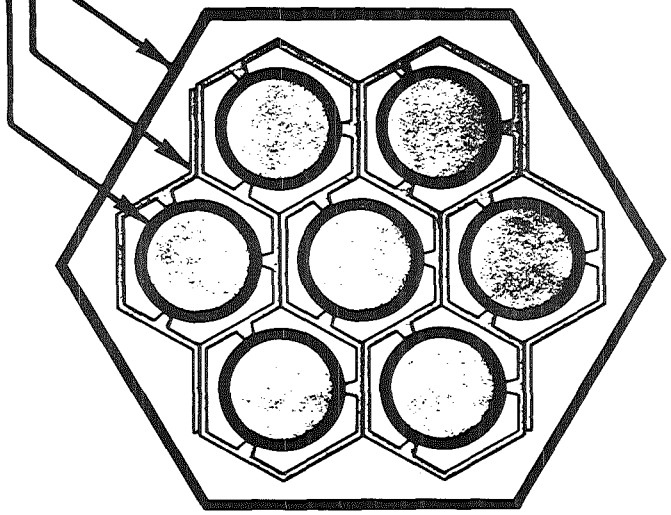

Strukturmaterial

- Na-Tank 1.4948 (Schild-Tank)
- Rohrleitungen 1.4948
- Zwischenwärmetauscher 1.4948
- Dampferzeuger 1.6770

$T = 400 - 600^{\circ}C$

$\phi_{tot} \cdot t = 5 \cdot 10^{20}$ $n \cdot cm^{-2}$

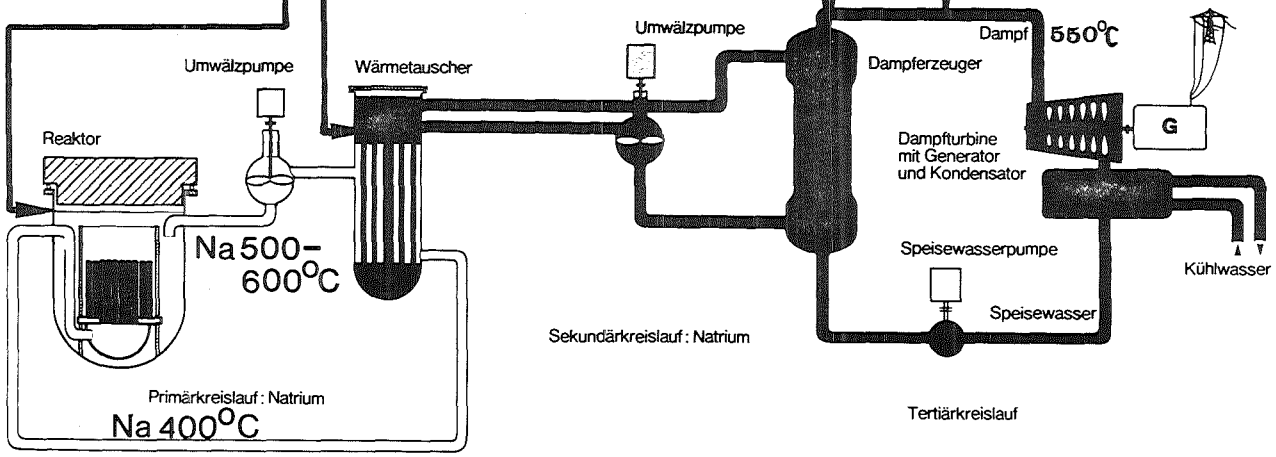

Fig. 2

Examples of loop- and pool-type reactors are given in Fig. 3 and 4:

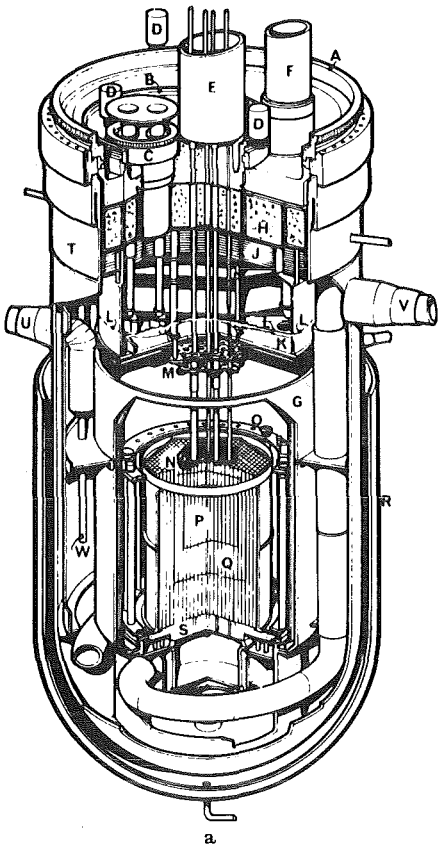

a

Fig. 3: SNR 300 (loop)

Reaktorbehälter mit Einbauten von Loop-Anlagen

a SNR-300

A Großer Drehdeckel
B Mittlerer Drehdeckel
C Kleiner Drehdeckel
D Drehdeckelantriebe
E Regelstabantriebe
F BE-Transferkanal
G Schildtank
H Basaltkästen
J Thermischer Schild
K Tauchplatte
L Na-Spiegel
M Haltestruktur der Instrumentierungsplatte
N Instrumentierungsplatte
O Ringlager
P Kern
Q Brutmantel
R Sicherheitstank (Doppeltank)
S Gitter-Trageplatte
T Reaktortank
U Na-Austritt
V Na-Eintritt
W Notkühler

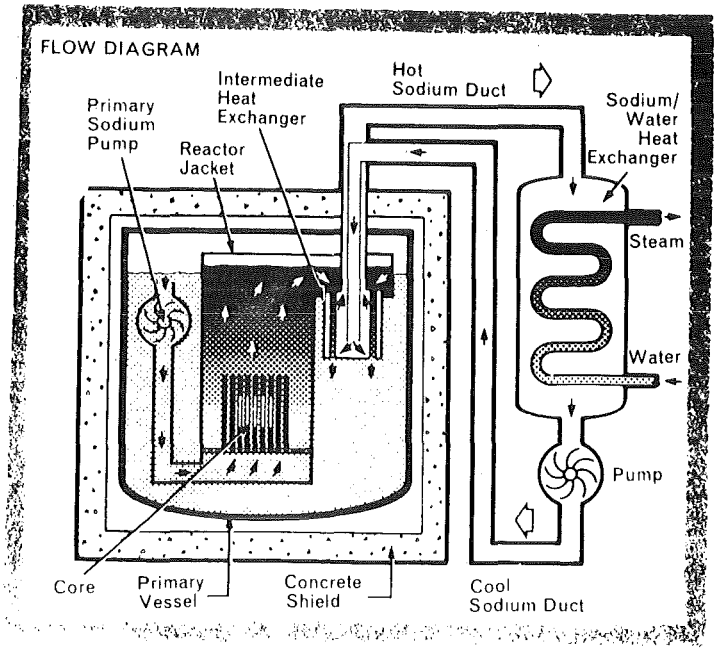

Fig. 4: PFR (pool)

In a fast breeder reactor, due to the higher operating temperatures and the high fast neutron flux, one has to deal with phenomena not occurring with LWR steels. The temperature levels, up to 680°C (0.57 T_m) for the cladding tubes and up to 550°C (0.50 T_m) for the sodium tank, are within the creep range. This makes necessary for many core positions the application of so-called inelastic analyses, considering time dependent processes. Those analyses are very expensive and one tries to avoid them wherever possible by proper material selection.

As to the irradiation effects and their temperature dependence, reference is made to p. 68.
At and above the temperature where volume diffusion starts (> 0.5 T_m) transmutation He (produced by thermal and/or fast neutrons, see chapter 4.21) may collect in grain boundaries. These are weakened by the bubbles or by the He-enhanced creep cavity formation, leading to the phenomenon of <u>He-embrittlement</u>

At temperatures where vacancies get mobile (0.3 T_m) <u>void formation and swelling</u> sets in under the influence of a fast neutron flux. The void formation fades away at temperatures above 0.55 T_m because then the point defects are removed by recombination or migration to sinks so quickly that a high supersaturation above the thermal vacancy concentration cannot be maintained.

Further conditions necessary for void swelling:

- Sinks must have a "bias" for interstitials so that the vacancy supersaturation can occur. This bias is

caused by the larger strain field around an interstitial; it causes an attraction of interstitials for dislocations)

- Trace quantities of insoluble gases (transmutation He) must be present to stabilize the embryo voids.)

The T-dependence of void swelling is shown in Fig. 5 .

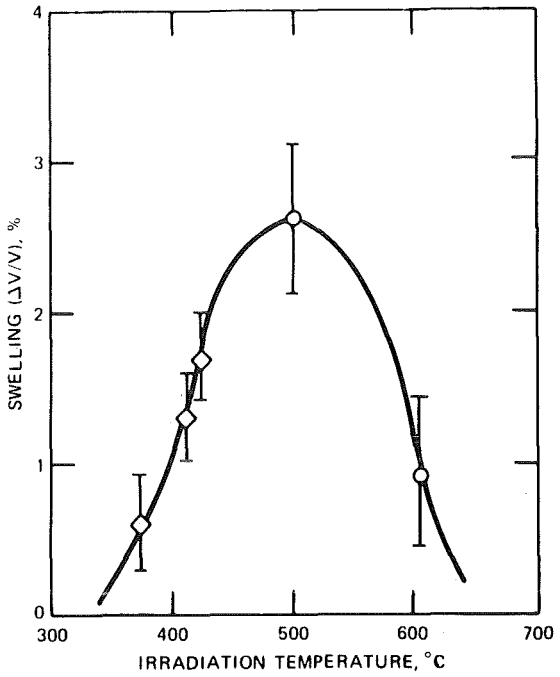

Fig. 5 Effect of irradiation temperature on swelling of type 304 stainless steel at a fluence of 5×10^{22} neutrons/cm^2. ○, transmission electron microscopy. ◇, immersion density. [After S. D. Harkness and Che-Yu Li, *Met. Trans.*, 2: 1457 (1971).]

At still lower temperatures, where only interstitials are mobile, the fast flux induced effect of irradiation creep is observed. As can be seen from the deformation maps of Fig. 6 and 7, taken from Gittus (1975), the irradiation creep regime takes much of the place of the elastic regime in non-irradiated materials.

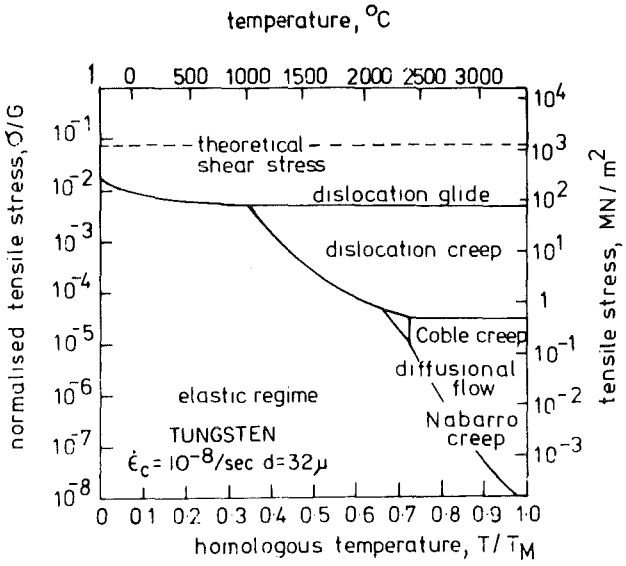

FIG. 6 Deformation map for tungsten. (After Ashby [1]. Courtesy *Acta Met.*)

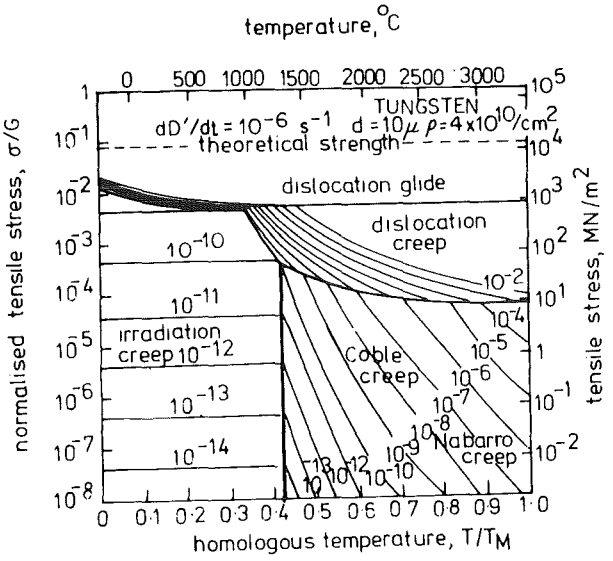

FIG. 7 Deformation mechanism map for tungsten of grain size 32 μ undergoing bombardment with energetic particles which displace each atom from its lattice site on one occasion in every million seconds.

For this comparison tungsten had to be chosen. A map for in-reactor creep of an austenitic steel is shown in Fig. 8 . On this map the region of T and stresses relevant for the operation of a fast breeder reactor is specially marked. One sees that 3 creep mechanisms are of importance here: irradiation creep, recovery-glide dislocation creep, and Coble creep.

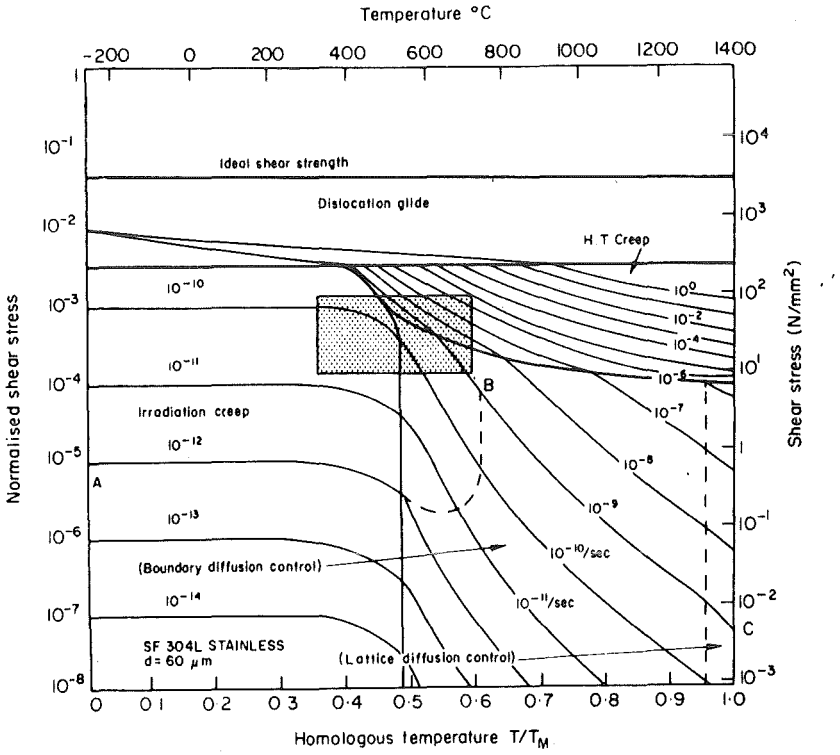

Fig. 8 Map for in-reactor creep of SF304 stainless steel with a grain size of 60μm. (The low temperature data correspond to yield. The diagram exactly describes the data of Beckitt and Gladman.) Solution strengthening has raised the yield stress and lowered the rate of power law creep of the stainless steel.

The irradiation creep rate increases in a fluence and temperature range where heavy void formation (which needs a incubation dose) sets in. Gittus suggested the equation

$$\dot{\varepsilon} = k_1 \dot{\phi} \sigma + k_2 \dot{S} \sigma$$

where k_1, k_2 are constants, $\dot{\phi}$ = displacement rate, $\dot{S}$ = swelling rate, σ = applied stress.

4.4.2 Fuel element (overview)

Fig. 1 shows the cross section of a fast reactor exhibiting around 200 fuel and 100 radial breeder elements (SNR 300, Mark Ia). The elements have hexagonal cross section with a "width over flats" of about 110 mm and contain 160 fuel pins each. The fuel pins have a diameter of 6 mm and a wall thickness of around 0,4 mm. The individual fuel element is envelopped by a wrapper which gives strength to the element and serves furthermore as duct for the sodium coolant.

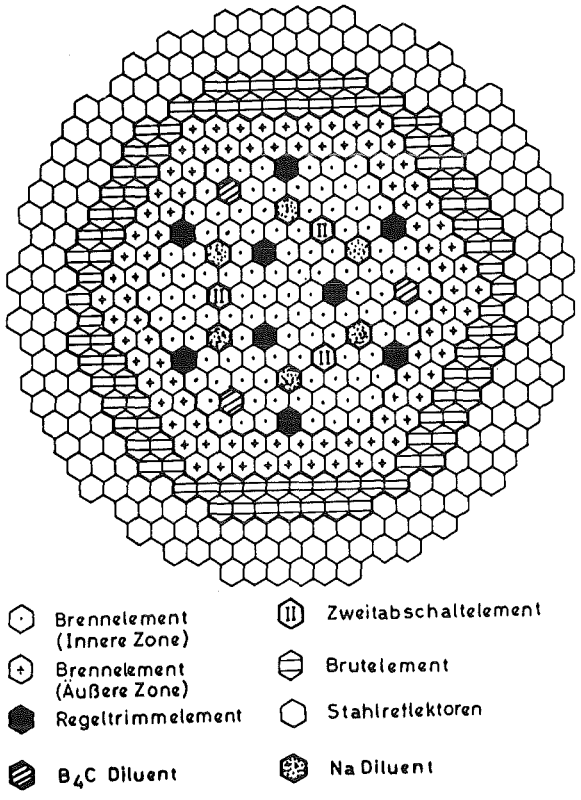

Fig. 1

Further details of a fuel element for a 300 MWe reactor (honeycomb-grid, double base plate) may be seen from Fig. 2 and 3 .

Fig. 2

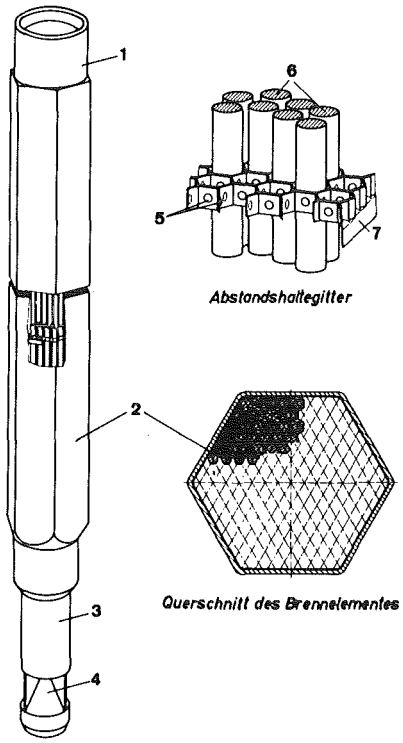

Brennelement eines natriumgekühlten schnellen Reaktors von 300 MWe [36]
1 Kopfstück
2 Brennelementkasten (Mantelrohr)
3 Zylindrischer Fluß
4 Kühlmitteleintritt
5 Noppen
6 Brennstäbe
7 Lasche zur Befestigung am Mantelrohr

Fig. 3

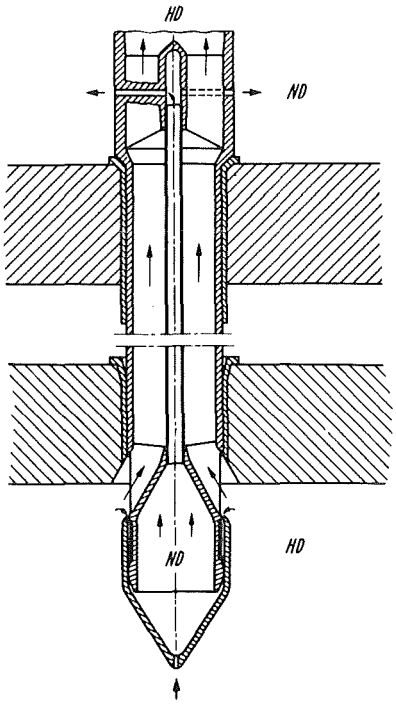

Hydraulische Niederhaltung
HD: Hochdruck
ND: Niederdruck

At mid-core, spacer pads on the wrapper hexagons are used to control thermal and irradiation induced bowing of the fuel elements.

Fig. 4 gives the dimensions (in mm) as well as the partition of fuel pin length (into fuel, breeder, gas plenum zones) of the main fast reactors.

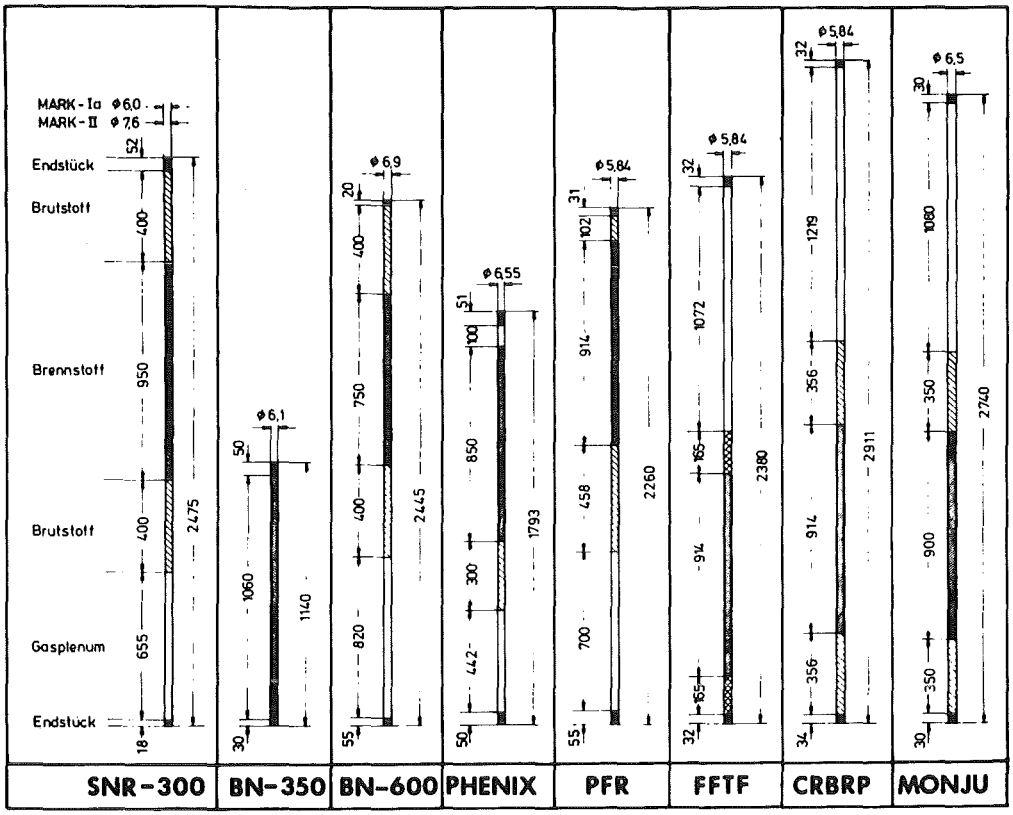

Fig. 4 Vergleich der Brennstababmessungen
(Zahlen in mm, einige Angaben näherungsweise)

Fig. 5 shows the typical axial temperature distribution along a fuel element in a fast reactor.

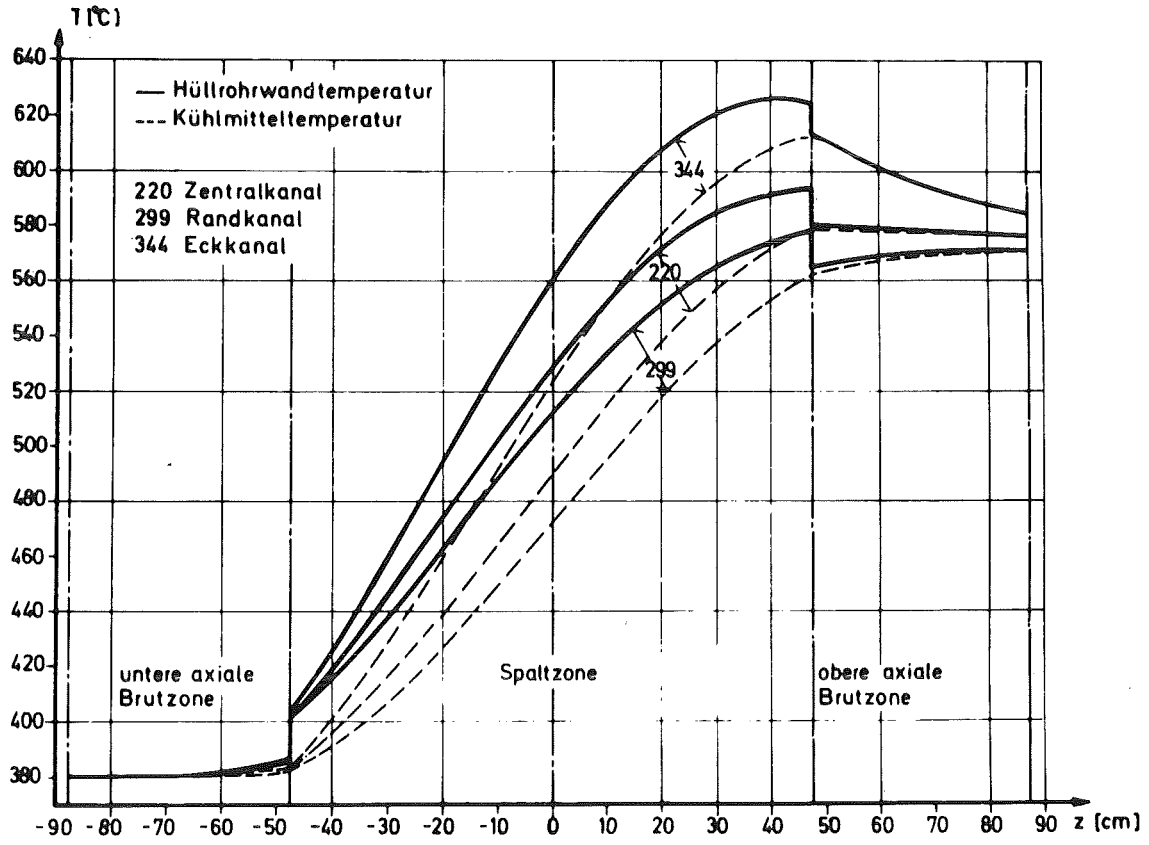

Fig. 5 Axialer Temperaturverlauf im MARK-I-Brennelement Nr. 616

In contrast to this, the neutron flux distribution shows a maximum at the core center ("0 cm").

4.4.3 Cladding and core structural materials

a) General remarks

A good cladding material must exhibit a combination of excellent (or at least fair) properties:

- Low neutron absorption
- Sufficient creep - and creep rupture strength up to 700 °C
- Sufficient tensile strength at medium temperatures (350 - 550 °C)
- Restricted embrittlement by neutron irradiation at temperatures between 200 and 700 °C
- Favourable swelling behaviour:
  Low swelling rate
  Low temperature dependence of swelling
- Restricted susceptibility to irradiation creep
- Corrosion resistance to liquid sodium
- Compatibility with (oxide) fuel as well as fission products
- Economical fabrication procedure

Most of these statements are also valid for wrapper (or duct) materials. Their peak temperature is, however, somewhat lower, say 600 °C.

For the prototype reactors (Phenix, PFR, SNR 300, Monjou, BN 350, BN 600, FFTF) austenitic steels have been worldwide chosen as cladding (and wrapper) materials.

Table I gives an overview on the reference materials for some of these prototype reactors and on developmental (advanced) materials as studied in 4 countries. In Table II nominal compositions of pertinent alloys are listed.

In the following some general comments on these alloys are made.

Table I

Overview on
reference (R) and developmental (D)
cladding and wrapper alloys

Country	Cladding R	Cladding D	Wrapper R	Wrapper D
France	316 316 Ti	40-60 % Ni	316 316 Ti	17 % Cr 12 % Cr 40-60 % Ni
Debene	X10 NiCrMo TiB 15 15 (1.4970)	.Disp.hardened ferritic .10Cr25Ni base	X8 CrNiMo Nb 16 16 (1.4981)	.1.4970 .X15 CrMoV Nb 11 2 (1.4914)
USA	316	HT 9 AISI 310 RA 330 A-286 M-813 Nimonic PE 16 Inconel 706 Inconel 718 and 8 developmental alloys	316	same as under "Cladding"
England	M 316	316 Ti, Si 17Cr12Ni 1.5Mo (FV 548)	Nimonic PE 16 (44Ni,17Cr)	321 FV 548 1.4970 10% Cr(FV448) 316 Ti,Si

Table II

Nominal compositions of
Austenitic alloys (Stainless steels and Ni-Base Alloys)

Designation	C	Cr	Ni	Mo	V	Mn	Si	Al	Ti	Nb	P	S	B
AISI 304	max. .08	19	10			max. 2	max. 1						
AISI 310	max. .25	25	20			max. 2	max. 1.5						
AISI 316	max. .08	17	12	2.5		max. 2	max. 1						
AISI 321	max. .08	18	10			max. 2	max. 1		min. 5 x C				
RA 330	.05	19	36			max. 2	1.1						
A 286	max. .08	15	26	1.25	0.3	1.35	0.50	0.25	2.0				.0060
Inconel 706	max. .06	16	42			0.35	max. 0.35	max. 0.40	1.8	3	max. 0.02	max. 0.015	max. 0.006
Inconel 718	max. .08	19	53	3			max. 0.35	0.5	1	5	max. 0.015	max. 0.015	max. 0.006
Nimonic PE 16	max. .10	16.5	44	3		max. 0.2	max. 0.3	1.3	1.3				
M-813													
1.4970 (12R72 HV [1])	.10	15	15	1.2		1.8	0.35		0.45		max. .030	max. .015	.0045
1.4981	.10	16.5	16.5	1.8		max. 1.5	0.45			max. 1.2			

1) Sandwik Steel Works designation
HV = High-vacuum remelting in arc furnace (after high frequency melting)

304 has a composition range including the classical 18 Cr 8Ni data. Due to a "borderline" Ni-content, 304 may form some martensite by cooling to subzero temperatures or by deformation at normal temperature ($M_d > M_s$). 316, due to its higher Ni and Mo contents, does not show this instability, which may be detrimental to the corrosion resistance. Due to its Mo content, 316 also has a better creep strength.

As can be seen, at 18 % Cr a minimum Ni-content is required to promote an austenitic structure at room temperature. Increasing the Cr-content therefore requires a higher Ni-content (AISI 310, and 1.4970, respectively).

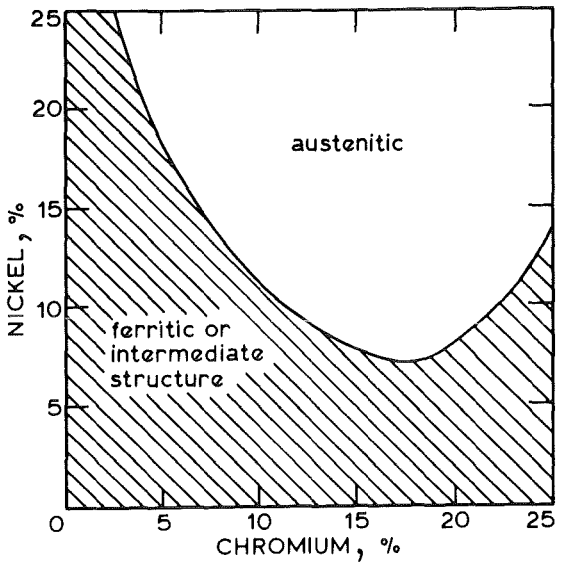

It is quite interesting to compare the stacking fault energy of the steels 316 and 1.4970. They are below 50 and 67 mJ/m^2, respectively.

The higher stacking fault energy of 1.4970 induces

- a higher tendency to form dislocation - substructure cells
- a lower twinning frequency (lower work-hardening rate)
- a higher tendency to recovery (and a lower tendency to recrystallisation).

Of course, the Ti-content of 1.4970 also adds to its high recrystallisation temperature.

A 286 belongs to the age-hardenable (γ' - NiAlTi) steels. A typical aging temperature is 750^{o}C. This steel forms a link to the γ' - hardened Ni - base alloys Inconel and Nimonic.

Up to now, with the "reference materials" ready for service, irradiation effects on the cladding and core structural materials (and not the fission product build-up in the fuel) limit the operational life time of fuel elements. Limiting data are, for instance, the volume swelling (Δ V/V) which must remain below 10 % and the thermal creep strain below 0.2 %. Nevertheless, the material requirements for the prototype fast reactors (Phenix, PFR, BN 300, SNR 300, Monju, FFTF) can be fulfilled by the reference materials (Phenix: 10 000 fuel pins have surpassed 65 dpa - NRT). With a preview to the next reactor generation, the commercial reactors, a parametric study (connecting thermohydraulic, mechanical and neutron physical design) has shown that strategical data,

like breeding rate and doubling time, can be much improved by using advanced alloys with better swelling and in pile creep properties (Heinecke, Dietz, Proc. Int. Conf. on Irradiation Behaviour of Metallic Materials for Fast Reactor Core Components, Ajaccio, France, 1979, Supplement, p.21-35).

For the first fast cores the favorite cladding steel was SS 316 (0.08 C, 17 Cr, 12 Ni, 2.5 Mo). This is still considered a good choice but there appears to be a growing tendency nowadays to turn to a stabilized version (316 Ti). For the Debene (Germany - Belgium - Netherlands) reactor SNR 300 the Ti-stabilized austenitic structure steel 1.4970 (X 10 NiCrMoTi B 15 15) has been specified in 1974.

b) Swelling Behaviour

Fig. 1 shows a comparison of the swelling behaviour of the two reference steels

cold worked SS 316, and

cold worked and tempered 1.4970.

Fig. 1

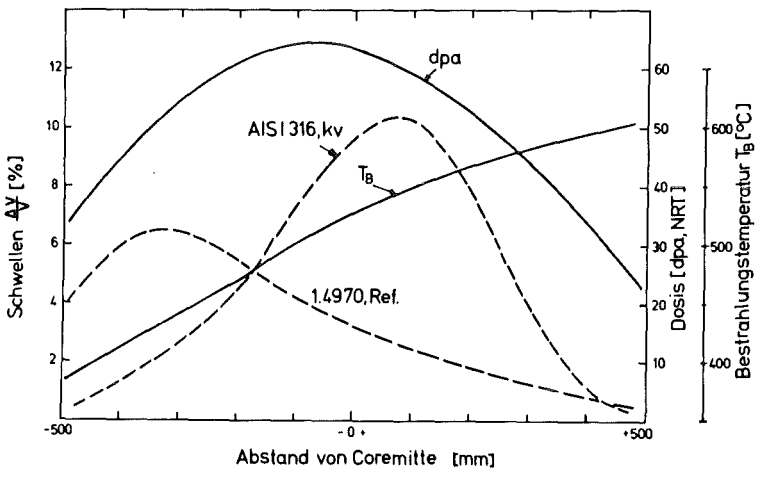

The maximum of swelling of 1.4970 is somewhat lower and occurs at a lower temperature as that of SS 316. The behaviour of 1.4970 is favourable since the temperature of the maximum is situated below the core centre where maximum flux occurs.

TEM allows an analysis of the swelling maximum. It can be seen that, besides the formation of dislocation loops and network, the average void radius increases and the void concentration decreases, with increasing temperature. (Fig. 2)

Fig. 2
Dose and temperature dependent microstructure of 1.4970

(KfK-IMF data, K.Ehrlich et al., 1981)

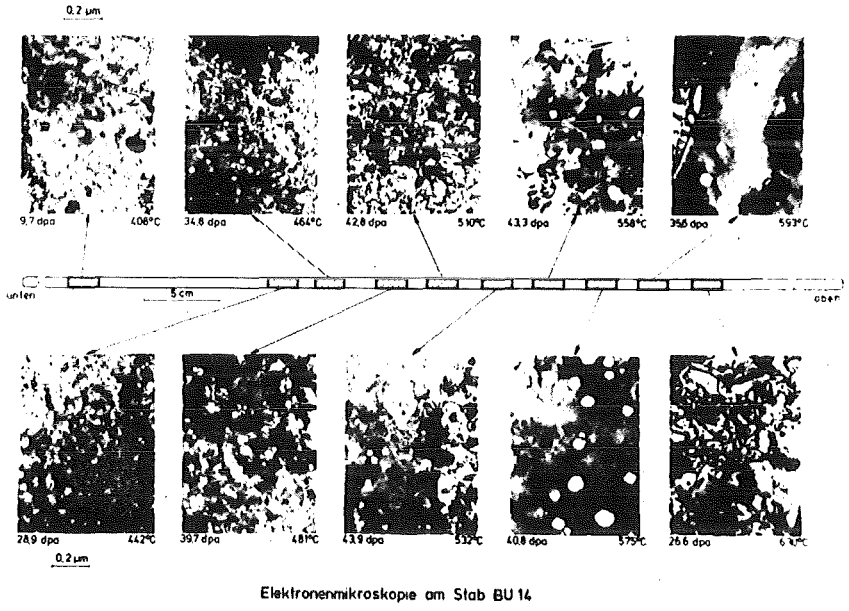

It is well known that swelling is low in a cold-worked steel, due to the sink function of dislocations which lowers the supersaturation of point defects.

This effect is shown in Fig. 3. The fluence dependence of swelling may be described by an incubation period followed by a linear increase of swelling with fluence. The "incubation fluence" increases with increasing cold work. It is not yet clear, however, how the extent of cold work influences the steady-state swelling rate.

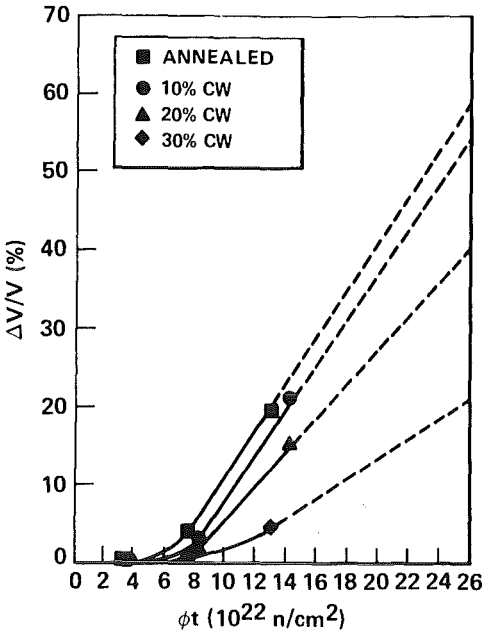

Swelling of Type-316 Stainless Steel at the peak swelling temperature, ~600°C, as a function of cold work level and fluence.

Fig. 3

(after Appleby et al., Scottsdale Conf., 1977)

Fig. 4

(after Brager et al., Scottsdale Conf., 1977)

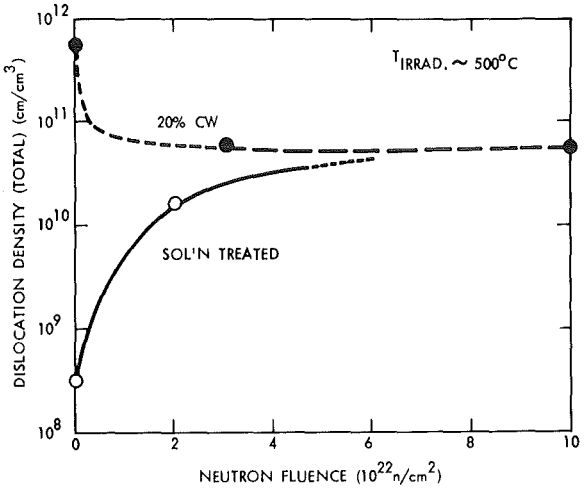

Total dislocation density in neutron irradiated 316 stainless steel tubing as a function of neutron fluence. The saturation density at high neutron fluence is independent of initial material condition.

Since the effect of cold working on the dislocation density fades away (Fig. 4), it may well be that the slope of the linear increase becomes independent of cold work at higher fluences.

Only recently an influence of stress on the void-swelling of austenitic could be clearly demonstrated. This σ - induced swelling portion depends linearly on stress but is independent of the overall (stress-free) swelling. Microstructurally the stress effect is observable as a change in the void size distribution (K. Ehrlich and co-workers, 1980).

Among the reference materials, Nimonic PE 16 presumably exhibits the lowest peak swelling and a relatively weak dependence of swelling on temperature. Its high Ni content, however, means a significant penalty in breeding performance.

What will be expected (US extrapolation) for the high-fluence swelling behaviour of advanced alloys may be seen from Fig. 5 .

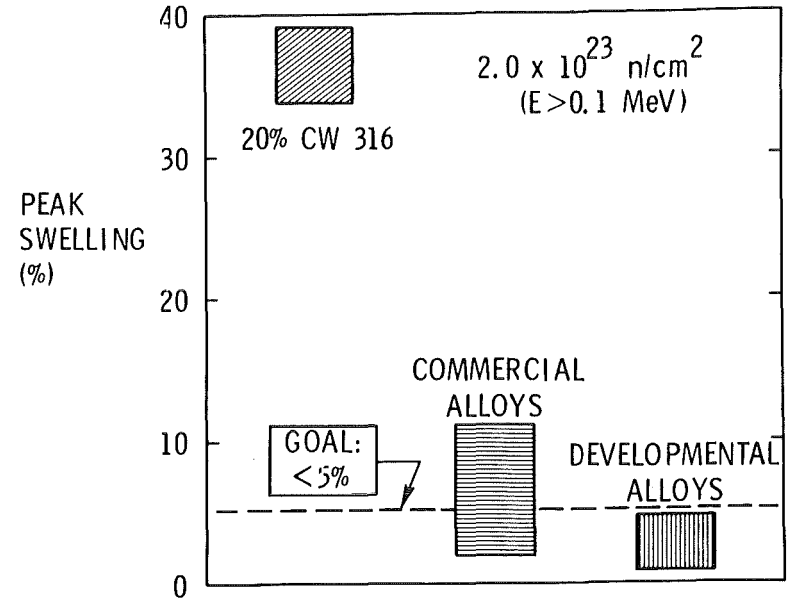

Fig. 5

The metallurgical background for this extrapolation has been discussed, for instance, by W.G. Johnston et al. (Radiation Damage in Metals, ASM, 1976, and Scottsdale Conf., 1977). Structural modifications (small grain sizes, high dislocation densities, optimum size precipitates) do not exhibit a high stability in an irradiation environment at elevated temperatures and therefore are not considered the most important method for controlling the swelling of commercial reactor alloys.

Help comes from the observation that swelling depends heavily on the base composition. Thus the swelling of simple ternary Fe-Cr-Ni alloys varies by 3 orders of magnitude over the austenitic range. The most swelling resistant simple alloys are those with low Cr and about 50 wt-% Ni.

The behaviour of commercial Fe-Cr-Ni-steels and of Ni-base alloys may be seen from Fig. 6 One sees that the austenitic steels (like SS 304, 316) are not situated in a favourable region.

The slightly better behaviour of 12 R72 HV (1.4970) may be due to its somewhat larger distance from the γ phase boundary.

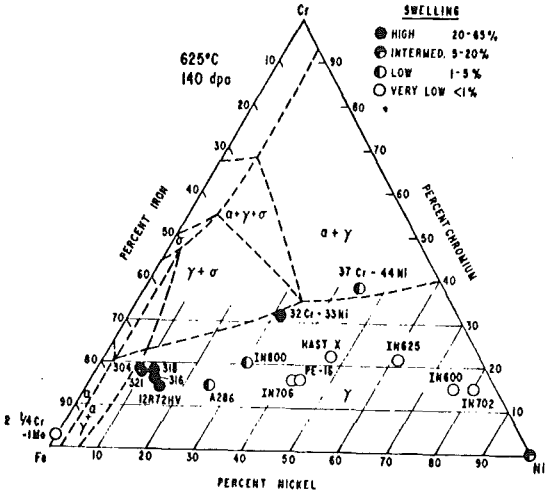

Fig. 6 Relative swellings of ion bombarded commercial alloys.

Pure ternary alloys swell appreciably more than the commercial alloys with a corresponding Cr and Ni content which implies that minor additions in commercial alloys may inhibit swelling.

A full explanation of the role of major composition and of minor additions cannot yet be given. The former has been correlated to the stability of the austenitic. A possible parameter is the "electron vacancy number" N_V (electron vacancies per atom), which has been useful in defining the stability of Ni-base super alloys against σ - phase formation. Many of the very high swelling steels, it is true, fell in the $(\gamma + \sigma)$ phase field, however, particularly at higher Ni concentrations, N_V is not a good measure of swelling resistance.

As to the effect of minor additions, one can think of impurities impeding dislocation climb thereby limiting the role of dislocations in biasing the defect populations. Or the mobility of point defects is reduced by impurity interactions, with the result of an increased recombination rate ($v + i = 0$) and, therefore, reduced loop and void formation.

The development of swelling resistant alloys is at full speed at many places. What has been reached end of 1980 by means of simulation experiments (He preimplantation; 70 dpa - Ni^{6+} - 46 MeV) at Karlsruhe may be judged from a graph taken from the IMF annual report 1980.

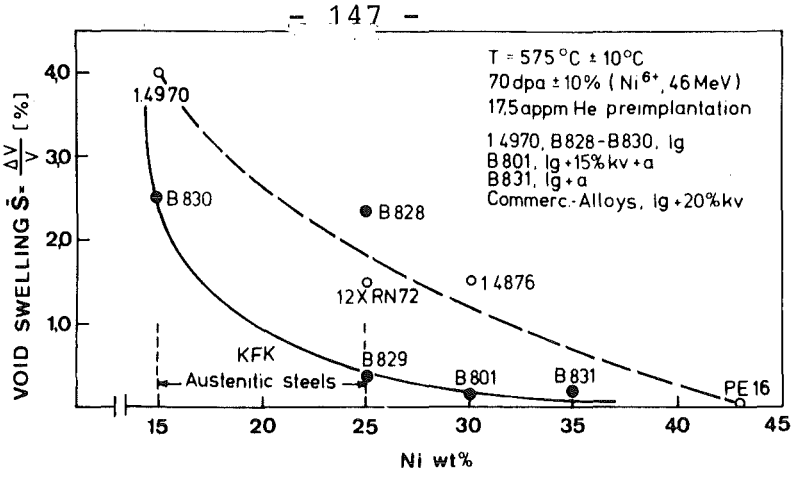

Schwellen als Funktion des Ni-Gehaltes für kommerzielle Austenite und Entwicklungslegierungen (B 800-Serie)

Reference is also made here to the good swelling resistance of (tempered) martensite 12 % Cr steels, which will be covered in a special lecture.

c) In-pile creep

Permanent deformation (at temperatures well below the thermal creep range) also occurs by the in-pile creep mechanism under fast neutron irradiation. A certain amount of this kind of deformation is welcome in that it helps to avoid stress concentrations. A too high in-pile creep rate must, however, be avoided because it would cause excessive "wrapper bulging" at the bottom of the fuel elements (high sodium pump pressure).

In-pile creep rates usually increase linearly with stress (Fig. 7).

Gilbert, Bates
(1977)

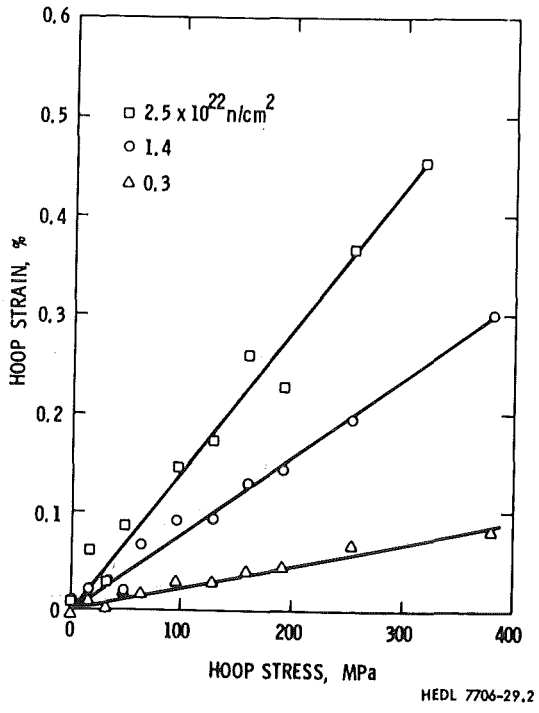

Fig. 7

Stress dependence of irradiation creep as determined from pressurized tubes of 20% cold worked Type 316 stainless steel at 475°C

Fig. 8 shows the dependency of IP-creep on the fluence and on the material state of SS 316. (Ordinate = Diameter increase minus $\frac{1}{3}$ of Volume Swelling gives the IP-Creep Deformation). As one sees, the creep rate (slope) increases with increasing fluence. The cold-worked state appears to have a somewhat higher creep deformation than the solution annealed one.

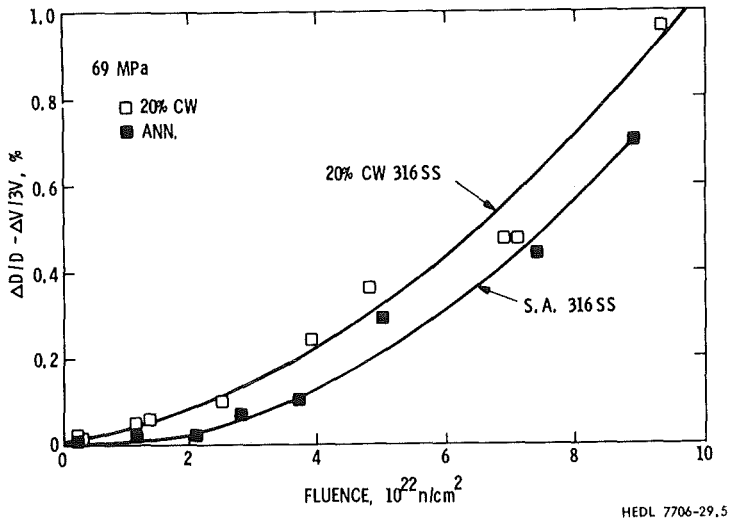

Irradiation creep in cold worked and solution annealed Type 316 stainless steel at 475°C.

Fig. 8

(Straalsund, Scottsdale Conf., 1977)

In-pile creep is only weakly temperature dependent and this dependence is not easily discernible at lower fluence levels (Fig. 9).

(there may be a correlation with the equally weak temperature dependence of irradiation induced loop - and dislocation line densities; SIPA model)

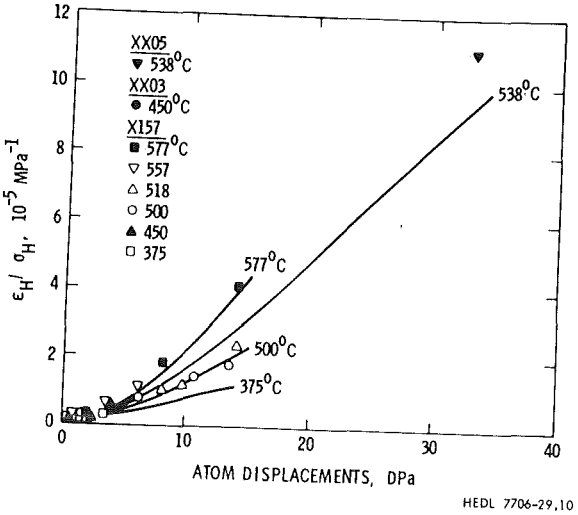

Dependence of irradiation creep on dose in 20% cold worked Type 316 stainless steel for different temperatures

Fig. 9

(after Gilbert, Bates, 1977)

The material behaviour under irradiation in the temperature regime where thermal creep mechanisms set in (above about 550 °C), is an interesting but still controversial field of research. It has recently been reviewed by K. Ehrlich (J.Nucl.Mat., 1981). Gilbert and Lovell reported a reduced in-reactor creep rate at 700 °C for SS 316 compared with data measured in pre- or post irradiation creep tests. They explain it by assuming a so-called "dynamic hardening" effect caused by irradiation-induced short-lived obstacles. In contrast to this, workers of KfK observed an enhanced creep deformation at 700 °C under irradiation (Fig. 10).

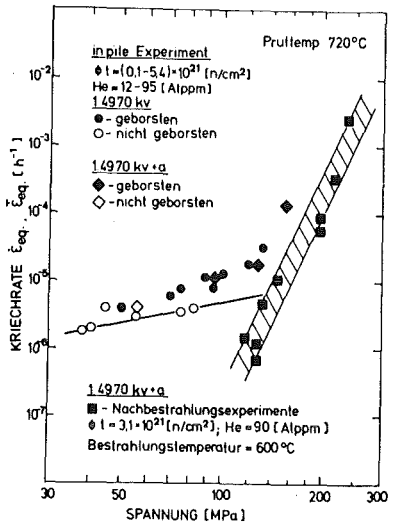

Minimale Kriechgeschwindigkeiten für den Werkstoff Nr. 1.4970, gemessen während bzw. nach der Bestrahlung

Fig. 10

This diagram leads over to the properties of cladding materials in the pre- and post irradiation state.

d) Tensile and creep properties

A comparison of the dependence of tensile yield strength and uniform elongation upon the fast neutron fluence between the two reference materials 1.4970 and AISI 316 has been made by Anderko et al. (Scottsdale Conf., 1977, p.65)

At testing temperatures of 570 $\pm$ 30 °C (Fig. 11), with the allowance made for a somewhat wider range of irradiation temperatures, the cold-worked and aged (sa + cw + a) 1.4970 still shows an initial slight increase in yield strength with increasing fast neutron fluence.

In contrast to this, the yield strength of AISI 316 decreases which is indicative of fast recovery processes. So at higher temperatures the steel 1.4970 compares favourably with AISI 316 ss as to microstructural stability. The decrease in ductility of the two materials due to irradiation embrittlement is quite similar.

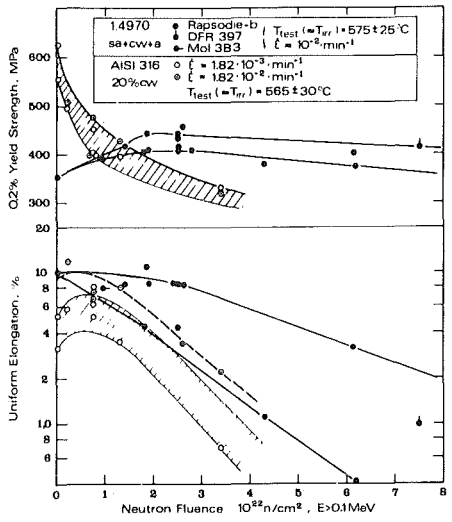

Fig. 11

Effect of fluence on the yield strength and the uniform elongation of type 1.4970 and AISI 316 (HEDL-TME 76-13)

Fig. 12 shows the tensile properties of 1.4970 as a function of the testing temperature ($\sim T_{irr}$). The results are as expected: the yield strength decreases with increasing temperature and the uniform elongation shows a maximum at approximately 550 ^{o}C. It is to be noted, however, that at $(1.6 \pm 0.9) \times 10^{22}$ fast neutrons/cm^2 the matrix hardening

leads already to a remarkable loss in ductility whereas a high temperature embrittlement effect is hardly to be seen at this fluence.

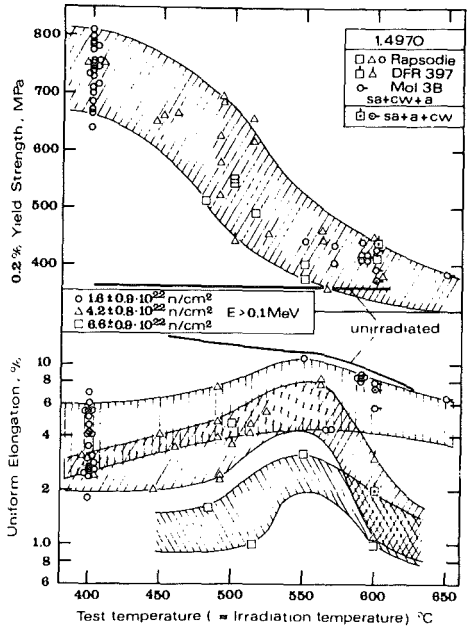

Fig. 12

Effect of test temperature on the yield strength and the uniform elongation of type 1.4970

The low uniform elongation at T below 500 °C can be understood as follows:

There is a classical criterion (Considère) for the onset of necking. It states that necking begins if the slope $d\sigma t/d\varepsilon t$ of the true-stress / true-strain curve becomes smaller than the true stress σ_t ("plastic instability"):

$$\frac{d\sigma t}{d\varepsilon t} \leq \sigma_t$$

Due to the strong irradiation-induced increase in yield strength (and the reduced ability to strain-hardening), necking begins shortly after the specimen departs from the line representing elastic straining.

As regards the influence of very high fluences of the order of $2.10^{23} n/cm^2$, E > 0.1 MeV (about 100 dpa), which is the target dose for commercial fast reactors, on the tensile properties, the following can be said:

As the yield strength "saturates" as a function of fluence at about $4.10^{22} n_f/cm^2$ one may assume that the embrittlement due to plastic instability will not reach "zero-ductility". A change in the fracture type, however, cannot a priori be excluded. In fact, such a change has been observed on annealed SS 304 (above $2.10^{22} n_f/cm^2$ and at temperatures below 480 ^{o}C). However, no normal-stress induced brittle fracture occured, but a shear-stress induced highly localized "channel fracture" as a consequence of dislocation channeling (an avalanche of dislocations can be released along the planar channels that have been cleared of (loop-) obstacles by the first dislocations). A minimum uniform elongation of 0.3 % could be measured.

At higher temperatures (above 600 ^{o}C) the transmutation helium determines the ductility. By irradiation in fast / thermal reactors one can simulate the target dose of fast reactors (about 100 appm He). The tensile ductility of such samples is at least 0,5 %.

Zero-ductility was measured in tensile testing at 650 °C of SS 316 tortured to 6000 appm He and 120 dpa (Bloom, Wiffen, J.Nucl.Mat. 58, 1975, 171), which corresponds to extreme and avoidable fusion reactor first wall conditions.

Turning to creep deformation it may be generally stated that austenitic steels are especially prone to intercrystalline fracture at higher temperatures. This tendency is much enhanced after a neutron irradiation, due to (n,α)- produced He diffusing to grain boundaries and supporting the formation of creep cavities.

As the transmutation He content is more important than dpa damage (fast fluence) for the creep behaviour at high temperatures, it is possible to simulate the post-irradiation behaviour of a fast reactor-treated material by an irradiation treatment of shorter duration in a mixed thermal / fast reactor which produces more He in a Ni (and especially B) bearing steel.

Fig. 13 shows the creep rupture strengths at 700 °C of 1.4970 in the reference state before and after such a simulation irradiation in the reactor BR2 (Mol, Belgium).

The decrease in rupture strength is due to a reduced ductility.

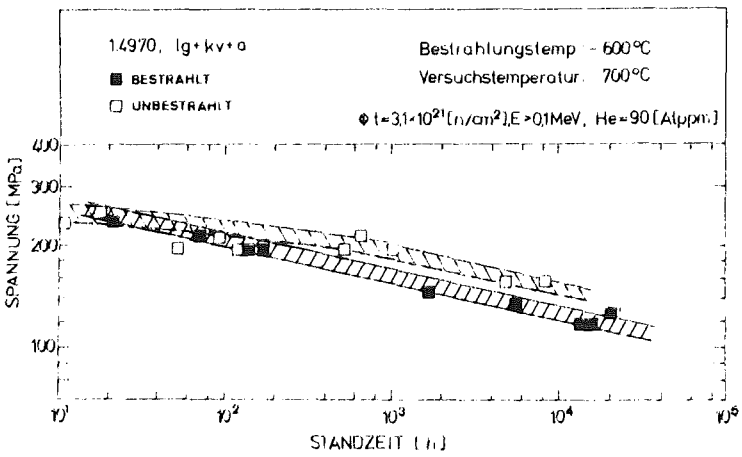

Fig 13

Example: Fission gas pressure may reach 90 bar = 9MPa in a fuel pin.

Azimutal stress in tube Da=6.0-S=0.4mm: $\sigma = \frac{p.d_i}{2s} = \frac{9 \times 5.2}{0.8} = 58$ MPa

This ductility reduction depends on pre-treatment and stress (or rupture time) as shown in Fig. 14

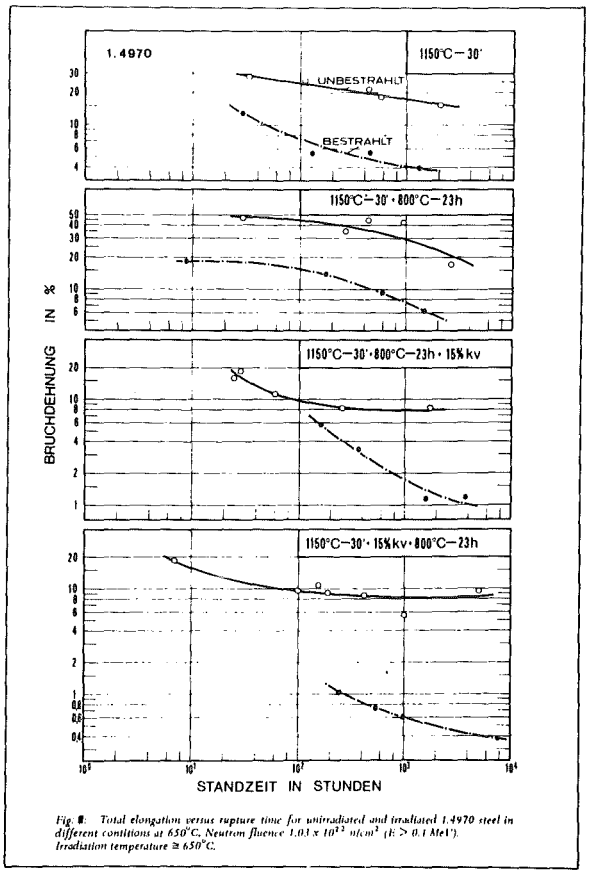

Fig. 8. Total elongation versus rupture time for unirradiated and irradiated 1.4970 steel in different conditions at 650°C. Neutron fluence 1.03×10^{22} n/cm² (E > 0.1 MeV). Irradiation temperature ≅ 650°C.

Fig. 14

A comparison of the post-irradiation creep rupture strength of the reference materials 1.4970 and AISI 316 can be seen in Fig. 15 and 16 (Anderko et al., 1976).

Fig. 15 shows the results after irradiation at 575 ± 25 °C with fluences of 0.3 to 6.2 x 10^{22} in the Rapsodie reactor and with

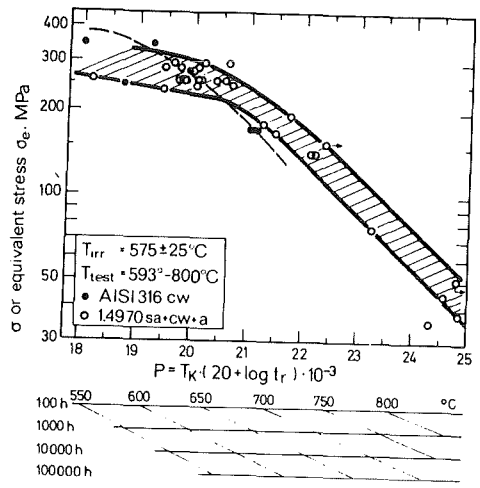

Creep rupture strength after fast neutron irradiation. A comparison between the reference materials 1.4970 and AISI 316 (ASTM STP-529, HEDL-TME 74-9, GEAP 14032)

Fig. 15

0.2 to 3.0 x 10^{22} n/cm^2 (E > 0.1 MeV) in the EBR-2, respectively. Testing temperatures and rupture times are correlated by the Larson-Miller parameter P. (1.4970 : internal pressurized tubes; AISI 316: uniaxial loading). At low values of P the cold worked AISI 316 offers the better strength; however, with increasing P the picture changes and at the 175 MPa stress level the 1.4970 yields the somewhat better results. This is obviously due to its

higher recovery resistance which is already known from the tensile results. It has been checked around the 175 MPa level that the separation of the two data groups is not due to fluence effects and that the groups cannot be merged by choosing a reasonable value (15 to 20) for the constant C in the Larson-Miller expression. The biaxial equivalent creep rupture strains of the 1.4970 specimens (Rapsodie-bundle) lay in a rather wide scatterband with the minimum above 0.2, 0.8 and 4 % at testing temperatures of 600, 700 and 800 ^{o}C, respectively.

For a further comparison of the creep rupture strengths of the two steels allowance had to be made for a somewhat wider range of irradiation temperatures, namely about 600 to 700 ^{o}C (Fig. 16). Irradiation of the 1.4970 samples occurred in the BR 2 reactor (Mol 3B $\sim$ 1 x 10^{22} n/cm^2, E > 0.1 MeV), resulting in a high helium level, up to 184 appm. The scarce data on AISI 316 from fast reactor irradiations usable for this comparison comprise fluences between 0.4 and 2.7 x 10^{22} n/cm^2 (E > 0.1 MeV). Fig. 16 shows the uniaxial stress rupture curves for testing temperatures of 600, 650 and 700 ^{o}C, respectively.

As to be expected from its higher recovery resistance, the steel 1.4970 offers the longer times to rupture at all three test temperatures. Within the Mol 3B data of test temperature 700 ^{o}C an influence of irradiation temperature on rupture life appears to be well established (Fig. 16). Samples irradiated at 610 ^{o}C (Mol 3B3) exhibit significantly higher times to rupture than the specimens irradiated at 640 ^{o}C

(Mol 3B2). This effect is due to the higher ductilities and the somewhat lower creep rates of the Mol 3B3 samples.

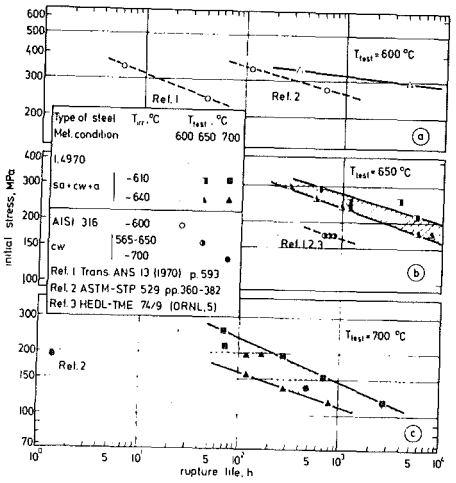

Fig. 16 Post-irradiation rupture life of types 1.4970 and AISI 316 stainless steels at 600, 650 and 700°C

Fig. 17 shows the influence of neutron spectrum and of irradiation temperature on the creep rupture ductility of 1.4970 after testing at 600 °C. The specimens DFR-irradiated at 490 °C exhibit improved ductility with increasing rupture time which proves that recovery effects during the creep test are stronger than the helium embrittlement of the grain boundaries. The high ductility at 7700 h is due to a distinct tertiary creep range. Specimens irradiated around 630 °C in the DFR or BR 2 reactors, however, yield falling ductility curves as a consequence of the helium embrittlement

effect which is of course stronger in the BR 2-irradiated specimens (far more helium, less recoverable displacement damage).

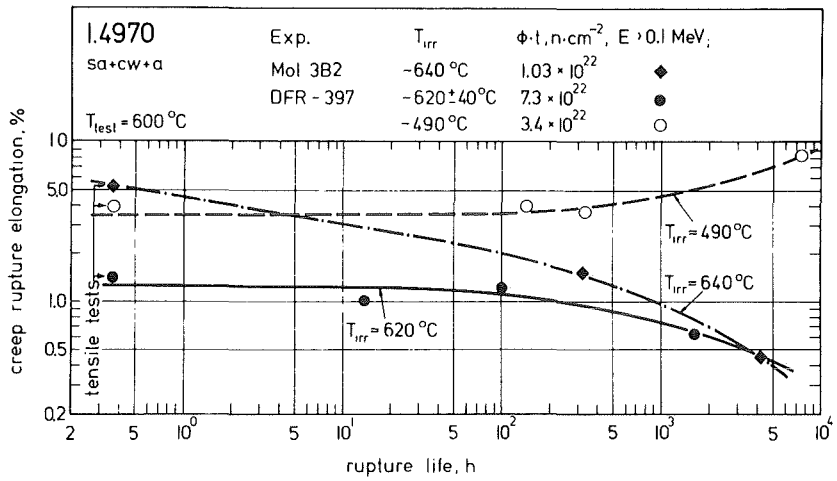

Fig. 17 Post-irradiation ductility of the type 1.4970 stainless steel at 600°C

The merging ductility curves prove the value of BR 2-irradiation for development work on creep resistant LMFBR-alloys.

The microstructural changes occurring in the DFR-irradiated specimens during the creep testing at 600 °C were followed by TEM investigations. The as-irradiated samples show high concentrations of voids and of planar faulted loops. The detailed data are shown in the Table. The nature of the loops was not determined.

Table: TEM-Investigation of DFR-Irradiated 1.4970

$T_{Irr.}$ °C	490	620
Neutron fluence, n·cm^{-2} (E > 0.1 MeV)	3.4x10^{22}	7.3x10^{22}
Loop concentration, cm^{-3}	2.0x10^{14}	3.0x10^{14}
Void concentration, cm^{-3} mean diameter, nm	3.0x10^{14} 20	6.5x10^{14} 35
Dislocation line density (without loops), 10^{10} cm·cm^{-3}	~ 2.5	not determined

The TEM results after the creep testing are described and discussed as follows:

a) After a test time of 13 h no loops could be detected anymore. The resolution of loops is therefore a fast process at 600 °C.

b) There is an annealing of voids during the creep test and this process is apparently accelerated by the applied stress. In the strained part of the sample irradiated at 490 °C practically all voids have disappeared.

In the specimens irradiated at 620 °C and exhibiting a higher initial void volume (1.6 %), voids do also anneal during creep testing as can be seen from the reduction of void concentration as a function of rupture life (Fig. 18). Since the mean void diameter is increasing, the amount of swelling does not change significantly in the gauge length within this time period. An explanation for this behaviour is that at high void concentrations the voids themselves are the most efficient sinks for the absorption of emitted vacancies. The illustrated changes in void concentration and void sizes lead to a reduction of the matrix hardening during creep testing, as can be calculated by an Orowan model. This decrease in strength is, however, not reflected in an improved ductility - due to the overriding effect of grain boundary helium embrittlement (Fig. 17).

c) The dislocation line density decreased in the specimens irradiated at 490 °C from $2.5 \cdot 10^{10}$ in the as-irradiated state to about $0.5 \cdot 10^{10}$ cm/cm^3 after creep testing (600 °C, 7644 h).

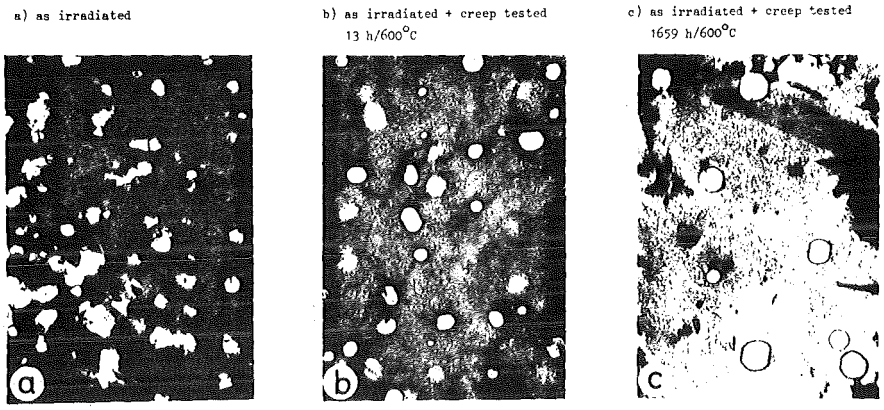

Annealing of voids in the gauge length of Type 1.4970 (sa+cw+a)

Fig. 18

A survey of the fracture types occurring in pre- and post irradiated austenitic stainless steels in tensile and creep testing is given in Fig. 19 and 20

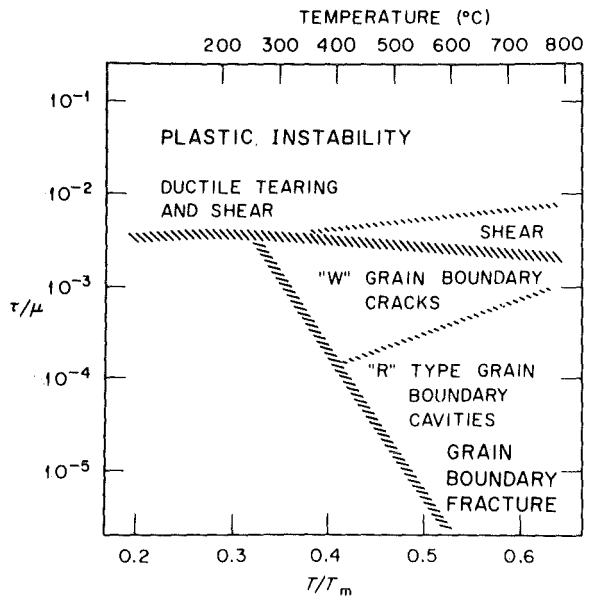

Fig. 19

Schematic Representation of the Fracture Behavior of Austenitic Stainless Steels. (From unpublished data of R. W. Sindenman and E. E. Bloom.)

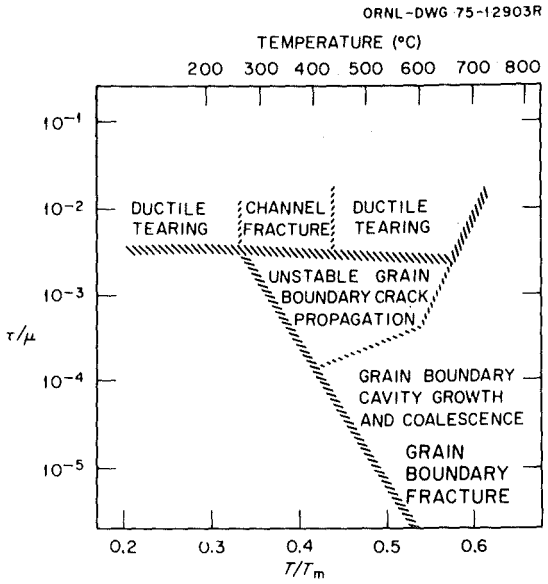

Fig. 20

Schematic Representation of the Fracture Behavior of Austenitic Stainless Steels After Irradiation to High Fast Neutron Fluences ($\geq 5 \times 10^{26}$ n/m^2 (E > 0.1 MeV). (From unpublished data of R. W. Swindeman and E. E. Bloom)

which were taken from M.L. Grossbeck et al., Scottsdale Conf., 1977, 95.

The influence of irradiation mainly shows up by

- a larger region of g.b. cavitation, since He pressure promotes growth of cavities
- Disappearance of the shear failure region leading to a slant fracture (low homogeneous deformation in irradiated material)
- the appearance of an entirely new phenomenon, the "channel fracture"

(Ductile tearing in short time tensile tests:
fracture surface $\perp \sigma$; internal cavities open at precipitate particles and failure occurs by tearing between them)

e) Phase Instabilities during high temperature service

As can be judged from the section through the Fe-Cr-Ni-C - phase diagram, a solution annealed austenitic Cr-Ni-steel, will precipitate (at least) carbide phases at temperatures corresponding to the operation of a LMFBR (400-700 ^{o}C). Due to the complex composition of technical steels also other phases (for instance nitrides, intermetallics) may form. This change may have a profound influence on the physical and mechanical properties.

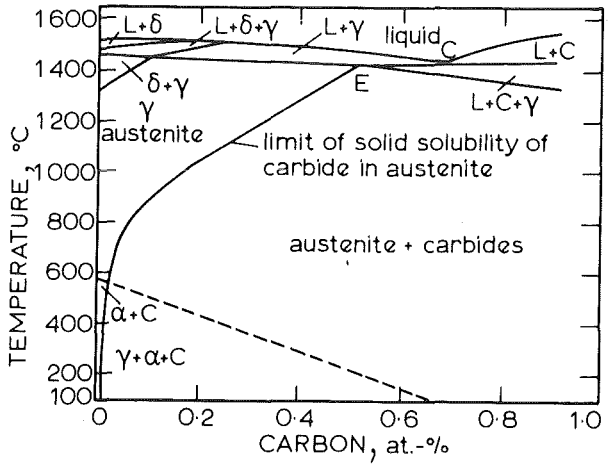

Effect of carbon on solubility of carbides in 18Cr-8Ni steels (from Chromium-nickel austenitic steels, F.H. Keating, Butterworths, London)

Looking at cladding and core structural materials, however, not only time and temperature have to be considered as parameters, but also the neutron fluence. In fact, irradiation induced phase changes form a fascinating field of metallurgical research nowadays.

The base for such studies are so-called TTP-diagrams, in which the effect of annealing time and temperature on a solution annealed microstructure has been plotted.

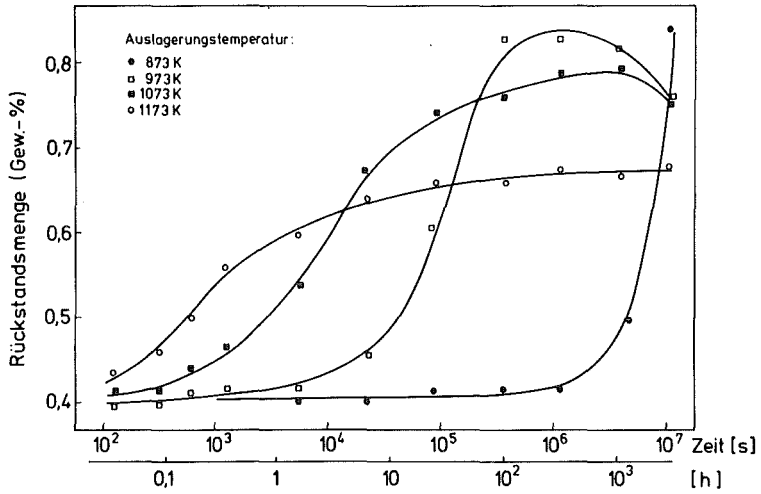

Abhängigkeit der Gesamtausscheidungsmenge von der Auslagerungszeit für die lösungsgeglühten Proben (25% kv + 1403 K-30 min.) (Charge B).

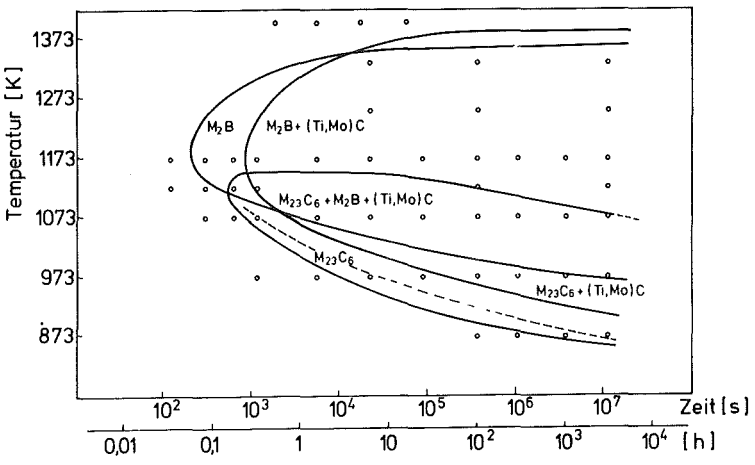

Zeit-Temperatur-Ausscheidungsdiagramm für die lösungsgeglühten Proben (25% kv + 1403 K-30 min.) des Stahles 1.4970 (Charge B).

Fig. 21

Fig. 21 shows the behaviour of the steel 1.4970 (0,09 C; Ti/C = 5,1; B = 45 ppm, A.F. Padilha et al., J.Nucl.Mat., 1982). The upper part gives the time and temperature dependence of the total amount of precipitate phases. Two of the curves exhibit a maximum indicating resolution processes.

The lower part of the figure shows that 3 phases precipitate: a boride M_2B = $(Cr, Fe)_2$ B, $M_{23}C_6$ = $(Cr, Fe, Mo, Ni)_{23}C_6$ and (Ti, Mo) C. Around 1100 K, $M_{23}C_6$ forms but after 100 h it goes into solution again and is replaced by the other two phases. How can this behaviour be understood? Fig. 22 shows the variation of the free formation enthalpy with temperature for TiC, $Cr_{23}C_6$ (and NbC). TiC is the stable phase in the whole temperature regime. The appearance of $M_{23}C_6$ at lower temperatures must therefore have purely kinetic reasons. Its nucleation must be easier (both carbides are initially coherent to the matrix) and its faster growth is reasonable considering the higher diffusion coefficient of Cr in comparison with Ti. ($D_{Cr} = 2.10^{-13}$, $D_{Ti} = 9.10^{-14}$ $cm^2 \cdot s^{-1}$ at 1073 K).

At higher temperatures ($\geq$ 1173 K) only the stable phases make their appearance.

It is remarkable, that even after prolonged annealing no intermetallic phases (like σ or Laves) occur in 1.4970. Such phases are unfavourable due to their embrittling effect. Since the σ - phase may form via δ - ferrite traces

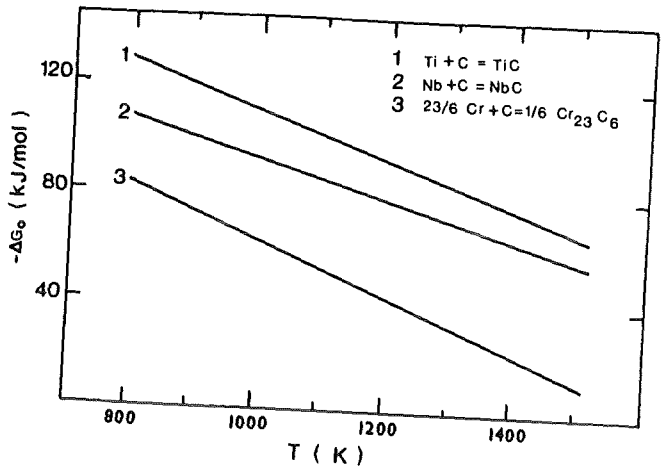

Variation der freien Bildungsenthalpien von TiC, NbC und $Cr_{23}C_6$ in γ-Eisen mit der Temperatur

Fig. 22

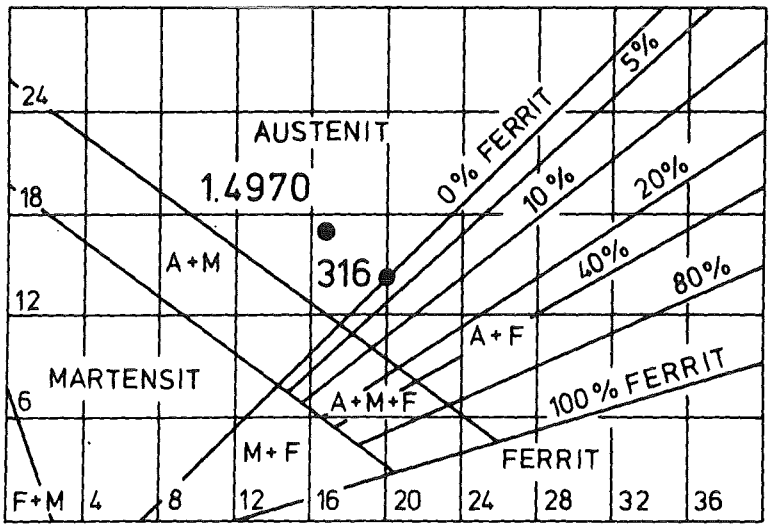

Fig. 23

in the microstructure, the position of 1.4970 well inside the austenitic field of the well-known Schaeffler-diagram (Fig. 23) explains this behaviour.

The results on 1.4970 were obtained mainly from X-ray diffraction analyses of bulk-extracted residues. In studying irradiated samples one must rely upon electron microscopic in situ - analyses (selected area diffraction, energy dispersive X-ray analysis EDAX). Herewith phase identifications are more difficult. Therefore it has not yet been conclusively established whether intermetallic phases will also not form in 1.4970 under heavy neutron irradiation. According to Weiss and Stickler (Met.Trans. 3, 1972, 851) the formation of intermetallic phases may be enhanced under neutron irradiation (accelerated substitutional diffusion kinetics, preferential nucleation by increased lattice distortion in the irradiated matrix).

A time-temperature-precipitation (TTP) diagram for the solution annealed steel AISI 316 (0.066 % C) is shown in Fig. 24 (Weiss and Stickler, loc.cit.).

Fig. 24

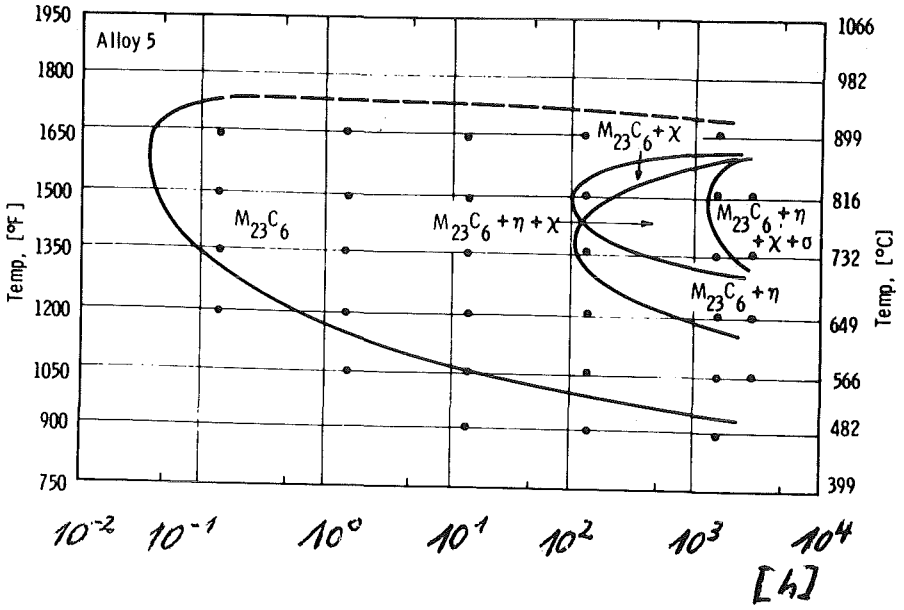

The $M_{23}C_6$ carbide appeared after very short aging times while the formation of intermetallic phases η (Laves), Chi (α-Mn-structure) and σ (tetragonal) occurred after more than 100 and 1000 h, respectively. A certain resolution of $M_{23}C_6$ could be observed because the intermetallics are thermodynamically the stable phases. (After precipitation of a certain amount of intermetallics, the C - solubility of the Mo - and Cr - depleted matrix increases which results in that resolution of $M_{23}C_6$.)

Thanks to a quite recent paper by Yang, Brager and Garner (1980), there is information on the irradiation effect on the phase stability of 316. These authors could show on 316 heats with C between 0.04 and 0.056 % (quite similar to Weiss and Sticklers heat), that irradiation ($1.4 \cdot 10^{23}$ n/cm^2, E > 0.1 MeV) does "modify both the stability of the austenitic matrix and the precipitation reactions. For instance, the phases γ′ (Ni_3Si) and G (Ni-silicide) are formed in 316 only during irradiation and would not otherwise be produced. The formation of these irradiation-induced precipitates has also been shown to affect the matrix composition by depleting it of certain solute elements (Ni, Si). A similar irradiation-induced concentration of these solutes in the thermally stable phases has also been observed. The development of these irradiation-induced and irradiation-altered phases is also expected to affect many properties of the material such as the mechanical properties, the creep and swelling behaviour, and possibly the corrosion resistance."

In total, after irradiation between 460 and 650 ^{o}C six precipitate phases were encountered:
γ' (Ni_3Si), G (Ni-silicide), η - silicide, $M_{23}C_6$, M_6C and Laves

The precipitates were classified as

- thermally stable, but modified
- irradiation - enhanced
- irradiation - induced and
- irradiation - transformed

As to the irradiation - induced phases (γ', G-phase), it has been observed that if the temperature is maintained but the irradiation ceases, both phases start to dissolve, indicating that they require irradiation for continued stability. These phases are naturally rich in Ni and Si. On the other hand, the $M_{23}C_6$ and Laves precipitates normally found in the thermally aged 316 contain only very low levels of Ni and Si; under the added influence of irradiation, however, Ni and Si are enriched in these precipitates ("infiltration - exchange").

Literature to 4.4.3 (e)

B. Weiss, R. Stickler, Phase Instabilities during high temperature Exposure of 316 SS, Metall. Trans. 3, 1972, 851

A.S. Grot, J.E. Spruiell, Metall. Trans. A, 6A, 1975, 2023

M.V. Vaidya, Über den Einfluss der Bestrahlung auf die Stabilität von Ausscheidungen, KfK 2567 (Kernforschungszentrum Karlsruhe), Dezember 1977

W.J.S. Yang, H.R. Brager, F.A. Garner, Radiation-Induced Phase Development in AISI 316, Symposium on Irradiation Phase Stability, Pittsburgh, Pa., USA, 1980

A.F. Padilha, G. Schanz, K. Anderko, Ausscheidungsverhalten des titanstabilisierten austenitischen Stahls 15 Cr - 15 Ni - 1 Mo - Ti - B (Din 1.4970), to be published in J. Nuclear Materials

f) Influence of sodium coolant

Generally speaking the following reactions may be expected if a liquid metal is in contact with a solid material:

1) Stagnant liquid metal:

Dissolution of the solid material is mainly controlled by the solubility of this material (or constituents thereof) in the liquid metal. An equilibrium is reached if the chemical potential of a specific element has the same value in the solid as in the liquid metal.

On the other hand, if the liquid metal contains as impurity elements like C or N, they may be taken up by the solid if the chemical potential difference points in this direction.

2) Recirculating (loop) systems:

Continuous mass transport: elements go into solution in high-temperature regions and deposit on or diffuse into the solid material in low temperature regions where the solubility in the liquid metal is lower. This process is self-sustaining as long as the temperature difference exists.

3) Liquid-metal embrittlement:

It requires the presence of tensile stress, similar to the case of stress-corrosion cracking. Cracks are initiated and propagate rapidly through the solid material.

Example: 4130 steel (0.3C, 1Cr, 0.2Mo) has been known to crack within 1 min at an applied stress of 103 MPa when contacted by liquid lithium.

What now occurs if liquid high-purity sodium is in contact with austenitic stainless steels as in a LMFBR reactor? The Na-coolant inlet and outlet temperatures are about 380 and 550 °C, respectively. The cladding (at hot spots) may reach 670 °C.

At first the statement can be made (from fuel pin examinations) that even heavy fast neutron irradiation obviously does not significantly change the corrosion behaviour of austenitic stainless steels in sodium. Thus the results of "cold loop" system studies are well suited for the evaluation of the material behaviour.

Fig. 25 shows the flow diagram of one of the Karlsruhe sodium high-temperature corrosion loops.

TI-III are three parallel test sections in the hot part, in which corrosion and internally pressurized tubular creep specimens were placed (6.0 mm diameter, 0.38 mm wall thickness).

Materials: Ti - or Nb - stabilized steels
1.4970 (X 10 NiCrMoTi B 15 15)
1.4981 (X 8 CrNiMoNb 16 16)
1.4988 (X 8 CrNiMoV Nb 16 13)

The overall corrosion of austenitic steels in sodium, as measured by weight loss, is mainly determined by the oxygen content of the sodium. There is a nearly linear dependence of corrosion rate on the oxygen concentration (Fig. 26):

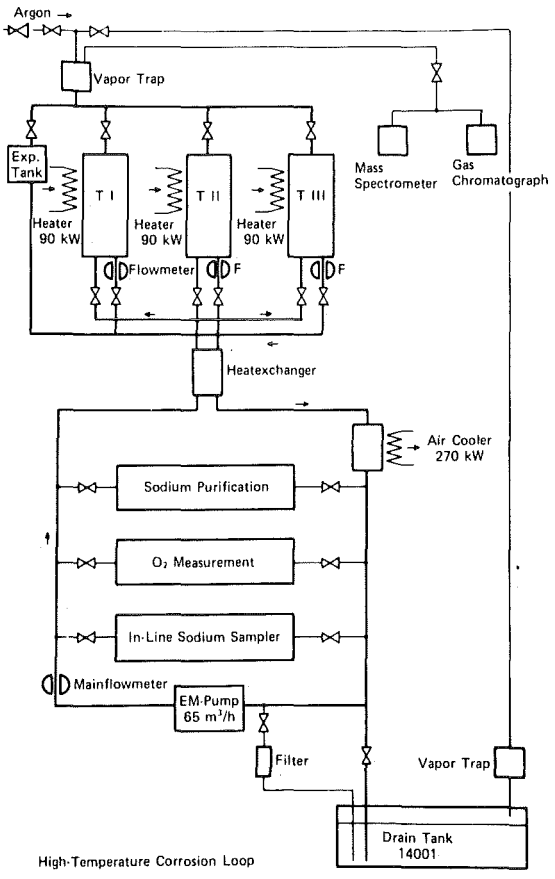

Fig. 25

Flow diagram of the sodium high-temperature corrosion loop.

Fig. 26

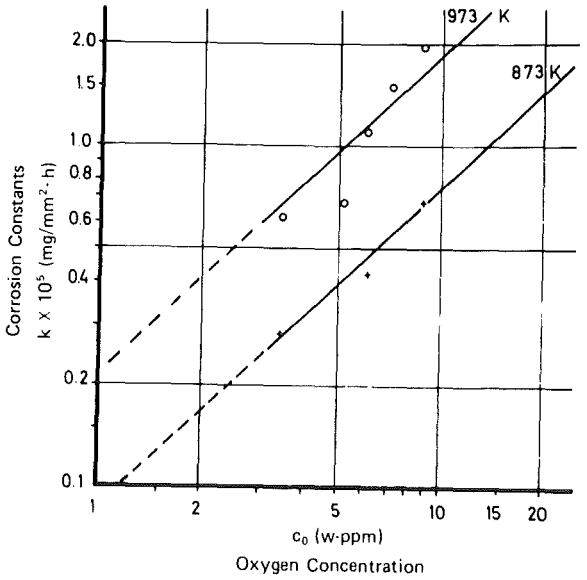

Relation of corrosion constants to oxygen concentrations of the sodium.

at 973 K:

$$\log k = 0.3385 + \underline{0.922} \cdot \log C_o$$

The weight loss is due to the selective leaching of substitutional alloying elements (Cr, Ni, Mn, V, Nb). This gives rise to structural changes in subsurface areas of the cladding tubes (Fig. 27).

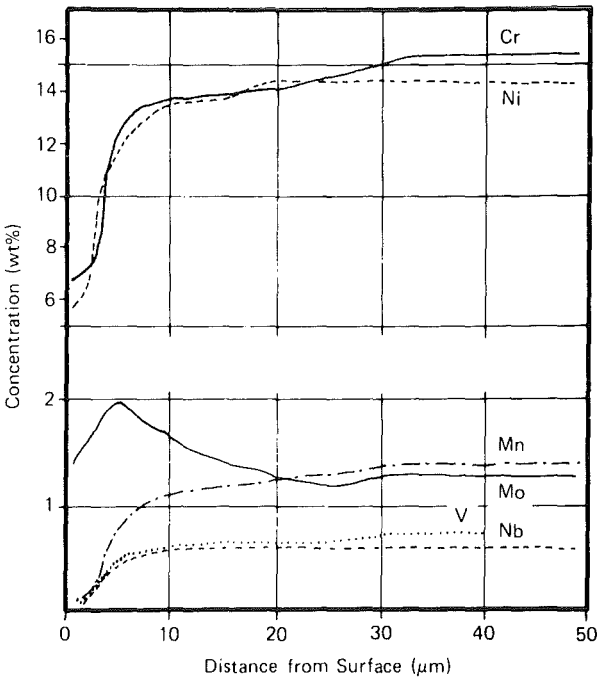

X8 Cr Ni Mo V Nb 16 13 (no. 1.4988)
Na; 5000 h, 973 K, 5 m/s, 5.5 ppm O.

Fig. 27

Depletion of substitutional elements in the surface near areas of a specimen of steel 1.4988 exposed 5000 h at 973 K.

A ferritic subsurface layer as well as ferritic zones at grain boundaries are formed. Mo is the only element being enriched in this area.

Although the carbon concentration in the sodium was kept low (0.1 - 0.2 ppm) there occurred a carbon uptake into the stabilized steels 1.4970 and 1.4981 (X 8 CrNiMoNb 16 16), up to the centre of the tube walls (Fig. 28):

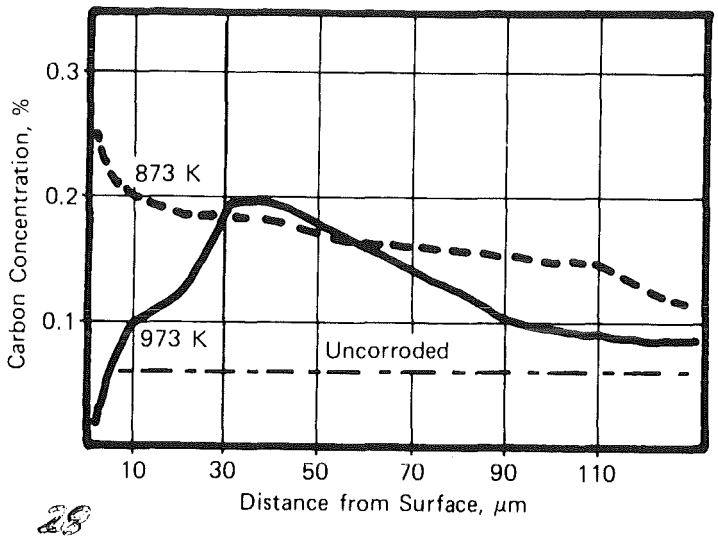

28

Fig. 110: Comparison of carburization profiles due to sodium exposure at 873 and 973 K (5000 h).

The increase of the carbon concentration corresponds to the difference in the chemical potentials for carbon in sodium and in the steels. In addition, even the carbon concentration profiles in the cross sections of the tubes are in accordance with the carbon activity changes due to the selective leaching of Cr and the stabilizing elements.

Fig. 29 summarizes the corrosion effects for cladding tubes of 1.4970 in Na of 700 ^{o}C.

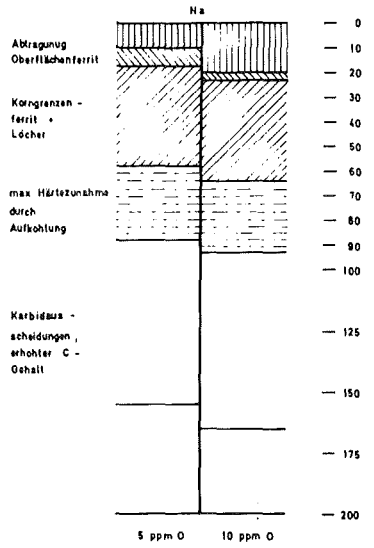

Fig. 29: Changes in the outer half of the wall thickness of 1.4970 - cladding tubes after 10 000 h in Na of 5 m/s flow velocity with 5 and 10 ppm oxygen, respectively, at 700 °C.

The removed material ("Abtragung") can be even further reduced by lowering the oxygen concentration level to about 1 ppm. This is not necessary for reasons of the life time of the fuel element, but may be attractive considering the transfer of activated elements into the reactor loop system.

An interesting point is also the behaviour of the element boron contained in steel 1.4970. After 5000 h in the sodium stream of 700 °C the bulk content in the tubes decreased from 54 to 22 ppm. This loss (which appears to increase with the

carbon content of the sodium: Borgstedt et al., 1977) is tolerable in view of the fact that 20 ppm B are sufficient to improve significantly the intergranular cohesion (Donati, et al., 1978).

Turning to creep behaviour in sodium it can be stated that the creep rate of austenitic cladding tubes is nearly unchanged. This may be commented by saying that the weakening effect by the depletion of substitutional elements in surface zone is obviously balanced by the bulk hardening due to carbon uptake.

A "liquid metal embrittlement" effect does not occur with austenitic steels. There is, however, an effect of Na on the creep ductility in that the tertiary creep range is somewhat shortened. This hardly affects the rupture time. We will return to this theme in discussing the tank and primary tubing material.

Some literature to 4.4.3 (f)

D.R. Olander, Fundamental Aspects of Nuclear Reactor Fuel Elements, Chapter 20: Interaction of Na and Stainless Steel, TID - 26711 - P1, 1976 (USA).

H.U. Borgstedt et al., Corrosion and Creep of Pressurized Stainless Steel Tubes in Liquid Sodium at 873 and 973 K, Nuclear Technology 34, 1977, 290-298

H.U. Borgstedt, W. Dietz, Korrosions- u. Kriecheigenschaften von Druckkapseln aus stabilisierten austenitischen Stählen im Na - Kreislauf bei 873 K und 973 K bis zu 10 000 Stunden, KfK 2516, Dezember 1977.

J.R. Donati et al., Influence de la teneur en bore sur les caractéristiques de fluage d'aciers 18-10 stabilisés au titane, Mém. Sci. Revue Mét., 75, 1978, 443 - 464

g) Application of high-strength alloy 718

Special mention should be made of the application of Inconel 718. Design needs in certain specialized areas in the upper (hot) internal core structure require a high-temperature, high strength alloy and can only be satisfied by alloy 718
(Upper contact pads, rods for emergency shut down system).

A comparison of the creep rupture strength with steel 1.4970 in the reference state is given in Fig. 30 :

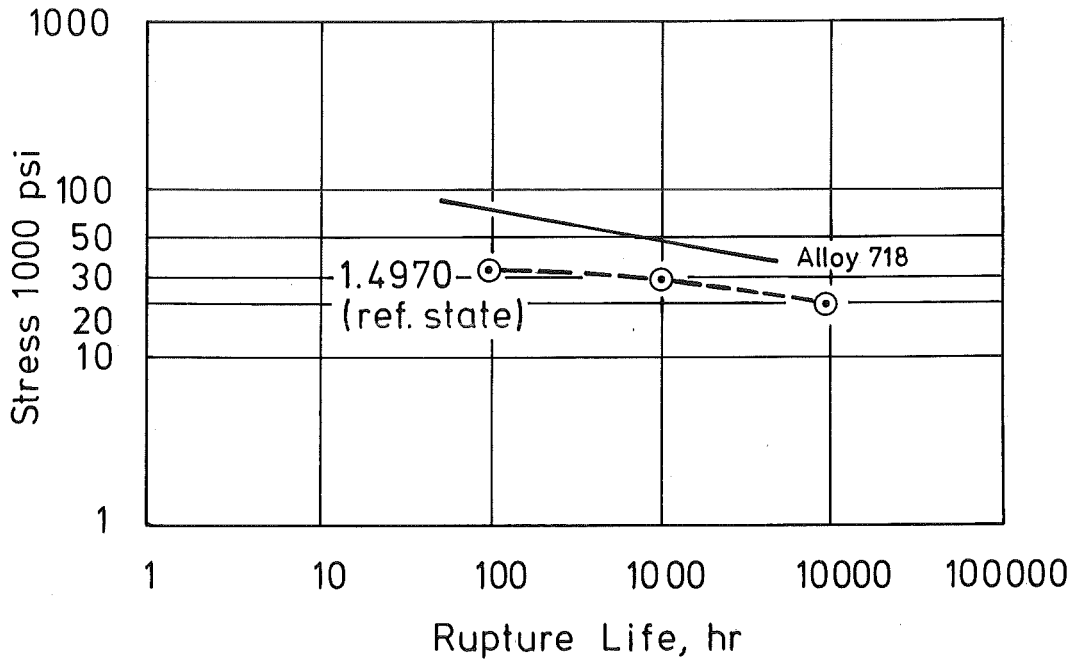

Fig. 30 Comparison of creep rupture strengths at 700 °C between Inconel 718 and 1.4970.
(718: W.Q. from 980 °C + 720 °C/8h, F.C. to 620 °
for total of 18 h
1.4970: cold-worked and annealed = "ref.state")

Whereas in 1.4970 the volume fraction of carbide available for hardening is limited by solubility considerations, the Ni - base alloy is age - hardened by a large volume fraction (~ 30 %) of the intermetallic γ' - phase Ni_3 (Al Ti). Moreover, the crystal structure (f.c.c.) and lattice parameters of γ' and matrix are similar, which leads to coherency and low energy interfaces (low coarsening rates according to the Lifschitz - Wagner equation).

Besides excellent creep strength up to 700 ^{o}C Inconel 718 exhibits also high fatigue strength. Another outstanding characteristic is its slow response to age hardening. The slow response enables the material to be welded and annealed with no spontaneous hardening unless cooled slowly. This alloy can also be repair-welded in the fully aged condition.

As stated above, alloy 718 is also in the US - development program for cladding.

4.4.4 Structural materials (Vessels and Primary Tubing)

In chapter 4.4.1 the two different types of LMFBR's (loop and pool) were characterized. In the following we will concentrate on the loop-system and preferentially on the SNR-300 reactor.

The core of this reactor is (see 4.4.1) enveloped by 3 vessels (tanks):

- Schildtank (shield vessel)
- Reaktortank (reactor vessel)
- Doppel(Sicherheits)-Tank (double or safety vessel)

The inner two vessels and iso-fluence lines in their region after 16 years of operation are shown in Fig. 1.

What are the functions of the shield vessel?

They are three-fold:

- Duct for the sodium flow under normal and emergency conditions (see Fig. 2)
- Neutron absorption (cover for the reactor vessel)
- Energy absorption (by plastic deformation) in case of a very hypothetical Bethe-Tait-accident (core melting)

It is quite obvious from what we have learned already that due to the rather low fluence regimes we will not have to tackle with problems like void swelling or in-pile creep. Furthermore, the elevated temperature levels present will prevent any strong hardening effects at those low fluences.

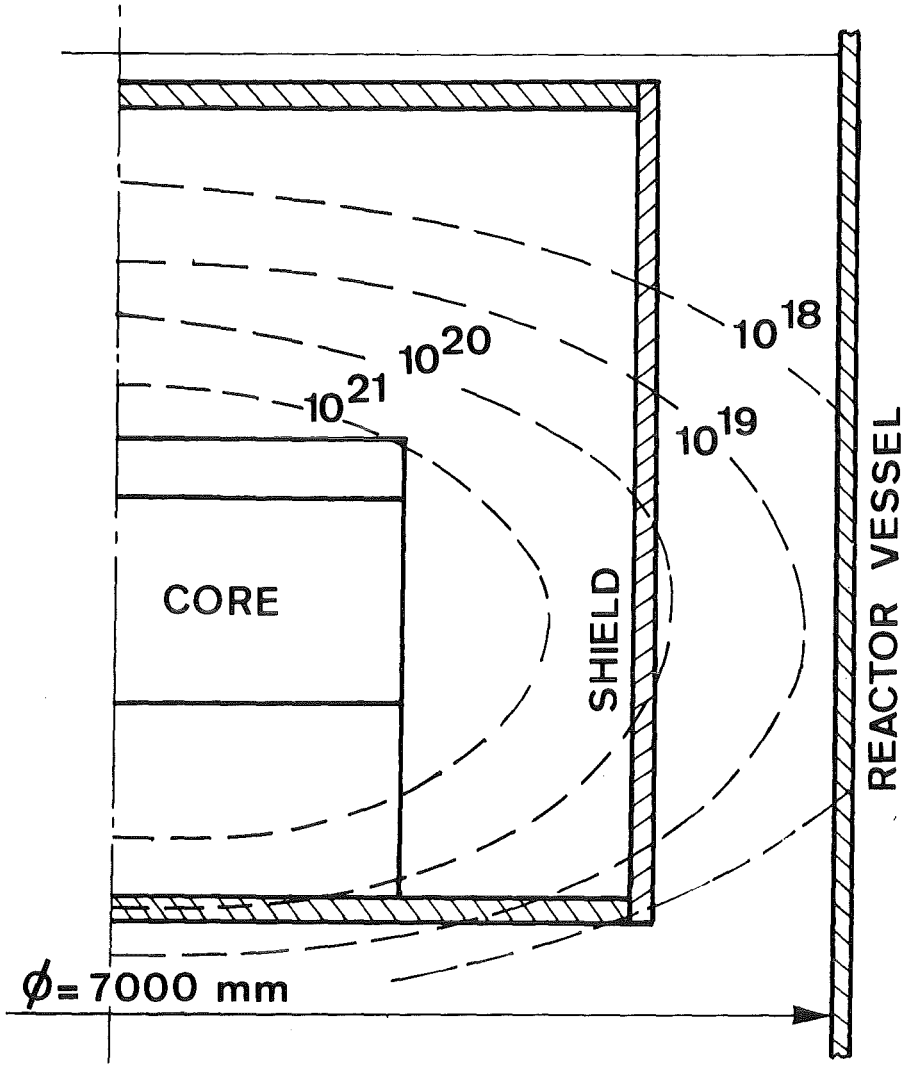

Fig. 1 Schematic drawing of the reactor core and its main surrounding components. The iso-fast-fluence (E > 0,1 MeV) contour lines, after 16 years of reactor operation, have been indicated with interrupted lines; fluence unit: $n.cm^{-2}$.

However, the He - embrittlement effect (high T embrittlement) will definitely have to be considered.

Extended parameter studies have been made, whereby the conditions existing during reactor operation served as a basis for establishing the test parameters. Irradiations were carried out at 450° and 550°C, the two temperatures being characteristic

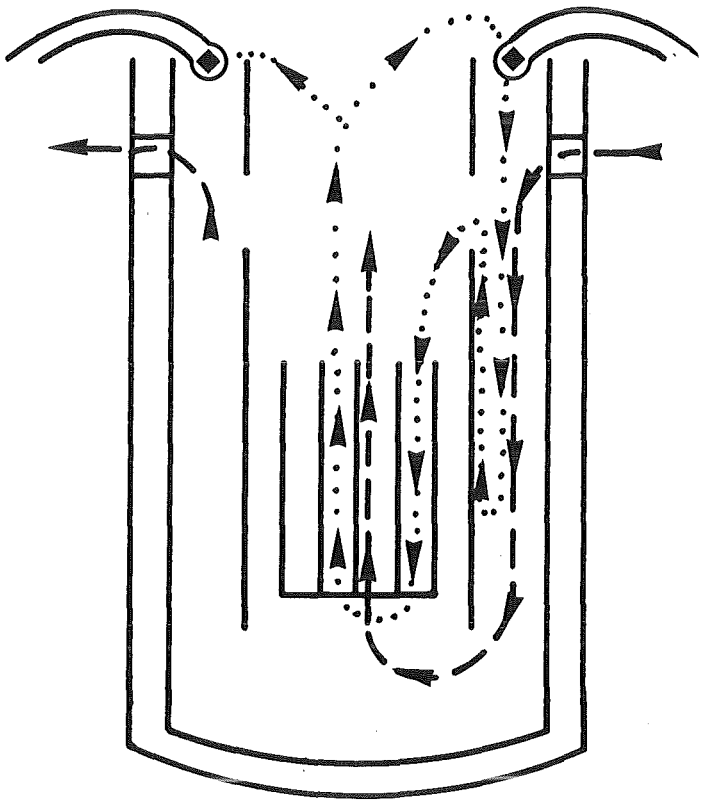

Fig. 2

for vessel and shield tank in the reactor core - midplane and for the reactor outlet, respectively. The neutron dose levels in the irradiation experiments were fixed at 10^{19} and 5 x 10^{20} n.cm^{-2} (E > 0.1 MeV). The former value will be reached at the end of reactor life in the midplane of the vessel, the latter in the shield tank - midplane and the center of the grid plate.

As a rule, test and irradiation temperatures were the same. However, for creep tests the temperature of 723 K (450°C) is too low to be of engineering significance and therefore only tests at 823 K (550°C) were carried out.

In the following we will consider the influence of irradiation on tensile, creep and fatigue properties.

The n-dose levels mentioned above (10^{19} and 5 x 10^{20} n/cm, E > 0.1 MeV) correspond to 0.3 and 7 appm He, respectively. This follows mainly from the B-content which is typically around 10 ppm. ^{10}B is by far the most important source of He ($^{10}B < n, \alpha > {}^{7}Li$ - reaction). The second largest He source, the 2-step transmutation of ^{58}Ni to ^{56}Fe, supplies two orders of magnitude less He in the fluence range investigated and is, therefore, to be neglected.

The onset of He embrittlement is at surprisingly low He-contents as may be seen from Fig. 3 (tensile) and Fig. 4 (creep).

The onset decreases with decreasing deformation rate: ~ 10^{-3} appm He (tensile), ~ 10^{-5} appm He (creep).

The corresponding thermal neutron fluences are ~ 10^{16} n/cm^2 and ~ 10^{14} n/cm^2.

On the other hand, the results indicate that above 0.5 appm He (5 x 10^{18} n/cm^2) the embrittlement does not further increase, at least not up to 10^{20} n_{th}/cm^2.

Without going into much detail the following relation between creep-extension vs. He-content will be presented (van der Schaaf et al., 1977):

$$\varepsilon = \sqrt{3} \times [d^3 \times (n_o + \frac{f \cdot n_{he}}{m_o})]^{-\frac{1}{2}}$$

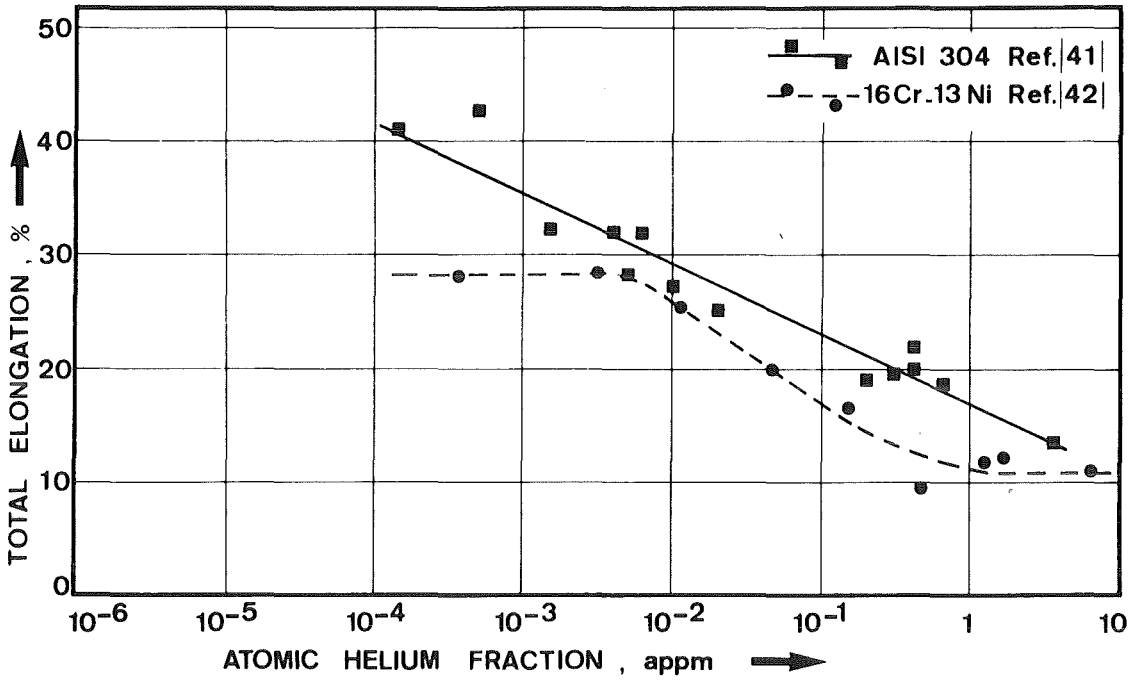

Fig. 3 Dependence of tensile elongations on helium content

where: ε = creep extension.

d = grain diameter.

n_o = density of critical sized cavities on the grain boundaries other than helium bubbles.

f = fraction of helium atoms in critical sized bubble on the grain boundaries.

n_{he} = number of helium atoms produced in the steel by thermal neutron reaction with ^{10}B per unit volume.

m_o = number of helium atoms in a bubble of critical size.

The fraction f will heavily depend on the initial distribution of B in the microstructure. That influence is nicely shown

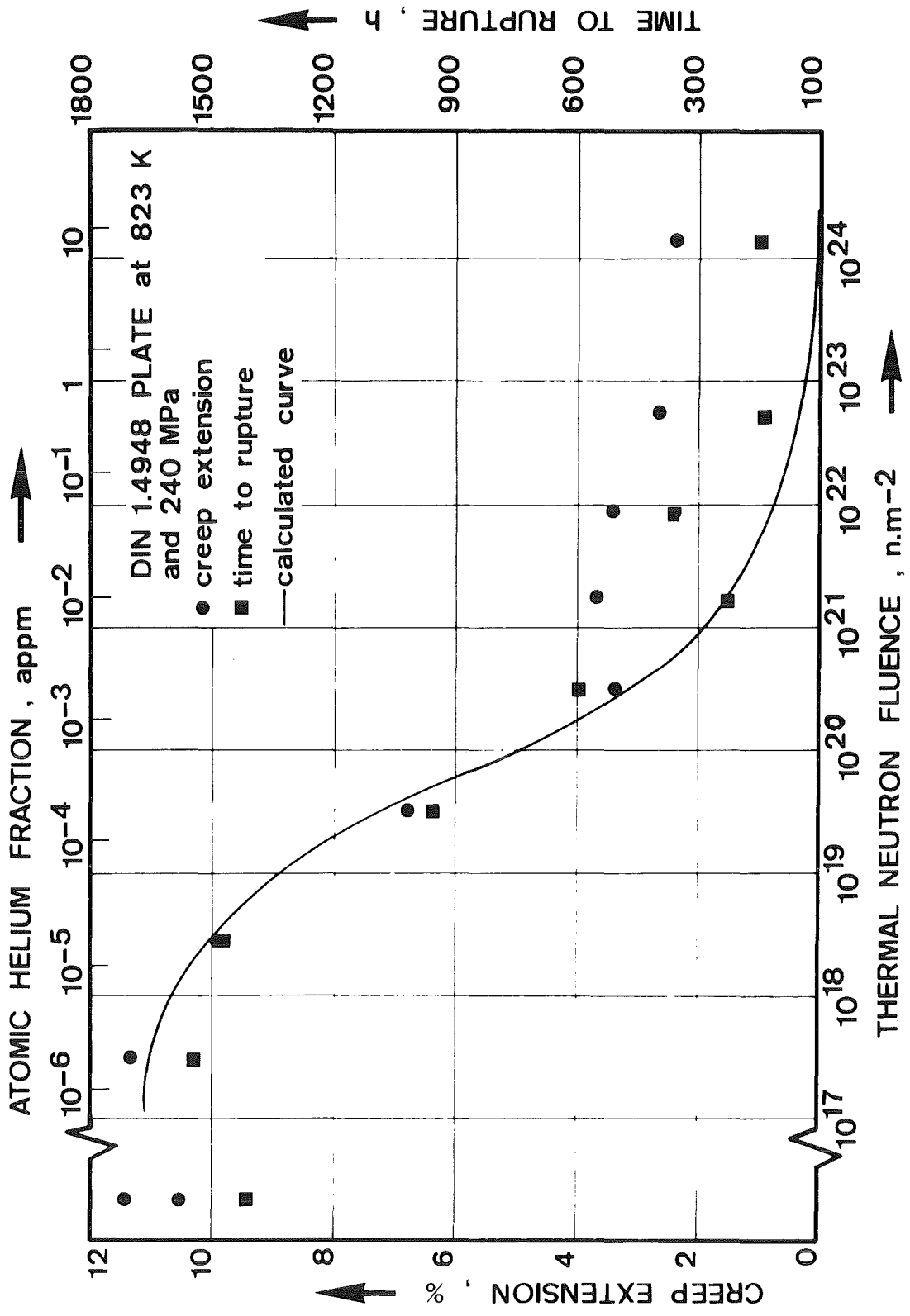

Fig. 4 The effect of helium content or thermal neutron fluence on the maximum creep extension and time to rupture for a stress of 240 MPa at 823 K.

when rupture stresses of base and welded material are compared. In the base metal B has segregated to a large extent on or near to grain boundaries, whereas in the dendritic weld metal B is distributed homogeneously due to the rapid quenching. In the unirradiated state, the base metal shows the higher rupture strength. After irradiation, however, this advantage is lost due to the relatively higher He-embrittlement of the base material. (Fig. 5)

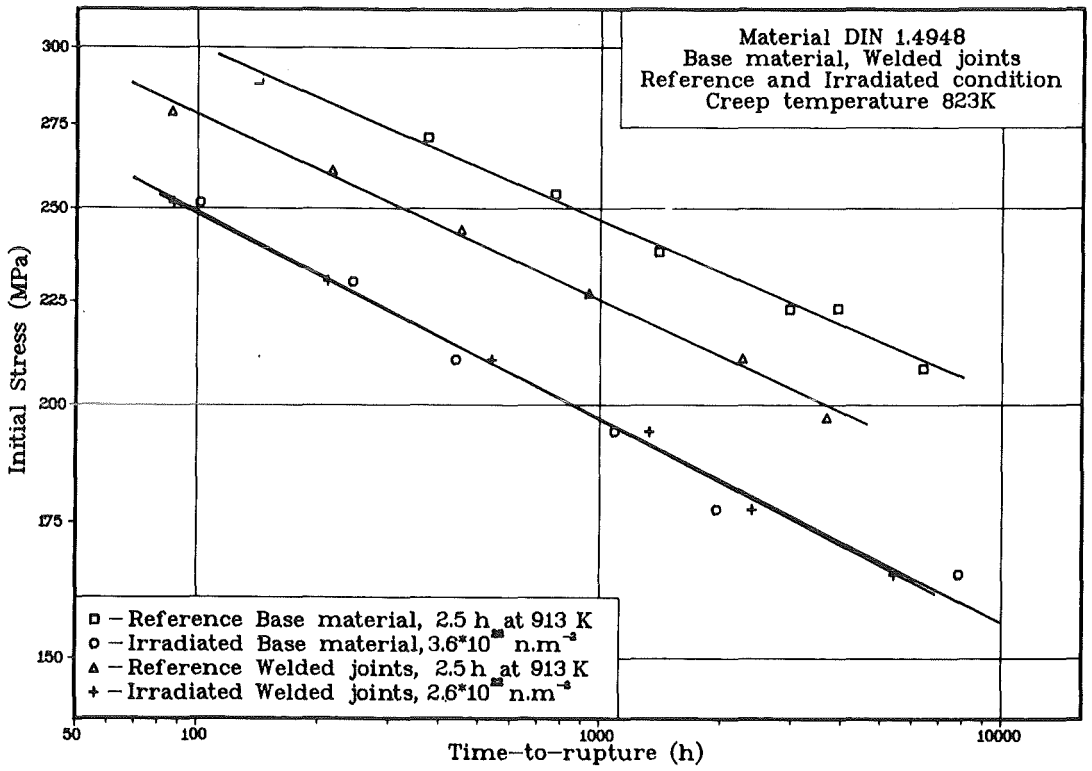

Fig. 5 Comparison of creep properties of parent metal and welded joints in irradiated 10^{23} $n.m^{-2}$ ($E > 0.1$ MeV) and reference condition 2.5 h at 913 K.

The relation also indicates that a grain- size reduction will yield an appreciable ductility improvement.

Since the structural components of a breeder reactor will have to withstand also instationary operational conditions, (low cycle-) fatigue damage besides and in addition to creep has to be considered.

Low cycle fatigue tests under constant strain range conditions are the appropriate investigation tool. Such results are shown in Fig. 6 .

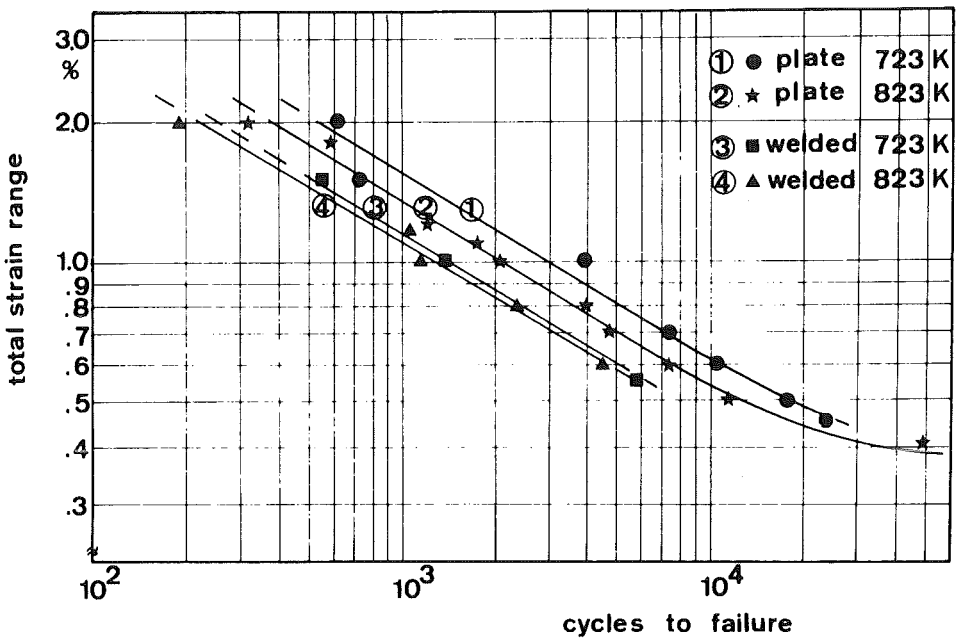

Fig. 6 Cyclic life curves of plate metal and welded joints DIN 1.4948. At 723 K and 823 K, tested at a strain rate of $3.10^{-3} s^{-1}$.

The fatigue lives at 550 °C (823 K) are shorter than at 450 °C (723 K) and the fatigue life of welded joints is about half that of plate metal.

The effect of irradiation on fatigue life of plate metal increases with increasing temperature and fluence. At 450 °C there is,

however, no effect of irradiation on cyclic life. Crack initiation of irradiated and unirradiated specimens is clearly transgranular.

At 550 ^{o}C and after irradiation to $5 \cdot 10^{20}$ n/cm^2 (E > 0.1 MeV) the fatigue life was about 20 % reduced and the scatter was significantly increased. This is due to subsurface local intergranular cracking events. The results gained with 1.4948 fit well into U.S. results on steels 304 and 316 (Fig. 7).

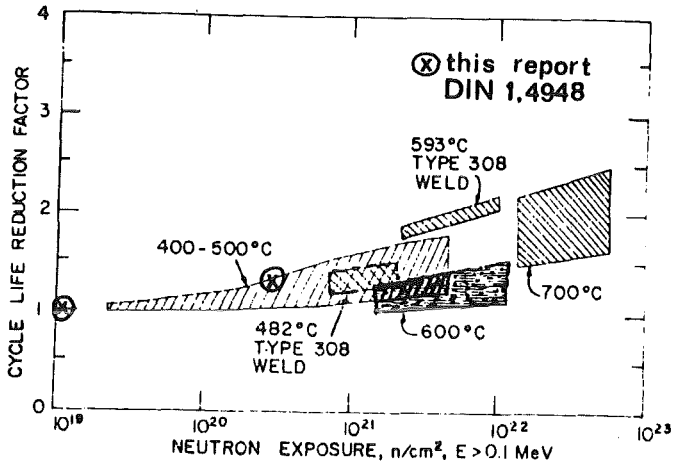

Fig. 7 Reductions in low cycle fatigue life of Type 304 and 316 stainless steel as affected by neutron exposure.

Figure from Michel, D.J.

As already mentioned, an important issue is the interaction of creep and fatigue damage.

For analyzing this high-temperature problem, several approaches are possible (L.F. Coffin et al., "Time Dependent Fatigue of Structural Alloys - a general Assessment", ORNL - 5073, Oak Ridge Nat. Lab., USA, 1977).

The method specified by the ASME Boiler and Pressure Vessel Code is based on the summation of cycle and time fractions resulting in the so-called linear damage rule

$$\sum_{j=1}^{P} \left(N/N_f \right)_j + \sum_{k=1}^{Q} \left(t/t_f \right)_k = D$$

There are several ways possible to carry out reasonable accelerated laboratory tests. It is, however, still an open question which of those tests allows the best extrapolation to real long-term service conditions.

An approach which has found extensive application with AISI 304 and 316 is the hold time test. For austenitic steels hold times within the tension-phase of a LCF loading represent the most severe loading conditions and the strain-controlled variant, called "cyclic relaxation", has been selected for the study of the behaviour of steel 1.4948 in the unirradiated and pre-irradiated states. For this type of test the cycle fraction in the equation becomes $\frac{N_h}{N_f}$, with N_h and N_f being the number of cycles to fracture in a hold time test and in a pure cyclic test (zero hold time), respectively (at zero hold time $N_h = N_f$). For a treatment of the more complicated time fractions, see

W. Scheibe et al., IAEA - Specialist Meeting on Properties of Primary Circuit Structural Materials Including Environmental Effects, Bergisch-Gladbach, West Germany, 1977 (IWGFR / 22), p. 210. In strain controlled tests stress relaxation occurs during each hold period and it is no easy task to define the stress and the corresponding creep rupture time t_f.

Fig. 8 shows the influence of hold-time and temperature on the number of cycles to fracture.

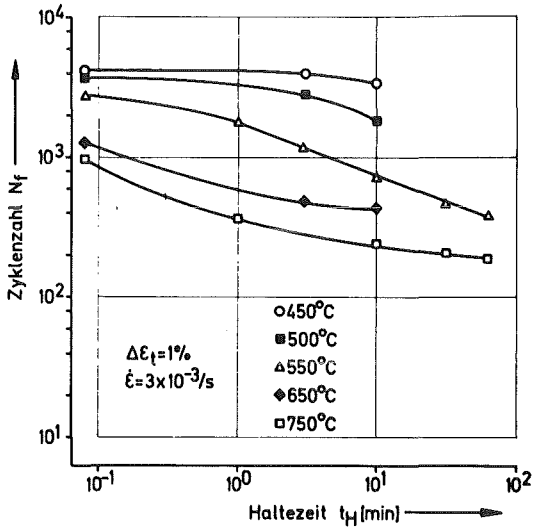

Fig. 8

It appears that the curves flatten out beyond a certain "saturation hold time".

In Fig. 9 a so-called interaction diagram is shown for 550 °C. The distance of the experimental rupture points from the design curve is a measure of the inherent safety factors. However, in actual reactor operation the strains will be smaller and the hold times will be longer which may lower the safety factors. Therefore more experimental and theoretical work is underway.

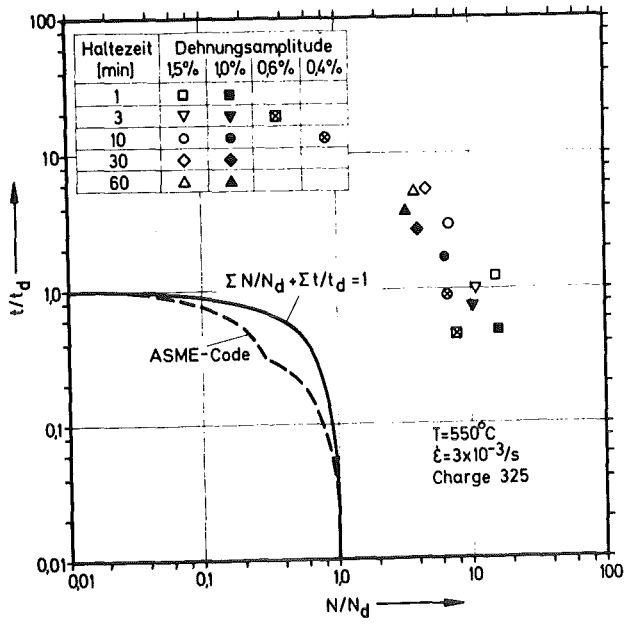

Fig. 9

Finally Fig. 10 shows the influence of irradiation on the hold-time behaviour. As is to be expected hold-times, leading to creep damage, cause a reduction of the cycles to fracture.

Fig. 10

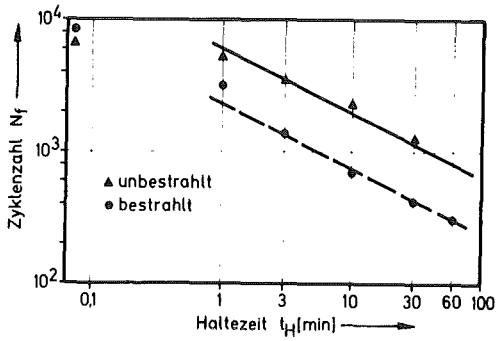

1.4948 $T = 550\,^{\circ}C$

$\Delta\varepsilon_t = 0.6\,\%$ $\dot{\varepsilon} = 3 \cdot 10^{-3}\ s^{-1}$

Fluence: $1 \cdot 10^{19}\ n \cdot cm^{-2}$, $E > 0.1\ MeV$

Especially for a loop type reactor with its extended primary tubing the question as to the possible failure mechanisms is an important one. If one can exclude a sudden fracture (instable crack propagation) then necessary safety measures can be minimized. A so-called "fail-safe" behaviour is exhibited if under most unfavourable operational conditions a crack nucleus grows until the tube wall is penetrated leading to a easy-to-detect sodium leckage. The crack length at the moment of penetration must be significantly smaller than the critical crack length for instable crack propagation ("Leckage-before-rupture"-criterion). Austenitic stainless steels (type 304, 1.4948, 316) have been shown to fulfill these requirements and, therefore, the above mentioned criterion

has already been acknowledged for several prototype reactors (including Superphenix, FFTF) by the regulatory commissions.

Literature to 4.4.4

B. van der Schaaf et.al., Radiation Effects in Breeder Reactor Structural Materials, Scottsdale, USA, 1977, p. 307-316

L.F. Coffin et.al., "Time Dependent Fatigue of Structural Alloys - A General Assessment", ORNL-5073, Oak Ridge Nat. Lab., USA, 1977

W. Scheibe, R. Schmitt, K. Anderko, IAEA - Specialists Meeting on Properties of Primary Circuit Structural Materials Including Environmental Effects, Bergisch-Gladbach, West Germany, 1977 (IWGFR/22), p. 210-218

R. Schmitt, W. Scheibe, K. Anderko, "Creep-Fatigue Interaction on 1.4948 Austenitic Stainless Steel, Including Irradiation Effects", Trans. 5th Intern. Conf. on Structural Mechanics in Reactor Technology, Berlin, Germany, 1979, Vol. L 12/7.

References to the sources of illustrations

(if not quoted in the text)

Page	Fig	Source
4	1)	
7	2,3)	
11	4)	Das Zustandsschaubild Fe-C. 4. Auflage.
12	5 (	Verlag Stahleisen mbH., Düsseldorf, 1961.
21	- (	
22	-)	
23	-)	
24	-)	
24a	-)	Physical Metallurgy Principles
25	9)	R.E.Reed-Hill, D.van Nostrand Co., 1973
44	-	
35	1	Constitution of Binary Alloys
38	3	M.Hansen, K.Anderko, McGraw-Hill, 1958, u. Supplements (R.P.Elliott, F.A.Shunk)
40	4	Ternäre Systeme, G.Masing, Leipzig 1949, Akad. Verlagsges.
41	-	
43	2	Metallographie, H.Schumann VEB Deutscher Verlag Grundstoffind., Leipzig, 10. Auflage, 1980
55	1-3	Metals Handbook (ASM) 9th ed., Vol. I
58	4)	Fundamental Aspects of Nuclear Reactor
64	- (	Fuel Elements, D.R.Olander, 1976.
65	-)	
71	1,2	Deutsche Risikostudie Kernkraftwerke, Verlag TÜV Rheinland, 1979.
80	6)	
81	7)	
82	8)	W.Debray, KWU-Erlangen,
84	9 (	Lecture at Dechema, Frankfurt/M, 1979
85	10 (	and Joint JEN-KfK-Seminar
86	-)	"Materials for Reactor Vessels and Components",
88	11)	Madrid, 1980
94	16)	

Page	Fig		Source
92	13,14	)	ASTM Standard Method, E 208-69
93	15	)	
107	25,26	)	Reaktorsicherheitstechnik, D.Smidt,
109	27	(	Springer-Verlag, 1979.
126	3	)	
113	28	)	
115	29	(	N.Wieling, KWU-Seminar, Erlangen, 1978.
116	30	)	
129	6,7	)	Creep, Viscoelasticity and Creep Fracture in
130	8	)	Solids, J.Gittus, Appl. Science Publ., London 1975.
131	1	)	
133	4	(	KfK-Bericht 1999, 1974.
134	5	)	
132	2,3		Reaktortechnik, D.Smidt, G.Braun, Karlsruhe, 1976.
139	-		Intern. Metals Reviews, Dec 1976.
144	5		S.S.Laidler et al., Radiation Effects in Breeder Reactor Structural Materials, Scottsdale, 1977.
183	1	)	B.van der Schaaf (ed.), ECN-4, 1976,
186	3	(	und ECN-61, 1979.
187	4	(	(Netherlands Energy Res. Found.)
188	5	)	
189	6	)	M.I.de Vries et al., ECN-67, 1979.
190	7	)	

PART II:

Nuclear moderator, absorber, shielding and coolant materials as well as nuclear fuels and fuel elements

K.R. Kummerer

A. MODERATOR MATERIALS

A.1. Survey on Moderator Materials

In thermal reactors the fast neutrons that are produced at the fission process are to be slowed down, this means, they have to loose most of their original kinetic energy. This slowing down process is performed by interaction with suitable materials, which are called moderators. As neutrons are not influenced by electrical forces, only a mechanical interaction can be effective, the most important process being the elastic collison between neutrons and moderator atoms. The energy transition in such a collision process depends primarily on the masses of the two collision partners. It is easily to be understood that only partners having equal or - at least - not too different masses are effective in this respect. This is the reason for the fact, that moderator materials are only to be found within the light elements at the beginning of the periodic table, e.g. in materials containing hydrogen, helium, lithium, beryllium, boron and carbon, the moderating efficiency decreasing with increasing mass number. Another important boundary condition for the selection of a moderator material is the absorption cross section for thermal neutrons, which has to be low enough with respect to the neutron economy of the reactor system.

If we consider the numerical values in Table A.1.I we have to drop the elements Li and B as potential moderator substances. On the other hand, the hydrogen isotope deuterium (abbreviation D) is in a top position. The absorption cross section of natural helium is also very low, the only contribution coming from the He-3 content.

To assess the nuclear properties of a moderator material quantitatively, the following definitions are introduced:

- The energy transition at the collision of a neutron with a moderator nuclide is described by the so-called "average logarithmic energy decrement" ξ

$$\xi = \ln (E_v/E_n)$$

where E_v, E_n is the neutron energy before and after the collision, respectively.

- The "slowing down power" BM ist dependent on ξ and also on the scattering potential Σ_s of the material

$$BM = \xi \cdot \Sigma_s$$

where the macroscopic scattering cross section $\Sigma_s = N \cdot \sigma_s$ is the product of microscopic scattering cross section σ_s and atom density N.

- The "moderating ratio"

$$BV = \xi \cdot (\Sigma_s/\Sigma_a)$$

additionally takes into account the reciprocal effect of thermal neutron absorption, $\Sigma_a = N \cdot \sigma_a$ being the macroscopic absorption cross section. Hence, BV is some sort of a quality number characterizing the practical usability of a moderator material.

The materials in gaseous state, hydrogen and helium, have a quite low slowing down power, as it is not feasible to increase too much the gas pressure and hence the atom density N. To overcome this limitation, hydrogen is only considered in the form of liquid or solid chemical compounds, e.g. water, organic compounds, metal hydrides. In case of the noble gas helium no such possibility exists.

The next Table A.1.II demonstrates for real moderator materials the properties and quality numbers introduced above. One realizes that helium also under high pressure does not present a sufficient slowing down power. The quality number BV is a misleading characterization in this special case.

There is some relation and similarity between the function of a moderator and the function of a reflector material. The reflector structure in a nuclear reactor has to impede the escape of

neutrons out of the reactor core, especially the loss of fast neutrons. For this purpose scattering processes in the reflector are necessary. Therefore, all moderator materials are applicable in reflectors. Above that, also good scattering heavy elements as e.g. nickel are suitable, because the energy transition at the interaction with neutrons is not relevant for the reflecting behaviour.

Table A.1.I: Neutron Absorption of the Light Elements

	Isotopic composition (NC = natural composition) (%)	Absorption Cross Section for Thermal Neutrons σ_a (barn)
Hydrogen	99,985 H, 0.015 D (NC)	0,332
	100 H	0·332
	100 D	0.00053
Helium	0,000138 He-3 99.999862 He-4 } (NC)	0,00735+)
	100 He-3	5327
	100 He-4	∿ 0
Lithium	7.5 Li-6, 92.5 Li-7 (NC)	70.7
Beryllium	100 Be-9 (NC)	0.0095
Boron	20.0 B-10, 80.0 B-11 (NC)	759
Carbon	98.90 C-12, 1.10 C-13 (NC)	0,0034

+) calculated value

Table A.1.II: Properties of Moderator Materials

	ξ	Σ_s (cm^{-1})	Σ_a (cm^{-1})	BM (cm^{-1})	BV
Natural Water	0.925	1.47	0.022	1.36	62
Biphenyl ($C_{12}H_{10}$)	0·812	0.88	0.00862	0.715	83
Zirconiumhydride (ZrH_2)	0.84	1.75	0.030	1.47	49
Heavy Water (∿ 99,75 % D_2O)	0.504	0.35	0.000036	0.18	5000
Helium at 100 bar	0.425	0.0022	0,00002	0.0009	45
Beryllium	0.206	0.76	0.0011	0.16	145
Graphite	0.158	0.38	0.00036	0.060	165

A.2 Natural Water

Natural water - which in reactor technology is also called "light water" - serves as a moderator material in many nuclear power reactors, the so-called "light water reactors (LWR)", and also in a variety of test reactors, e.g. in swimming pool reactors. In all cases, the water is simultaneously used as the coolant agent. As natural water has a quite low moderating ratio, in all LWR enriched uranium for fuel is necessary.

Water as a liquid material with its comparatively low boiling point allows only moderate operating temperatures. Further essential critical points at the technical application of this moderator are

- the corrosion attack on vessel and piping material,
- the radiolytic decomposition caused by reactor radiation.

Both effects - which appear, of course, in the same manner with heavy water - may be reduced substantially by excessive purification and proper conditioning of the water, but they cannot be suppressed completely. Hence an impurity level of, say, 1 ppm is considered to be the maximum tolerable limit.

The radiolytic decomposition of water results in a quite considerable amount of oxyhydrogen gas, the safe disposal of which is managed in the course of cover gas control.

Additional information on natural water is included in the forthcoming chapter C.3, where water is treated under the aspects of a coolant material.

A.3. Heavy Water

Heavy water in the pure form is the chemical compound D_2O between the hydrogen isotope deuterium D and natural oxygen. As it is very difficult to produce isotopically pure D_2O, always residuary amounts of light water are retained in industrial type heavy water. E.g., socalled heavy water of reactor quality has a D_2O content of, say, more than 99.7 mol-%. It should be recognized, that the residual light water in such a mixture of isotopes is not present in the form of H_2O molecules, but primarily as HDO according to the probability of formation.

Heavy water is in a top position concerning the moderating ratio compared to other moderator materials. Already slight impurities of H_2O diminish the quality substantially. Some of the physical and physico-chemical properties of D_2O are perceptibly different from light water. E.g. the density is higher by about 10 %, this fact being the reason for the name of the material.

The history of heavy water is strongly related to the development of nuclear physics and reactor technology. Deuterium was discovered in 1931 in the USA by Urey. In 1933, heavy water was separated and produced in pure form for the first time. In the following years, laboratory scale isolation was established as well as the production of kilogram amounts as a byproduct of industrial scale water electrolysis. After the discovery of nuclear fission in 1939 strong efforts came up for the technical production of tons of heavy water. Production plants were developed in Norway (Norsk Hydro), in the USA (within the military Manhattan project) and also in Canada. In 1952 the first large scale production began operation in the Savannah River Plant/USA, the capacity being about 500 tons per year. Since that time additional facilities in pilot plant and large scale were established mainly in Canada but also e.g. in India corresponding to the requirements of heavy water reactors.

The price of heavy water at the beginning of the fifties was in the region of 250 US-$ per kg dropping down to about 65 US-$

per kg by 1960. Presently (1982) the market price is again about 250 US-$ per kg.

There is a widespread natural abundance of deuterium: Every natural hydrogen compound contains about 0.015 % deuterium in the hydrogen component. Hence, natural water contains about 150 ppm D_2O, i.e. in about 7 m^3 of water there is 1 liter D_2O. It exists a slight variety in the D_2O content in water specimens of different origin, caused by meteorological influences within the water circuit in nature.

The physical and physico-chemical properties of D_2O and H_2O (i.e. natural water) are somewhat different, as it is demonstrated in Table A.3.I. Distinct and practically significant are the differences in density, in fusion and boiling point and in the heat of formation. Thus, it becomes understandable, that the chemical bonding with D is somewhat more stable than with H. The chemical reaction velocity of socalled deuterized compounds is a little bit smaller. The chemical equilibrium in H-D-mixtures is shifted in favour of the D-compound. This fact influences also the physiological compatibility in biological systems. In our present "H_2O-world", pure D_2O is a foreign body. D_2O is physiologically incompatible without being a poison in the real sense.

The recovery of heavy water is managed by different enrichment processes out of natural water, the general process scheme being outlined in Fig. A.3.1. In such a process the feed mixture F is separated into a light fraction L and a heavy fraction S. R means the atomic ratio of deuterium to hydrogenium:

$$R_F = \frac{D_F}{H_F}, \quad R_L = \frac{D_L}{H_L}, \quad R_S = \frac{D_S}{H_S} .$$

The efficiency of a separation process is characterized by the separation factor α, which is defined as follows:

$$\alpha = \frac{R_S}{R_L} = \frac{D_S \cdot H_L}{D_L \cdot H_S} .$$

In general, the separation factor does not depend on R_F, i.e. on the isotopic composition of the feed mixture. In Table A.3.II, the most important separation processes for deuterium enrichment are listed together with their separation factors.

In the course of the electrolysis of water, the D_2O is enriched in the residuum of the electrolytic cell. The very favorable separation factor on the one hand is to be compared with the high consumption of (costly) electrical energy. Hence, this process is primarily practicable in the highest steps of an enrichment cascade. An economically efficient operation requires the reflux of the continuously produced oxyhydrogen gas which is depleted in deuterium. The gas mixture is to be recombined to water and led back to the corresponding enrichment level of the cascade.

The destillation of water for D_2O enrichment is performed in rectifying columns, preferably under reduced pressure. This process requires energy in the form of low temperature heat only. Therefore, it is economically acceptable in spite of the low separation factor.

The chemical exchange processes are based on the shift of the chemical equilibrium towards the deuterized water, e.g. according to the following relationships:

- $H_2O + HD \rightleftharpoons HDO + H_2$

- $H_2O + HDS \rightleftharpoons HDO + H_2S$

The first mentioned water/hydrogen process is not used in technical application due to the fact that the catalyzers necessary for fast adjustment of the equilibrium are quite sensitive against humidity. The hydrogen sulfide process, however, does not require any catalyst. But H_2S is not available in unlimited amount for consumption in the process. Hence, it has to be recycled. Also in such a regime, a deuterium enrichment is possible due to the variation of the separation factor with temperature,

Fig. A.3.2. In the socalled hot-cold-regime - see Fig. A.3.3 -, the hydrogen sulfide releases deuterium to water within a cold counter current column and is reenriched in the following hot column due to the somewhat lower separation factor at higher temperatures. This H_2S-hot-cold-process is used in large scale, e.g. in the Savannah River Plant in USA, where it is realized for the enrichment up to about 15 % D_2O. A significant drawback of this process is the strong corrosion attack to structure metals and the enormous toxicity of H_2S.

In the last years, further chemical exchange processes with ammonia and methylamine proved to be technically and economically feasible. In both cases the deuterium has the tendency to be enriched in the organic phase.

The destillation of liquid hydrogen for deuterium enrichment makes use of a favorably high separation factor. It requires, however, the technological realization at extreme low temperatures. An operational scheme is sketched in Fig. A.3.4. At the enrichment of deuterium, there is to be applied an intermediate heating-up-step, because the primary compound HD turns over to H_2 and D_2 only at higher temperatures.

Gaseous diffusion and thermodiffusion were never applied in technical scale. In the field of thermodiffusion, there were substantial research work in the years around 1940 (separation pipe of Clusius and Dickel).

The determination of the D_2O content in heavy water is performed by mass spectrometry, infrared spectrometry and very subtle density measurements. An accuracy of, say, $\pm$ 0.002 mole % D_2O requires the density with a maximum error of $\pm$ 1 x 10^{-6} grams per cm^3. Another point of consideration is the shift in the oxygen isotopes parallel to the deuterium enrichment in aqueous medium.

There are also a lot of practical problems at the handling of heavy water:

- Heavy water is easily depleted in D_2O at any contact with the humidity in air. The same effect takes place in vessels,

containers and piping due to the molecular H_2O layers on the metal or glass surfaces. To avoid this problem it is necessary to "deuterize" the surfaces by multiple rinsing and drying.

- In a neutron flux, there is formed tritium T by the nuclear reaction $D(n,\gamma)T$. Tritium is the superheavy hydrogen isotope of mass number 3. It is radioactive and emits low energy beta radiation, half life about 12 years. Therefore, all biological systems are endangered due to their large water content and water exchange. In view of this fact, the maximum permissible amount of T in air and in water is very low. This has to be taken into account at the handling of heavy water that was already exposed to neutron flux in reactor operation.

Table A.3.I: Properties of D_2O and H_2O

	D_2O	H_2O
Molecular Weight	20.034	18.021
Density at 25 °C (g/cm^3)	1.104	0.997
Molecular Volume at 25 °C (cm^3)	18.139	18.074
Melting Temperature (°C)	3.81	0
Boiling Temperature (°C)	101.42	100.00
Temperature for Maximum Density (°C)	11.23	3.98
Viscosity at 25 °C (10^{-3}N s/m^2)	1.10	0.90
Index of Refraction at 20 °C for Na-Line	1.328	1.333
Dielectric Constant at 25°C	78.25	78.54
Heat of Formation (kJ/mol)	-296	-286
Ionization Constant at 24°C	$1.95 \cdot 10^{-15}$	$1 \cdot 10^{14}$

Table A.3.II: Enrichment of D_2O, Processes and Separation Factors

	Working Medium	Separation Factor
Electrolysis	Water	6 - 8
Destillation at 100 °C	Water	1.03
Destillation at 20 °C	Water	1.07
Chemical Exchange	Water/Hydrogen	2 - 4
	Water/Hydrogen Sulfide	1.7 - 2.6
	Ammonia/Hydrogen	2.5 - 5
	Methylamine/Hydrogen	2.5 - 5
Destillation at -253 °C	Hydrogen	1.81
Gaseous Diffusion	Hydrogen	1.20
Thermodiffusion	Hydrogen	1.052

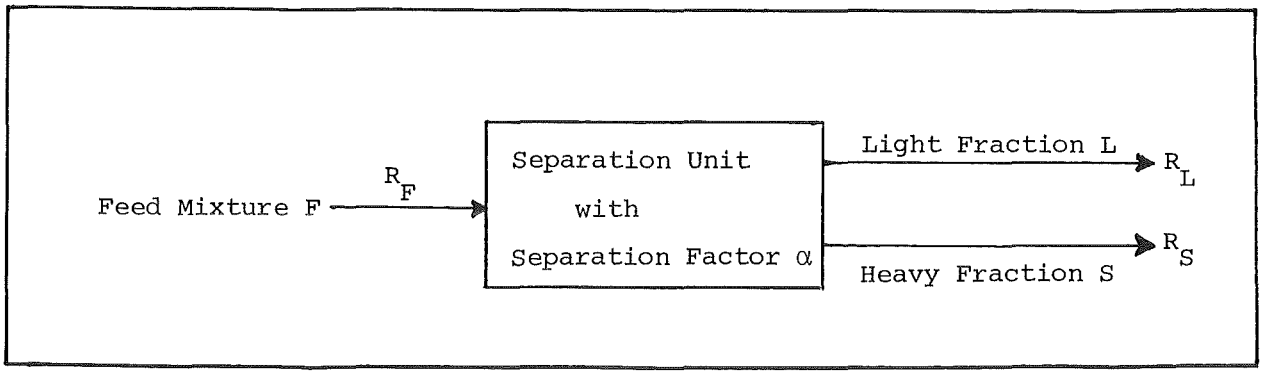

Fig. A.3.1: Enrichment of Deuterium, General Process Scheme

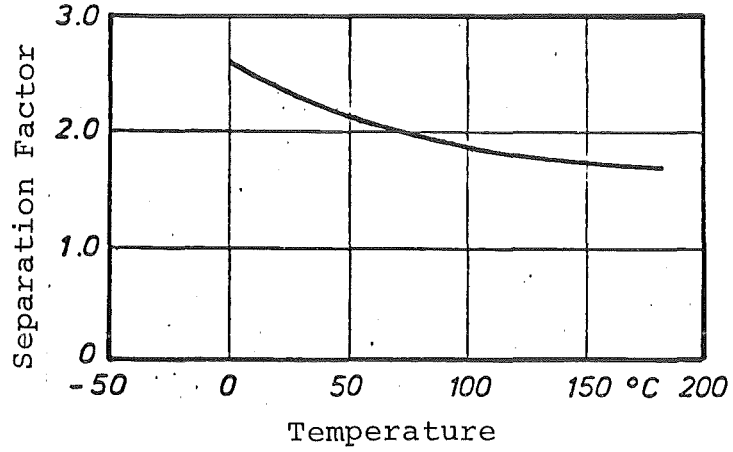

Fig. A.3.2:
Separation Factor in the H_2S/H_2O-System at 20 bar

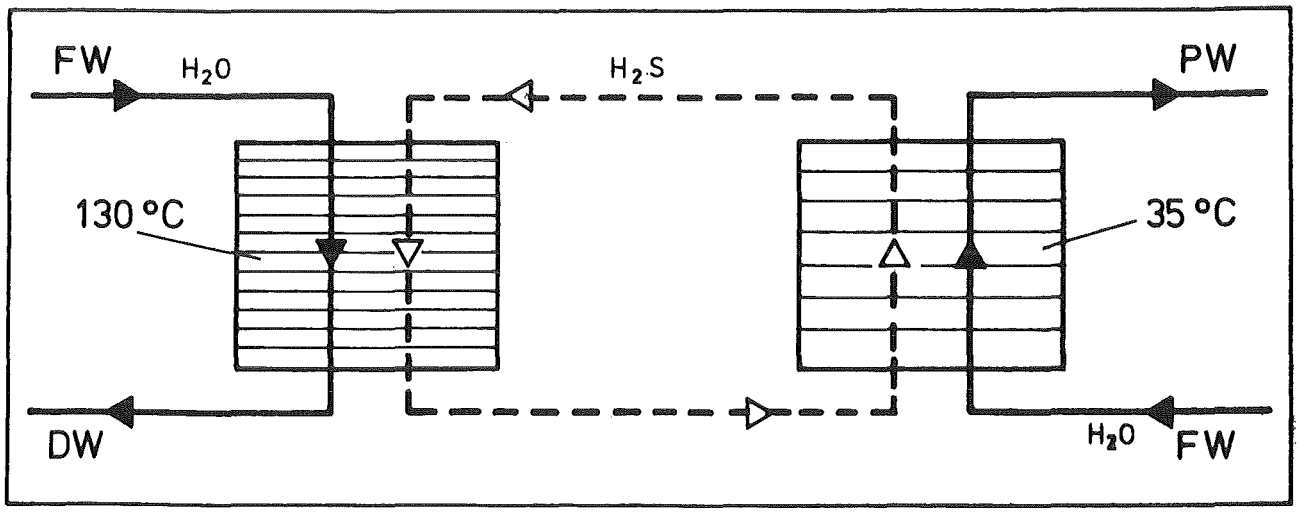

Fig. A.3.3: Hot-Cold-Process für Deuterium Exchange in Hydrogen Sulfide
FW Feed Water, DW Depleted Water,
PW Enriched Water

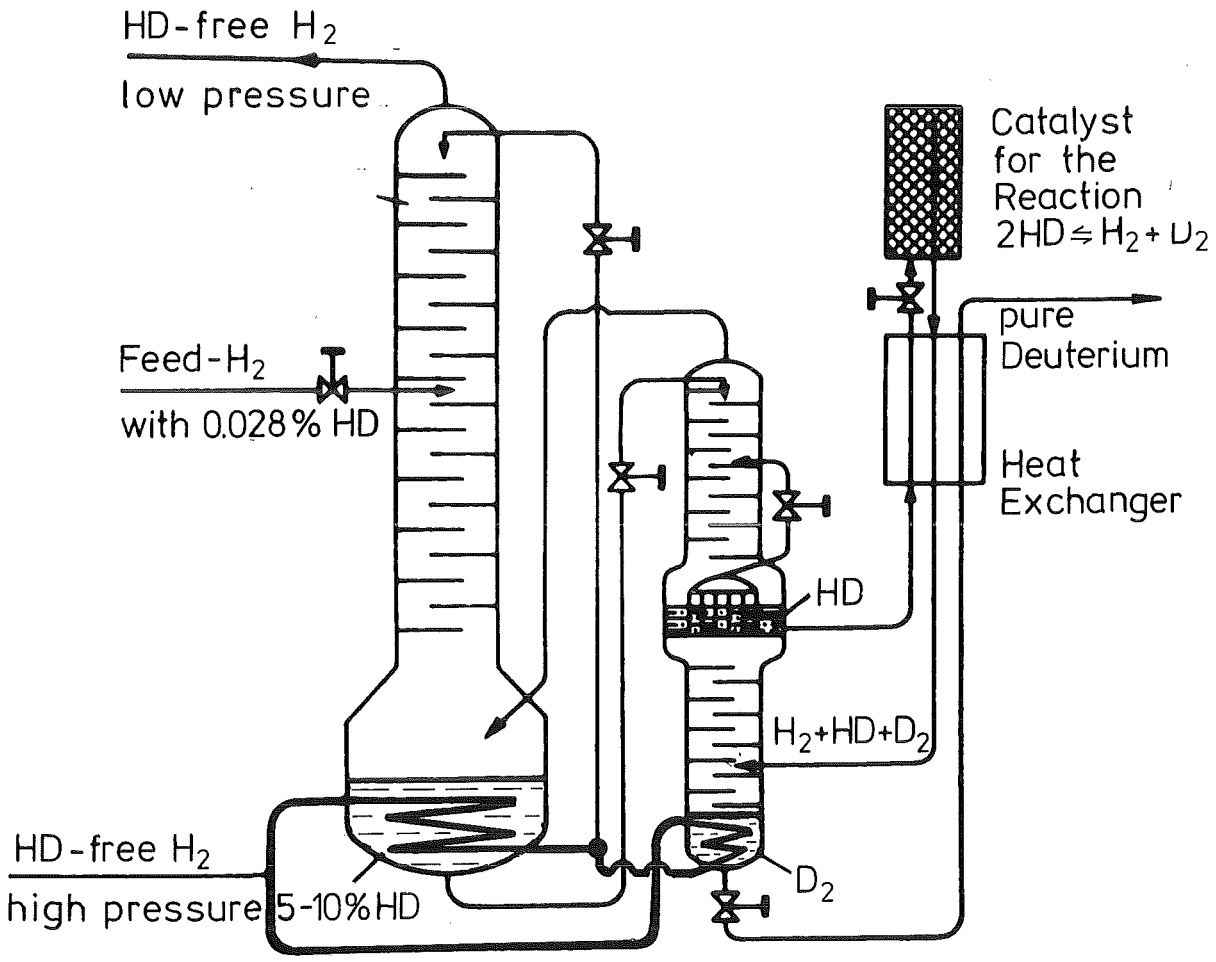

Fig. A.3.4: Destillation of Hydrogen, Process Scheme of Clusius and Starke

A.4. Other Hydrogen Compounds

For the employment of hydrogen containing materials as moderators the following viewpoints - in addition to the nuclear properties - are essential:

- Hydrogen density in the material
- Temperature limits of the physical condition
- Chemical stability in the relevant temperature level
- Stability against irradiation.

In Table A.4.I some significant data for hydrogen compounds are compiled. It is important to realize that in water and organic compounds also the relatively light nuclides C and O are contributing to the overall moderative effect, in addition to the hydogen atoms.

Out of the large number of organic compounds only a few were selected mainly considering the irradiation stability. In this respect the aromatic compounds are to be prefered, especially biphenyl and terphenyl due to the temperature range of liquid condition. Solid organic materials like paraffin and polyethylene are suitable at quite low temperatures only. They are used occasionally in the experiments in neutron physics.

A solid hydrogen moderator for high temperature is zirconium hydride. This material with an appearance similar to metals exhibits a rather high density in hydrogen. The hydrogen, however, is not bound very strongly in this compound, because there is a sensitive equilibrium to the hydrogen partial pressure in the gaseous environment. At 550 ^{o}C e.g., zirconium hydride with 61 at-% hydrogen (equivalent to $ZrH_{1.6}$) produces a partial pressure in H_2 of about 1 mbar. Zirconium hydride as a moderator was successfully tested in sodium-cooled prototype reactors up to temperatures in the region of 600 ^{o}C, e.g. in the Karlsruhe compact test device KNK I. The material is fully compatible with liquid sodium. The zirconium hydride blocks are canned with stainless steel sheets and there is an internal contact layer of sodium between hydride block and metal sheet in order to enhance thermal conductance. No corrosional interactions were observed.

All the hydrogen compounds exist, in principle, also with pure deuterium. There were already considerations to employ deuterized organic compounds for moderation. Economic calculations, however, prohibit definitely the practical application of such compounds in power reactor systems.

Table A.4.I: Hydrogen Compounds as Moderator Materials

	Composition	Physical Condition	Density (g/cm^3)	H-Density (g/cm^3)	Temperature Limits for Practical Use
Water	H_2O	liquid	1.0	0.11	below 100 °C at 1 bar up to 320 °C at 150 bar
Biphenyl	$(C_6H_5)_2$	liquid	1.01(90°C)	0.07	71 - 250°C at 1 bar
Terphenyl	$(C_6H_5)_2C_6H_4$	liquid	0.93(315°C)	0.06	up to 350°C at 1 bar
Paraffin	C_nH_{2n+2}, n=18-35	solid	0.9	0.14	below 50 °C
Polyethylene	$(CH_2)_n$	solid	0.95	0.14	below 100 °C
Zirconium Hydride	ZrH_2	solid	5.61	0.12	up to 600 °C

A.5. Beryllium as a Moderator Material

The element beryllium is a metallic material of low density and high mechanical strength. It exhibits excellent nuclear properties, especially a very low neutron absorption. In addition to that, the (γ-n)- and (n,2n)-reactions even support the neutron budget of a system. The essential properties of Be are composed in Table A.5.I. There are, however, some very important technological drawbacks in the behaviour of this metal, caused by the anisotropic crystalline form. This leads to marked texture formation in the course of fabrication. Above that, Be is quite toxic, especially in the form of little airborne particles that are unavoidable at machining. Furthermore, the metal shows some swelling under neutron irradiation, induced by the fast neutron (n,α)-reaction. The interaction with neutron leads to embrittlement, too.

Beryllium is gained out of the mineral beryl, which is a Be-Al-silicate, by chemical decomposition and fusion electrolysis. The careful purification is performed by vacuum melting. The fabrication of semiproducts is carried out by powder metallurgy mainly, because casting leads to coarse grain structure which is unsuitable for further processing. A typical composition of nuclear grade beryllium is written down in Table A.5.II.

Beryllium metal is used as a solid moderator in some material test reactors and also in submarine reactors. A very excellent application is featured in the Belgian reactor BR 2, where Be serves as a combined moderator and reflector material. The Be matrix in this test reactor is perforated by fuel and irradiation channels. Due to the material damage by neutrons, the Be matrix block must be replaced by a new one from time to time.

Besides the brittle and corrosion-sensitive Be metal, also beryllia (BeO) was taken into consideration. BeO is a ceramic material which can be shaped by powder-ceramic methods. Some of its properties are demonstrated in Table A.5.III. Quite conspicuous is the high thermal conductivity - see Fig. A.5.1 - which is higher than with common metals like iron. This is the reason for the endurance of BeO against thermal shocks.

While Be was promoted as a cladding material for gas cooled reactors in the early sixties, since about 1965 the further interest and development of Be as a reactor material is reduced to some few special applications.

Table A.5.I: Properties of Beryllium

Isotopic Composition		100 % Be-9
Nuclear Reactions		(γ,n), $(n,2n)$, (n,α)
Cross Section for Thermal Neutrons (barn)		0.01
Crystalline Form	α-Be	< 1250 °C: hexagonal
	β-Be	> 1250 °C: cubic body centered
Density (g/cm^3)	α-Be	1.84 at 20 °C
	β-Be	1.81 at 1260 °C
Linear Thermal Expansion of α-Be at 400 °C ($10^{-6}/K$)		$\parallel$ to the hexagonal axis: 15
		$\perp$ to the hexagonal axis: 18
Fusion Point (°C)		1285
Thermal Conductivity (W/m K)		125 - 170
Yield Strength at 20 °C (N/mm^2)		200 - 600

Table A.5.II: Composition of Nuclear Grade Beryllium Metal

	weight-%
BeO	0.9
Al	< 0.075
B	< 0.0002
C	< 0.10
Cr	< 0.01
Fe	< 0.075
Mg	< 0.03
Mn	< 0.012
Ni	< 0.02
Si	< 0.06
Be	> 99.0

Table A.5.III: Physical Properties of BeO

Crystalline Form	hexagonal
Crystalline Density at 25 °C (g/cm^3)	3.025
Fusion Point (°C)	2550
Linear Thermal Expansion ($10^{-6}/K$)	
for 25 to 100 °C	5.5
for 25 to 1000 °C	10.8
Thermal Conductivity (W/m K)	
at 25 °C	240
at 500 °C	65

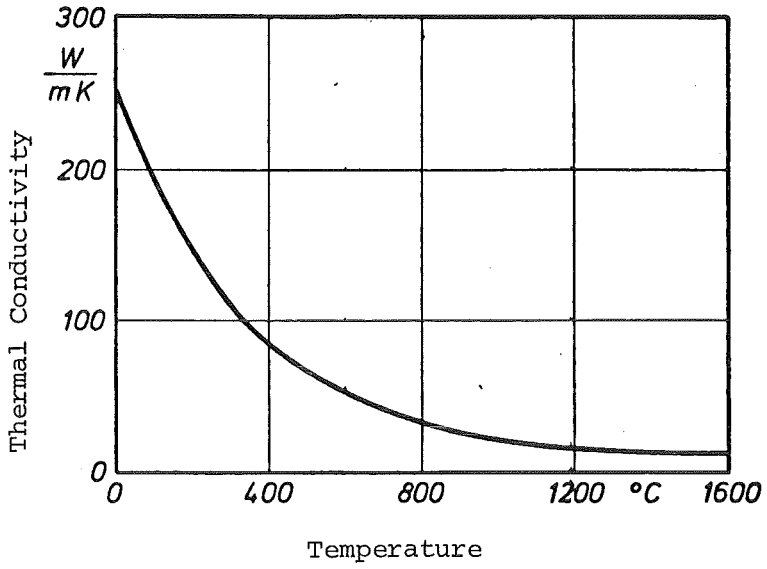

Fig. A.5.1: Thermal Conductivity of Sintered BeO with Density 2.8 g/cm^3

A.6. Graphite

One of the crystalline modifications of carbon, the graphite, is a material which is used in technology since a long time, e.g. for electrodes. The employment of graphite as a moderator material was suggested by the availability and especially by the quite low neutron absorption of technical graphite material. Already the first atomic pile in the world, the CP-1 in Chicago which became critical in 1942, was equipped with graphite as a moderator.

Pure carbon is distinguished by a very low absorption cross section for thermal neutrons. In the normally available technical graphite, however, there are a lot of high absorbent impurities as e.g. boron or rare earths. A boron content of 5 ppm e.g. doubles the neutron absorption of pure carbon. This fact initiated the development of special types of nuclear grade graphite, the absorption cross section of which is limited below a maximum of 5 millibarns.

The crystalline lattice of the graphite is a compilation of plane atomic layers and in these layers the carbon atoms are positioned within a hexagonal network, see Fig. A.6.1. The distance between the layers is substantially larger than the distance between the atoms within the layer. This anisotropic structure produces, of course, a marked anisotropy in some of the essential properties. Thus, in a graphite single crystal the thermal conductivity and the electrical conductivity exhibit high values parallel to the crystalline layers being in this direction comparable to a metal, while perpendicular to the layer planes the material behaves like a non-conductor. Vice versa, the thermal expansion parallel to the layers is almost zero, because the binding forces between the atoms are very strong in this direction. Perpendicular to the layers, however, there we have a rather high expansion coefficient.

This partly extreme anisotropy is substantially mitigated in technically formed graphite parts, but it still exists. In Table A.6.I a data comparison is shown between single crystal graphite and technical semiproducts. One realizes that the source material

and the production parameters are of some influence to the final material behaviour. Also the mechanical strength of a graphite part is correlated to the production routine and shows more or less anisotropy.

Graphite is a high temperature sustaining material. In general, the strength is even increasing with temperature. Also temperature shocks are sustained in a good manner. The chemical stability in air and carbon dioxide up to temperatures around 400 ^{o}C is excellent. Beginning at about 500 ^{o}C an oxide formation takes place. In contact to the cooling gas CO_2, there is an interaction according to the socalled Boudouard equilibrium:

$$C + CO_2 \rightleftarrows 2CO \quad .$$

This reaction with CO_2 normally becomes noticable above around 600 ^{o}C. Under irradiation in a reactor core, there is already a shift towards CO at lower temperatures.

Considering the origin of the source material for graphite production, one distinguishes socalled "artificial graphite" and "natural graphite". Natural graphite was found in some sedimentary deposits, e.g. in Sri Lanka, in U.S.A. and in Siberia. The minable material contains about 20 % graphite in the form of scale-like crystals up to dimensions of 1 mm. After separation and purification this graphite source material is mixed with an organic binder and pressed and hardened at 900 ^{o}C to pieces. Such semiproducts from natural graphite get always high density. The mechanical stability, however, is limited.

The production of artificial graphite ("Acheson-graphite") in most cases uses oil coke as source material. The crystallites in this coke have a dimension in the region of 50 Å. The fabrication scheme is drawn in Fig. A.6.2. The oil coke is gained by carbonizing heavy oil fractions. A simultaneous polymerisation and destillation at a temperature of about 450 ^{o}C leads to a crude coke containing about 95 % carbon (especially in benzene rings), up to 4 % sulfur and up to 2 % ash. The calcining of

this crude coke is carried out at about 1300 °C. At this temperature all hydrocarbons disappear and microcrystalline graphite is formed. After this, the material is milled and sieved. The powder particles differ more or less from ball shape due to the geometrical eccentricity of the single crystal. And these particles determine the anisotropic behaviour of the final product.

For the actual graphitation some coke powders of different grain size are mixed together at 150 - 200 °C with about 30 % pitch binder. This plastic conglomerate is formed to pieces by extrusion. In the course of this process, the crystallites get an orientation primarily parallel to the direction of extrusion. At forming by die-pressing the orientation becomes perpendicular to the direction of pressing. Afterwards, these green pieces are hardened by slowly up to 1000 °C increasing temperature. The pitch binder is polymerized between 300 and 500 °C. At this stage, large amounts of gases escape leading to a shrinking of the piece. If the final product is expected to get a density higher than, say, 1.6 g/cm^3, a special impregnation after the hardening step is necessary. For this purpose the hardened piece is immersed into hot pitch of 250 °C.

The final(and real) graphitation is performed within the electric furnace according to Acheson. The pile of green pieces is electrically heated up to temperatures between 2600 and 3000 °C within three to four days, the electric input being performed by graphite electrodes. In this period the graphite single crystals grow up to dimensions around 1000 Å supported by a catalyzing reaction with silicium. The effusing gases carry most of the impurities away. After that a slow cooling down period of about two weeks is followed. A final purification with halogen-containing gases leads to nuclear grade graphite, the residual impurities being e.g. 0.04 ppm boron and 0.005 ppm rare earths.

Normal graphite has a low tightness against gases. This can be improved markedly by impregnation with hydrocarbons.

The irradiation of graphite does not induce any ionization within the lattice, similar to the behaviour of a metal. Fast

neutrons, however, produce dislocations of C-atoms, the socalled Frenckel-defects. The dislocated C-atoms are primarily forced in between the layer planes, because there is available the largest space. In this manner, irradiation enlarges the distance between the layers, see Fig. A.6.3.

The dislocation of C-atoms to interstitial positions is accompanied by a storage of energy. This socalled Wigner energy initially increases with irradiation dose approaching, however, a limit value. This limit is the lower, the higher the irradiation temperature is applied. Fig. A.6.4.

The modifications within the single crystal due to irradiation cause macroscopic changes in the technical product. The strength of a graphite piece increases continuously accompanied by embrittlement. The "Wigner growth" perpendicular to the layer planes induces more or less anisotropic dimensional changes dependent on the grade of overall anisotropy of the piece. With technical graphite one has to take into account longitudinal growth up to 3 % perpendicular to the direction of extrusion. At higher working temperatures these elongations are reduced, some graphite types even shrink above 400 ^{o}C.

As a consequence of the lattice perturbations by neutron irradiation, the electrical and thermal conductivity decreases, because the free electrons partly lose their mobility within the lattice.

The developing of irradiation damage in graphite is continuously counterbalanced by a healing process, because the interstitials have a chance to move back into regular positions by further neutron knocks. This healing is favoured at higher temperatures, for higher thermal energies lower the potential barriers.

The Wigner energy may be piled up to a high level, especially within graphite reactors of low operation temperatures. This energy storage is a potential danger, as it may be released by a sudden temperature increase due to an operational transient. Therefore, with low temperature graphite reactors a careful healing-out procedure is necessary from time to time.

In modern graphite reactors, primarily electrographite is used. Large graphite configuration in and around the reactor core are compiled by single graphite blocks. The overall anisotropic dimensional changes can be minimized by a proper mode of compilation according to the anisotropy of the single blocks. To avoid the endangerment by stored Wigner energy a priori, the graphite temperature should be higher than 250 °C throughout the pile.

Table A.6.I: Properties of Graphite

	Single Crystal	Semiproduct out of	
		Oil Coke	Natural Graphite
Density (g/cm^3)	2.265	1.75	2.04
Thermal Expansion between 20 and 200 °C ($10^{-6}/K$) ∥	- 1.5	1-3	3.5
⊥	300	2.5-5	24
Thermal Conductivity ∥	> 350	200	
(W/m•K) ⊥	80	125	
Electric Resistivity ∥	0.05	1	1
(10^{-3} Ohm•cm) ⊥	5-10	1.5	5.5
Pressure Strength		35	20
(N/mm^2)		32	17
Sublimation Temperature (°C)	3650		
Absorption Cross Section for Thermal Neutrons (mbarn)	∿ 4		

∥ parallel
⊥ perpendicular
} to the main direction of the crystallites

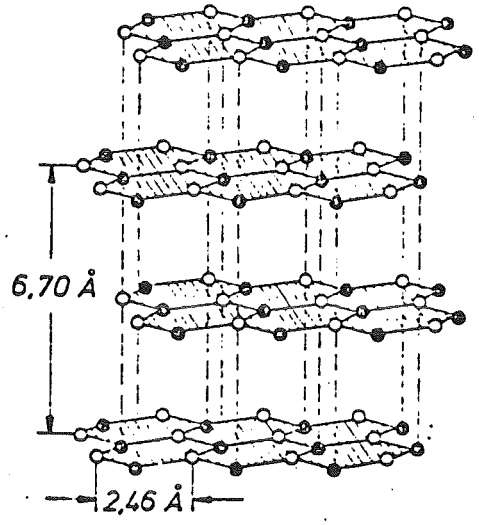

Fig. A.6.1:
Crystalline Lattice
of Graphite

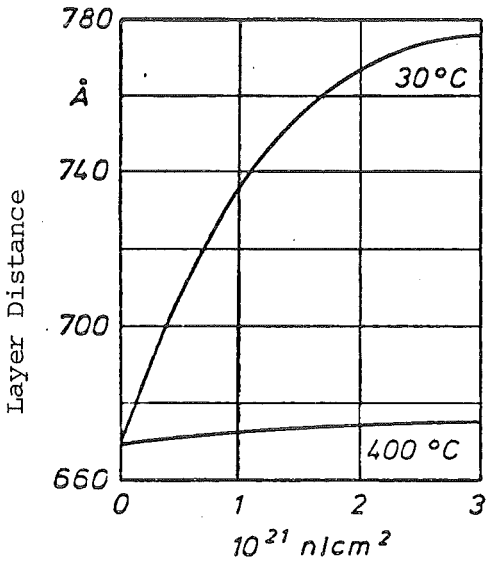

Fig. A.6.3:
Enlargement of the Layer
Distance by Irradiation

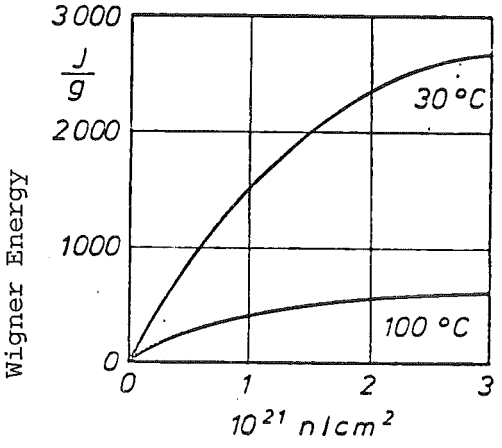

Fig. A.6.4:
Wigner Energy in Dependence
of Temperature and
Irradiation

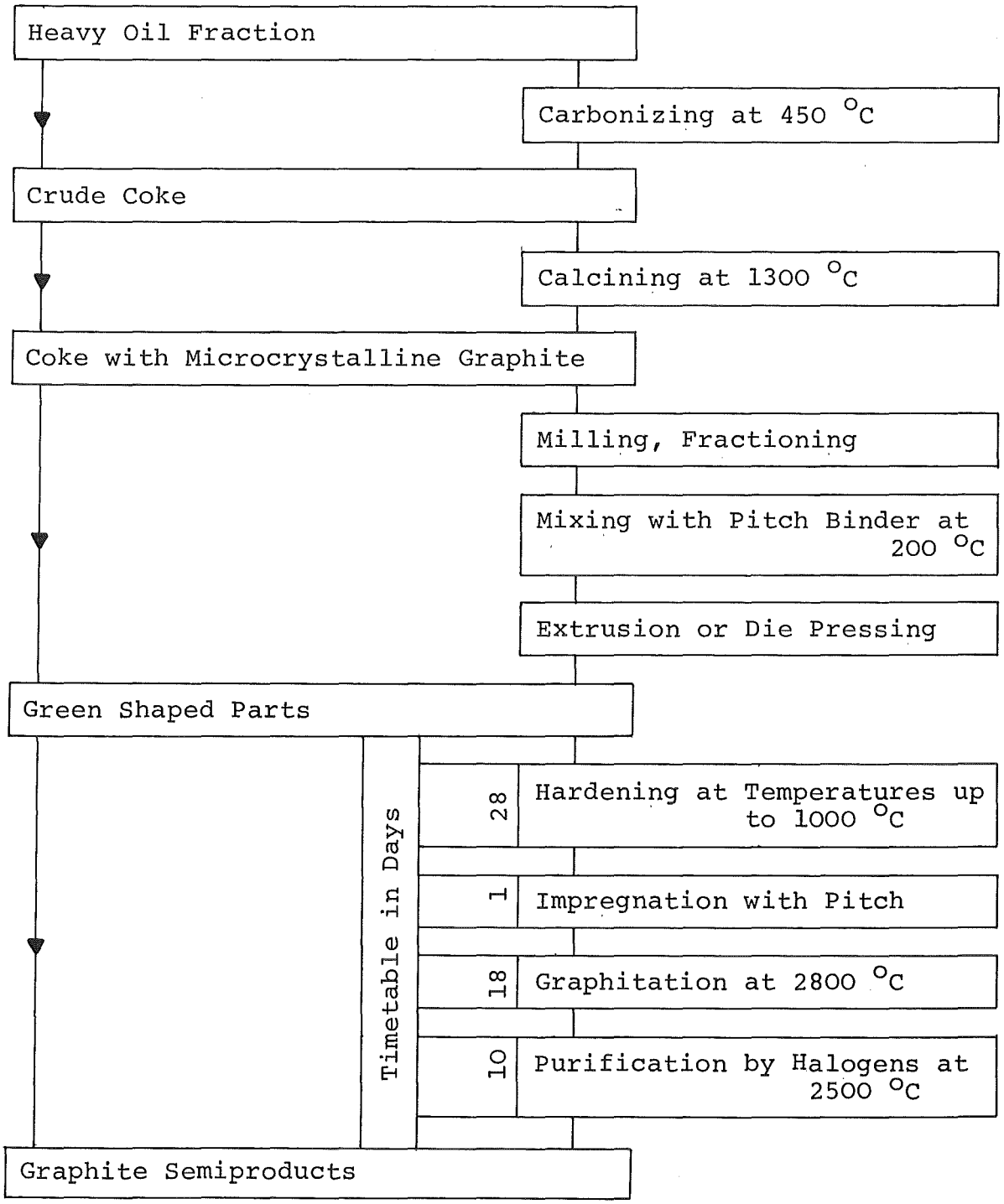

Fig. A.6.2 Fabrication of Artificial Graphite

B. NEUTRON ABSORBERS AND SHIELDING MATERIALS

B.1 MATERIALS FOR NEUTRON ABSORPTION

B.2 CADMIUM, INDIUM AND SILVER

B.3 BORON AND BORON-CONTAINING MATERIALS

B.4 HAFNIUM

B.5 RARE EARTHS

B.6 SHIELDING MATERIALS

B.1. Materials for Neutron Absorption

Neutron absorbing components are constitutive parts of a reactor core, mainly in the form of regulating or control rods, shim rods and safety rods. A further possibility for the longterm shimming of a reactor are homogeneous poisoning the liquid coolant and burnable neutron poisons in the fuel.

A first criterion for selection of a neutron absorber is the absorption cross section, which is extremely dependent on neutron energy. In order to get a first selection we take as a lower limit an absorption cross section of 60 barns for thermal neutrons. Hence, from all naturally occurrent elements there is a list remaining according to Table B.1.I. In addition to the thermal cross sections, the last column of this table contains the absorption cross sections for 100 keV fast neutrons. Out of this list only a few elements are really applicable for practical purposes. This is due to material properties like fusion point, chemical stability, availability and workability. Taking into account these practical viewpoints, a selection of materials according to Table B.1.II is remaining.

The mean kinetic energy of thermal neutrons is in equilibrium to the temperature of the surrounding medium, at 300 ^{o}C e.g. 0.05 eV. This low energy region is followed by the epithermal (up to some eV) and intermediary range. Many of the nuclides show here marked absorption peaks at discrete neutron energies, socalled absorption resonances. Further on the energy scale, there is the large range of fast neutrons, for which an energy of, say, 100 keV, is typical and often used for standardization.

The neutron energy distribution in a thermal reactor is widely spread into the epithermal range. Therefore, an absorber material is expected to exhibit a wide absorption spectrum. Additional important criteria are the type of the absorbing nuclear reaction and the succeeding nuclides. An absorbing reaction of the (n,α)-type produces finally helium, which can initiate damage and swelling within the absorber material, especially at higher

burnup. The expression "burnup" is used similar to the use for nuclear fuel, but the numerical figures are the dose of absorbed neutrons, expressed in n/cm^2.

In case the neutron absorbing reaction in an absorber material leads to a further nuclide of high absorption, the absorbing efficiency of the material remains more or less stable. Especially advantageous in this respect are nuclides which are followed by a chain of absorbing successors.

Table B.1.I: Elements with an Absorption Cross Section σ_{th} above 60 barns

Atomic No.	Element	σ_{th} (barn)	$\sigma_{100\ keV}$ (mbarn)
3	Lithium	71	1000
5	Boron	759	1600
45	Rhodium	150	490
47	Silver	64	440
48	Cadmium	2450	130
49	Indium	194	350
62	Samarium	5820	400
63	Europium	4400	750
64	Gadolinium	49000	400
66	Dysprosium	930	300
67	Holmium	67	950
68	Erbium	160	330
69	Thulium	103	650
71	Lutetium	108	1000
72	Hafnium	105	250
75	Rhenium	88	600
77	Iridium	440	300
79	Gold	99	300
80	Mercury	375	100

Table B.1.II: Selection of Materials for Neutron Absorption

Absorber Material	Suitable for Application in	
	Thermal Reactors	Fast Reactors
Cadmium and Alloys with Cd	X	
Boron and Boron Materials	X	X
Hafnium	X	
Rare Earths	X	X

B.2. Cadmium, Indium, Silver

Cadmium is a quite soft metal, that is often used in layers for rust protection. The fusion point is 321 °C. Therefore, this metal can be employed only at low temperatures. The pure cadmium metal - which is similar to zinc - is easy to be worked to semiproducts like sheets or pipes.

The natural Cd contains 8 isotopes of masses 106,108,110,111,112, 113,114, and 116. The relevant isotope for neutron absorption is Cd-113 with 12.3 % abundance and a thermal absorption cross section of 19910 barns. This cross section decreases rapidly above a neutron energy limit of 0.3 eV. There are no resonances in the epithermal range. The neutron absorptions is carried out according to the relation

$$^{113}_{48}Cd\ (n,\gamma)\ ^{114}_{48}Cd$$

with a subsequent gamma-emission.

While in former research reactors of low operation temperatures mostly pure Cd could be used as a neutron absorber, this is impossible with power reactors as because of the high temperature level. In LWR control rods, alloys with silver and indium primarily are taken. Above the stability against high temperatures, such alloys provide a widespread absorption spectrum, too, due to the resonances of Ag and In in the epithermal range, see Fig. B.2.1.

A standardized alloy for LWR application is based on the metal silver and has a composition of 80 % Ag, 15 % In, 5 % Cd. The alloy has a fusion point around 800 °C and is chemically stable in a water environment. The protection of the soft material against damage in the reactor is performed by a stainless steel cladding, e.g. in the control rods of a pressurized water reactor.

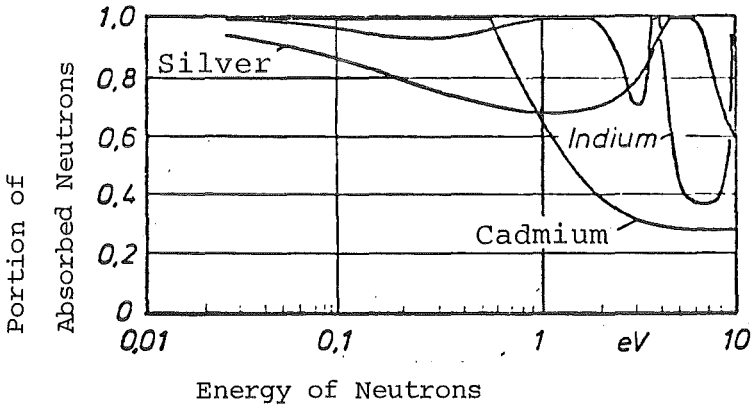

Fig. B.2.1: Neutron Absorption at about 5 mm Thickness

B.3. Boron and Boron-Containing Materials

The element boron with a fusion point of ca. 2050 °C is very hard and brittle and is - in pure form - not suitable for technical application. The natural boron is composed of two isotopes, namely 20 % B-10 and 80 % B-11, the isotope B-10 with a thermal neutron absorption cross section of 3836 barns being the decisive one. The neutron absorption takes place according to the relationship

$$^{10}_{5}B\ (n,\alpha)\ ^{7}_{3}Li.$$

As Li-7 does not absorb significantly, boron in a continuous neutron flux is burning out quite rapidly. Therefore, the material is better suitable for safety rods than for control or shim rods, which - at least partly - are continuously exposed to the neutron flux. A further successor with neutron absorption in boron (besides lithium) is helium. Especially, the He induces swelling of the absorber material, primarily at higher burnup. To increase the efficiency of boron absorbers, sometimes the isotope B-10 is enriched, e.g. up to 90 %.

The absorption cross section of boron decreases with increasing neutron energy in a mode which is reciprocal to the neutron velocity: Boron is a socalled 1/v-absorber. There are no resonances in the epithermal range. As Fig. B.3.1 demonstrates, the absorption for fast neutrons is still considerable. Besides that, the light element boron is moderating the fast neutrons quite effectively and, hence, can additionally act in this bypass. Therefore, boron is a standard absorber in thermal as well as in fast reactors.

The practical application of boron takes place in the form of boron carbide (possibly also boron nitride), furthermore as boron steel, borosilicate glass and boron-containing compounds and cermets:

- Boron carbide of composition B_4C has the highest boron density, fusion point around 2450 °C. The material is extremely hard and brittle and also very stable against

temperature and corrosion. Since a long time, B_4C is being used as a grinding material. It is very difficult to be worked and maschined. It is produced by melting in direct durrent. The crushing procedure afterwards delivers a sinterable powder or a coarse powder which is directly introduced in cermets. In absorber rods B_4C is contained either in form of sintered solids or as a vibrocompacted coarse powder.

- Boron nitride of composition B_3N is quite similar to B_4C, but is not used extensively in reactor technology up to now.

- Boron steel is an alloy that contains some few percents of boron. The absorption at a given thickness is strongly dependent on the total B-10-content as Fig. B.3.2 demonstrates.

- Borosilicate glass contains up to 12 % borontrioxide B_2O_3 and is used as absorber in pressurized water reactors. The glass pipes are enclosed in stainless steel, the free internal volume being available to the (n,α)-induced helium.

- Boral is a compound material - a cermet - in which B_4C is disperged within an aluminum matrix. These B_4C-Al-sheets or -plates are covered by thin layers of pure Al for protection of the internal mechanical mixture. Thus, the breaking-out of B_4C grains is impeded.

- Boron acid as a solution in the water circuit of a reactor is apt for a longterm regulation. The content in H_3BO_3 may be smoothly controlled via a slow continuous addition or removal (by destillation) in order to meet the reactivity status of the core.

- A newly developed material for fast reactor application is europium boride, see chapter B.5.

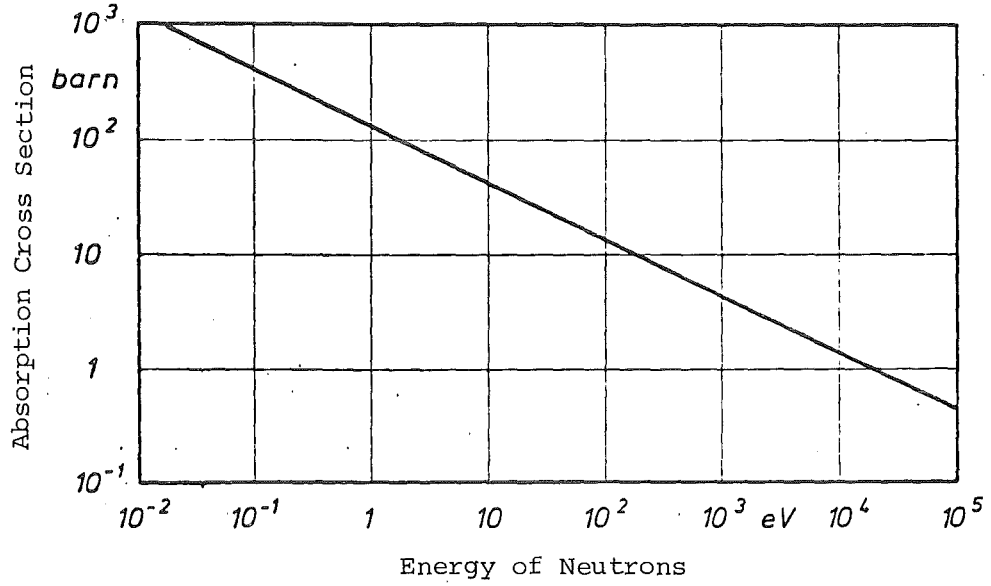

Fig. B.3.1: Neutron Absorption of Boron

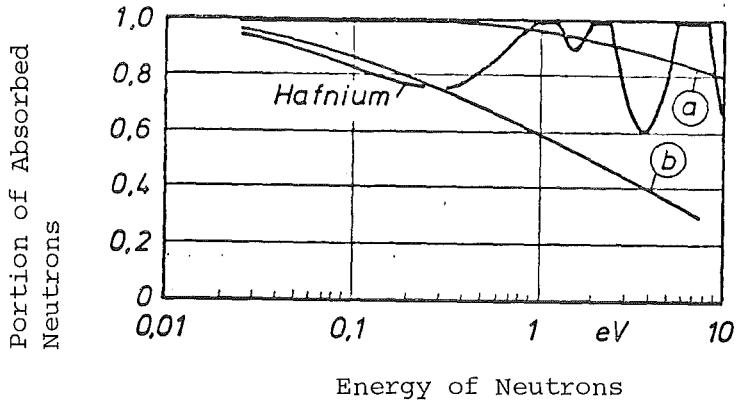

Fig. B.3.2: Neutron Absorption in 5 mm Thick Boron Steel Compared to Hafnium

- a) Boron Steel with 1 w/o B-10
- b) Boron Steel with 0.16 w/o B-10

B.4. Hafnium

Hafnium is a refractory metal, fusion point ca. 2200 ^{o}C. It is a by-product with the fabrication of zirconium. The available overall amounts are linked to the zirconium consumption and, hence, are limited.

The natural element hafnium, which is composed of 6 isotopes with mass numbers between 174 and 180, exhibits a wide absorption spectrum with resonances in the epithermal range, see Fig. B.3.2 in the preceeding chapter. The burnup in hafnium is very slow, too, due to efficient successors in the absorbing chain. On these grounds, hafnium is very suitable for shim and control rods, as their absorber materials is continuously exposed to the neutron flux.

The absorbing chain of the Hf isotopes is figured out in detail in Fig. B.4.1. One can realize, e.g., that the natural isotope Hf-177 may consecutively absorbe 4 neutrons up to the unstable Hf-181 which is quite inefficient in this respect.

Hafnium shows favourable mechanical and physical properties. The properly workable material is rather similar to zirconium. It is chemically stable in air and water. Hafnium can also be used for absorber purposes in the form of hafnium oxide.

Natural Hafnium				Absorption Chain	
0.18 %	174	390 b	n,γ →	175	unstable
5.2 %	176	38 b	n,γ →	177	370 b
18.5 %	177	370 b	n,γ →	178	86 b
27.2 %	178	86 b	n,γ →	179	45 b
13.8 %	179	45 b	n,γ →	180	13 b
35.1 %	180	13 b	n,γ →	181	unstable
Abundance	Isotope	Absorption		Isotope	Absorption

Fig. B.4.1: The Absorption Chains in Hafnium

B.5. Rare Earths

The rare earths are silvery metals, their preparation to pure form being quite difficult. Most of these very similar elements have a high absorption cross section for thermal neutrons. Up to now, only europium and gadolinium got some practical significance as a neutron absorber.

Europium consisting of the two isotopes Eu-151 (47.8 %) and Eu-153 (52.2 %) has a very wide absorption spectrum. Contrary to boron, the (n,γ)-absorption in Eu does not produce helium. Hence, no swelling of the material can develop. For the neutron absorbers in fast reactors it is intended to replace the boron absorbers by europium, totally or partly. For practical use, ceramic compounds like the oxide Eu_2O_3 or even the boride EuB_6 are envisaged.

The element gadolinium, in which the isotopes Gd-155 (14.9 %) and Gd-157 (15.7 %) are responsible for the extremely high absorption cross section, does not produce absorbing successors. Therefore, this element is suitable as a burnable poison. The newly specified fuel elements for LWR in most cases contain a few fuel pins with some percents of Gd_2O_3 in the UO_2. The mixture is to be properly adjusted so that during reactor operation the added absorption of burnable poison and developing fission products remain more or less constant.

B.6. Shielding Materials

The purpose of shielding materials in nuclear installations is to substantially reduce the intensity of radiation and - in many cases - to minimize the radiation to a very low level that is acceptable for biologic systems. From the different types of radioactive radiation only the penetrating species, i.e. the neutron- and gamma-radiation, are to be considered. The alpha- and beta-radiation (that e.g. in a reactor core exist simultaneously with neutrons and gamma's) are of short reach and are already totally absorbed by small layers of material.

The shielding of a reactor has to meet neutrons of different energy, e.g. thermal and fast neutrons, and gamma-radiation. In nuclear installations of the external fuel cycle (as e.g. reprocessing plant, hot cell, storage for used fuel) only gamma-radiation is existent.

The shielding design is functionally directed to the following items:

- The shielding of fast neutrons by direct absorption has a very low efficiency. The main shielding process is moderating by light elements followed by thermal absorption.

- The shielding of thermal and epithermal neutrons is performed by direct (n,α)- or (n,γ)-absorption.

- The shielding of gamma-radiation is effected by a high material density and, hence, by a corresponding wall thickness. The density of the material and the wall thickness are more or less reciprocal.

It is seen that different shielding materials act with selective efficiency. For a combined radiation, e.g. neutrons and gamma's out of a reactor core, material combinations are necessary for shielding. The design of a reactor shield distinguishes principally two sections of matter:

- The internal section, directly surrounding the core, is the "thermal shield", which reduces the radiation by a factor of about 100. Thus, in this thermal shield practically all the shielding heat due to the absorption processes is produced.

- In the external "biological shield" the radiation has to be diminished by some additional orders of magnitude to a biologically acceptable level (e.g. to a portion of 10^{-8} of the original radiation).

The practical requirements for shielding material, at first, aim for the shielding properties and, above this, for thermal conductance properties and finally for stability, endurance and fabricability. In Table B.6.I some practicable shielding materials are listed together with a qualitative assay of their efficiency.

The different materials are shortly characterized with respect to their application as follows:

- Steels (low alloyed and high alloyed) are the typical materials for the internal neutron and gamma shield of a reactor.

- Cadmium is - due to its low fusion point - suitable only for special purposes.

- Borated steel and Boral are high efficient neutron absorbers in the thermal shield, because they guarantee also a good thermal conductivity.

- Lead is very effective as a gamma absorber. This metal, however, is mechanically unstable and can be used at low temperatures only. In any case, a good heat transition out of the shield is necessary. Very pure lead con serve as a "neutron window" in experimental devices, because only the neutrons can pass.

- Leaded glass with lead content up to 30 w/o is suitable for gamma shielding in hot cell windows.

- Concrete is the typical material in the biological shield. It is hardly stable against heat. Concrete exhibits a combined efficiency against gamma radiation as well as against

neutrons due to the high materials density (compared to costs) and due to the relatively high content of crystal water. Extremely advantageous is the fact, that a concrete shielding can be fabricated on the construction site of the nuclear installation. Besides the normal concrete with a density of about 2.3, also special mixtures with additions of boron or socalled heavy concrete with additions of iron or barium minerals (magnetite, baryte) are employed.

- Water is an universal shielding material, too. In the LWR it forms the internal layer of the thermal shield. It is transparent also at a large thickness. Thus, in a storage pool for used fuel elements simple and safe manipulation is possible. Sometimes, also in hot cells liquid windows (water with additions of heavy salts) are used.

Table B.6.I: Materials for Shielding

Shielding Material	Efficient against		
	Thermal Neutrons	Fast Neutrons	Gamma-Radiation
Steels	X		X
Cadmium	X		
Boral	X	X	
Lead			X
Concrete	X	X	X
Water	X	X	X

C. REACTOR COOLANTS AND PROTECTIVE GASES

C.1 COOLANT MATERIALS, REQUIREMENTS AND SURVEY

C.2 GASEOUS COOLANTS

C.3 WATER

C.4 ORGANIC LIQUIDS

C.5 LIQUID METALS

C.1. Coolant Materials, Requirements and Survey

In the course of the operation of a power reactor the produced energy in the form of heat has to be removed out of the reactor core by a cooling medium. The heat release per unit volume in a nuclear reactor core is essentially higher than in a fossile plant, see the comparison in Table C.1.I. On these grounds, the cooling of nuclear reactors is a unique problem with respect to the design of the cooling circuits as well as with respect to the selection of coolant materials and the operation conditions.

The requirements for a cooling medium are based on conventional considerations according to the following items:

- Good heat transport properties, mainly thermal conductivity and specific heat per unit volume,
- Large temperature range, i.e. low fusion point and high boiling point,
- Thermal stability,
- No corrosion attack,
- Low energy consumption for circulation.

Additional requirements due to the conditions in a reactor core are:

- Low neutron absorption,
- Irradiation stability,
- No activation to radioisotopes (or at least only to isotopes with short half lives),
- Low mass number elements for moderation (in case of thermal reactors)
  or
- No or at least small moderation efficiency (in case of fast reactors).

For the practical application in the nuclear technology, three groups of coolants are to be distinguished, namely

- gaseous coolants,
- water and organic coolants,
- liquid metals.

Some years ago, there were also proposals, investigations and even experiments with other fluids like molten salts, e.g. Na-, K- and Be-fluorides. These salts have a fusion temperature in the region above 400 ^{o}C. A successful consequence in the sense of a real application in a reactor line, however, could not be drawn, mainly because of the extreme corrosion attack of these coolants on the structural material of the coolant circuit.

All the gaseous coolant materials are suitable as protective gases in hollow volumes, in-pile and out-of-pile. E.g., above the water surface of a D_2O moderated reactor, there is helium as a cover gas. The protective cover gas in sodium-cooled reactors may be argon. For the inertization of areas with sodium-filled equipment and piping often nitrogen is used.

Table C.1.I: Heat Release in Power Stations

	Heat Release in kW per Liter Core Volume
Fossile Power Station	∿ 1
Thermal Reactors with Gas-Cooling	1 - 5
with Water-Cooling	30 - 90
Fast Reactors with Na-Cooling	∿ 500

C.2. Gaseous Coolants

An important advantage of gaseous coolants is the fact, that there principally exists no limitation in the temperature range due to a phase transformation. The necessary pumping power in the circuit, however, is by far higher compared to a liquid, about by a factor of 10.

Some essential properties of gases (for cooling or for protective purposes) are compiled in Table C.2.I. Quite important is a high density and a high specific heat. Above that, a cooling gas should be chemically inert and resistant against irradiation. Mainly due to lack of irradiation stability,gaseous compounds with higher molecular weight cannot be employed.

In the first period of reactor technology, also air was used as a reactor coolant, mainly in reactors for military purposes. Besides the oxygen corrosion, the activation of argon to Ar-41 and the transformation of nitrogen to C-14 is very disadvantageous.

Nitrogen is suitable mainly as a protective gas, e.g. for inertization of empty volumes. It is not used within the reactor core. Nitrogen has a quite high neutron absorption which leads via a (n,p)-reaction to C-14, the last being biologically dangerous. There exists also the possibility that in-pile the very corrosive acid HNO_3 is synthetized.

Carbon dioxide has a high density and, hence, good thermal properties. The coolant gas - which is employed in the British Calder-Hall-type reactors - is stable up to about 600 ^{o}C, also under irradition. Above this temperature level, an increasingly perceptible transformation takes place, according to the relationship

$$C + CO_2 \rightleftarrows 2\ CO.$$

Above about 800 ^{o}C the CO-content is more than 10 %.

Dry Steam is the gaseous coolant in a conceptual reactor line which was developed on the basis of boiling water reactors. Dry

steam has very attractive cooling properties. A specific problem is the corrosive attack to stainless steels, which can only be controlled by a high nickel content in the structural material. In competition to the already introduced normal light water reactors, the dry steam reactor line was commercially not successful up to now.

Helium as a chemically and nuclearly inert medium is the given coolant for a high temperature reactor. An essential drawback are the high costs. Therefore, some special effort with respect to the tightness of the cooling circuit is necessary. Natural helium contains traces of He-3 which is transformed to tritium in neutron flux. This fact is to be considered in controlling leakages out of the circuit. At very high operation temperatures also some corrosive reactions may develop, which are caused by the very small, but unaviodable hydrogen and oxygen impurities in the helium.

Argon as a noble gas is also completely inert. The quite high neutron absorption and the transformation to Ar-41 favours the use as a protective gas only, e.g. in hot cells and in glove boxes for plutonium handling.

Table C.2.I: Gaseous Coolants

	Properties at 400 °C/100 bar				
	N_2	CO_2	Dry Steam	He	Ar
Density (kg/m^3)	49	80	38	8	77
Specific Heat ($10^3 J/kg\ K$)	1.13	1.21	3.10	5.20	0.52
Density x Spec.Heat ($10^3 J/m^3 K$)	55	97	118	42	40
Thermal Conductivity (W/m K)	4	3	7	28	3
Neutron Absorption Σ_{th} ($10^{-3}\ cm^{-1}$)	3.88	0.004	0.84	0.008	0.79

C.3. Water as a Coolant Material

The quite low boiling temperature of water under atmospheric pressure does not allow an economic operation of a steam turbine. Therefore, all power stations with water as a working medium utilize high pressure circuits. There are different types of water-cooled nuclear reactors. The extensively commercialized light water reactors (LWR) are built in two versions, namely the boiling water reactor (BWR) and the pressurized water reactor (PWR). With heavy water as coolant several versions of power reactors with pressure tubes, so-called pressure tube reactors, are in operation.

Water as a coolant material simultaneously acts as a moderator. It has good thermal properties, especially a uniquely high heat capacity. With respect to water corrosion, there are adequate materials available, the zirconium alloys and a variety of stainless steels. There is the problem of decomposition and irradiation, which was mention already in chapter A.2.

Typical cooling conditions are established for BWR and PWR as demonstrated in Table C.3.I.

Table C.3.I: Cooling Conditions in Light Water Reactors

LWR-Type	Pressure (bar)	Boiling Temperature (^{o}C)	Working Temperature (^{o}C)
BWR	70	286	265 - 286
PWR	158	346	291 - 326
Critical Point of Water	214.3	374.1	

C.4. Organic Liquids

The idea to use a special organic liquid as a reactor coolant stems from the fact that

- the boiling temperature is much higher than with water and, hence, no pressurization in the circuit is necessary,
- organic compounds are not (or less) corrosive against the structural material.

Organic compounds normally are not very stable at higher temperatures. Above 100 ^{o}C most of them decompose. Some aromatic hydrocarbons with benzene rings either in the main chain or in side chains show an exceptional behaviour. Within the group of such aromatic compounds the polyphenyls exhibit quite high boiling temperatures. Therefore, in conceptional designs and organic cooling experiments mostly biphenyl and terphenyl are employed. In these compounds in pure form, the high boiling point is always accompanied by a accordingly high fusion temperature. In order to get liquidization already at room temperature, special mixtures are selected, e.g. an eutectic mixture of biphenyl and biphenyl ether, called (with a US commercial name) Dowtherm A. The composition of Dowtherm A is

26.5 % Biphenyl $C_6H_5 \cdot C_6H_5$

73.5 % Biphenyl ether $C_6H_5 \cdot O \cdot C_6H_5$.

In Table C.4.I the relevant properties of Dowtherm A are listed in comparison to water. The specific heat as a typical coolant property is lower than with water, but the thermal conductivity is higher. Also the viscosity is higher, which influences unfavourably the pumping power.

The main and almost not solvable problem with organic coolants in reactor technology is the low radiation stability. Under irradiation, there continuously takes place a substantial decomposition and recomposition of organic matter leading to low molecular compounds (like H_2 and CH_4) as well as to high polymerized resins. On these grounds, a very effective purification

of the coolant during operation of the circuit is imperative. A special difficulty to be overcome is the blockage of heat transition areas by deposits of resins, the socalled "fouling".

Table C.4.I: Coolant Properties of an Organic Liquid Compared to Water

	Water	Dowtherm A
Fusion Temperature (^{o}C)	0	12.3
Boiling Temperature (^{o}C)	100	256
Vapor Pressure at 240 ^{o}C (bar)	33	0.7
Density at 25 ^{o}C (10^{3} kg/m^{3})	1.0	1.06
Specific Heat at 25^{o}C (10^{3} J/kg K)	4.18	1.59
Density x Spec. Heat (10^{6} J/m^{3} K)	4.18	1.67
Thermal Conductivity at 25 ^{o}C (W/m K)	0.60	1.38
Viscosity at 25 ^{o}C (10^{-3} N s/m^{2})	0.9	4.9
Neutron Absorption Σ_{th} (cm^{-1})	0.022	0.0008

C.5. Liquid Metals

Liquid metals are excellent heat transport media. They are thermally stable and completely insensitive to radiation, because the sensitive structure of the metallic crystal is not existent any more in the liquid state. Some problems arise with respect to the chemical affinity to air and water, which may induce violent chemical reactions. Liquid metals mostly are corrosive to structural metals, too.

The selection of suitable liquid metals or alloys is carried out considering primarily the fusion temperature and the neutron absorption. Both quantities should be low. There are a lot of elementary metals with fusion points up to about 300 ^{o}C. In addition to that, there are an immense amount of alloys, especially eutectic or near-eutectic alloys of two and more components with low fusion temperatures. Out of these alloys only a few can pass the selection criteria, because most of them contain the neutron absorber cadmium or another absorbing component. The practical consequence is that only Na-K-alloys and perhaps Bi-Pb-alloys are in further discussion.

Table C.5.I represents this selection of pure metals and binary alloys together with some relevant properties. An essential criterion is the activation potential in the neutron flux and the subsequent decay gamma radiation. The activation of bismuth to Bi-210 leads - via a beta decay - to Bi-210, an extensively alpha-active isotope.

The finally decisive criterion for the applicability of a low melting metal for cooling purposes is the question, whether or not there is available a resistant structural material for cooling components and piping. In most cases, at operation temperatures above about 400 ^{o}C - which is typical for liquid metal cooling - no commercial material is stable enough. The corrosion attack, especially the mutual solubility of the metals, limits drastically the life endurance of technical components.

Only for the alkaline metals sodium and potassium, there are suitable structural metals available, if special boundary conditions are met: The austenitic stainless steels and some nickel alloys resist corrosion up to temperatures above 600 ^{o}C, if the sodium impurities (mainly O, N, H, and C) are held within the ppm-range.

For practical application in a reactor cooling circuit only pure Na or a Na-K-alloy is being utilized. As the fusion diagram in Figure C.5.1 demonstrates, the fusion point decreases substantially with increasing K-content. The lowest fusion temperature, namely -12.3 ^{o}C, is reached at the eutectic alloy which is composed by 22.8 % Na and 77.2 % K. Besides the eutectic and the near-eutectic alloys, also alloys with higher Na-content are used, namely NaK-44 with 44 % K only and NaK-56 with 56 % K. In Table C.5.II the properties of some NaK-alloys compared to the pure metals are given.

Sodium and potassium are very reactive elements, K being even still more reactive than Na, according to its position in the electrochemical order. Also the NaK alloys are somewhat more reactive. For a survey, however, it is sufficient to consider Na to some more extent.

Na is spontaneously inflammable in air already at moderate temperatures (50 to 100 ^{o}C). At contact to water there is an abrupt chemical reaction. As protectives inert gases (He, Ar, and evtl. N_2) are to be used. Liquid sodium burns in any case at contact to open air. The reactive tendency is lower with different alcohols which are used for cleaning purposes.

Na forms alloys with many metallic elements, but not with Fe, Cr, and Ni. Iron, however, is soluble in liquid sodium, particularly if there are impurities present like Na_2O or NaOH. Liquid sodium may also penetrate into structural material to form solid solutions. This may lead to weld-type connections of structural components that are in mechanical contact.

Concerning the corrosion of materials in liquid sodium, different types of attack are to be distinguished. Contrary to water corrosion, in liquid metals no electrochemical corrosion effects take place. It is the dissolving attack that induces the unavoidable normal abrasion of surface material on the one hand, on the other hand an increased abrasion if O, N, H or C are present in the sodium. At the grain boundary corrosion the grain boundaries are dissolved selectively, hence weakening the mechanical properties of a structural part. Large difficulties may arise by the socalled mass transport which is based on the temperature dependent solubility of metallic elements in the sodium. This effect may also be triggered by a gradient in concentration, if e.g. an impurity in the liquid metal or a component in the circuit continuously traps the dissolved element. Finally, the corrosive erosion is a combined mechanical-chemical attack in which the chemical reactions are mechanically supported (e.g. by a too high flow velocity of the Na).

The corrosion in a stainless steel circuit and the mass transport from hot to cold parts remain within tolerable limits, if the oxygen content (or better the socalled oxygen equivalent formed by O, N, H, and C) is not higher than about 50 ppm. With refractory metals in the circuit, as e.g. vanadium base alloys, the oxygen content must be limited to 10 ppm. These extreme requirements in purity can be met only by a continuously working purification, e.g. in a bypass. In socalled "cold traps", where impurities like Na_2O are precipitated due to reduced solubility, an impurity level significantly below 100 ppm may be reached. For a level below 10 ppm additional "hot traps" with highly efficient getters are necessary.

There is already a lot of experience available with liquid metal circuits and their components. For low power loops, electromagnetic pumps (working without movable parts) were developed. Large circuits, however, use specially designed mechanical pumps. Special effort and care is necessary for the design of heat exchangers that arrange the energy transfer from liquid metal to water.

Table C.5.I: Liquid Metals for Cooling

		Fusion Temp. (^{o}C)	Thermal Conduct. (W/m K)	Properties at 600 ^{o}C: Density ρ (10^3kg/m^3)	Spezific Heat (10^3J/kg K)	$\rho \cdot c_p$ (10^6J/m^{3}K)	Neutron Absorption σ_{th} (barn)	Activation to	Half Life	Subsequent Emission α	β	γ
Mercury	Hg	-38,9	13	13.12+)	0.13	1.76	375	Hg-203	46.4d		x	x
Gallium	Ga	29.9	38	5.72	0.34	1.92	2.80	Ga-72	14.3h		x	x
Potassium	K	63.7	35	0.70	0.75	0.53	2.10	K-42	12.4h		x	x
Sodium	Na	97.8	63	0.81	1.25	1.02	0.53	Na-24	15.0h		x	x
Tin	Sn	232	33	6.71	0.29	1.97	0.63	Sn-121 Sn-123 Sn-125 Sb-125	27.0h 129.2d 9.6d 2.8a		x x x x	 x x
Bismuth	Bi	271	16	9.66	0.16	1.54	0.03	Bi-210 Po-210	5.0d 138.4d	x x	x	
Thallium	Tl	303	21	10.9	0.15	1.59	3.4	Tl-204	3.8a		x	
Lead	Pb	327	15	10.27	0.16	1.63	0.17	Pb-209	3.3h		x	
Na-K-Alloy with 22.8 % Na, 77.2 % K		-12.3	26	0.73	0.88	0.64	1.74	(according to Na and K)			x	x
Bi-Pb-Alloy with 44.5 % Bi, 55.5 % Pb		125	13++)	10.19++)	0.15++)	1.49++)	0.10	(according to Bi and Pb)		x	x	

+) at 200 ^{o}C, ++) at 400 ^{o}C

Leakages in sodium components and pipes cannot be completely excluded. Adequate provisions against sodium fires are necessary.

Table C.5.II: Properties of Na, K and NaK-Alloys

	Na	NaK-44	NaK-56	NaK-78	K
Potassium Content	0	44	56	78	100
Fusion Temperature (^{o}C)	97.8	18	6	-11	63.7
Volume Increase at Fusion (%)	2.6	2.5	2.5	2.5	2.4
Boiling Point (^{o}C)	881	825	812	784	758
Density at 20^{o}C (g/cm^3)	0.97	0.91	0.88	0.87	0.86
at 600^{o}C (g/cm^3)	0.81	0.77	0.75	0.73	0.70
Spezific Heat ($10^3 J/kg\ K$)	1.25	1.05	0.96	0.88	0.75
Thermal Conductivity at 600 ^{o}C (W/m K)	63	28	28	26	35
Viscosity at 600 ^{o}C ($10^{-3} N\ s/m^2$)	0.21	0.18	0.18	0.15	0.14
Neutron Absorption $\sigma_{100\ keV}$ (mbarn)	1.1	3.2	3.7	4.6	5.5

Fig. C.5.1:
Na-K-Fusion Diagram

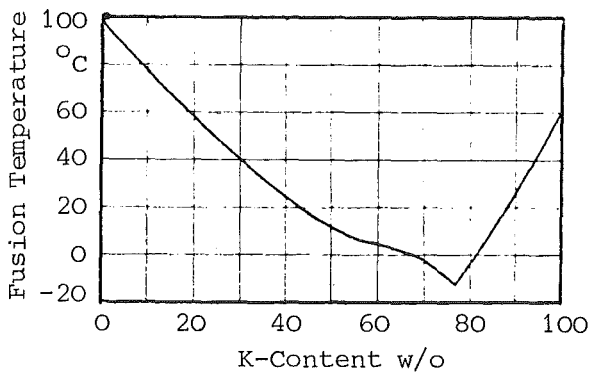

D. FUEL SOURCE MATERIALS

D.1. Demand for Fuel and Enrichment Services

All commercial nuclear power plants in the world presently are equipped with one out of three types of thermal reactors, namely with

- a gas-cooled graphite reactor (GGR) or
- a heavy water reactor (HWR) or
- a light water reactor (LWR).

The fuel for these reactor types is either natural or slightly enriched uranium.

Above that, there are many research and material test reactors that use highly enriched uranium. The utilization of thorium is restricted to high temperature reactors which are in a conceptual status in a few countries. Plutonium is required for fast breeder reactors, some such prototype reactors and power stations are already in operation or construction. Investigations and test irradiations for recycling plutonium into LWR are also in progress.

We concentrate here our deliberations to the demand of the commercial nuclear reactors. We have to distinguish between the primary demand of a reactor and the reload demand. This refers to the natural uranium source material and to the enriched uranium as well as to the enrichment services. The quantity for the enrichment is the "separative work unit SWU" (explained further in chapter D.4.).

In Table D.1.I a compilation of rough demand figures for power reactors is demonstrated. For a worldwide installed capacity at the year 2000 of - say - 1000 GWe, a yearly reload amount of about 150 000 tonnes of natural uranium is required. If this capacity is realized mainly by LWR the yearly reload requires more than 100 000 units of separative work. These figures do not include the first core equipment of the new reactors.

Assuming that by the end of the century fast breeder reactors will commercially penetrate the market, the consumption in natural uranium and separative work would stagnate with a further

tendency to fall, because the huge amounts of depleted uranium in the stockpiles of enrichment facilities could supply the needs for centuries.

Table D.1.I: Fuel Demand for Power Reactors

		1000 MWe Installed Capacity			
		GGR	AGR	HWR	PWR
Natural U	First Core (t)	1000	600	150	425
	Reload (t/a)	270	150	130	130
Enriched U	Enrichment (%U-235)	-	1,7	-	3
	First Core (t)	-	200	-	80
	Reload (t/a)	-	50	-	25
Separative Work	First Core (t SWU)	-	325	-	350
	Reload (t SWU/a)	-	80	-	110

D.2. Natural Occurrence of Uranium and Thorium

In the nature only long-living isotopes of Th and U occur. In nuclear technology, there is exclusively promoted the utilization of natural uranium, because this element contains about 0.7 % of the fissionable isotope U-235. More than 99 % in the element is U-238, which can serve as a breeding material only like the natural Th. Also some minor traces of U-234 exist. The isotopic distribution of U is equal in all deposits (with one exception), namely:

- 0.72 atom-% U-235 and
- 99.28 atom-% U-238.

The exception mentioned refers to a deposit in the African State Gabun, which was explored some years ago. The U-235 content in this deposit is markedly lower. The explanation may be, that in prehistorical time a naturally established nuclear chain reaction moderated by water took place forming a natural light water reactor.

Uranium is not a very rare element on earth. The earth's crust on average contains about 2.7 ppm U, which is more than for Ag, Hg or Cd. The main disadvantage in this connection is that there do not exist deposits with high U concentrations. A concentration of - say - 1 % U is already to be considered a rich ore.

There are to be distinguished primary and secondary deposits. Primary deposits include granite formations as well as ores with U as an accompanying element to basic metals. Secondary deposits are developed by surface weathering of primary deposed U followed by transportation in mechanical or dissolved form and final redeposition. In the secondary deposits U containing conglomerates, sandstone sediments, phosphate minerals or blackshale sediments may be found. Also fossile fuels like coal contain low amounts of U. Finally, very large amounts of U are dissolved in sea water, the concentration, however, being very low.

A compilation of the different types of deposits and the presently known resources in the western world is demonstrated in Table D.2.I. The main supply countries presently are USA, Canada, South Africa

and Australia. The mostly low grade ores in Europe (below 0.01 % U) are not worthwile to be mined under present conditions. Some higher grade deposits were found in France and in CSSR, the Bohemian pitschblende with its high U content became well known at the turn of the century when the phenomena of radioactivity were investigated. In South America as well as in other not thouroughly explored continents there are supposed to be large further resources.

The assured and estimated U reserves in the western world are presently calculated to be about 4 million tonnes. The recovery of these reserves is mainly a market and financial problem. While the U prices in the 1960'ties were in the range of 13 to 18 US-$ per kg of U_3O_8 raw material (yellow cake U_3O_8 with about 70 % U), the prices climbed up to about 100 US-$ per kg at 1977 followed by a reduction tendency to about 60 US-$ per kg (1982). At high U prices also the recovery out of low grade ores may become economical, in the future even out of sea water.

In all parts of the world, extensive prospecting and explorating activities are underway. Uranium deposits are identified at first by an increased level of gamma radiation induced by the isotopes of the U decay chain. The wide range prospection uses e.g. low flying planes that investigate large pieces of land by gamma monitoring. A roughly localized deposit is, of course, to be explored further for U concentration and total U amount by test drilling etc. There is to be distinguished between assured and estimated resources. Only the assured deposits are apt for a reliable calculation of the future U price. The time interval between prospection and practical utilization is about 8 years due to the long lead time for exploration and mining.

As U is chemically very active, this element exists only in the form of chemical compounds, mostly as oxide of the general formula U_xO_y. The following minerals are well known since a long time:

- Pitchblende — consists of the oxides UO_2, U_3O_8 in varying stoichiometric relation,
- Carnotite — is a mineral with K and V of composition $K_2O \cdot 2\ UO_3 \cdot V_2O_5 \cdot x\ H_2O$,

- Autonite is a mineral with Ca und P of composition $CaO \cdot 2\ UO_3 \cdot P_2O_5 \cdot x\ H_2O$.

The breeding material thorium is more frequent in the earth's crust than U, average 12 ppm. Up to now it was prospected not very much. The main resource presently is the mineral monazite, which mainly is composed by phosphates of rare earths and a minor percentage of Th. Monazite sands are available primarily in Brazil, India,Sri Lanka and USA. There exist also silicates with 50 to 70 % ThO_2, being named thorite and orangite. This minerals,however, are very rare.

Table D.2.I: Uranium Resources and Deposits

Deposit Type	Kind	Resources in	U-Content (%)	Total Amount (t U)
Primary Deposit	Granite	Solid Earth's Crust	10^{-4} to 10^{-3}	$\sim 10^{12}$
	Accompanying Element in Ores	South Africa, Namibia, USA, Canada, France	0.01 to $\sim$1	$\sim 10^6$
Secondary Deposit	Conglomerates	South Africa, Canada, Brazil, Australia	up to 0.1	$\sim 10^6$
	Sandstone Sediments	USA, Australia	0.1 to 0.2	$\sim 10^6$
	Black Shale Sediments	Sweden, USA	0.01 to 0.05	$\sim 10^6$
Solution in Water		Sea Water	$3 \cdot 10^{-7}$	$4 \cdot 10^9$

D.3. Recovery of Uranium

The uranium ore is gained mostly in surface mining. The first steps in ore processing are carried out directly at the mining site or nearby. It would be economically unbearable, to ship the ore (with a waste content of more than 99 %) over long distances. It is by far more advantageous to transport all chemicals (like acids or bases) necessary for the disintegration of the ore into the often quite remote places of an uranium mine.

The first goal of ore processing is extracting uranium concentrates, see Figure D.3.1. For this purpose, mechanical selection processes like e.g. flotation of crushed ore material are applied followed by solvent extraction with acids or bases. From these solutions the U concentrates are precipitated. These powdered concentrates contain 70 to 75 % U as uranate compounds. Due to their colour they are called "yellow cake" being the commercial product in the world uranium market.

At the nuclear fuel factory the yellow cake is converted to **nuclear grade U in technologically applicable form, i.e.**

- **sinterable UO_2 powder**
- **uranium metal as regulus or**
- uranium hexafluoride for the isotope separation.

There are different processes applied for the disintegration. In most cases the concentrate is dissolved in nitric acid followed by a liquid-liquid-extraction with tributylphosphate. The uranylnitrate remains in aqueous solution, while the impurities are separated in the organic phase. The so-called "ADU"-precipitation followed by thermal disintegration and reduction leads finally to sinterable UO_2-powder.

In order to gain U-metal out of UO_2 an intermediate step, i.e. the synthesis of UF_4 by treating the UO_2 with HF, is indispensable. This U-tetrafluoride subsequently may be reduced to pure U-metal by Ca or Mg. This "calciothermic" reaction is highly exothermic. Therefore, the reaction vessels are to be cooled properly.

The uranium hexafluoride UF_6 may be synthesized by an additional treatment with pure fluorine. All the chemical agents (NH_3, HF, Ca) taking part in the different steps of processing must be nuclear grade to maintain the level of chemical purity. This expression "nuclear grade" is not defined exactly. It means mainly that the neutron absorbing impurities (e.g. B, Cd, Rare Earths) must be held within a very low level - say - below 1 ppm boron equivalent. This "boron equivalent" of a neutron absorbing nuclide is equal to a boron content of equal neutron absorption.

The residual impurities in U or UO_2 as a source material for fuel elements are strongly specified, e.g. to a maximum of - say - 2000 ppm total amount and 1 ppm boron equivalent.

	U-Content
Uranium Ore	$\geq$ 0.1 %
Mechanical Segregation Extraction with Acids or Bases	
Uranium Concentrate, Yellow Cake	70 to 75 %
Dissolving in HNO_3	
Uranylnitrate $UO_2(NO_3)_2$+Impurities	70 to 75 %
Extraction with Tributylphosphate "TBP"	
$UO_2(NO_3)_2$ in Aqueous Solution	nuclear grade
Precipitation with NH_3 (or with H_2O_2)	
Ammoniumdiuranate "ADU" $(NH_4)_2U_2O_7$	nuclear grade
Thermal Disintegration by Calcining	
Oxide Mixture UO_3 + U_3O_8	nuclear grade
Reduction with Hydrogen at 700 ^oC	
Sinterable UO_2	nuclear grade
Hydrofluorination with HF	
Uraniumtetrafluoride UF_4 $(+F_2 \rightarrow UF_6)$	nuclear grade
Reduction with Ca (or with Mg)	
Uranium Metal	nuclear grade

Fig. D.3.1: Process Scheme for the Production of Nuclear Grade Uranium

D.4. Uranium Enrichment

The mixture of U-isotopes in nature with a content of about 0.7 % U-235 is sufficient for fuel only in graphite- and D_2O-moderated thermal reactors. In LWR an isotopic enrichment up to 2 - 4 % U-235 is necessary. For fuel elements in research and material test reactors an U-235-content up to even 90 % may be required.

The enriched U is produced out of natural U by isotope separation. The technically applicable physical separation processes require a gaseous U-compound. The heavy element U forms such gaseous compounds with halogens below 100 °C. Especially the fluorine compound UF_6 (sublimation temperature 56.5 °C) is preferred, as the natural F consists of 100 % F-19 thus avoiding multiple mass compounds with U.

Three different separation processes are presently applied in large scale or are in advanced technological development, namely

- the gaseous diffusion process,
- the gas centrifuge,
- the separation nozzle.

In the single separation modules of a gaseous diffusion cascade, the UF_6 is pressed through a diffusion barrier made from sintered metal with very small pores. The diffusion rate for the light gaseous component with U-235 is larger compared to the heavier component with U-238. Hence, the exit (low pressure side) of a diffusion module exhibits a somewhat higher content of the light U-isotope.

The separation effect in a gas centrifuge is based on the mass difference in the centrifugal field. The primary result is an enrichment of the heavy component on the cylindrical wall of the vessel rotating with high speed. At the technical implementation of this process a longitudinal temperature gradient is superimposed the cylindrical wall. In this way, a gas flux near the internal wall surface in upward direction is induced complemented by a downward flux in the center of the rotating vessel. Thus, in the

lower part an enrichment of the light component is being built up and, in the upper part of the vessel volume, an enrichment of the heavy component.

The separation nozzle process also uses the separation by centrifugal forces: A high speed gas flux consisting of hydrogen or helium with some percents of UF_6 is forced into a circle course. A "cutter" separates the light and heavy fractions.

Fig. D.4.1 demonstrates schematically the basic features of these 3 separation processes. Essential points of view - especially also with respect to economics - are the separation effect of a single module, the necessary number of stages for the required enrichment, the investment costs and the energy consumption, see Table D.4.I.

The objectives of new separation methods are to lower the investment costs and the energy consumption. A very low energy consumption is reached with the gas centrifuge. Furthermore, it is possible to operate a gas centrifuge plant in relatively small units in an economic manner and to enlarge it on short term demand. On the contrary, a diffusion plant is economically feasible only in very large units. The separation nozzle seems to be in between, a major technical advantage being the fact that a separation unit which comprises many single nozzles does not include any moving part.

An isotope separation device consists of an enrichment section (the rectifier) and a depletion section (the stripper). In the interconnection between both the feed material - e.g. UF_6 with natural U - is introduced. The stripper in the device is necessary for an economic yield of U-235 out of the feed, depleting e.g. natural U substantially down to a tails assay of - say - 0.2 % U-235.

A separation unit is composed of separation stages, that contain many separation modules. Each stage supplies a specified separation step, the first stage of the rectifier e.g. from 0.72 to 0.73 % U-235. The lower stages in the rectifier near the feed

input have to handle a large mass throughput. At further stages the throughput is decreasing successively. In such a way, a cascade type configuration of separation modules is formed. Rectifier and stripper together form a double cascade according to the scheme in Fig. D.4.2.

Quite important for such a cascade is the "non-blending-condition", which requires, that the depleted fraction of a stage may be added only to the feed of a lower stage having the same U-235-concentration: In such an "ideal cascade" no entropy increase may take place due to blending of unequal isotope concentrations.

The effort necessary for gaining a specified end product, e.g. uranium with 3 % U-235, is called "uranium separative work". This separative work T can be divided in the portions for the enrichment and the depletion section U_P and U_W, respectively:

$$T = U_P + U_W$$

A quantitative treatment leads for the desired product amount P to the following relation:

$$T = P \cdot V(N_P) + P \cdot (c-1) \cdot V(N_W) - P \cdot c \cdot V(N_O)$$

where V(N) is the value function $V(N) = (2N-1)\ \ell n\ N/(1-N)$ and $c = F/P$ is the relative amount of necessary feed material; it can be expressed by the enrichment figures N_O, N_P and N_W for natural uranium, product and waste, respectively, to:

$$c = \frac{N_P - N_W}{N_O - N_W}$$

The separative work formally has the dimension of mass or weight, in practical use is the expression "kg separative work" or "separative work unit SWU".

In Table D.4.II a series of numerical examples for separative work and demand of natural uranium is listed.

The commercial material leaving the enrichment plant is enriched UF_6. If the feed material (in the form of natural UF_6) is supplied,

the customer is charged only with the price of separative work. 1 SWU costs presently (1982) about 160 US-Dollars, the tendency being unstable.

There is an increasing separation capacity world-wide. The US-plants for commercial enrichment have a capacity of about 2.5×10^7 SWU per year. This capacity can supply the demands of 250 LWR power stations with 1000 MWe. The continuously increasing number of LWR plants requires additional separation capacity in the future. Besides the also existing smaller diffusion plants in France, Great Britain and USSR, there are the following enrichment installations under construction or preparation:

- A large gaseous diffusion plant in France,
- a German-British-Dutch gas centrifuge capacity,
- a separation nozzle plant in Brazil,
- a separation plant in South Africa (UCOR-process),
- gas centrifuge plants in USA.

Table D.4.I: Qualitative Assessment of Separation Processes

	Gas Diffusion	Gas Centrifuge	Separation Nozzle
Single Separation Effect	small	large	medium
Number of Stages for Enrichment to 3 % U-235	ca. 1200	10 to 20	ca. 300
Specific Energy Consumption	large no potential for reduction	small	large reduction possible ?

Table D.4.II: Separative Work and Demand in Natural Uranium
Natural U: N_O = 0.720 mol-% (≙ 0.711 w/o)
Tails Assay: N_W = 0.20 mol-%

U-235-Content N_P in the enriched U (mol-%)	Natural U Demand F/P (kg per kg enriched U)	Separative Work t (SWU per kg enriched U)
0.72 (Natural U)	1.00	0.00
1.0	1.54	0.37
2.0	3.46	2.16
3.0	5.39	4.25
4.0	7.31	6.47
5.0	9.23	8.76
10.0	18.85	20.68
30.0	57.31	70.50
50.0	95.77	121.40
70.0	134.23	172.98
90.0	172.69	225.64
99.0	190.00	251.11

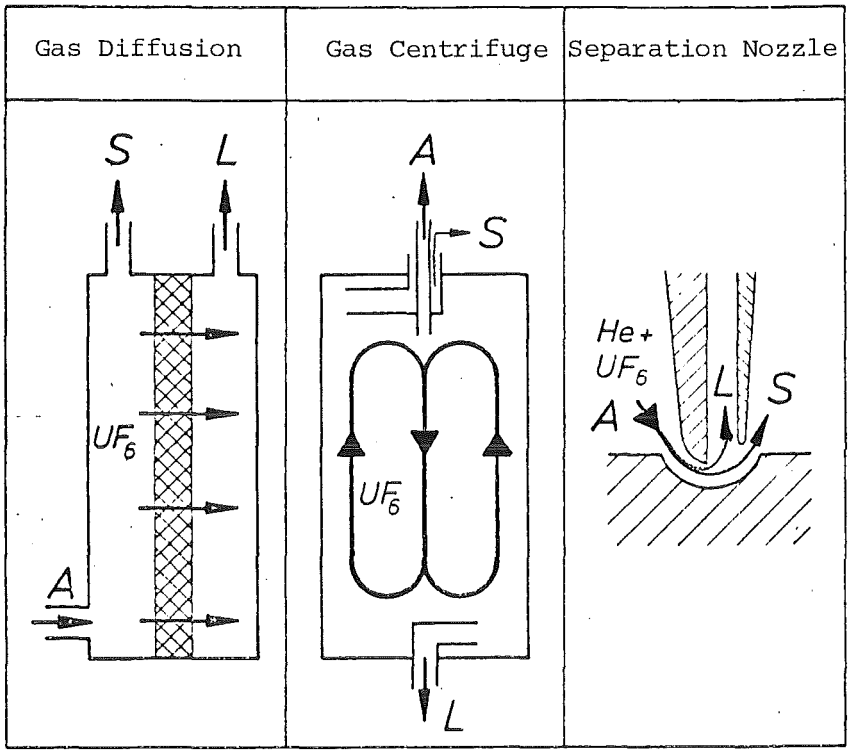

Fig. D.4.1: Separation Processes
A = Feed Gas, L = Light Fraction, S = Heavy Fraction

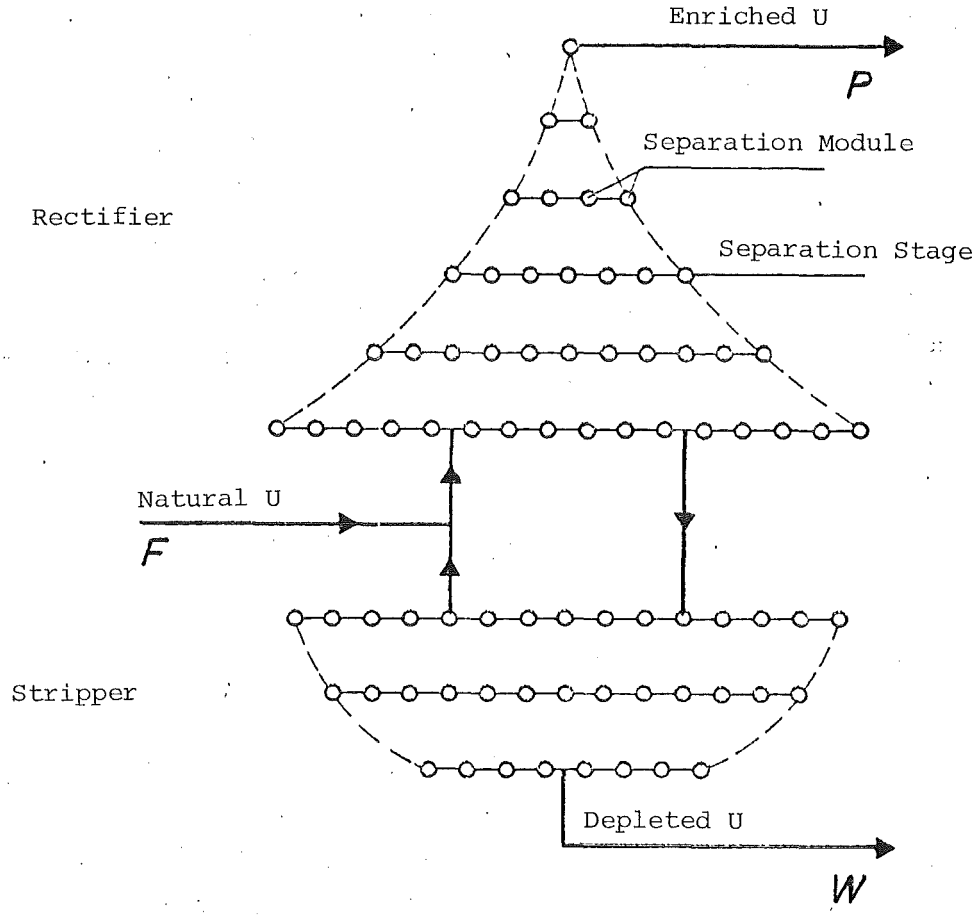

Fig. D.4.2: Scheme of an Enrichment Cascade

D.5. Plutonium Production and Separation

The element plutonium does not exist in nature. It is formed out of U-238 by the breeding process:

$$^{238}_{92}U + ^{1}_{0}n \rightarrow ^{239}_{92}U \xrightarrow{\beta} ^{239}_{93}Np \xrightarrow{\beta} ^{239}_{94}Pu$$

Therefore, irradiated uranium fuel contains Pu, the relative amount being dependent on burnup and conversion ratio. If e.g. in a reactor core, there is a conversion ratio of 0.5, then the fission

- of 1 % of the U-235 atoms should lead to 0.5 % Pu,
- of 10 % of the U-235 atoms should lead to 5 % Pu

in the irradiated fuel.

This quite simple picture, however, does not correspond fully to reality. For in the later operational phases also fissions in the Pu take place increasingly. Furthermore, some amount of higher Pu-isotopes is created according to the scheme:

$$^{239}_{94}Pu + ^{1}_{0}n \rightarrow ^{240}_{94}Pu + ^{1}_{0}n \rightarrow ^{241}_{94}Pu + ^{1}_{0}n \rightarrow ^{242}_{94}Pu$$

$$\downarrow \beta$$

$$^{241}_{95}Am$$

The halflife of Pu-241 is ca. 15 years, so that there is a sensible buildup of Am within relatively short time. Plutonium with a substantial content in higher Pu-isotopes (Pu-240 etc.) is called "dirty Pu". This designation was introduced as contrast to the "weapon grade Pu-239" which is desired for nuclear weapons. At an employment of Pu as reactor fuel the higher isotopes are practically of no detrimental influence.

There are produced increasingly substantial amounts of Pu. A large LWR power plant of 1000 MWe e.g. produces about 250 kg Pu per year.

The Pu is recovered out of the irradiated fuel in the course of reprocessing. In the technically and commercially matured

"Purex process" the pure Pu is gained in the form of Pu-nitrate after dissolution and separation from fission products and uranium, see Fig. D.5.1. This product in aqueous solution constitutes mostly the commercial form of Pu. Recently there is an increasing trend to produce the feed material for fuel fabrication directly at the reprocessing plant. For this intention, the oxalate precipitation process is applied leading to sinterable PuO_2 powder. A further rework to Pu-metal is - similar to the fabrication of U-metal - possible by taking the bypass over Pu-tetrafluoride.

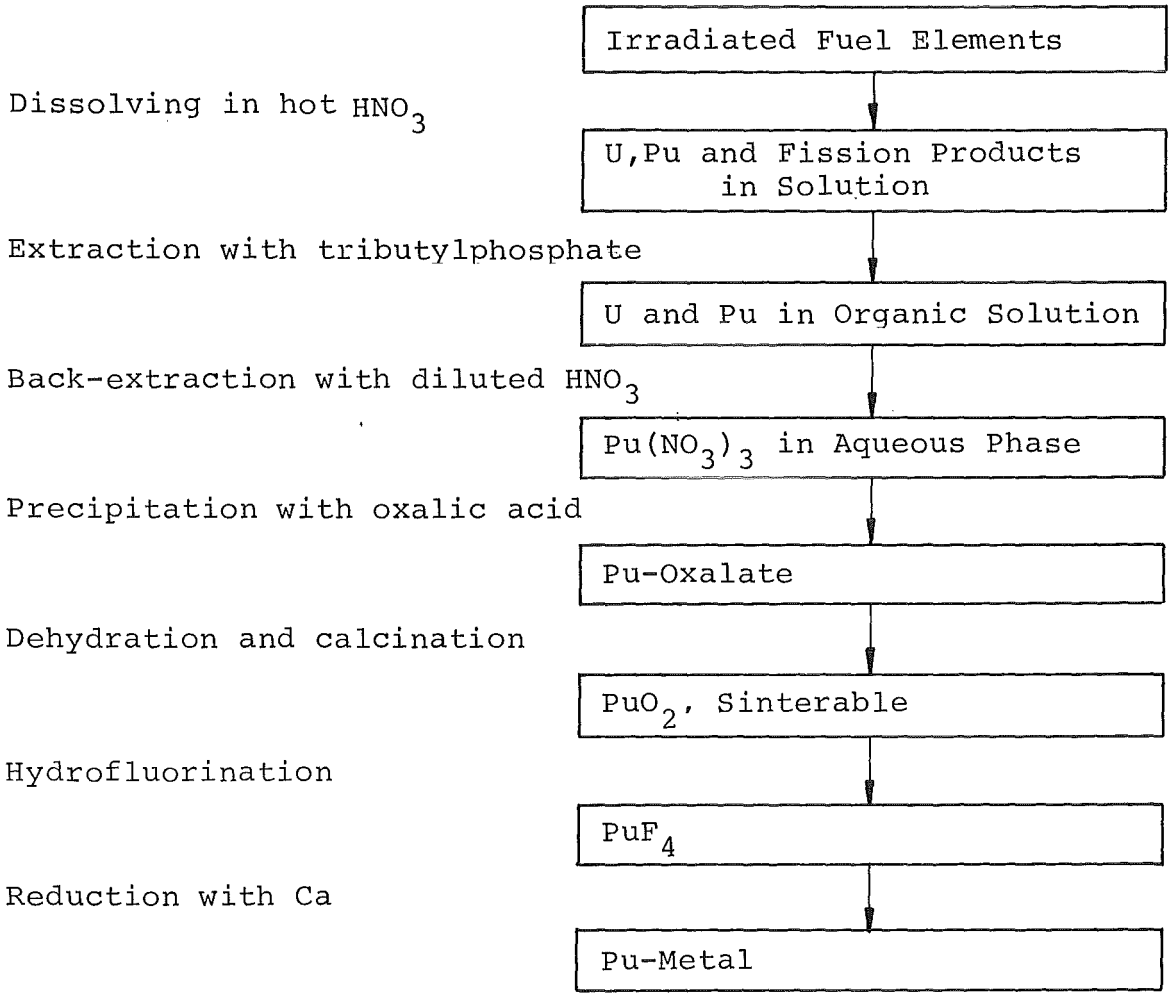

Fig. D.5.1: Recovery of Plutonium

D.6. Thorium and U-233

Source material for nuclear grade thoria or thorium-metal is monazite. Figute D.6.1 demonstrates the essential steps from monazite sand to the pure products.

The recovery process is quite similar to the U-recovery. The key intermediate product before final purification is Th-nitrate. For the reduction of thoria to the metal zinc chloride is introduced in order to get a low melting Th-Zn-alloy. Otherwise at the calciothermic reduction the melting point would not be achieved and the Th-metal would precipitate as powder. The separation of the Zn is easily performed by final destillation.

The artificial fissile nuclide U-233 is gained by breeding out of thorium. U-233 is present in irradiated Th-containing fuel and is disengaged in pure form in the course of the socalled "Thorex-process", see scheme in Figure D.6.2. This process is formally quite similar to the Purex-process. It leads to uranyl nitrate with U-233, which is further converted to oxide and metal. The Thorex-process is not yet verified and tested in technical scale. Special attention requires the buildup of U-232 - which is formed by a side reaction -,because this isotope initiates hard gamma radiation.

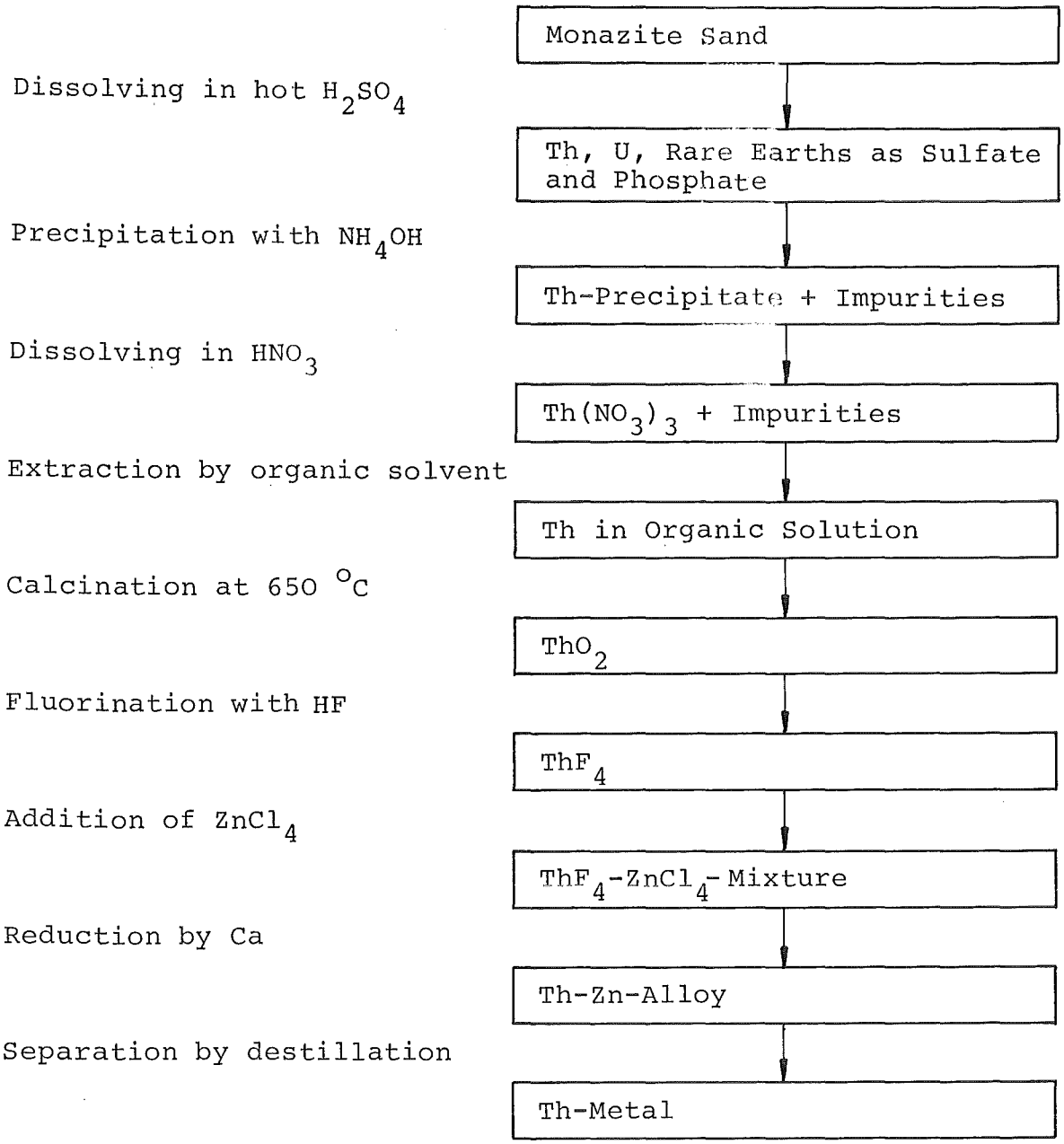

Fig. D.6.1: Scheme for the Recovery of Thorium

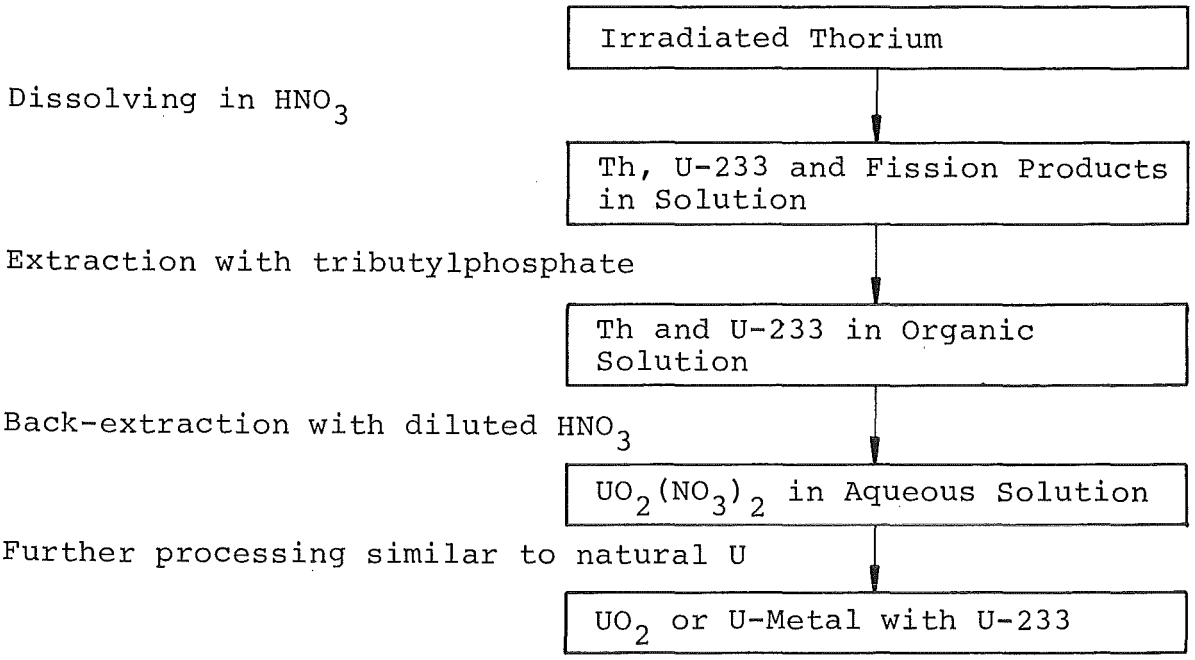

Fig. D.6.2: Scheme for the Recovery of U-233

E. FUEL TYPES AND FABRICATION

E.1. The Fuel Types in Research and Power Reactors

Principally there is to be distinguished between liquid fuel in homogeneous reactors and solid fuel in heterogeneous reactors. Nowadays only solid fuels are employed in power reactors and also - with very few exceptions - in research reactors.

The solid fuels may be subdivided into the following groups:

- Pure Metals and Alloys:
  for research reactors and CO_2-cooled power reactors as well as for early experimental fast breeders.
- Ceramic Compounds like oxide, carbide and nitride:
  Oxide for light and heavy water reactors, for AGR, for fast breeders, within the coated particles of high temperature reactors;
  Carbide also within coated particles and - possibly in the future - for fast breeders;
  Nitride has also some potential for fast reactor application.
- Metal-Ceramic-Compounds, Fuel Dispersions:
  for material test reactors and high flux reactors;
- Coated Particles:
  for helium-cooled high temperature reactors.

E.2. Survey on Fuel Properties

The basis for this survey and for comparison are the numerical data of some important material properties in Table E.2.I. The figures for ceramic fuel refer (if applicable) to 100 % dense material. This, of course, is the case for metallic fuel.

The density together with the heavy metal content defines the number of fissionable atoms per cm^3 and, hence, influences markedly the nuclear and thermohydraulic design of the reactor core. The density is slightly dependent on the isotopic composition which, however, is practically insignificant. Quite essential is for ceramic fuels the dependence of the density D from porosity P according to the relationship

$$D = D_{100}(1-P)$$

where D_{100} is the density of 100 % dense material, i.e. material of 100 % of theoretical density (≙ 100 % T.D.). The actual density of a ceramic mixture may be linearly interpolated from the figures of the components with sufficient accuracy.

The heavy metal density is, of course, highest at the pure metal and strongly reduced in compounds, see Table E.2.II.

The crystallographic form of the fuel metals is anisotropic at low temperatures, which induces macroscopic anisotropy. At higher temperatures also the metals change into cubic crystals. The ceramic compounds (except UC_2) are cubic face centered throughout the whole temperature range and, hence, isotropic.

The transition temperature designates the transition to another crystallographic form. At such a transition also the density of the material is altered.

The fusion point is the temperature limit, which governs the maximum permissible operation temperature. The latter is fair below this upper limit, the reasonable safety distance also taking into account hot spot considerations.

The thermal conductivity is a material property dependent on temperature. This property is responsible for the heat flux within the fuel and limits the maximum possible specific power of a fuel element. In Figure E.2.1 the quite different course of U-metal and U-ceramic is demonstrated. In addition to the temperature dependence, there is - for ceramic fuels - a non-negligible dependence on stoichiometry and porosity. For UO_2 e.g. the latter is approximated by the relation

$$k = k_{100} \ (1-P^{2/3}),$$

where k_{100} and k is the thermal conductivity of the 100 % dense material and the material of porosity P, respectively.

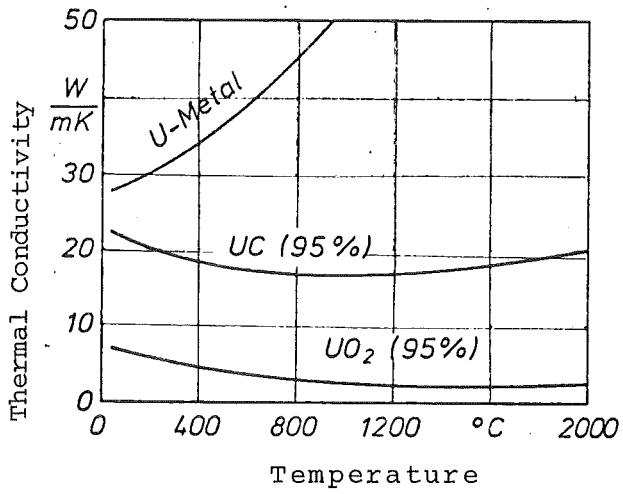

Fig. E.2.1: Thermal Conductivity of Nuclear Fuels

Table E.2.I: Material Properties of Nuclear Fuels
(Figures in brackets are applicable temperatures in ^{o}C)

	Density (g/cm^3)	Crystallographic Form	Transition Temperature (^{o}C)	Fusion Temperature (^{o}C)	Thermal Conductivity (W/m K)
U	19.04 (25) 18.11 (720) 18.06 (805)	α orthorhombic β tetragonal γ cubic b.c.	668 775	1132	25 (25)
Pu	19.82 (25) 17.82 (133) 17.14 (235) 15.92 (320) 16.00 (465) 16.48 (510)	α single monoclinic β monoclinic b.c. γ orthorhombic δ cubic f.c. δ' tetragonal ε cubic b.c.	126 209 316 456 484	641	8 (25)
Th	11.50 (25)	α cubic f.c. β cubic b.c.	1375	1750	38 (100)
UO_2	10.96 (25)	cubic f.c.		1850	8 (200)
UC	13.63 (25)	cubic f.c.		2370	24 (200)
UC_2	11.68 (25)	tetragonal cubic f.c.	1820	2470	6 (200)
UN	14.32 (25)	cubic f.c.		2840	13 (200)
PuO_2	11.46 (25)	cubic f.c.		2390	13 (200)
PuC	13.62 (25)	cubic f.c.	1654 (peritectic decomposition)		
ThO_2	10.05 (25)	cubic f.c.		3300	10 (100)
ThC	10.96 (25)	cubic f.c.		2620	8 (200)

Table E.2.II: Heavy Metal Density

	Metal Density (g/cm^3)	Metal Content (w/o)
U	19.04	100
UO_2	9.66	88.2
UC	12.97	95.2
UN	13.51	94.4

E.3. Metallic Fuels

Among the metallic nuclear fuels primarily pure uranium metal and uranium alloys are to be considered. Plutonium metal and alloys were extensively investigated in the course of nuclear weapon's development. For the energy production, however, they have no practical signifance. Thorium some time is employed in breeder pins.

Fuel metals offer high heavy metal density and high thermal conductivity compared to ceramics. At practical fabrication to shaped pieces all methods and procedures well known from convential metallurgy can be applied including powder metallurgy. Essential disadvantages are the limited corrosion resistivity to air and coolants and problems of compatibility with cladding materials, furthermore the crystalline anisotropy and the manifold phase transitions.

In the fabrication of U-metal or U-alloy mostly the metallurgical way of melting and casting is used followed by mechanical forming and treatment, see scheme in Figure E.3.1.

A special problem also at operation is the extensive anisotropy which is based on the complicated crystal structure of α-uranium, see Figure E.3.2. The atomic distances in the lattice differ with direction which influences remarkably some properties, e.g. the thermal expansion. In a single crystal - see Figure E.3.3 - for the direction of widest lattice distance the expansion coefficient is even negative.

The anisotropy decreases with higher crystallographic modification; the cubic body centered γ-uranium is fully isotropic.

It is, however, possible to get macroscopically isotropic material. Such socalled "texture-free" uranium is gained by procedural steps which arrange the anisotropic crystallites randomly. At an intermediate annealing step in the β-phase the original rolling texture is neutralized and at the following quenching into the α-phase no macroscopic rearrangement of the crystallites will take place.

At the fabrication of pure plutonium metal about the same procedures can be applied. There are, however, still more phase transitions. Most Pu-modifications are almost not workable. In addition to that, Pu must be handled in absolutely tight glove boxes due to the extreme radiotoxicity.

The behaviour of the pure metals U and Pu is often comparable. As far as practical application is concerned a list in Table E.3.I may demonstrate this similarity.

To improve some properties like anisotropy, corrosion, fabricability and irradiation damage the pure metals are alloyed. There are to be distinguished alloys with low and high amount of alloying partner. A status somewhat in between may be allocated to socalled "dispersion alloys".

Uranium alloys with low foreign additions (e.g. U-Nb 0.3; U-Mo5; U-Zr5-Nb1.5) are in the anisotropic α-state. At alloys with a higher foreign amount (like U-Nb10 or U-Mo10) the γ-state is quenchable and remains metastable at room temperature. U-alloys with Th are throughout soluble homogeneously, Pu is soluble in U up to a limit between 10 and 20 %.

Other alloying systems, e.g. with Al or Si, have no extended regions of solubility. They exist preferably as intermetallic compounds, like UAl_3, UAl_4 or U_3Si. These compounds often constitute the fuel component in dispersion alloys, e.g. UAl_4 in aluminum matrix.

In the case of Pu-alloys many systems were investigated in the course of weapon development. High-Pu as well as low-Pu alloys can be fabricated homogeneously with additions of Al, Zr, Fe, U, Th and others. The main goal in this context is always the stabilization of the isotropic δ- and ε-phases. Pu-U-alloys with an U-content above 25 % crystallize in the quite brittle socalled "zeta-phase". Also intermetallic compounds like $PuAl_4$ or $PuFe_2$ and their dispersion into Al or Fe were fabricated.

The metallurgy of thorium is basically more simple. The isotropic Th-metal is easily fabricable similar to steel. Alloying additions

like Zr or Mo improve selected properties like corrosion or weldability. Up to now, Th-metal was not applied very much, so that there could not be gained technical experience.

Table E.3.I: Behaviour of the Pure Metals U and Pu

Crystal Structure	anisotropic
Thermal Expansion	differs in direction
Phase Transitions	volume changes
Cyclic Temperature Change	anisotropic growth, cracks, surface roughening
Corrosion	not stable in air and water
Irradiation Damages	dimensional changes, swelling, loss in thermal conductivity
Problems at Fabrication	textures, embrittlement

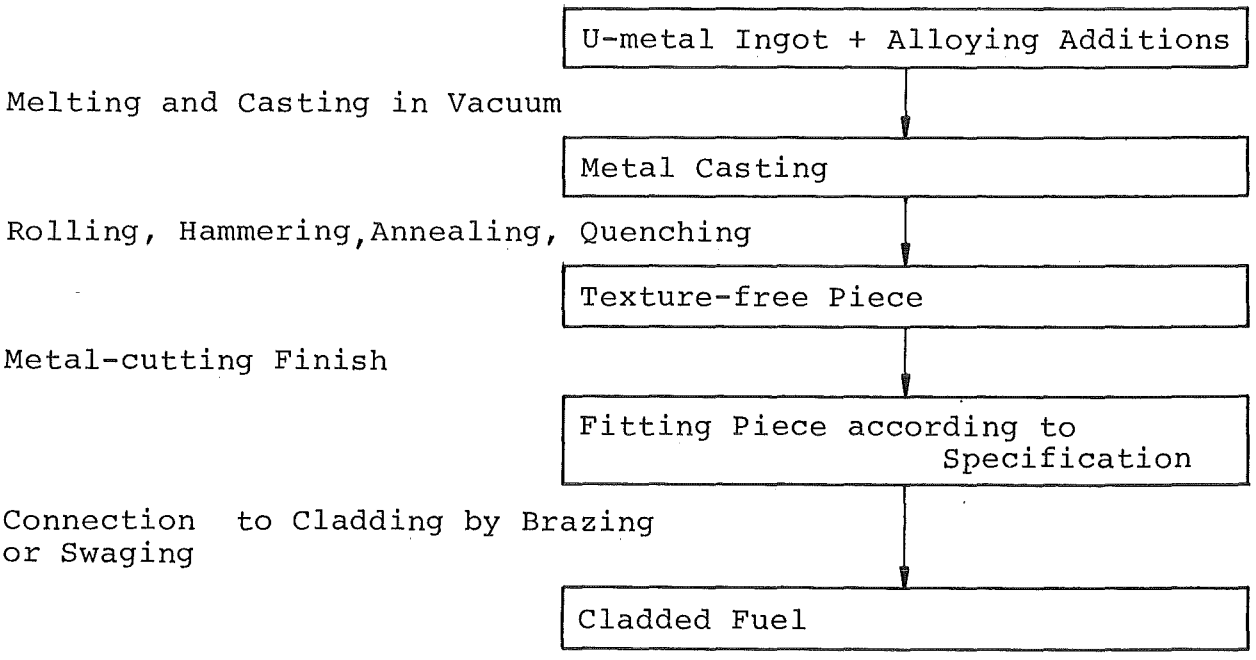

Fig. E.3.1: Fabrication of Fuel with Metallic Uranium

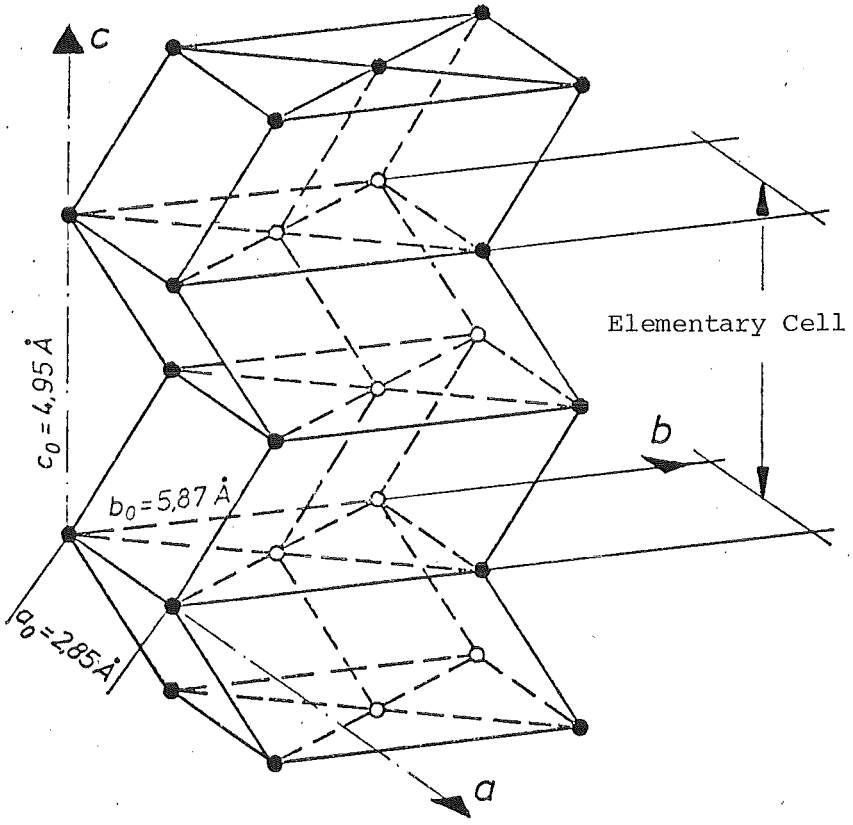

Fig. E.3.2: Orthorhombic Crystal Lattice of α-Uranium

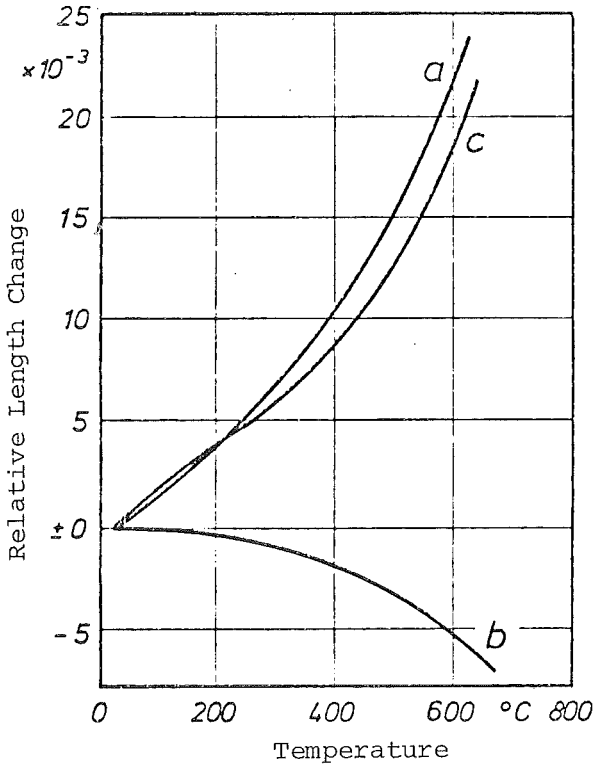

Fig. E.3.3: Thermal Expansion of α-U in the Crystallographic Base Directions

E.4. Ceramic Fuels

Ceramic nuclear fuels comprise the high-melting compounds of U and Pu, especially the oxides, carbides and nitrides. Also Th-compounds, which can serve as breeder materials, belong to this group. The high melting temperature allows principally a large temperature range of practical use. The ceramics throughout are isotropic in their properties and to far extent chemically resistant. On the other hand, the shaping requires powder ceramic methods at high temperatures. The thermal conductivity and the heavy metal density both are lower than with metallic fuel.

Out of the different ceramic compounds only UO_2 is produced and applied in large technical scale. All the LWR nuclear power plants are operated with UO_2 fuel. Carbide type fuel would constitute a safety risk in the presence of water coolant. Carbides (and perhaps also nitrides) may be a potential for future fast breeders because of their higher metal density and enhanced thermal conductivity. In laboratory scale also silicides, phosphides and sulfides were fabricated and tested. The silicide U_3Si was already irradiated, it may be a potential for thermal reactors.

The fabrication of UO_2 fuel for inserting into fuel pins starts always with nuclear grade sinterable UO_2, which is the final product of ore processing or isotopic enrichment. This UO_2 powder is processed into pellet fuel by a large scale powder ceramic procedure. These socalled "pellets" are cylindrical pieces with plane or "dished" top and bottom surfaces. The course of this process is characterized in Figure E.4.1; a sketch of sintered UO_2-pellets is shown in Figure E.4.2.

Another type of UO_2 fuel is particle fuel. Such particles necessarily have to have high density, in order to guarantee a sufficient high overall fuel density in view of the unavoidable cavities between them. For the fabrication of particles different ways are available, see the schemes in Figures E.4.3 and E.4.4.

There are to be distinguished dry and wet processes. In a dry process the sinter grade UO_2 powder at first is pressed and then

crushed and sintered. In the wet sol-gel-process at first a colloidal UO_2-sol ist generated out of uranyl nitrate by a complex-forming substance. By addition of a gelation agent compact little spheres are precipitated, which are finally sintered. These socalled "UO_2-kernels" have diameters below and around 1 mm.

Such a particle type fuel may be introduced into cladding tubes and further compacted by mechanical vibration. Also further compression of the particles in dyes seems to be feasible. But the "normal" pellet fabrication directly out of the sinterable powder is technically preferred for LWR fuel. A quite important application, however, is for high temperature reactors (HTR), where the particle fuel is used exclusively, see chapter E.6.

The UO_2 fuel in all phases of fabrication is accompanied by characterization and quality control. A few important characteristics are compiled in Table E.4.I.

The fabrication of pure PuO_2 or mixed UO_2-PuO_2-fuel follows a similar routine. On has to take into account, however, the special conditions of Pu-handling. In Figure E.4.5 a (simplified) process scheme for mixed oxide is demonstrated. In praxi there are many modifications applied in order to improve the homogeneity of the mixture. By far more satisfying compared to mechanically mixed fuel is the "coprecipitated" fuel, for which both the heavy metal components U and Pu are commonly precipitated out of the fluid phase into sinterable $(U,Pu)O_2$-powder.

One can expect, that in the future two principally different compositions of mixed oxide are required, that is the recycle fuel for LWR with a PuO_2-content below 10 % and the fast breeder fuel with a PuO_2-content around 20 %. Each of these fuel types makes necessary a specially adjusted fabrication process.

The fabrication of ThO_2 and its mixtures with UO_2 follows an analogous scheme. But ThO_2 may be sintered in air, while with UO_2 and PuO_2 an inert gas with hydrogen addition is necessary.

Carbide fuels of the type monocarbide MeC have the advantages of improved thermal conductivity (similar to the metals) and increased heavy metal density. They are, however, not resistant against air and water. Fine carbide powder is even pyrophoric and must be handled with great care. The vapour pressure at high temperatures is rather high, already below the fusion point. Pure PuC is decomposed at 1654 ^{o}C. The compatibility with cladding metals is good as long as the carbide is monophase. At a metal surplus in carbide, reactions with metallic components of the cladding take place, a carbon surplus lead to carburization of the clad.

The fabrication of U-monocarbide starts with U-metal or with sinterable UO_2. In any case, there is a two-step process necessary, namely at first the production of carbide raw material and then the further processing to pellets or other densified pieces. A simplified scheme of two processes is demonstrated in Figure E.4.6. A key characterization magnitude of the technical product is the impurity in higher carbides. While sesquicarbide Me_2C_3 in contents of some few percents is not detrimental to the properties, already a quite low impurity by dicarbide MeC_2 reduces the compatibility significantly.

The fabrication of Pu- und Th-monocarbides is carried out by similar processes.

A further ceramic fuel type already investigated thouroughly comprises the mononitrides MeN. They bring an improved chemical stability and compatibility compared to carbides, but the nitrogen content causes enlarged neutron absorption. The fabrication of UN out of UO_2 is performed by a carbothermic reduction at 1600 to 1800 ^{o}C in a N_2-atmosphere. Also mixed nitrides (U,Pu)N and carbonitrides were produced in laboratory scale and characterized and tested in irradiation experiments.

Table E.4.I: Characterization of UO_2 Fuel Pellets

UO_2 Powder	Composition Oxygen Content Specific Surface
Pressed Green Pellet	Geometry Density
Sintered Pellet	Geometry Density Stoichiometry Microstructure Behaviour at Repeated Sintering

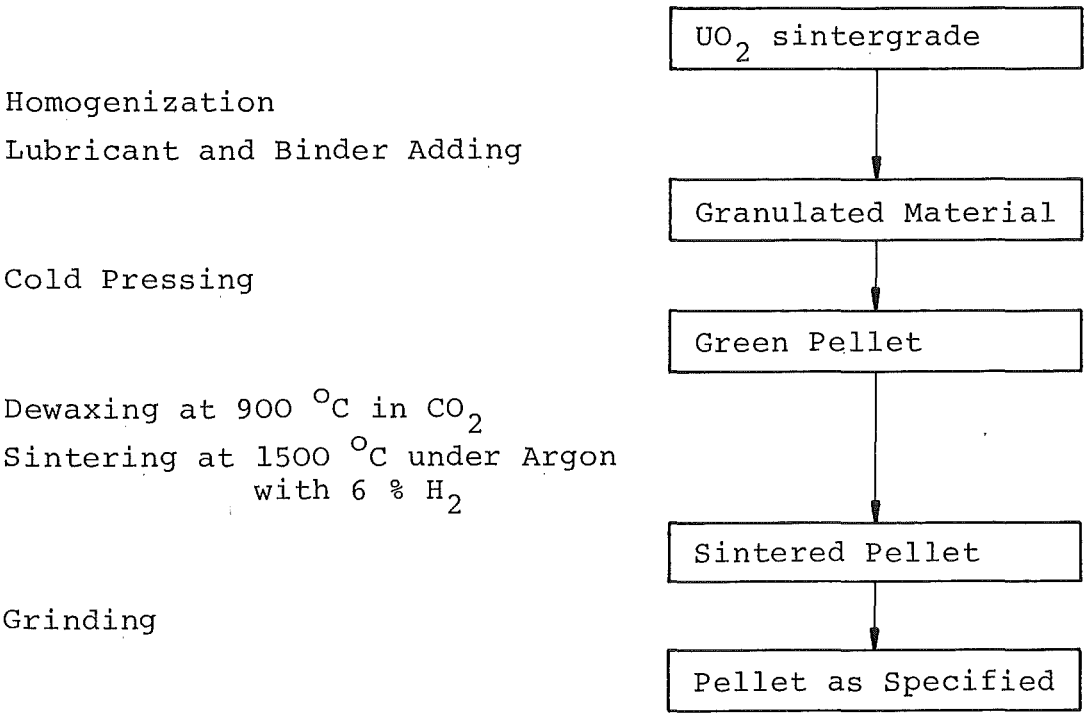

Fig. E.4.1: The Fabrication of UO_2 Pellet Fuel

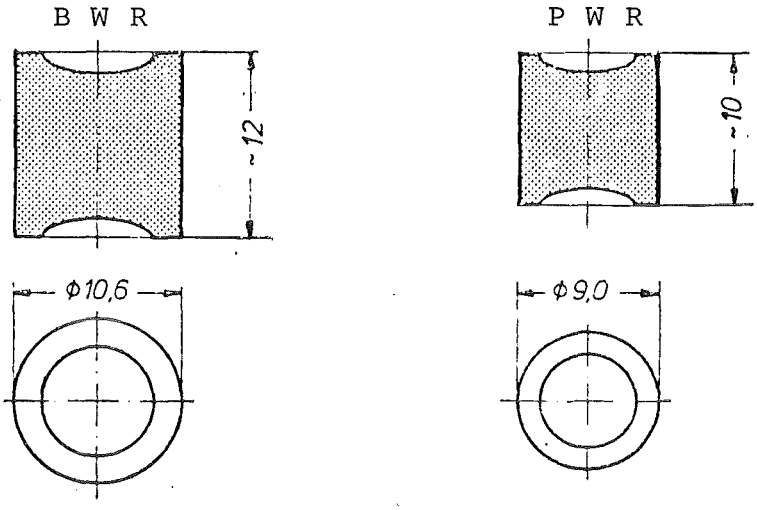

Fig. E.4.2: UO_2 Fuel Pellets with Dishing for BWR and PWR

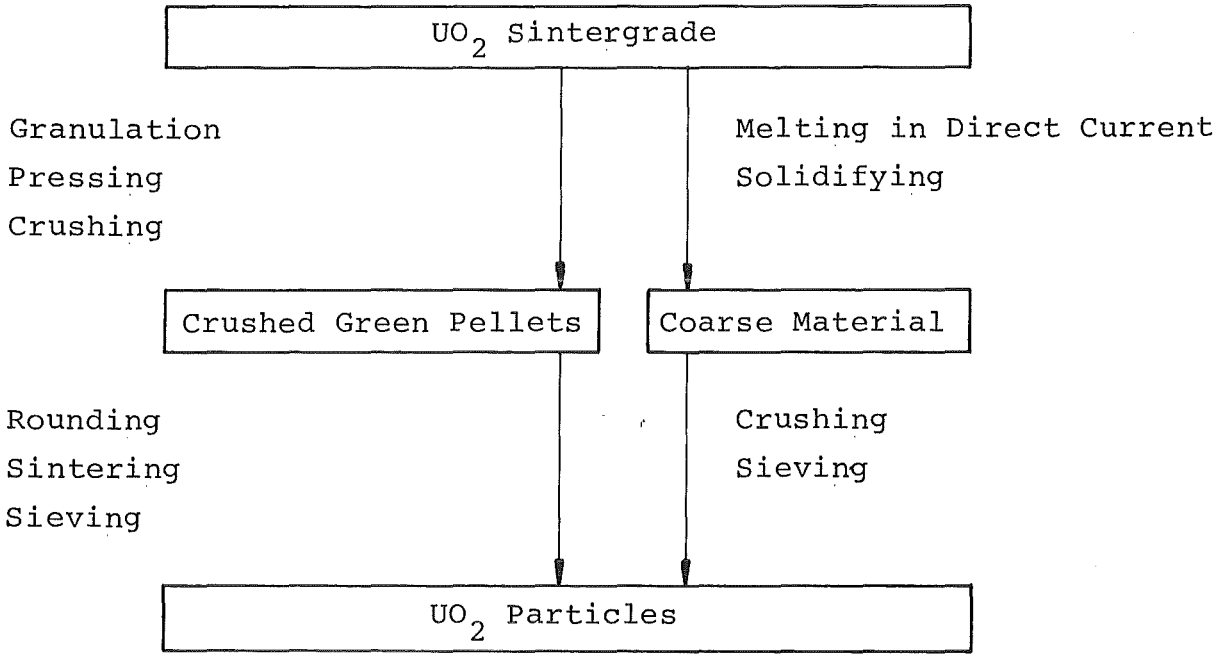

Fig. E.4.3: Dry Processes for UO_2 Particle Fabrication

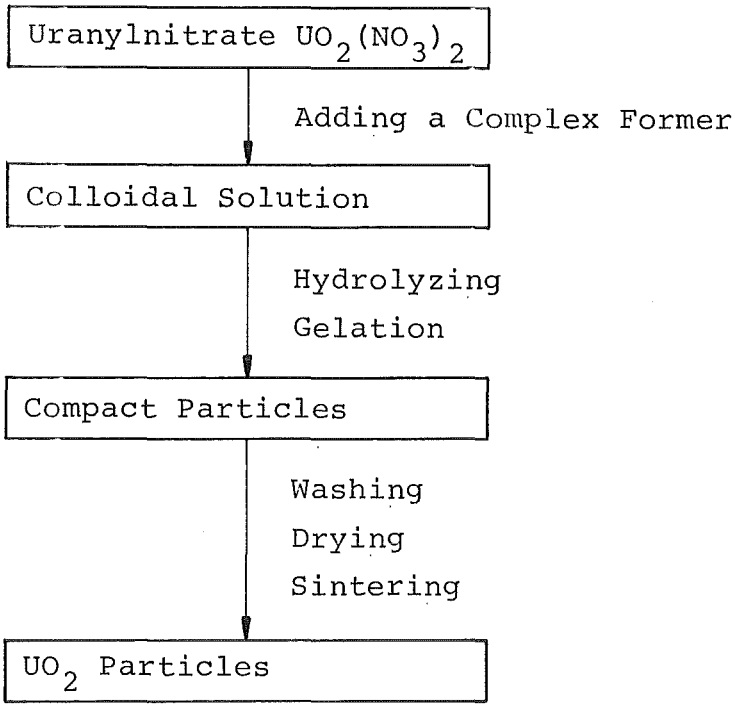

Fig. E.4.4: Sol-Gel-Process

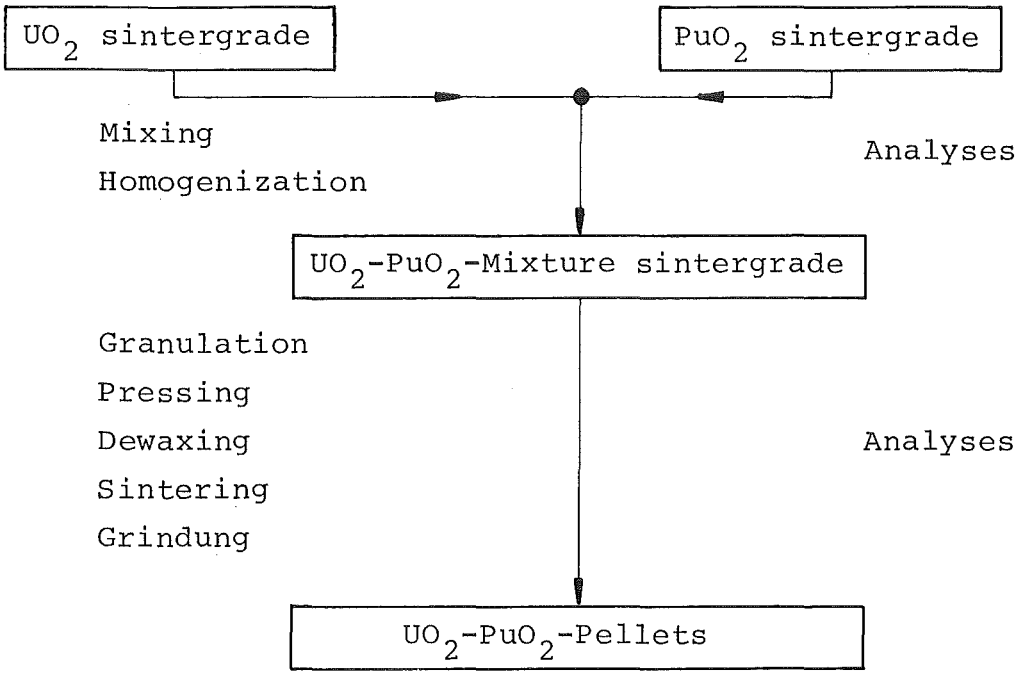

Fig. E.4.5: Fabrication of UO_2-PuO_2-Mixed-Oxide

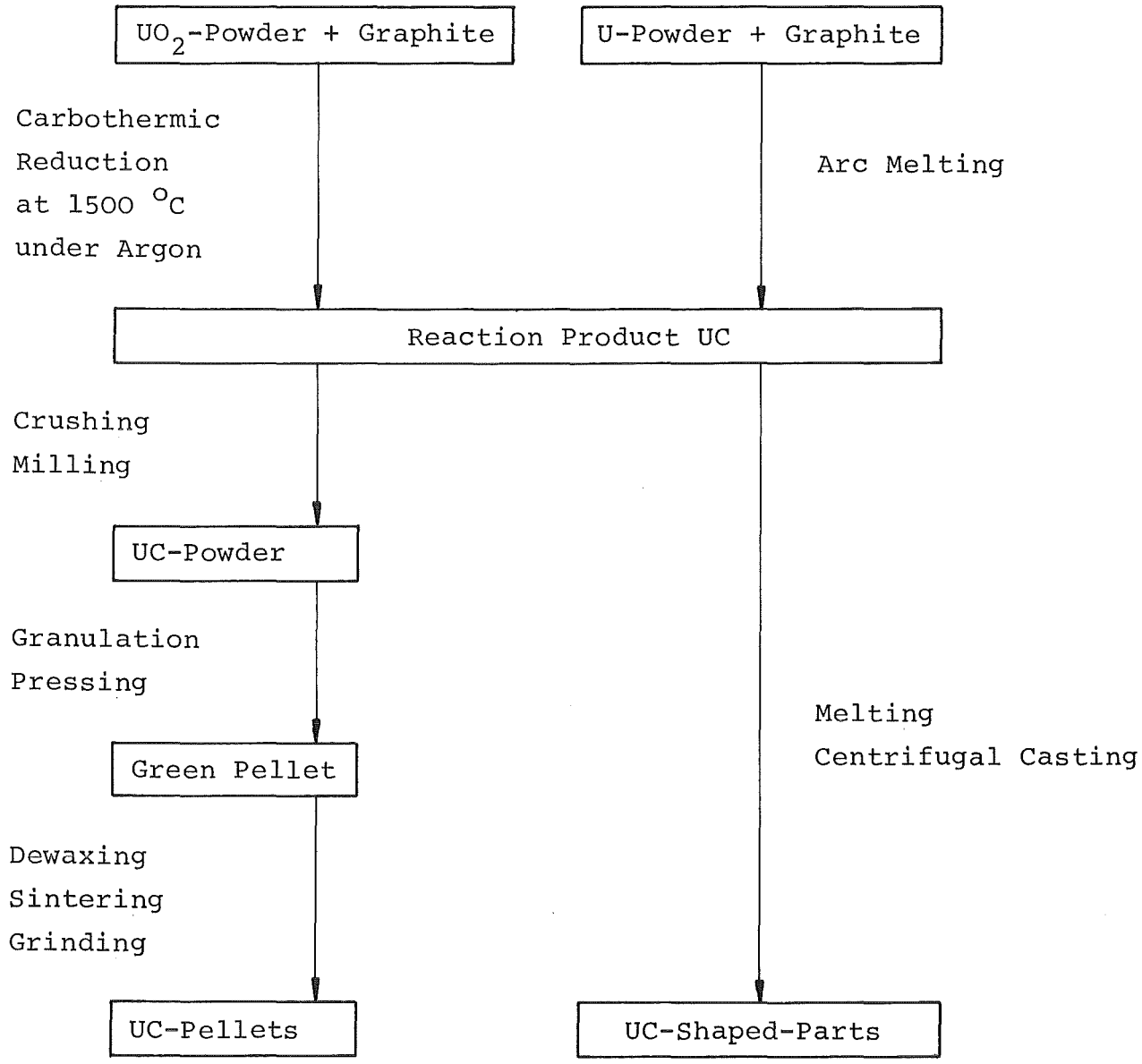

Fig. E.4.6: Two Different Processes for Fabrication of Uranium Monocarbide

E.5. Dispersion-Type Fuels

This not very exactly defined heading shall characterize compound fuels, that are composed of a metallic and a ceramic component. The fissionable material is always included in the ceramic, e.g. in UO_2, U_3O_8, UC_2 and this ceramic component is uniformly distributed throughout the metallic matrix. Therefore, these fuels are called "dispersion fuels" or"matrix systems". Another short designation is "cermet fuel".

The metallic matrix guarantees the metallic strength and thermal conductivity. Above that, metal work is more simple. Sometimes, the metallic component serves in highly concentrated fissionable material as a diluting agent which is permeable to neutrons. These compound fuels can be divided into cermets with low metal portion and cermets with high metal portion. There is some dependancy to dispersion alloys and fuel compounds out of ceramics and graphite, the latter being used in HTR's, see chapter E.6.

At cermets with low metal portion, the metal shall form a network of heat-conducting connections, a socalled "idealized structure". In such a structure, e.g. a molybdenum addition of 10 to 20 % to UO_2 already doubles the thermal conductivity. The overall behaviour remains defined by the ceramic component.

A dispersion fuel with high metal portion contains e.g.
- 35 v/o U_3O_8 in aluminum or
- 25 to 50 v/o UO_2 in stainless steel or
- 40 v/o UO_2 in refractory metals.

These compound fuels behave similar to the matrix metal with respect to mechanical and thermal properties. For fabrication either the ceramic fuel powder is disperged in the melted metal (e.g. U_3O_8 in Al) or both ceramic and metallic powders (e.g. UO_2 and steel powder) are mixed and densified by powder metallurgy applying common processes like cold and hot pressing, rolling, extruding, sintering.

Cermet-fuels can be formed to pellets by pressing and sintering, to rods and tubes by rolling and extruding. Very important,

however, is the fabrication of fuel plates. Especially for the fuel of material test reactors, that contains more than 90 % fissionable uranium isotopes, such plates are indispensable, because they make possible the design of compact reactor cores with large internal cooling surfaces.

For the cladding of fuel plates mostly the socalled "picture-frame-technique" is applied.

E.6. Coated Particles

In the coated particles a kernel of oxide or carbide fuel is surrounded with a solid and gas-tight coating. This coating consists of some separate layers of carbon and silicium carbide. The objective of this fuel concept is to guarantee the integrity of the envelopment of the fuel also at temperatures, to which metals do not withstand. The typical application for this concept is the helium-cooled high temperature reactor. The outside fuel element cladding of graphite is not sufficiently tight against fission products. The actual mechanical barrier against fission product release and fuel swelling is realized within the coating of the individual particle.

The fuel kernels consist of UO_2, UC of UC_2 or - in respective cases - of the same compounds with Th and Pu. The kernels are fabricated up to a size of about 1 mm

- by powder compaction, crushing, rounding and sintering,
- by arc melting or
- by a sol-gel-process.

For an envelopment of the fuel particles, basically also coatings of refractory metals like Mo and V are acceptable. But in practically all cases now multilayer-coatings of pyrolytic carbon - acronym PyC - are applied. One has to distinguish between two types of coatings, i.e. the "Biso"- and the "Triso"-coating. The Biso-coating is built up by 2 or 3 layers, namely:

- An internal porous layer of PyC serves as a buffer. It can absorb the fission product atoms that escape out of the surface of the fuel kernel.
- An external high-dense and high-tight layer (socalled HDI layer) provides a strong mechanical enclosement and tightness against fissionable material and fission products.
- Sometimes a "seal-layer" of anisotropic PyC is introduced between the two layers mentioned above.

Biso-particles provide sufficient restraint at not to high temperatures and only for oxide kernel fuel up to low or medium

burnup. At load conditions above these limits one has to take into account release of some metallic fission products like Cs, Sr, Ag by diffusion. An adequate protection is here established by a Triso-coating which contains an additional SiC-layer below the external PyC-layer. At an advanced state of development, in reality there are not three but four layers , because the high-dense PyC-layer is deposited two-times. In Figure E.6.1 the typical buildup of Biso- and Triso-particles is shown. The total thickness of such a multiple coating is between 100 and 300 µm and is therefore by far larger than the free migrational distance of recoil atoms.

The layers of pyrolytic carbon are produced by deposition out of hydrocarbons (methane, propene, acetylene) at high temperatures (1200 to 2100 ^{o}C) within a turbulance chamber. Dependent on temperature and organic gas density there are produced porous or highdense PyC-layers. Also an amorphous, laminary or columnary structure within the layers may be achieved at proper deposition parameters. The SiC-layers are gained by deposition out of methylsilicon trichloride CH_3SiCl_3 at about 1800 ^{o}C. Also layers of other carbides like ZrC and of coprecipitated PyC-SiC-mixtures have already been experimentally tested. In such a way it is possible to improve the strength and the geometric stability and to further reduce the diffusion of metallic fission products. Perhaps the total thickness of a coating may be reduced somewhat being favourable to the nuclear conversion rate in thermal breeding.

At the further processing to fuel elements, the coated particles are surrounded by a graphite envelopment,see H.5. For this purpose the particles either are filled into hollow graphite structures (e.g. a hollow ball) or are disperged into a graphite matrix. In preparation to such a dispersion procedure, the particles are equipped with an additional loose protection layer (e.g. of graphite powder), in order to protect the particle coatings during the workin up steps.

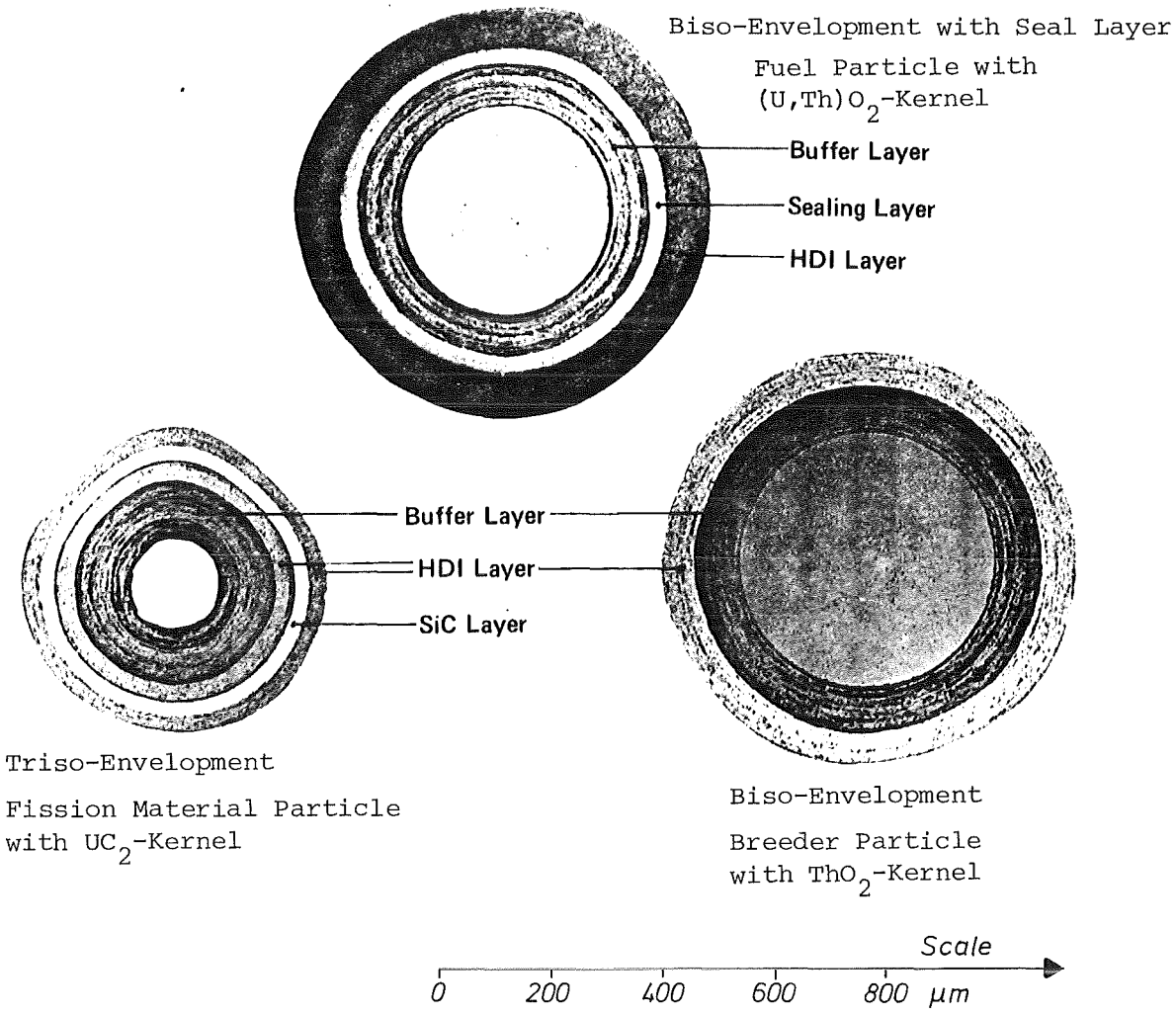

Fig. E.6.1: Coated Particles for the High Temperature Reactor THTR-300
(HDI means High Density Isotropic PyC)

E.7. Fuel Handling

Nuclear fuels principally constitute a hazard potential, be it for the nuclear installations and their employees themselves, be it for the environment and the general public. In this context the following points of view are primarily to be envisaged:

- health
- nuclear safety
- safeguarding against misuse
- safeguarding against actions from outside.

The dangers to health, which can be originated by nuclear fuels, refer to body damage by direct irradiation from outside or by incorporation. The endangerment by outside irradiation is primarily caused by the penetrating γ-radiation and - in some special cases - by neutron radiation. Concerning the incorporation, mainly the α-emitters that produce high energy doses within short reach are to be considered.

An extraordinarily large intensity of hard γ-radiation is emitted by burnt nuclear fuel, wherefore irradiated fuel elements can be handled only behind huge shieldings (about 2 meters of concrete). Also unirradiated fuels emit some γ-radiation. But only higher Pu-isotopes and U-232 may lead under special circumstances to a radiation load which requires a definite shielding.

All the isotopes of nuclear fuels are toxic. The chemical toxicity is similar to the toxicity of other heavy metals e.g. lead. The specific endangerment stems from the radiotoxicity which is induced by the α-radiation. In Table E.7.I, for the fuel isotopes a compilation of the most important data relevant in this respect is brought.

The protection measures against radiotoxicity are generally based on cleankeeping of air and water and on avoiding direct incorporation. At the professional handling of nuclear fuels the following provisions and measures are indispensable:

- protective clothing, evt. special breath protection,
- personal dosimetry,

- surveillance of working spaces with respect to contamination by radioactive material, especially on surfaces and in the air,
- an ergonomically favourable layout of the working process,
- precaution and care and clean working conditions,
- medical surveillance of workers.

Irradiated fuel can be manipulated only in a hot cell using remotely operating tools. Such a cell is surrounded by a very thick shield made of normal or heavy concrete. Besides that, the cell has to be α-tight, too. For visual connection to the operators there are installed thick windows of leaded glass.

Unirradiated natural U (and also depleted U) principally can be handled in open air. But with fine powdered material (e.g. sintergrade UO_2) some dust protection is required in order to keep the air properly clean. Also direct contact must be avoided. Enriched U requires improved breathing protection because of the higher α-activity.

Plutonium is to be enclosed into absolutely tight boxes, the socalled "glove boxes", see figure E.7.1. The manipulation is carried out via rubber gloves or remotely. The glove boxes have internally a slight underpressure compared to outside. Thus, at an occasional untightness - e.g. in a rubber glove - the aircurrent is directed into the box.

The sanitary consequences of inadmissibly high irradiation or incorporation may be shortterm or longterm. A shortterm consequence is the socalled radiation sickness, a "radiation syndrom", longterm consequences are possibly leucemy, cancer and genetic damage. Such sanitary damages, however, were observed (e.g. at animal tests or at radiation accidents) only at actual doses which were by some orders of magnitude above the legally admissible limits.

The item nuclear safety refers to the danger, that there is formed unintentionally a critical device. In such an incident, not the energy release would be of primary concern, but the push of radiation. The formation of a critical device is safely avoided by

- precautions concerning geometry ("safe geometry"),
- concentration limits of fissionable material or

- mass limitation ("safe mass").

The mass limitation as an inherently safe method is oriented on the minimal critical mass. The maximum allowable amount in handling and fabrication is always less than the half of the critical mass, see Table E.7.II.

The safeguarding against misuse, e.g. for fabrication of nuclear explosives is based on the international system of non-poliferation control. A prerequisite for the efficiency of such a system is the availability of measuring methods and equipment as well as a complete mass control and accountance for the fissionable material.

The safeguarding against actions from outside, which is necessary especially at the handling of large amounts of Pu, requires resistant buildings, e.g.against earthquake and air crash and, in addition, administrative protection and personal guarding, e.g.against sabotage.

Table E.7.II: Mass Limits for Fissionable Isotopes

	U-233	U-235	Pu-239
Minimal Critical Mass			
in Solution with Reflector	590 g	820 g	510 g
as Metal with Reflector	7.5 kg	22.8 kg	5.6 kg
Maximum Allowable Amount			
in Solution	250 g	350 g	220 g
as Metal	3.2 kg	10.0 kg	2.6 kg

Table E.7.I: Radiation of Fuel Isotopes and Permissible Activity in Air and Water

	Th-232	U-235	U-238	Pu-239	Pu-240
Halflife (a) Radiation	$1.41 \cdot 10^{10}$ α	$7.04 \cdot 10^{8}$ α	$4.47 \cdot 10^{9}$ α	$2.44 \cdot 10^{4}$ α,γ	6537 α,γ,n
Specific (μCi/g) Activity (l/s g)	0.11 $4.04 \cdot 10^{3}$	2.16 $7.99 \cdot 10^{4}$	0.34 $1.24 \cdot 10^{4}$	61300 $2.27 \cdot 10^{9}$	227800 $8.43 \cdot 10^{10}$
1 Curie is equivalent to	9152 kg	463 kg	2976 kg	16.3 kg	4.4 g
Permissible Limit of Activity - in Water (Ci/m^3) ($l/s\ m^3$)	$9.0 \cdot 10^{-8}$ $3.3 \cdot 10^{3}$	$2.3 \cdot 10^{-7}$ $8.3 \cdot 10^{3}$	$3.5 \cdot 10^{-8}$ $1.3 \cdot 10^{3}$	$2.8 \cdot 10^{-7}$ $9.8 \cdot 10^{3}$	$2.8 \cdot 10^{-7}$ $9.8 \cdot 10^{3}$
- in Air (Ci/m^3) ($l/s\ m^3$)	$6.6 \cdot 10^{-14}$ $2.5 \cdot 10^{-3}$	$2.6 \cdot 10^{-13}$ $9.6 \cdot 10^{-3}$	$1.5 \cdot 10^{-13}$ $5.5 \cdot 10^{-3}$	$3.6 \cdot 10^{-15}$ $1.3 \cdot 10^{-4}$	$3.6 \cdot 10^{-15}$ $1.3 \cdot 10^{-4}$
Maximum Allowable Amount - in Water ($\mu g/m^3$)	800000	100000	100000	4.5	1.2
- in Air ($\mu g/m^3$)	0.6	0.1	0.5	$5.9 \cdot 10^{-8}$	$1.6 \cdot 10^{-8}$

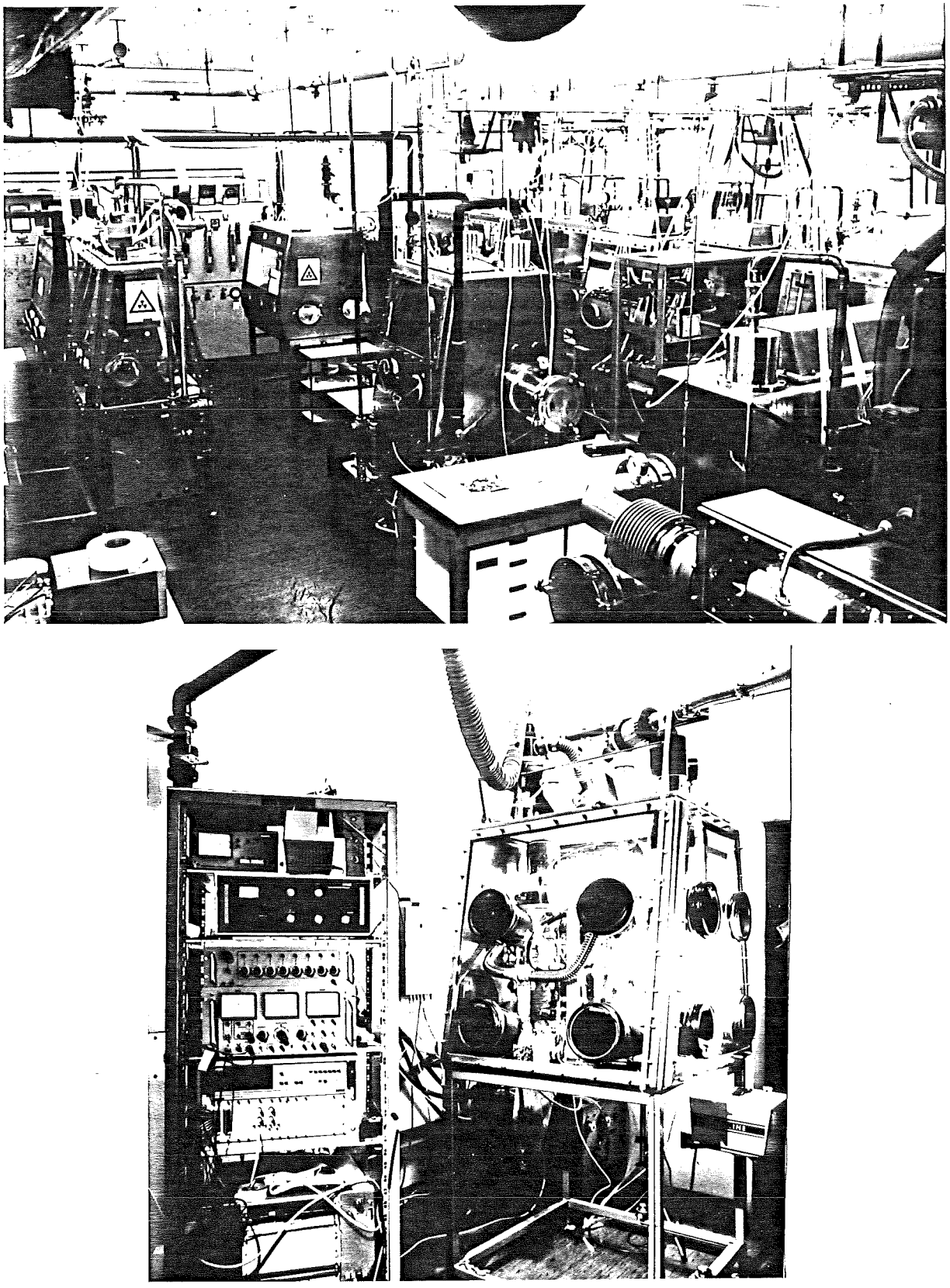

Fig. E.7.1: Glove-Box in a Pu Fabrication Line

F. NUCLEAR FUELS UNDER IRRADIATION

F.1 IRRADIATION CONDITIONS AND DEFINITIONS

F.2 STRUCTURAL CHANGES IN THE FUELS

F.3 THE BEHAVIOUR OF THE DIFFERENT FUEL TYPES

F.1 Irradiation Conditions and Definitions

The statements for power and energy in the fuel always refer to the transformed and released amount of heat. This is true for the power as well as for the burnup (if the latter contains an energy measure).

Two kinds of power measures are to be distinguished, namely

- the mass specific magnitude "specific power" b_{fis}, measured in watts per gram fissionable atoms

and

- the power in relation to geometry, measured in
  watts per cm^3 fuel
  or megawatts per m^3 core volume
  or watts per cm fuel rod length
  or kilowatts per m fuel rod length.

The last mentioned magnitude applicable to fuel pins is designated as linear rod power χ. It is connected to the specific power b_{fis} by the formula

$$\chi = [\rho_{th} \cdot \frac{d_{Br}}{100} \cdot f_{Me} \cdot \gamma \cdot R^2 \pi] \cdot b_{fis}$$

with ρ_{th} ≙ theoretical density,
d_{Br} ≙ % of theoretical density,
f_{Me} ≙ weight portion Me in fuel,
γ ≙ weight portion of fissionable nuclides,
R ≙ fuel radius.

As a measure for the fuel burnup either the number of nuclear fissions per specific amount of fuel or the total energy generated by fissions and released is used. Therefore, we have the following burnup definitions:

- Number of fissions per cm^3 fuel,
- burnup in % = 100 x (number of fissions per number of initial heavy metal atoms) = 100 x fima-value,
- fima = fissions per initial metal atoms,
- fifa = fissions per initial fissile atoms,

- Megawattdays (MWd) per kg fuel,
- Megawattdays per kg or tonne heavy metal.

In this context "heavy metal (Me)" means Th, U and Pu. In case of U-235 as fissionable material, the following correlations are exactly fulfilled, for the other fissionable materials they are a very good approach:

- 1 Watt = $3.25\ 10^{10}$ fissions per second,
- 1 % Burnup = 9.13 MWd per kg Me = 9130 MWd per t Me,
- 1 MWd per kg Me = $2.81 \cdot 10^{18} \cdot Q$ fissions per cm^3 fuel with

$$Q = \frac{\rho_{th} \cdot d_{Br} \cdot f_{Me}}{100} \quad .$$

The correlation between fima and fifa is

$$\text{fima-value} = \frac{\text{fifa-value}}{1 + y} \quad , \text{ where } y = \frac{\text{breeder amount}}{\text{fissionable amount}} \quad .$$

F.2. Structural Changes in the Fuels

Exposed to the neutron flux of a reactor, the chemical composition of a nuclear fuel as well as the structural constitution is changed. These mostly irreversible alterations are the irradiation damages, which may lead finally to the failure of a fuel element. Within the fuel under irradiation the following primary processes are effective:

- The fission product atoms carrying primarily the largest portion of the fission energy are interacting strongly with the surrounding lattice atoms by ionization and knock processes up to a reach of about 10 µm. There is taking place a cascade of hundreds of single reactions up to the final slowing down. Every fission product atom leaves behind a trace of lattice damage in the solid body.
- There is a continuous change of the chemical composition. Fissionable atoms (as e.g. U-235) disappear and instead of them a variety of other chemical elements come into existence: the fission products. U-fuel after a burnup of 3 atom-% contains e.g. about 3 weight % foreign material. About 15 % of these portion are the noble gases Kr and Xe. Some of the elements like Cs and I are easily volatile, most of them are solid.

These primary effects produce alterations and damages in the fuel, namely

- nuclear alteration: The fissionable content decreases, the neutron absorption by the fission products increases significantly;
- lattice and structure changes: Lattice extensions, empty lattice positions, grain boundary deposits and finally pores and cracks;
- segregations: The noble fission gases are partly released, the fission products and also the fissionable atoms may migrate as a consequence of the temperature gradient;
- thermal alterations: Due to the lattice damages the thermal conductivity is reduced, also the heat transition out of the fuel decreases;

- changes in stoichiometry: The fission product mixture exhibits another chemical valence compared to the disappeared fissionable atoms. E.g. in oxide fuel the oxygen potential is increasing, the fuel becomes hyperstoichiometric in the course of irradiation;
- corrosion attack on the cladding: Some special fission products as well as the change in stoichiometry may induce enhanced chemical attack, the compatibility between fuel and clad decreases;
- mechanical alterations: As a consequence of the lattice damages the fuel embrittles further,accompanied by a reduction in strength;
- dimensional changes: Instead of the fissionable atoms a double number of fission product atoms are produced. Their space needs lead to fuel swelling. Local differences in swelling amount or anisotropic behaviour of lattice may lead to changes in the geometric shape.

All these alterations are influencing the lifetime of a nuclear fuel. Basically two types of life limits are to be distinguished, namely

- the nuclear life limit, that is defined by the reduction in fissionable content and by the fission product poisoning,
- the technological life limit, that is reached by thermomechanical degradation of the lattice and the structure and by the swelling.

In thermal reactors with natural U often the nuclear life limit is decisive, in thermal reactors with enriched fuel and in fast reactors practically always the technological life limit is the more important criterion.

F.3. The Behaviour of the Different Fuel Types

The primary processes and the secondary effects - as described in the preceding chapter - are more or less the same in all fuel types. But there are quite large differences concerning the quantitative changes of technological properties induced by these effects.

In metallic fuel the irradiation damages cause distinct alterations in structure already after small burnup (e.g. 0.1 %). The scarcely soluble fission gas produces pores. These pores - together with the solid fission products which cannot be accomodated in the dense metal body - cause swelling expansion. The ductility declines, there are cracks being developed within the fuel. Especially in case of cyclic operation, in an anisotropic structure an anisotropic swelling may take place. A coarse grain metal structure may be roughened on the surface. The lifetime with pure U-metal fuel is limited to about 1 % burnup. Some alloys, however, achieve the range of 3 % burnup, e.g. Mo-alloys. There are also special alloys - e.g. a ternary U-Pu-Zr-alloy - which sustain even higher burnups. But the overall irradiation behaviour of metal fuel is not satisfactory with respect to technical applications.

For high burnup regions ceramic fuels are the given nuclear materials. UO_2 in LWR-fuel pins achieves maximum burnups of 5 %, mixed oxide in fast breeder fuel more than 10 %. In ceramic fuels high central temperatures and large radial temperature gradients are being developed. These gradients generate cracks in the ceramically brittle material, primarily in radial direction. While the structure of LWR-fuel shows only minor alterations in the course of the burnup (see Figure F.3.1), the UO_2-PuO_2-mixed-oxide fuel for fast breeders develops strongly differentiated structure zones (Figure F.3.2). There is a correlation between structure profile and temperature profile, the structure limits approximately refer to specified temperatures.

LWR oxide fuel in pellet shape demonstrates only a very low fission gas release; in fast breeder fuel, however, up to 90 % of the generated gas amount is released. The fuel swells, because the

fission products need space. At lower burnups, the pore volume is partly used for swelling accomodation, at high burnups external volume increase takes place. The increasing amount in free oxygen - which is partly somewhat counterbalanced by the radial oxygen gradient - may lead to cladding attack, this attack being even promoted by some special fission product elements.

In high burnup mixed oxide fuel for fast breeders the migration and segregation phenomena are marked, see Figure F.3.3. Some of the fission products, like especially Cs, migrate in the axial and radial temperature gradient. In the same manner some segregation of UO_2 and PuO_2 takes place.

Oxide fuel in the form of vibrated particles exhibits a large fission gas release under irradiation. In the radially outside portions of the fuel, the particle structure remains more or less unchanged, while in the center the particle fuel becomes quite similar to irradiated pellets.

Carbide fuel (which is an option for future fast reactors) sees at the same power a substantially lower temperature gradient. Therefore, only a few cracks develop and practically no structural changes. Also the fission gas release is very low. This increased restraint, on the other hand, results in a larger swelling rate compared to oxide. The higher heavy metal density acts in the same direction. Nitride fuel which is basically quite similar to carbide and the carbonitrides show swelling rates in between. In table F.3.I some rough swelling figures are compiled for orientation. In any case, one has to take into account, that this roughly linear swelling becomes observable outside not before an incubation period (at oxide not before about 2 % burnup).

In metal-ceramic fuel the metallic matrix surrounding the ceramic fissionable regions is being damaged by high energy ions of the fission products to a depth of about 10 µm. Further damage develops as a consequence of the space requirements of the fission products. Hence pore formation develops as well as internal stresses and cracks, especially in spots with peak temperatures and steep gradients. Cermets from UO_2 and stainless steel achieve burnups

of 20 % fima, always related to the U content. In such a fuel, the temperature within the steel matrix is limited to about 600 ^{o}C. The Al-matrix in a U_3O_8-Al-cermet may loose its integrity already somewhat above 100 ^{o}C. With this cermet, however, burnups of 60 % fima were already achieved at low temperatures.

The main point of view with coated particle fuel is the mechanical strength of the coating and its tightness against solid and gaseous fission products. An useful measure for the release of fission products is the R/B-ratio, which symbolizes the ratio "release/birth". This R/B-ratio is different for different fission products and, above that, specific for the special layer considered. Single layers of PyC e.g. exhibit a ratio R/B = 10^{-3} for fission gases, twin layers show a ratio R/B = 10^{-5}. This tightness remains unchanged as long as the coating is mechanically intact. The increasing internal pressure buildup finally blows up the coating, thus reaching the technological lifetime. At high concentrations of fissionable isotopes (e.g. about 90 % U-235) burnups of 50 % fima and more are achievable. But often the lifetime is limited by an one-sided attack of the kernel to the coating. Such a phenomenon (which is also called "amoeba-effect") is linked to a temperature gradient in the particles at a high temperature level: The kernel penetrates the coating at the hot side, see Figure F.3.4. This migration of the kernel is initiated by a chemical interaction between fuel and PyC, where the carbon of the PyC-layer is isolated and deposited on the opposite side of the kernel. Within a particle with a carbide kernel the carbon is assumed to diffuse directly, while in the presence of an oxide kernel the diffusion seems to operate via the gaseous phase CO_2 and CO. In the latter case the oxygen potential and the retransport of oxygen is important. Suitable additives to the fuel may suppress the whole effect up to high burnup. In oxide kernel e.g. special getter for reduction of the oxygen potential are effective in this respect.

Table F.3.I: Fuel Swelling under Irradiation

	Volume Increase in % at 10 000 MWd/t Me Burnup
Metals	3
Oxides	1
Carbides	2
Nitrides	1.5

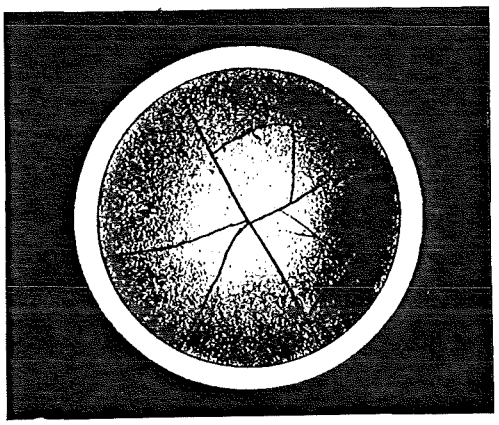

Fig. F.3.1:
Cross Section of a UO_2 Pellet after 2 % Burnup under LWR-Conditions
- Diameter 10 mm

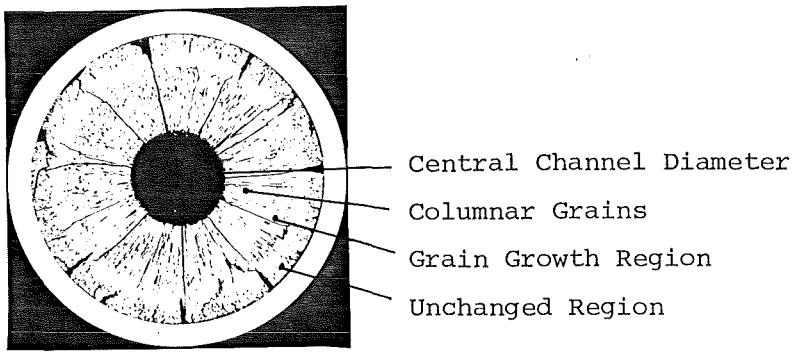

Fig. F.3.2: Cross Section of a UO_2-PuO_2-Pellet after 5 % Burnup under Fast Reactor Conditions
- Diameter 6 mm

a)
The micrograph of the pin cross section shows the fuel structure after irradiation.

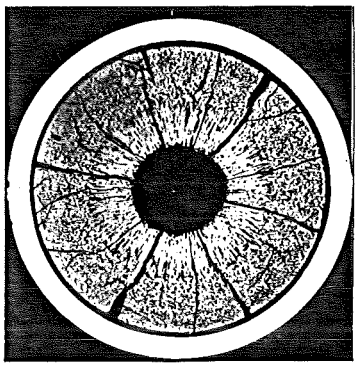

b)
The Alpha-Autoradiography shows the migration of the PuO_2 radially to the center.

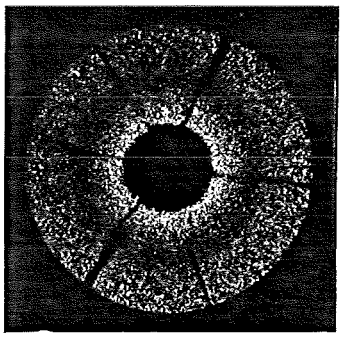

c)
In the Beta-Gamma-Autoradiography the accumulation of fission products in the fuel ring around the central channel becomes visible.

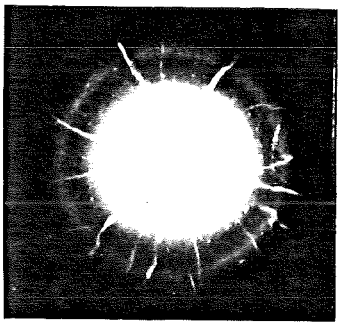

Fig. F.3.3: Migration Phenomena in High Burnup Mixed Oxide - Fuel Diameter 6 mm, Burnup 90 MWd/kg Me -

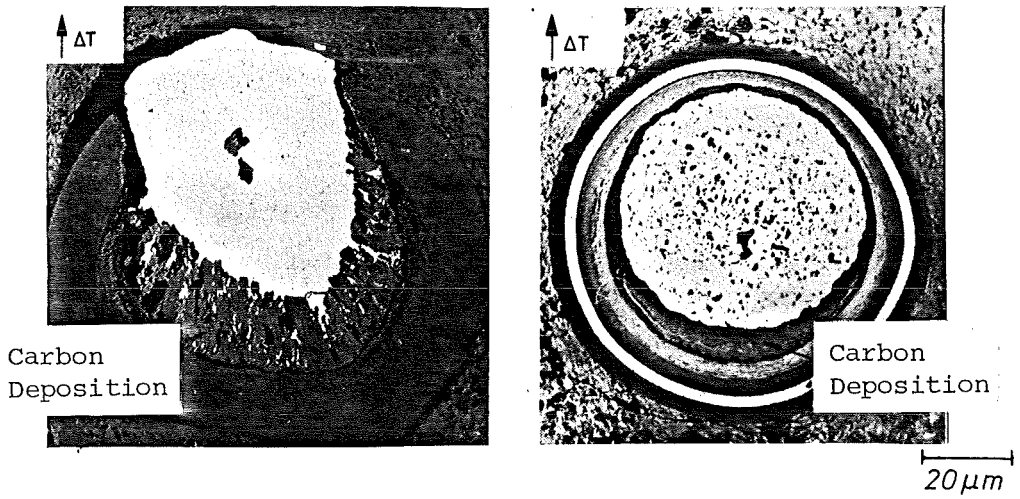

Fig. F.3.4: Amoeba-Effect in Coated Fuel Particles

G. FUEL ELEMENT DESIGN AND FABRICATION

G.1 SURVEY ON FUEL ELEMENT TYPES

G.2 PIN LAYOUT AND BUNDLE STRUCTURE

G.3 BASIC RELATIONS FOR PIN DESIGN

G.4 SPECIFICATIONS FOR PIN AND BUNDLE

G.5 A TYPICAL FABRICATION ROUTINE

G.1. Survey on Fuel Element Types

A fuel element can be defined as fuel carrier, that is manipulated closely within a reactor core. We distinguish

- pins, individually inserted and manipulated,
- pin bundles,
- plate bundles,
- ball type fuel, socalled "pebbles",
- prismatic blocks with fuel channels.

The orientation of the different types within the reactor core and the reactor designs concerned are compiled in Table G.1.I.

Single fuel pins with U metal form the core of the Gascooled Graphite Reactors (GGR). Every cooling channel contains some few pins, one above the other. The High Temperature Reactor (HTR) is cooled by helium, the fuel elements being arranged in "pebble beds" or in graphite blocks with fuel channels. All other power reactors are equipped with pin bundles: The Advanced Gascooled Reactor (AGR), the Heavy Water Reactor (HWR), the Light Water Reactor (LWR) in both versions (Boiling Water Reactor BWR and Pressurized Water Reactor PWR), the Fast Breeder Reactor (FBR). In Table G.1.II a compilation is presented comparing the data of the different pin bundle types in power reactors. It is to be mentioned that in pin bundles mostly not all the positions are occupied by fuel pins. E.g. in a PWR bundle 20 pin positions remain free being reserved for the control rods.

Table G.1.I: The Fuel Element Types and Their Application

	Orientation in Reactor Core	Reactor Type
Single pins	vertical	Gascooled graphite reactors, research reactors
Pin bundle	vertical	Light water reactors, heavy water reactors (KWU), advanced gascooled reactors, fast Na-cooled reactors
	horizontal	Heavy water reactors (CANDU)
Plate bundle	vertical	Materials test reactors, high flux reactors
Pebbles	pebble bed	Heliumcooled high temperature reactors
Blocks with fuel channels	vertical	

Table G.1.II: Typical Data for Pin and Bundle Design in Power Reactors

	Power Plant	Calder	Hinkley Point B	Philippsburg 1	Biblis B	Pickering-1	Phénix
	Location	Calder Hall	Hinkley Point	Philippsburg	Biblis	Pickering Township	Marcoule
	Country	Great Britain		Germany		Canada	France
	Reactor Type	GGR	AGR	BWR	PWR	HWR	FBR
	Power (MWe)	220	621	900	1300	542	250
Outer Dimensions	Length (mm)	1115	996	4088	4407	495	1793
	Diameter (mm)	29.2	15.2	14.3	10.75	15.2	6.55
Fuel	Material	U-Metal	UO_2	UO_2	UO_2	UO_2	UO_2-PuO_2
	Diameter (mm)	27.6	14.5	12.4	9.1	14.4	5.5
Clad	Material	Magnox	Stainless Steel	Zircaloy	Zicaloy	Zircaloy	Stainless Steel
	Wall Thickness	0.8	0.38	0.81	0.72	0.38	0.45
Bundle	Arrangement	(Single Pins)	3 Rings	Square	Square	3 Rings	Hexagon
	Number of Pins		36	49	236	28	217
Bundle (or Single Pins) per Core Position		(7)	8	1	1	12	1

G.2. Pin Layout and Bundle Structure

A fuel pin contains always

- nuclear fuel, i.e. fissionable material + breeding material + alloying or compound elements,

surrounded by

- a can or cladding, i.e. a cylindrical tube with end caps.

Fuel pins that are due for higher burnup often have a

- fission gas plenum, i.e. an empty volume within the can mostly secured by a support spring.

Fuel pins for breeder reactors have

- breeding sections forming axial breeder blankets within the reactor core.

Between fuel and clad there is either

- metallic contact, e.g. if metal fuel is directly connected to the cladding

or

- a more or less loose mechanical contact

or

- a defined and specified radial gap.

A gap between fuel and clad is filled up with a protective gas (mostly helium) at the final steps of fabrication, as is done with every other hollow space within the pin. There are considerations and also some experiments, where instead of a gas bonding a bonding with liquid Na was used as contact material with highly improved thermal conductance. A typical example for such a concept is the Na bonding between fuel and clad in a carbide pin.

The pin layout for 3 different pin types is demonstrated schematically in Figure G.2.1, namely for pins of LWR, FBR and GGR. All these pins are vertically oriented within the reactor core. There are also reactors, the pins of which are positioned horizontally, the most important example being the canadian CANDU-type heavy water reactors.

The fuel pins of all power reactors are assembled in bundles. With respect to the geometry of the bundle cross section one can distinguish square, circular and hexagonal bundles, see Figure G.2.2.

Furthermore, there are also more complicated cross sections, especially for research and test reactors.

In a square bundle the possible number of pin positions is given by the square numbers. They need not to be occupied completely. Typical for a boiling water reactor (BWR) are 7 x 7 = 49 pin positions, for a pressurized water reactor (PWR) 16 x 16 = 256 positions. The possible positions in a hexagonal bundle are 7, 19, 37, 61, 91, 127, 169 etc.

The pins of a bundle are to be positioned and mechanically fixed against each other. The whole bundle is to be integrated into the reactor core. For this purpose a special bundle structure is necessary that has also to guarantee the proper coolant flow. Generally, this structure is composed of foot endpiece, head endpiece, wrapper tube and spacers, see Figure G.2.3. In LWR, for fuel pin spacing only spacer grids are in use. For FBR also wire spacing, i.e. wires helically surrounding every single pin, is a experimentally proven option. Also cladding tubes with integrated fins for spacing were already tested successfully.

Numbers mean mm, scale for diameter enlarged 15 fold compared to length scale

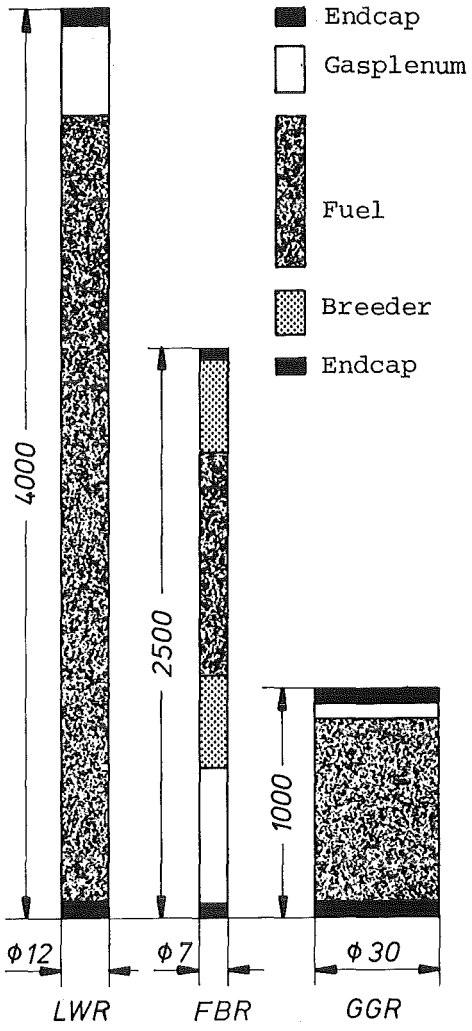

Fig. G.2.1: Layout and Approximate Dimensions of Different Pin Types

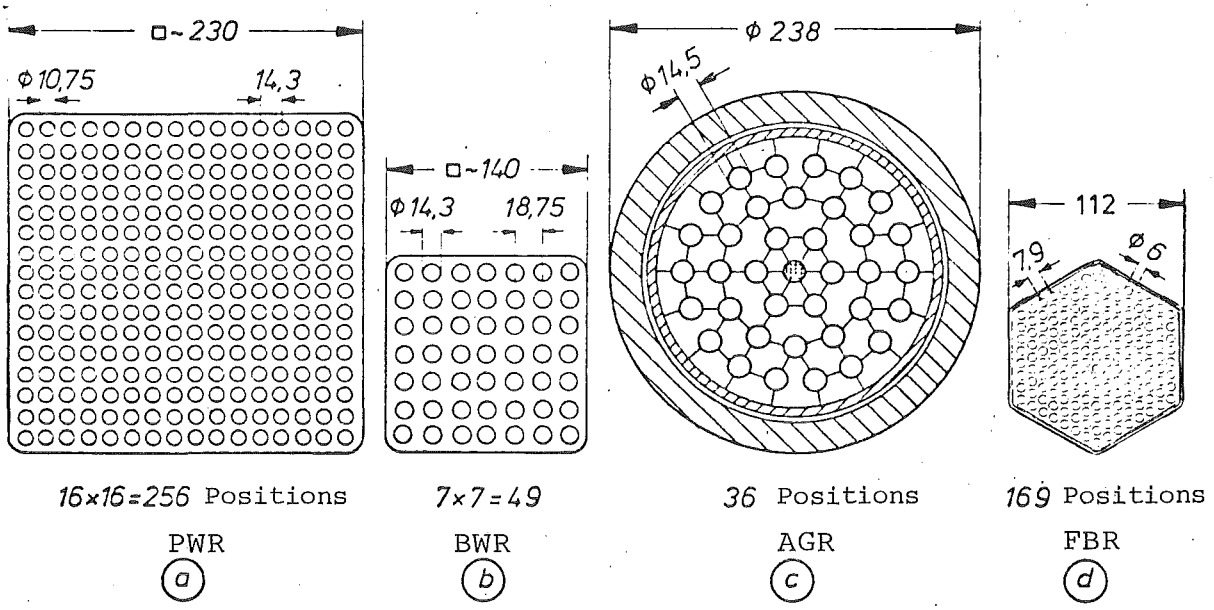

Fig. G.2.2: Cross Sections of Typical Fuel Bundles

a) Pressurized Water Reactor (PWR)
b) Boiling Water Reactor (BWR)
c) Advanced Gascooled Reactor (AGR)
d) Sodiumcooled Fast Breeder Reactor (FBR)

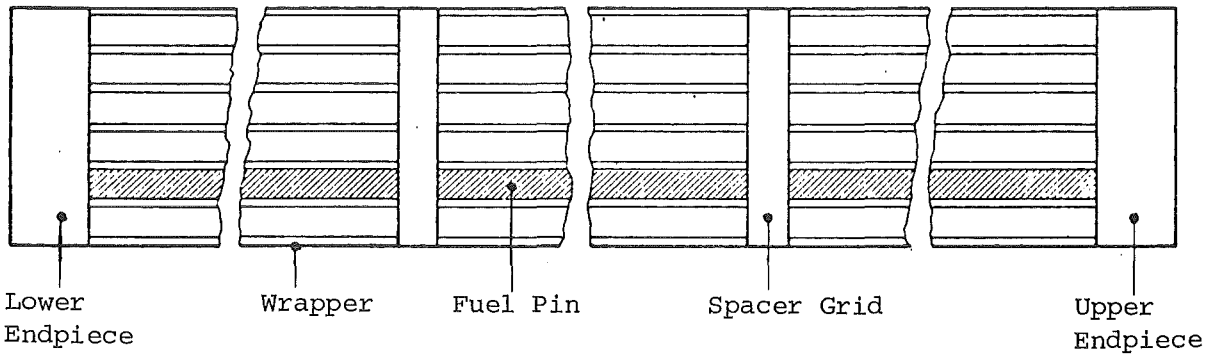

Fig. G.2.3: Structure of a Fuel Pin Bundle, Example BWR

G.3. Basic Relations for Pin Design

In the numerical effort for pin design, there are to be used some special definitions as outlined in Table G.3.I.

The coherence between the power measures is given by (R ≙ fuel radius):

$$\chi = \pi R^2 \cdot b_{fis} \cdot \rho_{fis} = \pi R^2 \cdot b_f \cdot \rho_f = b_f \cdot L \qquad (1)$$

The linear rod power and the radial temperature distribution in the fuel are connected via the thermal conductivity k. In the simple case of constant heat source density within the fuel, the integration of the heat conductance equation leads to

$$\chi = 4\pi \int_{T_a}^{T_i} k(T)\,dT \qquad (2)$$

with T_a ≙ temperature on the fuel surface,
T_i ≙ internal fuel temperature in the center,
$k(T)$ ≙ thermal conductivity of fuel.

This relation is strongly applicable for homogeneous fuel cylinders in fast flux; it also approximates more or less the conditions in thermal flux, but only for low enriched fuel.

From formulae (1) and (2) the radial <u>temperature distribution</u> can be calculated. In order to do so, a radial fuel portion with radius r is considered, see Figure G.3.1. With temperature T on the cylinder surface, the rod power χ' of the inner fuel part can be expressed by both formulae as follows:

$$\chi' = \pi r^2 \cdot b_{fis} \cdot \rho_{fis} = 4\pi \int_{T}^{T_i} k(T)\,dT$$

For a rough approximation we set k(T) = constant; hence:

$$T = T_i - r^2 \frac{b_{fis} \cdot \rho_{fis}}{4\,k}$$

This is a parabolic temperature distribution, Fig. G.3.1.

The maximum possible linear rod power in a fuel is (theoretically) defined by its thermal conductivity and the fusion or transition temperature. The fusion point shall not be achieved during operation. The same is due concerning a phase transition, because there would be substantial alterations in properties. From these considerations, limitations for the maximum rod power can be derived, see Table G.3.II. Of course, this compilation is based on some rough simplifications.

The heat transition between fuel and clad is mostly a complex process (only at a completely metallic contact the conditions are more simple). This transition is described in approximation using the heat transition coefficient β_{FC}:

$$\chi = 2 \pi R \cdot \beta_{FC} \cdot (T_{F,s} - T_{C,i})$$

with $T_{F,s}$ ≙ temperature on the fuel surface,
$T_{C,i}$ ≙ temperature on the inner clad surface.

Rough figures for the heat transition coefficient are given in Table G.3.III.

The radial temperature decrease within the clad is expressed by (provided the wall thickness is small compared to the pin diameter):

$$\chi = \frac{2 \pi \cdot \bar{k}_C}{\ell n \, (r_{C,O}/r_{C,i})} \, (T_{C,i} - T_{C,O})$$

with

$\bar{k}_C$ ≙ average thermal conductivity of cladding,
$r_{C,O}$, $r_{C,i}$ ≙ clad radius outside, inside,
$T_{C,O}$, $T_{C,i}$ ≙ clad temperature outside, inside.

Due to an internal gas pressure p there are established stresses in the cladding. It is to be distinguished between

- the hoop stress $\sigma_t = \frac{p \cdot r_{C,i}}{s}$ and
- the axial stress $\sigma_a = \frac{p \cdot r_{C,i}}{2s}$.

These relations correspond to the "vessel formula" and are applicable only at a small wall thickness s. Above that, there are thermal stresses and evt. mechanical stresses caused by interaction with the fuel. The cladding of a pin may also be burdened mechanically by a coolant outside pressure (e.g. in a PWR). Such external forces may lead to creep buckling damages.

Table G.3.I: Definitions for Pin Design

Term	Symbol	Dimension
Linear Rod Power	χ	W/cm or kW/m
Specific Power, in relation to fissionable material amount	b_{fis}	W/g fissionable material
Specific Power, in relation to fuel amount	b_f	W/g fuel
Fissionable Material Density	ρ_{fis}	g fissionable mat./cm^3
Fuel Density	ρ_f	g fuel/cm^3
Linear Density of Fuel	L	g fuel/cm

Table G.3.II: Linear Rod Power Ranges for Fuels in Cylindrical Geometry

	Temperature Range outside T_a (°C)	inside T_i (°C)	Average Thermal Conductivity k (W/m K)	Maximum Linear Rod Power χ_{max} (W/cm)
U-Metal	300	600	35	1200
UO_2	400	2000	3	600
UO_2-PuO_2	700	2500	3	570
UC-PuC	800	1600	17	1700

Table G.3.III: Heat Transition Coefficients

	$\beta_{F,C}$ (W/cm^2 K)
100 µm He-Gap	0.5
Contact at He-Bonding	1
100 µm Na-Gap	50
Contact at Na-Bonding	200
Metallic Bond	(very large)

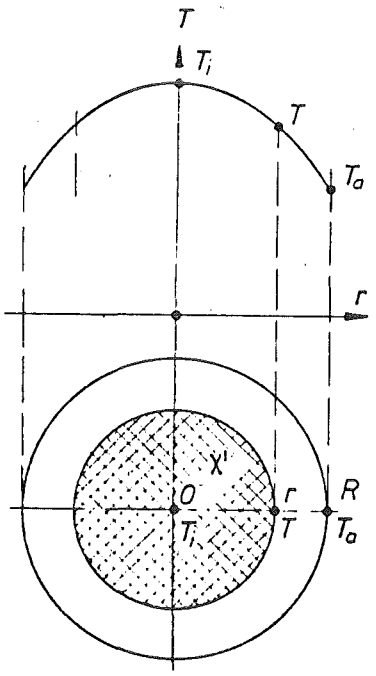

Fig. G.3.1: Radial Temperature Distribution in the Fuel

G.4. Specifications for Pin and Bundle

The technical specifications for the fuel pin comprise statements on fuel, on cladding, on internal structure and on the whole pin itself. A further very important part refers to the bundle with statements on the bundle design and bundle structure.

In Table G.4.I we have compiled a more detailed list according to this scheme. At all numerical data the corresponding tolerances are most essential. Furthermore, one has to pay attention, that all specifications are consistent and complete. It is advisable to include statements on fabrication methods, test methods, test volume as well as on designation and packaging, in addition to the bare materials specifications. Finally, it is often agreed, what paperwork and test certificates are to be supplied at delivery.

Table G.4.I: List of Specifications

Fuel	Type and Shape Chemical Composition Isotopic Composition Stoichiometry Water and Gas Content Chemical Impurities	Homogeneity Pellet Density Pellet Geometry Pellet Stack Test Lists and Certificates
Cladding Tube	Material, Name and No. Fabrication Method Metallurgical Pretreatment Chemical Composition Grain Size Mechanical Properties	Tube Geometry Ovality, Straightness Surface Roughness Surface Purity Annealing Colours Stock Length Tests and Certificates
End Caps, Internal Structure	Type and Shape Material, Composition	Geometry Tests and Certificates
Fuel Pin	Internal Geometry External Geometry Filling Gas Welding Procedure	Surface Status Tightness Outside Contamination Tests and Certificates
Structural Parts for the Bundle	Design Material, Compositon Mechanical Strength	Welding Procedure Tests and Certificates
Bundle	Design Fabricational Sequence	Tests and Certificates

G.5. A Typical Fabrication Routine

In the course of the fabrication of fuel elements, the fuel and the structural parts for pin and bundle are at first manufactured and supplied. For pin compilation the cladding tube is closed on one side by welding an end cap and then filled with fuel pellets together with additional parts of internal pin structure. Before closing the pin, a thorough rinsing with inert gas takes place. Finally the pin is closed by a second end cap welding.

The spacer grids and support rods are fixed together forming the bundle skeleton, in which the finished fuel rods are inserted. Finally the bare bundle is mounted into a wrapper tube (if applicable).

In Figure G.5.1 such a fabrication procedure for PWR fuel elements is outlined. Actually, there are by far more single steps. Especially the intermediate and final tests require very much effort. In this context all measures for quality control and assurance are to be considered, mainly those, which are carried out in preceding and parallel actions.

There is a great difference between fabrication in laboratory scale and an industrial production. The latter uses increasingly procedural steps that are partly or even fully automized, especially at the quality control. For the fabrication of Pu-containing fuel pins the incentive for automization is particularly large, because the improvement compared to manual work in glove boxes may be quite high.

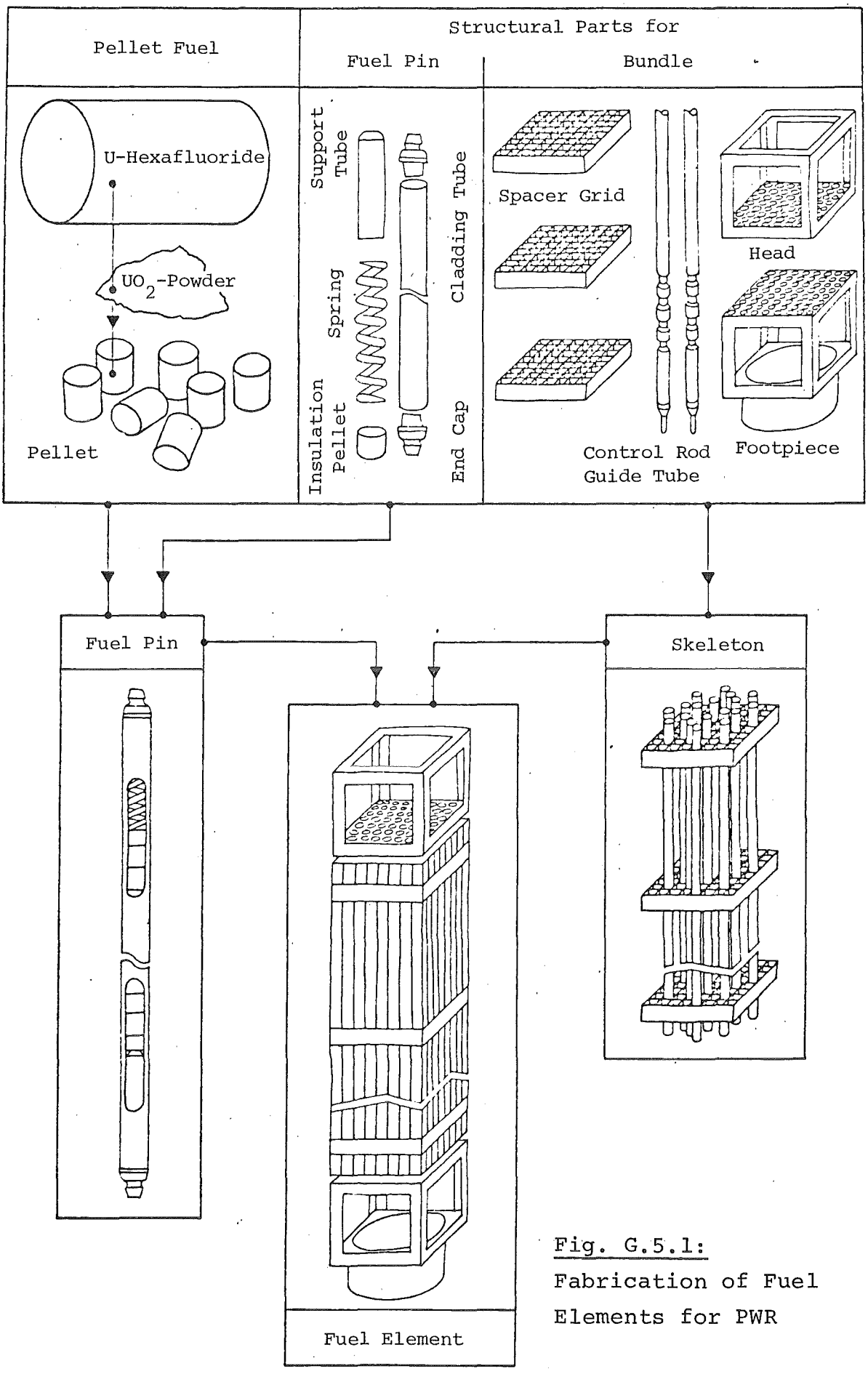

Fig. G.5.1:
Fabrication of Fuel Elements for PWR

H. THE FUEL ELEMENTS IN RESEARCH AND POWER REACTORS

H.1 FUEL ELEMENTS FOR CO_2-COOLED REACTORS

H.2 FUEL ELEMENTS FOR LIGHT WATER REACTORS

H.3 FUEL ELEMENTS FOR HEAVY WATER REACTORS

H.4 FUEL ELEMENTS FOR FAST BREEDER REACTORS

H.5 FUEL ELEMENTS FOR HIGH TEMPERATURE REACTORS

H.6 PLATE-TYPE FUEL ELEMENTS

H.1. Fuel Elements for CO_2-cooled Reactors

There are two different fuel pin types to be distinguished, namely

- pins with natural U-metal as fuel and a cladding made from a Mg-alloy,
- pins with enriched U in the form of UO_2 and a stainless steel cladding.

The first mentioned pins are used in the core of gas-graphite-reactors (GGR), as they are constructed since 1957 in Great Britain (Calder Hall was the first one!) and also in France. The pins with enriched urania belong to a concept with higher CO_2-temperature, called "Advanced Gas-cooled Reactor" (AGR). Some of the design data for both concepts are brought in Table H.1.I.

For the "magnox-pins", the large fuel diameter is characteristic as well as the extensively roughened clad surface with cooling fins. Some of these about 1 meter long pins are positioned one above the other in a coolant channel of the graphite block that forms the reactor core. The achievable burnup throughout is quite small. There are existing a variety of differently detailed designs. Two of them are demonstrated in Figure H.1.1. There are also tube-type U-metal pins, e.g. in French designs.

The AGR fuel pins are very much thinner; they are always assembled in bundles. The fuel element of the AGR Windscale e.g. contains 21 pins positioned in two rings and surrounded by a graphite wrapper tube. The newer unproved design provides three circular rings with a total of 36 pins in the bundle. An example is given in Figure H.1.2 demonstrating the fuel element for a British AGR-power plant. In every single cooling channel of this reactor 8 such fuel elements are positioned above each other.

Table H.1.I: Fuel Pins for CO_2-cooled Reactors

		GGR-Type	AGR-Type
Pin Diameter	(mm)	ca. 30	ca. 11
Pin Length	(mm)	ca. 1000	ca. 1000
Fuel		U-Metal	UO_2
U-235-Enrichment		Natural-U	2.5 %
Cladding Material		Magnox-Alloy	Cr-Ni-Steel
Average Linear Rod Power	(W/cm)	200	60
Average Heat Flux	(W/cm^2)	20	20
Maximum Clad Temp.	(^oC)	450	650
Average Burnup	(MWd/t M)	3000	10000

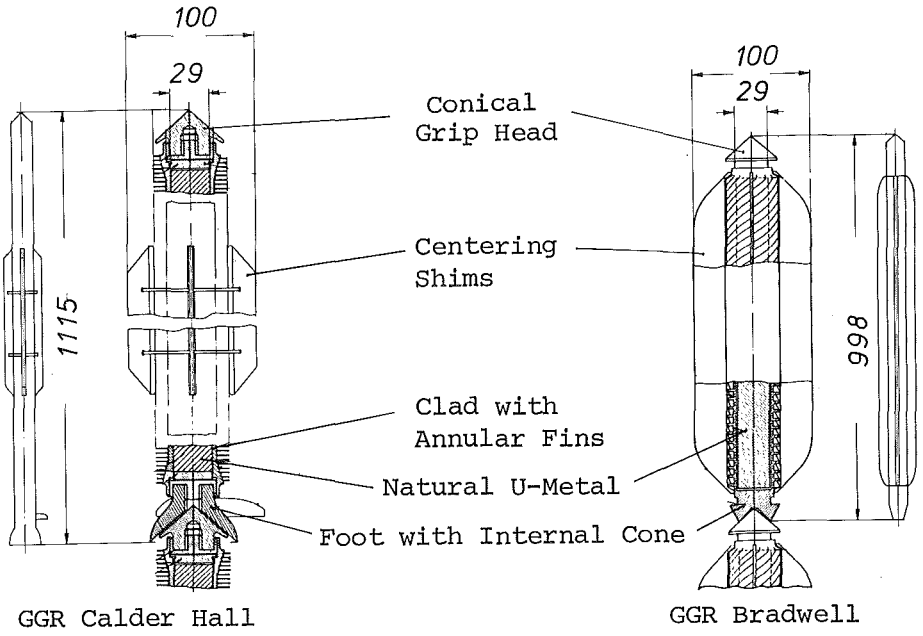

Fig. H.1.1: Fuel Elements with U-metal for CO_2-cooled Reactors

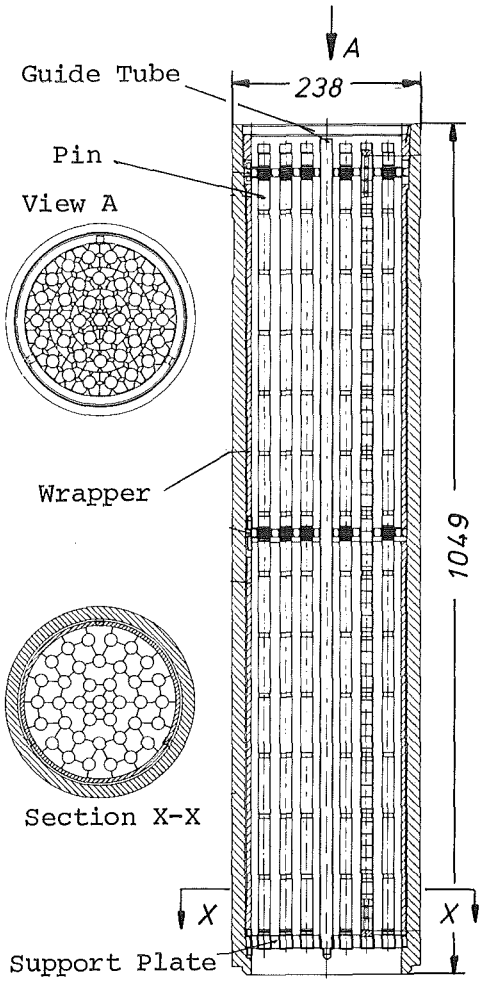

Fig. H.1.2: Fuel Element of the AGR Hinkley Point B

H.2. Fuel Elements for Light Water Reactors

Both variants of the commercialized light water reactors, the PWR and the BWR are equipped with quite thin fuel pins which are assembled to bundles with a square cross section. Typical design data are compiled in Table H.2.I. Both the pin concepts include a slightly enriched UO_2-fuel (U-235 content 2.5 - 4 %) and cladding from zircaloy. Some particulars of the pin design can be realized in Fig. H.2.1. Both reactor types operate under very high coolant pressure, the PWR at ca. 150 bars, the BWR at ca. 70 bars. In order to prevent creep buckling caused by external overpressure, the PWR pin design provides now an initial internal gas pressure of - say - 25 bars.

The bundle designs for each of the LWR-types is specifically different. The PWR fuel element in its square cross section includes 15 x 15 to 18 x 18 pin positions, a major number of which being occupied by guide tubes for control rods. This fuel element wears no wrapper tube. Being completely open, the heat exchange also in radial direction is facilitated.

The BWR fuel element contains by far fewer pins according designs from 6 x 6 to 8 x 8 positions. The element is surrounded by a wrapper. The layout and dimensions including some details are shown in the drawings of Figure H.2.2 and the accompanying Table H.2.II. In the PWR bundle the spacer grids are fixed and positioned by the control rod guide tubes, in the BWR bundle this fixation is performed by an empty pin, the socalled "water pin".

Table H.2.I: UO_2 Fuel Pins for Light Water Reactors (typical design examples)

		PWR	BWR
Pin Diameter	(mm)	10.75	12.5
Pin Length	(mm)	4400	4100
Pin Arrangement		16x16	8x8
Cladding			
Material		Zircaloy-4	Zircaloy-2
Wall Thickness	(mm)	0.75	0.85
UO_2-Fuel in Pellets			
Density	(g/cm^3)	10.3	10.4
Dishing		on both sides	on both sides
Diametral Gap	(µm)	∿200	∿200
Linear Rod Power			
Average	(W/cm)	210	180
Maximum	(W/cm)	450	440
Maximum Clad Temperature	(^oC)	340	370
Maximum Local Burnup	(MWd/kg U)	∿45	∿45

Table H.2.II: Structural Data of LWR Fuel Elements

		PWR of class 1300-MWe	BWR of class 900-MWe
Pin Array		16 x 16	8 x 8
Fuel Pin	(No.)	236	63
Control Rod Guide	(No.)	20	-
Water Pin	(No.)	-	1
Spacer	(No.)	9	7
Pin Length	(mm)	4407	4088
Active Length	(mm)	3900	3760
BE Total Length	(mm)	4835	4470

Fig. H.2.1:
PWR Fuel Pin Sketch
(Type Biblis)

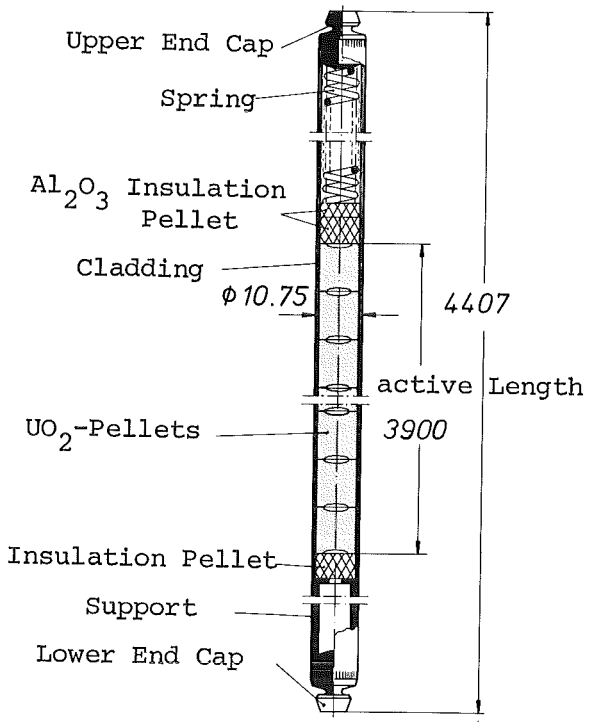

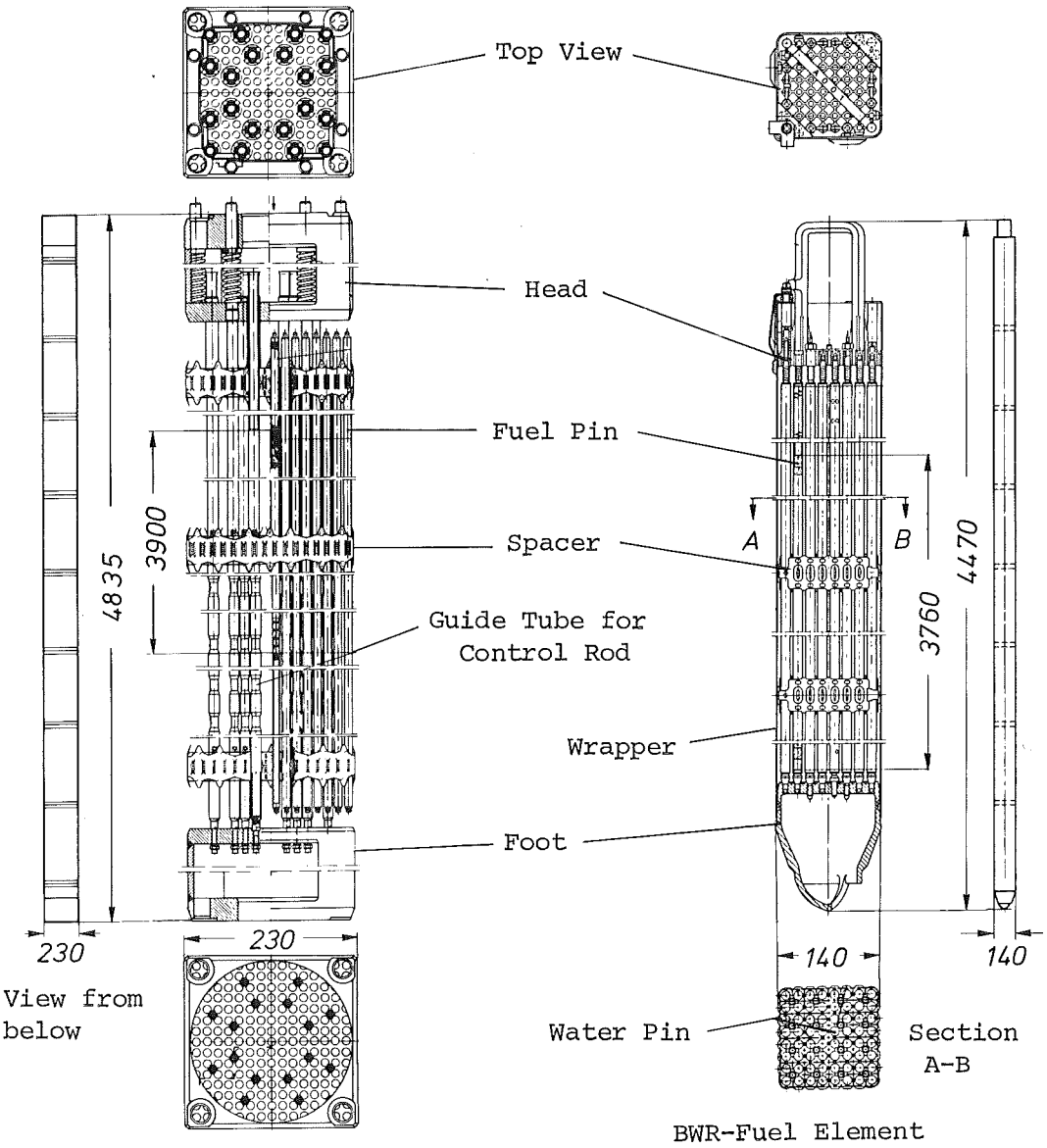

Fig. H.2.2: Design of Typical LWR Fuel Element

H.3. Fuel Elements for Heavy Water Reactors

The first heavy water reactors were designed for research purposes, e.g. the NRX in Canada and the FR 2 in Karlsruhe/Germany. The fuel pins for the first cores of the FR 2 were quite thick rods of U-metal canned with aluminum.

Heavy water reactors for power plants have fuel pin bundles containing oxide pins with zircaloy cladding. In the prototype reactor MZFR in Karlsruhe as well as in the Atucha power plant in Argentine the bundles are vertically positioned in the core. Parallel to this, there is an alternate design, the CANDU type, where the bundles are horizontally arranged. Table H.3.I contains a data list of the different fuel pins. The drawing of a MZFR-bundle is presented in Figure H.3.1, of an Atucha-bundle in Figure H.3.2 and of a CANDU-type bundle in Figure H.3.3.

Table H.3.I: Fuel Pins for Heavy Water Reactors

	MZFR Karlsruhe	ATUCHA I Argentine	CANDU Canada
Pin Diameter (mm)	11.7	11.9	15.2
Pin Length (mm)	1845	ca. 5400	495
Pin Arrangement	37 pins in ring element	36 pins in ring element	19 pins in ring element
Fuel			
Material	UO_2	UO_2	UO_2
Form	pellets	pellets	pellets
Density	10.6	10.4	10.4-10.7
Clad			
Material	Zircaloy-2	Zircaloy-4	Zircaloy-2
Thickness (mm)	0.6	0.5	0.38
Linear Rod Power			
Average (W/cm)	116	218	200
Maximum (W/cm)	360	575	500
Maximum Clad Temp. (^{o}C)	306	323	302
Maximum Burnups (MWd/kgU)	5	9	ca. 10

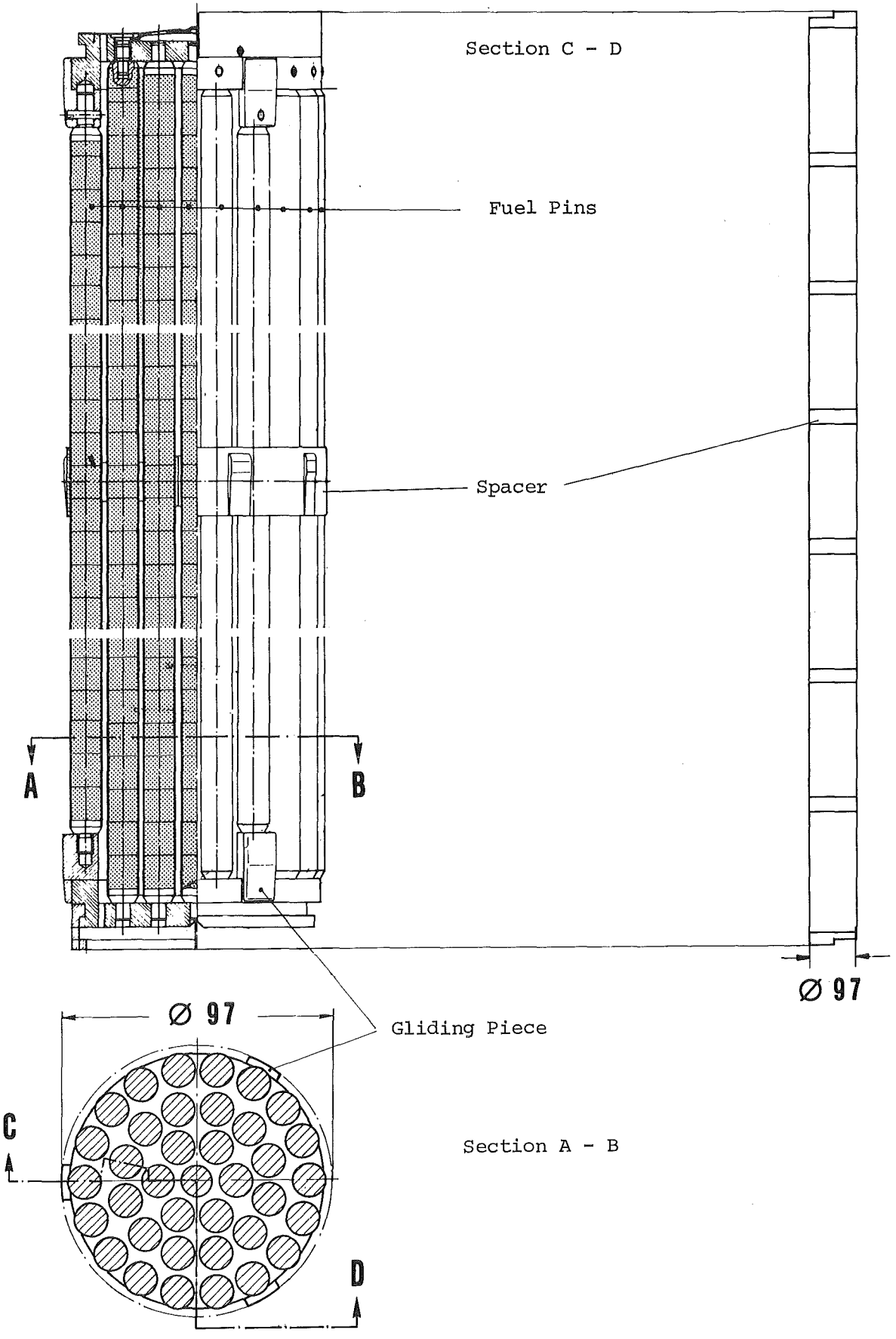

Fig. H.3.1: MZFR Fuel Element

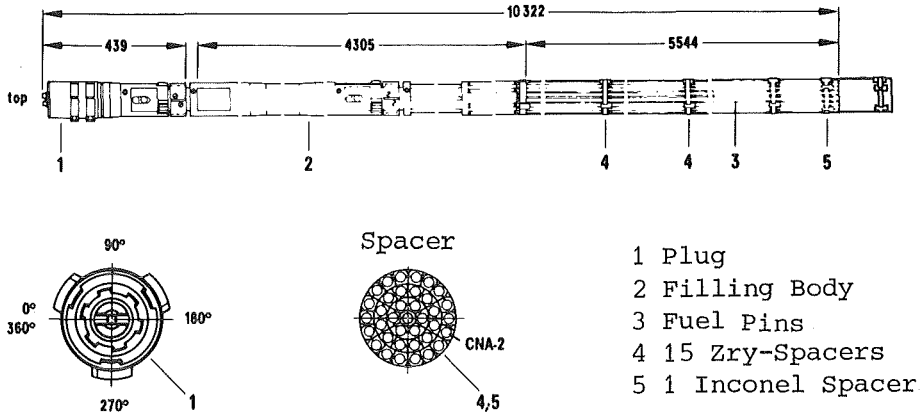

Fig. H.3.2: Fuel Element Column of ATUCHA I

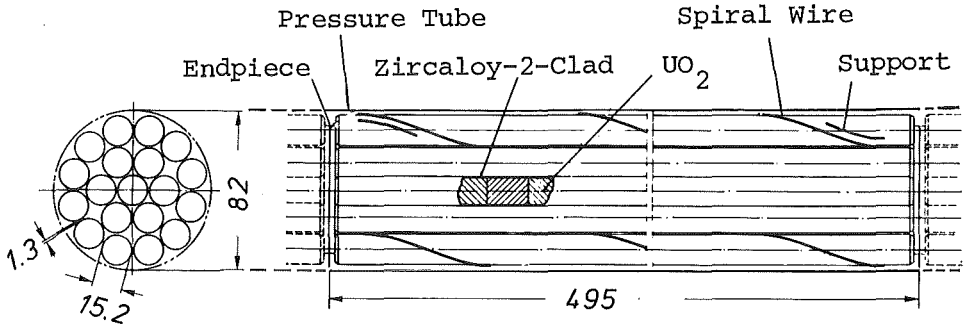

Fig. H.3.3: CANDU Fuel Element

H.4. Fuel Elements for Fast Breeder Reactors

The fuel pins in fast breeder fuel elements contain in addition to the fuel zone axial breeder zones and a fission gas plenum. The volume of this plenum is nearly as large as the fuel volume, so that the fission gas pressure buildup can be limited to acceptable values also at high burnups typical for fast breeders. The pin layout of the diverse development groups is quite similar, see the comparison in Figure H.4.1 and Table H.4.I.

Nevertheless there are essential differences in some details, e.g. in the distribution of the axial pin zones. The main portion of the gas plenum is positioned either at the bottom (coolant entrance) or at the top of the pin (hot end). PHENIX and PFR include only the lower breeding zone within the pin, while the upper axial breeder blanket is formed by separate breeder elements. In the Russion prototype BN-350, the pin contains only fuel. In the American test reactor FFTF, the axial breeder is replaced by reflector material.

The fuel pins in all reactor designs are assembled to hexagonal bundles. For the pin spacing either spacer grids or spiral wires are used. Such spiral wires surround every single pin and support each other.

In all fast breeder pins up to now oxide fuel is provided and actually used, in most cases UO_2-PuO_2-mixed oxide. This fuel is basically similar to the UO_2-fuel of LWR. The fuel density is somewhat lower. The pin diameter is considerable smaller, so that there is an essentially increased specific power in the fuel at about the same linear rod power.

The actual design of the SNR-300 pin and bundle is given in the Figures H.4.2 and H.4.3. This fuel element belongs to the German-Belgien-Dutch fast prototype reactor in Kalkar, the first version Mark Ia for the first core having a pin diameter of 6 mm.

Advanced pin developments which are listed in Table H.4.II aim for larger pin diameters with oxide fuel and also for carbide fuel. Fuel

elements with carbide fuel promise a distinctly increased linear rod power as well as a higher breeding ratio. The fast reactor variant with He-cooling employs a quite similar pin design, the clad temperatures to be expected is, however, considerably higher.

Table H.4.II: Pin Concepts for Advanced Fast Breeders

	Na-Cooled Fast Breeders			Pins for Helium-Cooling
	SNR-300 Mark Ia	Pins with Larger Diameter	Pins with Carbide Fuel	
Fuel Clad	UO_2-PuO_2 S.S.	UO_2-PuO_2 S.S.	UC-PuC S.S.	UO_2-PuO_2 S.S.
Pin Diameter (mm)	6.0	7.6	8.5	8.2
Max. Lin. Rod Power (W/cm)	355	450	800	430
Max. Clad Temperature (^oC)	620	620	620	630
Max. Burnup (MWd/kg M)	85	100	100	100
Possible Variants		Finned Tubing	Na-bonding	Carbide Fuel, Fission Gas Release

Table H.4.I: Fuel Pins of Fast Prototype Reactors, Design and Operational Data

	SNR-300		BN-350	PFR	PHENIX	FFTF	MONJU
	Mark Ia	Mark II					
Fuel Pin							
Diameter (mm)	6.0	7.6	6.1	5.84	6.55	5.84	6.5
Length (mm)	2475	2475	1140	2260	1793	2380	2740
Fuel	UO_2-PuO_2	UO_2-PuO_2	UO_2, enriched	UO_2-PuO_2	UO_2-PuO_2	UO_2-PuO_2	UO_2-PuO_2
Breeder	UO_2	UO_2	-	UO_2	UO_2	-	UO_2
Cladding							
Material (No. AISI)	1.4970	1.4970	Type 316	Type 316	Type 316	Type 316	Type 316
Wall Thickness (mm)	0.38	0.50	0.35	0.38	0.45	0.38	0.45
Fuel Pellets							
Diameter (mm)	5.09	6.41	5.1	4.95	5.5	4.94	5.4
Pellet Shape	Dishing	Dishing	Central Hole	Central Hole	Full Cylinder	Dishing	
Material Density (% T.D.)	86.5	92	95.8	95.7	85	90.4	85
Smeared Density (% T.D.)	80	85	73	80	80	85.5	
Lin. Rod Power, max.[1] (W/cm)	355/500	450/600	440/500	450/	430/	430/	450/
Clad Temp. max.[1] (°C)	620/685	620/685	/675	/700	650/700	610/670	/700
Target Burnup (MWd/kg M)	85	85	50	70	50	80	80
Pins per Bundle	169	127	169	325	217	217	169
Spacer	Grid	Grid	Wire	Grid	Wire	Wire	

[1] Nominal/Hot channel conditions

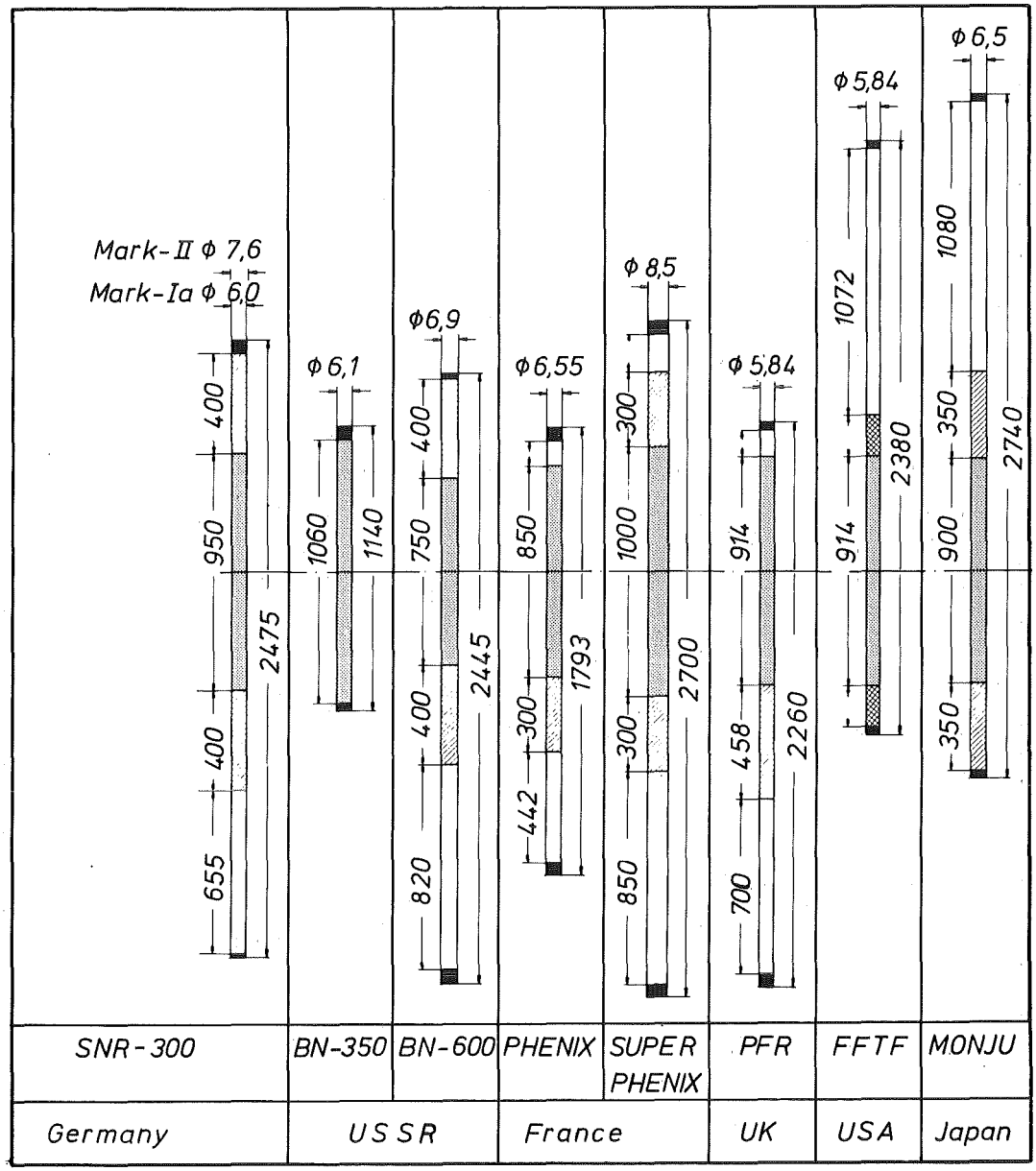

Fig. H.4.1: Fuel Pins of Fast Reactors

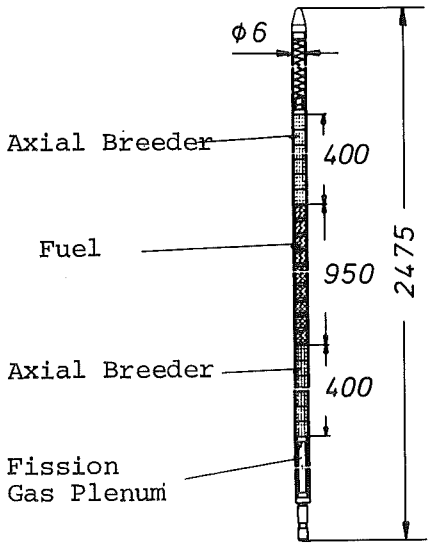

Fig. H.4.2: Fuel Pin Mark Ia of SNR-300

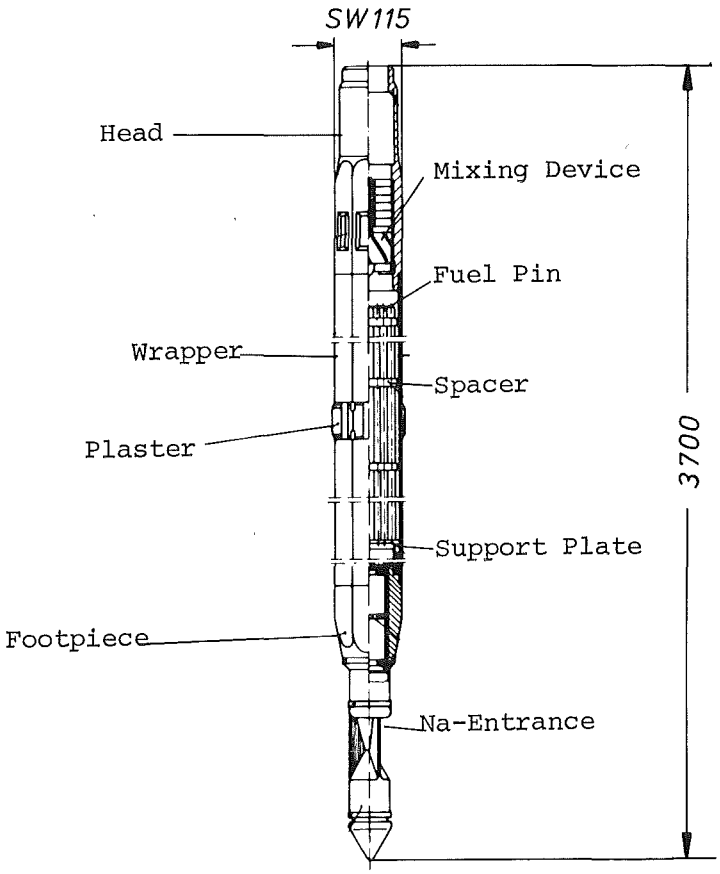

Fig. H.4.3: Fuel Element of SNR-300

H.5. Fuel Elements for High Temperature Reactors

The helium-cooled High Temperature Reactors (HTR) employ graphite as a moderator. Therefore, it is obvious to use graphite as temperature-resistant cladding material, too. There are two fuel element designs essentially different in geometry: The ball-shaped "pebbles" and the block element. Both element designs use coated particles with UO_2 or UC_2 as fuel carrier. In addition to this ceramic fuel (mostly highly enriched), there are also pure breeder particles, e.g. containing ThC_2, in use.

The pebble element, as it was developed in Germany for the pebble bed reactor (AVR Jülich, THTR Schmehausen), is a 60 mm ball diameter, the thickness of the fuel-free graphite shell being 5 mm. The interior of such a pebble contains fuel particles with highly enriched U and also breeder particles. One pebble contains about 1 g U-235 and 10 g Th.

There were different ball designs continuously developed, see Figure H.5.1. The first design was a hollow ball, in which coated particles homogeneously mixed with graphite powder were filled. In an advanced type the fuel particles are glued to the internal surface of the ball, the hollow space being filled up with graphite powder. The final standard design is fabricated by isostatic pressing. In this process the core of the ball containing fuel particles and graphite is prepressed, then surrounded by a fuel-free graphite shell and pressed for a second time. A final heat treatment produces a compact binding of the ball.

The block element developed in USA is a prismatic graphite block with hexagonal cross section, see Figure H.5.2. In this block, there are numerous longitudinal channels alternately for particle fuel and for cooling purposes. In the American HTR in Fort St. Vrain six such block elements are stacked in a core position. The fabrication of the elements is performed by machining of graphite blocks or by a powder-press process similar to the pressed ball-type element.

The function of the graphite in the HTR elements is limited to the mechanical configuration and strength and to the heat transition from the fuel particles to the coolant gas. The tightness against fission products is already guaranteed by the coating of the particles. Special care at the fabrication is to be expended, in order to keep the graphite mantle free of heavy metal, otherwise during reactor operation the coolant will be contaminated by fission products.

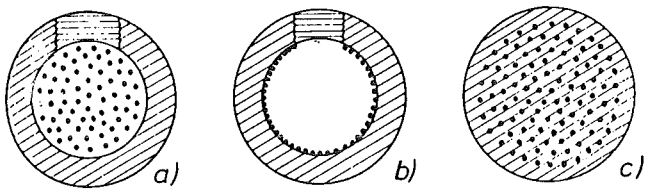

Fig. H.5.1: Ball-shaped Fuel Element for HTR

a) Hollow ball element with homogeneously distributed fuel particles

b) Hollow ball element with particles glued on the inner surface

c) Isostatically pressed ball element

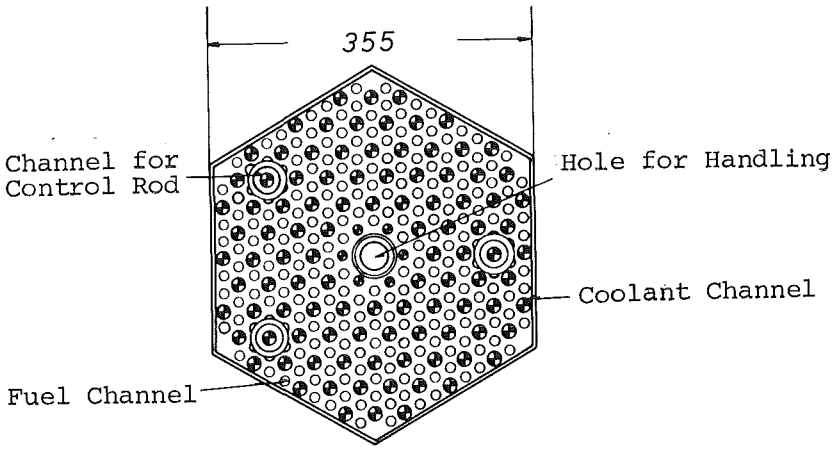

Fig. H.5.2: Cross Section of the Block-Element of HTR Fort St. Vrain (Longitudinal Dimension 792 mm)

H.6. Plate-Type Fuel Elements

In a plate-type fuel element a quantity of single fuel plates is combined to a bundle. Such a geometry makes possible a very intensified cooling, because the relation between cooling surface and fuel volume becomes more favourable. Therefore, this fuel element type is especially suitable for thermal high flux reactors and material test reactors (MTR). A typical design of a MTR element is shown in Figure H.6.1. In this design, 19 somewhat curved fuel plates are assembled to a bundle with square cross section, spaced by side support plates and completed by head-and footpieces.Another design is demonstrated in Figure H.6.2 representing a fuel element of the Belgian test reactor BR 2. Here 18 fuel plates are curved forming a concentric ring element with a central irradiation channel of very high neutron flux.

The fuel in the plates consists of an alloy or a cermet with highly enriched U. The plates mostly are covered with Al. The fabrication of such plates often is carried out applying the socalled "picture-frame-technique". In this technique a plane fuel layer of - say - dispersion-type fuel is surrounded by an Al frame and then covered on both sides with an Al-sheet, Figure H.6.3. This arrangement is finally joined by rollplating at 600°C. Afterwards this plates (about 70 cm long, 8 cm wide and 1 mm thick) are curved and fixed into the bundle structure.

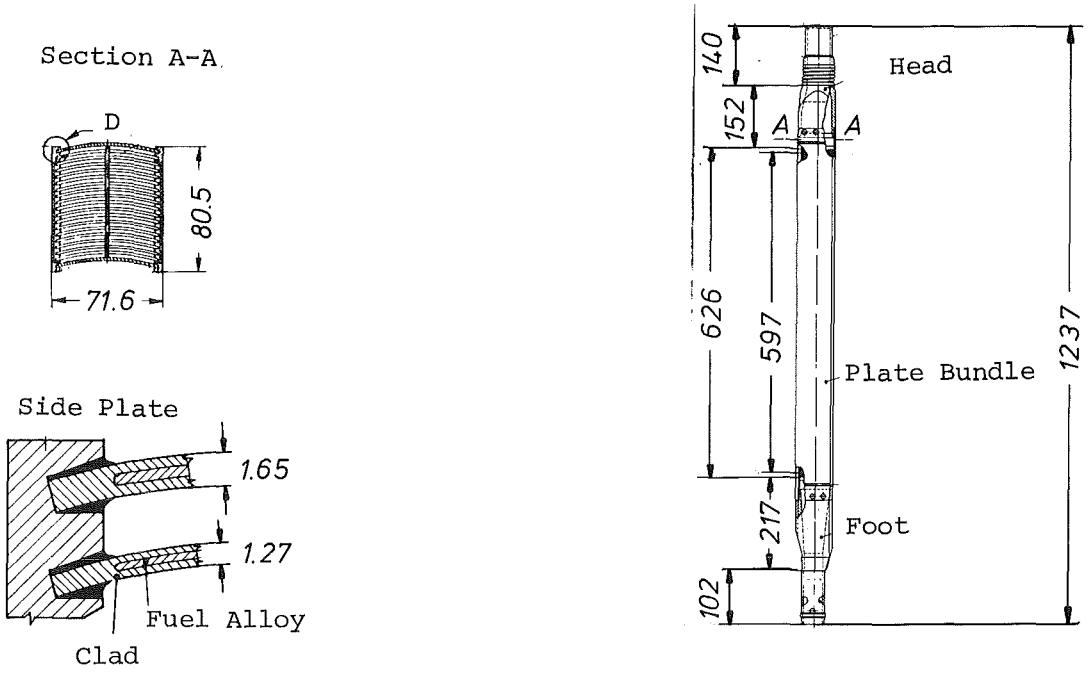

Fig. H.6.1: Fuel Element of the Materials Testing Reactor in Idaho Falls, USA

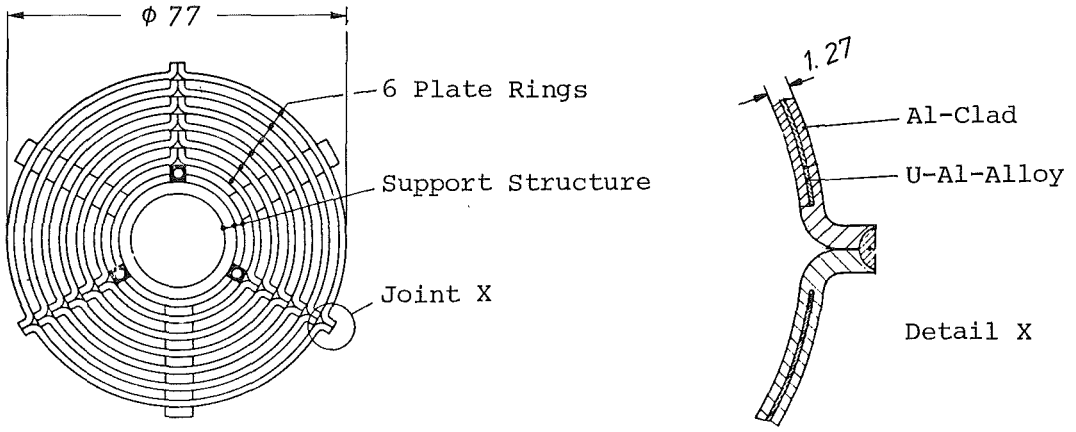

Fig. H.6.2: Cross Section of the Plate Type Element in BR 2 in Mol/Belgien (Total length 965 mm, active length 763 mm)

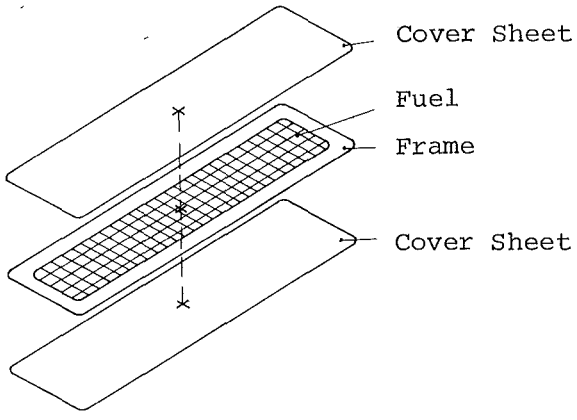

Fig. H.6.3: Scheme of the Picture-Frame-Technique

J. FUEL CYCLES

J.1 THE DIFFERENT TYPES

J.2 THE U-PU-FUEL CYCLES

J.3 THE HTR-FUEL CYCLE

J.4 COST CONSIDERATIONS

J.1. The Different Types

According to definition, a cycle is a closed formation. In spite of this logical fact, we consider in nuclear technology also an socalled "open fuel cycle" as well as the closed fuel cycle.

While in the closed cycle the consecutive steps are principally repeated, this continuity is not performed in the open cycle. The open cycle renounces the reprocessing and waste treatment. The finally burnt fuel elements are stored in longterm installations after some conservative measures or without any further conditioning. In the open cycle, no further use is made of the remaining fissionable and breedable nuclides in the burnt fuel.

In practice we have to consider 3 different types of closed fuel cycles, namely

- the LWR fuel cycle,
- the fuel and breeder cycle for fast reactors,
- the HTR fuel cycle.

J.2. The U-Pu-Fuel Cycles

The essential steps in the LWR cycle - see Figure J.2.1 - are the conditioning of fuel source material, the U-235-enrichment, the fuel element fabrication, the burnup in the reactor core and the reprocessing. This cycle is connected to the outside via the U recovery and ore treatment, via the delivery of depleted U and of produced Pu and via the delivery of radioactive waste. In the special case of a "Pu recycling regime" no Pu is delivered to the outside. The gained Pu replaces partly the enriched U in new fuel elements. All these steps are to be connected by transport actions, unless there are some steps "collocated".

The cycle scheme for a fast breeder comprises two separate cycles, see Figure J.2.2. The specific fuel cycle and the breeder cycle are in contact within the reactor core. Feed material from outside is only U-238 (e.g. as depleted U). Delivered to the outside is surplus Pu and radioactive waste.

Both cycles,the LWR-cycle and the FBR-cycle base on the U-Pu-chain. Their features are similar. Major differences are in that the FBR fuel has higher Pu-content and higher burnup. On the other hand, the FBR cycle do not need U enrichment. In a commercialized power reactor economy of the future, the single steps of a fuel cycle are not established separately for every reactor. They are collected into enrichment facilities, fuel fabrication and reprocessing plants. A special connexion between LWR- und FBR-cycle exists in the depleted U, which is of no value for the LWR, but can feed the FBR exclusively.

The practical realization of the steps in the U-Pu-cycles is very advanced. The fabrication of oxide type fuel is carried out in large technical scale. For the chemical reprocessing the PUREX process is applied world-wide. Also the large scale waste treatment and disposal is exercised with promising results.

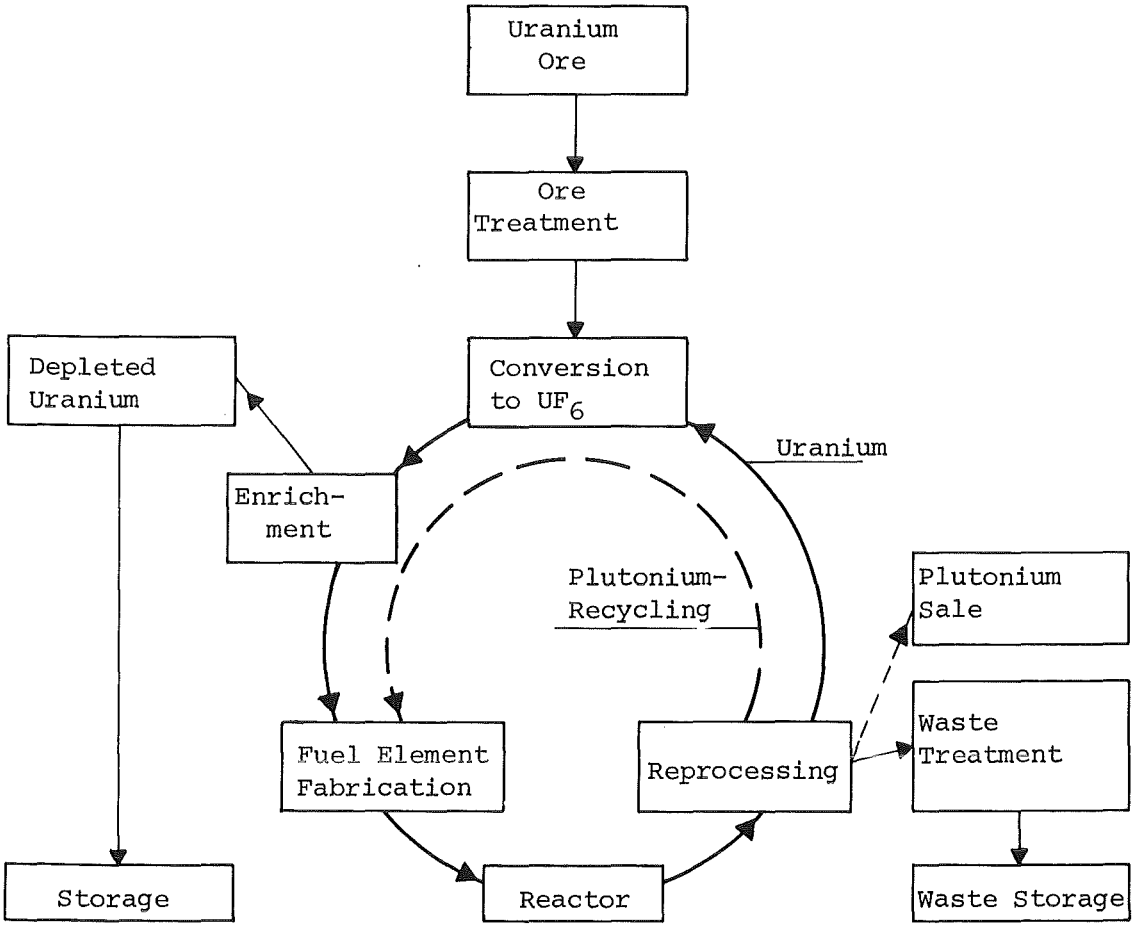

Fig. J.2.1: The Fuel Cycle for Light Water Reactors

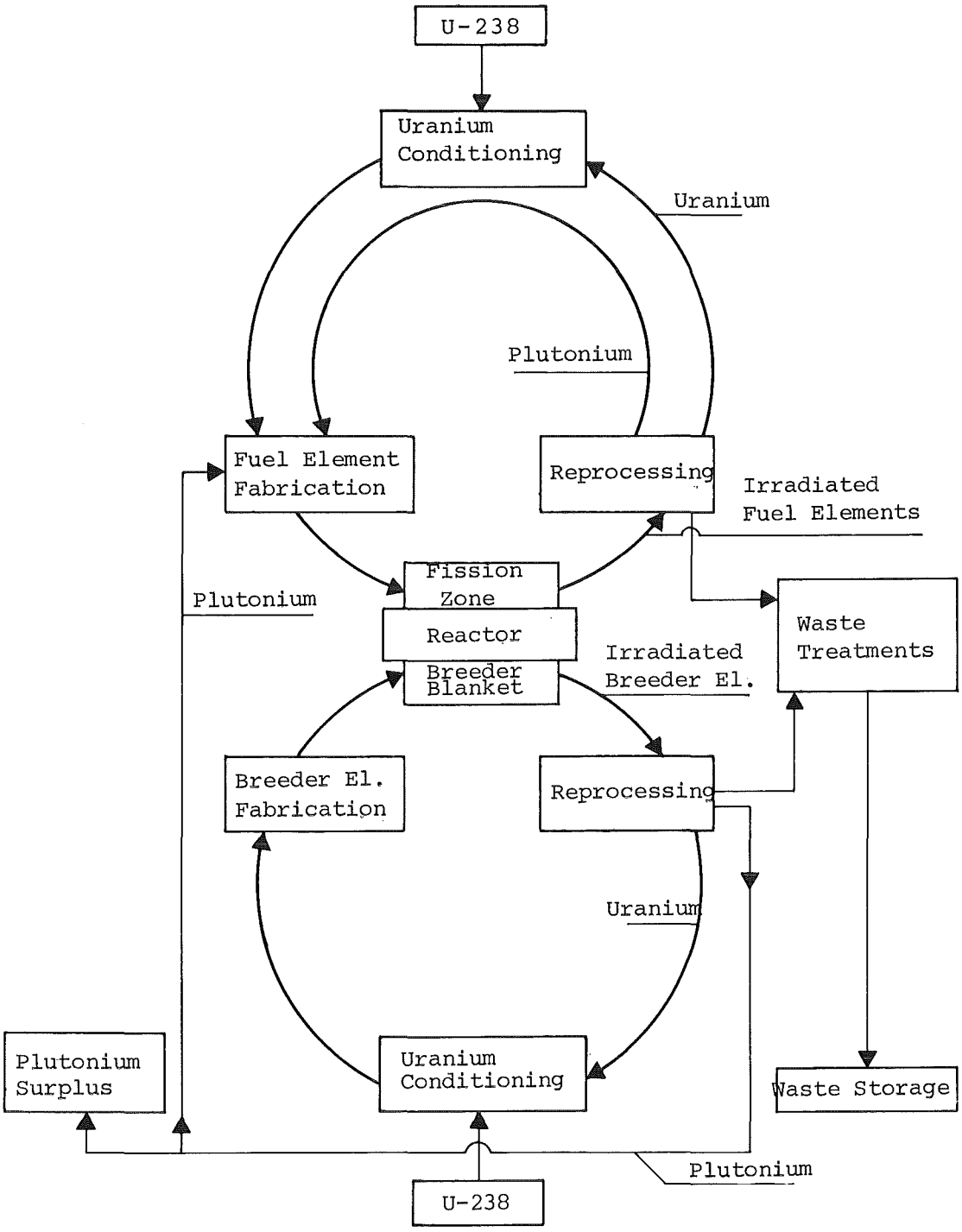

Fig. J.2.2: Fuel and Breeder Cycle for Fast Reactors

J.3. The HTR-Fuel Cycle

The HTR-fuel cycle based on the Th-U-chain is demonstrated in Figure J.3.1. For the reprocessing of the burnt fuel the so-called "THOREX"-process is applied. This process is schematically very similar to the PUREX-process but there exists more or less no larger technical experience. A major problem is the headend, where the large portions of carbon (as graphite and PyC) have to be removed, e.g. by burning. The primary fabrication of HTR fuel is well established. There may arise an increasing problem at repeated refabrication: Besides of the regular breeding result U-233, there is also some U-232 produced in a side reaction. This isotope as an impurity causes a very hard γ-radiation, so that shielding and remote refabrication may become necessary.

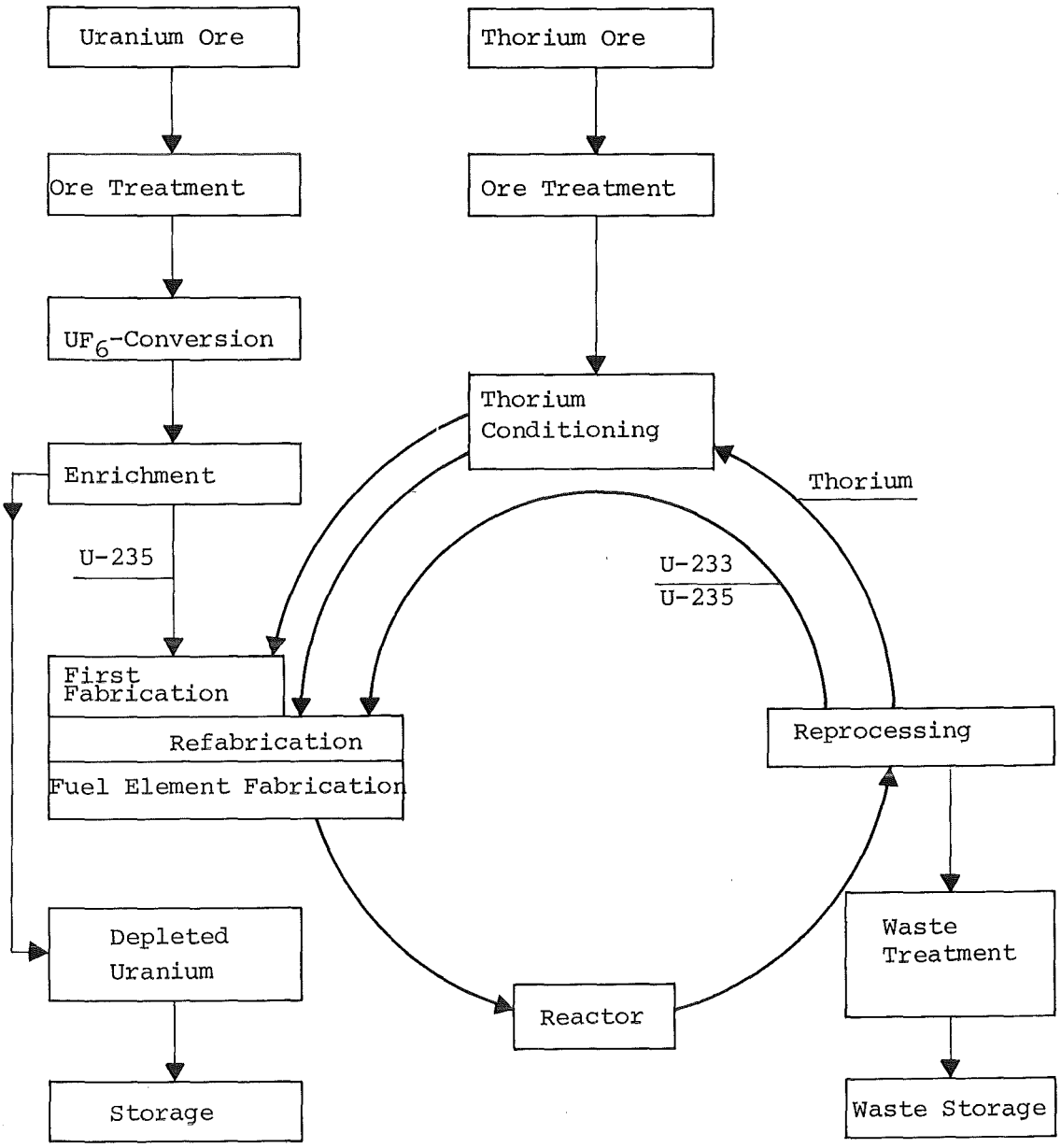

Fig. J.3.1: The Fuel Cycle for High Temperature Reactors

J.4. Cost Considerations

The costs of the fuel cycle amount to a portion of - say - 30 % of the total electricity costs of a nuclear power plant. As a very rough estimate for LWR power plants the following relative cost distribution may be a base for discussion, see Table J.4.1. In this consideration the recycling of Pu is not taken into account. The Pu recycling may lead to some reduction of the total sum by - say - 10 %. But this is still open to the future, it mainly depends on the handling and fabrication penalty for Pu.

The comparison of the single cost contributions show that the supply of natural U and the enrichment amount to about half of the total sum. The further development of these cost ingredients decides, if and when Pu-recycling in LWR and full use of U in FBR will become economical in large scale.

Table J.4.I: Cost Distribution in the LWR-Fuel Cycle

	Cost Portion %	%	
Uranium Supply	30	25	Yellow Cake
		5	Conversion to UF_6
Fabrication	35	25	U-235-Enrichment
		10	BE-Fabrication
Reprocessing and Waste Disposal	35	20	Reprocessing
		10	Waste Treatment
		5	Final Storage
Fuel Cycle	100		

K. FUEL PIN MODELING

K.1 DEFINITION AND PURPOSE

K.2 THE STRUCTURE OF FUEL PIN CODES

K.3 REVIEW OF FUEL PIN CODES

K.1. Definition and Purpose

The goal of modeling treatment of a fuel pin is to describe theoretically the overall behaviour in the course of scheduled and also non-scheduled reactor operation as well as the detailed behaviour of the pin components. Especially, there are to be investigated such quantities that are important as criteria for economic and safe operation, like temperature distribution, migrational effects, deformations, stresses and strains. The comparison of such calculational results to established failure limits may lead to maximum tolerable operation conditions. The problem definition of modeling is schematically demonstrated in Figure K.1.1. Principially it could be expressed by the following equation:

$$L = f\ (A,B,M) \overset{<}{=} S$$

The symbols L, A, B. M and S represent groups of parameters,namely:

- L Load quantities
- A Design parameters
- B Operation conditions
- M Material quantities
- S Failure limitations

These parameter groups are detailed to some extent in Table K.1.I.

Table K.1.I: Parameter Groups in Modeling

Design Parameters A	Materials Composition State of Fabrication External Geometry Internal Geometry etc.
Operation Conditions B	Linear Rod Power Neutron Flux Coolant Temperature etc.
Material Quantities M of Fuel and Clad	Mechanical Properties Thermal Conductivity Heat Transition Fuel/Clad Swelling Behaviour Pore Migration Fission Gas Release etc.
Load Quantities L	Temperature Distribution Stresses and Strains Material Distribution Corrosion Attack etc.
Failure Limitations S	Allowable Maximum of — Temperatures — Stresses and Strains — Burnup etc.

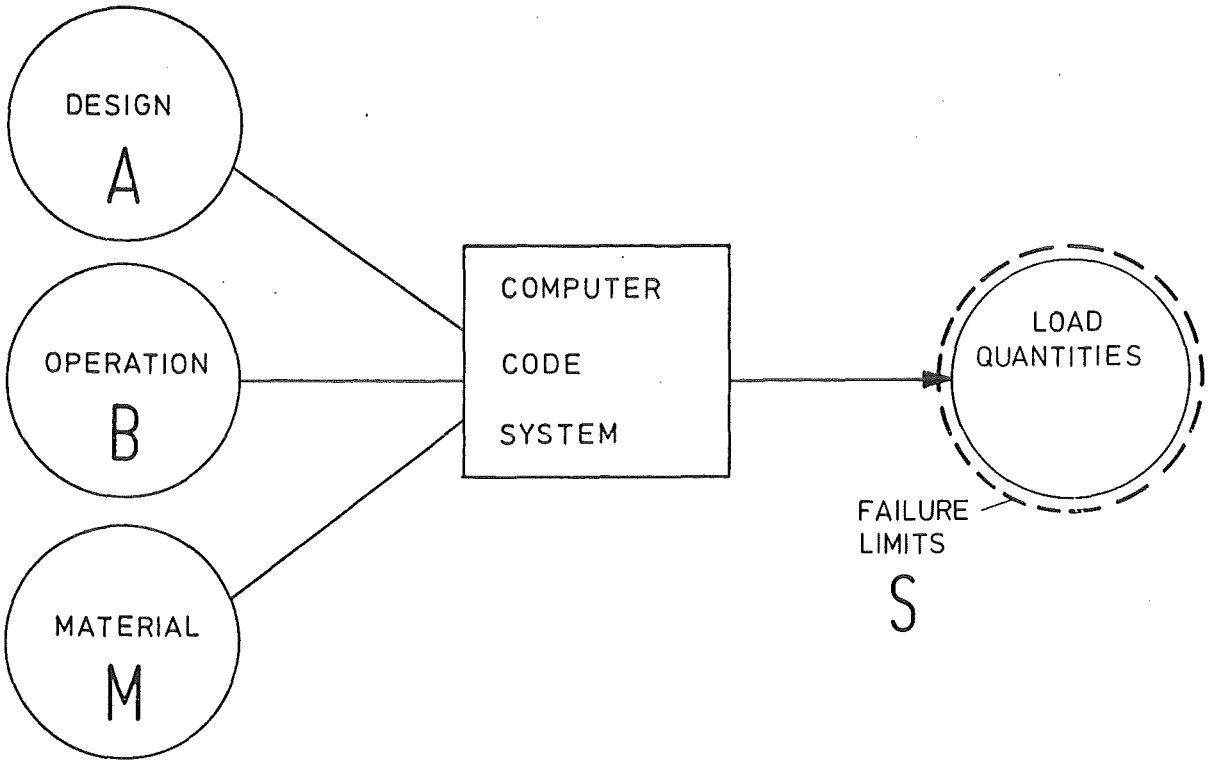

Fig. K.1.1: Scheme of Fuel Pin Modeling

K.2. The Structure of Fuel Pin Codes

The mathematical description uses as a basis physical laws and empirical relationships concerning the mechanical, physical and chemical behaviour of the pin components. All these features are connected within a computer code. In a socalled "analytical code" everything is expressed in a comprehensive matrix of analytical equations. If e.g. you want to know the cladding hoop stress at 5 % burnup at the position of coolant exit, you have to feed in the numerical values of all parameters and get the desired result by analytical dissolving the applicable set of equations.

This analytical procedure would be scientifically satisfying, but is not practicable due to the tremendous complexity of the problem. Only in very simplified cases it could be applied.

The normal way of modeling is establishing a "numerical code". A practical approach for solution is to separate the space structure and time structure within the formalism. This means that the pin lifetime is divided into consecutive time intervals following each other stepwise. For each of these time steps a thermomechanical calculation, including all space induced influences, is carried out.

To treat the space structure, different methods are applicable, namely

- fully analytical procedures,
- partially analytical methods with iterative corrections,
- finite element methods.

It is clear that the mathematical tools for these different modes of treatment are quite different. Mostly, combinations are applied, e.g. an analytical term for a special volume element is iterated with respect to time.

The equations and terms in the fully analytical procedures describe completely the thermomechanics including all geometrical quantities and the motion and segregation of material components. The partially analytical methods - which are by far more applied - take into account the fact that all analytical work is an approach that needs

corrections, and these corrections are performed by iterations. The finite element method is also an analytical tool allowing to treat geometrical sections of the pin consecutively which are interconnected by boundary conditions. The different methods of dealing with the space structure must be adapted to the single problem. As shown in Table K.2.I, the analytical procedures are mainly applied to symmetrical problems, while finite element methods have their domain in non-symmetric configurations.

The time structure is demonstrated in the scheme of Fig. K.2.1. Each state L_{n+1} is produced by the preceding state L_n using analytical relations and approximations. In order to achieve a requested accuracy, the results obtained for each time step are iterated until they become consistent. The time intervals may be different in their lengths. In steady state operation the changes within the pin are small and long time steps are sufficiently accurate. For startup or power cycling periods and especially for transient conditions the time intervals must be chosen to be sufficiently short.

As an example the SATURN-1 code, which was developed for fast reactor pins, is presented. In this code, the schematic diagram of Fig. K.1.1 was implemented by most of the essential phenomena of mixed oxide fuel and stainless steel cladding. The structure diagram of this program, which postulates axial symmetry, is shown in Fig. K.2.2. One realizes that there are some iterative loops in the course of calculation. In SATURN-1 cracked and plastic fuel is dealt with by using a simplified "plane stress" approach. Geometry changes occur around a reference point or line which coincides with the center or center line of mass of coherent parts of the fuel pellet.

The problem of cracking and crack healing of oxide fuel pellets has been solved in the SATURN-1 code system by a first simple approximation. The fuel pellet is assumed to crack when the hoop stress in a fuel zone exceeds the fracture strength. It forms so many cracks that volume changes can take place free of stress. Crack healing is allowed due to thermal expansion and swelling, respectively. When the cracks have been healed up to a certain

boundary, the fuel is assumed to be capable of being stressed and mechanical analysis is resumed. The model applied in SATURN-1 to calculate geometry changes of a cracked fuel pellet includes the effect of radial relocation on power cycling.

Table K.2.I: Treatment of the Space Structure

SUBJECT	METHOD	Already Tested
Fuel Pin, axially symmetrical r-Geometry r-z-Geometry	Analytical Method	X
	Iteration	X
Fuel Pin, non axially symmetrical r-φ-Geometry	Analytical Method	X
	Finite-Element-Method	X
Spacer	Finite-Element-Method	X
Wrapper Tube	Finite-Element-Method	X
Total Subassembly	Finite-Element-Method	

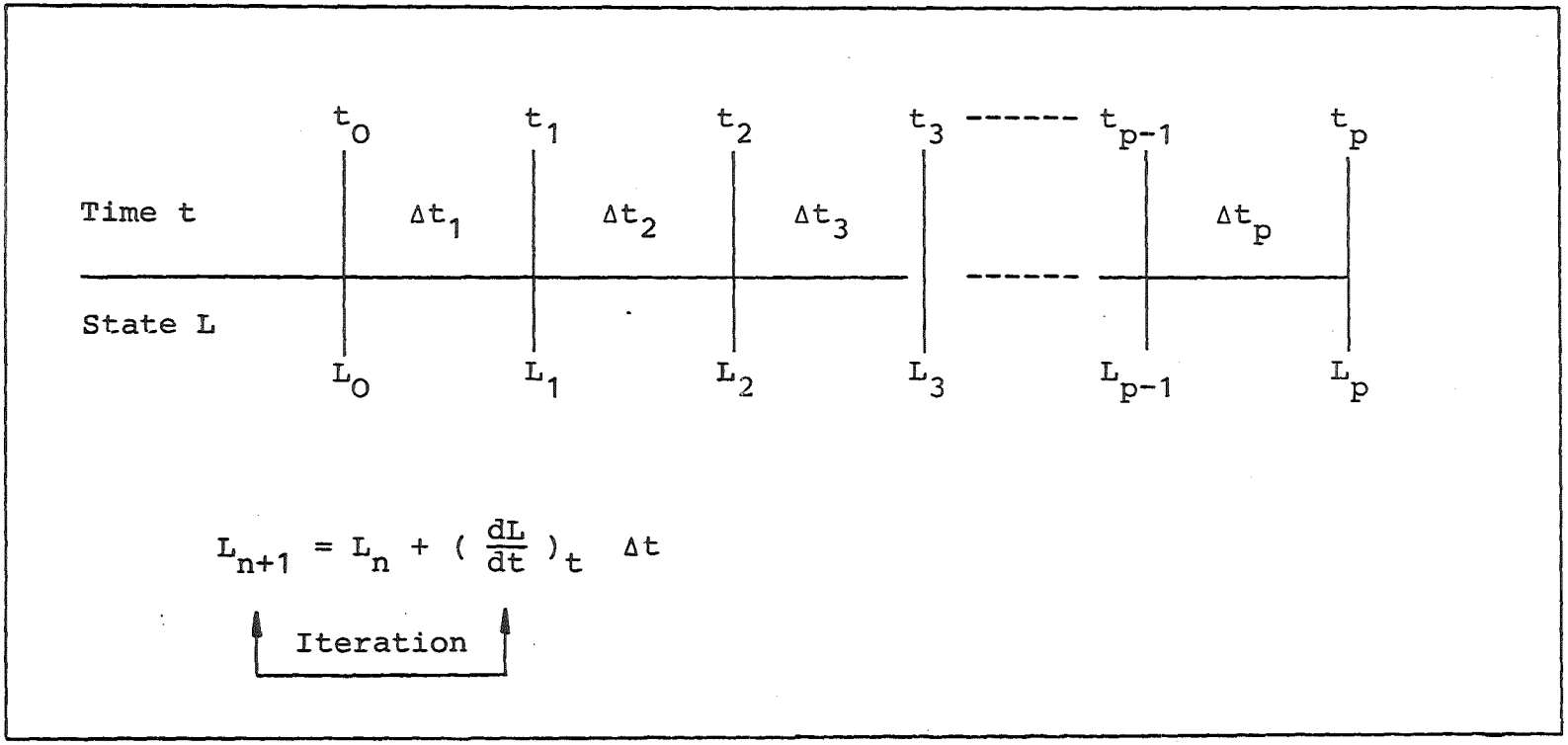

Fig. K.2.1: Time Structure in the Computer Code

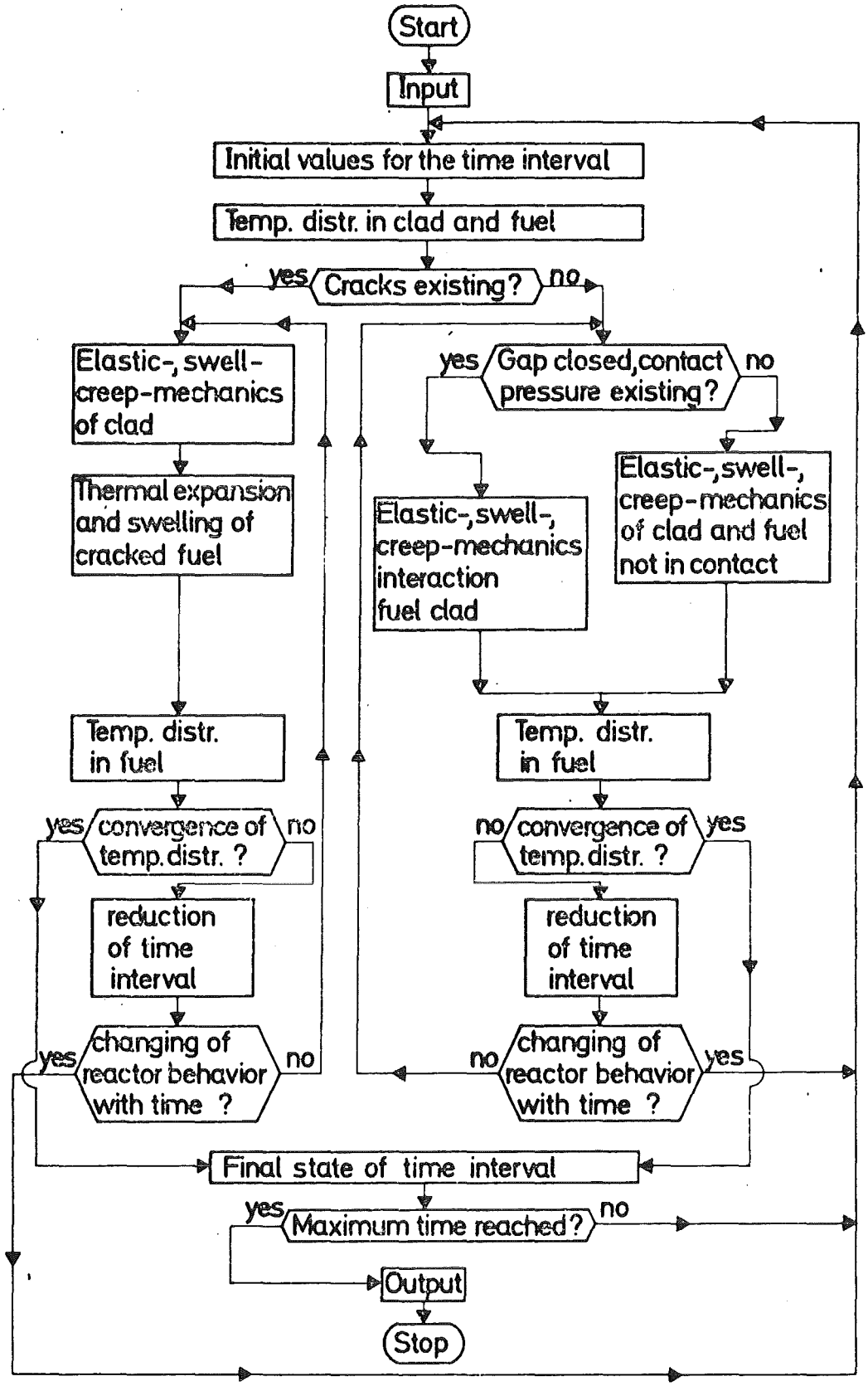

Fig. K.2.2: Structure Diagram of SATURN-1

K.3. Review of Fuel Pin Codes

In order to demonstrate the details of a code to some more extent, a review of fuel pin codes is brought in a comprehensive Table K.3.I. (This compilation is of 1976, meanwhile some progress especially in transient codes is achieved). All important features are listed.

None of the different codes considered includes everything. It should be mentioned, however, that every additional approach to ideal complexity requires more computer calculation time and causes more difficulties in handling such a code.

Table K.3.1: Review of Fuel Pin Codes

	Code Name	BREDA	SATURN-1	SATURN-3	URANUS	IAMBUS	COMETHE	FRUMP	BEHAVE	CYGRO	DEFORM	FMODEL	LIFE-III	SIEX
General Characteristics	Applicable to pin cross section	x	x	x	x	x	x	x	x	x	x	x	x	x
	Applicable to total pin	o	o	x	x	x				o		o	x	o
	Applicable to steady state conditions	o	x	x	x	x	x	x	x	x	o	x	x	x
	Applicable to ramps and power cycling	o	x	x	x	x	x	x			o		x	
	Applicable to transient conditions	x	o	o	o	o		x	x		x		x	o
	Pin Type - LWR oxide pins	o	x	x	x	x	x			x	o		o	o
	Pin Type - FBR oxide pins	x	x	x	x	x	x	x	x	x	x	x	x	x
	Pin Type - FBR carbide pins	o	x	x	x	o					o			o
	Axial symmetry	x	x	x	x	x	x	x	x	x	x	x	x	x
	Stress-strain Configuration - plane strain	x	x	x	x	x	x	x	x	x	x	x	x	
	Stress-strain Configuration - plane stress	o	x	x	o	x		x			o			
	Axial coupling	o	o	x	x	x				o	x	o		o
	Radial modeling zones in fuel	3	3	1	20	x				1		2		3
	Radial calculational mesh points	x	50	30	200	x	50	x						x
	Axial zones in fuel	10	x	20	30	x				x				21
Mathematical Methods	Numerical iterative	o	x	o	o	x		o	o	o	o	o	x	o
	Analytical iterative	x	o	x	x	o		x	o	o	x	o	o	o[1)]
	Finite differences	o	o	o	o	o		o	o	o	o	x	o	o
	Finite elements	o	o	o	o	o		o	x	x	o	o	o	o

Table K.3.1: Continuation

	Code Name	BREDA	SATURN-1	SATURN-3	URANUS	IAMBUS	COMETHE	FRUMP	BEHAVE	CYGRO	DEFORM	FMODEL	LIFE-III	SIEX
Fuel Mechanics Take into Account	Thermal expansion	X	X	X	X	X	X	X	X	X	X	X	X	X
	Creep	O	X	X	X	X	X	X	X	X	O	X	X	O
	Plastic flow	X	X	X	X	X	X		X		X	X	X	O
	Hot pressing and sintering	O	O	O	X	X	X		O	X	O	O	X	O
	Swelling	O	X	X	X	X	X	X	X	X	X	X	X	X
	Crack formation and healing	O	X	X	X	X	X	X	X	X	O		X	O
Migration and Segregation of Fuel Components	Pore migration	O	X	X	X	X	X	X		X	O	X	X	O
	Fission gas release	O	X	X	X	X	X		X		X	O		X
	Oxygen redistribution	O	X	O	O	O		X		O	O	X	O	O
	Pu migration	O	X	O	O	O		O		O	O	X	O	O
	Fission product migration	O	O	O	O	O		O		O	O	O	O	O
	Axial transport	O	O	O	O	O		O		O	O	O	O	O
Fuel/Clad Interaction	Radial interaction	X	X	X	X	X	X	X	X	X	X	X	X	X
	Axial interaction, friction	O	O	X	X	X					X	O	X	O
	Fission gas pressure buildup	X	X	X	X	X	X		X		X	O		X
	Inner corrosion	O	O	O	X	X			O		O	O	O	O
Clad Mechanics Take into Account	Thermal expansion	X	X	X	X	X	X	X	X	X	X	X	X	X
	Creep	O	X	X	X	X	X	X	X	X	O	X	X	O
	Plastic flow	X	X	X	X	X			X		X	X	O	O
	Swelling	O	X	X	X	X	X	X	X	X	O	X	X	X
	Corrosion	X	O	O	X	X			O		O	O	O	O
Temperature Calculations Take into Account	Fuel thermal conductivity	X	X	X	X	X	X	X	X	X	X	X	X	X
	Heat transfer in fuel/clad gap	O	X	X	X	X	X	X	X	X		X	X	X
	in contact zone	O	X	X	X	X	X		X	X			X	X
	Clad thermal conductivity	X	X	X	X	X	X	X	X	X	X	X	X	X
	Clad/coolant heat transfer	O	O	X	X						O			X
External and External Controling Parameters for the Calculation	Time	X	X	X	X	X	X	X	X	X	X	X	X	X
	Linear rod power	X	X	X	X	X	X	X	X	X	X	X	X	X
	Temperature	X	X	X	X	X	X	X	X	X	X	X	X	X
	Neutron flux	O	X	X	X	X		X	X	X	X			X
	Neutron fluence	O	X	X	X	X	X	X	X	X	X			X
	Fuel burnup	O	X	X	X	X	X	X	X		O			X
Calculational Output	Temperature profiles	O	X	X	X	X	X	X		X	O	X	X	X
	Clad stresses	X	X	X	X	X	X	X	X	X	X	X	X	O
	Fuel/clad contact pressure	X	X	X	X	X	X	X	X	X	X	X	X	X
	Fission gas pressure	X	X	X	X	X	X				X	O		X
	Clad strain - pin diameter	X	X	X	X	X	X	X	X	X	X	X	X	X
	Clad strain - pin length	O	O	X	X	X			X					O
	Fuel/clad gap width	X	X	X	X	X	X	X		X	X	X	X	X
	Gas composition	O	X	X	X	X	X				O			X
	Fuel structure - structure zones	X	X	X	X	X	X	X		X	X		X	X
	Fuel structure - porosity distribution	O	X	X	X	X	X	X	X	X	O		X	O
	Fuel structure - crack distribution	O	X	X	X	X	X	X	X		O			O
	Fuel structure - Pu distribution	O	X	O	O	O		O		O	O			O
	Fuel structure - O/Me distribution	O	X	O	O	O				O	O			O
	Fuel structure - fission product distrib.	O	O	O	O	O				O	O			O
Failure Criteria / Damage Limits included		X	O	O	O	X		X		X	X		X	O

LITERATURE

O. Survey on Reactor Materials

O.1 E. Gebhardt, F. Thümmler, H.D. Seghezzi: Reaktorwerkstoffe Teil 1 und 2. Stuttgart, 1964/1969

O.2 C.R. Tipton (editor): Reactor Handbook, 2nd edition, Vol. I, Materials. New York, 1960

O.3 C.J. Rodden (editor): Analysis of Essential Nuclear Materials. USAEC, New Brunswick, 1964

O.4 A. Boltax: Nuclear Materials (Book IV of Nuclear Engineering Fundamentals). New York, 1964

O.5 Génie Atomique Tome IV, Volume I et II: Les Propriétés des Matériaux des Réacteurs Nucléaires. Saclay, 1965

O.6 Génie Atomique Tome V: Elaboration des Matériaux Nucléaires de Base, Elaboration et Utilisation des Elêments Artificiels. Saclay, 1965

O.7 C.O. Smith: Nuclear Reactor Materials. Reading/Mass., 1967

O.8 T.J. Thompson, J.G. Beckerley (editors): Reactor Materials and Engineering (Vol. 2 in: The Technology of Nuclear Reactor Safety). Cambridge/Mass., 1973

O.9 J. Weissman (editor): Elements of Nuclear Reactor Design, Chapter 2. Amsterdam/Oxford/New York, 1977

O.10 Proceed. of the Second United Nations International Conference on the Peaceful Uses of Atomic Energy, Vol. 2-6. Genf, 1958

O.11 Proceed. of the Third International Conference on the Peaceful Uses of Atomic Energy, Vol. 9-12. Genf, 1964

O.12 Proceed. of the Fourth International Conference on the Peaceful Uses of Atomic Energy, Vol. 8-10. Genf, 1971

O.13 Proceed. of an International Conference on Nuclear Power and Its Fuel Cycle, Vol. 2-3. Salzburg, 1977

O.14 C. Keller, H. Möllinger (Herausgeber): Kernbrennstoffkreislauf Bd. I und II. Heidelberg, 1978

O.15 K. Kummerer: Werkstoffe der Kerntechnik. Karlsruhe,1980

A. Moderator Materials

A.1 E.M. Simons: Review of Moderator Materials, Chapter 41 in: Reactor Handbook, Vol. I Materials, p. 835-837. New York, 1960

A.2 C.R. Breden:Light and Heavy Water, Chapter 42 in: Reactor Handbook, Vol. I Materials, p. 838-887. New York, 1960

A.3 D.W. Kuhn: D_2O-H_2O Separation, Chapter 3 in: Reactor Handbook, Vol. I Materials, p. 53-63. New York, 1960

A.4 E.W. Becker: Heavy Water Production, IAEA Review Series No. 21. Wien, 1962

A.5 A.I. Schatenstein et al.: Isotopenanalyse des Wassers. VEB Deutscher Verlag der Wissenschaften, Berlin, 1960

A.6 I.F. Zartmann: Organic Materials, Chapter 45 in: Reactor Handbook, Vol. I Materials, p. 943-954. New York, 1960

A.7 M.W. Mallett, J.H. Stang: Hydrides and Hydroxides, Chapter 46 in: Reactor Handbook, Vol. I Materials, p. 955-973. New York, 1960

A.8 O. Kubaschewski (editor): Zirconium: Physico-Chemical Properties of Its Compounds and Alloys, Atomic Energy Review, Spec. Iss. No. 6. IAEA, 1976

A.9 W.W. Beaver, D.W. Lillie: Beryllium Metal, Alloys and Compounds, Chapter 44 in: Reactor Handbook, Vol. I Materials, p. 897-942. New York, 1960

A.10 L.D. Loch: Graphite, Chapter 43 in: Reactor Handbook, Vol. I Materials, p. 888-896. New York, 1960

A.11 A.R. Ubbelohde, F.A. Lewis: Graphite and Its Crystal Compounds. Oxford, 1960

A.12 P.L. Walker, Jr., P.A. Thrower: Chemistry and Physics of Carbon, A Series of Advances, Vol. 1-12. New York/Basel, 1965-1975

B. Absorber Materials

B.1 R.W. Dayton: The Engineering Requirements for Control and Burnable-Posion Materials, Chapter 35 in: Reactor Handbook, Vol. I Materials, p. 777-782. New York, 1960

B.2 B.T. Kelly, R.A. Murgatroyd: Technology and Assessment of Neutron Absorbing Materials, Atomic Energy Review, Vol. 15, p. 3.74, IAEA, 1977

B.3 K.F. Smith: Cadmium, Chapter 38 in: Reactor Handbook, Vol. I Materials, p. 806-809. New York, 1960

B.4 E. F. Losco: Silver, Chapter 40 in: Reactor Handbook, Vol. I Materials, p. 823-832. New York, 1960

B.5 W.K. Anderson: Boron, Chapter 37 in: Reactor Handbook, Vol. I Materials, p. 790-805. New York, 1960

B.6 L.B. Prus: Hafnium, Chapter 36 in: Reactor Handbook, Vol. I Materials, p. 783-789. New York, 1960

B.7 W.K. Anderson: Rare Earths, Chapter 39 in: Reactor Handbook, Vol. I Materials, p. 810-822. New York, 1960

B.8 H.E. Hungerford: The Nuclear, Physical and Mechanical Properties of Shielding Materials, Chapter 51 in: Reactor Handbook, Vol. I Materials, p. 2027-1101. New York, 1960

C. Coolants and Protective Gases

C.1 R.N. Lyon: Introduction to Coolant Materials, Chapter 47 in: Reactor Handbook, Vol. I Materials, p. 977-978. New York, 1960

C.2 P.C. Davidge et al.: Gas Coolants, Chapter 48 in: Reactor Handbook, Vol. I Materials, p. 979-993. New York, 1960

C.3 C.R. Breden: Light and Heavy Water, Chapter 42 in: Reactor Handbook, Vol. I. Materials, p. 838-887. New York,1960

C.4 I.F. Zartmann: Organic Materials, Chapter 45 in: Reactor Handbook, Vol. I Materials, p. 943-954. New York, 1960

C.5 M.T. Simnad: Fuel Element Experience in Nuclear Power Reactors. New York, 1971

C.6 R.N. Lyon (editor): Liquid Metals Handbook, NAVEXOS p.-733 (Rev.). Washington, 1955

C.7 C.B.Jackson (editor): Liquid Metals Handbook, Sodium NaK Supplement, TID 5277. Washington, 1955

C.8 R.N. Lyon: Liquid Metals, Chapter 49 in: Reactor Handbook, Vol. I Materials, p. 994-1020. New York, 1960

C.9 M. Hansen, K. Anderko: Constitution of Binary Alloys. New York etc. 1958, First Suppl. 1965, Second Suppl. 1969

D. Fuel Source Materials

D.1 W.-J. Schmidt-Küster, H.-F. Wagner: Probleme des Kernbrennstoffkreislaufs, Chapter II in: Kernbrennstoffkreislauf Bd. I. Heidelberg, 1978

D.2 Gmeling Handbuch der Anorganischen Chemie, Uran Ergänzungsband A1. Berlin/Heidelberg/New York, 1979

D.3 Gmelin Handbuch der Anorganischen Chemie, Band: Thorium und Isotope. Weinheim, 1955

D.4 F. Klein, G. Lange: Die Versorgung mit Uran, Chapter V in: Kernbrennstoffkreislauf Bd. I. Heidelberg, 1978

D.5 C. Keller: Das Oklo-Phänomen - Vorgeschichtlicher Kernreaktor in Gabun, Chapter XVI in: Kernbrennstoffkreislauf Bd. II. Heidelberg, 1978

D.6 H. Geier: Übersicht über Verfahren der Uranerzverarbeitung, Chapter VI in: Kernbrennstoffkreislauf Bd. I, p. 108-130. Heidelberg, 1978

D.7 Gmelin Handbuch der Anorganischen Chemie, Uran Ergänzungsband C8: Verbindungen mit Fluor. Berlin/Heidelberg/New York, 1980

D.8 W. Ehrfeld, U. Ehrfeld: Uranisotopentrennung, Chapter VII in: Kernbrennstoffkreislauf Bd. I. Heidelberg, 1978

D.9 W. Ehrfeld, U. Ehrfeld: Anreicherung von Uran-235, in: Gmelin Handbuch der Anorganischen Chemie, Uran Ergänzungsband Teil A2, p. 57-149. Berlin/Heidelberg/New York, 1980

D.10 O. Kubaschewski (editor): Thorium: Physico-Chemical Properties of Its Compounds and Alloys, Atomic Energy Review Spec. Iss. No. 5, IAEA, 1975

D.11 O. Kubaschewski (editor): Plutonium: Physico-Chemical Properties of Its Compounds and Alloys, Atomic Energy Review Spec. Iss. No. 1, IAEA, 1966

D.12 O.J. Wick (editor): Plutonium Handbook - A Guide to the Technology Vol. II. New York, 1967

D.13 Gmelin Handbuch der Anorganischen Chemie, Ergänzungsbände Transurane. Weinheim, 1972/73, Berlin/Heidelberg/New York, 1974/75

D.14 M. Taube: Plutonium - A General Survey. Weinheim, 1974

D.15 G. Koch: Chemische Aufarbeitung der bestrahlten Kernbrennstoffe, Chapter XI in: Kernbrennstoffkreislauf Bd. II. Heidelberg, 1978

E. Fuel Types and Fabrication

E.1 M.T. Simnad: Fuel Element Experience in Nuclear Power Reactors. New York, 1971

E.2 M. Taube: Plutonium - A General Survey. Weinheim, 1974

E.3 O.J. Wick (editor): Plutonium Handbook - A Guide to the Technology, Vol. I and II. New York, 1967

E.4 D.R. Olander: Fundamental Aspects of Nuclear Reactor Fuel Elements, TID-26711-P1. USA-ERDA, 1976

E.5 B.G. Ryle et al.: Uranium, Chapter 7 in: Reactor Handbook, Vol. I Materials, p. 147-210, New York, 1960

E.6 H.S. Kalish et al.: Uranium Alloys, Chapter 8 in: Reactor Handbook, Vol. I Materials, p. 147-210. New York, 1960

E.7 T.C. Runion et al.: Thorium, Chapter 9 in: Reactor Handbook, Vol. I Materials, p. 211-226. New York, 1960

E.8 A.S. Coffinberry et al.: Plutonium and Its Alloys, Chapter 11 in: Reactor Handbook, Vol. I Materials, p. 248-290. New York, 1960

E.9 C.C. McBride et al.: Fabrication of Fuel Elements, Chapter 14 in: Reactor Handbook, Vol. I Materials, p. 331-352. New York, 1960

E.10 E. Gebhardt, H.D. Seghezzi: Metallische Werkstoffe (Teil 1 von E.Gebhardt, F. Thümmler, H.D. Seghezzi: Reaktorwerkstoffe). Stuttgart, 1964

E.11 L.D. Loch, J.F. Quirk: Ceramics, Chapter 12 in: Reactor Handbook, Vol. I Materials, p. 291-303. New York, 1960

E.12 F. Thümmler, E. Gebhardt: Keramische und pulvermetallurgische Werkstoffe (Teil 2 von Gebhardt, F. Thümmler, H.D. Seghezzi: Reaktorwerkstoffe). Stuttgart, 1969

E.13 V.W. Schneider, F. Plöger: Herstellung von Brennelementen, Chapter VIII in: Kernbrennstoffkreislauf Bd. I. Heidelberg, 1978

E.14 D.L.Keller: Dispersion Fuels, Chapter 13 in: Reactor Handbook, Vol. I Materials, p. 304-330. New York, 1960

E.15 S. Nazaré, G. Ondracek, F. Thümmler: Die Technologie von Cermets, High Temperatures - High Pressures, Vol. 3, p. 615-634, 1971 (KfK Report No. 1738)

E.16 R.G. Post, K. Wirtz, T.D. Gulden, H. Nickel (editors): Coated Particle Fuels, Nuclear Technology Vol. 35, No. 2 (Special Issue), 1977

E.17 T.D. Gulden, H. Nickel: Coated Particle Fuels, Nuclear Technology Vol. 35, p. 206-213, 1977

E.18 W. Delle et al.: Graphitische Werkstoffe für den Einsatz in Kernreaktoren, Teil 1, Thiemig-Taschenbuch Bd. 81. München, 1978

E.19 W. Stoll: Plutonium - Ziel und Problem des Brennstoffkreislaufes, Chapter XIV in: Kernbrennstoffkreislauf Bd. II. Heidelberg, 1978

F. Nuclear Fuels under Irradiation

F.1 H.S. Rosenbaum: Microstructures of Irradiated Materials. New York/ San Francisco/London, 1975

F.2 D.R. Olander: Fundamental Aspects of Nuclear Reactor Fuel Elements, TID-26711-P1. USA-ERDA, 1976

F.3 D. Geithoff: Das Bestrahlungsverhalten von Brennstäben in Leistungsreaktoren, Chapter IX in: Kernbrennstoffkreislauf Bd. I. Heidelberg, 1978

F.4 W. Delle et al.: Graphitische Werkstoffe für den Einsatz in Kernreaktoren, Thiemig-Taschenbuch Bd. 81. München, 1978

G. Fuel Element Design and Fabrication

G.1 A. Klusmann, H. Völcker: Brennelemente von Kernreaktoren, Thiemig-Taschenbuch Bd. 25. München, 1969

G.2 J. Lopez-Jimenez: Diseño de barras combustibles para reactores rápidos refrigerados por sodio, Energia Nuclear 1977, España, 159 ff.

G.3 V.W. Schneider, F. Plöger: Herstellung von Brennelementen, Chapter VIII in: Kernbrennstoffkreislauf Bd. I. Heidelberg, 1978

G.4 D. Vollath, K. Kummerer (editors): Characterization and Quality Control of Nuclear Fuels, Proc. of the Conference 1978. Amsterdam, 1979

G.5 D. Vollath, K. Kummerer (editors): Characterization and Quality Control of Nuclear Fuels, Proc. of the Conference 1981. Amsterdam, 1982

H. The Fuel Elements in Research and Power Reactors

H.1 IAEA: Directory od Nuclear Reactors, Vol. I . Wien, 1971

H.2 IAEA: Directory of Nuclear Reactors, Vol. II. Wien, 1959

H.3 IAEA: Directory of Nuclear Reactors, Vol. IV. Wien, 1962

H.4 IAEA: Directory of Nuclear Reactors, Vol. X . Wien, 1976

H.5 A. Klusmann, H. Völcker: Brennelemente von Kernreaktoren, Thiemig-Taschenbuch Bd. 25. München, 1969

H.6 M.T. Simnad: Fuel Element Experience in Nuclear Power Reactors. New York, 1971

H.7 R. Holzer: Konstruktion des Reaktorkerns, Beitrag IV in: Druckwasserreaktoren für Kernkraftwerke (herausgegeben von W. Oldekop), 2. Auflage, Thiemig-Taschenbuch Bd. 51. München, 1979

H.8 R. Holzer et al., Atomwirtschaft 10, S. 355-357, 1965

H.9 K. Kummerer: Brennelemente für Brüter-Kraftwerke, Chapter in KfK-Report No. 2416, p. 20. Karlsruhe, 1976

H.10 J. Höchel et al.: The Status of the Fuel Elements for SNR-300 with Consideration of the Technical and Economical Aspects, Chapter in: Proceedings of the International Conference on Fast Reactor Power Stations, p. 335. London, 1974

H.11 J. Lopez-Jimenez: Diseño de barras combustibles para reactores rápidos refrigerados por sodio, Energia Nuclear 1977, España, 159 ff.

H.12 K. Kummerer: Programa alemán de irradiación de barras combustibles de óxidos para reactores rápidos, Energia Nuclear, 1981, España, 44 ff.

H.13 E. Merz: Brennstoffkreislauf beim gasgekühlten Hochtemperaturreaktor (HRT), Chapter X in: Kernbrennstoffkreilauf Bd. I. Heidelberg, 1978

H.14 H. Nickel, E. Balthesen: Stand und Möglichkeiten der HTR-Brennelement-entwicklung in der BRD für nukleare Prozeßwärme-Reaktoren, Kerntechnik 17, S. 205, 1975

J. Fuel Cycles

J.1 Some contributions in C. Keller, H. Möllinger (editors): Kernbrennstoff-kreislauf Bd. I and II. Heidelberg, 1978

J.2 P. Schmiedel, E. Schwarz: Brennstoffkreislauf und Brennstoffkosten, Chapter VII in: Druckwasserreaktoren für Kernkraftwerke (edited by W. Oldekop), 2. Auflage, Thiemig-Taschenbuch Bd.51. München, 1979

K. Fuel Pin Modeling

K.1 H. Kämpf, H. Elbel, K. Kummerer: Brennstabmodelltheorie, Modelle und Materialdaten, KfK 1400. Karlsruhe, 1971

K.2 D.R. Olander: Fundamental Aspects of Nuclear Reactor Fuel Elements, TID-26722-P1. USA-ERDA, 1976

PARTE III:

Desechos nucleares: un problema de materiales

(Nuclear Waste Materials)

G. Ondracek

(Traducción U. Röser)

Sumario

El objeto de este estudio sumario es tratar en tres partes

- la caracterización y el almacenamiento de desechos radiactivos de actividad alta
- la estructura de embalages de desechos (≙ producto + envuelta)
- la tecnologîa de los embalajes de desechos (formas de almacenamiento)

asî como sus conexiones. No intentamos comunicar datos especiales para condiciones especîficas, por los cuales les recomendamos la literatura indicada.

En la primera parte de este trabajo damos una exposición sobre la formación de los desechos radiactivos de actividad alta y su caracterización. La discusión de las posibilidades para su aislamiento permanente o a largo plazo respectivamente de la biosfera nos lleva a formaciones geologicas continentales como instalaciones de almacenamiento definitivo. En el caso de la República Federal de Alemania éstas son formaciones de sal gema, cuyas condiciones de estado y sus modificaciones debido a la introducción de embalajes de desechos altamente radiactivos definen las exigencias mînimas que tienen que cumplir las estructuras de las formas de almacenamiento que convienen para el almacenamiento definitivo.

En la segunda parte tratamos esta estructura de embalajes posibles de desechos (≙ producto de almacenamiento definitivo + envuelta) del sistema de barreras multiples. Se comparan vitrios, supercalcinados, titanatos y Synroc como alternativas en cuanto a su equilibrio termoquîmico interior y exterior (formación de fases, cristalización, reacciones de superficie lîmite, corrosion y lixiviación, estabilidad mecánica).

Por fin se discute en la tercera parte el tratamiento tecnologico de fundición y de polvos de los desechos para la fabricación de embalajes de desechos, con respecto al condicionamiento casi homogéneo así como heterogéneo del desecho altamente radiactivo fijado en vidrio, supercalcinados o Synroc.

I. Caracterización y almacenamiento de los desechos de actividad alta

I.1 Formación y composición de los desechos de actividad alta

Para la producción de energía nuclear, el combustible nuclear se consume en los elementos combustibles de los reactores nucleares. Las medidas necesarias para el tratamiento del combustible consumido se llaman gestión de los desechos (Fig. I.1). Como el combustible consumido de un reactor de agua ligera se compone en gran parte de uranio y plutonio recuperables (≥ 95% en peso), se lo reelabora. Para ello, se cortan las agujas de combustible, almacenadas provisionalmente después de extraerlas del reactor nuclear, y se disuelve el combustible en ácido nítrico (Fig. I.2). Por adición de tributilfosfato (TBP) se puede extraer casi completamente (≥ 99%) el plutonio y uranio (relación Pu/U ≤ 1:100) contenidos en el combustible consumido (proceso PUREX), y se puede recuperarlo para el aprovisionamiento del reactor nuclear (ciclo del combustible, Fig. 1,2). En el desecho radiactivo que sobra (Radwaste) algúnos componentes insolubles, de más baja actividad, forman los lodos activados de alimentación que son - junto con los fragmentos de vainas de zircaloy no solubles - el desecho de actividad media (Medium Activity Waste, MAW), mientras que a partir de los desechos altamente radiactivos (High Activity Waste = HAW) los productos de fisión gaseiformes (que corresponden juntos a aproximadamente 15-20% en peso; p. ej. Kr, Xe, J, Br, $^{3}_{1}H$) se escapan y tienen que recojerse en filtros. Aquí se tiene que prestar atención especialmente al yodo 129 aún en concentraciones mínimas, porque tiene un período muy grande (> 10^{7} años). Por ello, durante grandes espacios de tiempo, pequeñas cantidades por unidad de tiempo pueden acumularse en la atmósfera a cantidades que tienen una radiactividad no despreciable. El efluente líquido nítrico de actividad alta que sobra (High

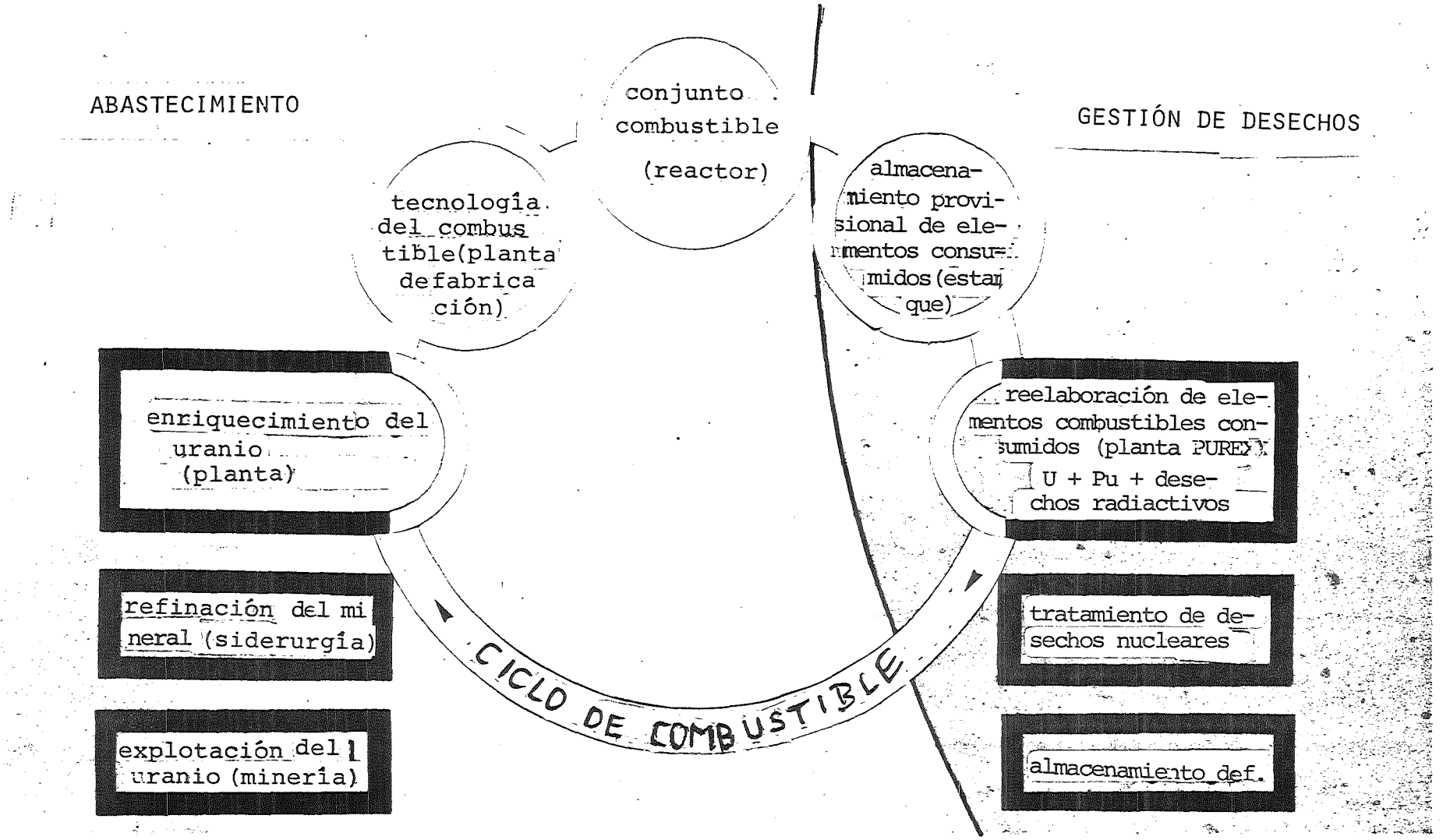

FIG. I.1: CICLO DE COMBUSTIBLE NUCLEAR

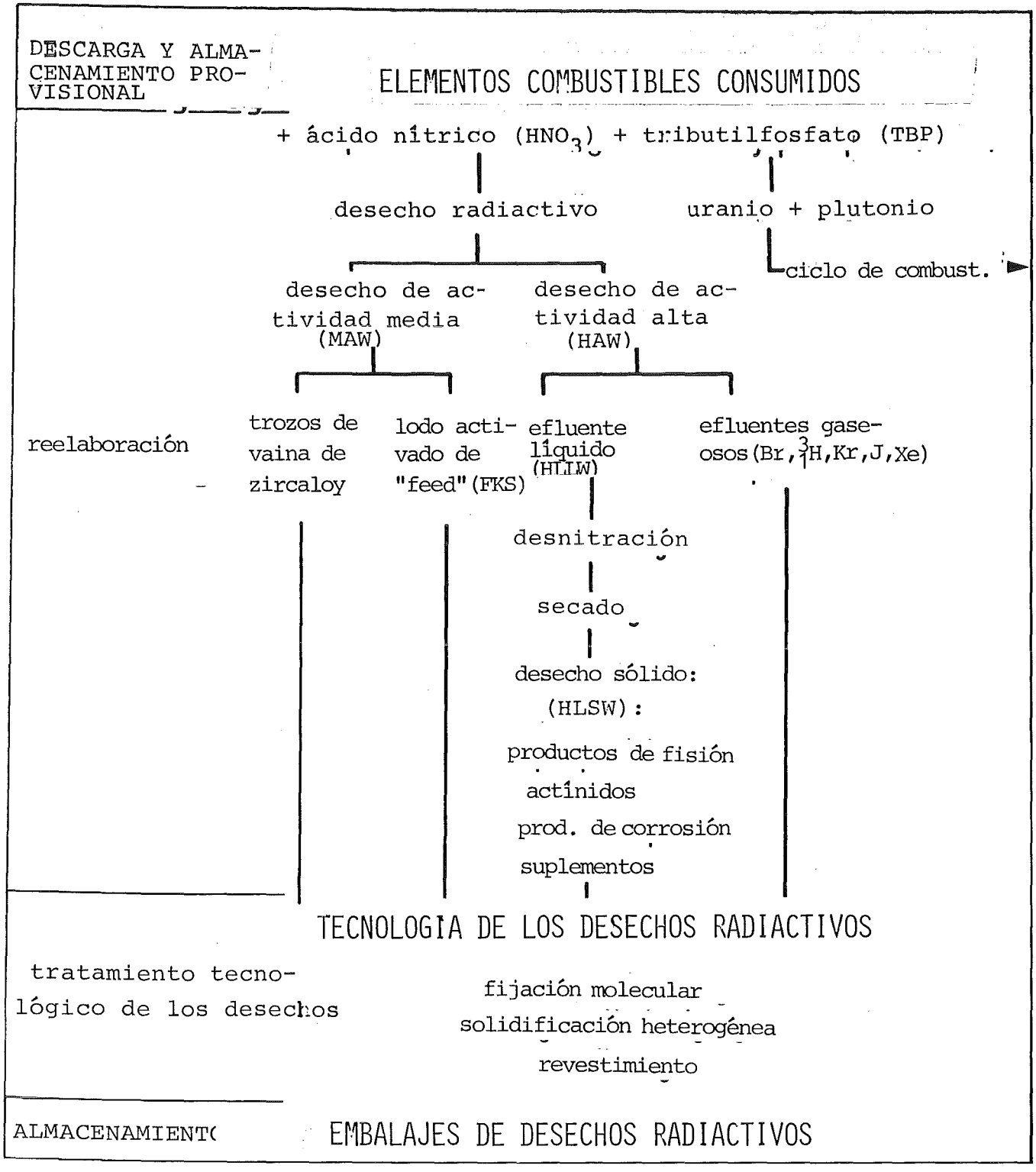

FIG. I.2: ORGANIGRAMA DE LA REELABORACION Y DEL TRATAMIENTO DE LOS DESECHOS DEL COMBUSTIBLE NUCLEAR

Level Liquid Waste = HLLW) [50] puede denitrarse, secarse en el aire y con esto parcialmente oxidarse y de este modo dar lugar al desecho sólido de actividad alta (High Level Solidified Waste = HLSW). Este se compone de tres grupos de materia [116] que son:

- productos de fisión sólidos (nucleídos provenientes de la fisión nuclear sin gases de fisión)
- los actínidos (uranio y plutonio no extraido así como elementos transuránicos formados por captura de neutrones)
- productos de corrosión y sustancias accesorias [21], que inicialmente no estaban contenidos en el combustible, pero que debido al proceso llegan a los desechos (Fe, Ni, Cr procedentes de componentes de disolución y evaporación de la planta de reelaboración por interacción con HNO_3, fósforo como producto de descomposición del TBP y gadolineo adicionado eventualmente al HLLW como veneno de neutrones para evitar la criticalidad).

La composición del desecho sólido de actividad alta depende:

- del tipo de reactor del cual proceden los elementos combustibles consumidos; estándar : LWR = reactor térmico de agua ligera
- de la composición iniciál del combustible; estándar : UO_2 (o MOX, ver mas abajo), enriquecimiento 3,5% U-235
- del grado de quemado; estándar : 36.000 MWd/t $\hat{=}$ 3,9%
- del momento de la reelaboración después de la descarga del reactor; estándar : $\leq$ 10 años [28]
- de la eficacia y del número de los ciclos de extracción; estándar : = 1
- del "tratamiento posterior técnico" eventual; estándar : ninguno.

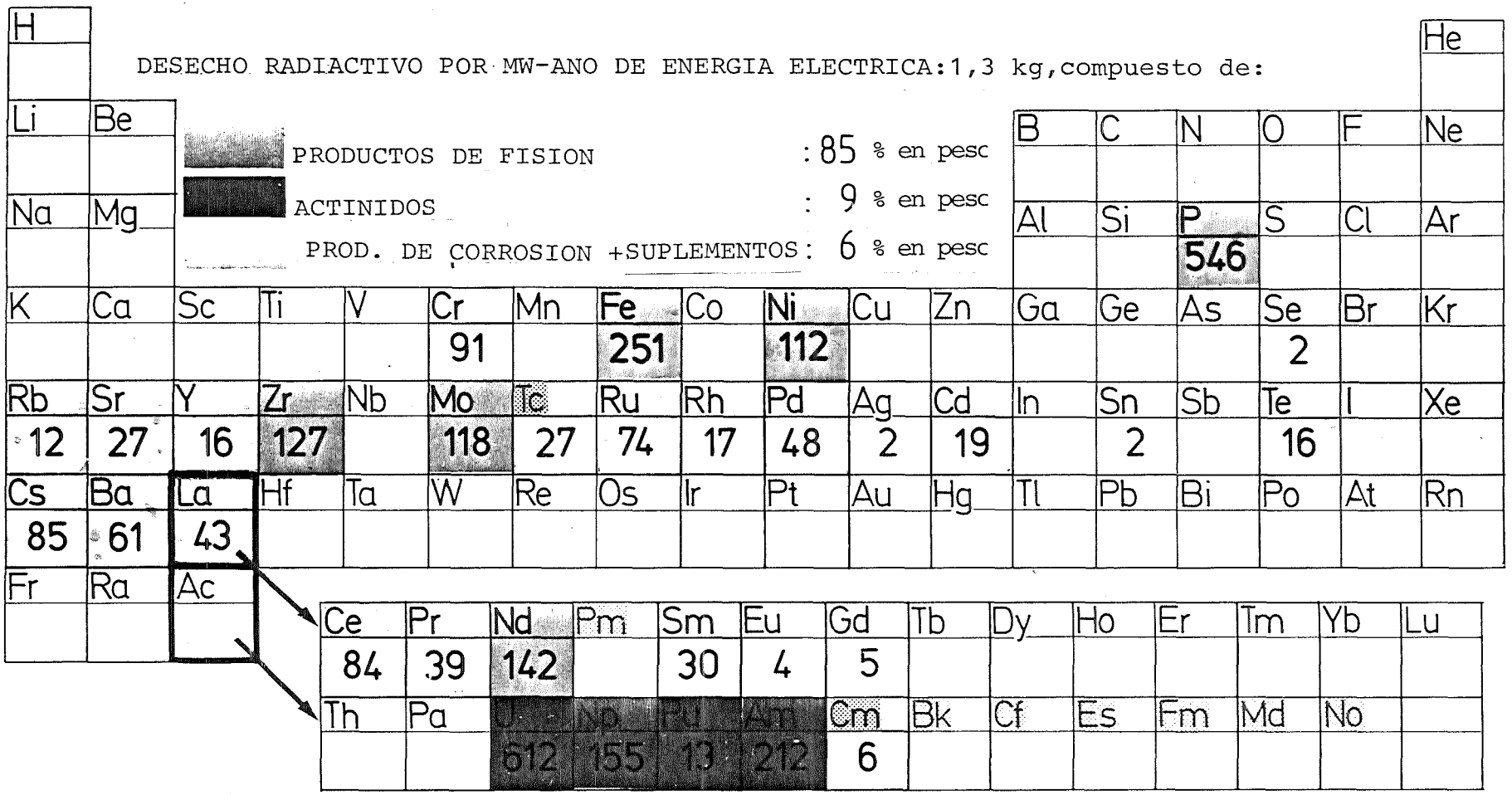

FIG. I.3: COMPOSICION MATERIAL DE DESECHO ESTANDAR DE ACTIVIDAD ALTA

(INDICACIONES EN % EN PESO)

Las "condiciones estándar" citadas dentro del marco de este artículo sumario son valores de orientación para los cuales se tienen que admitir variaciones mayores. Siempre que en el texto que sigue nos refieramos a un "desecho estándar", estas dispersiones están implicadas, por lo que las curvas en las representaciones gráficas muchas veces no están representadas como líneas sinó como "bandas". Las marchas - y no los valores absolutos - ocupan el primer lugar.

Para un desecho sólido de actividad alta formado bajo condiciones estándar, se indica en la Fig. I.3 la composición según los grupos de sustancias elementos, despreciando los elementos que tienen un porcentaje en peso muy pequeño (< 0,2% en peso). El empleo del combustible de óxido mixto U-Pu (MOX) en lugar del dióxido de uranio no tiene ninguna influencia fundamental sobre la composición del desecho sólido de actividad alta. En cambio, la fecha de la reelaboración (10 años después de la descarga del reactor, para la Fig. I.3) es muy importante, lo que prueba p.ej. la parte del isótopo Am-241, al que se desintegra el plutonio 241 después de un período de semidesintegración relativamente corto (aproximadamente 15 años). El americio 241 por su parte tiene un período casi 30 veces más grande y proporciona bajo condiciones estándar en el desecho sólido de actividad alta aproximadamente la mitad de la parte de radiactividad que el grupo de los actínidos contribuye a la radiactividad total (ver Fig. I.5). Por ello, más pronto - y más completamente - se extrae el Pu-241, más pequeña es la parte del Am-241 en el desecho sólido altamente radiactivo.

El posible "tratamiento posterior técnico" arriba mencionado del desecho sólido altamente radiactivo se refiere a consideraciones de separar determinados elementos - p.ej. transuránicos - y de fisionar nucleos de actínidos con períodos muy largos ($\gtrsim 10^6$ años) por "transmutación", es decir por

bombardéo neutrónico o de transformar por captura de neutrones productos de fisión con períodos largos en isótopos pesados con períodos más cortos. El cambio de la composición del desecho así producido sirve para desplazar los períodos de los elementos radiactivos de tal modo que la duración del aislamiento del desecho radiactivo de la biosfera necesaria para reducir los riesgos, pueda reducirse a un valor uniforme ($\leq$ 1000 años).

En la fig. I.4 se ha representado la actividad térmica, en la fig. I.5 la radiactividad del desecho sólido altamente radiactivo procedente de combustible reelaborado. En el intervalo de tiempo de 1 hasta 10 años la potencia térmica de desintegración (y) puede representarse bien en función del tiempo (t) por la ecuación

$$y_{rel} \sim \frac{9{,}37 \cdot 10^{5} \cdot (t-1{,}83)^{-0{,}858}}{e^{6{,}452} \cdot x^{-0.086}} \qquad (1)$$

(Magnitud de referencia: 10 años), y en el intervalo de tiempo de 10 hasta 100 años, esta potencia térmica de desintegración según la fig. 4 puede describirse aproximadamente por la ecuación

$$y_{rel} \sim \left(\frac{59{,}7}{t + 49{,}7}\right)^{1{,}73} \qquad (2)$$

La contribución de los actínidos aumenta con la duración de tiempo tanto para la potencia térmica de desintegración (3,4% dos años después de la descarga del combustible del reactor; 10,7% 10 años después de la descarga del combustible del reactor) como para la radiactividad. - La mayoría de los productos de fisión son emisores β con períodos relativamente pequeños (<100 años), la mayoría de los actínidos son emisores α. Aproximadamente tres cuarto de la radiactividad de los productos de fisión será proporcionada dos años después

de la reelaboración por isótopos de los cinco elementos que son el rutenio, radio, cesio, cerio y praseodimio, 10 años después de la reelaboración por los isótopos de los cuatro elementos estroncio, itrio, cesio y bario, donde el itrio y el bario metaestable resultan como productos de desintergración inmediatamente del estroncio y cesio.

I,2 Posibilidades de contención durable del desecho de actividad alta: almacenamiento provisional y definitivo

Como lo muestran las consideraciones sobre la radiactividad en la parte 1, el riesgo del almacenamiento definitivo del desecho altamente radiactivo emana de su radiactividad. Para poder evaluar este riesgo cuantitativamente, se utiliza el índice de radiotoxicidad (fig. I.6). Establece una relación entre el volumen de agua necesario para la dilución del desecho nuclear con la cual se obtiene la calidad de agua potable, y la dilución correspondiente (10^5 : 1) para el mineral uranífero natural (0,2% en peso de U) [24]. Hasta ahora no se sabe hasta qué punto esta normalización está justificada desde el punto de vista médico.

Para eliminar este peligro se necesita aislar durante un período muy largo el desecho altamente radiactivo de la biosfera. El almacenamiento a largo plazo que conviene para este aislamiento durable puede realizarse

- en zonas extraterrestres
- en el hielo antárctico
- en el fondo del mar y
- en formaciones geológicas continentales,

donde - globalmente - siempre hay que tener en cuenta el riesgo

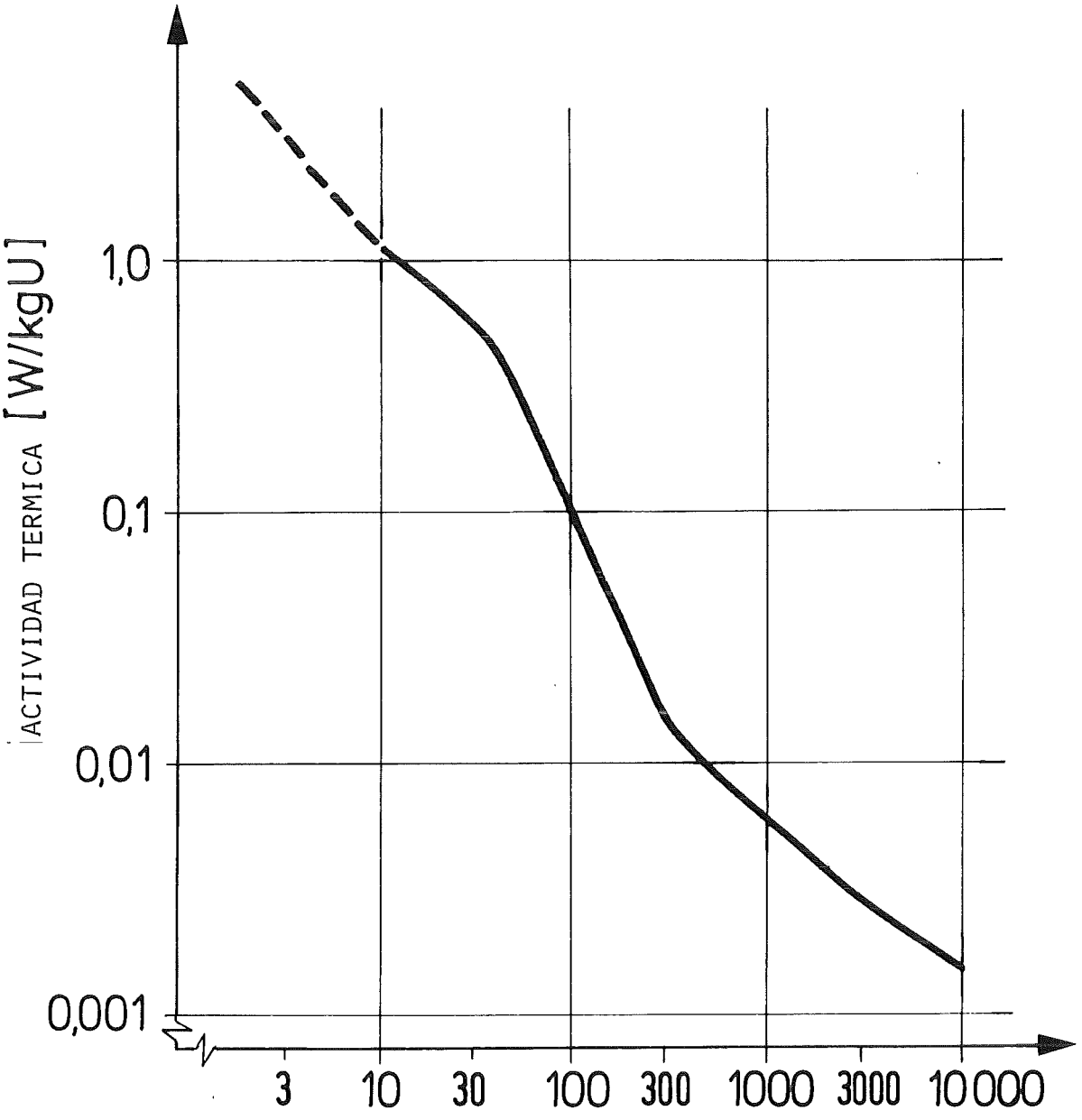

FIG. I.4: LIBERACION NORMALIZADA DE CALOR DEL DESECHO ESTANDAR DE ACTIVIDAD ALTA EN FUNCION DE LA DURACION DEL ALMACENAMIENTO DESPUES DE LA DESCARGA DEL REACTOR /5, 28/

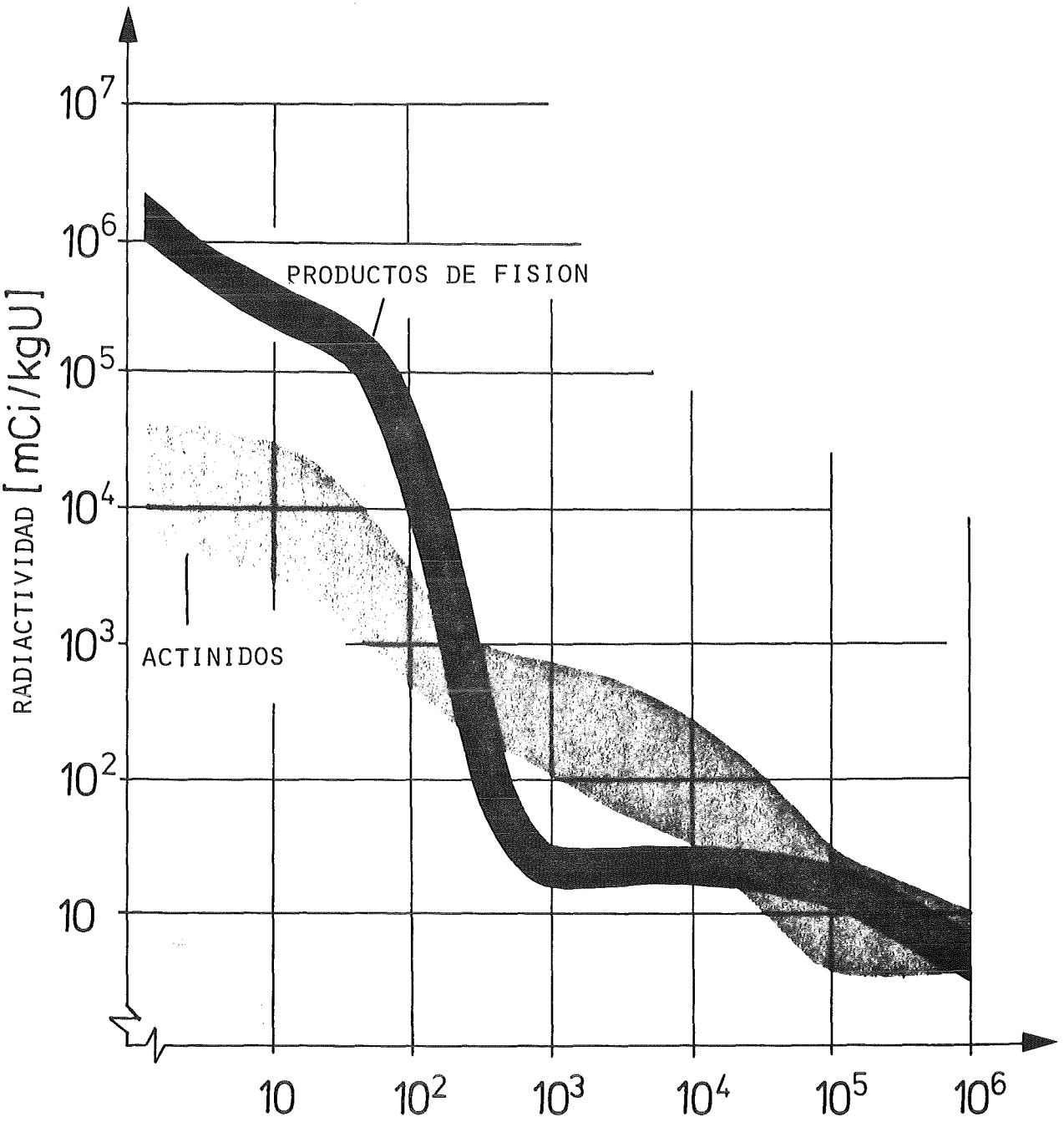

FIG. I.5: RADIACTIVIDAD DE DESECHO DE ACTIVIDAD ALTA (LWR; ENRIQUECIDO DE 3,3 % EN U-235; QUEMADO 34 000 MWD; REELABORACION 150 DIAS DESPUES DE LA DESCARGA DEL REACTOR /24/.

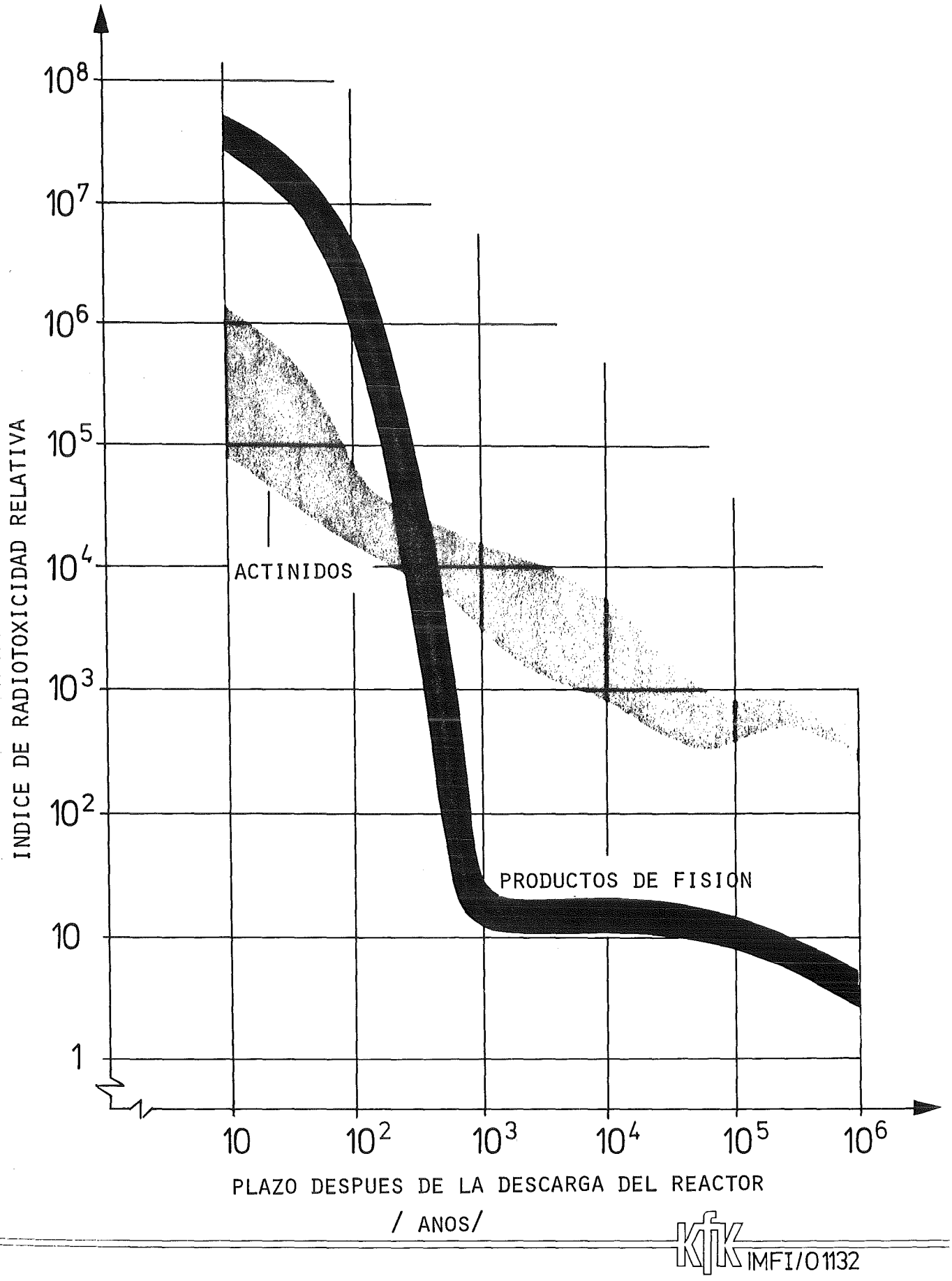

FIG. I.6: INDICE DE RADIOTOXICIDAD RELATIVA PARA PRODUCTOS DE FISION Y ACTINIDOS EN EL DESECHO RADIACTIVO /24/

- de un accidente con liberación de radionucleidos
  - en la vía de transporte
  - durante la introducción al almacenamiento o
  - durante el almacenamiento definitivo
- de una intervención no autorizada especialmente durante el almacenamiento definitivo.

Así la idéa simpática de un "basurero atómico" fuera de la tierra no se ha desvanecido hasta ahora a causa de la posible realización o del balance de energía (relación entre la energía por unidad de masa de desecho radiactivo que se consumiría durante el transporte al espacio y aquella energía que ha sido producida por unidad de desecho radiactivo cuando este se formó), sinó a causa del riesgo de accidente ligado con el empleo de vehículos espaciales en largas vías de transporte [24].

El almacenamiento del desecho radiactivo sobre, en o bajo el hielo antárctico - en el fondo del mar - sería también realizable técnicamente, p.ej. por introducción automática por fusión debida a las temperaturas elevadas del desecho [18, 52]. Pero además del riesgo de accidente general durante largos transportes, al almacenamiento definitivo sobre el hielo se opone además el problema de la protección contra la intervención no autorizada, al almacenamiento definitivo en el hielo él del riesgo de accidente aumentado debido al desconocimiento de los movimientos posibles del hielo durante períodos más largos.

El almacenamiento a largo plazo parece favorecido por la estructura en aquellas regiones del fondo del mar que presentan una estructura geológicamente muy estable de las capas y que coinciden además con regiones biológicamente poco activas. La capa superior de arcilla cubre una segunda capa de

sedimentos petrificados bajo la cual se encuentra la roca de base de basalto. En el caso del almacenamiento definitivo en la roca de base - que parece ser posible técnicamente en orificios taladrados o introducidos por impacto - esta capa formará junto con la capa sedimentaria que funciona como intercambiador de iones de alta capacidad y con la capa límite de arcilla, un sistema de tres barreras frente al agua del mar [52], que reduce el riesgo de accidente del almacenamiento definitivo. Es cierto que - en el caso de la rotura de una barrera - se dispondría inmediatamente de agua como medio de transporte más importante para la difusión rápida de los radionucleidos en la biosfera. Pero la dilución sería muy alta y el riesgo de accidente bajo condiciones de almacenamiento definitivo sería relativamente pequeño. El riesgo de accidente sobrante en largas vias de transporte junto con el hecho de que el fondo del mar queda insuficientemente investigado, comparado con formaciones geológicas continentales, favorece hasta ahora a éstas últimas para el almacenamiento definitivo y la contención del desecho radiactivo frente a la biosfera.

En casos especiales, estas formaciones geológicas continentales constituyen capas de roca naturales con gran extensión, altamente porosas y acuíferas ("Aquifers", approx. 1000 m de profundidad) o cavidades producidas "artificialmente", por "hidrofractura" ("Hydrofers", 200-300 m de profundidad), que están protegidas por capas de base y de recubrimiento poco permeables, tectónicamente estables y que no comunican con capas que llevan agua subterranea. Por hidrofractura se entiende aquí el desdoblamiento horizontal de capas de roca mediante lodo de arena bajo presión ($\sim$20 MPa) [45, 46, 52, 54]. Después del desdoblamiento el lodo de arena se evacúa por bomba, y la cavidad se rellena de una mezcla de desecho radiactivo y de cemento [56].

Al contrario de este almacenamiento en Hydrofers, para el almacenamiento en Aquifers el efluente líquido nítrico viene inyectado directamente (10 MPa [29, 45, 46] y es absorbido por la roca.

Pero existen solamente pocas formaciones geológicas disponibles como Aquifers o que pueden desdoblarse hidrostáticamente en el sentido horizontal y que estén aisladas de modo suficientemente seguro del medio de comunicación que es el agua subterranea. En cambio, se dispondría de bastantes capas de roca de granito o sal gema que convienen para el almacenamiento durable de desechos radiactivos, siendo seguro que formaciones salinas en regiones desérticas serían una combinación casi ideal: "Donde hay sal, no hay agua subterranea"! Para la introducción temprana de desechos altamente concentrados de actividad alta en estas rocas se ha considerado la incrustación directa en la roca. Las cápsulas que contienen el desecho, debido al calor de desintegración, desarrollan en su superficie temperaturas tan elevadas (1100 K para sal; 1500 K para granito), que la roca ambiente se funde. Cuando se introducen estas cápsulas en perforaciones profundas, bajan por sí mismo tras algunos decenios hasta profundidades de vários kilómetros, con una velocidad de > 100 m por año.

El concepto más adaptado a la práctica - porque se domina la técnica minera y porque es controlable - es el concepto que por estas razones ha sido lo más perfeccionado y que preve el almacenamiento de desechos radiactivos en sistemas de galerías en granito o sal (en 500-1000 m de profundidad). Aquí también no se puede excluir totalmente el riesgo de una intervención no autorizada o de un accidente en la vía de transporte y durante el almacenamiento definitivo - pero se puede limitarlo. Desde el punto de vista de la organización y de la técnica de la maquinaria pueden realizarse cortas

vías de transporte y contenedores de transporte seguros bajo condiciones atmosféricas. El máximo accidente previsible que es la penetración de agua en el almacenamiento definitivo durante la fase introducción, puede probablemente dominarse por medios técnicos mineros mediante una disposición especial de los pozos y galerías, y por la técnica de los materiales mediante embalajes de desechos resistentes a la corrosión por lo menos a corto plazo, es decir que no hay que contar con un transporte rápido de radionucleídos a la superficie. Así queda finalmente el problema del contacto de elementos radiactivos con el agua subterranea a través de la difusión en la roca [25, 26, 57] y/o lixiviación, eventualmente como consecuencia de la inundación durante la introducción, antes de lograr una duración de almacenamiento definitivo segura para este acontecimiento (>1000 años) [6, 33, 37, 40, 43]. Se tiene que prevenir este riesgo, desarrollando embalajes de desechos integros a largo plazo!

Para el almacenamiento de embalajes de desechos altamente radiactivos en formaciones de sal gema, estos se introducen en forma de bidones cilíndricos (≤30 cm de diámetro, 100-300 cm de alto) en taladros de perforación que tienen que disponerse geométricamente de modo que el calor de desintegración producido no afecte la estabilidad mecánica de la roca, es decir que no se sobrepase una densidad máxima de la fuente de calor. Por consiguiente, la disposición geométrica de los embalajes de desechos radiactivos (producto de desecho + envuelta) en el almacenamiento definitivo depende de su calor de desintegración, es decir de su composición y con esto - además de la reelaboración y del tratamiento técnologico de los desechos - también de los tiempos de almacenamiento provisional.

En principio el almacenamiento

- de los elementos cumbustibles consumidos [12] antes de la reelaboración

- o de los desechos después de la reelaboración

da la posibilidad de variar la composición y con esto la actividad térmica y la radiactividad y de utilizar aún el calor de desintegración - por lo menos dentro del marco de reflexiones.

Este almacenamiento provisional es imaginable tanto para los efluentes líquidos como para los sólidos. Pero el almacenamiento provisional de efluentes líquidos radiactivos tiene el inconveniente que

- el ácido nítrico altamente contaminado se evapora continuamente y tiene que ser retornado a los tanques de almacenamiento a través de sistemas de condensación cerrados;
- fenómenos de corrosión vienen reforzados por segregación y condensación;
- se necesita mucho volumen de almacenamiento.

A esto hay que añadir el riesgo general de contaminación que también en el almacenamiento provisional - practicado - de embalajes de desechos [35, 51] con refrigeración por agua o por aire dificulta la utilización del calor perdido procedente de depósitos intermédios después de la reelaboración.

La cuestión de si y para cuánto tiempo se tiene que almacenar provisionalmente, depende tanto de aspectos de política social como técnicos y económicos. Bajo los aspectos de política social, la necesidad de la seguridad toca un papel esencial. Por motivos técnicos, la duración del almacenamiento provisonal para elementos combustibles consumidos no tendría que ser demasiado grande, porque en la desintegración del plutonio 241 con período corto (15 años) se forma el americio 241 con

período mucho más largo (433 años) que aumenta considerablemente el plazo de la radiactividad de los productos almacenados definitivamente. Desde el punto de vista económico se tiene que considerar también la pregunta del almacenamiento provisional de desechos altamente radiactivos después de la reelaboración, teniendo en cuenta que la disposición geométrica, es decir la compacidad de los embalajes de desechos en el almacenamiento definitivo puede hacerse tanto más económica cuanto más bajo sea el calor de desintegración. Por consiguiente, los gastos del almacenamiento definitivo bajan proporcionalmente con la actividad térmica, excepto los gastos fijos que valdría un almacenamiento definitivo - hipotético - para embalajes de desechos no activos térmicamente. Para un desecho procedente de un combustible reelaborado 10 años después de la descarga del reactor, la evolución de los gastos de un almacenamiento definitivo sigue en primera aproximación la función de tiempo dada por la ecuación 2 para la actividad térmica. La proporcionalidad de la actividad térmica y los gastos dependen entonces de diferentes hipótesis que se refieren a los gastos reales de construcción y de mantenimiento y que se han extraido de la literatura para un caso especial representado en la fig. I.7 [51]. Los cálculos correspondientes han sido efectuados por J. Ehni dentro del marco de un trabajo de estudios (Universidad de Karlsruhe; asignatura: ciencia de los materiales para ingenieros economistas). La conclusión esencial es que los gastos del almacenamiento definitivo bajan con la duración de tiempo que sigue a la descarga del reactor. Utilizando provisoriamente un almacenamiento provisional en vez de un almacenamiento definitivo, los gastos de un almacenamiento definitivo ulterior serán más bajos, pero en vez de esto resultarán gastos para el almacenamiento provisional. Estos se subdividen en gastos fijos para la construcción y los gastos corrientes del mantenimiento del almacenamiento provisional, y han sido indicados también en la fig. 7 como evolución de

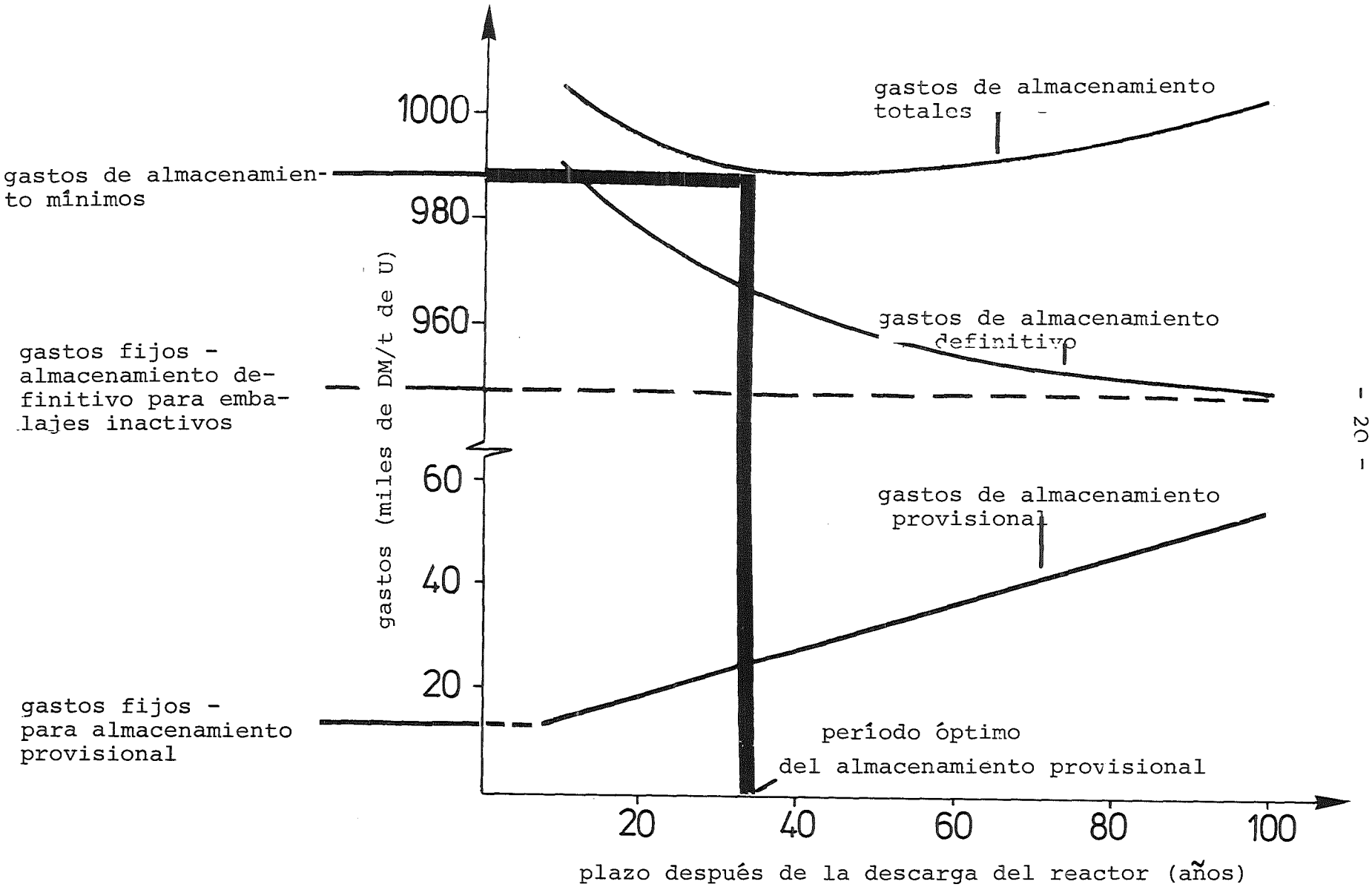

FIG. I.7: ESTIMACION DEL DESARROLLO DE LOS GASTOS PARA EL ALMACENAMIENTO PROVISIONAL Y DEFINITIVO COMBINADO DE EMBALAJES DE DESECHOS NUCLEARES

los gastos sobre la duración de tiempo después de la descarga del reactor. Otra vez, la conclusión esencial en este contexto es que los gastos de almacenamiento provisional aumentan con la duración de tiempo. En el caso especial la correlación gastos-duración de tiempo es lineal y tiene una pendiente determinada.

Los gastos totales para una combinación del almacenamiento provisional y definitivo resultan entonces de los gastos de almacenamiento provisional y definitivo en el momento considerado. Su evolución está indicada también en la fig. 7 para el ejemplo estudiado. Es posible que el mînimo indicado allî coincida bajo otras hipótesis con el comienzo de la curva de los gastos totales o que se desplace a la derecha. Es también posible que salga aún más plana que en el ejemplo. Pero otras condiciones de gastos de almacenamiento provisional y definitivo y la consideración de intereses de capital tampoco no cambian el resultado de principio

- que este mînimo existe
- que la marcha de la curva de los gastos totales después del minimo es relativamente plana y
- que por ello el almacenamiento provisional y definitivo combinado en el órden de magnitud de decenios es economicamente justificable - posiblemente aún más económico - que el almacenamiento definitivo inmediato de embalajes de desechos después de su fabricación.

Terminamos aquî el capîtulo de la influencia del almacenamiento provisional sobre el almacenamiento definitivo de embalajes de desechos radiactivos en la sal gema o granito.

Para garantizar una transmisión uniforme del calor desde el embalaje de desechos al ambiente en el almacenamiento defini-

tivo, conviene rellenar los taladros de perforación después de introducir los embalajes. Como material de relleno en formaciones de granito se preve entre otros la bentonita, una mezcla de arena y arcilla (proporción volumétrica 80 : 20) [36], que es un intercambiador de iones relativamente bueno y que por otra parte se hincha al contacto con agua y que de este modo obtura grietas eventuales en la roca. Ambas propiedades retardan el transporte de radionucleídos a la biosfera y representan reacciones de autoprotección del sistema. Para el relleno de taladros de perforación en la sal gema, solamente la primera propiedad sería importante, porque generalmente la obturación de grietas se produciría espontáneamente debido a la plasticidad de la sal. Pero se ha señalado varias veces que existen excepciones [25, 26].

Cuando se resumen todas las posibilidades del almacenamiento definitivo de desechos radiactivos, resulta como concepto actualmente alcanzable el enterramiento en formaciones geologicas en la base de un sistema con barreras multiples (fig. I.8), donde

- el desecho radiactivo viene primero fijado de modo generalmente molecular (p.ej. vitrificación) (barrera molecular);
- el desecho fijado de modo molecular está granulado y - de modo heterogéneo - introducido en una fase de matriz (barrera microestructural);
- el producto heterogéneo está revestido de modo macroscópico, p.ej. en recipientes (1a barrera macroestructural);
- los embalajes de desechos radiactivos son introducidos en posiciones de almacenamiento definitivo (material de relleno = relleno de sal, eventualmente con suplementos que favorecen la adsorción [2, 36] = 2a barrera macroestructural);
- las posiciones de almacenamiento definitivo se encuentran en roca de granito o salina (barrera geológica).

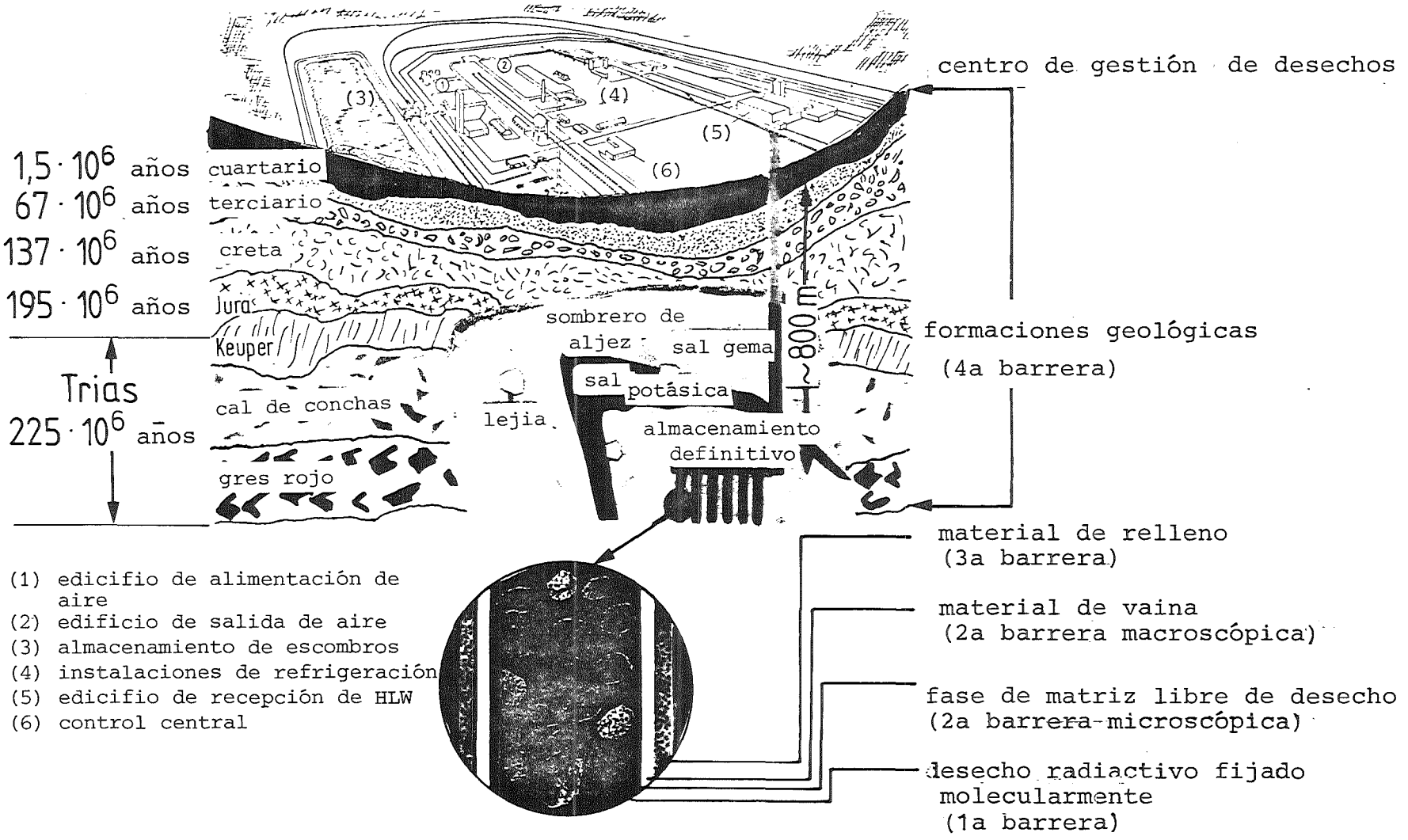

fig. I.8: Esquema de un centro de gestión de desechos con almacenamiento definitivo

I.3 Condiciones de estado en el almacenamiento definitivo

Antes de la introducción de embalajes de desechos radiactivos en formaciones geológicas éstas son cuasi estables, es decir están - aproximadamente - en equilibrio. El hecho de que este "cuasi-equilibrio" admite movimientos de materia, ha sido confirmado varias veces por las geociencias [25 - 57]. Para las condiciones de estado correspondientes de formaciones de sal gema (profundidad 500-1000 m) se tienen aproximadamente los datos representados en la fig. I.9 .

La introducción de embalajes de desechos radioactivos cambia las condiciones de estado del sistema - nuevamente formado - de barreras multiples, por lo que este está en un estado de desequilibrio durante largos periodos. Los transportes de materia en la roca ya mencionados (transformaciones de minerales, redistribución de elementos) tiene en este contexto una importancia especial, por lo que hasta ahora la estabilidad de formaciones de sal gema no puede considerarse como dada [25, 26, 57].

La composición viene modificada sobre todo por los componentes del desecho altamente radiactivo cuya composición en elementos está dada en la fig. I.3 bajo condiciones estándar y que cambia contínuamente, según los procesos de transformación radiactiva. A esto hay que añadir los elementos de los componentes introducidos en el tratamiento tecnológico de los desechos para la fijación molecular, la solidificación heterogénea y el revestimiento, es decir para la fabricación del embalaje de desechos (ver fig. I.2). La simulación de la composición del desecho sólido de actividad alta no está basada generalmente en los elementos, sinó en los óxidos y/o nitratos.

La actividad térmica específica del desecho sólido de actividad alta tiene como consecuencia temperaturas del embalaje de desechos que dependen de la "dilución" del desecho por los componentes del embalaje y de la evacuación del calor al ambiente del embalaje en el almacenamiento definitivo. Está última origina la formación de gradientes de temperatura. En la fig. 10 se han introducido estimaciones de los gradientes de temperatura para un embalaje de desechos nucleares bajo condiciones pesimistas, basándose en datos de la literatura [38], donde

- 15% en peso de desecho estándar altamente radiactivo está fijado de modo molecular en vidrio ($\triangleq$ 17,5 · 10^{-3} W/cm^3-producto);
- el desecho solidificado está envuelto de un recipiente de acero (espesor de pared: 1 cm; diámetro interior: $\sim$30 cm);
- se ha utilizado sal granulada para rellenar el taladro de perforación.

La estimación corresponde a condiciones pesimistas en cuanto que el relleno admitido del taladro de perforación posee la peor conductividad térmica debido al esponjamiento de sal. Por ello, los gradientes de temperatura obtenidos son más elevados bajo condiciones realistas, si entre el embalaje y la pared del taladro existe un entrehierro, y son más bajos en el caso de un contacto inmediato entre el embalaje y la sal compacta.

Debido al gradiente geotérmico, la evacuación del calor va a largo plazo completamente hacia la superficie terrestre. Pero el gradiente de temperatura que se forma en el ambiente del embalaje de desechos depende también de la distancia entre dos embalajes en el almacenamiento definitivo. Pero esta influencia se hace despreciablemente pequeña por encima de

distancias calculables entre dos embalajes [32]. Por ello no tiene que tomarselo en cuenta para la distancia admitida en la fig. I.10 ($\gtrsim$ 20 m) de dos embalajes de desechos (una coquilla por taladro de perforación).

Composición [3, 48, 51]	Halita (NaCl; componente principal) Carnalita ($MgCl_2 \cdot KCl \cdot 6\ H_2O$; suplemento) Anhidrita ($CaSO_4$; inclusiones) Gotas alcalinas (0,1-1% vol., pH_{RT} = 6,5; inclusiones): BO_3 1 200 ppm Br^- 400 ppm Ca^{2+} 600 ppm Cl^- 190 000 ppm HCO_3^- 700 ppm J^- 10 ppm K^+ 30 000 ppm Mg^{2+} 35 000 ppm Na^+ 42 000 ppm SO_4^{2-} 3 500 ppm Sr^{2+} 5 ppm
Temperatura [39]	$\sim$ 310 K
Presión (litostática) [55]	12 - 30 MPa

Fig. I.9: Magnitudes de estado en formaciones de sal gema (500-1000 m de profundidad)

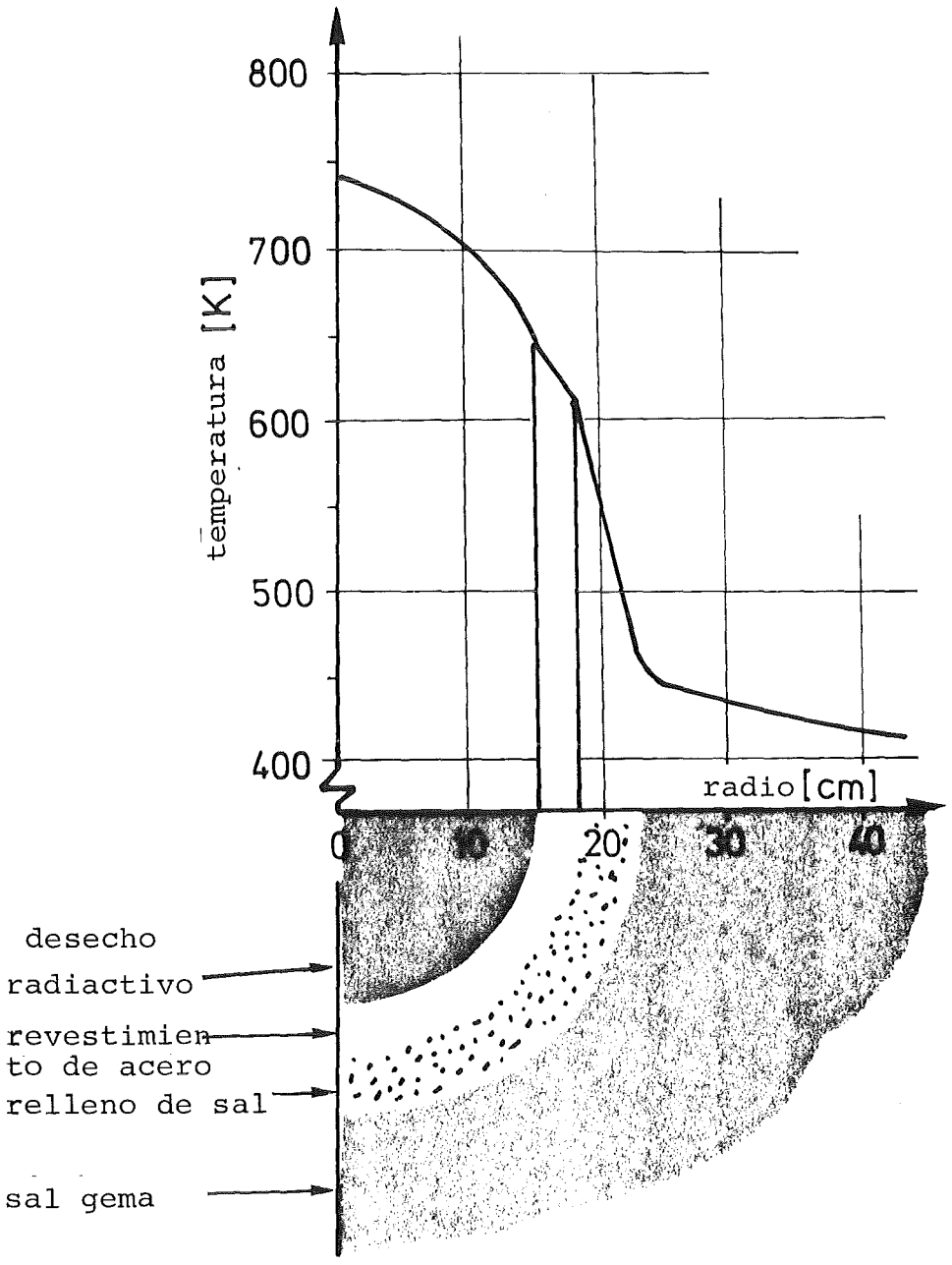

FIG. I.10: DISTRIBUCION DE LAS TEMPERATURAS EN EL EMBALAJE DE DESECHOS Y EL AMBIENTE PARA UN DESECHO ESTANDAR DE ACTIVIDAD ALTA DESPUES DE CINCO AÑOS DE ALMACENAMIENTO /38/

Así como las temperaturs sobre el embalaje y en su ambiente inmediato pueden variarse por su composición y geometría, así las temperaturas en el almacenamiento definitivo y su ambiente pueden influenciarse por medios de la técnica de ingeniería por su diseño, sobre todo la compacidad de almacenamiento de los embalajes de desechos [12, 31, 32, 39]. De este modo, las temperaturas pueden adaptarse, dentro del marco de un cierto ancho de variación, a condiciones que resultan de las consecuencias de aumentos de temperaturas sobre el ambiente indirecto y directo así como sobre el embalaje de desechos mismo. Estos últimos suponen un producto definido desde el punto de vista de la ciencia de los materiales, con una envuelta, lo que será el téma de nuestras consideraciones en la parte III de este trabajo. En cambio, consideramos que son conocidos los efectos de un aumento de temperatura sobre el ambiente inmediato del embalaje de desechos, que se refieren a

- la disolución parcial o completa de la estructura cristalina de la sal
- la formación de grandes cantidades de lejía salina.

La fig. I.11 presenta el análisis térmico de sal de ASSE [19], cuya estructura cristalina - especialmente a más de 500 K - es cambiada térmicamente de tal modo que se libera agua de cristalización, se puede formar ácido clorhídrico (HCl) y que pueden aparecer cambios dramáticos de la capacidad calorífica y de la conductividad térmica del ambiente inmediato del embalaje [41]. Como lo muestra la comparación con la fig. 10, bajo condiciones marginales realistas - en vez de pesimistas - podrán probablemente evitarse temperaturas máximas de sal >500 K, lo que por cierto queda todavía demasiado alto para algunas consideraciones geocientíficas [25, 26].

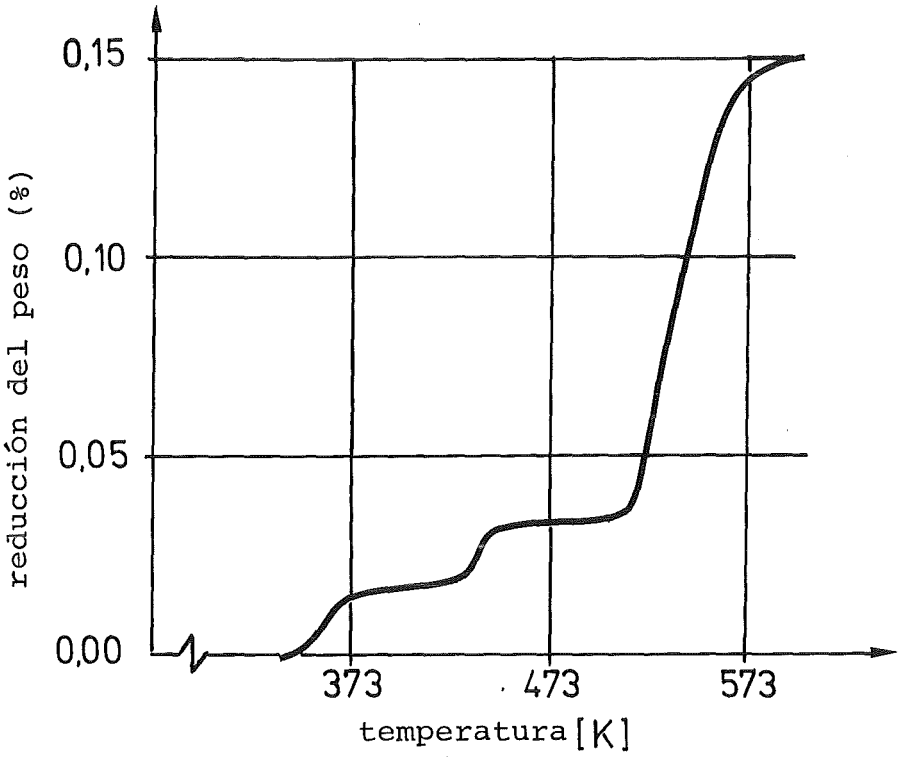

FIG. I.11: ANALISIS TERMICO DE SAL DE ASSE

En cambio, no se puede evitar que las gotas de lejía incluídas en sal (0,1-1% vol., ver fig. 9) se deplacen en el gradiente de temperatura hacia el embalaje de desechos y que pueden acumularse allí en cantidades de litros, cuando los diámetros de las gotas no son demasiado pequeños [3, 17, 28, 31, 48]. Este diámetro de la gotas que limita la acumulación de lejía es tanto más pequeño cuanto más elevado es el gradiente de temperatura hacia el embalaje, y para gradientes que corresponden a la fig. I.10 está en el órden de magnitud de 10^{-2} mm. La causa de la migración de las gotas es el efecto que en el lado más caliente de una gota se disuelve más sal que en el lado más frío. Por ello, en aquel lado se separa sal que viene redisuelta en el lado más caliente, por lo que las gotas en el gradiente de temperatura se desplazan en dirección del embalaje y se acumulan allí. Otra posibilidad de contacto, aúnque poco probable, entre la lejía de sal y el embalaje de desechos resulta de la presencia de inclusiones mayores de agua en formaciones salinas [10, 25, 26].

Además de estas consecuencias sobre el ambiente inmediato de los embalajes de desechos pueden calcularse aquellas que actúan a través del ambiente inmediato hacia la superficie terrestre, debido a la evacuación del calor, como p.ej.

- el calentamiento de capas que llevan aguas subterráneas;
- la dilatación térmica en la región de las cavidades de almacenamiento definitivo ("estabilidad de la minas") y de la superficie terrestre ("eminencias del terreno").

Cuando, debido a la inestabilidad térmica de la sal (>500 K, ver. fig. I.11) e inseguridades geocientíficas [25, 26] se considera una temperatura máxima admisible ($\lesssim$ 375 K) para ésta, resulta aproximadamente [28, 31, 32, 39, 51, 52], que

- se tiene que fijar una temperatura média máxima de los embalajes de desechos ($\lesssim$ 500 K);

- los aumentos de temperatura máximos causados por ella no tendrían que ser $\gtrsim$ 100 K en ningún sitio del almacenamiento definitivo y en ningún momento;

- la densidad del flujo térmico en el almacenamiento definitivo tiene por consiguiente que limitarse (según cálculos americanos basados en 175 K como aumento de temperatura máximo, es $\lesssim$ 37 W/m^2 [32]);

- el aumento de temperatura de lás aguas subterráneas no tendría que sobrepasar $\leq$ 6 K;

- el aumento de temperatura en la superficie terrestre tendría que ser $\leq$ 0,5 K;

- la eminencia del terreno inducida térmicamente en la superficie terrestre sobre el almacenamiento definitivo tendría que ser $\leq$ 1,5 m.

Además de la composición y temperatura, la presión representa una variable de estado en el almacenamineto definitivo (ver fig. 9), pero que debido a la plasticidad de la sal frente a la formación geológica no cambia practicamente sin embalaje de desechos. Pero otra magnitud de estado suplementaria que hay que considerar es la radiactividad que, como ya lo hemos mencionado, puede originar la radiolisis de lejías de sal y con esto la formación temporaria de ácido nítrico así como de hidrogéneo, oxigénio y gas cloro [8, 31].

Además sería posible acumular y por consiguiente "represar" energía de radiación en defectos de construcción inducidos por radioación de los materiales de embalaje. En el caso de una liberación espontánea de estas energías como calor a partir de sal y/o vídrio no ocurre sin embargo ningún aumento de temperatura que tenga una importancia práctica [22, 31, 49].

Literatura

/1/ Allard B. et.al. in G.J. McCarty (ed) Scientific Basis for Nuclear Waste Management Vol. 1, Plenum Press, New York (1979) 403

/2/ Allard B. IAEA-SM-246/13 (1981)

/3/ APS Study Group, Report to the American Physicyl Society by the Study Group on Nuclear Fuel Cycles and Waste Management, Review of Modern Physics 50 (1978) S1

/4/ Battelle Columbus Laboratories, NASA-CR-161419 (1980)

/5/ Bechthold W in H. Grupe (ed) "Wie sicher ist die Entsorgung?" Kernforschungszentrum Karlsruhe (1980) 35

/6/ Bertozzi G. et.al in OECD Nuclear Energy Agency (ed) Risk Analysis and Geologic Modelling in Relation to the Disposal of Radioactive Wastes in Geological Formations (1977) 13

/7/ Blomeke J.D. et. al., Nucl. Techn. 56 (1982) 361

/8/ Bradshaw R.L. et.al., ORNL-4555 (1971)

/9/ Braithwaite J.W. et. al. in G.J. Mc Carty (ed) Scientific Basis for Nuclear Waste Management Vol. 1, Plenum Press, New York (1979) 283

/10/ Bannert B., Mitteilungen aus dem Römermuseum 30 (1928) 1

/11/ Clauss J., Atom und Strom 24/4 (1978) 98

/12/ Closs K.D. et.al., KFK 3000 (1980)

/13/ Com. Europ. Communities, Community action in radioactive waste management, Director-General for Res.,Science and Education (1980)

/14/ Croff A.G., Actinide Transmutation, Fission or Fusion Reactors Studies: A Review, American Nuclear Society 1976 Annual Meeting, Toronto, Ontario, Kanada, CONF-760622--3 (1976)

/15/ Dosch R.G. in G.J. McCarthy (ed) Scientific Basis for Nuclear Waste Management Vol. 1, Plenum Press, New York (1979) 395

/16/ Fischer u., H. Wiese, KORIGEN - ein Programm zur Bestimmung des nuklearen Inventars von Reaktorbrennstoffen im Brennstoffkreislauf, KFK 3014 (in Vorbereitung)

/17/ Gaffney E.S. et.al., UCRL--15102 (1979)

/18/ Gera F., IAEA-CN-36/313 (1977)

/19/ Gesellschaft für STrahlen- und Umweltforschung (GSF):Jahresbericht 1978

/20/ Grupe, H. W. Koelzer, Fragen und Antworten zur Kernenergie, Info-Zentrale der Elektrizitätswirtschaft (1980) 37

/21/ Guber W. et.al., KfK 2721 (1979)

/22/ Hall A.R., et.al., IAEA-SM-207/24 (1976)

/23/ Hamastra J., IAEA-SM-207/42 (1976)

/24/ Haug H.O., KfK 2022 (1975)

/25/ Herrmann A.G., Fortschritte der Mineralogie 58 (1980) 169

/26/ Herrmann A.G., Z. dt. geol. Ges. 131 (1980) 433

/27/ Hyland et.al.: Feasibility of Space Disposal of Radiactive Nuclear Waste, NASA TM X-2912, Col. 2 (1974)

/28/ IAEA, Report of INFCE Working Group 7: Waste Management and Disposal, STI/PUB/534 (1980)

/29/ Kelly K.L. et.al. in J.G. Moore (ed) Scientific Basis for Nuclear Waste Mangement Vol. 3, Plenum Press, New York (1981) 189

/30/ Kienzler B., et.al., KfK 3013 (1980)

/31/ Koplik, C.M., PB--293403 (1979)

/32/ Llewellyn G.H., ORNL/ENG/TM-7 (1978)

/33/ Logan S.E. et.al. in OECD Nuclear Energy Agency (ed) Risk Analysis and Geologic Modelling in Relation to the Disposal of Radioactive Waste in Geological Formations (1977) 77

/34/ Memmert G., Jül-Conf-42 (1981) 873

/35/ Moncouyoux J.P. et.al., Jul-Conf-42 (1981) 12

/36/ Nowak E.J., SAND--79-0990C (1979)

/37/ Oak Ridge National Laboratories (ed), CONF-760701 (1976)

/38/ Platt A.M. et.al., PNL-SA-7072 (1978)

/39/ Ploumen P., et.a., Atomwirtschaft/Atomtechnik 24 (1979) 85

/40/ Ringwood A.E. et.al., Jül-Conf-42 (1981) 495

/41/ Russell J.E., Y/OWI/TM-37 (1979)

/42/ Schneider K.J. (IAEA), IAEA-SM-246/63 (1981)

/43/ Schwedisches Indistrieministerium, Yttranden över statens vattenfallsverks ansökan enligt villkorslagen i, tillstand att tillförd reaktoranläggningen Ringhals 3 kärnbräsle, Ds I 1978:29 (1978)

/44/ Scott T.E., CONF-800305--7 (1980)

/45/ Spitsyn V.I. et.al. in G.J. McCarthy (ed) Scientific Basis for Nuclear Waste Management Vol. 1, Plenum Press, New York (1979) 237

/46/ Spitsyn V.I. et.al., IAEA-CN-36/245 (1977)

/47/ State of New Mexico, Governor's Energy Task Force (1975)

/48/ Stewart D.B. et.al. in G.J. McCarthy (ed) Scientific Basis for Nuclear Waste Management Vol. 1, Plenum Press, New York (1979) 297

/49/ Tyler L.D. et.al. in OECD Nuclear Energy Agency (ed) In Situ Heating Experiments in Geological Formations (1978) 31

/50/ US-Department of Energy (DOE), Environmental Aspects of Commercial Radioactive Waste Management, DOE/ET-0029 (1979)

/51/ US-DOE: Technology for Commercial Radioactive Waste Management, DOE/ET-0028 (1979)

/52/ US-Energy Research and Development Administration (ERDA), Alternatives for Managing Waste from Reactors and Post-Fission Operations in the LWR Fuel Cycle, ERDA-76-43 (1976)

/53/ US-Environmental Protection Agency (EPA, ed.), State of Geological Knowledge Regarding Potential Transport of High-Level Radioactive Waste from deep Continental Repositories, PB-289947 (1978)

/54/ US-Nuclear Regulatory Commission, NUREG-0043 (1976)

/55/ US-Office of Waste Isolation (OWI), Y-OWI/TM-44 (1978)

/56/ Weeren H.O. et.al. in G.J. McCarthy (ed) Scientific Basis for Nuclear Waste Management Vol. 1, Plenum Press, New York (1979) 257

/57/ Zeipert C., H. Wondratschek, N. Jb. Miner. Mh. 9 (1981) 407

II. La estructura de embalajes de desechos de actividad alta

II.1 Productos del almacenamiento definitivo en el sistema con barreras múltiples

La caracterización del desecho de actividad alta y del peligro que procede de él, tema de la Parte 1 de este trabajo, tenía como resultado la necesidad de su contención a largo plazo (> 1000 años) frente a la biosfera. - El análisis de las alternativas de almacenamiento definitivo de la Parte I de estos estudios tuvo como resultado la selección de formaciones geológicas continentales como lugar del almacenamiento definitivo, y trataba de las condiciones de estado después de la introducción de embalajes de desechos de actividad alta. El concepto de embalaje de desechos - o forma de depósito - comprende aquí el producto que conviene para el almacenamiento (definitivo) y su envuelta. Para garantizar el aislamiento durable del desecho de actividad alta frente a la biosfera durante su almacenamiento definitivo en formaciones salinas, el sistema de barreras múltiples es considerado como el concepto mejor realizable.

Conforme a las condiciones de estado - el sistema global que es el almacenamiento definitivo está en desequilibrio - no pueden existir barreras absolutas ilimitadas en el tiempo, sin embargo su eficacia con respecto a un retardo de la liberación de elementos altamente radiactivos es diferente. Pensamos que el producto más eficaz, es decir una primera barrera casi absoluta durante largos períodos, será él que fija el desecho en su mayoría de modo molecular y que está en equilibrio termoquímico interior; es decir que las fases formadas por interacción con componentes del desecho así como las fases formadas a partir de los componentes de desechos sobrantes, no disueltos, serán estables. Si este sistema

estuviera además en equilibrio con el material de una fase de matriz libre de desechos (barrera microestructural) y/o con el material de vaina (1a barrera macroestructural), el embalaje de desechos en su conjunto estuviera en equilibrio interior y proporcionaría entonces un sistema absoluto de barreras, si se pudieran excluir también interacciones posibles del material de vaina y/o de la fase de matriz libre de desechos o respectivamente de las fases de producto con sal y lejías de sal (ambiente inmediato del embalaje). En este caso - ideal - la función de barrera de la formación geológica (adsorción de radionucleídos liberados) frente a la superficie terrestre no sería necesaria. Debido a la complejidad material del desecho altamente radiactivo, su cambio con el tiempo debido a la desintegración, así como su actividad térmica y su radiactividad, no se puede realizar sin embargo este estado de equilibrio ideal. Interacciones entre los componentes del sistema que cambian con el tiempo debido a la desintegración, así como la difusión y la corrosión (lixiviación) bajo el efecto del ambiente originarán a largo plazo la liberación limitada de los elementos radiactivos del desecho. Por ello el concepto de barreras multiples tiene que realizarse de modo que retarde el acceso de estos elementos a la biosfera durante aquel período (> 1000 años) en que existe una alta radiotoxicidad (ver fig. 5, 6, Parte I de este trabajo) y incluye por ello las formaciones geológicas como barrera con alta potencia de adsorción para elementos de actividad alta [3, 10, 22, 31, 46, 52, 53]. - Hasta ahora los productos siguientes han sido desarrollados para la fijación - homogénea y heterogénea - de desechos de actividad alta y han sido estudiados:

- vidrios
- supercalcinados
- titanatos - zeolitas
- Synroc
- monazita (solamente para actínidos!).

II.2 Equilibrio interior: componentes, fases, superficies límites del producto

II.2.1 Vidrios

Entre los vidrios han sido probados y considerados como convenientes los vidrios de borosilicato [15] y de hipersilicato [23, 29]. Los vidrios tienen la tendencia y la capacidad de disolver la mayor parte de los componentes altamente radiactivos del desecho. Aún para condiciones de estado (473 K; 20 MPa) que las que hasta ahora han sido consideradas como posibles en el almacenamiento definitivo, se puede detectar que el vidrio, ya después de períodos relativamente cortos (1500 horas) entra en interacción con una parte de los componentes del desecho sólido de actividad alta (ver fig. II.1). El resto - especialmente Ru, Rh, Pd, Ag así como algunos compuestos de Ce, Zr, Ti y Te [14] - forma fases propias.

En la fig. II.2 se ha comparado la composición material de un vidrio de hipersilicato, un vidrio de borosilicato y un vidrio de feldespato de bario facilmente cristalizable ("cerámica de vidrio"). Como lo muestran los diagramas de estado correspondientes (fig. II.3), tiene que basarse en un estado de equilibrio con varias fases, aún para el sistema con dos componentes dióxido de silício-diborotrióxido. La adición de los componentes del desecho altamente radiactivo aumentará el órden del estado polifásico [38, 56], y en el estado líquido las tendencias de segregación de las fases, es decir hará más probable la inhomogeneidad macroscópica del producto solidificado [38, 49, 56] (ver figs. II.4, II.5).

Una singularidad de todos los vidrios es la que con un enfriamiento normal a partir de la fase líquida generalmente no alcanzan el estado de equilibrio estable. Esto se refiere menos o no solamente a las fases de vidrio mismas, sinó a su estructura fina: aúnque sea cristalina para el estado

de equilíbrio, el vidrio queda amorfo hasta casi-amorfo (orden próximo), es decir en el estado de desequilibrio o respectivamente de equilibrio metaestable de una fase líquida sobreenfriada. El plazo hasta la cristalización depende del tipo de vidrio y de las condiciones de estado durante la fabricación y en el almacenamiento definitivo [7]. Los vidrios de feldespato de bario (ver fig. II.2) y vidrios comparables se cristalizan ya durante un enfriamiento lento [37] y pueden transformarse directamente en "cerámica de vidrio" [8] para evitar la desvitrificación incontrolada. Entonces los límites de solubilidad para los componentes radiactivos de los desechos en las distintas fases cristalizadas son diferentes, pero para las concentraciones de desechos usuales (< 20% en peso) son alcanzadas solamente en casos excepcionales. Para otros vidrios y bajo condiciones de estado correspondientes, se tiene que contar con un principio de cristalización (p.ej. 7% vol. de fase cristalizada después de 10^{15} años para $\sim 0{,}6 \cdot T_E$; T_E = temperatura de ablandamiento K) y con la cristalización completa solamente después de períodos muy largos (10^{30} años [17, 24]. Pensamos sin embargo que el almacenamiento de desecho de actividad alta originará siempre el aumento de la tendencia a la cristalización [7], porque los componentes insolubles, cristalizados del desecho como p.ej. el rutenio, rodio o paladio actúan para la cristalización como gérmenes extraños, lo que ha sido probado experimentalmente para tipos de vidrio con gran aptitud de cristalización (fig. II.6) [38]. En cambio, para los componentes de desecho solubles en el vidrio, su estructura fina amorfa está probablemente favorable, porque permite una amplia adaptación al cambio inevitable de la composición material causado por la desintegración radioactiva. Este cambio afecta tanto la desintegración de los productos de fisión como el helio formado en la desintegración de los actínidos. Se supone que debido a la estructura fina amorfa del vidrio, su

capacidad como solvente es tan alta que no aparecen ni acumulaciones de helio y con ello centros de presión de vidrio (para 10^{19} α/g) ni efectos negativos de los elementos de productos de fisión (para 25% en peso de contenîdo de productos de fisión, 11 años) [49]. Por ello, el vidrio amorfo parece en principio ser relativamente insensible a los cambios materiales del desecho altamente radiactivo.

El estado polifásico (lîmites de fase) y la cristalización (bordes de grano) tienen como consecuencia superficies lîmites interiores que aparecen y se terminan en la superficie del vidrio. Allî forman gérmenes activos catalíticamente para la interacción del vidrio que contiene el desecho con el ambiente [16]. Su aumento, dificilmente previsible, con el tiempo debido a tendencias de desvitrificación representa un factor suplementario que favorece los procesos cinéticos en el vidrio que contiene el desecho debido a su estado de desequilîbrio termoquímico bajo condiciones de almacenamiento definitivo.

Mientras que la magnitud de estado temperatura - aumentada - en el almacenamiento definitivo para desecho altamente radiactivo introducido en vidrio favorece su tendencia a la estructura fina cristalina, la otra - nueva - magnitud de estado radiactividad actúa en el sentido opuesto: la radiación viene por lo menos parcialmente absorbida y causa con esto cambios de la estructura del vidrio. Especialmente la radiación α de los actînidos produce a lo largo de la órbita de la partículas en el vidrio defectos suplementarios, también en la red amorfa (zonas de recoil, thermal spikes), que ya no se restablecen espontâneamente en regiones de baja temperatura (< 350 K). La formación de "redes de órbitas defectuosas y su penetración hasta la superficie del vidrio tendrîa consecuencias comparables a las de las superficies lîmites que penetran a la superficie del vidrio (lîmites de fase, bordes de grano), pero según los resultados obtenidos

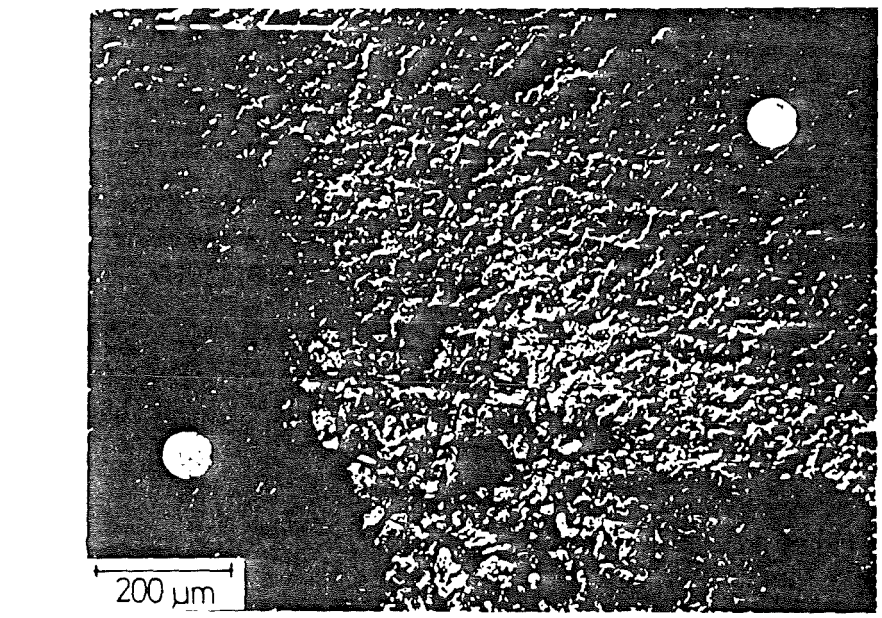

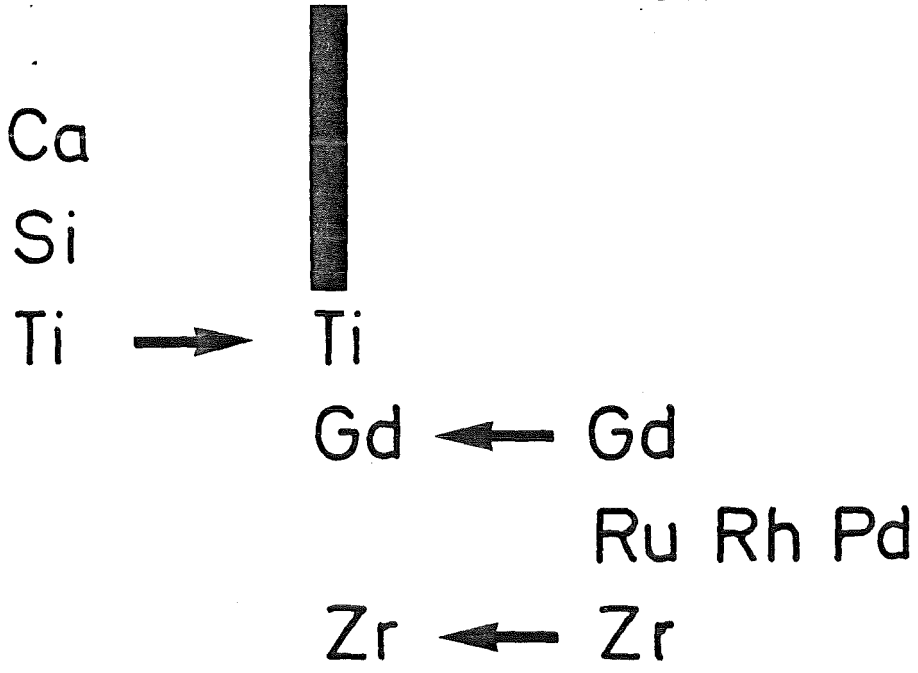

fig. II.1: Interacciones del vidrio con desecho altamente radiactivo simulado (473 K;, 20 MPa, 1 500 h)

componente	porcentaje (% en peso)		
	vidrio de hiper-silicato CUA	vidrio de boro-silicato KfK GP 98/12	vidrio de feld-espato de bario (HMI)
Al_2O_3	6	2,6	12-16
B_2O_3	4	12,3	2-9
BaO			16-20
CaO		4,1	0-7,5
Li_2O			1-4
MgO		2,1	
Na_2O		17,5	0-3
PbO			0-4
SiO_2	96	57	27-35
TiO_2		4,6	4-5
ZnO			4-6

fig. II.2: Composición material de varios vidrios
[1, 8, 14, 15, 23, 29, 39]

Schmelze= material fundido o fase líquida

Quarz= cuarzo

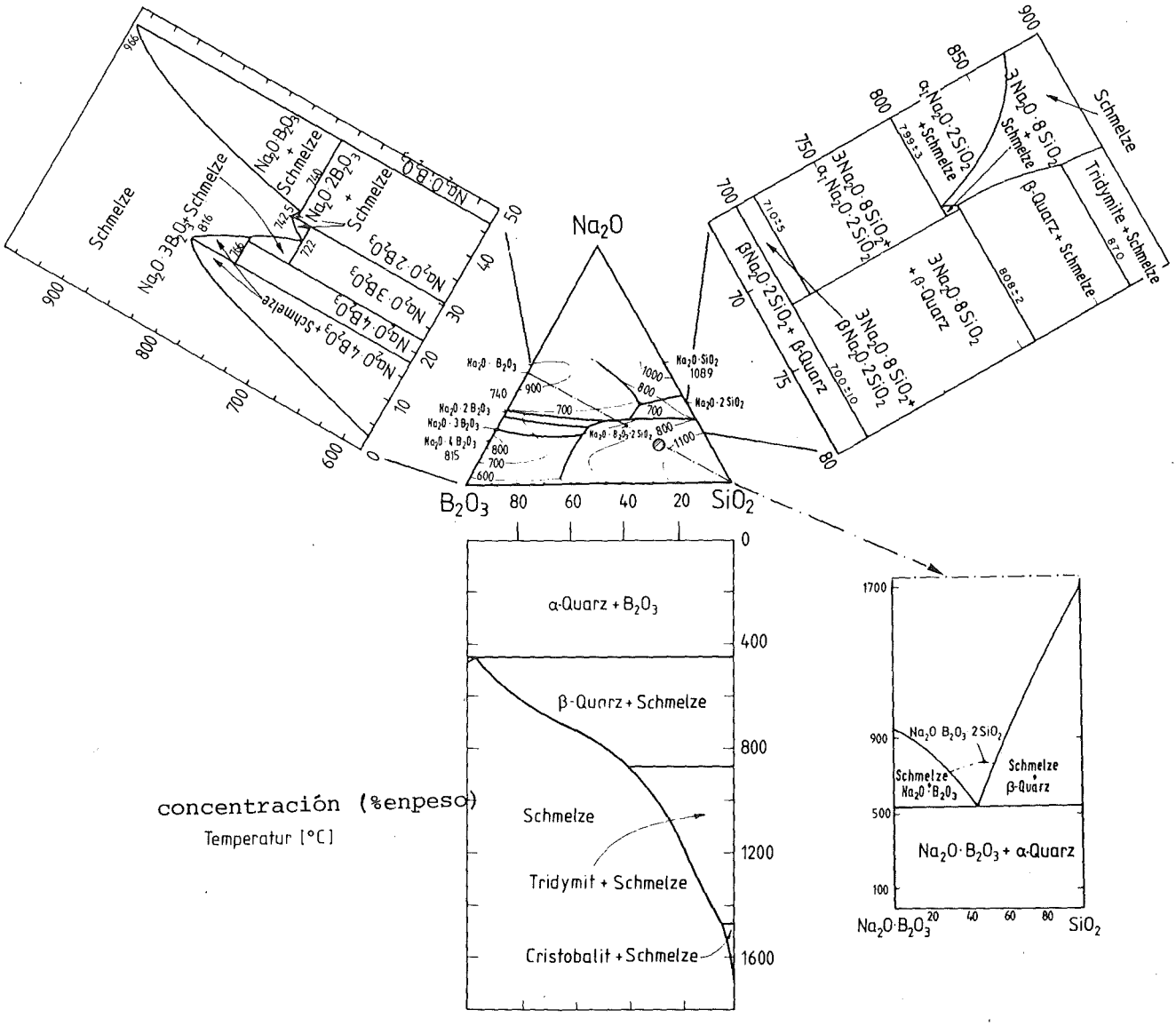

fig. II.3: Secciones conocidas del diagrama de estado (cuasi) ternario de B_2O_3-Na_2O-SiO_2 /21,34,35,47,58 /

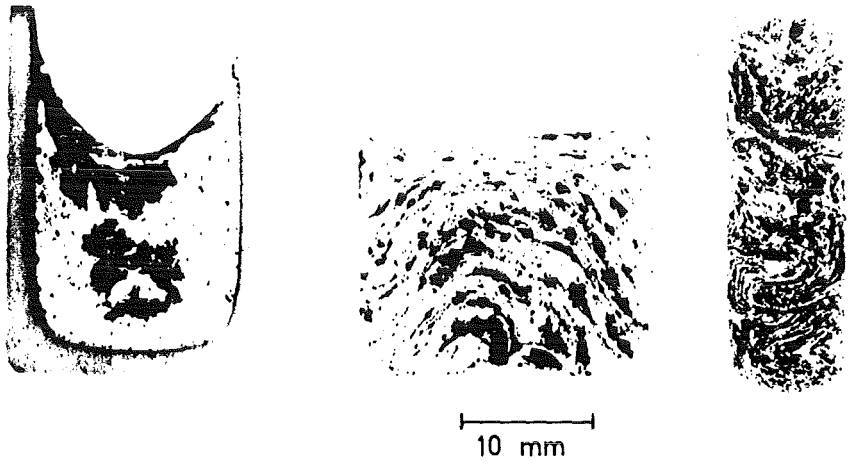

fig. II.4: Segregaciones en productos de vidrio fundido con desecho altamente activo simulado (15 % en peso)

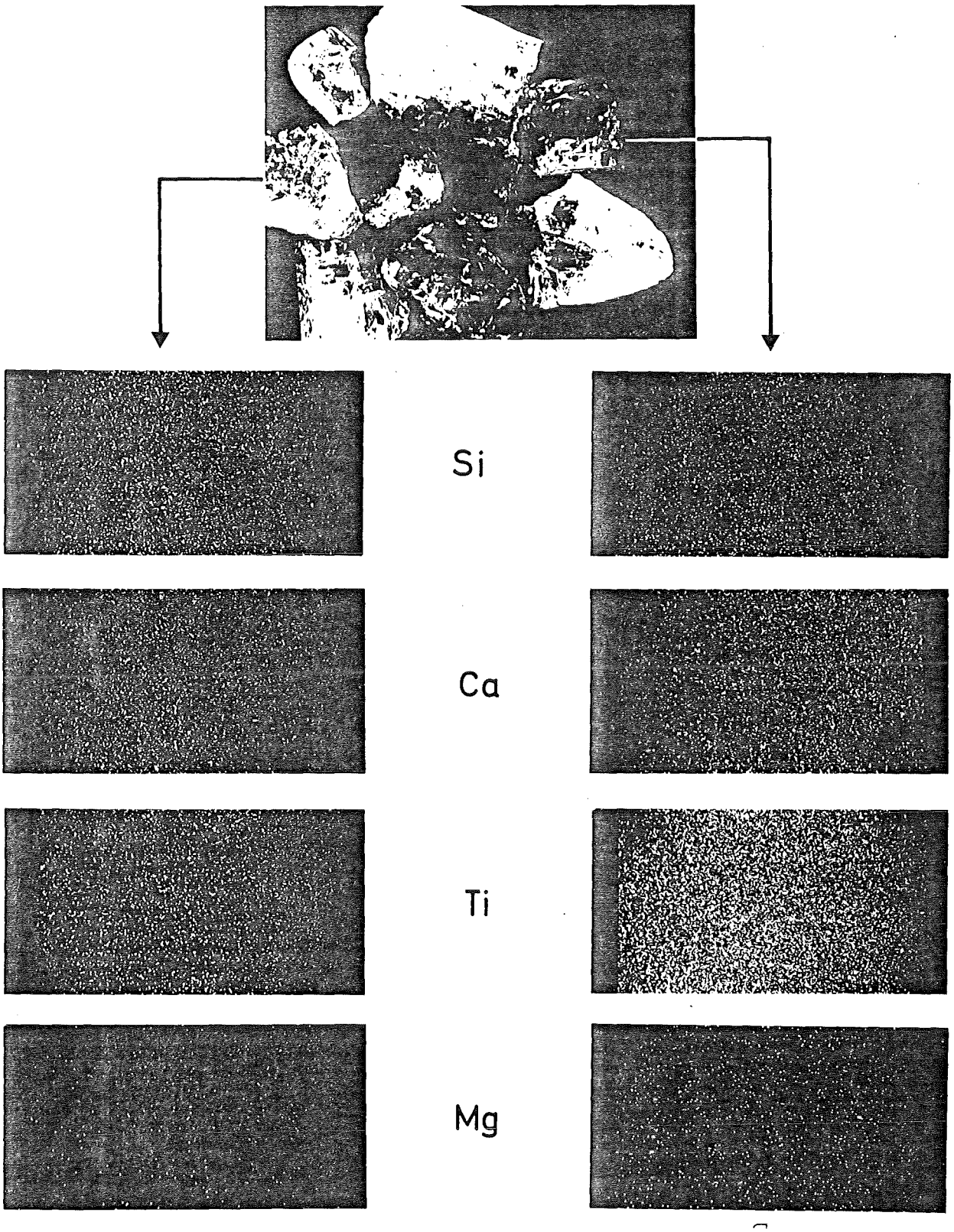

fig. II.5: Componentes de vidrio de borosilicato que contiene desecho (claro/oscuro-ver arriba) y su composición con respecto a algunos elementos, según análisis con microsonda (abajo).

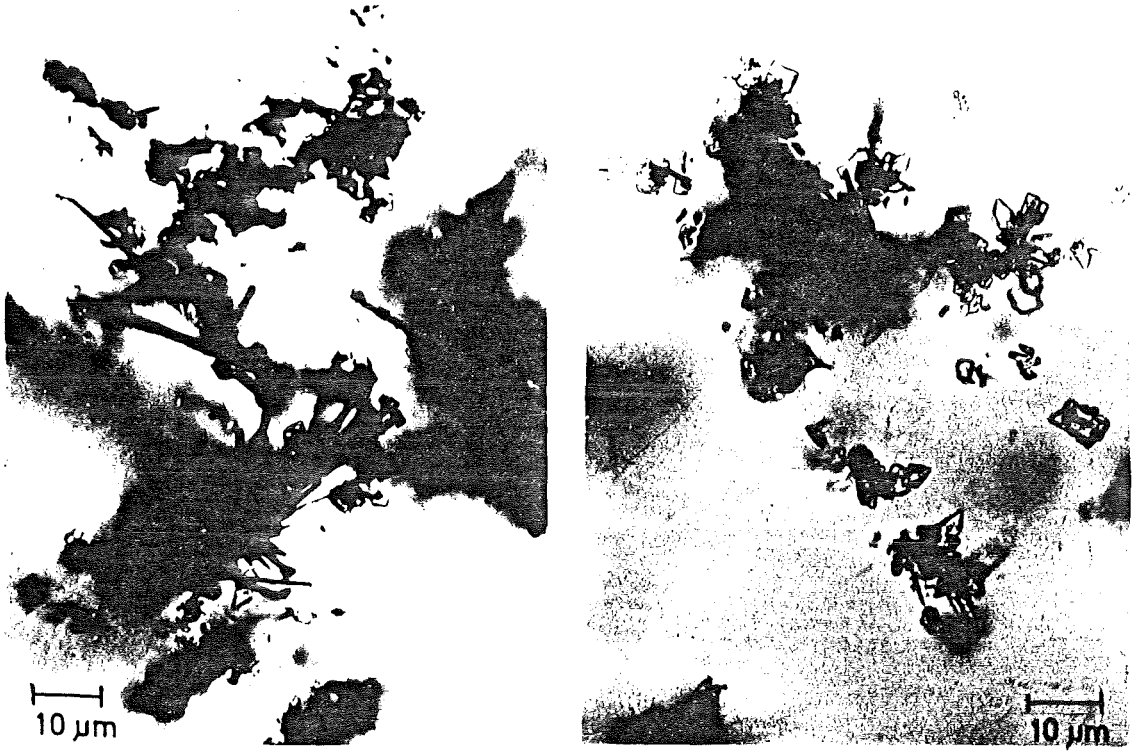

VG 12

VG 17

fig. II.6: Principio de cristalización en productos de borosilicato que contienen desechos simulados

hasta ahora no tiene ninguna importancia primaria [11]. - Otra consecuencia de la formación de defectos por absorción de radiación en el vidrio es la acumulación temporaria de energía cuya liberación repentina como calor no originaría sin embargo ningún aumento de temperatura peligroso [33, 40].

II.2.2 Supercalcinados

Como resulta de lo antes dicho, la tendencia de los vidrios - inmanente al sistema - al estado de desequilibrio termoquímico en el caso de una combinación con el desecho altamente radiactivo, complejo materialmente, entraña consecuencias difíciles de evaluar para el comportamiento a largo plazo de los productos bajo condiciones de almacenamiento definitivo. Por lo tanto la investigación de alternativas está concentrada a sistemas que están en equilibrio termoquímico interior. Con los vidrios cristalizados (cerámica de vidrio) se ha dado ya un primer paso en esta dirección. Como lo muestra la fig. II.7 también para más productos, consistía sobre todo en reducir el contenido en SiO_2 que favorece el estado de vidrio - amorfo. Con los supercalcinados se prosigue este desarrollo: con los componentes altamente radiactivos calcinados de los desechos se adicionan aquellos óxidos en cantidad, que hacen falta para la formación de un sistema cerámico polifásico de minerales conocidos (ver fig. II.8). Además de ocho fases cristalinas se ha encontrado una fase de matriz amorfa (6-10% vol.). Contiene el cesio no disuelto en la polucita (0,5-10% en peso) [30].

Para las fases cristalinas en el supercalcinado, los componentes del desecho altamente radiactivo tienen la función de formar redes huéspedes, por lo que influencian considerablemente el equilibrio polifásico. Por ello, el sistema es sensible frente a variaciones de la composición del desecho altamente radiactivo. Como ésta cambia inevitablemente con el tiempo debido a la desintegración radiactiva, esto es un

componentes	composición (% en peso)				
	vidrio de silicato	vidrio de boro-silicato	vidrio de feld-espato de bario (cerámica de vidrio)	supercal-cinato	Synroc
Al_2O_3		2,2	13,5	4,4	16
B_2O_3	3,4	10,5	5		
BaO			17,5		17
CaO		3,5	3,5	4,9	6
Li_2O			2,5		
MgO		1,8			
Na_2O		14,9	1,5		
PbO			2		
SiO_2	81,6	48,2	30	19,1	0
SrO				1,2	
TiO_2		3,9	4,5		60,4
ZnO			5		
ZrO_2					9,9
desecho rad.	15,0	15,0	15,0	70,4	10,7

fig. II.7: Composiciones de productos de desechos radiactivos [8,15,23,25,26,29,42,44]

COMPONENTES		FASES			
Composición	cantidad (% en peso)	Composición			
		nombre	fórmula	elementos principales	elementos-traza
Al_2O_3	4.4	apatito (A_{ss})	$(CsSr)_2SE_6(SiO)_6O_2$	O,Si,Ca,Gd,Nd,La,Ce,Pr,Y	St,Zr,[Al]
CaO	4.9	fluorita (F_{ss})	$(UCeZrSE)O_x$	O,U,Zr,Gd,Ce,Y,Sm	
SiO_2	19.1	corindón ($Fe_2O_{3\_ss}$)	$(Fe,Cr)_2O_3$	O,Fe	Cr
SrO	1.2	monazita (M_{ss})	$SEPO_4$	O,P,Nd,Gd,La,Pr	
		poluzita (P)	$(Cs,Rb,Na)AlSi_2O_6$	O,Cs,Al,Si	[Ca] , [Fe]
HLSW	70.4	rutilo (RuO_2)	RuO_2	O,Ru	
		scheelita (S_{ss})	$(Ca,Sr,Ba)MoO_4$	O,Mo,Ca,Sr, [Ba]	
		espinela (SP_{ss})	$(NiFe)(Fe,Cr)_2O_4$	O,Fe	Ni [Cr]
		fase amorfa	SiO_2-Al_2O_3-Fe_2O_3	O,Si,Al,Fe,Cs,Sr,SE	

fig. II.8: Componentes y fases de supercalcinato SPC 2 (SE = tierras raras; los elementos en corchete pueden faltar).

punto débil del producto. Hay que añadir que la fase amorfa está en desequilibrio termoquímico por lo menos por lo que a su estructura fina se refiere. Con respecto a la influencia de las magnitudes de estado temperatura y radiactividad, vale lo mismo que lo que hemos dicho para los vidrios. Para la mayoría de las fases cristalinas - especialmente para apatito - aparece bajo el efecto de radiaciones radiactivas metamictización, una destrucción comparable al efecto producido por radiactividad en el vidrio (zonas de recoil, thermal spikes), del órden cristalino por colisión de átomos con partículas α. De este modo el apatito ha sido completamente amorfizado (dosis 10^{18} α/g) [51], mientras que la fluorita y sobre todo la monazita presentan una alta resistencia a los rayos α. Así por ejemplo la monazita con grandes porciones de óxidos de actínidos disueltos (-42% en peso) en minerales naturales (edad $5 \cdot 10^8 \div 2 \cdot 10^9$ años) no presenta ninguna metamictización [45, 48], y por ello parece convenir particularmente bien para la fijación a largo plazo de los actínidos.

II.2.3 Titanatos, zeolitas y Synroc

Para reducir la sensitividad del producto frente a cambios de la composición del desecho altamente radiactivo así como para disminuir el número de las fases, la función que determina el equilibrio de fases del componente del desecho tiene que reemplazarse por una función de los suplementos.

La combinación de componentes de desecho altamente radiactivos (< 25% en peso) con titanato de sodio o respectivamente de calcio ($NaH/CaTi_2O_5$) [54] y con zeolita ($Na_2/K_2/ca/Ba/Cs_2/SrAl_2O_3 \cdot 6\ SiO_2 \cdot x \cdot H_2O$) por intercambio de iones daba lugar - también para un desecho no simulado - a un producto polifásico, conteniendo silicatos [9, 54], en los cuales aparecían entre otros aquellas tres fases que - por sí sola - determinan el producto de Synroc que resulta.

Los componentes de Synroc y sus fases están representados en la fig. II.9 [2, 42, 43]. Para obtener la función de los suplementos que forma la red huésped y que determina las fases, está limitada la solubilidad para componentes radiactivos de desechos (∿10% en peso). Por ello, el cambio con el tiempo de la composición debido a la desintegración radiactiva no tendría que tener una influencia decisiva sobre el equilibrio de fases. En cambio, se ha notado metamictización sobre todo para circonolita, pero también para holandita y perovskita [57].

II.3 Equilibrio exterior: interacciones entre producto-ambiente, producto-fase de matriz/material de vaina y fase de matriz/material de vaina y ambiente

II.3.1 Interacciones entre el producto y el ambiente

En el caso de un accidente bajo condiciones de almacenamiento definitvo, cada uno de los productos estudiados puede entrar en contacto directo con el ambiente de los embalajes de desechos. Para un almacenamiento definitivo en formaciones salinas esto significa que contactos entre el producto y

- sal
- lejía de sal así como
- agua neutral hasta ácida

tienen que tomarse en cuenta.

Los resultados disponibles hasta ahora se refieren a la compatibilidad, es decir al equilibrio exterior de los productos con la lejía de sal y el agua, y están resumidos en la fig. II.10. Para poder indicar grados de lixiviación selectivos, hemos tomado los elementos cesio, estroncio, plutonio y uranio, porque por una parte se trata de productos de fisión representativos (Cs, Sr) y de actínidos (Pu, U), y por otra parte porque - por los menos para vidrio - la tendencia a la

COMPONENTES		FASES		
Composición	Cantidad (% en peso)	nombre	fórmula	elementos disueltos del desecho altamente radiactivo
Al_2O_3	16	holandita (35% vol.)	$BaAl_2Ti_6O_{16}$	Ba^{2+}, Cr^{3+}, Cs^{+}, Fe^{2+}, K^{+}, Mo^{4+}, Na^{+}, Ni^{2+}, Rb^{+}, Tc^{4+}
BaO	17			
CaO	6	perovskita (32% vol.)	$CaTiO_3$	actínidos $^{3+}$, actínidos^{4+}, lantánidos^{4+}, Sr^{2+}
TiO_2	60,4			
ZrO_2	9,9	circonolita (31 % vol.)	$CaZrTi_2O_7$	actínidos^{3+}, actínidos^{4+}, lantánidos^{3+}, Na^{+}, Th^{4+}, Zr^{3+}, Y^{3+}
componentes altamente radioactivos	10,7	fase residual (12 % vol.)	$Al_2O_3 + TiO_2$	

fig. II.9: Componentes y fases de Synroc B

lixiviación disminuye en el órden

Cs > Sr > Co > Sb > Mn > Pu > Eu > Cm > Ce

Así por ejemplo el cesio tiene una tendencia aproximadamente cuatro veces más grande a la lixiviación que el cerio. Los datos relativos al grado de lixiviación global de vidrio de hipersilicato han sido medido solamente una vez, por lo cual tienen que considerarse como provisonales, pero están debidos probablemente al mineral natural tectita que casi no ha sido corrodida o respectivamente erosionada en diferentes aguas desde hace más de varios millones de años [24, 29, 39]. La cerámica de vidrio no mencionada no distingue del vidrio de borosilicato con respecto al órden de magnitud, y a partir de resultados mineralógicos y de laboratorio se sabe solamente de la fase de monazita, rica en actínidos, que existe en supercalcinatos y en minerales naturales, que presenta un grado de lixiviación por lo menos una dimensión más pequeña que el vidrio de borosilicato. Los grados de lixiviación del vidrio pueden aumentarse por medios de lixiviación ácidos y alcalinos [55].

Con grados de lixiviación de 10^{-5} para cesio o respectivamente de 10^{-7} $g/cm^2 \cdot d$ para plutonio, menos de 10% de la radiactividad inicial está liberada tras algunos decenios o respectivamente algunos siglos [15], pero grados de lixiviación global de productos de vidrio de $>10^{-4}$ $g/cm^2 \cdot d$ originan una desintegración volumétrica de aproximadamente 50% en algunos decenios y comprometen así la cohesión mecánica de tal producto. La cristalización aumenta este efecto de la destabilización mecánica y del aumento de la lixiviación [28, 41]. Por lo tanto, se ha estudiado varias veces la construcción de una segunda barrera alrededor del producto. Esta segunda barrera (ver fig. 8, Parte I de este trabajo) puede realizarse en forma de una fase de matriz microscópica, libre de desecho activo, y/o de envuelta macroscópica (coquilla de contenedor).

II.3.2 Interacción entre el producto y las fases de matriz - y/o el material de vaina así como las fases de matriz - o respectivamente los materiales de vaina con el ambiente

Técnicamente, la introducción de partículas conteniendo desechos altamente radiactivos en una fase de matriz libre de desechos es posible tanto para el vidrio como para todos los otros productos de desechos estudiados hasta ahora. Para esto, estos productos están generalmente granulados, y se prefieren partículas esféricas: Las esferas presentan una relación mínima entre la superficie - lixiviable - y el volumen - conteniendo el desecho. Las partículas de producto que contienen el desecho pueden entonces revestirse del material de la fase libre de desechos y/o mezclarse con la fase de matriz líquida o sólida (pulverizada) y compactarse. Entonces el equilibrio termoquímico está determinado - adicionalmente - por la compatibilidad de las fases de producto con las fases de peso o respectivamente de matriz y/o el material de vaina por un lado y las interacciones posibles con sal, lejía de sal y agua por otro lado.

Hasta ahora se han revestido (espesor de capa $\sim$ 50 µm) partículas de supercalcinado y de vidrio esféricas con óxido de aluminio y dióxido de silicio así como partículas esféricas de vidrio, supercalcinado y de Synroc con carbono pirolítico. Las densidades de las capas están limitadas, porque por una parte las temperaturas relativamente elevadas favorables para la densificación pueden originar grietas en la capa debido a los coeficientes de dilatación diferentes del material de capa y de partículas, y porque por otra parte serían favorecidas interacciones entre el material de partículas y el material de vaina [36, 50, 51].

Como fases de matriz para el vidrio se han empleado carbono, aleaciones de plomo así como una aleación de estaño [5, 13, 51, 57], y partículas de supercalcinado han sido incluídas en fases de Al-Si-, Cu y Pb-Zn [6, 26, 50, 51]. Además, los

PRODUCTO	CONDICIONES DE LIXIVIACION MEDIO TEMPERATURA [K]	ELEMENTO LIXIVIADO [gr/cm^2.d] Cs	Sr	Pu	U	global
VIDRIO DE BORO-SILICATO	AGUA ~300	10^{-6}	10^{-7}		10^{-8}	
	AGUA ~375	10^{-3}-10^{-4}	10^{-4}		10^{-4} - 10^{-5}	10^{-3} - 10^{-4}
	LEJIA DE SAL ~525					10^{-3} - 10^{-4}
	LEJIA DE SAL ~625	10^{-3}	10^{-4} - 10^{-5}		10^{-6}	10^{-2} - 10^{-3}
SUPERCALCINADO	AGUA ~375	10^{-3} - 10^{-4}	10^{-3} - 10^{-4}			10^{-4}
TITANATO-ZEOLITA	AGUA 375					10^{-3} - 10^{-4}
	LEJIA DE SAL 525	$<10^{-5}$				
Synroc	AGUA 375		10^{-7}	10^{-7}	10^{-8}	10^{-7}

fig. II.10: Grados de lixiviación del producto (g /cm^2.día)

componentes del desecho altamente radiactivo se han incluído directamente en una fase de matriz rica en SiO_2 [1, 57] y - con suplementos - en una aleación de base de hierro-niquel [18]. Esta inclusión de componentes altamente radiactivos de desecho originará en principio la formación de compuestos de calcinado y con esto interacciones con el material de la fase de matriz. Entre el vidrio y el plomo y resp. aleaciones de plomo así como el vidrio y el hierro, se han notado interacciones no solamente para altas temperaturas (775 K, 240 horas) [51], sinó tambien bajo condiciones simuladas de almacenamiento definitivo (ver fig. II.11), mientras que no se han encontrado interacciones entre el supercalcinado y el carbono pirolítico tampoco para temperaturas más elevadas [27].

En la fig. II.12 hemos resumido grados de corrosión conocidos en el caso de una interacción con el ambiente para agua y soluciones salinas. El plomo reacciona tambien con la sal bajo condiciones simuladas de almacenamiento definitivo (ver fig. II.11).

Para productos revestidos de capas, debido al pequeño espesor y a la pequeña densidad de las capas, se ha observado no solamente corrosión, sinó tambien lixiviación selectiva de los productos revestidos. En estos casos las capas de carbono sobre partículas de supercalcinado pueden por ejemplo aún aumentar el grado de lixiviación selectiva para el cesio, mientras que capas de Al_2O_3 lo reducen por lo menos en un órden de magnitud para todos los elementos altamente radiactivos estudiados hasta ahora [26, 51]. Generalmente estas capas no tienen el mismo efecto de barrera que las fases de matriz o las envueltas compuestas del mismo material.

Todas las fases de matriz metálicas y todos los materiales de vaina se metamictizan a partículas de producto altamente radiactivas en las superficies límites, donde el plomo

absorbe considerablemente la radiación γ (26% [13]). Los grados de corrosión bajo irradiación aumentan por ejemplo para "ticodes" con 10^7 γ-rad/h hasta el doble valor. Pero todas las fases de matriz metálica y todos los materiales de vaina mejoran también la estabilidad mecánica (seguridad del transporte) y la conductividad térmica (comportamiento al enfriamiento; por ejemplo desecho altamente radiactivo = 0,5 W/mK [32]; vidrio de borosilicato con 15% en peso de desecho altamente radiactivo = 1 W/mK [15]; vidrio vitromet en plomo = 12 W/mk [13]). En total se puede decir que no disponemos de resultados suficientes sobre la interacción en las superficies límites, la influencia de la temperatura y el cambio de la composición material del desecho altamente radiactivo así como sobre los efectos de radiación. Pero con respecto a la lixiviación, Tiedoch y Zircaloy y el grafito - en tanto que se presente en forma altamente densa y sin porosidad contínua - así como cerámicas de oxido como por ejemplo Al_2O_3 parecen ser potenciales materiales de segunda barrera altamente eficaces.

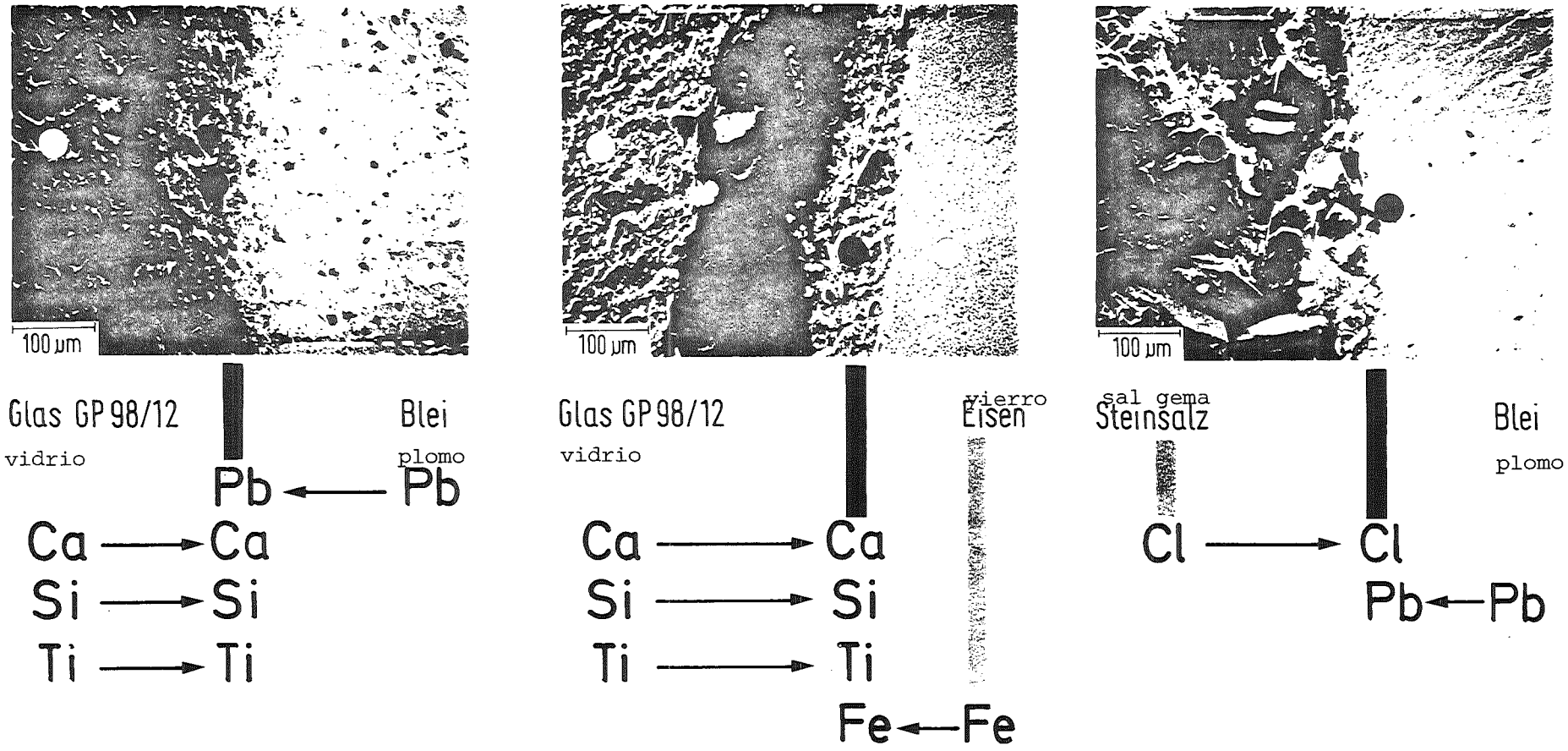

fig. II.11: Interacciones entre vidrio-plomo, vidrio-yierro, sal gema-plomo bajo condiciones máximas simuladas del almacenamiento definitivo (473 K, 20 MPa, 1500 h)

material de la 2a barrera	forma de la 2a barrera	grado de corrosión (g/cm^2d)				
		agua		solución salina		
		300 K	375 K	375 K	525 K	625 K
óxido de aluminio (Al_2O_3)	capa vaina		10^{-5}	10^{-5}		
vidrio (96% SiO_2)	capa fase de matriz vaina	10^{-7}	10^{-5}-10^{-6}		10^{-7}	
grafito (C)	capa (PyC) fase de matriz		10^{-9}			
aleaciones de aluminio (88 Al+12 Si)	fase de matriz					
aleaciones de plomo (97,5 Pb+2,5 Sb; 90 Pb+10 Sn; 84 Pb+12 Sb+4 Sn Pb-Zn)	fase de matriz vaina	10^{-4}	10^{-4}			
aleaciones de base de hierro-niquel	fase de matriz	10^{-4}-10^{-6}	10^{-5}			10^{-2}
Hastelloy (59 Ni+17 Mo +15 Cr+5 Fe+4 W)	vaina				10^{-7}	
Inconel 600 (76 Ni+15,5 Cr +8 Fe+0,2 Si +0,2 Mn+0,04 C)	vaina				10^{-7}	
cobre (Cu)	fase de matriz					
acero SS 304L (67,2 Fe+19 Cr +10 Ni+2 Mn +1 Si+0,8 C)	vaina				10^{-7}	
titanio CP (99,5 Ti)	vaina				10^{-8}	
Ticode 12 (98,718 Ti+0,84 Ni +0,34 Mo+0,09 Fe +0,012 C)	vaina				10^{-8}	
aleaciones de estaño (96 Zn+4 Al)	fase de matriz					
Zircaloy 2 (98,23 Zr+1,5 Sn +0,12 C+0,1 Cr+0,05 Ni)	vaina				10^{-8}	

Fig. II.12: Grados de corrosión de materiales de capa, de fase de matriz y vaina [1,4,6,12,13,18,19,20,26,36,39,50,51,57]

Literatura

[1] American Nuclear Society (ANS), CONF-780304 (1978) X1-15

[2] Angelini P., et.al., ORNL-WS-7530 (1979)

[3] Bertozzi, G., et.al. in OECD Nuclear Energy Agency (ed) Risk Analysis and Geologic Modelling in Relation to the Disposal of Radioactive Wastes in Geological Formations (1977) 12

[4] Braithwaite J.W., et.al., SAND--79-2023C (1980)

[5] Brummer H., H. Vietzke, DP 3018 746 (1981)

[6] Cornman W.R., DP--79-157-3 (1980)

[7] Dalton J.T., Boult K.A., Chambolain H.E. Int. Seminar Jülich (1981)

[8] De A.K., et.al., Ceram. Bull. 55 (1976) 500

[9] Dosch R.G., Ceramic Forms for Nuclear Waste, ACS Symposium Series, No. 100 (1979)

[10] Dosch R.G. in McCarthy (ed) Scientific Basis for Nuclear Waste Management Vol. 1, Plenum Press, New York (1979) 395

[11] Dran J.E., et.al., Science 209 (1980) 1518

[12] Gesellschaft für Strahlen- und Umweltforschung (GFS), GSF-T84 (1978)

[13] Geel J. von., IAEA-SM-207/83 (1976)

[14] Guber W.,et.al., CONF-970420 (1979) 188

[15] Guber W., et. al., KfK 2721 (1979)

[16] Hirsch E.H., Science 209 (1980) 1520

[17] King E.A. in E. Virgil et.al. (ed) Tektites, Dowden, Hutchinson and Ross Inc., Stroudsburg, Pennsylvania (1973) 51

[18] Kobisk E.H., et.al., ORNL/TM-7395 (1980)

[19] Larker H., Schwedisches Patent Nr. 7614376-7, KFK-TR-651 (1976)

[20] Larker H., Schwedisches Patent Nr. 7704488-1, KFK-TR-652 (1977)

[21] Levin E.M., Robbin C.R., McMurdie H.F., Phase Diagrams for Ceramists The Am. Ceram. Soc. 1959-1964

[22] Logan S.E. et.al. in OECD Nuclear Energy Agency (ed) Risk Analysis and Geologic Modelling in Relation to the Disposal of Radioactive Waste in Geological Formations (1977) 77

[23] Macedo P.B., et.al., CONF-970420 (1979) 321

[24] Macedo P.B., et.al., PB-294865 (1979) 81

[25] Malow G., et.al., HMI-B-218 (1977)

[26] McCarthy G.J., et.al., COO-2510-15 (1979)

[27] McElroy, J.L., BNWL--1826 (1974)

[28] McElroy, J.L., PNL-2265-2 (1978)

[29] McElroy, J.L., et.al., PNL-3050-1 (1979)

[30] McElroy, J.L., et.al., PNL-3050-2 (1979)

[31] Memmert, G., Jül.-Conf.-42 (1981) 873

[32] Mendel, J.E., et.al., BNWL-1666 (1972)

[33] Mendel, J.E., et.al., BNWL-SA--5534 (1976)

[34] Morey, G.W., H.E. Merwin, J. Am. Chem. Soc., 58 (1936) 2252

[35] Morey, G.W. J. Soc. Glass Techn. 35 (1951), 270

[36] Neumann, W., et.al., CONF-790420 (1979) 150

[37] Oguino, N., et.al., CoNF-790420 (1979) 143

[38] Ondracek, G., KFK 2940 (1980) 278

[39] Page, L.E., et.al., UCID-18873 (1980)

[40] Platt, A.M., et.al., BNWL-1788 (1973)

[41] Projekt Wiederaufarbeitung und Abfallbehandlung Kernforschungszentrum Karlsruhe, KfK 2940 (1980)

[42] Ringwood, A.E., Safe Disposal of High-Level Nuclear Reactor Wastes, A New Strategy, Australian National University Press, Books Australia, Norwalk, CT (1978)

[43] Ringwood, A.E., et.al., Geochemical Journal 13 (1979) 141

[44] Ringwood, A.E., et.al., CONF-790420 (1979) 174

[45] Ringwood, A.E., et.al.: Immobilization of High Level Nuclear Reactor Wastes in Synroc, Publ. No. 1475, Research School of Earth Sciences, Australian National University (1981)

[46] Ringwood, A.E, et.al., Jül-Conf-42 (1981) 495

[47] Rockett, T.J., W.R. Foster, J. Am. leram. Soc., 48 (1965) 78

[48] Römpp, H., Chemie Lexikon, Franckh'sche Verlagshandlung, Stuttgart (1966)

[49] Ross, W.A., et.al., PNL-2625 (1978)

[50] Ross, W.A., et.al., PNL-3060 (1979)

[51] Rusin, J.M., et.a., PNL-2668-1/2/3 (1978/1979)

[52] Schwedisches Indistrieministerium, Yttranden över statens vattenfallsverks ansökan enligt villkorslagen o, tillstand att tillförd reaktoranläggningen Ringhals 3 kärnbränsle, Ds I 1978:29 (1978)

[53] Scott, T.E., CONF-800305--7 (1980)

[54] Simonen, F.A. et.al., PNL-3036 (1979)

[55] Stewart, D.B., et.al., in G.J. McCarthy (ed) Scientific Basis for Nuclear Waste Management Vol. 1, Plenum Press, New York (1979) 297

[56] US-Energy REsearch And Development Administration (ed), CONF-770102 (1977)

[57] US-Department of Energy (DOE),DOE/TIC--10228 (1979)

[58] Williamson, J., F.P. Glasser, Science, 148 (1965) 1589

III. Tecnología de los productos de actividad alta almacenados definitivamente

III.1 Fijación cuasi-homogénea

Como lo muestra el diagrama de la fig. III.1, los productos adaptados al almacenamiento definitivo pueden en principio realizarse por métodos tecnológicos de fundición y de polvo.

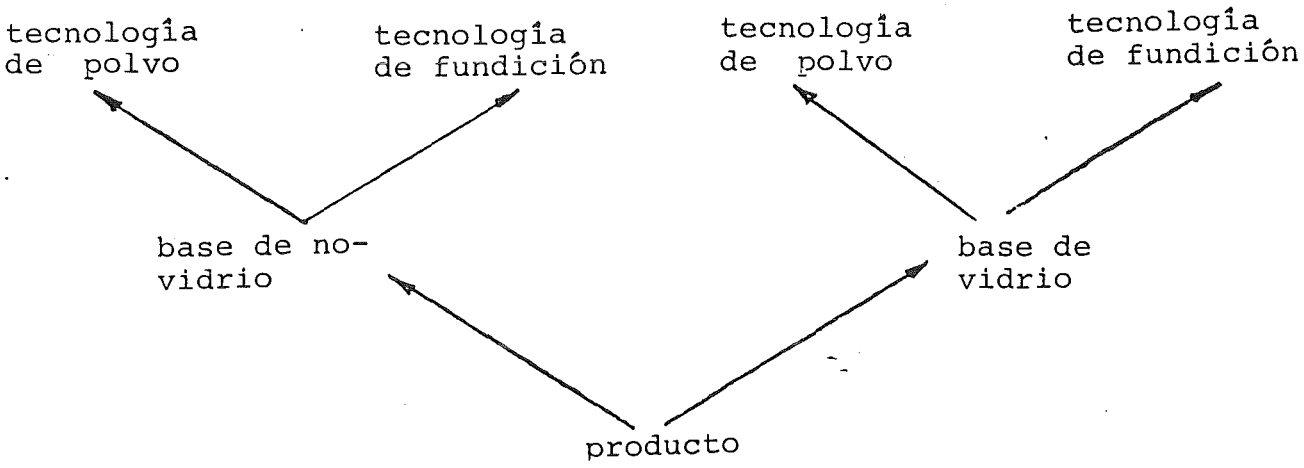

fig. III.1: Alternativas del material y de la tecnología de los productos

En la fig. III.2 presentamos las estapas tecnológicas de fundición del proceso. La desnitración puede realizarse en el efluente líquido de actividad alta (ver fig. I.2) por adición de, p.ej., formaldehido o ácido fórmico o por evaporación del solvente y calentamiento del sobrante. Esto significa la combinación del secado (∿ 400 K), de la desnitración y calcinación (900-1000 K), como la que se realiza en los procesos de vitrificación desarrollados en los Estados

PROCEDIMIENTO	ETAPAS DEL PROCEDIMIENTO							
	desnitración	secado	calcinación	mezclado	introducción	fundición	trasiego (coquilla)	obturación
SC-ICM (Spray Calciner-In Can Melter)	secado desnitración calcinación			mezclado introducción-trasiego fundición				obturación
AVM/H (Atelier de Vitrification Marcoule/La Hague)	secado calcinación desnitración			mezclado introducción		fundición	trasiego	obturación
LFCM (Liquid Fed Ceramic Melter)	introducción secado desnitración calcinación fundición mezclado						trasiego	obturación
HARVEST	introducción-trasiego mezclado secado desnitración calcinación fundición							obturación

fig. III.2: Etapas del procedimiento y su combinación para la fabricación tecnológica de fundición de productos que contienen desechos radiactivos

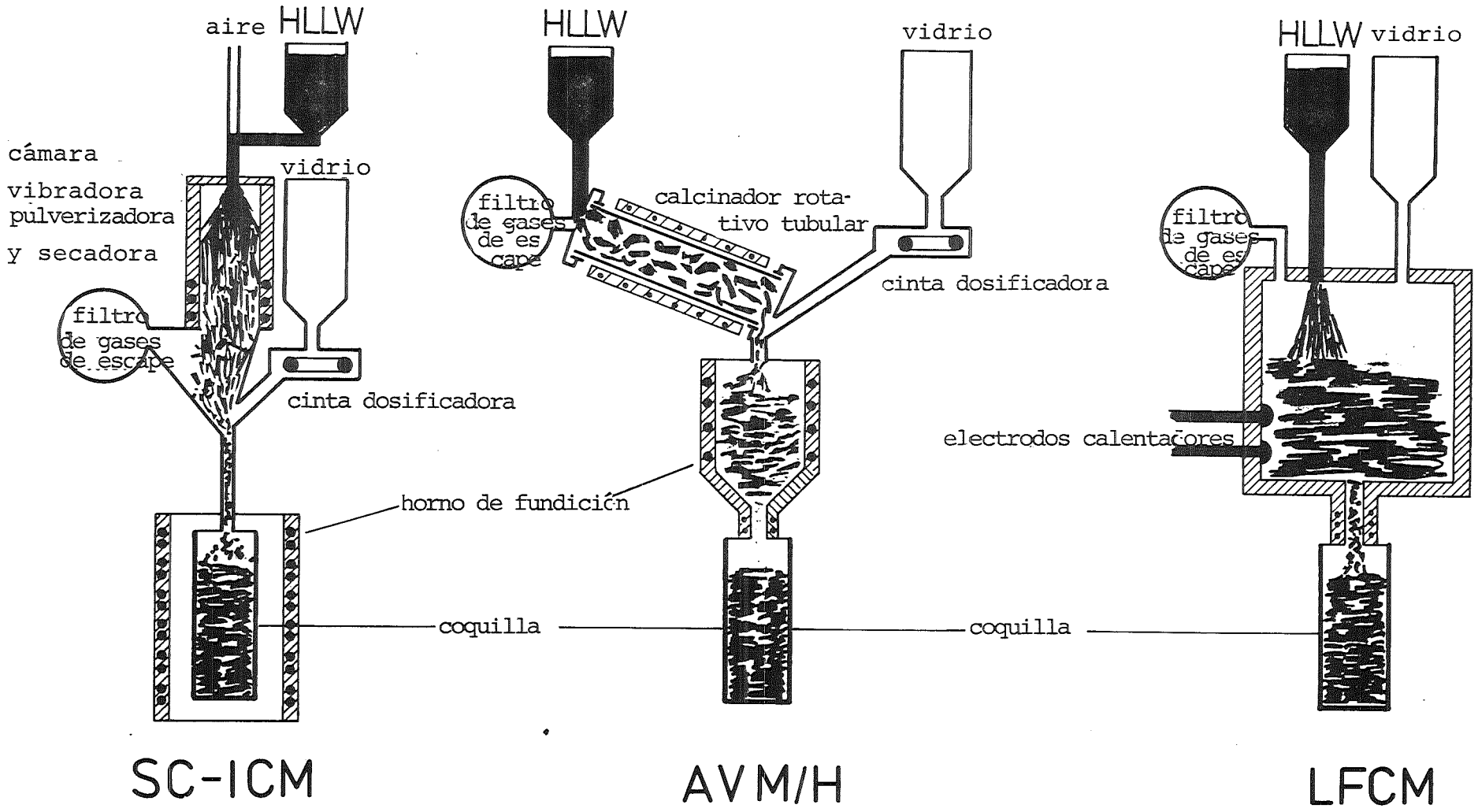

fig. III.3: Representación esquemática de diferentes procedimientos tecnológicos de fundición para la fabricación de productos que contienen desechos

Unidos (SC-ICM) [3, 4, 7, 15, 27], Francia (AVM-H) [6, 20], Alemania (LFCM) [18, 28] y Gran Bretaña (HARVEST). Estos procedimientos tecnológicos de fundición para la vitrificación de los desechos de actividad alta reunen entonces solamente algunas otras etapas del proceso que se suceden diferentemente. La fig. 3 muestra esquemáticamente las diferencias entre los procedimientos SC-ICM, AVM/H y LFCM. Mientras que en los dos primeros procedimientos el primer tratamiento térmico (secado, desnitración, calcinación) se realiza separadamente de la segunda etapa (fundición), en el procedimiento LFCM todas las etapas están reunidas y se realizan con temperaturas aumentadas. Por otra parte el procedimiento AVM/H y LFCM tienen en común que se hace la fundición en un horno separado (crisol) y que se cuela entonces en coquillas, mientras que en el procedimiento SC-ICM (y HARVEST) el crisol y la coquilla son idénticos. Los grupos de tratamiento térmico para el secado, la desnitración y calcinación pueden ser cámaras de calefacción con aspersión (SC-ICM), hornos rotativos tubulares multipaso (AVM/H) o secadores de cilindros (FIPS: cilindros y desmoldeadores calentados, ver fig. III.7), los grupos de fundición pueden permitir el calentamiento indirecto (SC-ICM, AVM/H) también multipaso (HARVEST) o directo de la fundición (LFCM; p.ej. electrodo de Inconel). En todos los procedimientos tecnológicos de fundición, el nivel de temperatura (> temperatura de ablandamiento del vidrio), determinado por la técnica del proceso, es un punto problemático (ver fig. III.4):

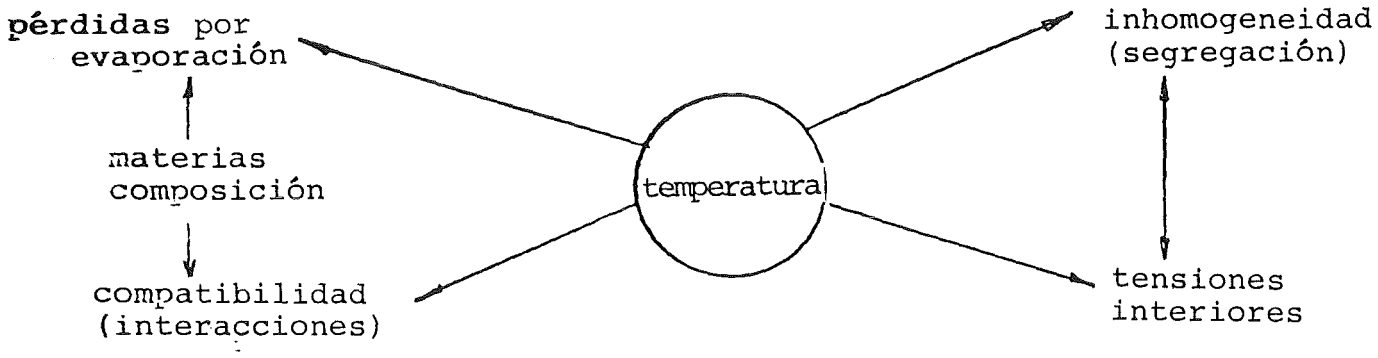

fig. III.4: La función de la temperatura en la tecnología de fundición

- Las pérdidas por evaporación que aparecen a altas temperaturas (funciones T de las presiones de vapor) cambian la composición material del producto y producen desechos secundarios: La fig. III.5 muestra grados de evaporación globales para un producto simulado altamente radiactivo de desecho (HAV) sin vidrio, para vidrio sin producto simulado altamente activo de desecho, y vidrio con producto simulado altamente radiactivo de desecho (15% en peso) después de experiencias de laboratorio (16-24 horas). En todos los casos la evaporación aumenta fuertemente para más de 1200 K, y para temperaturas de sinterización es claramente menor que para temperaturas de fundición del vidrio. Hasta aproximadamente 700 K el grado de evaporación del producto simulado altamente radiactivo de desecho está determinado por la descomposición de nitratos y el escape de gases nitrosos. Los gases de escape que corren hacia el filtro contienen sobre todo rutenio, cesio así como telurio y molibdeno (ver fig. III.5, curva HAV). La fijación molecular del desecho altamente radiactivo (15% en peso) en vidrio (ver curva de evaporación vidrio + HAV, fig. III.5) disminuye visiblemente su escape por evaporación, como se ha podido prever. Como las mediciones han sido realizadas con conjuntos específicos de probetas, no pueden extrapolarse los valores absolutos de los grados de evaporación; sirven solamente para demostrar cualitativamente el comportamiento de evaporación.

- Las interacciones entre la fase fundida y el material del crisol o respectivamente del horno de fundición que aparecen con temperaturas elevadas cambian la duración de los aparatos y originan también un cambio dificilmente controlable de la composición material del producto.

- El estado de agregación líquido que existe para temperaturas elevadas permite segregaciones y, como consecuencia, pertur-

baciones en el desarrollo del procedimiento así como inhomogeneidades macroscópicas del producto: Así p.ej. en el procedimiento LFCM la fase líquida se presenta con tres capas ya en el horno de fusión; al efluente líquido en la parte superior sigue el desecho calcinado, y la capa inferior es de vidrio fundido conteniendo desechos. La escoria formada que no escurre y la segregación que bloquea las salidas, pueden afectar la capacidad de funcionamiento de los hornos de fusión, y elevaciones en la coquilla debidas a la segregación de fases han sido observadas varias veces.

- El enfriamiento a partir de temperaturas elevadas origina un aumento de las tensiones interiores. Como la superficie del producto se enfría primero, se forman - según la velocidad de enfriamiento - gradientes de temperatura cuya compensación al final del enfriamiento da lugar a tensiones de tracción en el interior y tensiones de compresión en las zonas exteriores del producto. Pueden calcularse mediante los coeficientes de dilatación térmica, las conductividades térmicas y las velocidades de enfriamiento, y están representadas en la fig. III.6 sobre el radio del cuerpo del producto para vidrio de borosilicato con desecho altamente radiactivo (15% en peso). Solamente determinadas velocidades de enfriamiento, es decir aquellas con las que las dilataciones calculadas son inferiores al alargamiento de rotura del cuerpo del producto, garantizan que no aparezcan grietas en el vidrio. Al mismo tiempo se puede observar que las inhomogeneidades macroscópicas arriba mencionadas aumentan las tensiones interiores, que de todos modos aparecen durante el enfriamiento [9, 19], debido a su dilatación térmica - diferente - y que los coeficientes de dilatación diferentes del producto y de la envuelta (coquilla) pueden producir en esta última tensiones que en las envueltas de acero han provocado una sensibilidad aumentada frente a la corrosión por tensofisuración [19, 23].

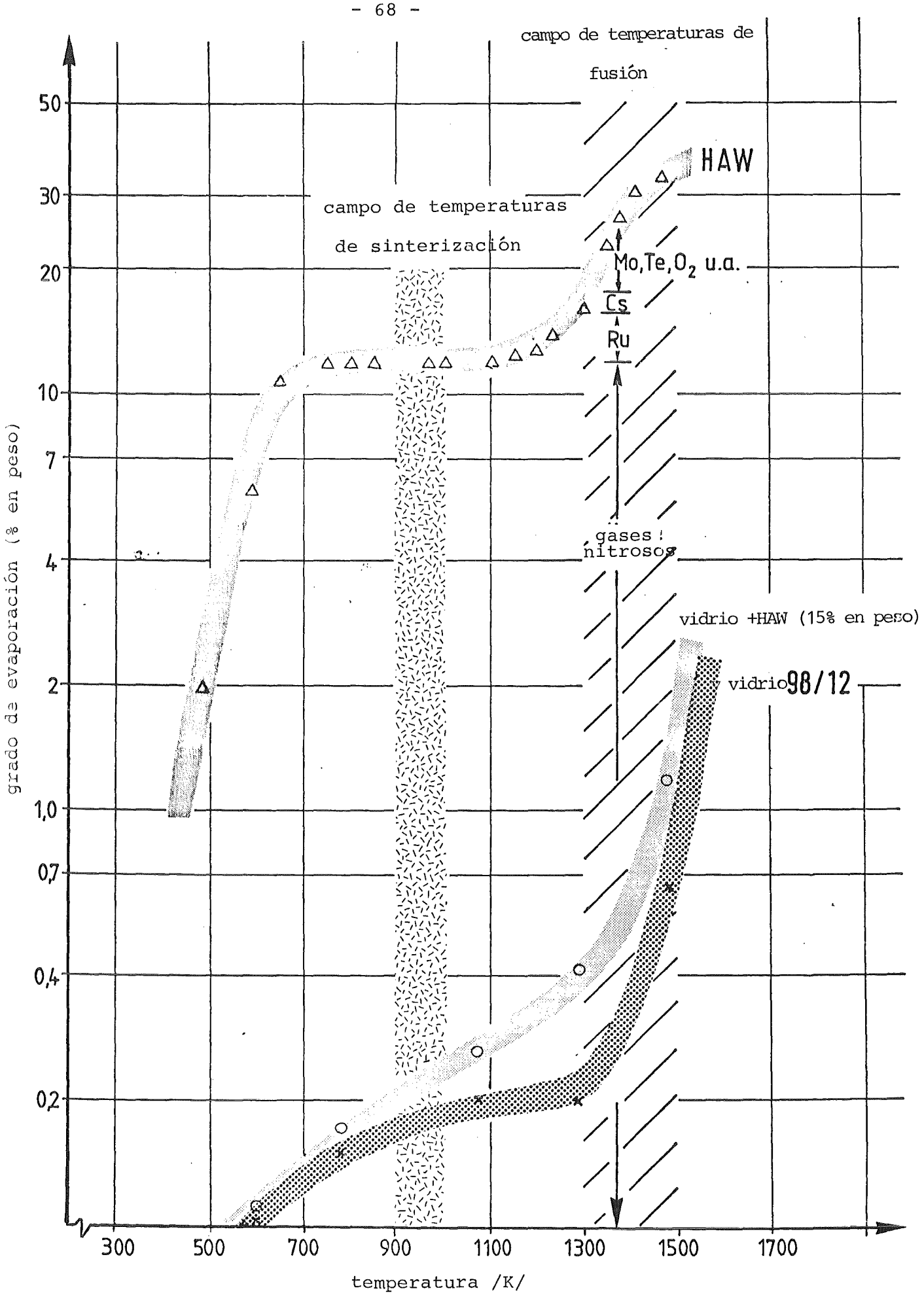

fig. III.5: Grados de evaporación globales en función de la temperatura, a partir de ensayos de laboratorio con vidrio con desecho radiactivo simulado y libre de desecho

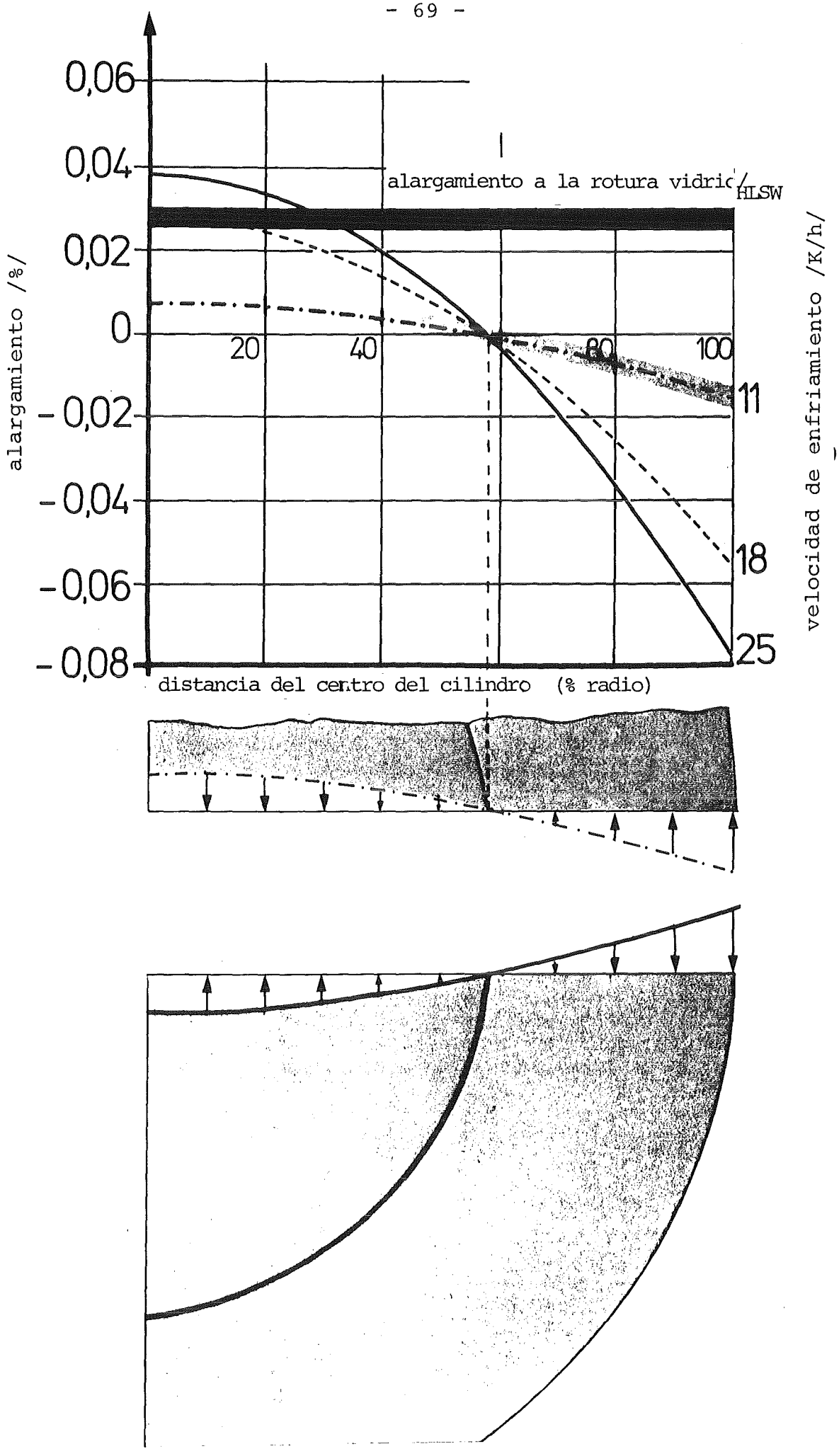

fig. III.6: Alargamientos y recalcados calculados en productos de vidrio

Para reducir las pérdidas de evaporación, es decir la producción de desecho secundario altamente radiactivo, las interacciones con el material de crisol o de coquilla y las tensiones interiores, y para excluir la formación de escorias y la segregación de fases, se ha fijado pulvitecnológicamente desecho altamente radiactivo en vidrio. Comparado con las etapas tecnológicas de fundición del procedimiento de la fig. 1, se reemplaza aquí en principio solamente la fundición por el prensado y la sinterización. Esta última etapa puede reunirse en la sinterización por presión, aplicando la presión de modo uniáxico o isostático. La fig. III.7 muestra esquemáticamente la marcha del procedimiento.

La mezcla del vidrio con los componentes altamente radiactivos de desechos en los procedimientos pulvitecnológicos puede realizarse de diferente manera. La fig. III.7 muestra el método de la mezcla directa en húmedo-seco, que en principio puede sustituirse por el método AVM/H a través de calcinadores rotativos tubulares que se ha probado ya para el desecho altamente radiactivo (ver fig. III.3). Es también posible empapar de efluente líquido altamente radiactivo partículas porosas de vidrio [1, 22]. La mezcla de componentes altamente radiactivos de desecho con titanatos-zeolitas [8, 16, 26] se hace por empapado de polvos ultrafinos de titanato-zeolita (50-100 Å), que absorben la mayoría de los elementos de desecho a través del intercambio de iones y que entonces se secan (900 K), se incluyen y se sinterizan por presión (7-14 MPa, 1200-1500 K). La desventaja que tienen las mezclas de empapado y adsorción es la producción de desecho secundario residual. - La mezcla de los componentes mediante la solución química fue demostrada para un caso especial eventualmente prometedor: Los actínidos - sin productos de fisión - en solución nítrica se precipitan con fosfato dicarbonatado de amonio y urea. El secado (700 K), el calcinado (1100 K) y la sinterización por presión (1300 K; 28 MPa)

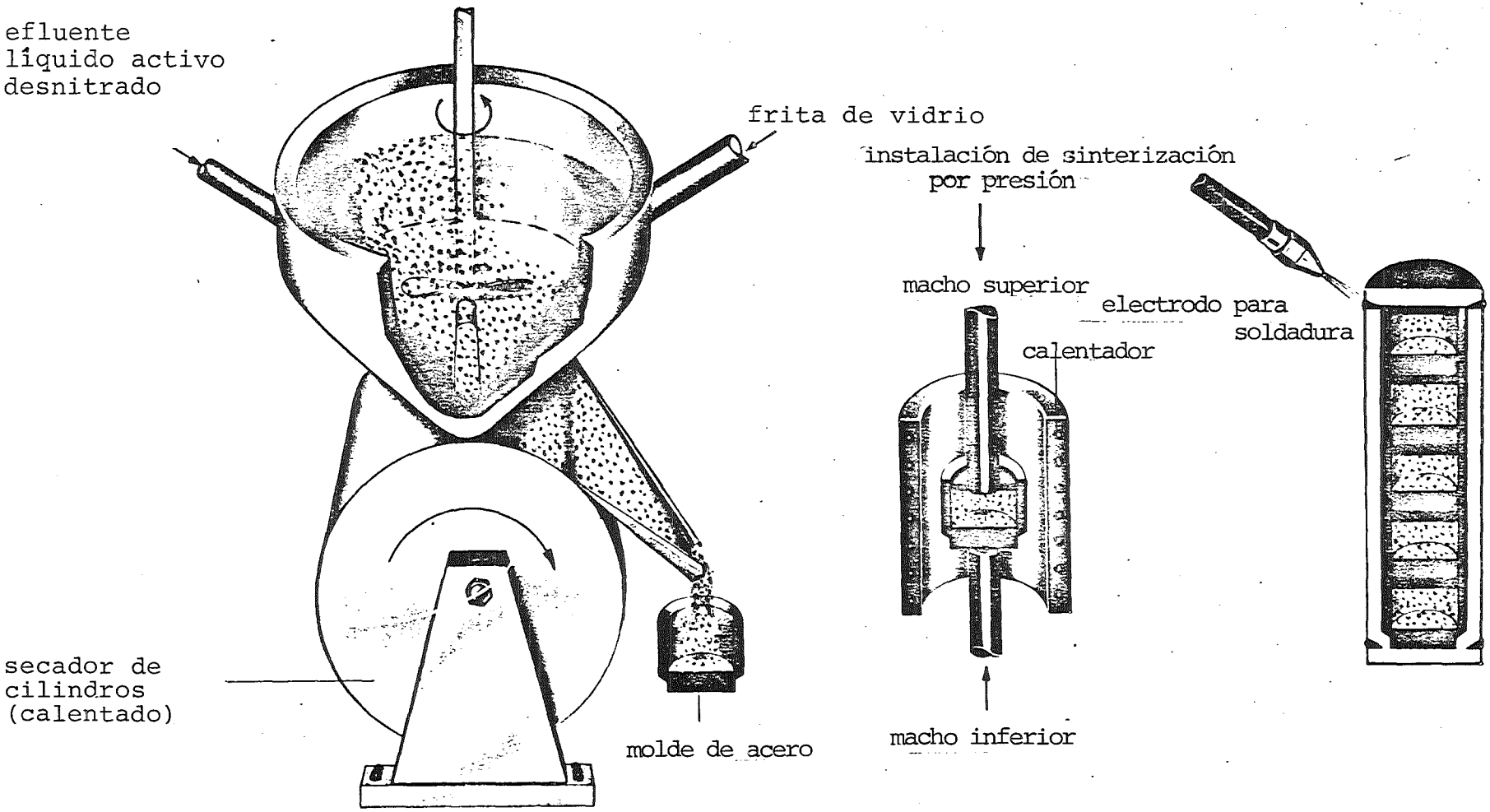

fig. III.7: Esquema del procedimiento para el condicionamiento pulvitecnológico de desechos nucleares

	UNIÁXICO	ISOSTÁTICO
PRENSADO EN FRÍO Y SINTERIZACIÓN	p (MPa) : 100 ÷ 200 T (K) : 750 ÷ 900 t (min) : 200 ÷ 600 $\frac{\Delta T}{\Delta t}\left(\frac{K}{h}\right)$: 50 ÷ 5 SEGÚN ϕ (10÷5) ATMÓSFERA : AIRE	
SINTERIZACIÓN POR PRESIÓN	p (MPa) : $\leqq$ 1,0 T (K) : 850÷900 t (min) : 5÷ 60 $\frac{\Delta T}{\Delta t}\left(\frac{K}{h}\right)$: 50÷ 5 ATMÓSFERA : AIRE	
DENSIDAD (g/cm^3)	92 - 98 % TD	

fig. III.8: Datos de compactación pulvitecnológicos

dan lugar a la formación de monacita que contiene actínidos (fosfato de lantanidos, p.ej. $CePO_4$), cuya forma mineral es altamente resistente a la lixiviación y radiación [17]. La condición previa de esta combinación de componentes es la separación de los elementos de desecho en elementos que contienen actínidos y elementos que no los contienen.

Con las condiciones pulvitecnológicas representadas en la fig. III.8 (polvo de vidrio $\sim$ 40 µm de cuerda) se han fabricado embalajes de desechos apilables con desecho de actividad alta (y media),

- cuyas pérdidas de evaporación son menores (ver fig. III.3),
- que no plantean problemas de compatibilidad con, p.ej., matrices de acero o de grafito y que no dan lugar a la segregación de escorias o fases macroscópicas y
- cuyas tensiones interiores no afectan la integridad mecánica tampoco en el ensayo de caída [2].

Hay que mencionar aquí que pequeñas porosidades como las que existen generalmente en el producto en el procedimiento pulvitecnológico bloquean la propagación de grietas y que por ello tienen que considerarse como favorables! - De una manera semejante, por sinterización por presión (180-300 MPa, 1500-1800 K), se condicionaron componentes altamente radiactivos de desechos en Synroc y envueltas de níquel [24].

III.2 Condicionamiento heterogéneo

Para la preparación de partículas de producto para la inclusión en fases de matriz libres de desecho como barrera microscópica se aplican también métodos tecnológicos de fundición y de polvo.

En el procedimiento PAMELA se hace gotear un vidrio fundido que contiene desecho (1300-1600 K) sobre un disco rotatorio [11]. Se forman perlas de vidrio. La fabricación pulvitecnolo-

gica de partículas de supercalcinado o de Synroc que contienen desecho puede hacerse por preparación de pellets o en el procedimiento sol-gel. En la preparación de pellets, los componentes altamente radiactivos de desecho se conforman y se tratan térmicamente (1500 K) juntos con los componentes del producto y con aglomerantes en tambores rotatorios inclinados mediante una especie de efecto de bola de nieve por aglomeración. En el procedimiento sol-gel, un sol - es decir un sistema altamente disperso de partículas de sólido es transformado en un líquido a un gel, en que interacciones entre las partículas y el sol originan la gelatinización [5]. Synroc se gelatiniza p.ej. en sol HNO_3, que sale goteando a través de una tobera y cuyas gotas se estabilizan en una atmósfera definida (NH_3) y/o un líquido (NH_4OH). Las gotas son secadas en vapor (500 K) y comprimidas con temperaturas de sinterización (1500 K; H_2 + 4% de atmósfera de Ar) [14].

La inclusión heterogénea de las partículas de vidrio, supercalcinado o Synroc en una fase de matriz libre de desecho puede también hacerse mediante tecnologías de fundición y de polvo. En el procedimiento PAMELA las perlas de vidrio que contienen el desecho se introducen en plomo fundido (625 K) de la manera esquematizada en la fig. III.9a. Debido a la diferencia de densidad entre el vidrio y el plomo las esferas de vidrio en la coquilla interior suben hasta arriba y finalmente la llenan completamente después de quitar el tubo de llenado. Al mismo tiempo, debido a la coquilla de doble pared se ha formado una envuelta de plomo libre de vidrio [10-12, 25]. Es también posible llenar la coquilla interior con esferas de vidrio e introducir el plomo a través del intersticio anular (ver fig. III.9b).

Las partículas de vidrio, supercalcinado o Synroc que contienen desecho pueden recubrirse con capas mediante el pre-

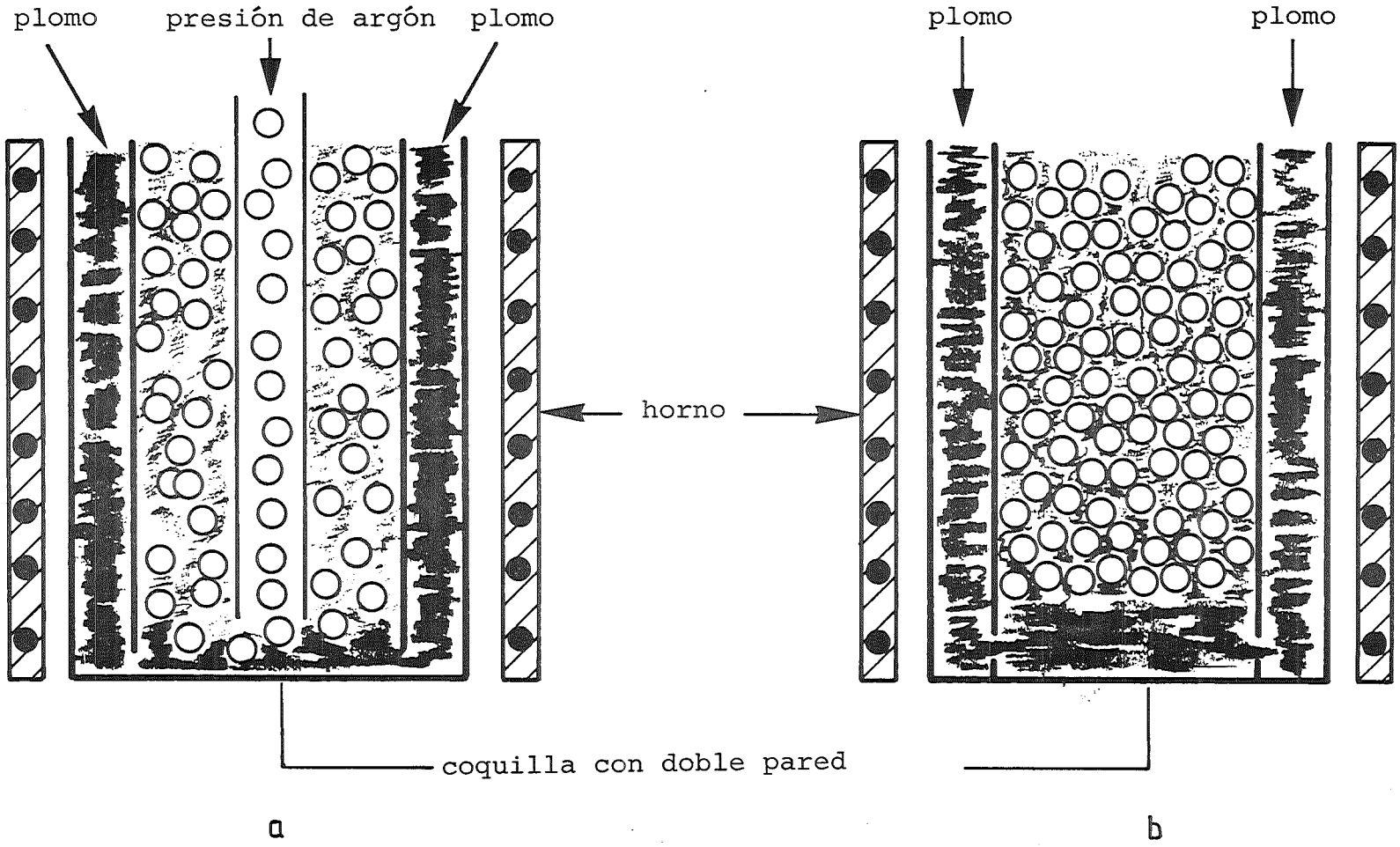

fig. III.9: Principio del procedimiento Pamela para la fabricación de Vitromet

cipitado a partir de la fase gaseosa (CVD = Chemical Vapor Deposition) de compuestos evaporados y descompuestos o por recubrimiento por laminado [21, 25]. En el último procedimiento se adicionan a las partículas que contienen el desecho polvos finísimos y aglomerantes en tambores rotatorios que se adhieren en la superficie de las partículas y que de este modo forman capas. La adición de mayores cantidades de estos polvos, el mezclado, prensado y la sinterización dan entonces lugar a la realización pulvitecnológica de la segunda barrera, microscópica.

Con un método pulvitecnológico comparable se han incluído partículas de supercalcinado en fases de matriz metálica y partículas de vidrio con desecho en una fase de matriz de vidrio-hipersilicato libre de desecho (temperatura de sinterización: 1200 K) [1, 22].

Finalmente se ha obtenido una formación de fase de matriz pulvitecnológica "in situ" por mezcla de los componentes altamente radiactivos de desecho con úrea y polvos metálicos (Fe, Cu, Ni, Co, Al, Si, Ti) [13]. La sinterización (1100 K) y la extrusión y prensado por impacto en atmósfera reductora (1500 K, H_2) han dado lugar a la formación "in situ" de una aleación metálica, posiblemente polifásica.

Al igual que para la comparación de procedimientos tecnológicos de polvo y de fundición para la fijación cuasi homogénea de componentes altamente radiactivos de desechos, la tecnología de polvos tiene también sus ventajas para la fabricación de productos heterogéneos:

Mientras que la inclusión del desecho fijado de modo molecular en una fase de matriz libre de desecho (p.ej. procedimiento Vitromet/Pamela) por métodos tecnológicos de fundición

- admite solamente fases de matriz cuyo punto de fusión es inferior al punto de ablandamiento o resp. al punto de fusión de las partículas que contienen desecho
- no admite la inclusión discontínua de las partículas que contienen desecho en la fase de matriz (el contacto con las partículas disminuye los aspectos de seguridad en la lixiviación)
- plantéa problemas de mojabilidad entre la fase de matriz y las partículas que contienen desecho y limita el juego de adaptación con respecto a los diferentes coeficientes de dilatación térmica del material de fase de matriz y de partículas,

se puede decir que con una inclusión pulvitecnológica del desecho vitrificado en una fase de matriz libre de desecho

- pueden utilizarse también materiales cuyos puntos de fusión son más elevados que los de las partículas que contienen desecho, porque solamente su temperatura de sinterización tiene que ser inferior al punto de fusión de las partículas a incluir, o resp. en el caso del vidrio inferior al punto de ablandamiento del vidrio,
- pueden incluirse las partículas de modo discontínuo, es decir sin contacto entre ellas, en una fase de matriz contínua, lo que aumenta la seguridad en el caso de una rotura parcial de la barrera,
- los problemas de mojabilidad entre la segunda fase heterogénea y los componentes de desecho no tienen casi ninguna importancia técnologica, y las tensiones interiores están considerablemente reducidas.

Hay que mencionar en este contexto que no es irrealista suponer que se producirán tipos de desecho con composición

distinta que necesitarán métodos de tratamiento diferentes, específicos. En suma, las condiciones tecnológicas determinadas por el proceso de fundición no tienen que ser generalmente más desfavorables, y los productos pulvitecnológicos no tienen que ser en cada caso cualitativamente mejores. Un tratamiento de desechos adaptado al desecho, es decir la adaptación tecnológica a diferentes tipos de desecho como objetivo del desarrollo en lugar de una sola tecnología de referencia sin alternativa parece sin embargo actualmente ser el concepto más flexible y mejor justificado desde el punto de vista científico-técnico.

Literatura

[1] American Nuclear Society (ANS), CONF-780304 (1978) X1-15

[2] Barblan, F.F., Schweiz. Mineral. Petrogr. Mitt. (1943) 295

[3] Blair, H.T., PNL-SA-6768 (1979)

[4] Bonner, W.F., et.al., BNWL-2059 (1976)

[5] Cecille, L., IAEA-SM-246/22 (1981)

[6] Chotin, M.M., et.al., CONF-790420 (1979) 73

[7] Christian, J.D., et.al., PNL-2486 (1977)

[8] Dosch, R.G., Ceramic Forms for Nuclear Waste, ACS Symposium Series, No. 100 (1979)

[9] Ewest, E., et.al. IAEA-SM-207/18 (1976)

[10] Geel, J. van, Jül-Conf-42 (1981) 205

[11] Heimerl, W., CONF-790420 (1979) 97

[12] Jardine, L.J., et.al., ANL-78-19 (1978)

[13] Kobisk, E.H., et.al., ORNL/TM-7395 (1980)

[14] Lackey, W.J., et.al., Nucl. Technology 49 (1980) 321

[15] Larson, D.E., et.al., BNWL-SA--5968 (1976)

[16] Lynch, R.W., et.al., SAND-75-0255 (1975)

[17] Mattson, E. in G.J. McCarthy (ed) Scientific Basis for Nuclear Waste Management Vol. 1, Plenum Press, New York (1979) 271

[18] McElroy, J.L., et.al., PNL-3050-2 (1979)

[19] Mendel, J.E., PNL-2764 (1978)

[20] Moncouyoux, J.P., et.al., Jül-Conf-42 (1981) 12

[21] Neumann, W., et.al., CONF-790420 (1979) 150

[22] Page, L.E., et.al., UCID-18873 (1980)

[23] Ramm, E.J., et.al., Demonstration of Synroc Fabrication Scaleup on a Non-Radioactive Basis, Australian Atomic Energy Commission Research Establishment (1982, preprint)

[24] Ringwood, A.E., et.al., Geochemical Journal 13 (1979) 141

[25] Rusin, J.M., et.al., PNL-2668-1/2/3 (1978/1979)

[26] Simonen, F.A., et.al., PNL-3036 (1979)

[27] US-DOE: Technology for Commercial Radioactive Waste Management, DOE/ET-0028 (1979)

[28] Weisenburger, S., et.al., CONF-7904200 (1979) 86